INŻYNIERIA MINERALNA

CZASOPISMO POLSKIEGO TOWARZYSTWA PRZERÓBKI KOPALIN

2(52) 2023

NR 2(52) 2023, LIPIEC – GRUDZIEŃ

PL ISSN 1640 - 4920

JOURNAL OF THE POLISH MINERAL ENGINEERING SOCIETY

NO. 2(52) 2023, JULY – DECEMBER

INŻYNIERIA MINERALNA

Czasopismo Polskiego Towarzystwa Przeróbki Kopalin

JOURNAL OF THE POLISH MINERAL ENGINEERING SOCIETY

INŻYNIERIA MINERALNA JEST DOSTĘPNA (OPEN ACCESS) NA STRONIE WYDAWCY | WHOLE ISSUES OF INZYNIERIA MINERALNA ARE AVAILABLE (OPEN ACCESS) ON PUBLISHER WEBSITE: POLSKA WWW.POTOPK.COM.PL/ARCHIWUM
ENGLISH WWW.POTOPK.COM.PL/AN_ARCHIWUM
www.inzynieriamineralna.com.pl

INŻYNIERIA MINERALNA JEST INDEKSOWANA I ABSTRAKTOWANA | INŻYNIERIA MINERALNA IS INDEXED AND ABSTRACTED:
SCOPUS (ELSEVIER), WEB OF SCIENCE, MASTER JOURNAL LIST – EMERGING SOURCES CITATION INDEX (CLARIVATE ANALITICS), POL-index, EBESCO, BAZTECH, Chemical Abstracts, Реферативный Журнал.
Inżynieria Mineralna is a member of CROSSREF.

ADRES REDAKCJI | CORRESPONDENCE ADDRESS:
POLSKIE TOWARZYSTWO PRZERÓBKI KOPALIN | POLISH MINERAL ENGINEERING SOCIETY
MICKIEWICZA 30, 30-059 KRAKÓW
MAIL: im@agh.edu.pl, inzynieria_mineralna@agh.edu.pl, tora@agh.edu.pl

SKŁAD/ŁAMANIE/UKŁAD TYPOGRAFICZNY/OBSŁUGA: NOWY WSPANIAŁY HOLDING (NWH)
KONTAKT: C@NWH.PL
DRUK: DRUKARNIA TYPOGRAFIA — WWW.TYPOGRAFIA.COM.PL
KONTAKT: TYPOGRAFIA@TYPOGRAFIA.COM.PL
NAKŁAD: 50 egz.

INŻYNIERIA MINERALNA
CZASOPISMO POLSKIEGO TOWARZYSTWA PRZERÓBKI KOPALIN

Distinguished participants,

As we gather for the prestigious POL-VIET 2023 — the 7th International Conference POL-VIET, dedicated to fostering scientific and research cooperation between Vietnam and Poland, we embark on a journey of discovery, collaboration, and innovation in the realms of Industry and Earth Sciences.

This conference stands as a beacon of opportunity for scientists and experts alike, offering a platform for the exchange of knowledge and experiences that span the breadth of these fields. At the core of our discussions will be subjects that delve into the heart of contemporary scientific and technological advancements, all of which are intrinsically tied to the pursuit of sustainable and responsible industry practices.

At POL-VIET 2023, we bring together not just expertise but also a collective determination to address the challenges that lie before us. It is here that we will explore the frontiers of innovation, forge collaborations, and lay the groundwork for a future where industry practices align harmoniously with environmental preservation.

We are providing a collection of papers that were submitted to the conference and successfully reviewed and we invite you to engage with us in thoughtful deliberation and exchange of ideas. Each presentation and discussion will contribute to the set of insights that will shape the future of mining and Earth sciences.

Thank you for being a part of POL-VIET 2023, and we look forward to the valuable contributions and enriching discussions that await us.

Sincerely,

Marek Borowski
Conference Chair
POL-VIET 2023

AGH

Geological Controls on Evolution of Submarine Channels in Song Hong Basin, Offshore Vietnam

Anh Ngoc LE[1)], Hoa Minh NGUYEN[2)], Muoi Duy NGUYEN[3)], Ngan Bui THI[4)]*

[1)] Petroleum Geology Department, Faculty of Petroleum and Energy, Hanoi University of Mining and Geology; Basin, stratigraphy and sedimentary process group (BSSP), Hanoi University of Mining and Geology, 18 Vien Street - Duc Thang Ward - Bac Tu Liem District - Ha Noi – Vietnam; https://orcid.org/0000-0002-1607-9388
[2)] Petroleum Geology Department, Faculty of Petroleum and Energy, Hanoi University of Mining and Geology; Basin, stratigraphy and sedimentary process group (BSSP), Hanoi University of Mining and Geology, 18 Vien Street - Duc Thang Ward - Bac Tu Liem District - Ha Noi – Vietnam; https://orcid.org/0000-0002-6555-662X
[3)] Petroleum Geology Department, Faculty of Petroleum and Energy, Hanoi University of Mining and Geology; Basin, stratigraphy and sedimentary process group (BSSP), Hanoi University of Mining and Geology, 18 Vien Street - Duc Thang Ward - Bac Tu Liem District - Ha Noi – Vietnam; https://orcid.org/0009-0005-1964-1048
[4)] Petroleum Geology Department, Faculty of Petroleum and Energy, Hanoi University of Mining and Geology; Basin, stratigraphy and sedimentary process group (BSSP), Hanoi University of Mining and Geology, 18 Vien Street - Duc Thang Ward - Bac Tu Liem District - Ha Noi – Vietnam; https://orcid.org/0009-0004-6188-3246
* Correspondence author: Nguyen Duy Muoi, nguyenduymuoi@humg.edu.vn; lengocanh@humg.edu.vn

http://doi.org/10.29227/IM-2023-02-07

Submission date: 19-08-2023 | Review date: 06-09-2023

Abstract

Song Hong basin is a very large basin with complicated onshore to offshore geological structure. The basin comprises the pre-Tertiary basement and Kainozoi sequences. This study focused on the evolution of submarine channel in Miocene sequence. The study interval is the major reservoir of the basin characterized as submarine channel complex and lower to Middle Miocene carbonates with the porosity of 15–25%. The channel is highly eroded into the substrate with c. 7 km wide and 20 km long, trending northwest-southeast. They are 'U' to 'V' shape, sub-parallel to deep faults which reactivated in the Early and Mid-Late Miocene. The channel deposit is characterized by cut and fill architecture and can be seen as high amplitude, bi-directional downlap. The channels are likely to be controlled by the two inverted phases in Late Oligocene and Middle-Late Miocene. The tectonic events are not only controls the flow directions but also modified the shape of the channels. The occurrence of well-developed submarine channel give a great hydrocarbon potential for the Song Hong basin.

Keywords: *Song Hong basin, submarine channels, channel complex, 3D seismic*

1. Introduction

During the past few years, submarine channel has been significantly getting interest from scientists due to the development of 3D seismic techniques. This advance techniques allow us to get inside the channel image and thus understand the channel evolution and also its spatial and temporal distribution (Gee et al., 2007; Posamentier and Kolla, 2003; Kolla et al., 2007). Despite this, many elements of channel development and the processes that define their geometry remain unconstrained (Gee et al., 2007).

Submarine channel evolution is a result of sea-level change, sediment gravity flows, tectonics, and climate and plays an important element in the sedimentary basins (Satterfield and Behrens, 1990; Covault et al., 2016). The channel can extend up to thousands of kilometers. The channel fills reveal different stages from early channel incision to lateral migration to late-stage aggradation (Covault et al., 2016). They were proved to be very important in oil and gas exploration as the sand-rich channel filled that have high porosity and thus can store large amount of hydrocarbon (Kolla et al., 2001).

Submarine channels have been documented in the Song Hong basin (Hiep, 2019). The channels are not just simple with straight planform, they are highly complex with deeply incised channels. Due to this complexity, many aspects of channel evolution and the processes that control channel geometry remain unconstrained and have not been studied. In this paper, we use 3D seismic data to investigate the channel evolution and its associated depositional elements in conjunction with the tectonic regime in the northern part of the Song Hong basin. The channels are in Mid-Miocene in age and buried a few hundred meters below the present-day seafloor.

2. Geological setting

The Song Hong basin, situated on the northern part of the Vietnam continental shelf, is an extended basin trending NW--SE direction containing a small onshore area (Hanoi trough) and a large offshore area in the Gulf of Bac Bo from the NE to offshore Central Vietnam with more than 10 km of sediment thickness in the central basin area (Fig. 1).

Song Hong basin is the second largest sedimentary basin in Vietnam with complicated onshore to offshore geological structure, varying from the NW to the SE and from North to the South. The rhombic shape extended along the basin axis suggests that the basin had a strike-slip origin related to the Red River fault system, which was initiated by the collision between the Indian and the Eurasian plates in Eocene - Early Oligocene times (Tapponnier et al., 1986, 1990, Nguyen et al., 1999). Left-lateral strike-slip movement and pull-apart extension are the main geodynamic factors that form the Song Hong basin. After that, tectonic inversion in Late Oligocene

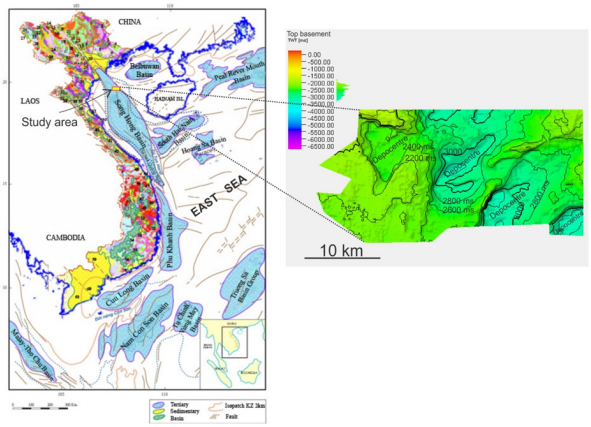

Fig. 1. (a) Study area in the Song Hong basin, one of the tertiary Sedimentary Basins in Vietnam, (b) Time structure map of the top basement of the study area – visible 4 depocentres with a thickness of up to 400 ms TWT

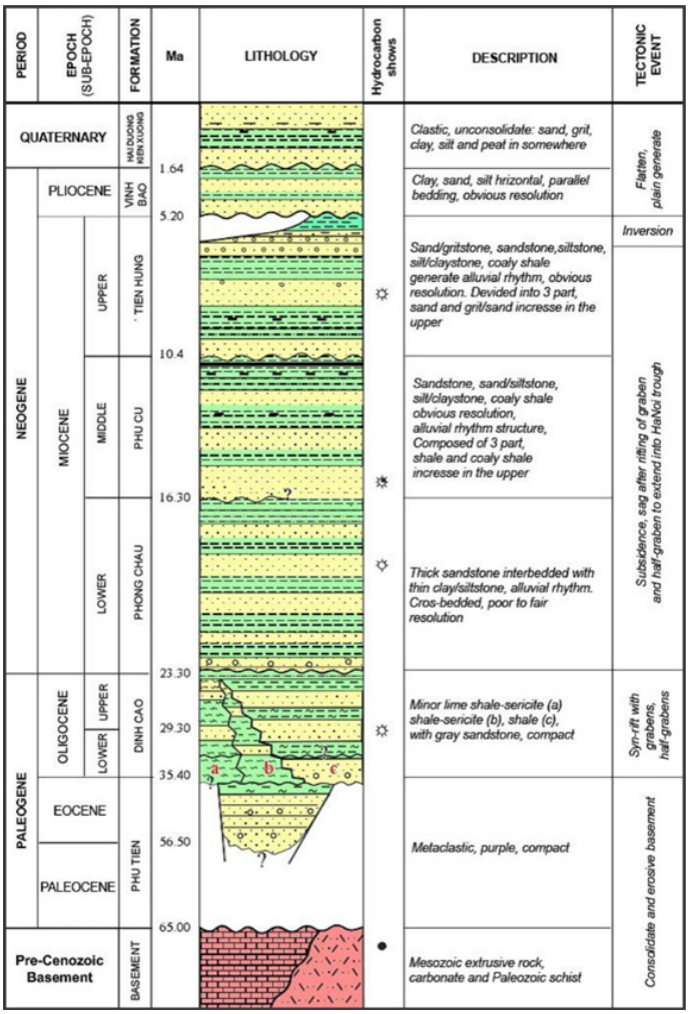

Fig. 2. Generalized stratigraphic column of NW Song Hong basin (Hiep, 2019)

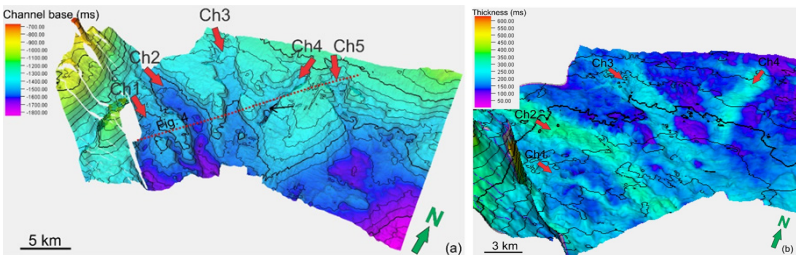

Fig. 3. (a) A map, 3D view of the channel base, shows the occurrence of five channel in the same stratigraphy level corresponding to Mid–Miocene in age. (b) Thickness maps between the channel base and the top of Mid–Miocene sequence reveal the channel thickness is up to 350 ms

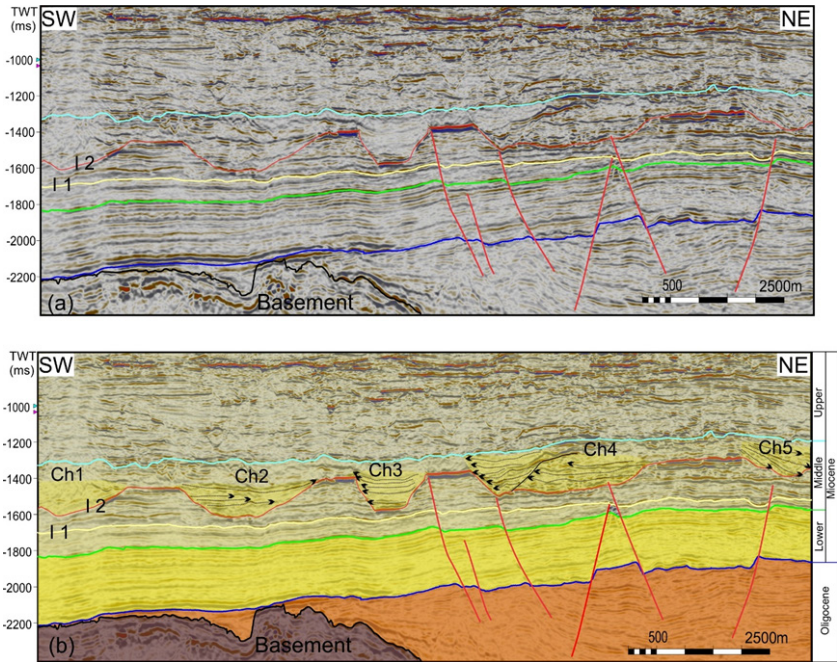

Fig. 4. The un-interpreted seismic section (above) and interpreted seismic section (below) to show the five channels in the cross section

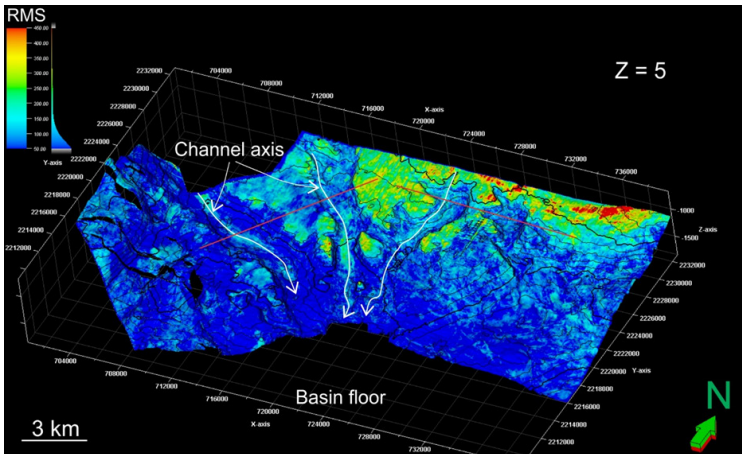

Fig. 5. RMS attribute map of the Mid Miocene channel base in 3D view

caused by northwest–southeast opening of East Vietnam Sea and the Middle-Late Miocene tectonic inversion partly contributed to the hydrocarbon trapping mechanism in the Song Hong basin (Vo et al., 1999).

The stratigraphy of the Song Hong basin is relatively complex, including the Pre-Tertiary basement and Kainozoic sequences – Paleogene, Neogene, and Pliocene-Quaternary sediments (Fig. 2).

Geological structures in the Song Hong basin, which involved the hydrocarbon accumulation, were formed in different stages, including (1) buried basements, (2) Oligocene tilted fault blocks or flower fault systems, and (3) Oligocene –Early Miocene inverted structures. Hydrocarbon migrated from Eocene–Oligocene source rocks vertically along faults, then secondary migration was mainly lateral. However, to some extent, fault systems would facilitate the leakage hydrocarbons from the traps (Hiep, 2019).

3. Dataset and methodology

In this study, we use high-resolution 3D seismic data covering an area of 936 km² (39 km long and 24 km wide) from the northern part of the Song Hong basin. The dataset has inline and crossline spacing of 12.5 m. Dominant frequency is c. 44 Hz and the velocity is 2000 m/s, the vertical seismic resolution defined as a quarter of the dominant wavelength, will be 11 m. The study focused on the Lower–Middle Miocene sequence, corresponding to the interval from 560 ms to 2740 ms.

The seismic interpretation have carried out using the Schlumberger™ Petrel software to determine the key sequence stratigraphy boundaries, geometry, and internal structure of channels. The seismic interpretation started with line by line interpretation, auto-tracking, and seismic facies identification. Detail time structural, thickness, gradient, and attribute maps were generated to visualize the channel image in 2D and 3D map view. The study used the sequence stratigraphy method of Vail and Mitchum (1977) to detect the channel. The reflection terminations are the key to breaking up the seismic sequences by identifying their unconformities and their correlative unconformity. Channel is recognized as a set of onlap or bidirectional down termination reflections onto the erosional base.

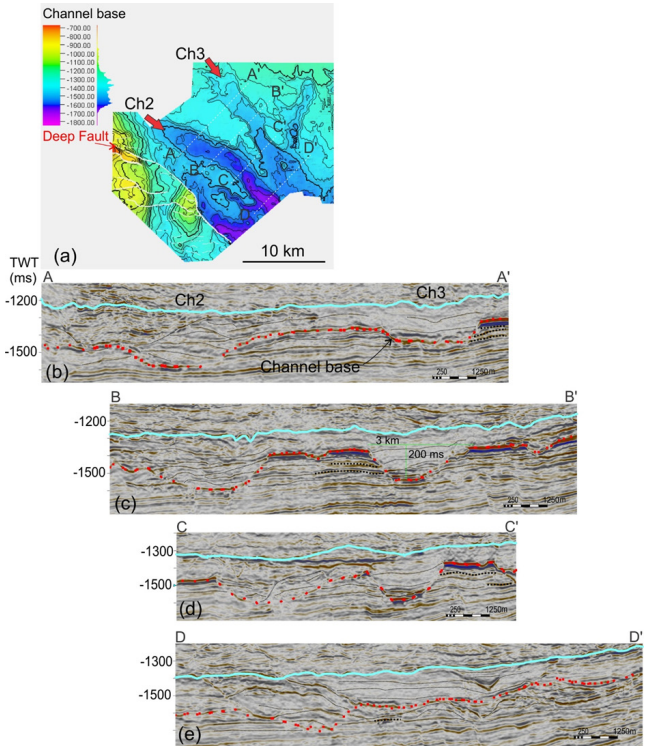

Fig. 6. (a) Time structure map of the base of the Mid Miocene channels, (b–e) seismic cross sections along the channel 2 and 3 to illustrate the channel variation and evolution downstream

4. Results and discussion

In the Miocene sequence, the channels are intensively developed at the Mid–Miocene level in which the channel base has been mapped to analyze the channel morphology (Fig. 3 & 4). Five channels have been detected, marked as channel 1 (Ch1) to channel 5 (Ch5) from West to East respectively. The channels are rather straight, derived from the north, and northwest, flowing down to the central of the basin to the southeast. The channels have 'U' to 'V' shape, up to 20 km long, 7 km wide, and 350 ms deep (Fig. 4). They intensively developed in the same stratigraphy level, spacing of c. 5 to 10 km. The channels tend to remain dimension until some of them join together downslope.

Three elements to describe channel characteristics include (i) channel axis, (ii) channel fills, and (iii) levees.

The base of channels is wide and relatively flat. The channel axis is often associated with high amplitude at the base of the channel and can be well observed in channel 2, 3, and 4 (Fig. 5). These high amplitudes change to low when the channel move further down toward the basin floor.

The channel fill is characterized as low to moderate amplitude with discontinuous to continuous reflections, complex geometries. This is interpreted to be sandy deposits. Among those channels, channel 3 is dominantly by low amplitude to transparent amplitude reflections, high amplitude reflections only observed at the channel base. This suggests that the channel had mainly been supplied by a muddy source system and thus gradually derived very fine-grained sediments. The internal architecture of the channels is progradation or aggradation fills which tends to convex up (Fig. 6 & 7). These folding shapes may be caused by a period of high sedimentation rate or more likely be a result of the inversion tectonic uplift in Mid-Late Miocene, leading to sediment compression.

Levee is the last channel element, it commonly shows aggradational and low to high amplitude reflections. High amplitude reflections appeared to be seen near the channel and decreasing amplitude away from it. The maximum levee height is approximately 20 ms, decreasing thickness away from the channel. The amplitude gradually changes to low away from the channel indicating the finer grain size in this direction.

The channels are highly incised into the substrate and conduit the sediment downward to the basin floor. These sediments were deposited in a deltaic or shallow marine setting (Hiep, 2019). The occurrence of all channels in the same stratigraphy level corresponds to the Mid-Miocene time. The basin experience an uplift and inversion in the Early Oligocene to Mid-Late Miocene, and even to the Early Pliocene in some places. Miocene sediments were strongly compressed, uplifted, and truncated. As a result, a thick section of approximately hundreds to thousands of meters was eroded; non-deposition possibly lasted for several million years (Hiep, 2019). The channel image of this study area confirmed for the tectonic inversion by the convex up of internal channel fill reflections.

Tectonic inversion was triggered by the right lateral movement of the Red River fault system at the end of the Miocene (Hiep, 2019). Therefore, channels developing in the highly tectonic area are experienced many phases of dynamic adjustment in their cross-channel geometry. The internal structure of the channel varies along the channel profile from aggradation to progradation. Channels are highly incised into the substrate with muti-stage of cut and fill (Fig. 6 & 7). The channels are straight indicating for high-energy environment. They are more likely to conduit turbidity current flows, transporting sediments further downslope to deposit in the depocentres.

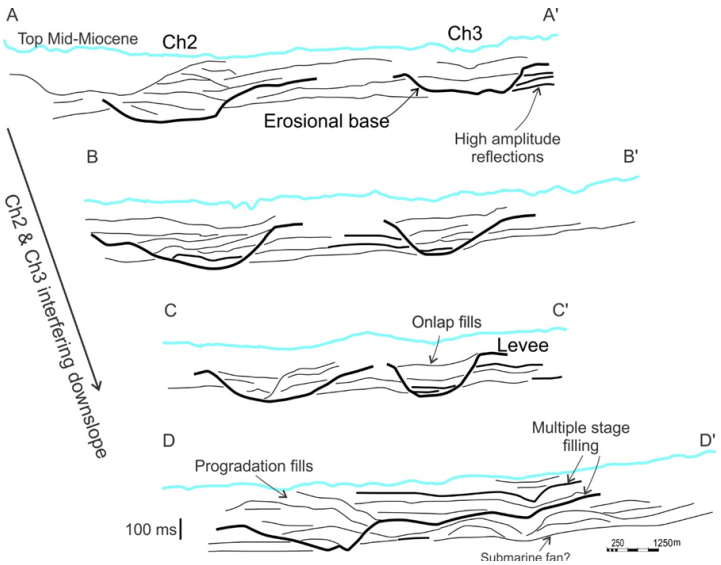

Fig. 7. Seismic facies diagram of the channels 2 and channel 3. Channels 2 and 3 tend to join together downslope, toward the basin floor (see seismic section in Fig 6)

The rifting phase creates the basin and forms many grabens corresponding to the four depocentres on the Basement map (Fig. 1b). These depocentres are overfilled in Oligocene time. Some deep basin opening faults dominantly in the eastern part of the study area (Fig. 6a) reactivate and penetrate through Oligocene and Miocene with the offset up to c. 50 ms, trending northeast–southwest. These faults tend to parallel with the channel paths. All of the channels are derived from the north and northwest which is the basin margin direction. The channel seems to follow the basement structure, the deep fault of the basin (Fig. 6a). There is no connection between the depocentre on the top basement and the Mid–Miocene channel system.

The amplitude attribute is an indicator to predict the strata lithology. In this area, the channels are filled by medium to high-amplitude seismic reflections, suggesting sandy channel deposits. Among those, channel 3 has muddy filled at the late stage with low to transparence amplitude. This indicates for more than one sediment source supplying for this channel system. Channel 3 is mainly supplied by the muddy sediment source.

According to Hiep (2019), the porosity of Miocene sandstones and sandstone-claystones usually varies from 15% to 25% increasing towards the upper section. The intensively developed channel system in the Mid-Miocene, which tends to be merged downslope, shows a widespread and stable distribution of the sand-rich channel deposits. This channel system may provide good reservoir quality for the Mid-Miocene sequence, giving a great hydrocarbon potential for the area.

5. Conclusions

Mid-Miocene channels are a complex channel system located on the margin of the Song Hong basin. The channels developed intensively on the same stratigraphy, highly incised along its pathway. The geometry of the channels almost remains 'U' to 'V' shape, channel width, and thickness along its profile. The channels have been built gradually by progradation or aggradation. The channels may have undergone some postdepositional deformation due to the mid to late Miocene tectonic inversion, resulting in the relatively doming channels. Channels run northeast–southwest which has a similar direction to the deep faults which have been reactivated in early and Mid-late Miocene time. The occurrence of submarine channels which are interpreted to be sand-rich deposits (except channel 3) at large scale give high-quality hydrocarbon reservoirs for the study area.

6. Acknowledgments

This paper has been interpreted in the lab of the Petroleum and Energy Faculty, Hanoi University of Mining and Geology by Basin, stratigraphy, and sedimentary process group (BSSP). We thank to Schlumberger for software support.

Literatura – References

1. Covault, J. A., Sylvester, Z., Hubbard, S. M., Jobe, Z. R. & Sech, R. P. 2016. The Stratigraphic Record of Submarine-Channel Evolution.
2. Gee, M., Gawthorpe, R., Bakke, K. & Friedmann, S. 2007. Seismic geomorphology and evolution of submarine channels from the Angolan continental margin. Journal of Sedimentary Research, 77, 433-446.
3. Hiep, N. 2019. The petroleum geology and resources of Vietnam. Publishing House for Science and Technology Hanoi, 552pp.
4. Kolla, V., Bourges, P., Urruty, J.-M. & Safa, P. 2001. Evolution of deep-water Tertiary sinuous channels offshore Angola (west Africa) and implications for reservoir architecture. AAPG bulletin, 85, 1373-1405.
5. Kolla, V., Posamentier, H. & Wood, L. 2007. Deep-water and fluvial sinuous channels—Characteristics, similarities and dissimilarities, and modes of formation. Marine and Petroleum Geology, 24, 388-405.
6. Nguyen, V. G., Rabinowitz, P. D. (1999). Gravity Modeling of the Song Hong Basin, Offshore Vietnam. Offshore Technology Conference.
7. Posamentier, H. W. & Kolla, V. 2003. Seismic geomorphology and stratigraphy of depositional elements in deep-water settings. Journal of sedimentary research, 73, 367-388.
8. Satterfield, W. M. & Behrens, E. 1990. A late Quaternary canyon/channel system, northwest Gulf of Mexico continental slope. Marine Geology, 92, 51-67.
9. Tapponnier, P., Peltzer, G., Armijo, R., 1986. On the mechanisms of the collision between India and Asia. In: Coward, M.P., Ries, A.C. (Eds.), Collision Tectonics. Geological Society of London Special Publication, 19, 115–157.
10. Tapponnier, P., Lacassin, R., Leloup, P.H., Scha¨ rer, U., Zhou, D., Wu, H., Liu, X., Ji, S., Zhang, L., Zhong, J., 1990. The Ailo Shan/Red River metamorphic belt: Tertiary left-lateral shear between Indochina and South China. Nature, 343, 431–437.
11. Vail, P. R., and R. M. Mitchum, 1977, Seismic stratigraphy and global changes of sea-level - Part 1: Overview, in C. E. Payton, ed., Seismic stratigraphy — Applications to hydrocarbon exploration: AAPG Memoir 26, 51–52.
12. Vo, T. H. Q & Pham, H. G. (1999). Geochemical evaluation of shale formations in the northern Song Hong basin, Vietnam. Journal of Petroleum Exploration and Production Technology, 9, 1839–1853.

Simulation on Flyrock due to Blasting Using Smoothed Particle Hydrodynamics (SPH) with LS-Dyna software

Bao Tran DINH[1)], Trieu Do VAN[3)], Viet Pham VAN[2)], Nguyen Dinh AN[4)]*

[1)] Hanoi University of Mining and Geology, 18 Vien street, Hanoi 100000, Vietnam; Innovations for Sustainable and Responsible Mining (ISRM) Research Group, Hanoi University of Mining and Geology, 18 Vien street, Hanoi 100000, Vietnam; email: trandinhbao@humg.edu.vn, https://orcid.org/0000-0003-1801-1165

[2)] Hanoi University of Mining and Geology, 18 Vien street, Hanoi 100000, Vietnam; Innovations for Sustainable and Responsible Mining (ISRM) Research Group, Hanoi University of Mining and Geology, 18 Vien street, Hanoi 100000, Vietnam; email: phamvanviet@humg.edu.vn, https://orcid.org/0009-0003-3345-9328

[3)] Institute of Mining Science and Technology – Vinacomin; dovantrieu15091996@gmail.com, https://orcid.org/ 0009-0007-7887-9034

[4)] Hanoi University of Mining and Geology, 18 Vien street, Hanoi 100000, Vietnam; Innovations for Sustainable and Responsible Mining (ISRM) Research Group, Hanoi University of Mining and Geology, 18 Vien street, Hanoi 100000, Vietnam; email: nguyendinhan@humg.edu.vn, https://orcid.org/0009-0003-2156-6011

* Corresponding author: trandinhbao@humg.edu.vn

http://doi.org/10.29227/IM-2023-02-08

Submission date: 18-08-2023 | Review date: 11-09-2023

Abstract

In surface mining operation, blasting method has been commonly used and accounted highly for breaking waste rock and mineral. The main goal of the activity is fundamental fragmentation by energy generation due to blasting. However, only 20% to 30% blasting energy is generated to fragment rock. The remain energry is wasted for flyrock, ground vibration, air overpressure, dust and too fine fragmentation. Flyrock in blasting is large risk for surface mines and occupies more than a half of incidents relating to blasting at surface mines, because this is a severe issue and causes negative reaction of the surrounding residients. However, studies on flyrock-phenomenon prediction methods for blasting in Vietnam have been also limited. In the study, simulation analysis method on induce-blasting-induced flyrock experiment using Smoothed Particle Hydrodynamics (SPH) with LS-Dyna software. Two-dimension modelling was built and practically applied for B2 cross section of Mong Son quarry in Yen Bai province. The result showed that the ability of Smoothed Particle Hydrodynamics (SPH) in analysizing flyrock trajectory distance in blasting. By using the modelling with field-site parameters, the researcher monitored flyrock velocity at installed time periods, such as 1.5 second when the flyrocks fly with a maximum distance of 85 m from blasting site and their average velocity of 40 m/s.

Keywords: *flyrock, smoothed particle hydrodynamics, simulation, blasting, LS-Dyna*

1. Introduction

In open-pit mining, the blasting method (Blasting) is widely used and has a significant proportion in breaking rocks and extracting valuable minerals. Blasting is the initial and crucial technological step in the mining process, directly influencing the effectiveness of subsequent technological stages.

The main objective of blasting is to efficiently break rocks and extract valuable minerals while ensuring the optimal quality of fragmentation with the lowest possible cost and minimal negative impact on the surrounding environment [1, 2, 3, 4, 5]. To achieve these goals, accurate calculation of the design parameters for blasting and the application of modern blasting techniques are necessary. The blasting operation must fulfill the requirements for the volume of rocks to be broken, the size of rock fragments according to production needs, cost optimization for the entire mining operation, and the minimization and control of harmful effects on the environment. In summary, optimizing the degree of rock fragmentation, displacement distance, geometric size of rock piles after blasting, while ensuring safety in terms of ground vibrations, airblast waves, and flyrock, is the primary objective in any blasting operation.

In the process of blasting operations, it should be noted that only 20% to 30% of the blasting energy is utilized for rock fragmentation. The remaining energy is wasted in the form of flyrock, ground vibrations, airblast waves, dust generation, and excessive fragmentation [6, 7, 8, 9]. Flyrock is the most significant hazard in open-pit mining blasting operations. It accounts for about half of all mining-related accidents. A study [10] has shown that over 40% of fatal accidents and over 20% of serious accidents in mining operations in India are caused by flyrock. Another study [11] revealed that flyrock exceeding the hazardous zone is the cause of 25% of open-pit mining accidents in the United States. According to statistical accident data [12], flyrock is responsible for 20–40% of mining-related accidents. The dangers and damages caused by flyrock are a serious issue that has been present since the use of blasting in mining operations. Some consequences of flyrock include severe injuries or fatalities, damages to structures and equipment, and even mine closures.

The causes of flyrock phenomenon in mining blasting can include both controllable and uncontrollable factors. Inaccurate blasting design parameters, improper stemming, insufficient burden height, inaccurate hole spacing, excessive explosive charges, unfavorable geological conditions (such as fractures, voids, layering, weak geological formations, etc.), time delays and sequencing inconsistencies, rock fractures and falls, [10, 11, 13, 14], are some of the causes leading to flyrock phenomenon. Therefore, efforts to prevent conditions

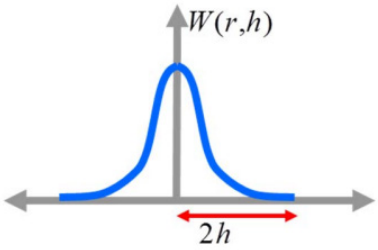

Fig. 1. Interpolation position of kernel function 2D [42]

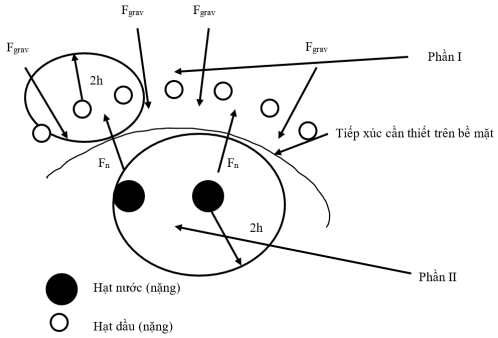

Fig. 2. Particle-particle interactions [43]

that may lead to flyrock phenomenon are an urgent issue that needs to be addressed in current research.

Currently, mining operations are expanding closer to residential areas, increasing the safety risks associated with blasting activities. If issues related to blasting, such as ground vibrations, airblast waves, dust, and especially flyrock, are not properly controlled, they can lead to severe consequences. Until now, many researchers have attempted to predict blasting-related issues through various experimental equations [22, 23]. However, the performance of these models has been unsatisfactory on a large scale, resulting in inaccuracies and a lack of scientific basis. In recent years, various modeling techniques have been applied to predict flyrock distances. Monjezi et al. [24, 25, 26], Rezaei et al. [27], and Ghasemi et al. [28, 29] have utilized artificial neural networks and fuzzy logic techniques for flyrock prediction. Amini et al. [30] employed a machine learning technique called Support Vector Machine (SVM). Raina et al. [31] used a probabilistic method to delineate the hazardous area of flyrock in an open-pit mine. With the emergence of scientific tools, engineering techniques, and advancements in hardware and software in recent decades, the accuracy of predictions has improved [32]. Lastly, the use of AI techniques, including data training and testing from blasting events and comparing results using different algorithms, has gained significant importance in the past decade. AI techniques such as Fuzzy Inference System (FIS), Artificial Neural Networks (ANN), and Adaptive Network-based Fuzzy Inference System (ANFIS) have been successfully applied to solve complex geotechnical problems [33, 34]. These methods have been widely used to mitigate blasting-related issues [35, 36] as AI analysis models leverage the flexible nature of data, allowing easy adjustments as a predictive tool for any new data. This advantage makes AI a fast and powerful tool in addressing non-linear relationships between input and output parameters that are not well-known [37]. However, alongside these advantages, models using AI techniques require a large amount of input data, and measuring flyrock distances from blasting events is complex and challenging. To date, there has been limited research on using simulation models to predict flyrock phenomena in blasting operations.

In this study, a new method is proposed to predict flyrock distances. The model is developed based on the Smoothed Particle Hydrodynamics (SPH) method, originally developed by Lucy, Gingold, and Monaghan (1977). This method was developed to overcome limitations encountered in extreme deformation problems through the finite element method. The main difference between SPH and conventional methods is that SPH does not divide the nodes. The particles represent the elements that have both general and specific characteristics depending on the declared properties [38, 39].

Until now, several studies have explored the application of the SPH method in simulating blasting operations using LS-Dyna software. Among them, the studies by Jing Gao et al. [40] on "2D Simulation of Blasting Process with 5 Blastholes under Various Horizontal Pressure Coefficients" and Gaohui Wang et al. [41] on "Assessment of Blast Protection and Dam Safety against Explosion Energy" can be mentioned.

Today, simulation has become a reliable solution for studying, analyzing, and evaluating mechanical impact models. This paper performs a simulation analysis of flyrock resulting from blasting using the SPH method in the LS-Dyna software for a 2D model constructed from the B2 cross-section of the Mông Sơn limestone quarry. The results of the model demonstrate the capability of the SPH method in analyzing the details of blasting operationsSouth-central Vietnam is situated in the Indochina block of Southeast Asia and abundantly occurs Cretaceous granitic batholiths [1–3]. The formation of Cordilleran-type granitic batholiths mainly shows a close correlation with the subduction of oceanic crust beneath the continental crust, and they can be products of crustal recycling and the presence of liquid water [4–11]. Generally, cordilleran granitic batholiths consist of different chemical characterizations due to they are formed by melting of sedimentary rocks (i.e., S-type granites), differentiation

Fig. 3. The border of Mong Son mine [46]

of mafic parental magmas (i.e., A-type granites), and partial melting of dehydrated middle/lower crust (i.e., I-type granites) [11–13]. In south-central Vietnam, granitic batholiths have been considered to be contemporaneous with the granitoid of the South China block. However, only a few studies were carried out on granitic batholiths in this area for investigating Cretaceous magmatism and granite composition [2, 14, 16, 17, 18]. Therefore, Cretaceous magmatism and the formation of granitic batholiths (subducted material (basalt + sediment) or melted basement rock) is still unclear. In this study, granitic rocks of the Deoca, Ankroet, and Dinhquan complexes are collected for zircon U–Pb analysis to investigate Cretaceous magmatism and granite composition in south-central Vietnam.

2. Research Methods

In this section, the authors will provide an overview of the Smoothed Particle Hydrodynamics (SPH) method, the interaction between particles in SPH, as well as the constitutive equation of materials specific to rocks and explosives for simulating blasting operations on a 2D model.

2.1. Standard formula of fine particle dynamics (SPH) method

The SPH method is expressed based on the second-order formula of moving particles (xi(t), wi(t)) for i ∈ P, where P is the set of particles, xi(t) represents the position of the i-th particle, and wi(t) denotes the weight of the i-th particle. The second-order formula for a function can be written as follows:

$$\int_{\Omega} f(x)dx = \sum_{j\in P} W_j(t).f\left(x_j(t)\right) \tag{1}$$

The second-order formula (1), along with the smoothing kernel, forms the definition of an approximate value function for the particles. The interpolated value of the function u(x) at position x using the SPH method is given by:

$$\Pi^h\left(u(x_i)\right) = \sum_{j\in\Omega} w_j(t).u\left(x_j\right).w\left(x_i - x_j, h\right) \tag{2}$$

Where Σ is taken over all particles within Ω and within a radius of 2h, W is the position of the smoothing kernel based on the "spline" curve with a radius of 2h, and h is the smoothing length in both time and space. The kernel function is defined as follows:

$$w\left(x_i - x_j, h\right) = \frac{1}{h}\theta\left\{\frac{x_i - x_j}{h(x,y)}\right\} \tag{3}$$

$W(x_i–x_j,h)$ tends to δ as h approaches 0, where δ is the Dirac function, and h is a function of x_i and x_j, known as the smoothing length of the kernel function.

The spline curve construction function is defined as follows:

$$\theta(d) = Cx\begin{cases} 1-\frac{3}{2}d^2+\frac{3}{4}d^3 & \text{Khi } 0\le d\le 1 \\ \frac{1}{4}(2-d)^3 & \text{Khi } 1\le d\le 2 \\ 0 & \text{Khac} \end{cases} \tag{4}$$

With d being the spatial dimension, the gradient of the function u(x) is obtained by applying the derivative operator to the smoothing length:

$$\nabla\Pi^h\left(u\left(x_i\right)\right) = \sum_j w_j.u\left(x_j\right).\nabla w\left(x_i - x_j, h\right) \tag{5}$$

The evaluation of an inner product interpolation of two functions is given by the product of their interpolated values (Fig 1).

2.2. Continuity equations and momentum equations of particles in the smoothed particle dynamics method

The approximate value of the particle in the continuity equation is determined as follows:

$$\frac{d\rho_i}{dt} = \rho_i\sum_j \frac{m_j}{\rho_i}\left(v_i^{\beta} - v_j^{\beta}\right)w_{ij},\beta \tag{6}$$

It is Galilean invariant, as the position and velocity of particles only appear in the form of differences, where is the velocity component at the i-th particle.

The discrete form of the SPH momentum equation is developed as:

$$\frac{dv_i^{\alpha}}{dt} = -\sum_j \frac{m_j}{\rho_i\rho_j}\left(\sigma_i^{\alpha\beta} \pm \sigma_j^{\alpha\beta}\right)w_{ij},\beta \tag{7}$$

The formula ensures that the stress is automatically continuous on the material's interface. Different types of SPH

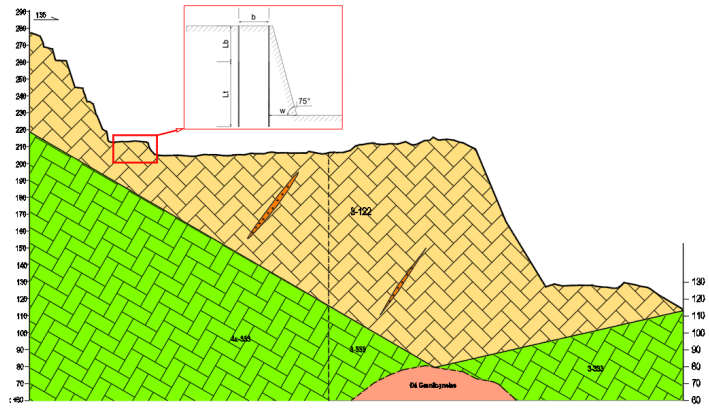

Fig. 4. Section of B2 line of Mong Son mine and explosive loading diagram used to simulate blasting on LS-Dyna software

momentum equations can be achieved by applying different consistency equations to the standard SPH momentum equation. The symmetry of the SPH momentum equation helps to reduce errors arising from particle inconsistency issues.

From equation (7), the components of the forces acting on each particle can be determined.

$$F_i^{pressure} = -\sum_j m_j \frac{\rho_i+\rho_j}{2\rho_j}\nabla w\left(r_{ij},h\right)$$
$$F_i^{viscosity} = \mu\sum_j m_j \frac{v_i+v_j}{2\rho_j}\nabla^2 w\left(r_{ij},h\right) \quad (8)$$

Where: $r_{ij} = xi - x_j$, μ is the viscosity coefficient of the material. The pressure pi is calculated through the equation of state:

$$p_i = k(\rho_i - \rho_0) \quad (9)$$

Where: k is the stiffness of the material and B is its initial density. Finally, for the acceleration of particle i, we have:

$$a_i = \frac{1}{\rho_i\left(F_i^{pressure} + F_i^{viscosity} + F_i^{external}\right)} \quad (10)$$

where: $F_i^{external}$ is represents external forces such as forces acting on the body or contact forces.

2.3. Interactions between particles in simulation

Fig 2 illustrates that all SPH interpolations are performed within the local domains of each SPH particle. Contact forces will be applied to external forces as described in equation 10.

In this system, the contact force acting on the particles due to contact, Fc, is proportional to the displacement or overlap between the particles, δ.

$$F_c = K_l\delta \quad (11)$$

Where δ = d-2d and Kl is the linear spring constant or stiffness. If the contact point is modeled using only this linear spring, no energy will be dissipated and the contact will be perfectly elastic. In reality, some kinetic energy is dissipated through plastic deformation, either converted into heat or sound energy. To account for these energy losses, a damping source based on the dashpot model is defined:

$$F_d = \eta v \quad (12)$$

The damping force is proportional to the relative velocity of the contacting particles, where the proportionality constant η is called the damping coefficient, $v = v_1 - v_2$.

2.4. Characterization equation of the materials used in the simulation

Alongside the development of the SPH method, material models have been constructed and advanced to address issues within the simulation framework of LS-Dyna software. In the scope of studying rock fragmentation caused by blasting, the research group utilizes characteristic models for soil and rock: the Riedel-Hiermaier-Thoma (RHT) model and the High Explosive Burn (HEB) model, which incorporates the Jones-Wilkins-Lee (JWL) stress wave propagation equation for the explosive material.

- Rock Material Model (RHT)

The characteristic of rock is its brittle behavior [44]. Therefore, the suitable material model in LS-Dyna is the Riedel-Hiermaier-Thoma (RHT) material model, developed by Riedel, Hiermaier, and Thoma [45]. RHT consists of three pressure-dependent yield surfaces in the stress space, representing different limiting states, namely the yield limit, elastic limit, and ultimate failure limit.

The failure limit Yphá hủy is defined as a function of pressure p, angle θ, and strain rate ε, and is determined by the formula.

$$Y_{phahuy}(p^*,\theta,\dot{\varepsilon}) = Y^*_{TXC}(p^*).R_3(\theta).F_{tile}(\dot{\varepsilon}) \quad (13)$$

Where p* is the pressure normalized by the function fc, $p^* = p/f_c$, where p is the hydrostatic pressure, f_c is the compression strength; $R_3(\theta)$ is a function defining the invariant dependence of a shape; Fstrain is the strain rate, expressed through the increase in fracture toughness with plastic strain rate; Y^*_{TXC} is the equivalent stress intensity factor on the compressive meridian.

The elastic limit is determined based on the ratio of the fracture surface area, defined by the formula [9]:

$$Y_{đàn\ hồi} = Y_{phá\ hủy} \,.\, F_{đàn\ hồi} \,.\, R_3(\theta) \,.\, F_{CAP}(p^*) \quad (14)$$

Where, $F_{đàn\ hồi}$ – the ratio between the elastic limit and the failure limit; $F_{CAP}(p^*)$ is the function of the elastic limit deviation stress when subjected to hydrostatic compression, with values in the range (0,1).

Tab. 1. Drilling and blasting parameters on simulation model

Parameters	Symbol	Unit	Value
Bench height	h	m	8
Burden	b	m	2.6
Stemming	L_b	m	3.2
Explosive Charge	L_t	m	5.8
Hole Diameter	d_k	mm	76
Bottom-Hole Burden	w	m	2.6
Type of explosives			Anfo
Delay time		ms	17

Tab. 2. Key parameters of the materials used in the simulation model

Parameters	Values	Parameters	Values
RHT material model			
Mass density, g/cm^3	2,72	Crush pressure, Pa	$4{,}00^{e+7}$
Tensile strength, kg/cm^2	60,77	Break compressive strain rate	$3{,}00^{e+19}$
Compression resistance strength, kg/cm^2	750,77	Break tensile strain rate	$3{,}00^{e+19}$
Angle of internal friction, độ	$34^0 35'$	Reference tensile strain rate	$3{,}00e^{-6}$
Deformation modulus, kg/cm^2	4,08	Reference compressive strain rate	$3{,}00e^{-5}$
Elastic modulus, Pa	$2{,}47^{e+10}$	Shear modulus reduction factor	0,5
Porosity	1,94	Minimum damaged residual strain	0,015
JWL stress wave equation			
Mass density, kg/m^3	931	Chapman-Jouget pressure	$5{,}15e^{+9}$
Detonation velocity, m/s	4.200		
Equation of state coefficien (A), Pa	$4{,}95e^{+10}$	Equation of state coefficien (A), Pa (R2)	1,118
Equation of state coefficien (B), Pa	$1{,}89e^{+9}$	Equation of state coefficien (A), Pa (ω)	0,33
Equation of state coefficien (R1)	3,907	Detonation energy per unit volume and initial value for E. See equation in Remarks, Pa, Pa/m^3	$2{,}48e^{+9}$

Secondary fragmentation is used to describe the strength of completely crushed rock, and it is determined by the following expression:

$$Y^*_{phahuythupha} = B.p^{*M} \quad (15)$$

Where B is the constant of secondary fragmentation, and M is the exponent of secondary fragmentation.

- The stress wave propagation equation of the explosive material (JWL)

For the explosive charge inside the borehole, the high explosive burn (HEB) material model used in LS-Dyna utilizes the Jones-Wilkins-Lee (JWL) stress wave propagation equation, which is defined by the equation [45]:

$$P = A(1-\frac{\omega}{R_1V})e^{-R_1V} + B(1-\frac{\omega}{R_2V})e^{-R_2V} + \frac{\omega E}{V} \quad (16)$$

In which, P represents the stress wave, A, B, R_1, R_2, and ω are constants, V is the specific volume, and E_0 is the initial internal energy with a value of E_0.

3. Results and discussions

3.1. Characteristics of the study area

a. Geographical location

The Mong Son limestone quarry is located in Mong Sơn commune, Yen Binh district, Yen Bai province. The total licensed area for zones A and B of the quarry is 13.9 hectares (Fig. 3). The geological structure of the mining area is relatively simple, primarily consisting of white weathered limestone. The limestone is pure white with a fine crystalline structure and relatively large particle size.

b. The current state of mining technology and drilling and blasting operations at the Mong Son limestone quarry [47]

The Mong Sơn quarry is currently focused on mining Area A, which covers an area of 11.81 hectares. The mining method employed is layer-by-layer extraction from top to bottom, with each layer being 8.0 meters in height. The slope angle of the layers is α = 750. The rock in the quarry is fragmented using the drilling and blasting method, with drill holes having a diameter of 76 mm. The blasting technique used is full electric delay blasting, with delay times of 17 ms and 42 ms. The explosive material used is Anfo in the form of D60 bags, and the emulsion explosive is D60, initiated by a 400ms electric detonator and an MN31-175g booster (for the first mining blast). The majority of the explosive charge is continuously structured within the blast column.

3.2. Simulation model of blasting process at B2 section at Mong Son limestone quarry using LS-Dyna software

Currently, at some production blasting sites in the quarry, the applied drilling and blasting parameters have increased the risk of flyrock hazards. Therefore, in order to assess the impact of flyrock on production, the paper conducted a simulation of the blasting process using LS-Dyna software on the cross-sectional profile B2 of the quarry (Fig. 4).

The drilling parameters on the 2D model are presented in Tab. 1.

The materials representing the geological environment, as well as the explosives compatible with the properties of RHT and JWL materials in LS-Dyna, are determined based on the geological data of the Mong Son limestone quarry and existing studies on the mechanical properties of limestone with a density of 2.72 g/cm^3. The key parameters of the materials are shown in Tab. 2.

The computer specifications used for simulating the blasting work are as follows: Intel(R) Core(TM) i7-10700 CPU @ 2.90GHz and 16.0 GB of RAM. With a result recording time

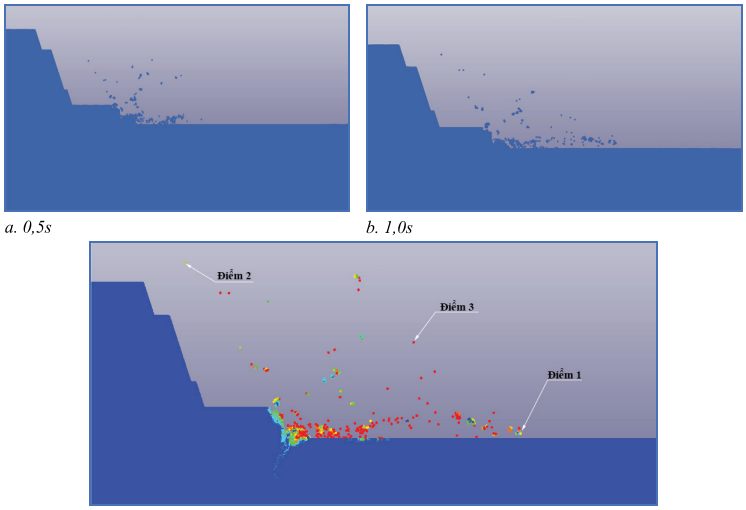

a. 0,5s *b. 1,0s*

c. 1,5s

Fig. 5. Simulation of the blasting process using LS-Dyna software

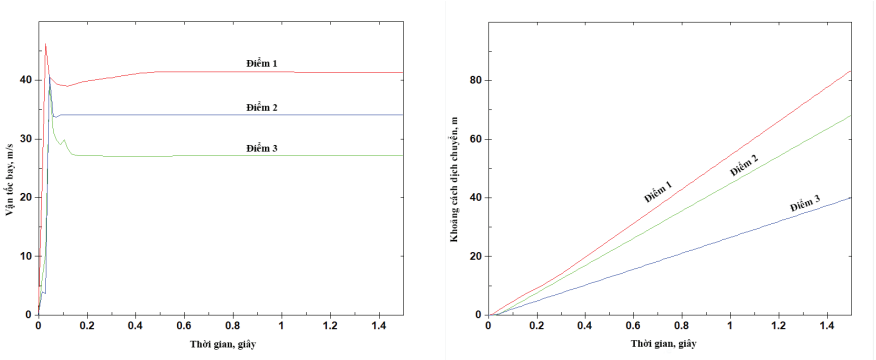

a. Speed of flying rocks over 3 survey points *b. Flight distance over 3 survey points*

Fig. 6. Velocity (a) and distance (b) flying from 0 ÷ 1.5 seconds

of 1.5 seconds, the simulation completed its calculations after 12 hours using the LS-Dyna software.

3.3. Simulation results of flying rock for Mong Son limestone quarry by SPH method on LS-Dyna software

The article sets up data measurements for simulating the rock fragmentation phenomenon during the blasting process on a 2D model of cross-section B2 at Mong Son limestone quarry after 1.5 seconds. The obtained results are recorded at time intervals of 0.5 seconds, 1.0 second, and 1.5 seconds, as shown in Fig. 5.

To assess the distance of flyrock and the velocity of flyrock after 1.5 seconds of detonating the explosive charge, three measurement points were set in the simulation model (Fig.5c). The monitoring results are presented in Fig. 6.

The measurement results at the monitoring points show that with the blast network parameters as shown in Tab.1, after 1.5 seconds, the farthest flyrock from the blast center reached a distance of 85 meters, corresponding to an average velocity of 40 m/s. Therefore, the blast network parameters pose a potential risk of flyrock hazards for the Mong Son quarry. It is necessary to calculate and select the blast network parameters based on the safe criteria for flyrock.

4. Conclusions

The simulation method for the blasting process and the determination of the trajectory and flyrock distance of the rock and soil using simulation tools is not widely used in our country at present. The use of empirical formulas to determine flyrock distances is not suitable for real blasting conditions, while applying machine learning algorithms and AI models requires collecting a large amount of input parameters. On the other hand, measuring and documenting flyrock distances caused by blasting events is extremely complex and challenging.

Numerical modeling methods have become a reliable solution for studying, analyzing, and evaluating mechanical impacts. The results of the model demonstrate the capabilities of the Smoothed Particle Hydrodynamics (SPH) method in analyzing blasting operations in depth. The use of this method enables mining engineers and safety managers to preliminarily predict flyrock distances for each blast under realistic blasting conditions at the mine by inputting the required simulation parameters.

Based on the analysis of the blasting effects using the 2D SPH method constructed from the B2 cross-section of the Mông Sơn limestone quarry, it is evident that the current design parameters for the blast network (KNM) pose a potential risk of flyrock hazards. Therefore, it is necessary to further study, calculate, and select appropriate KNM parameters. However, more detailed and in-depth research is required on the application of the SPH method in LS-Dyna software for 3D models with multiple realistic blastholes according to ac-

tual construction plans and supplementary experiments that consider additional mechanical properties specific to the rock and soil characteristics at the quarry. This will enhance the accuracy of the simulations and establish longer observation periods to fully understand the flyrock phenomena in different directions and at different time points during the blasting events.

5. Acknowledgements

The authors would like to sincerely thank Assoc. Prof. Dr. Dam Trong Thang from the Military Technical Academy for his assistance during the simulation of the mining blasting using the licensed software LS-Dyna/Ansys. Additionally, the authors express their gratitude for the support and scientific advice provided by the scientists from the Strong Research Group "Advancements in Sustainable and Responsible Mining" – ISRM, during the execution of this research.

The paper was presented during the 6th VIET-POL International Conference on Scientific-Research Cooperation between Vietnam and Poland, 10-14.11.2021, HUMG, Hanoi, Vietnam.

Literatura – References

1. Kahriman, A., Ozer, U., Aksoy, M., Karadogan, A., Tuncer, G. (2006). Environmental impacts of bench blasting at Hisarcik Boron open pit mine in Turkey. Environmental Geology, 50 (7), 1015-1023.
2. Uysal, O., Cavus, M. (2013). Effect of a pre-split plane on the frequencies of blast induced ground vibrations. Acta Montanistica Slovaca, 18(2), 101-109.
3. Karadogan, A., Kahriman, A., Ozer, U. (2014). A new damage criteria norm for blast induced ground vibrations in Turkey. Arabian Journal of Geosciences, 7(4), 1617-1627.
4. Gorgulu, K., Arpaz, E., Uysal, O., Duruturk, Y.S., Yuksek, A.G., Kocaslan, A., Dilmac, M.K. (2015). Investigation of the effects of blasting design parameters and rock properties on blast-induced ground vibrations. Arabian Journal of Geosciences, 8(6), 4269- 4278.
5. Kulekci, G., Alemdag, S. (2016). The investigation of blasting effect on natural heritages in quarries: Registered rock room sample. Proceedings of the 8th International Aggregates Symposium, 13-14 October, Kutahya, Turkey, 498-504.
6. Singh, T.N., Singh, V. (2005). An intelligent approach to prediction and control ground vibration in mines. Geotechnical and Geological Engineering, 23(3), 249-262.
7. Rezaei, M., Monjezi, M., Varjani, A.Y. (2011). Development of a fuzzy model to predict flyrock in surface mining. Safety Science, 49, 298-305.
8. Hajihassani, M., Armaghani, D.J., Sohaei, H., Mohamad, E.T., Marto, A. (2014). Prediction of airblast-overpressure induced by blasting using a hybrid artificial neural network and particle swarm optimization. Applied Acoustics, 80, 57-67.
9. Sadeghi, F., Monjezi, M., Armaghani, D.J. (2020). Evaluation and optimization of prediction of toe that arises from mine blasting operation using various soft computing techniques. Natural Resources Research, 29(2), 887-903.
10. Bhandari S (1997) Engineering rock blasting operations. A. A. Balkema, Rotterdam.
11. Fletcher, L. R., D'Andrea, D. V. (1986): Control of flyrock in blasting. Proc., 12th Conf. on Explosives and Blasting Technique, Atlanta, Georgia, 167-177.
12. Raina AK, Murthy VMSR, Soni AK (2015) Flyrock in surface mine blasting: understanding the basics to develop a predictive regime. Curr Sci 108:660–665.
13. Workman, J. L., Calder, P. N. (1994): Flyrock prediction and control in surface mine blasting. Proc., 20th Conf. on Explosives and Blasting Technique, Austin, Texas, 59-74.
14. Kopp, J. W. (1994): Observation of flyrock at several mines and quarries. Proc., 20th Conf. on Explosives and Blasting Technique, Austin, Texas, 75-81.
15. Lundborg N, Persson PA, Ladegaard-Pedersen A, Holmberg R (1975) keeping the lid on flyrock in opencast blasting. Eng Min J 95–100.
16. Roth J (1979) A model for the determination of flyrock range as a function of shot conditions, final report contract no. J03872A2. Management Science Associates, Los Altos.
17. Hillier DE, Holywell PD, Jeffries RM, Scott IMB (1999) Limiting the instance of flyrock from quarry operations, research report. WS Atkins Consultants Ltd., Warrington.

18. Schneider L (1997) Back to the basics, flyrock (part 2: prevention). The Journal of explosives engineering 14:1–14 quarry blasting. Appl Acoust 71:1169–1176. doi:10.1016/j.apacoust.2010.07.008

19. Adhikari GR (1999) Studies on flyrock at limestone quarries. Rock Mech Rock Eng 32:291–301. doi:10.1007/s006030050049

20. Mishra AK, Mallick DK (2012) Analysis of blasting related accidents with emphasis on flyrock and its mitigation in surface mines. In: Proceedings of the 10th International Symposium on Rock Fragmentation by Blasting, New Delhi, India. pp. 555–563

21. Bajpayee TS, Rehak TR, Mowrey GL, Ingram DK (2004) Blasting injuries in surface mining with emphasis on flyrock and blast area security. J Saf Res 35:47–57. doi:10.1016/j.jsr.2003.07.00

22. Kulekci, G., Yilmaz, A.O. (2018). Roadway tunnel construction with drilling-blasting method; Gümüşhane environment road example. Int. Journal on Mathematic, Engineering and Natural Sciences, 4, 34-39.

23. Kulekci, G., Yilmaz, A. (2019). Investigation of the effect of activities in a coper mine on historical works, an example of Gümüşhane Süleymaniye. Journal of Underground Resources, 16(8), 1-14.

24. Monjezi, M., Amini Khoshalan, H., Yazdian Varjani, A. (2010a). Prediction of flyrock and backbreak in open pit blasting operation: a neuro-genetic approach. Arabian Journal of Geosciences, 5(3), 441-448.

25. Monjezi, M., Bahrami, A., Yazdian Varjani, A. (2010b). Simultaneous prediction of fragmentation and flyrock in blasting operation using artificial neural networks. International Journal of Rock Mechanics and Mining Sciences, 47(3), 476-480.

26. Monjezi, M., Mehrdanesh, A., Malek, A., Khandelwal, M. (2012). Evaluation of effect of blast design parameters on flyrock using artificial neural networks. Neural Computing and Applications, 23(2), 349-356.

27. Rezaei, M., Monjezi, M., Varjani, A.Y. (2011). Development of a fuzzy model to predict flyrock in surface mining. Safety Science, 49, 298-305.

28. Ghasemi, E., Sari, M., Ataei, M. (2012a). Development of an empirical model for predicting the effects of controllable blasting parameters on flyrock distance in surface mines. International Journal of Rock Mechanics and Mining Sciences, 52, 163-170.

29. Ghasemi, E., Amini, H., Ataei, M., Khalokakaei, R. (2012b). Application of artificial intelligence techniques for predicting the flyrock distance caused by blasting operation. Arabian Journal of Geosciences, 7(1), 193-202.

30. Amini, H., Gholami, R., Monjezi, M., Torabi, S.R., Zadhesh, J. (2011). Evaluation of flyrock phenomenon due to blasting operation by support vector machine. Neural Computing and Applications, 21(8), 2077-2085.

31. Raina, A.K., Chakraborty, A.K., Choudhury, P.B., Sinha, A. (2011). Flyrock danger zone demarcation in opencast mines: a risk based approach. Bulletin of Engineering Geology and the Environment, 70(1), 163-172.

32. Alemdag, S., Zeybek, H.I., Kulekci, G. (2019). Stability evaluation of the Gümüşhane-Akçakale Cave by numerical analysis method. Journal of Mountain Science, 16(9), 2150-58.

33. Momeni, E., Nazir, R., Armaghani, D.J., Maizir, H. (2014). Prediction of pile bearing capacity using a hybrid genetic algorithm-based ANN. Measurement, 57, 122-131.

34. Mohamad, E.T., Armaghani, D.J., Hajihassani, M., Faizi, K., Marto, A. (2013a). A simulation approach to predict blasting-induced flyrock and size of thrown rocks. Electronic Journal of Geotechnical Engineering, 18, 365-374.

35. Monjezi, M., Dehghani, H. (2008). Evaluation of effect of blasting pattern parameters on back break using neural networks. International Journal of Rock Mechanics and Mining Sciences, 45(8), 1446-1453.

36. Esmaeili, M., Osanloo, M., Rashidinejad, F., Bazzazi, A.A., Taji, M. (2014). Multiple regression, ANN and ANFIS models for prediction of backbreak in the open pit blasting. Engineering with Computers, 30(4), 549-558.

37. Garret, J.H. (1994). Where and why artificial neural networks are applicable in civil engineering. Journal of Computer in Civil Engineering, 8, 129-130.

38. Tran Thanh Thung.(2017). Study of the SPH method for Simulation in LS-Dyna

39. L.B. Jayasinghe. (2020). Numerical investigation into the blasting-induced damage characteristics of rocks considering the role of in-situ stressed and discontinuity persistencd. Nanyang Centre for Underground Space, School of Civil and Environmental Engineering, Nanyang Technological University, Singapore 639798.

40. Jing Gao, Shizhen Xie, Xiantang Zhang, Hongli Wang, Wenle Gao, và Hongmin Zhou. (2020). Study on the 2D optimization simulation of complex five-hole cutting blasting under different lateral pressure coefficients. Hindawi Complexity. Volume 2020, Article ID 4639518, 12 pages

41. Gaohui Wang, Sherong Zhang, Yuan Kong, and Hongbi LI. (2013). A comparative sudy on the dynamic response of concrêt gravity dams sybjected to underwater and air explosions. Journal of Performance of Constructed Facili-

ties. Submitted October 22, 2013; accepted January 29, 2014; posted ahead of print January 31, 2014. doi:10.1061/(ASCE)CF.1943-5509.0000589.

42. Jingxiao Xu, Jason Wang. (2013). Interaction Methods for the SPH Parts (Multiphase Flows, Solid Bodies) in LS-Dyna. Livermore Software Technology Corporation.
43. PGS.TS. Đàm Trọng Thắng, PGS. TS. Bùi Xuân Nam, TS. Trần Quang Hiếu. (2015). Nổ mìn trong ngành mỏ và công trình. NXB Khoa học tự nhiên và công nghệ. Hà Nội
44. Jing Gao, Shizhen Xie, Xiantang Zhang, Hongli Wang, Wenle Gao, và Hongmin Zhou. (2020). Study on the 2D optimization simulation of complex five-hole cutting blasting under different lateral pressure coefficients. Hindawi Complexity. Volume 2020, Article ID 4639518, 12 pages
45. Riedel, W., Thoma, K., Hiermaier, S. (1999). Numerical analysis using a new macroscopic concrete model for hydrocodes. In Proceedings of 9th international symposium on interaction of the effects of munitions with structures (pp. 315–322). Strausberg, Germany
46. Satellite Images of Mong Son quarrz.
47. Illustration of Mining Production Adjustment of Mong Son Quarry, Mong Son Ward, Yen Binh District, Yen Bai Province

Current Situation of State Management on Mineral Mining in The North Eastern Vietnam and Tasks Proposal for Audit Activities

BUI Thi Thu Thuy[1)], Pham Thu Huong[1)], DUONG Quang Chinh[2)], DUONG Duc Trung[2)]*

[1)] Faculty of Economics and Business Administration, Hanoi University of Mining and Geology, 18 Vien Street, Ha Noi, Viet Nam; *email: buithithuthuy@humg.edu.vn; BUI Thi Thu Thuy: ORCID 0009-0003-4374-0500; Pham Thu Huong: ORCID 0009-0002-6580-9532; Duong Quang Chinh: ORCID 0009-0009-5488-372X

[2)] State Audit, 116 Nguyen Chanh Street, Ha Noi, Vietnam; Duong Duc Trung: ORCID0009-0009-1250-2845

http://doi.org/10.29227/IM-2023-02-09

Submission date: 17-08-2023 | Review date: 12-09-2023

Abstract

Vietnam is a country with abundant mineral resources, in recent years, the minerals mining (MM) has affirmed its very important position in contributing to the development of the national products, alleviate Vietnam's economy to a higher level at a rapid pace in recent years. However, the MM in recent years has caused many negative impacts on long-term economic and social development, posing unpredictable consequences on the environment... This leads to the need to strengthen the Government's management work. In the effort to manage mining extraction, this is considered a complex field that has not been uniformly understood, and there remains several inadequacies and insufficient support in the process of performing management procedure. Therefore, although the Government requires to tighten the management of mineral exploitation, the effectiveness and efficiency are not reached, and many mistakes occur in the process of the procedure. Given the mentioned challenges of the management of control and the audit results of the State Audit on internal audit in recent years, there are a number of important tasks that need to be focused on auditing, including (i) Audit of mining license; (ii) Audit of mined reserves and output; (iii) Audit of environmental safety protection and inspection of mining activities.

Keywords: *minerals mining, audit, north-eastern Vietnam*

Introduction

The Northeast is one of the richest regions in terms of mineral resources in our country. Here there are important minerals such as coal, apatite, iron, copper, lead, zinc, tin... Minerals are distributed in the Northeast such as: Coal (Quang Ninh, Thai Nguyen); Copper, gold (Thai Nguyen), minerals for building materials such as stone, limestone, mineral water, clay (Hai Phong, Hai Duong, Quang Ninh). Mineral exploitation is considered the strength of this region. However, in recent years, this activity has caused many adverse impacts on the sustainable development of the economy and society as well as environmental consequences... This leads to the need to strengthen the state management of mineral exploitation.

State management of mineral resource exploitation and environment is a complex field, not uniformly understood, and at the same time facing many shortcomings and overlapping issues in the process of performing the functions of management. Despite tightened state management efforts, the effectiveness has been limited, resulting in numerous irregularities in mineral exploitation, leading to resource waste, loss of state budget revenues, uncontrolled mining activities, land expropriation from many households for mining purposes, negative public perception in society and alarming environmental consequences (Chinh et al, 2022).

With approaches from the perspective of management science, combined with relevant laws on mineral exploitation, the authors focus on the following main contents:

- Point out fundamental and important contents in the state management of mineral exploitation;
- Collect and analyze actual data to clarify inadequacies in the state management of mineral exploitation in localities in the Northeast;
- Propose audit tasks that the State Audit Office of Vietnam (SAV) needs to focus on auditing mineral resources

1. Study area and data collection

Study area: The localities having data collected for research and evaluation include 5 provinces in the Northeast Vietnam: Quang Ninh, Thai Nguyen, Hai Duong, Hung Yen and Hai Phong.In recent years, in the Northeast, mining projects have been implemented in thousands of mines and mining sites, with a wide range of mineral types. Figures are shown in table 1.

Data collection: To analyze and evaluate the current situation of state management on mineral exploitation, the authors rely on the provisions of the Law on Minerals (National Assembly, 2010) to determine the content of the state management on mineral exploitation. Accordingly, the State management on mineral exploitation includes the following basic contents:

- Build and promulgate legal documents, create a legal framework for mineral exploitation activities;
- Build mineral exploitation strategy/planning;
- Promulgate and enforce policies on issuance of mining licenses; recognition and approval of mineral reserves according to its competence;
- Promulgate regulations on fulfillment of financial obligations, enforcement of measures to protect the environment, ensure security, social order and safety in the locality where the mineral exploitation project is located;

Tab. 1. Mining projects and mineral types of the Northeast in 2017–2021 period (Chinh et al, 2022)

No.	Provinces and cities	Mineral type	Mining projects	Typical mineral types
1	Quang Ninh	33 mineral types	243 mines and mine sites	- Coal - Stone for building material - Clay for roofing tiles - Construction sand, pyrophyllite - Cement limestone - Clay for cement production - Mineral water
2	Hai Phong	21 mineral types	201 mines and mine sites	- Cement stone - Stone for building material - Clay, kaolin - Sand
3	Hai Duong	24 mineral types	186 mines and mine sites	- Upper cement stone - Stone for building material - Clay, kaolin - Sand
4	Hung Yen	14 mineral types	126 mines and mine sites	- Clay, kaolin - Sand
5	Thai Nguyen	16 mineral types	342 mines and mine sites	- Coal, manganese - Clay, brick, tile - Sand and gravel, backfill soil; - Promising mineral resources primarily distributed in mountainous districts, such as copper, gold, lead-zinc.

- Propagate and disseminate laws on minerals and environment;
- Inspect, examine, supervise and handle violations of the law on mineral exploitation.

With data collected from the scientific research project of the authors, thematic reports of the State Audit Office of Vietnam for each locality on state management on mineral exploitation in the period of 2017–2021, combined with the collection of practical information from the reports of the Government Inspectorate, the indictment of the Supreme People's Procuracy on the wrongdoings of mining enterprises discovered and made public in 2022 and 2023, the article does not present each content of state management on mineral exploitation, but focuses on pointing out the shortcomings and typical existing problems in the promulgation and enforcement of the law on mineral exploitation management, thereby highlighting the research results.

2. Results and discussions

2.1. Inadequacies in the state management on mineral exploitation in localities in the Northeastern Vietnam

a. Shortcomings in the promulgation and enforcement of the law on the issuance of mineral exploitation licenses

The Law on Minerals (National Assembly, 2010) stipulates the auction of mineral exploitation rights, which is established to help enterprises and individuals participate in the exploitation of mineral resources, create jobs, contribute to budget revenues, etc. Accordingly, in order to ensure publicity, transparency and increase revenue for the State budget, the issuance of mineral exploitation licenses, enterprises are required to auction mineral exploitation rights. However, according to Article 78 of this Law, "Auction of mineral exploitation rights shall be carried out in areas of mineral activities, except for areas designated by competent state agencies as areas where mineral exploitation rights are not auctioned" (National Assembly, 2010). This provision is understood to mean that the auction of mineral exploitation rights is carried out only in areas where mineral activities are located, for areas where there are no mineral activities (even if minerals are determined), they are entitled not to auction mineral exploitation rights. The provisions of the Law did not specify the criteria for delineating auction areas and non-auction areas, but assigned the Government to detail them." This has led to a situation where the criteria for delineating non-auction zones are too broad and the fact that the vast majority of mineral deposits are classified as non-auctions.

To date, the Law on Minerals has come to life for almost 13 years. The law stipulates that only certain special cases are not subject to auction. This is a content that was considered a breakthrough when it was first introduced into the Law on Minerals. However, according to a report summarizing 10 years of law enforcement, the Ministry of Natural Resources and Environment (Ministry of Natural Resources and Environment, 2022) gave disappointing figures:

- Accordingly, until June 2021, the Ministry of Natural Resources and Environment successfully auctioned 6 mineral areas, accounting for 1.4% of total 421 issued licenses. Thus, at the Central level, more than 98% of licenses are issued in a begging-giving fashion.
- The situation at the local level is not much different. Just over 9% of the nearly 4,280 licenses were issued by auction. Thus, 91% of licenses are also issued in a begging-giving fashion. For provinces in the Northeast, the proportion of licenses issued by auction in the period of 2017–2021 was higher, but still low, only 18.5%, as shown in Table 2.

Many enterprises do not have expertise in mineral exploitation, or are incompetent but still issued mining licenses, so when issued, (i) either do not carry out the mining; or (ii) resell to another investor; or (iii) waste resources due to inefficient business. (Chinh et al, 2022).

In many localities, as soon as mineral deposits are discovered, the managing authorities issue licenses to individuals and businesses to exploit the resources without considering future needs (SAV region 6 pointed out that in Quang Ninh, out of 11 additional mineral exploration sites, 10 new mining licenses were issued.

b. Shortcomings in reserve management

The current recognition and approval of mineral reserves also face significant contradictions due to the inaccurate methods of determining reserves (According to the provi-

Tab. 2. Situation of issuance of mineral exploitation licenses in localities in Northeastern Vietnam. Source: Thematic Audit Report on Mineral Resources of SAV Specialty 2, SAV Region 6) [4],[7]

No.	Provinces and cities	Number of licenses issued through auction of mineral exploitation rights	Number of licenses issued without auction	Total number of issued mineral exploitation licenses	Percentage of licenses issued through auction
1	Quang Ninh	5	19	24	20.8%
2	Hai Phong	0	6	6	0
3	Hai Duong	0	11	11	0
4	Hung Yen	0	16	16	0
5	Thai Nguyen	16	40	56	28.6%
	Amount	21	92	113	18.5%

Tab. 3. Increased state budget revenue from resource taxes through auditing and tax reconciliation activities in Quang Ninh and Hai Phong by SAV Region 6. Unit: million VND. Source: Chinh et al, 2022 [1]

No.	Provinces and cities	2017	2018	2019	2020	2021
1	Quang Ninh		875		1,589	3,983
2	Hai Phong	635	35	3.7	118	83,883

sions of Circular No. 60/2017/TT-BTNMT, the highest level of geological certainty for mineral reserves, level 111, can still have a geological error of up to 20%). In practice, the following issues have arisen:

- The approved reserves are much larger than the actual exploitable output;
- Approved reserves are much smaller than the exploitable output.

As a result, some entities suffer losses due to the issuance of mining rights, while others benefit greatly, causing unfairness. Moreover, this situation leads to resource wastage and loss of state budget revenue.

Typically, Vinh Tien Coal Mine (Thai Nguyen), with approved coal reserves of 200,000 tons, but only from March 2019 to August 2021, Dong Bac Hai Duong Company illegally exploited over 3.1 million tons of coal and accompanying minerals, 23.4 times higher than total licensed output of 18-year term; with a capacity 115 times higher than the approved level (Do Tan, 2023)

Or at the limestone mine of Thuy Nguyen District (Hai Phong), SAV Zone VI used drone technology to restore the mining terrain, determined that the mining output of this mine exceeded many times the approved reserves (Chinh et al, 2022).

c. Shortcomings in management of mining output

Since 2011, the scope of entities engaged in mineral exploitation has expanded to include many private individuals and businesses. These entities go to great lengths to obtain mining licenses and, once they have them, they often operate at alarming levels of production. The current situation of exceeding mining licenses, exceeding usage needs, or mining after the expiration of licenses is common (The audit report on mineral resources by the State Audit Office during the period 2017–2021 [6] pointed out the following: In Trang Kenh quarry (Hai Phong), Vicem Hai Phong Cement Company Limited has exceeded the licensed capacity of 84,572 tons for cement and clinker production in 2021; At Vicem Hai Phong, the licensed output and capacity exceeded the demand. Currently, this company has been granted two limestone mining licenses for cement production with a capacity of 2.8 million tons of limestone per year. According to their report, the maximum usage demand for limestone (4,000 tons of clinker per day) is equivalent to 1.8 million tons of limestone/ year. Therefore, the company's limestone demand is lower than the granted mining capacity by about 1 million tons/ year.

In Quang Ninh: Excessive mining operations were observed at Hon Gai Coal Company – TKV, Mong Duong Coal Joint Stock Company – Vinacomin, Quang Hanh Coal Company – TKV, Cao Son Coal Joint Stock Company – TKV. Furthermore, there were instances of mining activities that continue after the mining licenses expires, have not been renewed at Uong Bi Coal Company – TKV. Additionally, Quang Hanh Coal Joint Stock Company – TKV exceeded the permitted exploration capacity. (Thematic report on the audit of mineral resources at TKV Group of SAV Specialty 6, [5]).

Currently, natural resources tax is collected based on the output of mined resources (self-declared by enterprises), which causes great inadequacies, because the nature of natural resources tax must be collected based on resource reserves. As a result, in practice certain phenomena occur (Chinh et al, 2022):

- Enterprises only choose places with favorable conditions for mining, which causes loss and waste of resources;
- Due to the fact that the declared mining output much smaller than the actual mining output, resources are lost, the budget is reduced.

During the years of auditing, it has been observed that the number of cases where resource tax revenue increases due to underreporting the output by enterprises tends to increase. In 2021, when strengthening the audit work for the field of mineral resources, SAV Region 6 changed the method of determining the output of mined resources, found a very large volume of mined resources but did not declare and pay taxes, therefore the increase in resource tax revenues increased very high in this year.

Unfortunately, in the audits of Mineral Resource by SAV, the scope of audits is often limited, and the determination of reserves for already exploited mines is not thoroughly audited, which results in the accurate determination of the mining output.

d. Environmental protection

There are still some investors (such as Cat Ne Coal Mine, Phu Tien iron-manganese mine, Phu Van commune sand-

stone quarry, Linh Nham iron mine in Thai Nguyen) who have not completed the environmental protection works and measures as committed, but started exploitation (Government Inspectorate, 2022), violating Articles 26 and 27 of the Law on Environmental Protection No. 55/2014/QH13 (National Assembly, 2014).

Many projects have expired their mining licenses, but local authorities have not been strict in demanding investors to carry out mine closure procedures. The exploitation of minerals in these projects not only posed safety risks but also caused losses, resource depletion, and failure to comply with regulations on environmental restoration after mineral exploitation (observed in all localities during inspections and audits). Although administrative fines had been imposed, they were not strong enough to deter investors, and some were willing to pay fines and continue illegal mining.

Local authorities still allowed situations where businesses owed environmental protection deposits and under-declared environmental protection fees (During the period 2017-2021, the Audit Delegation of SAV recommended Quang Ninh to collect a fee of VND 1.3 billion for environmental protection; in Hai Phong, when selecting the sample for inspection, out of 5 mining projects, 1 project still owed the deposit, and 4 projects were delayed in paying the environmental protection deposit in all years) (State Audit Office of Vietnam Region 6, 2022).

Some enterprises have not conducted environmental monitoring and sampling on time as required (State Audit Office, specialized in Region 6, 2022), and the local authorities had not yet come up with effective solutions to manage this activity properly.

e. Inspection and Audit of Mineral Exploitation Activities

Inspection and audit activities are carried out annually at both central and local levels, based on specific topics related to each type of mineral, mining operation, or management area, depending on the practical situation or in response to complaints, accusations, or recommendations from organizations, citizens, or authorized agencies;

Despite the inspection and audit results, many localities continue to face numerous violations in state management of mineral exploitation, especially in the procedures for granting mining licenses, illegal mining activities, non-compliance with payment obligations to the state, and violations related to environmental issues. However, the measures to handle these violations have not been thorough and decisive enough, leading to the prevalence of violations of mineral exploitation laws (State Audit Office of Vietnam specialty 2, specialty 6, region 6, 2022).

2.2. Proposed tasks for the audit of mineral resources

a. For audit of mining licensing

In order to ensure openness, transparency, create fairness among investors, and increase revenue for the state budget, the proposed tasks for the state audit are:

- Create motivation to promote the number of projects licensed to exploit minerals through auction: Strengthen the audit of openness and transparency at the Ministry of Natural Resources and Environment as well as localities on (i) Mineral planning, (ii) The process of issuing, extending and revoking licenses for mineral activities, (ii) The process of appraisal and approval of mineral reserves and closure of mineral reserves, (iii) The process of auctioning mineral rights and delineating prohibited zones and areas temporarily prohibited from mineral activities, (iv) Administrative procedures on minerals and comments on the implementation of administrative procedures; (v) The process by which the State identifies areas not subject to mineral auctions, (vi) Information about enterprises licensed for mineral activities and the process of mineral exploitation.

- Focus on auditing at mineral exploitation projects licensed without auction:

+ Audit the capacity and expertise of investors, compare to conclude on deep expertise, experience, technique and financial capacity;

+ Audit the compliance of the Ministry of Natural Resources and Environment as well as the People's Committee of the provinces with the order and regulations in issuing mineral exploitation licenses;

+ Promptly detect acts of corruption, waste and violations in the management and licensing of mineral exploitation.

b. Audit and approval of reserves and management of mining output

- Expand the scope of audits, if in the past, audits were limited to exclude the management of reserves and mining output. However, it is now necessary to include these two areas in the audit scope and make them a focal point of audit activities;

- Use advanced audit methods such as remote sensing method, expert method, select the most accurate reserve calculation method, thereby redefining mineral reserves, as a basis for increasing state budget revenue, while avoiding loss and waste of resources;

- Inspect, compare and conduct audits at mining sites, measure to determine the actual exploited mineral output, compare with the declared output of enterprises, thereby having information and sanction forms on the level of violations of mineral exploitation projects;

In fact, when applying the Remote sensing method, using unmanned aerial vehicles (UAVs) at Trai Son limestone quarry, Tan Xuan mine (Hai Phong), SAV Region 6 Team found that the difference in mining output was over 10 million m3 of limestone, it is proposed to increase revenue for the state budget over VND 1000 billion.

c. Audit on environmental protection, inspection and examination in mineral exploitation:

- It is necessary to organize independent audits on environmental protection in mineral exploitation, (currently environmental audits are integrated in financial audits); Where:

+ Audit the implementation of reasonable and effective procedures and measures to remediate the environment with mining projects;

+ Inspect the observance of regulations on deposit and use of environmental rehabilitation funds under approved schemes;

+ Inspect and compare the actual environmental protection activities during and after the exploitation process at mineral reserves.

- Focus on building and strengthening the capacity of environmental audit auditors in both quantity and quality, ensuring that the requirements of the audit are met.

- Add qualified auditors with deep expertise in minerals to inspection teams and inspect mineral exploitation activities in localities.

3. Conclusions

The research results show that the state management of mineral exploitation activities in Vietnam in general and in the Northeast in particular in recent years has revealed many shortcomings and limitations.

The article outlines the most typical shortcomings that have been pointed out in the report of the State Audit Office of Vietnam and the Government Inspectorate. Shortcomings in the management of issuance of mining licenses, calculation of reserves and management of mining output as well as environmental management, carrying out inspections on mineral exploitation activities in localities may entail severe consequences, leading to revenue loss for the state budget, depletion and wastage of mineral resources and significant environmental degradation in mining areas.

With many limitations pointed out in the state management of mineral exploitation, the State Audit Office of Vietnam, when conducting the audit, needs to detect limitations and irrationalities of mechanisms, policies and acts and violations of corruption at state agencies and enterprises; clearly define the responsibilities of collectives and individuals, propose to handle violations in accordance with law; propose remedies and handle violations; Provide reliable information and data to the National Assembly and the Government in order to enhance the efficiency and effectiveness of state management in mineral exploitation management.

Literatura – References

1. Duong Quang Chinh et al, 2022, Renovating the audit organization of mineral resources management under the condition of technology application, Ministerial-level scientific project, Hanoi.
2. Do Men, "Illegal coal mining and trillion invoice sales line,VnEconomy.com, May 9, 2023, https://vneconomy.vn/vu-khai-thac-than-trai-phep-va-duong-day-mua-ban-hoa-don-nghin-ty.htm.
3. Ministry of Natural Resources and Environment, 2022, Report on 10-year review of implementing the Law on Minerals, Hanoi.
4. State Audit Office of Vietnam specialty 2, 2022, Thematic audit report "State management audit of mineral resources in the period 2017-2021" at People's Committee of Thai Nguyen province.
5. State Audit Office of Vietnam specialty 6, 2022, Thematic audit report "State management audit of mineral resources in the period of 2017-2021 at Vietnam National Coal and Mineral Industries Group - Vinacomin".
6. State Audit Office of Vietnam specialty 6, 2022, Thematic audit report "State management audit of mineral resources in the period of 2017-2021 at Vietnam National Cement Corporation (Vicem).
7. State Audit Office of Vietnam region 6, 2022, Thematic audit report "State management audit of mineral resources in the period of 2017-2021 in region 6".
8. National Assembly, Law on Minerals (No. 60/2010/QH12), 2010,
9. National Assembly, Law on Environmental Protection (No. 55/2014/QH13), 2014.
10. Government Inspectorate, 2022, Inspection Conclusion No. 1113/TB-TTCP, Thai Nguyen.

A New Approach on Improving The Operation of Over-Current Relays in 6kV Mining Grids of QuangNinh, VietNam

BUN Ho Viet[1)], THANH Le Xuan[2)]

[1)] Department of Electrification; HaNoi University of Mining and Geology, HaNoi, VietNam
[2)] Department of Electrification; HaNoi University of Mining and Geology, HaNoi, VietNam; email: lexuanthanh@humg.edu.vn

http://doi.org/10.29227/IM-2023-02-10

Submission date: 18-08-2023 | Review date: 12-09-2023

Abstract

Over-current relays (OCR) are the most popular protecting devices utilized in 6kV mining grids of open-pitch mines, QuangNinh province, VietNam. Depending on time of operation of OCR, there are many operating mode catergorized as: Instantaneous OCR, Inverse time OCR, Inverse definite minimum time (IDMT) OCR, Very invese relays, Extremely Inverse relays. Nowaday, to give protection against: Phase faults, Earth faults, Winding faults (in transformer), most of mining companies using Over-current relays with instantaneous characteristic. This charactersitic has the following important features: i) Operates in a definite time when current exceed relay's pick-up/setting up values, ii) Relay's operation is mainly relied on current magnitude, iii) Operating time is constant, iv) There isn't any intentional time delay, v) The operating currents are progressively increased for the other relays when moving towars the source. Apart from many advantages, there is a significant disavantage of the relays's operation: when there are faults at the beginning of feeders, OCR with instantaneous characteristic usually has a big-time tripping. Moreover, sometimes there are false trip of OCR because of improper set-up. In this study, an offline method is proposed with simulation in ETAP software to overcome these issues. With Gurobi-Optimizer application, an algorithm for identifying Time Multiplayer Setting (TMS) will be employed to generate inverse-time characteristic/inverse definite minimum time charactersitic for improving the performance of over-current relay with better discriminative tripping. The proposed method is simulated on ETAP with a 6kV sample skeleton distribution network (in QuangNinh province of VietNam). The demonstrating results are: the prevention of false trip of OCR and the operating time of OCR is reduced.

Keywords: *over-current relays, open-pitch mines, instantaneous time characteristic, false trip, Time Multiplayer Setting*

1. General introduction of Over-Current relays in 6kV mining grid

1.1 The advantages of ORC in mining electric system

For supplying energy, most coal mines in Vietnam utilize 6kV skeleton grids. 6kV electricity is normally feed to distribution boxes for energized motors, pumping system, ventilating system or coal-processing system. Because of high request in energy-supplying reliability, all of 6kV feeders contain at least 2 type of protection relays, among them OCR is the key one that responsible for fast and secured isolating the faults. Like normal medium voltage grids in urban areas, ORCs of 6kV networks must contain the following requirements and advantages [1], [26–29]:

+ Simplicity with reasonable cost: The design of OCRs is relatively simple; their implementation is not so complicated when compared to more other kind of complex protection schemes. They are really cost-effective solutions for detecting and responding to excessive current levels in mining grids.

+ Wide Range of Protection Settings: The protection setting of OCRs is wide and flexible, they could offer a wide value of adjustable settings, allowing customization based on the specific requirements and characteristics of the mining grid. These flexible characters enable operators/engineers to optimize the relay's performance for different fault levels.

Versatility: The utilization of OCR is wide with various types of electrical apparatus and systems, making them versatile in mining grid applications. Some popular utilization could be: motors protection, transformers protection, feeder protection, and other components within the mining infrastructure.

High-speed tripping: OCRs could provide rapid fault detection and response. When properly coordinated and set, they can quickly isolate faulty sections and minimize downtime, reducing the risk of equipment damage and improving the reliability of the grid.

Compatibility with digital control Systems: Most new modern ORC could be integrated with digital control/monitoring systems, such as annunciators or remote monitoring devices. This integration is important and allows the operator for real-time monitoring and abnormal/fault identification, aiding in troubleshooting and maintenance activities within the mining grid. According to [1], [31] OCRs installed in 6kV feeder must be integrated with SCADA systems, providing remote monitoring and control capabilities. This integration enables real-time monitoring of relay status, fault indications, and alarms, allowing operators in mines to promptly respond to abnormal conditions or faults in the mining grid. Hence, they enhance situational alarming and facilitates efficient decision-making.

1.2 The problems of present ORCs system in 6kV grid of Vietnamese coal mines

Because of insufficient investment, 6kV grids of most Vietnamese coal mines are equipped ORCs with instantaneous time-characteristics. Because of the containing multi-level tripping, the operation of 6kV feeders OCRs has many disadvantages, particularly the wrong tripping could sometimes arise that lead to big economical damage caused by de-energized.

Other disadvantages of OCRs in 6kV grid of Vietnamese coal mines could be listed as follow:

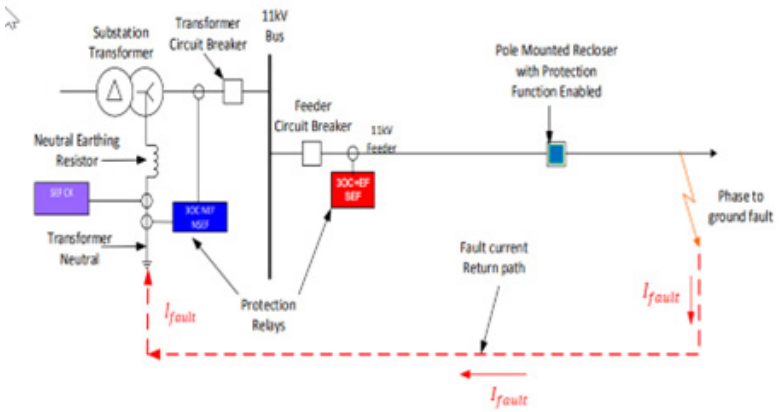

Fig. 1. Routine of earthing current in MV grids

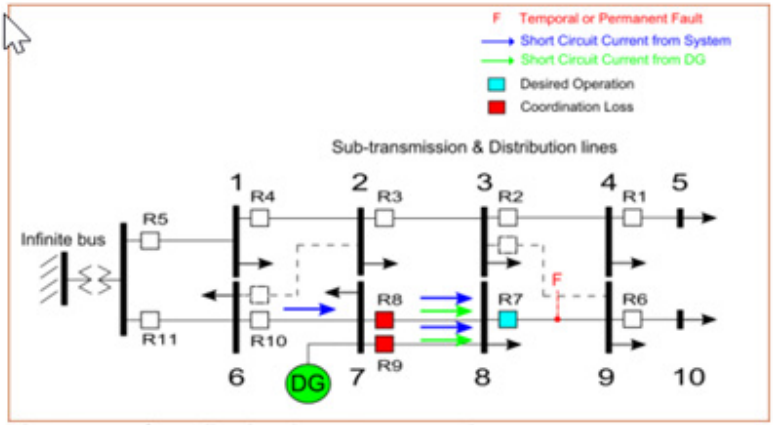

Fig. 2. Directional fault currents with distributed source

+ Delayed response time: OCRs operate based on the detection of current levels exceeding a predefined threshold [12, 13, 30]. However, depending on time-characterized [12, 30], the relay could perform a delayed response time before initiating a tripping procedure. This delay can be problematic in situations where a quick and immediate response is required, such as during fault conditions.

+ Discriminative tripping/Inaccurate coordination: Because OCRs are typically coordinated to ensure selective operation, it means that only the OCR closest to the fault must detect and send tripping signal to circuit breaker to isolate the faulty part of system. However, achieving criminative tripping could be great challenge due to the OCRs employed different time characteristics of relays and the complexity of 6kV mining network configurations. Improper OCR coordination might result in unnecessary or wrong tripping. Consequently, the overall 6kV system reliability and performance are significantly affected.

+ Limited sensitivity: OCRs have a predefined pick-tripping-up current threshold above which they initiate the trip signal. However, the threshold may not be sensitive enough to detect low-level faults (earthing current) [2, 3, 4] or incipient faults (for instance earthing current which is over 90% of the total faults in 6kV mining grids). Consequently, these relays may not obtain adequate protection in certain scenarios. Figure 1 presents the routine of earthing current in MV [2] (11kV-similarly in 6kV of coal mines). Depending on connection diagram of 35/6kV transformer's neutral point (delta connection [1]), detecting current value could not initiate the relay located at the beginning of feeder.

The sensitivity of OCRs is also affected by direction of fault current [16,17], in Figure 2 [16], because of distributed generator, value and direction of fault currents might not be "strong" enough for initiate the OCRs. This fact is similar to the manner of 6kV surface mines, where there are dozens electric excavators operated as distributed generator [32].

+ Lack of directional sensing: OCRs typically do not have or incorporate directional sensing capabilities themselves. They cannot distinguish between fault currents flowing into or out of the protected zone. This limitation [16, 18, 19] can result the incorrect tripping during faults heppenning on the non-protected side, causing to inefficient fault isolation and leading to potential damage of parts of the system.

+ Vulnerability to power system changes: OCRs are designed most relied on specific system parameters. Under certain condition, if the structure of the system is, such as the addition of new equipment or system islanding configuration, the relay settings may become inpropriate or inadequate. Consequently, OCRs' the reliability and effectiveness might be compromised.

+ Hardly detect high-impedance faults: When there is a poor connection between conductors or a short circuit containing a high resistance, OCRs could get challenges in detecting high-impedance faults. Since the rms of current in these occasions are relatively small, OCRs may not be able to identify them precisely, leading to potential safety hazards [4, 14].

Despite of above-mentioned disadvantages, in electric grids of Vietnamese mines OCRs are still widely utilized and

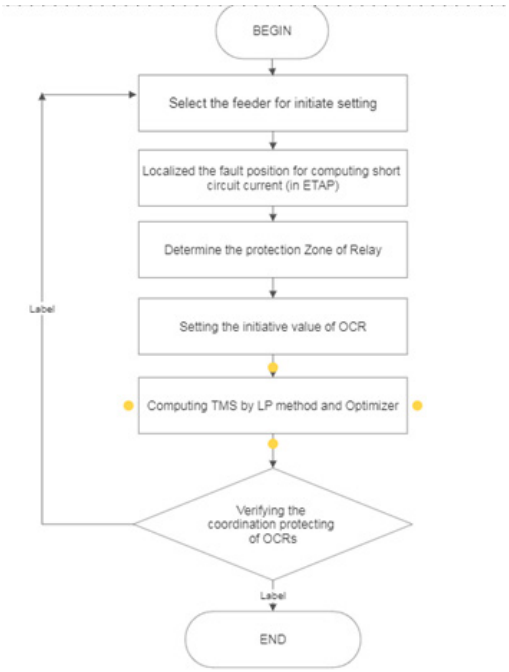

Fig. 3. Proposed Algorithm for identifying TMS of OCRs

provide essential protection in feeders, transformers, 6kV motors. Some technical weaknesses that OCRs must be improve are:

1. Discriminative tripping because of OCRs multi-ladder employed in 6kV networks;
2. Directional tripping if the impact of electric excavators is great.

There are many methodologies [5-11] to compute or optimize the operation of OCRs for logical coordination. But with skeleton grids, choosing the appropriate time curve from 4 basic type of curves [14, 29, 30] could be implemented by combination of Matlab programming and ETAP utilization. The following parts of this paper present an algortithm using Gurobi Optimizer combined with ETAP simulation to calculate the time factors for all OCRs installed in 3 or 4 layers of 6kV grids. The testing results will be simulated for obtaining time curves which is suitable for relay setting which protect both feeders and transformers of mines.

2. Identifying Time Multiplayer Setting (TMS) of OCRs

At present, in Vietnamese 6kV mining grids, because of many historic reasons, most of OCRs settings are difinte time characters for all protection level. Consequently, the time delayed tripping is the greatest issue that must be solved.

Other challenge is the identification of Time Multiplayer Setting (TMS) as wel as time ladding interval (Δt) of OCRs. Proper TMS identification could avoid the wrong tripping (backup OCR trips before essential OCR. Many researches shown in [5-10] focus on indentifying TMS as well as finding method for optimal coordination of OCRs. Each above propose has their individual advances, however refer to the skeleton structure of 6kV mining grids this part propose Linear Programming Algorithm, it will be embeded into Gurobi Optimizer in ETAP software [21] for testifying. According to [22] tripping time of OCR installed in skeleton feeder is calculated as equation (1):

$$t = \frac{0,14}{(I_{nm}/I_s)^{0,02}-1}.TMS \quad (1)$$

Whereas: I_{nm}-3-phase short cirtcuit current
I_s-Setting value

For identifying the value of TMS, a Linear Programme Algorithm is applied, in which an objective function f(x) (equa. (2)) is solved to obtain its minimum value, the constraint of the function is shown in equation (3) [19, 20].

$$f(x) = \sum_{j=1}^{n} c_j x_j \rightarrow \min \quad (2)$$

$$\sum_{j=1}^{n} a_{ij} x_j = b_i; \quad x_j \geq 0 \quad (3)$$

Where:
a_{ij} is the element of constraint matrix A;
b is the vector of freedom parameter;
x = (x1, x2, ... xn) is the optimal results of equation (2) which meet the constraint (3).

For satisfying the discriminative tripping, other constraints are considered [15, 21, 22, 23]:

Additional constraint 1: time bias between essential OCR (TiN) and back up (TjN) when there is a fault at N.

$$T_{jN} - T_{iN} \geq \Delta t \Rightarrow K_{jN}TMS_j - K_{iN}TMS_i \geq \Delta t \quad (4)$$

Additional constraint 2: TMS of each relay:

$$TMS_{min\_i} \leq TMS_i \leq TMS_{max\_i} \quad (5)$$

Additional constraint 3: TMS must be in the range of Tmin_i and Tmax_i which are listed in specification of each OCR:

$$T_{min\_i} \leq T_i \leq T_{max\_i} \quad (6)$$

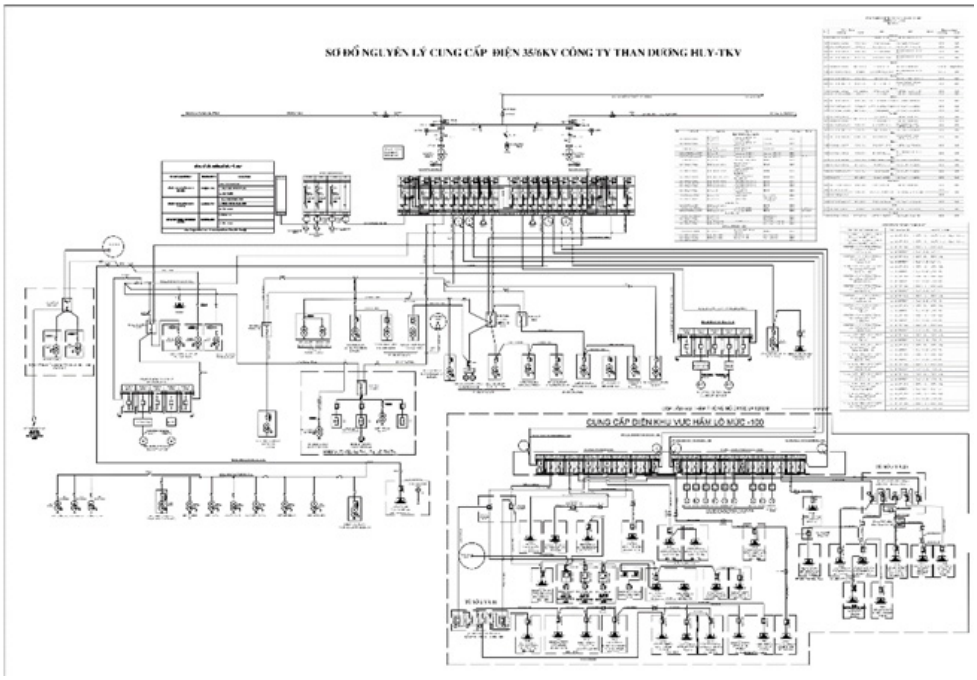

Fig. 4. Single line diagram of 6kV grid of DuongHuy coalmine (VietNam)

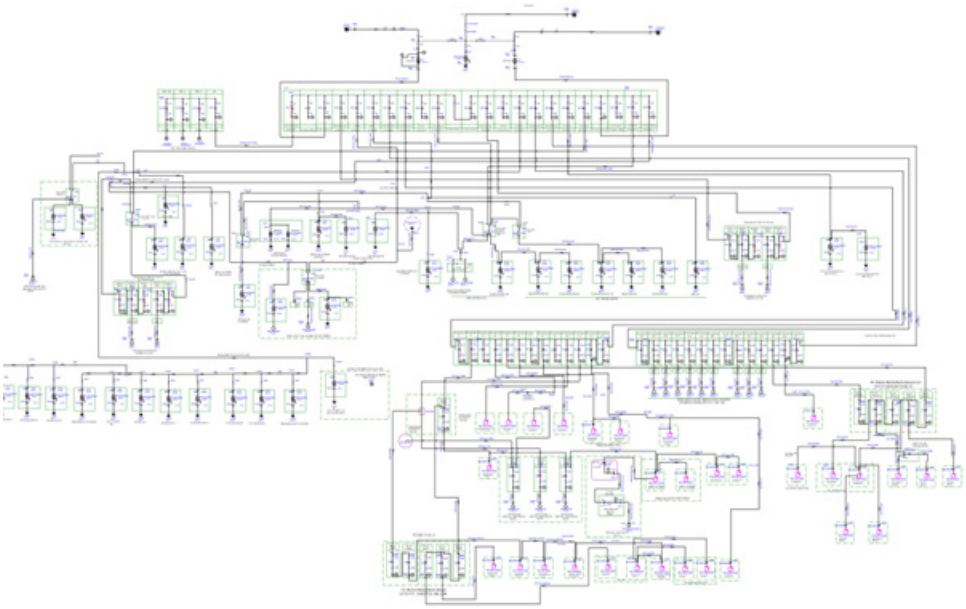

Fig. 5. Simulation diagram in ETAP of 6kV grid of DuongHuy coalmine (VietNam)

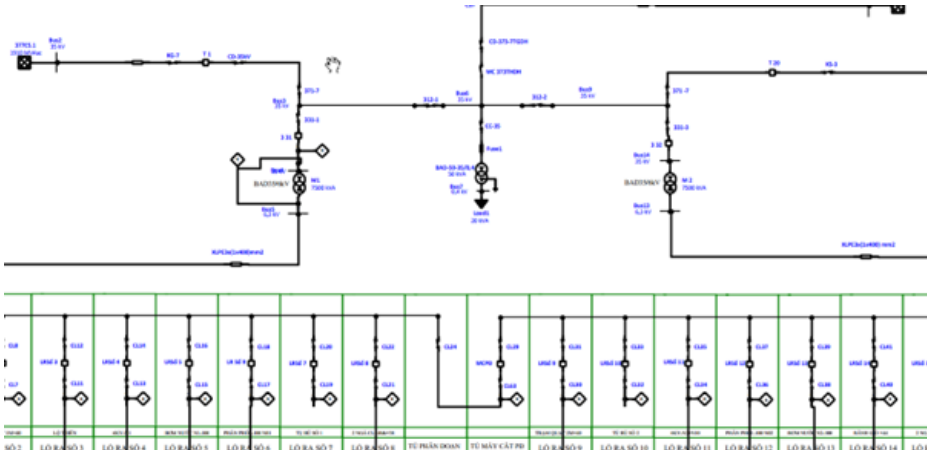

Fig. 6. The first OCRs employed in 6kV feeders

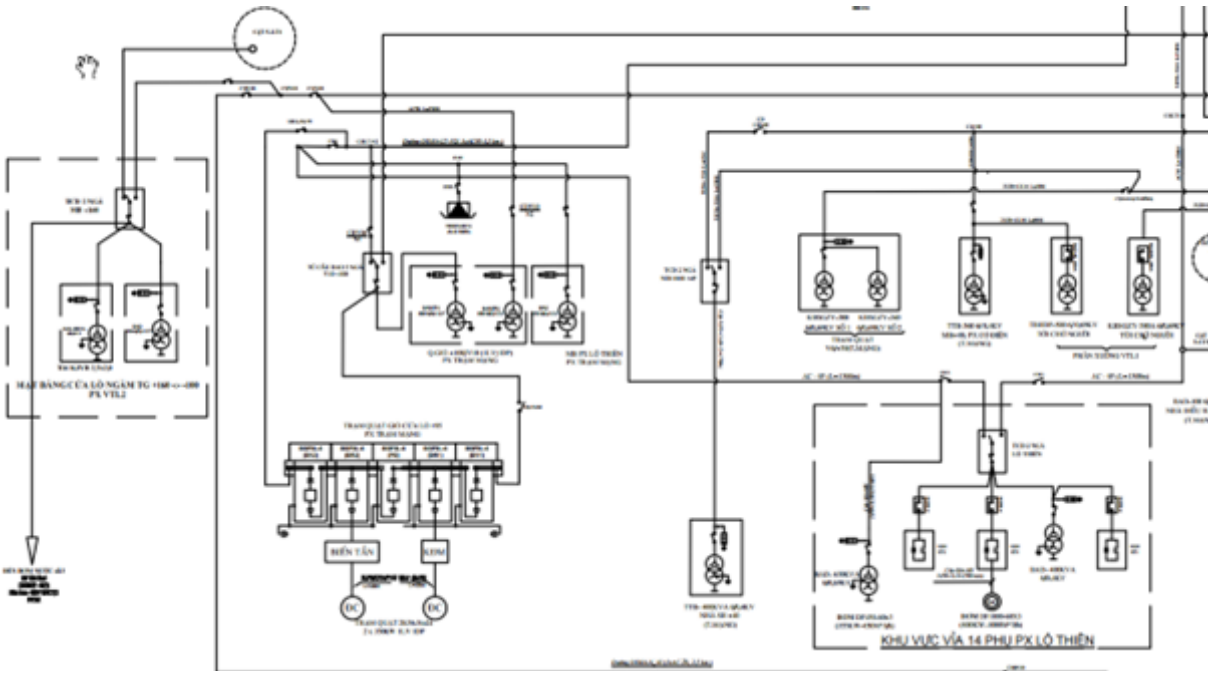

Fig. 7a. Single line diagram of 2nd OCRs layer in 6kV feeders

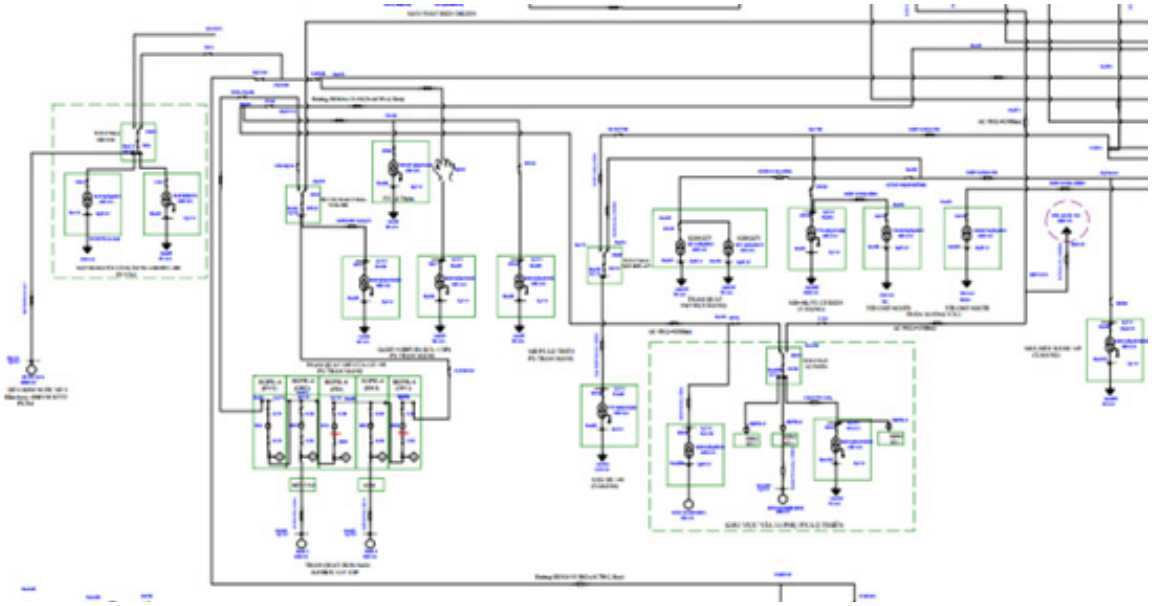

Fig. 7b. Simulation diagram of 2nd OCRs layer

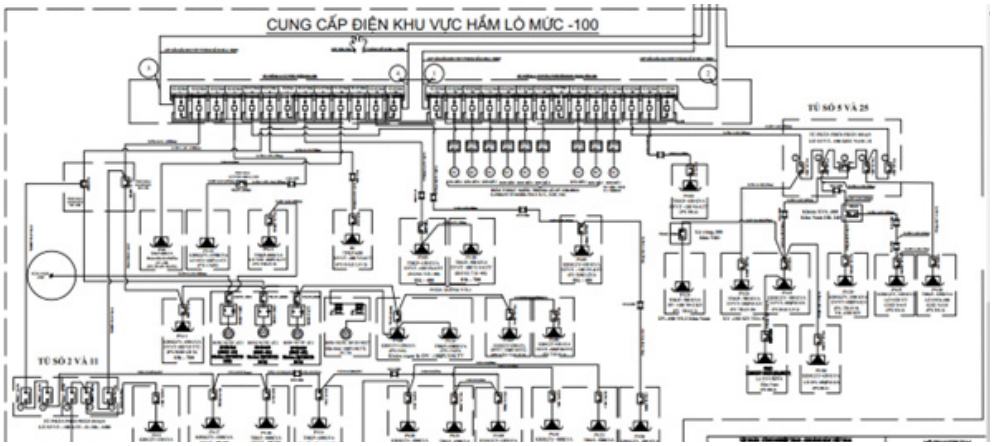

Fig. 8a. Single line diagram of 3rd OCRs layers in 6kV feeders

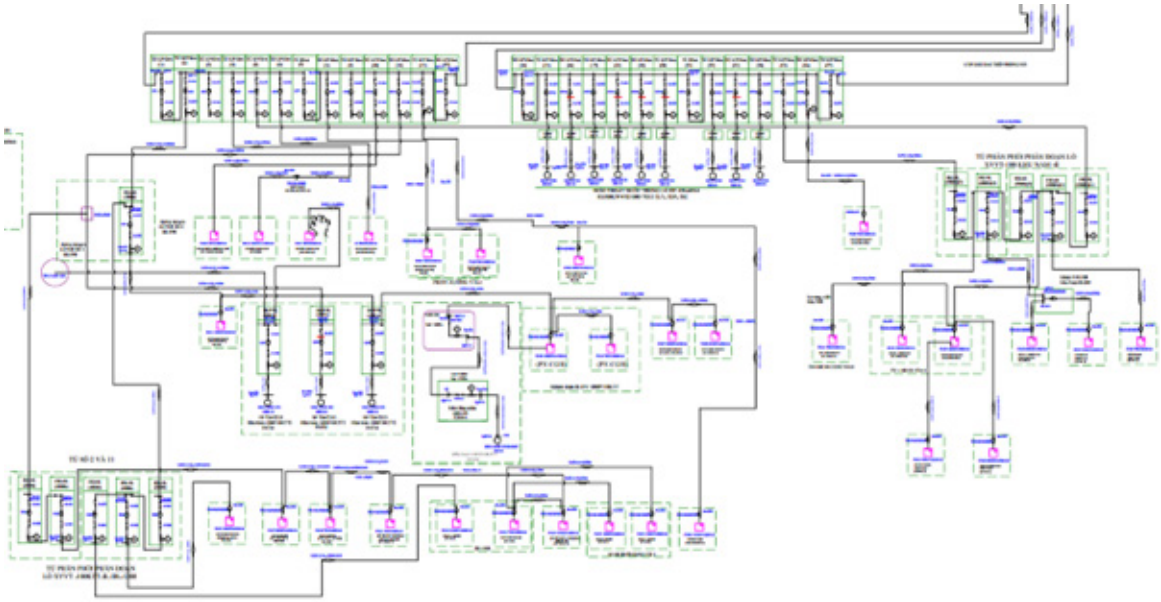

Fig. 8b. Simulation diagram of 3rd OCRs layer

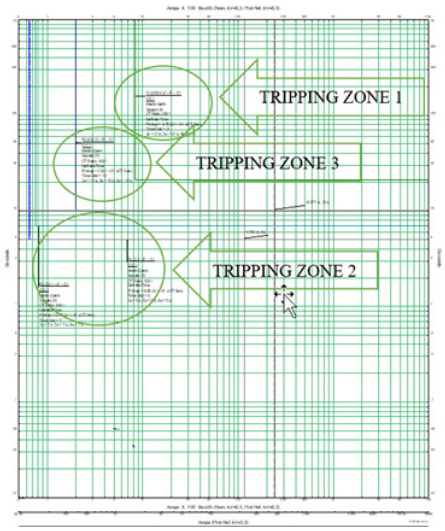

Fig. 9. The Definite Time Curve of OCR showing huge delay tripping

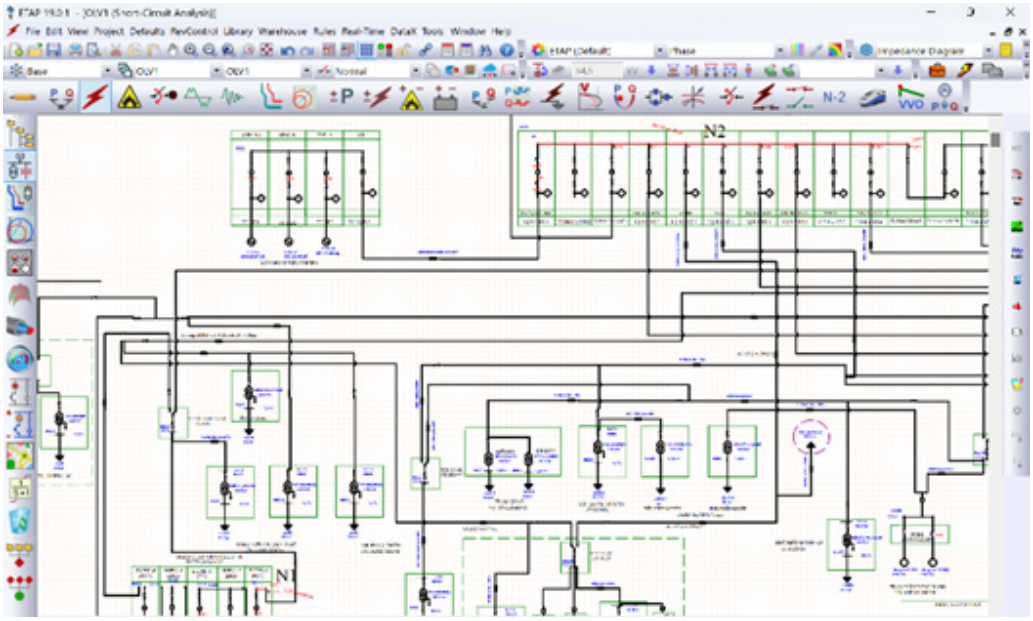

Fig. 10. Simulation of Fault currents calculation

Fig. 11. Simplization of the routine and value of fault currents

Tab. 1. Value of matrix converted into simplex-method

Relay	RLQ2 (Zone 1)	RLDV1 (Zone 2)	RLKH15 (Zone 3)	51(35kV)2 (Back up at transformer substation)
TMS	0,1	0,13	0,2617	0,345
t	t_1=0,1316	t_2=0,4315	t_3=0,7316	

Tab. 2. Values of TMS obtained from Simplex-Method

TMS1	TMS2	S1	S2	S3	P	b
-1,316	1,649	-1	0	0	0	0,3
1	0	0	-1	0	0	0,1
0	1	0	0	-1	0	0,1
1,316	1,39	0	0	0	1	0

If the time-curve characteristic is Definite Time (DT) or Inverse definite minimum time (IDMT), Objective function f(x) epressed in (1) is solved as:

$$\min C = \sum_{i=1}^{n} t_i = \sum_{i=1}^{n} K_{iN} TMS_i \tag{7}$$

Basing on above equations, an algorithm is proposed in figure 3. In the figure, if there are multi-layers OCRs in a feeder, a factor K of OCR numbered I is calculated as equation (8) [21, 23].

$$K_{iN} = \frac{0,14}{(I_{iN} / I_{si})^{0,02} - 1} \tag{8}$$

Where: Ii_N – Fault current of OCR numbered i;
I_si-Setting current of OCR numbered i.

3. Simulation and results

3.1 A case study for a typical 6kV grid of DuongHuy coal mine of VietNam

Algorithm in figure 3 will be applied for 6kV of Duong-Huy coal mine. The criminative operation of relays is proved and verified with simulation in ETAP. Single line diagram of the mine is presented in figure 4. A Simulated diagram on ETAP is expressed in figure 5.

Simulation parameters of the grid are: 2 main 35/6kV transformers with each one capacity of 7,5MVA, the low voltage of transformers is 6kV, total LV load is 5MW. There are four layers of OCR which located at the beginning feeders shown in Figure 7, 8, 9 and 10.

In these figures: 7a, 8a present single line diagram of the grid, 7b 8b corresponding are Simulation diagrams in ETAP.

At present, DuongHuy coal mine company utilize Sepam S20 relay [24, 25] for over current protection. The relay exhibits DT curves [30], the tripping time at 2nd layer (figure 7b) is 10 second, consequently the tripping time at 1st layer (figure 6-6,3kV bus bar) is 21 second. Hence, when there is a short-circuit at 15-distribution box (ending of 1st layer), the OCR of second layer denies its trip. This fact leads to the fact that the eliminate time of fault current is so great that could harm to 6kV cables and transformer. The expression of curves is shown in figure 9. Other consequence is the relay discriminative operation, the tripping time of zone 3/layer 3 is bigger than one of zone 2/layer 2. This fact is really very "annoyed" to operator because of wrong isolation the fault parts of the system.

To avoid this huge delay-tripping as well as criminative tripping, applying the algorithm presented in part 2, IDMT curves are employed. The task of LP method is to determine TMS values of all 3 layers. The provement rely on the following steps:

(1) Calculate the fault currents at beginning of layer 1 and layer 2 (two biggest values of all layers);
(2) Perform objective function and constraint matrix;
(3) Employing the Optimizer for identifying TMS;
(4) Simulate in ETAP for identify the series of IDMT curves for visual provement of relays in all layers.

3.2 Simulation and Results

In figure 10, locations of fault currents are exhibited, N1 and N2 are the beginning point of each feeder, relays R1 and R2 are correspondingly main protection one and back up one of each routine. The the results of faults currents and simplization of the routine is shown in figure 11.

* Step (1): Utilizing equation (8) [21], [23], when faulted at N_1, K factors of main relay R_1 and back up relay R_2 are computed as:

$$K_{11} = \frac{0,14}{(I_{N1} / I_{S1})^{0,02} - 1} = \frac{0,14}{(11754 / 75)^{0,02} - 1} = 1,316$$

$$K_{21} = \frac{0,14}{(I_{N1} / I_{S2})^{0,02} - 1} = \frac{0,14}{(11754 / 200)^{0,02} - 1} = 1,649$$

When faulted at N_2, K factors of main relay R_2:

$$K_{22} = \frac{0,14}{(I_{N2} / I_{S2})^{0,02} - 1} = \frac{0,14}{(24277 / 200)^{0,02} - 1} = 1,39$$

* Step (2) Forming the constraint matrix.
The Objective function is:
$\min C = K_{11} \times TMS_1 + K_{22} \times TMS_2$

With constraint:
$K_{21} \times TMS_2 - K_{11} \times TMS_1 \geq 0,3$
$TMS_1 \geq 0,1$
$TMS_2 \geq 0,1$

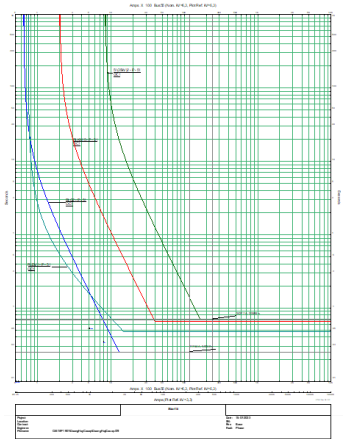

Fig. 13. The provement of criminative tripping of OCRs on 6kV grid

Tab. 3. Results of TMS indentification-Algorithm (TIA) for some typical mines in VietNam

Name of coal mines In VietNam	Tripping time before applying TIA (s)	Discriminative problem	Tripping time after applying TIA	Number of protection zones	Tripping time of Zone/layer 1	Tripping time of Zone/layer 1	Tripping time of Zone/layer 1
HaLam	16	YES	0,862	2	0,236	0,862	-
NuiBeo	15	NO	2,063	3	0,166	0,568	2,063
ThongNhat	20	NO	0,968	2	0,663	0,968	-
CaoSon	22	YES	1,267	3	0,568	0,969	1,267
CocSau	16	YES	1,689	3	0,656	1,086	1,689
QuangHanh	18	YES	2,078	3	0,985	1,389	2,078

Adding an auxiliary variable P, and S_1, S_2, S_3 (which are not negative) to transfer the above math inequality become an equality:

1,316×TMS1+ 1,39×TMS2 + P = 0

1,649×TMS2–1,316×TMS1– S1 = 0,3

TMS1 – S2 = 0,1

TMS2 – S3 = 0,1

Four equality equations exhibite values shown in table 1 which express the simplex-method.

From Table 1 values of factors matrix could be obtained:

C = [1,316 1,649 0 0 0];

B = [0,3 0,1 0,1];

$$A = \begin{vmatrix} -1,316 & 1,649 & -1 & 0 & 0 \\ 1 & 0 & 0 & -1 & 0 \\ 0 & 1 & 0 & 0 & -1 \end{vmatrix}$$

* Step (3): Finding TMS by Optimizer Linprog in Matlab:

options=optimset('LargeScale','off','Simplex','on');

[TMS,FVAL,EXITFLAG,OUTPUT]=linprog(C,[],[],A,B,zeros(size(C)),[],[],options).

*t1 = 1,316.*TMS(1)*

*t2 = 1,649.*TMS(2)*

Δt = t2 - t1

Results are deducted as:

TMS = [0,1 0,2617]

t1 = 0,1316

t2 = 0,4315

Δt = 0,3

Those values are immersed into ETAP, curves are performed in figure 13. Values of TMS for 3 protection zones/layers are given in table 2. It is easily seen in table 2 that the delayed time is reduced significantly (only 0,7316s compared with 21s in above analysis). Corresponding to 1 value of fault current (IN) the computing process of TMS showed that the tripping times (t_1, t_2, t_3) are logically criminative ($t_1 < t_2 < t_3$).

Implementing this Algorithm to other 6kV mining grids, the effect of IDMT curves is shown in table 3.

4. Conclusion

Overcurrent relays play very important role in 6kV mining grids of VietNam. Along with reforming process for replacing electromechanics relays by digital ones, the requirements of relay system smart utilization are the big matters that all mines must solved. By applying the programming in Matlab, combined with simulation in ETAP based on proposed TMS Identification Algorithm (TIA), the paper shown the following advantages on the field of improving the operation of OCRs in VietNam coal mines:

+ The proposed TIA is suitable for all skeleton 6kV mining grid despite of the complexity of protection zone;

+ TIA could help operator/technician in mine to transfer IT curves of overcurrent relay into its IDMT without any wrong operation;

+ The problem of delayed-tripping and discriminative tripping are completely cleared in all biggest coal mines in VietNam.

+ Results deducted from ETAP are visualable for operating, monitoring and designing the relay system in 6kV grids.

Literatura – References

1. QCVN 01:2011/BCT, 2011. Vietnam National regulation on safety Mining, http://www.kiemdinh.vn/upload/files/QCVN%2001-2011-BCT%20An%20toa%CC%80n%20trong%20khai%20tha%CC%81c%20than%20h%C3%A2%C-C%80m%20lo%CC%80.pdf
2. Narayan, Sanjay (2019) Earthing Systems and Earth Fault Protection in Power System Distribution Network. Research Project report, University of Southern Queensland. https://eprints.usq.edu.au/43125/12/Narayan_S_Quinton_Redacted.pdf
3. Ghanbari, T., Samet, H., & Ghafourifard, J. (2016). New approach to improve sensitivity of differential and restricted earth fault protections for industrial transformers. IET Generation, Transmission & Distribution, 10(6), 1486-1494. https://doi.org/10.1049/iet-gtd.2015.1343
4. Topolánek, D., Toman, P., Orságová, J., Kopička, M., & Dvořák, J. (2014). The evaluation of overvoltage during short-time additional earthing of healthy phase for fault location in MV networks. Developments in Power System Protection, 48-56. https://doi.org/10.1049/cp.2014.0160
5. A. E. Emanuel and E. C. Lalas, "Evaluation of Overcurrent Relay Settings Using a Genetic Algorithm," IEEE Transactions on Power Delivery, vol. 17, no. 1, pp. 85-91, Jan. 2002.
6. Y. M. Atwa, E. F. El-Saadany, and M. M. A. Salama, "Optimal coordination of overcurrent relays using a fuzzy-based immune algorithm," IEEE Transactions on Power Delivery, vol. 22, no. 4, pp. 2283-2290, Oct. 2007.
7. H. R. Hedayati-Dehkordi and G. R. Yousefi, "Optimal coordination of overcurrent relays using a novel hybrid approach based on improved particle swarm optimization and harmony search algorithms," International Journal of Electrical Power & Energy Systems, vol. 54, pp. 94-103, May 2014.
8. M. J. Hossain and M. A. Mahmud, "Optimal coordination of overcurrent relays using particle swarm optimization," IEEE Transactions on Power Delivery, vol. 27, no. 2, pp. 984-992, April 2012.
9. S. K. Goswami and S. Das, "Overcurrent relay coordination using bacterial foraging optimization algorithm," IET Generation, Transmission & Distribution, vol. 6, no. 12, pp. 1186-1197, Dec. 2012.
10. S. G. Haghjoo and H. Lesani, "A new protection coordination algorithm for microgrids using overcurrent relays based on harmony search," IEEE Transactions on Smart Grid, vol. 5, no. 6, pp. 3012-3020, Nov. 2014.
11. K. S. Pandya, R. K. Saket, and V. R. Prajapati, "Optimal coordination of overcurrent relays using artificial bee colony algorithm," International Journal of Electrical Power & Energy Systems, vol. 70, pp. 192-200, Jan. 2015.
12. Overcurrent relay and its characteristic, Electrical concept, Internet access at https://electricalbaba.com/over-current-relay-and-its-characteristics/
13. Type of overcurrent relay, Electrical Deck, Internet access at:
14. https://www.electricaldeck.com/2021/09/types-of-overcurrent-relay.html
15. Vincent Nsed Ogar, Sajjad Hussain, Kelum A. A. Gamage, (2023), The Use of instantaneous overcurrent relay in determining the threshold current and voltage for optimal fault protection and Control in transmission line, Signals-Volume 4 (1), page 137-149.
16. https://doi.org/10.3390/signals4010007
17. 15. Mahdi Ghotbi-Maleki, Reza Mohamadi Hamid Javadi, Method to solve false trip of Non-Directional overcurrent relays in radial networds equiped with distributed generator, IET Generation, Transmission and Distribution 13 (4) DOI: 10.1049/iet-gtd.2018.5610
18. https://ietresearch.onlinelibrary.wiley.com/doi/full/10.1049/iet-gtd.2018.5610
19. Meng Yen Shih, Arturo Conde, "An Adaptive Overcurrent Coordination Scheme to improve relay sensitivity and overcome drawbacks due to distributed generation in smart grids", IEEE Transaction on Industry Applications, 2016 DOI: 10.1109/TIA.2017.2717880
20. https://ieeexplore.ieee.org/document/7954715
21. Cheung, H., Hamlyn, A., Wang, L., et al.: 'Investigations of impacts of distributed generations on feeder protections'. Proc. IEEE Power & Energy Society General Meeting, Canada, 2009, pp. 1–5
22. Saleh, K.A., Zeineldin, H.H., Al-Hinai, A., et al.: 'Optimal coordination of directional overcurrent relays using a new time-current-voltage characteristic', IEEE Trans. Power Deliv., 2015, 30, pp. 537–544
23. Sarang V. Khond and Gunwant A. Dhomane, Optimum coordination of directional overcurrent relays for combined overhead/ cable distribution system with linear programming technique, Protection and Control of Modern Power Systems, 2019.

24. SKeith Brown, Herminio Abcede, Farrokh Shokooh, “Interactive simulation of power system & ETAP application and Techniques” IEEE operation Technology, Irvine, California.
25. Keith Brown, Herminio Abcede, Farrokh Shokooh, “Interactive simulation of power system & ETAP application and Techniques” IEEE operation Technology, Irvine, California.
26. Nguyễn Xuân Hoàng Việt, Rơle bảo vệ và tự động hóa trong hệ thống điện. Nhà xuất bản Đại học Quốc Gia TP.HCM, 2005.
27. A. Akhikpemelo, M. J. E. Evbogbai and M. S. Okundamiya, Overcurrent relays coordination using MATLAB model, Journal of Engineering and Manufacture Technology JEMT 6 (2018) 8-15.
28. https://www.se.com/vn/vi/download/document/PCRED301005EN/
29. https://www.se.com/vn/vi/download/document/PCRED301006EN/
30. IEEE Standard C37.112: "IEEE Guide for the Application of Protective Relays Used for Abnormal Frequency Load Shedding and Restoration."
31. IEC 60255-151:2019: "Electrical relays - Part 151: Power system protection and control devices."
32. IEEE Standard C37.2: "IEEE Standard Electrical Power System Device Function Numbers, Acronyms, and Contact Designations."
33. IEC 60255-1:2018: "Measuring relays and protection equipment - Part 1: Common requirements."
34. R. R. Williams, G. Benmouyal, and A. D. Singh, "Understanding overcurrent coordination curves," IEEE Transactions on Power Delivery, vol. 17, no. 3, pp. 724-729, July 2002.
35. Coal Mining Safety and Health Regulation 2017, Part 4 Electrical activities, equipment and installations. https://www.legislation.qld.gov.au/view/pdf/asmade/sl-2017-0165
36. Thanh, L.X., & Bun, H.V. (2022). Identifying the factors influencing the voltage quality of 6kV grids when using electric excavators in surface mining. Mining of Mineral Deposits, 16(2), 73-80. https://doi.org/10.33271/mining16.02.073

Prediction of Tunnel Cross-Sectional Area After Blastin

Chi Thanh NGUYEN[1)], Nghia Viet NGUYEN[1)]*

[1)] Faculty of Civil Engineering, Hanoi University of Mining and Geology, 18 Vien Stress, Hanoi, VietNam
*Corresponding author: nguyenthanh.xdctn47@gmail.com, nguyenchithanh@humg.edu.vn

http://doi.org/10.29227/IM-2023-02-11

Submission date: 12-08-2023 | Review date: 09-09-2023

Abstract

In this paper, two methods to predict and calculate the area of the tunnel face after the blasting were used. The first one is an artificial intelligence method using an artificial neural network system (ANN) model, and the second one – the support vector regression (SVR). After building predictive models for the area of the tunnel face after blasting by both methods, on the basis of comparing the results obtained in both methods, the performance of these models was assessed through the root mean square error RMSE and the coefficient of determination R^2. RMSE and R^2 values of the artificial neural network system (ANN) model were obtained as 0.1473 and 0.903 in training datasets, respectively. These values are 0.1497 and 0.9107 in testing datasets. In the SRV model, RMSE and R^2 were equaled to 0.1228 and 0.9331 in training datasets, respectively. These values are 0.1708 and 0.9055, respectively in testing datasets. It can be concluded that artificial intelligence using ANN and SVM models can be used to predict the area of the tunnel face after blasting with high accuracy.

Keywords: *ANN, SVR, tunnel, the drilling-blasting method, the cross-sectional area of tunnel, prediction*

1. Introduction

The method of drilling-blasting to break up rocks during the construction of tunnels is one commonly applied method in Vietnam due to its advantages, including cost effectiveness, simplicity, and fast progress. Several parameters affect the quality of the drilling and blasting method, with the cross-sectional area of the tunnel after blasting being crucial. Currently, there are few analytical methods available to predict and calculate the post-blasting tunnel area. Typically, the post-blasting tunnel area is taken within the range of (1÷1.25) times the design area of the tunnel face. Some scientists have statistically analyzed key parameters affecting the post-blasting tunnel area. However, accurately predicting the post-blasting tunnel area remains challenging using analytical methods. Some studies have successfully utilized artificial intelligence, specifically ANN and ANFIS models, to accurately predict and calculate the post-blasting tunnel area compared to actual values. In this study, the authors applied artificial intelligence, employing ANN and support vector regression (SVR) models, to build accurate prediction models for the post-blasting tunnel area. The study utilized a dataset of 110 regression data points obtained during the construction of the Deo Ca traffic tunnel. For the ANN models, the data in the dataset were randomly shuffled to create different models, each with training and testing datasets in a 4:1 ratio. The training dataset accounted for 80% of the total database, while the testing dataset accounted for 20%. Both the ANN and SVR models used the cross-validation algorithm (K-fold cross-validation) with the total database divided into k equal parts. The model was trained using (k-1) parts, and the remaining part was used to check model accuracy. The study compared the predicted post-blasting tunnel area from the models with measured data obtained during tunnel construction using the drilling and blasting method. The results revealed that the SVR model demonstrated high applicability in accurately predicting the post-blasting tunnel area. These findings serve as a foundation for applying ANN and SVR to build artificial intelligence models capable of accurately calculating and predicting other drilling and blasting parameters.

2. The ANN model and SVM model

2.1. Support Vector Machine SVM

Support Vector Machine (SVM) are supervised learning models. In the SVM, associated learning algorithms that analyze data for classification or regression analysis (in case of used to analyze data for regression, SVM as SVR- Support Vector Regression). According Aref A., et al., 2021, Support Vector Regression could use the training dataset to build the predicting model.

In regression, the SVM maps the input vectors to a multidimensional feature space. Next, the SVM creates a hyper plane that separates the input vectors with the maximum possible distance.

With the database $\{x_k, y_k\}$, k = 1,2, ... s, $x_k \in R^m$ is the input vector, $y_k \in R^n$ is the corresponding value of the desired model output, s is the number of samples. SVM is simulated using the following function:

$$f(x)=<w, x> +b \quad (1)$$

where: w, $x \in R^m$, <w, x> is the input data mapping function of the model, b is estimate bios, w is weight vector values.

The optimal hyperplane was elicited to maximize the distance between the data layers in terms of w and b, satisfying the equation:

$$\min \left(\frac{1}{2}\|w\|^2 + C\sum_{k=1}^{s} \varepsilon_i + \varepsilon_k^*\right) \quad (2)$$

With the following conditions to be satisfied:

$$\begin{cases} y_k - (w.\varphi(x) + b \leq \in +\varepsilon_k \\ (w.\varphi(x) + b) - y_i \leq \in +\varepsilon_k^* \\ \varepsilon_k, \varepsilon_k^* \geq 0, k = 1, 2, \ldots s \end{cases} \quad (3)$$

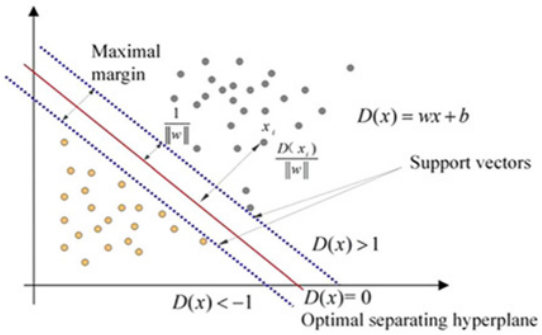

Fig. 1. Algorithm to support vector machine SVM (Aref A., et al., 2021)

Fig. 2. Deo Ca traffic tunnel

Where, C is capacity or penalty parameter, C>0; ε_k,ε_k^* are slack variables, $\in$ is the coverage area. Using the Lagrange method in equation (1):

$$f(x) = \min\left(\sum_{k=1}^{s}(a_k - a_k^*)K(x, x_k) + b\right) \quad (4)$$

Where: a_k và a_{ik}^* are Lagrange coefficients, K is Kernel function. Expand equation (3) as follows:

$$W(a_k, a_k^*) = \sum_{k=1}^{s} y_i(a_k - a_k^*) - \epsilon\sum_{k=1}^{s}(a_k + a_k^*) - \frac{1}{2}\sum_{k=1}^{s}\sum_{t=1}^{s}(a_k - a_k^*)(a_t - a_t^*)K(x_k, x_t) \quad (5)$$

The above equation must satisfy the conditions:

$$\sum_{k=1}^{s}(a_k - a_k^*) = 0; 0 \le a_k \le C, k = 1, 2, \ldots s; 0 \le a_k^* \le C, k = 1, 2, \ldots s. \quad (6)$$

2.2. Artificial Neural Network (ANN)

An Artificial Neural Network (ANN) is an information processing model of a computer based on the way biological neural systems in the human brain process information. An artificial neural network ANN is made up of a definite number of elements (Hecht-Nielsen R, 1987; Simpson PK, 1990). The elements of the artificial neural network are connected to each other through links (called link weights). A neuron is considered a basic component of a neural network (a structural element of a neural network) and an information processing unit. A model of working together between neurons in hidden layers with input signals processing neurons (Input) and output signals processing neurons (Output) - The ANN model to determine the relationship between desired input data and output data.

An ANN artificial neural model consists of the following main components (Esmaeili, M. et al., 2014; Koopialipoor, M. et al., 2017):

- Set of input signals of the model: these are the input signals of artificial neurons, these signals are usually put in the form of a vector with m-dimensionality;
- Set of links: each link is represented by a weight (Synaptic weight). The effect of weighting is to create a link between the jth input signal and the k neuron, usually denoted wjk. When the network initialization, weights were randomly initialized and were continuously updated during the training of the network.
- Summing function: this Summing function was used to count the sum of the product of the inputs data with the corresponding Synaptic weights.
- Bias: in the transfer function, bias is defined as a component.
- Transfer function (Activation function): the transfer function was used to limit the output range of each neuron in the ANN model. The transfer function takes as input the result of the given sum and threshold function. These transfer functions can be linear or nonlinear.

3. Data to build ANN and SVR models

In order to build ANN and SVM models, capable of predicting and calculating the cross-sectional area of the tunnel after blasting with high accuracy, it is necessary to use the data collected on actual construction sites. In this paper, 110 construction data at Deo Ca traffic tunnel construction site, Phu Yen, Vietnam has been collected, processed, and used to train and test ANN and SVR models. These data include the design area of the tunnel face S_{tk} (m^2); the average boreholes length l (m); The rock mass rating (RMR); specific charge q (kg/m^3). The above-mentioned parameters are evaluated as those that have a great influence on the value of the cross-sectional area of the tunnel after blasting during construction.

In order to be reasonable for the use of data in building artificial intelligence models for the purpose of predicting and calculating the cross-sectional area of the tunnel after the blasting with high accuracy, the data should be processed and returned to the range of [-1, 1] according to the formula:

$$X_n = \frac{X - X_{min}}{X_{max} - X_{min}} \quad (7)$$

Tab. 1. Parameters of data in building ANN and SVR models

Parameters	The symbol	Unit	Category	Min	Max	Average
The design cross-sectional area of tunnel	S_{tk}	m^2	Input	49,26	64,86	52,52
The average boreholes length	l	m	Input	1,0	3,2	1,75
The rock mass rating	RMR	-	Input	5	67	45,76
The specific charge	q	kg/m^3	Input	0,32	2,51	1,31
The cross-sectional area of tunnel after the blasting	SC	m^2	Output	50,276	71,049	56,6

Tab. 2. The results of R^2 in ANN models for different neuron numbers in the hidden layer

The neuron numbers in the hidden layer	Model 1		Model 2		Model 3		Model 4		Model 5		Average R^2	
	Training	Testing	Training	Testing	Training	Testing	Training	Testing	Training	Testing		
	R^2	R^2	R^2	R^2	R^2	R^2	R^2	R^2	R^2	R^2	Training	Testing
4	0.9001	0.8371	0.8457	0.7855	0.9012	0.8466	0.9005	0.8658	0.9063	0.8782	0.890766	0.842634
5	**0.9267**	**0.7740**	**0.8955**	**0.8819**	**0.9030**	**0.9107**	**0.9301**	**0.8726**	**0.8903**	**0.9170**	**0.909122**	**0.871239**
6	0.9128	0.5749	0.9035	0.7643	0.9695	0.9163	0.9090	0.8658	0.8850	0.9137	0.915949	0.806986
7	0.9065	0.7088	0.9094	0.6581	0.8915	0.8722	0.9090	0.8751	0.8952	0.9191	0.902315	0.806689
8	0.8910	0.6123	0.8873	0.6147	0.8480	0.8935	0.9026	0.8079	0.8726	0.8538	0.880296	0.756452

Tab. 3. The results of RMSE in ANN models for different neuron numbers in the hidden layer

The neuron numbers in the hidden layer	Model 1		Model 2		Model 3		Model 4		Model 5		Average RMSE	
	Training	Testing	Training	Testing	Training	Testing	Training	Testing	Training	Testing		
	RMSE	RMSE	RMSE	RMSE	RMSE	RMSE	RMSE	RMSE	RMSE	RMSE	Training	Testing
4	0.1646	0.2261	0.1895	0.2163	0.1543	0.1972	0.1449	0.2078	0.1411	0.1895	0.158869	0.207387
5	**0.1378**	**0.1700**	**0.1606**	**0.1729**	**0.1473**	**0.1497**	**0.1225**	**0.2236**	**0.1526**	**0.1487**	**0.144178**	**0.17297**
6	0.1500	0.2202	0.1483	0.2300	0.1575	0.1559	0.1360	0.2078	0.1562	0.1565	0.149605	0.194097
7	0.1612	0.2522	0.1432	0.2683	0.1694	0.1786	0.1360	0.2128	0.1533	0.1616	0.152629	0.214703
8	0.1673	0.2522	0.1600	0.2985	0.1852	0.1587	0.1510	0.2236	0.1676	0.2177	0.166232	0.230151

Tab. 4. The rank of models obtained from five different datasets for different neuron numbers in the hidden layer

The neuron numbers in the hidden layer	Average R^2				Average RMSE				Sum Rank
	Training	Rank	Testing	Rank	Training	Rank	Testing	Rank	
4	0.890766	4	0.842634	2	0.158869	4	0.207387	3	13
5	**0.909122**	**2**	**0.871239**	**1**	**0.144178**	**1**	**0.17297**	**1**	**5**
6	0.915949	1	0.806986	3	0.149605	2	0.194097	2	8
7	0.902315	3	0.806689	4	0.152629	3	0.214703	4	14
8	0.880296	5	0.756452	5	0.166232	5	0.230151	5	20

Tab. 5. Model selection for optimal results in ANN models

The neuron numbers in the hidden layer, n=5	Training				Testing				Sum rank
	R^2	Rank	RMSE	Rank	R^2	Rank	RMSE	Rank	
Model 1	0.9267	2	0.1378	2	0.7740	5	0.1700	3	12
Model 2	0.8955	4	0.1606	5	0.8819	3	0.1729	4	16
Model 3	**0.9030**	**3**	**0.1473**	**3**	**0.9107**	**2**	**0.1497**	**2**	**10**
Model 4	0.9301	1	0.1225	1	0.8726	4	0.2236	5	11
Model 5	0.8903	5	0.1526	4	0.9170	1	0.1487	1	11

Where X and X_n represent the measured and normalised values, respectively. X_{min} is the minimum measured parameters value and X_{max} is the maximum measured parameters value, respectively. X_{min}=-1 and X_{max}=1 (Esmaeili, M., et al., 2014).

To evaluate the accuracy of the ANN and SVR models for predicting the cross-sectional area of tunnel after the blasting, the paper compared the prediction values obtained from the models. The author evaluated the accuracy of the models through two coefficients, the coefficient of determination R^2 and the root mean square error (RMSE).

$$RMSE = \sqrt{\frac{1}{N}\sum_{i=1}^{N}((y_i - y_i')^2} \quad (8)$$

$$R^2 = \left[\frac{\sum_{i=1}^{N}(y-\bar{y})(y'-\bar{y}')}{\sum_{i=1}^{N}(y-\bar{y})^2 \sum_{i=1}^{N}(y'-\bar{y}')^2}\right]^2 \quad (9)$$

Where y_i are the observations, y'_i predicted values of a variable, and n the number of observations available for analysis.

4. Results and discussion

ANN and SVR models were built to predict and calculate the cross-sectional area of a tunnel during tunnel construction. In this paper, 110 data were obtained during the actual construction of the Deo Ca tunnel, including relevant evaluated parameters that had the greatest influence on the cross-sectional area of the tunnel after the blasting. These data were determined, collected, processed, and used to build

Tab. 6. Results of SVR models with different parameter C values

C	Training		Testing	
	R^2	RMSE	R^2	RMSE
10.5	0.89861893	0.151327	0.913373	0.149332
10	0.8989008	0.150997	0.913737	0.149332
9	0.89874298	0.151327	0.91334	0.149666
8	0.89843964	0.151327	0.91299	0.149666
7	0.89855903	0.151327	0.913697	0.149332
6	0.89913427	0.150997	0.913264	0.150333
5	0.89886603	0.151658	0.910816	0.154272
4	0.89840493	0.151658	0.909924	0.155242
3	0.89853552	0.151658	0.909979	0.155242
1	0.89257087	0.156844	0.91136	0.156205
0.5	0.89296119	0.160624	0.911244	0.164924
0.25	0.8924826	0.176918	0.910708	0.186279
0.15	0.86392173	0.244336	0.876024	0.260192
0.05	0.64571197	0.37229	0.684102	0.379868
0.03	0.53810729	0.413884	0.589071	0.416893

Tab. 7. The rank of SVR models with different C parameter values

C	Training Rank		Testing Rank		Sum Rank
	R^2	RMSE	R^2	RMSE	
10.5	5	5	3	3	16
10	**2**	**1**	**1**	**1**	**5**
9	4	4	4	4	16
8	8	5	6	4	23
7	6	6	2	3	17
6	1	3	5	6	15
5	3	7	9	7	26
4	9	8	12	9	38
3	7	9	11	9	36
1	11	10	7	10	38
0.5	10	11	8	11	40
0.25	12	12	10	11	45
0.15	13	13	13	13	52
0.05	14	14	14	14	56
0.03	15	15	15	15	60

Tab. 8. Survey results of SRV models with different Kernel values with C=10.5

Kernel	Training		Testing	
	R^2	RMSE	R^2	RMSE
5	0.90187817	0.14866069	0.91340272	0.15033296
4	0.91649036	0.13747727	0.90625765	0.16000000
3	0.93311381	0.12288206	0.90552194	0.17088007
2	**0.95402171**	**0.10198039**	**0.89597588**	**0.17748239**
1	0.97650525	0.07280110	0.79020098	0.23515952
0.5	0.98330894	0.07280110	0.65963997	0.32171416
0.25	0.98760436	0.06082763	0.10956368	0.44497191
0.075	0.98840993	0.06324555	0.05317605	0.46141088
0.05	0.98838461	0.06324555	0.03312009	0.46658333
0.03	0.98834682	0.06324555	0.02283761	0.46989360
0.02	0.98834230	0.06324555	0.02152737	0.47233463
0.01	0.98834288	0.06324555	0.02153341	0.47655010

Tab. 9. Ranking of SVR models by surveyed Kernel parameter values

Kernel	Training Rank		Testing Rank		Sum Rank
	R^2	RMSE	R^2	RMSE	
5	12	12	1	1	26
4	11	11	2	2	26
3	10	10	3	3	26
2	**9**	**9**	**4**	**4**	**26**
1	8	8	5	5	26
0.5	7	7	6	6	26
0.25	6	6	7	7	26
0.075	**1**	**2**	**8**	**8**	**19**
0.05	2	3	9	9	23
0.03	3	4	10	10	27
0.02	5	5	11	11	32
0.01	4	6	12	12	34

Note: As per the ranking in Table 9, models with Kernel values of 0.075 and 0.05 have the lowest SumRank, with values of 19 and 23 respectively. However, these values are rejected due to the coefficient of determination R^2 in the test dataset being less than 0.6.

ANN and SVR models. Input data for the ANN and SVR models included the rock mass rating RMR, the design area of the tunnel face S_{tk} (m^2), the average boreholes length l (m); specific charge q (kg/m^3). The K-Means Clustering Algorithm was used to train and test the model, ensuring the accuracy of the model results. Here, the total database was divided into 5 equal parts, with each part containing 22 data points. Four parts were used to build and train the ANN and SVM prediction models, while the remaining part was used as testing data for the built models.

4.1. Result of Artificial Neural Network models

In the ANN algorithm, one hidden layer is used to build models capable of predicting the cross-sectional area of a tun-

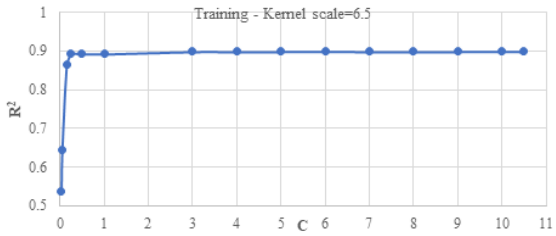

Fig. 3. The graph shows the dependence of the coefficient of determination R^2 with the regularization parameter C in the training dataset of the SVR optimum model

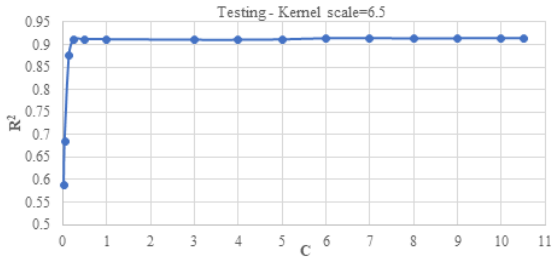

Fig. 4. The graph shows the dependence of the coefficient of determination R^2 on the regularization parameter C in the testing dataset of the SVR optimum model

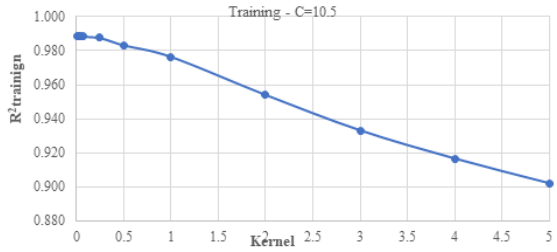

Fig. 5. The graph shows the dependence of the coefficient of determination R^2 on the Kernel scale in the training dataset of the optimal SVR model

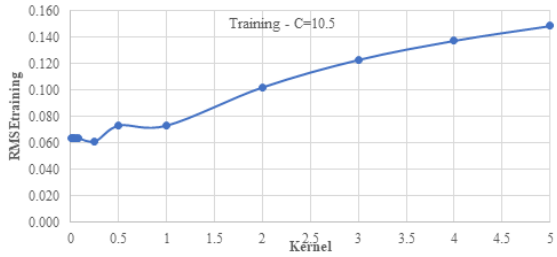

Fig. 6. The graph shows the dependence of the RMSE on the Kernel scale in the training dataset of the optimum SVR model

nel after blasting. With a hidden layer, the accuracy of ANN models still ensures accuracy when predicting only one output variable and reduces the complexity and processing time of the model (Chi T.N., et al., 2022). The transfer function used in ANN models is tanh(x). Run the ANN models with different neuron numbers in the hidden layer to select the optimal neuron numbers that can ensure the highest accuracy for the ANN models. According to Mohammad. E., et al., 2014, the neuron numbers in the hidden layer must be less than or equal to (2*N+1), where N is the number of input variables of the model.

Based on the results of ANN to predict and calculate the area of the tunnel face after the blasting in tables 2÷5, the ANN models had the optimal value when the neuron numbers in the hidden layer is n=5. When the neuron numbers in the hidden layer n=5, the coefficient of determination R^2 had the maximum value and the original mean the root mean square error RMSE of ANN models is the smallest (with the ranking value SumRank being the smallest). In Table 5, Model 3 with the corresponding databases is the optimal model.

4.2. Result of Support Vector Regression (SVR) models

Building predictive models of the cross-sectional area of a tunnel after blasting using Support Vector Regression (SVR) with different parameter values. Conducting a trial and error method to identify the optimal parameter values for the model (parameters include Kernel ratio, C-Regularization parameters). Through the aforementioned trial and error method, the optimal model was determined based on the parameters and characteristics of the model, including: Gaussian Kernel function (RBF Kernel - radial basis function) – the most commonly used function in SVR models as it yields highly accurate results (Aref A., et al., 2021; Nguyen H., et al., 2019), with a Kernel scale value of γ=2.0; Regularization parameter C=10.

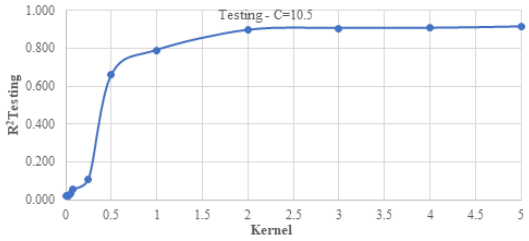

Fig. 7. The graph shows the dependence of R^2 on the Kernel scale in the testing dataset of the SVR optimum model

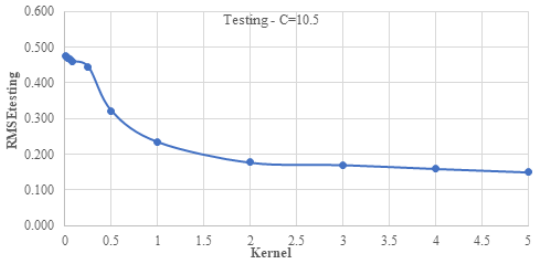

Fig. 8. The graph shows the dependence of RMSE on the Kernel scale in the SVR optimum model's testing dataset

4.3. The results of predicting the cross-sectional area of tunnel after the blasting are obtained from optimum models

Based on the results obtained from the ANN models in Table 2–5, it can be seen that model number 3 with the corresponding database is the model with the best predictive results for the cross-sectional area of the tunnel after the blasting. Using model 3 has been selected with the model's parameters such as 1 hidden layer, the number of neurons in the hidden layer is 5, the tanh function is used as the transfer function in the model to predict the cross-sectional area of the tunnel after the blasting. The obtained coefficient determined in the training dataset is $R^2_{training}$=0,903; the coefficient of determination in the test dataset is $R^2_{testing}$=0.9107; the root mean square error in the training dataset is $RMSE_{training}$=0.1473; the root mean square error in the testing data set is $RMSE_{testing}$=0.1497 (Figures 9, 10), when comparing the model's predictive results with the corresponding actual measured values (Figures 11, 12).

For the SVR optimum model that has been built and selected, based on the results obtained when using the model to estimate the cross-sectional area of the tunnel after the blasting in Tables 6–9 and Figures 13–16. It can be found that the model can predict the cross-sectional area of the tunnel after the blasting with high accuracy ($R^2_{training}$=0.9331; the coefficient of determination in the testing data set is $R^2_{testing}$=0.9055; root mean square in the training dataset $RMSE_{training}$=0.1228; root mean square error in the test dataset $RMSE_{training}$=0.1708). Based on the graphs showing the correlation between RMSE and R^2 of the training and testing data sets with the Kernel scale value, it is found that a Kernel scale value of 2 meets the accuracy of the results of the SVR model. At the Kernel scale value of 2, the RMSE and R^2 of the model with the testing dataset and training dataset are almost unchanged and reach good values (RMSE is small and R^2 is close to 1) and the RMSE values are also good (Figures 5 ÷ 8). For the investigation and determination of the optimal C - the regularization parameter, based on the obtained results and the graph in Figures 3, 4, it is found that in both the training dataset and the testing dataset, C=10 for the biggest values of the coefficient of determination R^2.

According to the results of this investigation, the cross-sectional area of the tunnel after the blasting values was found to be homogeneous in both models: ANN and SVR. There was no significant difference between the cross-sectional area of the tunnel after the blasting, as indicated by R^2 and RMSE, in the training dataset and the testing dataset.

5. Conclusion

The drilling-blasting method was one of the main methods used to construct tunnels and underground works in Vietnam because of the advantages of this method, such as low cost and no high technical requirements. This method can be used in most geological conditions in the area where underground works are arranged. Among the parameters that can be evaluated for the effectiveness of tunnel construction and underground works, the area of the tunnel face after the blasting is one of the most important parameters. This parameter determines the volume and properties of other works during the construction of underground work.

In practice, determining the cross-sectional area of the tunnel after the blasting has been extensively studied. However, due to its dependence on several parameters, such as the characteristics of the drilling-blasting method, the type of explosives used, the equipment employed in the construction process, and the tunnel's features, accurately determining the cross-sectional area of the tunnel after the blasting is challenging. This paper researched and applied artificial intelligence models, specifically ANN and SVR techniques, to develop predictive and calculation models for the cross-sectional area of the tunnel after the blasting. The models were constructed and chosen based on actual data collected during the construction of the Deo Ca traffic tunnel in Phu Yen. They exhibit high accuracy in predicting and calculating the cross-sectional area of the tunnel after the blasting, based on the comparison of the prediction results of these models with the values of the cross-sectional area of the tunnel after the blasting obtained from the actual construction with the help of various graphs and some statistical parameters. The following conclusions can be drawn from the results obtained using ANN and SVR models for predicting and calculating the

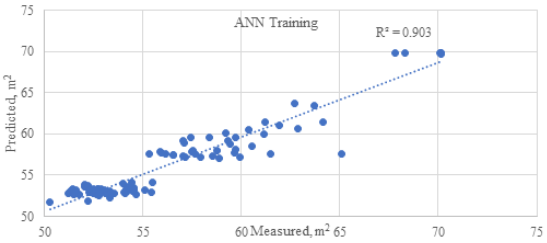

Fig. 9. The coefficient of determination R^2 of the ANN model selection at training step

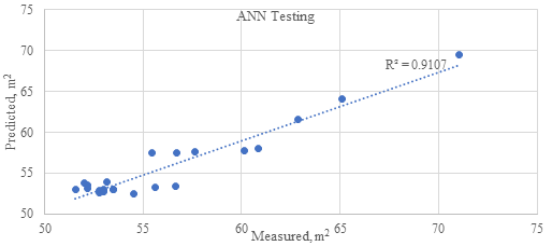

Fig. 10. The coefficient of determination R^2 of the ANN model selection at testing step

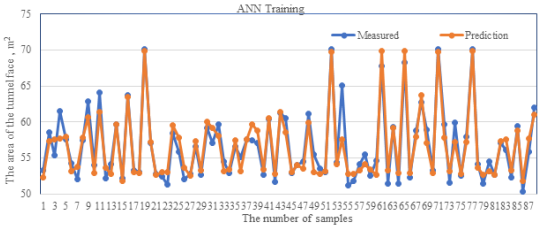

Fig. 11. Measured and predicted the values of the cross-sectional area of tunnel after the blasting obtained through the ANN model for training dataset

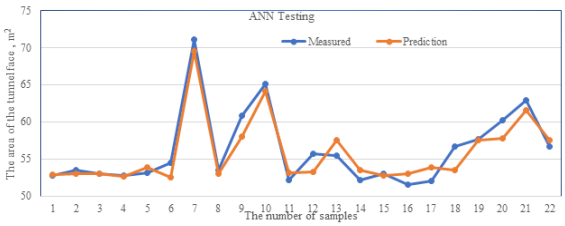

Fig. 12. Measured and predicted the values the cross-sectional area of tunnel after the blasting obtained through ANN model for testing dataset

cross-sectional area of the tunnel after the blasting:

- The accuracy of the models in the ANN artificial neural network depends a lot on the number of hidden layers and the neuron numbers in the hidden layers;
- The artificial neural network ANN model is capable of predicting and calculating the cross-sectional area of the tunnel after blasting. The coefficient of determination in the training dataset is $R^2_{training}$=0,903, and in the testing dataset it is $R^2_{testing}$=0.9107. The root mean square error in the training dataset is $RMSE_{training}$=0.1473, and in the testing dataset it is$RMSE_{training}$=0.1497;
- The SVR models depended a lot on the value of influential parameters during the model-building process, including the Kernel function, Kernel scale, and the regularization parameter C;
- In the case of the Kernel scale decreasing, the accuracy of the model in the training dataset increases; however, the accuracy of the model in the testing dataset decreases. Therefore, it is necessary to run SVR models with different values of Kernel scale, evaluate, and rank the results of the models to find the suitable Kernel scale value;
- If the Kernel scale decreases, the model's accuracy on the training dataset increases while its accuracy on the testing dataset decreases. Thus, it's vital to run SVR models with various Kernel scale values, assess their results, and rank them to determine the appropriate Kernel scale value.;
- The SVR model is capable to predict and calculate the cross-sectional area of the tunnel after the blasting with high accuracy. ($R^2_{training}$=0.9331; $R^2_{testing}$=0.9055; root mean square error in training dataset $RMSE_{training}$=0.1228; root mean square error in testing dataset $RMSE_{training}$=0.1708);

The rock mass rating RMR, the design area of the tunnel face S^{tk} (m^2), the average boreholes length l (m); specific charge q (kg/m^3) are important parameters that greatly influence the performance of ANN and SVR models. These models can predict the cross-sectional area of the tunnel after blasting accurately. The results of the ANN and SVR mod-

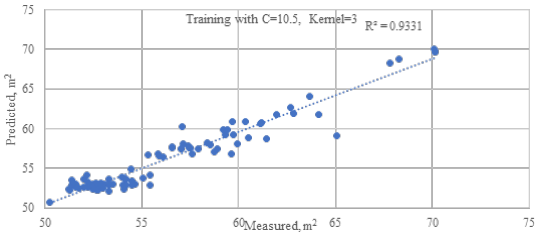

Fig. 13. The coefficient of determination R^2 of the SVR optimum model in training step

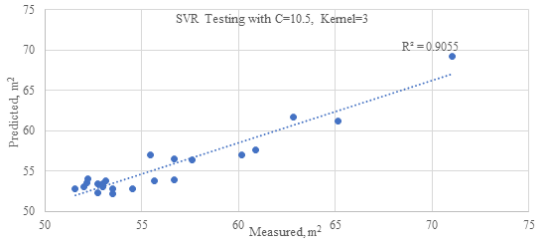

Fig. 14. The coefficient of determination R^2 of the SVR optimum model in testing step

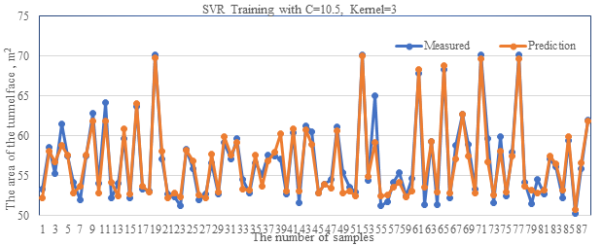

Fig. 15. Measured and predicted the values of the cross-sectional area of tunnel after the blasting obtained through the SVR model for training dataset

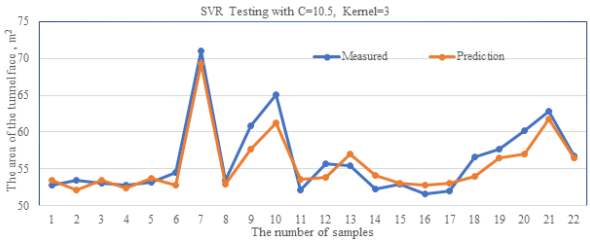

Fig. 16. Measured and predicted the values of the cross-sectional area of tunnel after the blasting obtained through the SVR model for testing dataset

els confirm the significance of these parameters in building accurate prediction models for the tunnel's cross-sectional area after blasting. Additionally, other parameters such as the cross-sectional shape of the tunnel, the characteristics of the drilling equipment used in the tunnel construction process, and the detailed characteristics of the borehole system arranged on the cross-section of the tunnel (quantity, distance, and angle of inclination created with the horizontal plane of boreholes) should also be mentioned and considered when building ANN and SVR models to predict and calculate the cross-sectional area of the tunnel after blasting in future studies. For different projects, it is necessary to update and change the actual values of the inputs in the data sets used to build predictive ANN and SVR models to ensure the accuracy and reliability of the model.

6. Acknowledgement

This research was supported by Vietnamese Ministry of Education and Training and Hanoi University of Mining and Geology.

7. Contributions of authors

Thanh Nguyen Chi: Data curation, Formal analysis, Funding acquisition, Investigation, Methodology, Writing - original draft. Nghia Viet Nguyen: Conceptualization, Supervision, Writing – review.

Literatura – References

1. Armaghani, D.J., Hajihassani, M., Mohamad, E.T., Marto, A., Noorani, S.A., (2014). Blasting-induced flyrock and ground vibration prediction through an expert artificial neural network based on particle swarm optimization. Arabian J. Geosci. 7 (12), 5383–5396.
2. Aref A., Mojtaba, M.A , Mostafa, A., (2021). Support Vector Machines for the Estimation of Specific Charge in Tunnel Blasting. Periodica Polytechnica Civil Engineering, 65(3), 967–976, 2021.
3. Dey, K., Murthy, V.M.S.R., (2012). Prediction of blast induced over break from un-controlled burn-cut blasting in tunnel driven through medium rock class. Tunn. Undergr. Space Technol. 28, 49–56.
4. Esmaeili, M., Osanloo, M., Rashidinejad, F., Aghajani, A.B., Taji, M., (2014). Multiple regression, ANN and ANFIS models for prediction of backbreak in the open pit blasting. Eng. Comput. 30 (4), 549–558.
5. Hecht-Nielsen R., (1987). Kolmogorov's mapping neural network existence theorem. In: Proceedings of the first IEEE international conference on neural networks, San Diego, CA, USA, pp 11–14.
6. Jang, H., Topal, E., (2013). Optimizing over break prediction based on geological parameters comparing multiple regression analysis and artificial neural network. Tunn. Undergr. Space Technol. 38, 161–169.
7. Koopialipoor, M., Armaghani, D.J., Haghighi, M., Ghaleini, E.N., (2017). A neuro-genetic predictive model to approximate overbreak induced by drilling and blasting operation in tunnels. Bull. Eng. Geol. Environ.
8. Chi T. N., Do N. A, Pham V. V., Nguyen P. T., Gospodarikov. A., (2022). Prediction of blast-induced the area of the tunnel face in underground excavations using fuzzy set theory ANFIS and artificial neural network ANN. International Journal of GEOMATE, 2022, 23(95), 136-143.
9. Nguyen H, Bui XN, Tran QH, Moayedi H., (2019). Predicting blast-induced peak particle velocity using BGAMs, ANN and SVM: a case study at the Nui Beo open-pit coal mine in Vietnam. Environmental Earth Sciences 78(15). DOI:10.1007/s12665-019-8491-x.
10. Mahtab, M.A., Rossier, K., Kalamaras, G.S., Grasso, P., (1997). Assessment of geological over break for tunnel design and contractual claims. Int. J. Rock Mech. Min. Sci. 34 (3–4).
11. Mohammad Esmaeili, Morteza Osanloo, Farshad Rashidinejad, Abbas Aghajani Bazzazi, Mohammad Taji (2014). Multiple regression, ANN and ANFIS models for prediction of backbreak in the open pit blasting. Engineering with Computers. 30, 549–558
12. Mottahedi, A., Sereshki, F., Ataei, M., (2018). Development of overbreak prediction models in drill and blast tunneling using soft computing methods. Eng. Comput. 34 (1), 45–58.
13. Simpson PK (1990) Artificial neural system: foundation, paradigms applications and implementations. Pergamon, New York.

Research on the Effect of the Mine Waste Dump on the Stability of Tunnels Below in the Quangninh Coal Area by Numecical Method

Dang VAN KIEN[1)], Vo TRONG HUNG[1)], Bui XUAN NAM[1)], Nguyen HUU SA[1)]*

[1)] Hanoi University of Mining and Geology, 18 Vien street, Hanoi, 100000; email: dangvankien@humg.edu.vn

http://doi.org/10.29227/IM-2023-02-11

Submission date: 10-08-2023 | Review date: 19-09-2023

Abstract

Nowadays, there are many underground coal mines in Quang Ninh, Vietnam have been exploiting coal seams below the mine waste dump such as Khe Cham II, Mong Duong, Mao Khe, and Ha Lam… Coal Company. Many mine waste dumps have reached the height of dumping from 400m, especially up to over 400m. The rock mass pressure due to the weight of the rock mass in the mine waste dump is considered an artificial pressure formed from the process of dumping soil and rock, it will be part of the pressure acting on the furnace lines located under the mine waste dump. The paper presents the current status of the mine waste dump and the coal seams that have been and will be exploited located below the mining waste dump in Cam Pha Quang Ninh and based on the actual conditions of the Bang Nau, Khe Cham II coal mine waste dump. The studies used the 2D FEM RS2 program to create simulation models with the mine waste dump to study the primary stress distribution in the rock mass. The objective of this study is to highlight the influence of the relationship location of tunnels below with the inclined coal/rock mass layer on the rock support behavior of the underground tunnels in the Quang Ninh coal area. The simulation results will help the consulting and construction companies to calculate the rock pressure acting on the tunnels located under the mining waste dump.

Keywords: *Mine Pressure, mine waste dump, rock support behavior, inclined coal/rock mass layer, yielded zone*

1. Introduction

Currently, the largest dumping site in Cam Pha area is Dong Cao Son landfill (with a capacity of 295 million m^3) which is being used by 3 open-pit mines Deo Nai, Coc Sau and Cao Son. In which, the volume of waste rock from Deo Nai, Cao Son, Coc Sau, Khe Cham II and Dong Da Mai mines accounts for over 94% of the total volume of waste rock in the whole region. In the period 2013–2020, the volume of waste rock in the region has reached over 1.9 billion m^3 (Figure 1). The soil and rock of the landfill is in a discrete state, including fragments, broken lumps of sandstone, siltstone, siltstone, claystone, coal clay and quaternary cover soil, size D = 0.1 mm ÷1000 mm (Figure 1 ÷ Figure 3).

The tunnels along the rock seams at Khe Cham III coal mine usually have a cross-sectional area designed according to the purpose of use and suitable according to the exploitation output of each area. In Fig.4.d shows the excavated cross-sectional dimensions of the trench along the rock seam at -190 of the seam 14.5 and the profile along the tunnel after being compacted. Currently, the underground coal mines in the area below the mine waste dump are mainly excavated by drilling and blasting and supported by CBII steel frames. The tunnels in the study area of the seam 14.5 include tunnels through the coal seam or through rock layers with poor stability. The temporary rock support is CBII steel frames will be replaced by permanent concrete lining. Special locations where the floor tunnel may be grow up are also fixed by reinforced concrete anti-reinforced shells combined with inverted arch beams to prevent growing up of floor tunnel.

2. The current status of the rock support of tunnels Below Mine Waste Dump in Quang Ninh coal area

High in situ stress of deep underground tunnel Below Mine Waste Dump in Quang Ninh coal area:

The TVT 14.5 tunnel in the Southeast area, Khe Cham III is deformed. According to the design of the tunnel, which is supported by SVP 22 steel, with a cross section of 9.4 m^2, the roof is sealed, both sides of the tunnel are staggered by precast reinforced concrete inserts placed and floor tunnel are support by the foundation beams. But due to the time and influence of the upper layer of rock pressure and the landfill area, many tunnels in this area were strongly compressed. The tunnel DVTG 14.4-2, built by Khe Cham Coal Company in 2019, was compressed and cracked, causing the steel frame to crack. To ensure the safety and usability of the tunnel, the Company has resisted cropping to bring the tunnel back to its original cross-section. However, the tunnel continued to be compressed, deformed, pushed both sides of the tunnel to break the entire P24 rail platform, reducing the tunnel cross-section, the actual used section to 5.4 m^2, affecting the ventilation, transportation and drainage of the area (Fig.4b) (Fig.5 ÷ Fig.7). Through the assessment of the causes of tunnel destruction, it was found that the selection and calculation of the rock support based on the traditional calculation hypotheses is no longer appropriate because through the process of re-evaluating the structure, the structure is still durable enough in theory.

The study area belongs to the seam 14.5 with the following characteristics: The seam 14.5 is located from 30 m to 60 m away from the reservoir 14.4. The seam 14.5 occurs mainly in Khe Cham I, III and Cao Son open pit mining (Khe Cham IV). The thickness of the entire reservoir varies from 0.24 m (BKC09) to 38.84 m (NKC67), with an average thickness of 5.72 m. The specific thickness of coal varies from 0.00m to 27.37 m (NKC67), averaging 4.99 m. The seam has a very complicated structure, in the reservoir there are from 1÷9 layers of clamped rock, the thickness of clamped rock is from 0.0 m ÷ 11.50 m (NKC67), with an average of 0.53 m. The slope of the seam is from 30÷ 600, the average is 270. The thickness of

Tab. 1. Summary of current situation of Mine Waste Dump in Vietnam

N⁰	Name of Mine Waste Dump	Volume of waste (x10⁶) m³	Current elevation (m)	Waste floor height (m)	Waste floor slope angle (Degree)	Waste dump heigh (m)	Slope angle of Mine Waste Dump (⁰)	Width of floor surface (m)	Landfill background structure
1	East of Cao Son Mine Waste Dump	539.7	+310	50÷150	36÷40	210	28÷36	30÷50	Stable
2	North of Bang Nau Mine Waste Dump	963.7	+190	40÷180	34÷36	180	30÷36	30÷50	Stable
3	Southwest Khe Tam Mine Waste Dump	296	+320	30÷60	33÷35	200	30÷32		Stable
4	East of Khe Sim Mine Waste Dump	150	+250	30÷50	34÷37	200	30÷32		Stable
5	Chinh Bac Mine Waste Dump	53	+256	7÷70	30÷36	186	25÷31	30	Stable
6	Khanh Hoa Mine Waste Dump	526	+195	11÷81	30÷40	153	25÷33	20÷25	Survey drilling needed
7	Na Duong Mine Waste Dump	25	+365	4÷16	25÷35	80	15÷25	20÷30	-
8	Phan Me Mine Waste Dump N03	16	+190	30÷50	130	130	30	25÷30	Weak background
9	Waste dump of ash and slag of thermal power plants		+410	5÷50	30÷36	60÷80	20	15÷30	Weak background
10	Mong Gioang Mine Waste Dump			20÷30		170	18÷22	20÷30	Stable
11	Lo Phong Mine Waste Dump (Finished)			40	30	200	24÷27	35	Stable

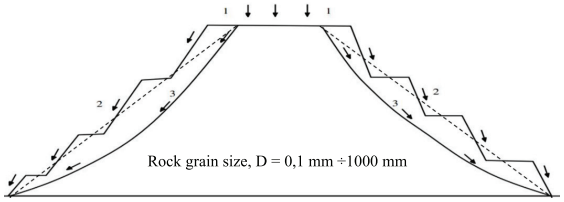

Fig. 1. Diagram of the process of stabilizing the soil and rock of the landfill

Fig. 2. Plane of Bang Nau Mine Waste Dump, Quangninh coal area

Fig. 3. The surfce Plane of Bang Nau Mine Waste Dump, Quangninh coal area

the seam 14.5 gradually decreases from the south to the north. Seam 14.5 has 317 drilling works to control the deep seam, 39 excavation works to control the seam. Soil and rock walls, coal seam pillars are layers of siltstone, claystone, dirty coal or coal clay and the aggregates are often located close to the coal seam wall, this is an easy to recognize sign. Compared to the 2008 conversion report, the average thickness of coal seam 14.5 has decreased from 6.77 m to 4.99 m.

The research results show that the rock support structure is calculated by structural mechanics method or numerical model. However, the above calculation methods have not paid much attention to the influence of the mine waste dump on the surface, or the large surface structures such as the vertical shaft tower, the office building of the mine as well as the upper layers of compacted soil left by the previous mining floors. In addition, the above calculation methods have not paid attention to the special geological conditions of the strongly compressed rock mass. Therefore, studying the influence of the mine surface waste dump on the mechanical behavior of the tunnels below in the Quang Ninh coal region will be very necessary and urgent to find new solutions to improve the stability of the tunnels in order to improve the efficiency of coal mining in the whole corporation, and at the same time apply scientific research achievements in countries with a developed coal mining industry in the world. The study diagram of the influence of the relationship between the tunnel position below the mine surface dump on the mechanical behavior of the tunnel support structure is shown in Figure 8. According to Figure 8, there are two locations that need attention, namely the tunnel located in area (I) – the center of the mine waste dump and the side of the mine waste dump (Area II). The objective of this paper is to highlight the influence of the relationship location of tunnels below with the inclined coal/rock mass layer on the rock support behavior of the underground tunnels in the Quang Ninh coal area.

3. A case study at Khe Cham II coal mine

Introduction to the Khe Cham II Coal Mine:

The Khe Cham III Coal Mine is in Cam Pha City, Quang Ninh Province, 200 km from Hanoi capital, Viet Nam. It is

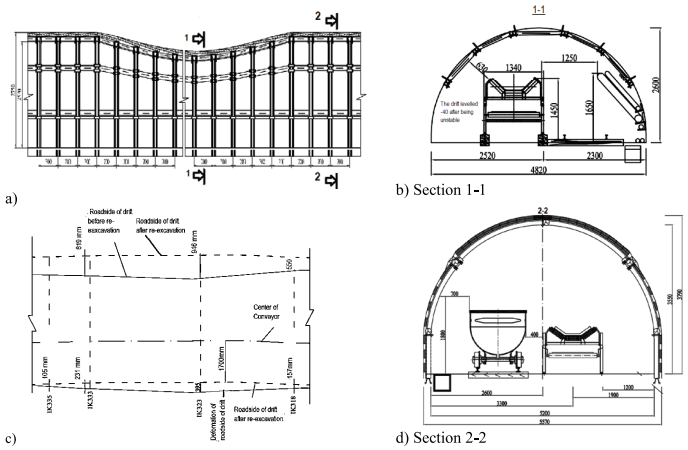

Fig. 4. Failure of the tunnel levelled -40 in the Nam Mau coal company through complex geology conditions below mine surface waste dump

Fig. 5. The collapses of deep underground tunnel floor seam 14.5 southeast area at Khe Cham III coal mine in Quang Ninh coal mine area at 12/05/2021 [1]

Fig. 6. Some typical failures in DVTG 14.4-2 tunnel at Khe Cham III coal mine in 12/05/2021 in Quang Ninh coal mine area at [1] (by authors)

Fig. 7. The collapses of TVT tunnel seam 14.5 southeast area at Khe Cham III coal mine in Quang Ninh coal mine area at 12/05/2021 [1]

one of the big coal mines owned by TKV group, that provides an important energy source for the rapid sustainable economic growth of Viet Nam, producing an annual coal output of more than 30 million tons (Mt) since 2009, reaching a maximum of 3.5 Mt/year.

Geological profiles of deep underground mine tunnel:

The haulage and rail DVTG 14-2 tunnel at Khe Cham III coal mine levelled – 150, with a horizontal width of 5.0÷6.0 m in the first mining level of – 150 m, playing a pivotal role in the sustainable development of the Khe Cham II coal mine with high output. The geological profiles of deep underground mine tunnel structures exist that are extremely complex, as shown in Table 1. The area of haulage and rail DVTG 14.4-2 tunnel at Khe Cham III coal mine is located near 14.5 seam. Water depth varies with seasons from 0.3m ÷ 1.0 m. The average flow is 2÷128.8 l/s in the dry season, but the speeed of water is very fast in the rainy season. The average thick of stratified rock seam is (0.4÷0.6) m with the rock consolidating coefficient by M.N. Protodyakonov: f=6÷8, and f=8÷10, some sections was through coal seams with the consolidating coefficient of rock by M.N. Protodyakonov: f=2÷3.

Numerical model building process

Based on the actual tunnel excavation data and the processing phases in the simulation, the modeling computation

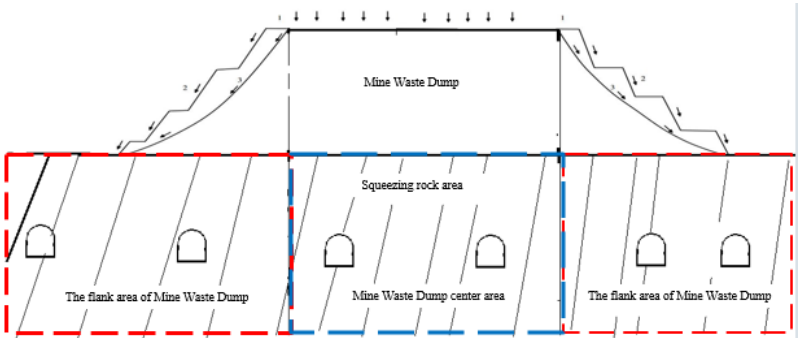

Fig. 8. Diagram of the study of the influence of the mine surface waste dump on the stability of the tunnel below
1. Surface subsidence – vertical displacement; 2. Surface erosion due to the impact of exogenous phenomena; 3. Landslide – landslide mass due to exogenous impact)

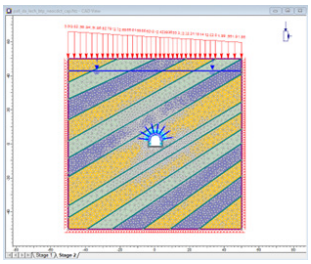

Fig. 9. Numerical model of the DVTG 14-2 tunnel at Khe Cham III

Tab. 2. Analysis Sequence

Phase	Description
Step 1	Initial Stress
Step 2	Initialize displacement
Step 3	Install SVP steel frame
Step 4	Install supports (Rock bolt & Shotcrete)
Step 5	Hardened shotcrete

phases are simplified to the following steps. Numerical model of the DVTG 14-2 tunnel at Khe Cham III are presented on Figure 9, the tunnel is located in area II. Flowchart of this study are presented on Figure 10. Analysis sequence of model are presented in Table 2. Properties of the rock mass and joints are presented in Table 3.

Floor grouting reinforcement technique with pressurization and progressive depths:

The floor heave of the underground tunnel is critical. The floor must be reinforced given the destructive floor heave. However, the holes drilled in the floor are always subjected to collapse because of the soft broken coal seams with the rock consolidating coefficient by M.N. Protodyakonov: f=2÷3. The bolts and cables cannot be installed in the floor. Based on the industrial testing of the floor reinforcement during working of tunnel, we proposed the floor grouting reinforcement technique with pressurization and progressive depths. Grouting depths in the floor successively increased from shallow to deep, and the corresponding grouting pressure also progressively increased (see Figure 8). The array pitch and the water-to-cement ratio for 1.5 m-deep holes grouting was 1:1. The earlier shallow holes grouting not only reinforces the shallow rock mass but also forms a stop-grouting layer for subsequent deeper drilling holes grouting and solves the problem of wall collapse in deeper holes. The 6 m-deep holes with grouting with superfine cement reinforces the deep rock mass in the floor and forms a large joint bearing ring with the reinforced deep rock mass in the roof and sidewalls. The displacement velocity of the floor decreased, providing a foundation for secondary enclosed support measures for the long-term stability of the surrounding rock.

Shallow holes post-grouting with superfine cement:

Shallow holes pre-grouting with superfine cement was completed (Figure 8). The lengths of the grouting pipes and boreholes were 1500 mm, and the array pitch was 1000 mm. Grouting pressure was generally not more than 3.0 MPa. The strength of the superfine cement was 62.5 MPa. The water-to-cement ratio was 0.8–1.0. The distance of shallow holes pre-grouting relative to the tunneling face was less than 6.0 m.

Deep holes post-grouting with superfine cement:

Deep holes post-grouting with superfine cement were bored after secondary shotcrete (see Figure 9). The lengths of grouting pipes and boreholes were 6000 mm. The array pitch average was 1000 mm. The grouting pressure was 6.0÷8.0 MPa.

To improve the grouting effect, deep post-grouting was conducted by a repeated grouting method with alternating intervals; i.e., the odd array holes grouting was first completed along the opening axis direction. Afterward, the grouting of the remaining even array holes was conducted. In addition, the deep holes post-grouting sequences at the same cross-section were from holes No.1 and No.9 on the sidewalls; then holes No. 2 and No. 8 in the shoulders, to the last hole No.3 to No.7 in the arch crown; No.10 and No.11in the floors (see Figure 9).

4. Numerical model the post-grouting to improve the stability of the underground mine tunnel

Tab. 3. Properties of the rock mass and joints

No	Parameters	Symbol	Values		Units
			Sandstone	Siltstone	
1	Unit weight of rock	γ	0.026	0.027	MN/m^3
2	Uniaxial compressive strength of intact rock	σ_{c1}	60; 70	45; 50	MPa
3	Tensile strength	σ_t	0.5	0.7	MPa
4	Cohesion	χ	2	4	MPa
5	Friction angle	φ	30	35	Degree
6	Young modulus	E	1500	2000	MPa
7	Poisson ratio	μ	0.3	0.28	-
8	Dilation angle	ψ	0	-	Degree
9	Residual tensile strength	φ_{pc}	28	32	Degree
10	Residual friction angle	χ_{pc}	1	0.5	MPa
11	Span of adits	B	5	-	m
12	Criterion of material	M–X	-	-	-
13	Ratio of initial stress	σ_3/σ_1	1	1	-
14	Depth of adits	H	100	-	m
15	Incline angle of rock mass layers	α	45	45	Degree
16	Thickness of rock mass layer	Δ	2; 4; 8; 16	2; 4; 8; 16	m
17	Strength tensile on the surfaces between two layers Sandstone / Siltstone	$\rangle'$	0		MPa
18	Friction angle on the surfaces between two layers Sandstone/Siltstone	φ'	35		Degree
19	Normal stiffness on the surfaces between two layers Sandstone / Siltstone	σ_j	100000		MPa/m
20	Shear stiffness on the surfaces between two layers Sandstone/Siltstone	τ	10000		MPa/m

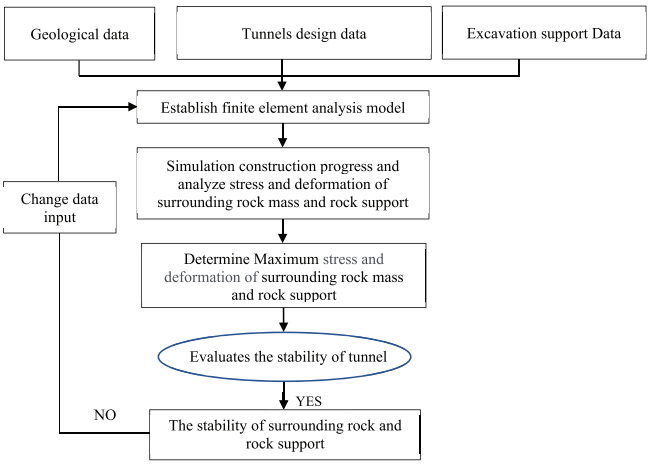

Fig. 10. Flowchart of the study

Numerical simulations were performed using the Finite Element Method with the Phase 2.0 software. The 2D model were used in this research. Using 2D models permits to validate the mesh and investigate some parameters of the model. The rock mass was modeled using the elastic perfectly plastic constitutive model (with a Mohr-Coulomb failure criterion). The parameters of the rock mass see in Table 1. Result of numerical simulations of before post-grouting and after post-grouting are presented from Fig. 10 to Fig. 15. The model is studied on 3 stages: stage 1 – before post-grouting; stage 2 – The grouting work has just been completed; stage 3 – The grouting work has been completed in a time. Parameters of rock mass after being reinforced by grouting using as input ones are friction angle (resid) and cohesion (resid), also Young's modulus (E). The cohesion (resid), Young's modulus (E) is increased by post-grouting process, the rock mass surrounding the tunnel can be able to carry of self loading after grouting.

The criteria to determine whether a tunnel has sufficient capacity to sustain the external load effects is strength factor of rock mass. The strength factor is calculated by dividing the rock strength (based on failure criteria, the model used Mohr-Coulomb failure criterion) by the induced stress at every point in the mesh. All three principal stresses have an influence on the strength factor (Sigma 1, Sigma 3 and Sigma Z).

By the numerical model, the efficiency of grouting solution has been investigated. The result of numerical model on Fig.10 to Fig. 12 shows the stress and displacement induced in the rock mass surrounding the tunnel. The friction angle (resid) and cohesion (resid), also Young's modulus (E) is increased by post-grouting process. It also shows that Young's modulus (E) is increased 1.25 times higher than before grouting by shallow holes post-grouting with superfine cement (Stage 2) and increased 1.5 times higher than before grouting by deep holes post-grouting with superfine cement (Stage 3). Displacement around the tunnel after post-grouting are presented on Figure 13. The strength factor of rock mass after grouting is prented on Fig.14. Strength factor of rock mass at roof, shoulder of tunnel in stage 2 is more than 1.0, but the strength factor of rock mass on some points at left floor is less than 1.0 (Fig.14). Strength factor of rock mass of stage 3 in which the grouting work has been completed in a time is higher than stage 2. All of them are higher than 1.0.

Tab. 1. Physiccomechanical parameters of surrounding rock before post-grouting

Parameters	Symbol	Value	Unit
Unit weight	γ	0,26	MN/m^3
Tensile Strength	σ_k	0,5	MPa
Cohesion	c	0,025	MPa
Friction angle	φ	35	Deg.
Young's modulus	E	1000	MPa
Poisson's ratio	μ	0,30	-
Dilation angle	ψ	0	Deg.
Friction angle (resid)	φ_{re}	28	Deg.
Cohesion (resid)	c_{re}	0,02	MPa
Material type	-	Elastic-Plastic	-
Failure criterion	Mohr-Coulomb	-	-

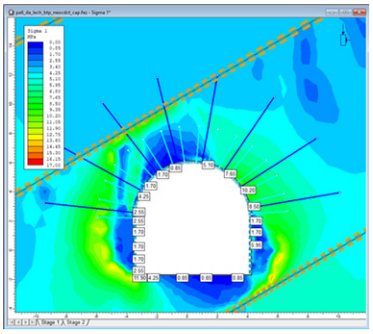

Fig. 10. Damaged zones around the tunnel before post-grounting

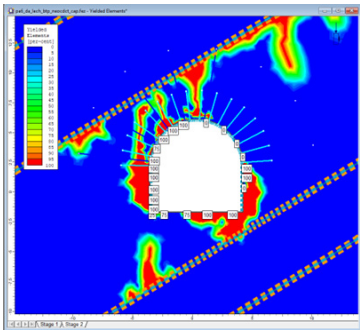

Fig. 11. Stress around the tunnel before post-grounting

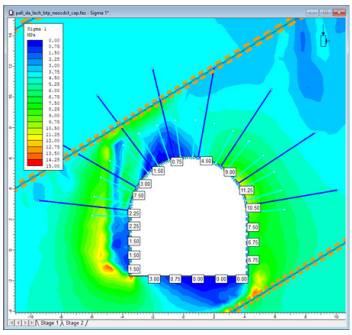

Fig. 12. Stress around the tunnel after post-grounting

The paper also conducts research for a case of tunneling along the seam dug in coal seam 14.5 of Khe Cham III coal mine. The location of the tunnel is located on the slope of the mine waste dump - pressure deflection is a dangerous state with 3 different cases of rock support. The numerical model results show that the rock support case 3 that uses SVP 27 steel frame with distance bettwen each steel frame 0.8 m; rock bolt with length L =2.4 m (axa = 0.8x0.8 m); Cable bolt L = 6 m (axa = 1.6x1.6 m) for the smallest displacement compared to other alternatives. Therefore, the case 3 and the proposed plan is used to prevent the pit lines in the 14.5 reservoir area dug in coal under the Khe Cham III mine surface waste dump area.

5. Conclusions and Proposals

The stability of tunnel under mine waste dump during operation determines the sustainable safety production in underground coal mines. This work was a case study on the stability control of DVTG 14.4-2 tunnel at Khe Cham III coal mine is located near 14.5 seam, Campha, Quang-ninh, VietNam. The results were based on the analysis of long-term engineering practices and numerical model that provide valuable practical guidance for the stability control of deep underground mine tunnel in other coal mines with similar geological conditions, such as the Mao Khe, Nam Mau coal mine. Some conclusions and research prospects are summarized below:

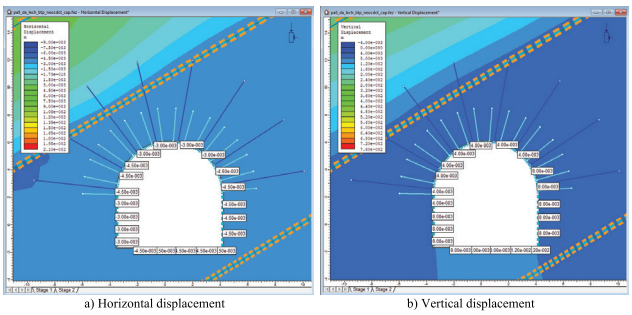

a) Horizontal displacement b) Vertical displacement

Fig. 13. Displacement around the tunnel after post-grouting

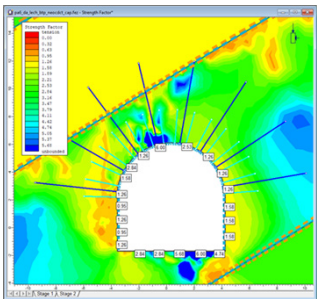

Fig. 14. Strength factor of rock mass

Mine surface waste dumps have a great influence on the mechanical behavior of the tunnels below. Depending on the position of the tunnel relative to the mine surface waste dump site, the pressure acting on the tunnel can be evenly distributed with the tunnel located center area of the mine surface waste dump (I) or skewed with the slope of the mine surface waste dump (zone II), affecting the working of the rock support.

The phenomenon of tunnels being destroyed and distorted, the rock support is quickly destroyed after digging, leading to re-excavate the tunnel many times, affecting transportation the coal, especially for main tunnels. The deformation of the areas around the tunnel appears to be large even though the calculated supporting structures are used, the durability test shows that the traditional calculation hypotheses are no longer correct, these calculation methods have not considered the influence of the mine waste dump as well as the broken loose rock layers in the upper mining strata.

The use of a numerical model built on the Finite Element Method through the Rockscience – RS2-Phase2 software allows effective simulation of pressure, calculation of internal forces and behavior of the rock support, including consideration of the influence of the mine surface landfill, and the stratigraphic characteristics of the research tunnel area.

- Minimum range of pre-grouting and post-grouting reinforcement for deep underground tunnel through complex geology. According to engineering practices and numerical model, the minimum pre-reinforcement range around the proposed deep underground opening through complex rock mass should be 15 m. Moreover, the minimum reinforcement range of deep holes post-grouting should be completed to improve the strength and intactness of the 6-8 m-deep surrounding rock mass.
- Influencing Factors: The main factors influencing safe excavation and the stability of deep underground mine tunnels include high in situ stress, poor mechanical properties and engineering performance of the argillaceous surrounding rock mass, groundwater inrush.
- Pre-Grouting and deep holes post-grouting: The experimental results at DVTG 14.4-2 tunnel at Khe Cham III coal mine shows that the pre-grouting and deep holes post-grouting with superfine cement should be used to block fracture water from seeping, and prevent the deep complex rock mass. Numerical model indicated that deep holes post-grouting with superfine cement were able to improve the intactness of deep rock mass but also improves the bearing load-ability of rock mass.
- Suggestions of coordinated control techniques: According to the deformations and failure characteristics of the surrounding rock, the factors influencing the safe excavation and the stability and geo-hazards encountered, coordinated control techniques, including regional strata reinforcement technique such as Pre-grouting and deep holes post-grouting, primary enhanced control measures of the surrounding rock, floor grouting reinforcement technique with pressurization and progressive depths, and secondary enclosed support are proposed and should be adopted to ensure the tunnel safety and long-term stability of deep underground openings through complex geology.
- The strength factor of rock mass: The criteria to determine whether a tunnel has sufficient capacity to sustain the external load effect is strength factor of rock mass. The result of numerical model show that strength factor of rock mass at roof, shoulder of tunnel in stage 2 in which the grouting work has just been completed is more than 1.0, but the strength factor of rock mass on some points of left floor is less than 1.0. Strength factor of rock mass of stage 3 in which the grouting work has been completed in a time is higher than stage 2. All of them are higher than 1.0. It shows that the capacity to sustain the external load effects of rock mass after grouting is guaranteed.

Literatura – References

1. Institute of Science and Technology- Vinacomin - 2015, Final Report TKV group project "Research, develop standards and inspection procedures for rock support in undergound mining in Quang Ninh area", Hanoi, Vietnam, 2015.
2. Tran Tuan Minh. Research on choosing reasonable and flexible steel-resistant structures for basic stone kilns in thick seams and steep slopes, applied to Uong Bi-Quang Ninh coal area. Ministry of education and tranining level project. B2018.MDA. Hanoi, Vietnam, 2018.
3. Institute of Mining Science and Technology - Vinacomin. The final report on the topic at the level of TKV Group. "Study on stability, selection of parameters, discharge sequence, drainage solutions and protection works suitable to climate change situation at opencast coal mine dumps of TKV". Hanoi, 2016.
4. Pham Minh Duc, Nguyen Van Phuong, Nong Viet Hung, Trinh Dang Hung, Nghiem Xuan La, Ngo Van Dinh et al. Report on the TKV group project "Research and application of technical and technological solutions to prevent coal mines in conditions of high mine pressure in some Quang Ninh underground mines". Institute of Mining Science and Technology. Hanoi- 2005.
5. E. Hoek, P.K. Kaiser, W.F. Bawden, Support of underground excavation in hard rock. Rotterdam, Balkema, 1995.
6. Gale W. J. and Fabianczyk M.W. Design approach to assess coal mine roadway stability and support requirements. Australia 1993.
7. Sicherheit gegen Niederbruch im Untertagebau. Alexander H. Schneider. ETH Zürich, 2002
8. Paul Avinash et al., Design of Support System and Stability Evaluation for Underground Workings of Gare Palma Coal Mine - A Case Study. Modelling, Measurement and Control C. September 2018.
9. Walawska B, Szymanek A, Szymanek P. Impact of decomposition temperature on the surface area of sodium bicarbonate Przemysł Chemiczny 2012, pp.1049-1052

Industrial Symbiosis Applied to Vietnam Coal Mining Industry to Promote the Circular Economic Model towards Sustainable Development Goals

DINH CHIEU Le[1)], NGA Nguyen[1,2)], THI BICH Dong[1)], MINH THONG Le[1)]*

[1)] Hanoi University of Mining and Geology, 18 Vien street, Hanoi, Vietnam
[2)] Innovations for Sustainable and Responsible Mining (ISRM) Research Group, Hanoi University of Mining and Geology, Hanoi, 100000, Vietnam
* Corresponding Author: ledinhchieu@humg.edu.vn

http://doi.org/10.29227/IM-2023-02-12

Submission date: 11-08-2023 | Review date: 15-09-2023

Abstract

Industrial symbiosis associated with the eco-industrial parks is the cooperative activities between businesses to optimize using of inputs and outputs such as raw materials, energy, water, waste materials, etc. in the orperation of businesses. In the industrial symbiosis model, the overall benefits of the symbiosis activities are more than the ones when working individually. Applying the model could help to reduce the demand of raw materials and increase the waste that be treated – an important part of the circular economy model. The coal mining industry includes many different stages from exploration, exploitation, processing, and trading. Each stage could be performed by different businesses which could corporate with each other. Besides the contributions to the socio-economic development, the industry also emits lots of waste into the environment to cause environmental pollution that needs to be treated. The paper summarizes the theoretical basis of the industrial symbiosis, the circular economy and clarifies the relationship between the industrial symbiosis, the circular economy and the sustainable development goals. From analyzing some typical situations of industrial symbiosis activities in Vietnamese coal mining industry; analyzing some characteristics and potential application of industrial symbiosis in the industry, the paper proposes the model of industrial symbiosis for Vietnamese coal mining industry. The paper also proposes some solutions to promote symbiotic activities in the industry.

Keywords: *coal mining industry, industrial symbiosis, circular economy model, sustainable development*

1. Introduction

Industrial symbiosis is the collective approach to competitive advantage in which separate industries create a cooperative network for the exchange of materials, energy, water or by-products (Baldassarre et al., 2019). The keys of industrial symbiosis are the cooperation and synergistic possibilities offered by geographical proximity (Chertow, 2008). Industrial symbiosis associated with the treatment, recycling, reuse of waste and other undesirable outputs that has close relationship with the circular economy to achieve the sustainable development goals. It is the tool to realize the circular economy to achieve the goals.

The traditional mining production is operating in the model: mineral exploration – exploitation – primary product processing – fine product manufacturing – product consumption – waste dumping (Mu QJ, 2003). For each country, especially the developing countries, mineral resources including coal resources plays an important role in providing mineral materials for the need of development of the national economy. It is even more important in the context of resource depletion, environmental pollution and climate change. However, with the traditional approach, we will quickly face to the problem of resource depletion and environmental pollution. In the coal mining industry, the approach would cause increased resource loss, and also increasing of environmental pollution due to deeper and further mining operation. Therefore, it is urgent to promote industrial symbiosis in coal mining industry towards the circular economy and sustainable development goals.

The application of industrial symbiosis in the coal mining industry could not be separated from the formation of the industrial symbiosis model, which were built from synthesizing of the relevant theories and analyzing the characteristics and potentials to apply the model.

2. Theoretical basis

2.1. Industrial symbiosis

"Symbiosis" is a concept that is built on the notion of biological symbiotic relationships in nature, in which at least two unrelated species exchange materials, energy or information in a mutually beneficial manner – the specific type of symbiosis known as mutualism (Miller & Spoolman, 2012). The concept of industrial symbiosis originates from the field of industrial ecology (Chertow, 2008); The underlying concept of industrial symbiosis is the metaphor of an industrial ecosystem that mimics a natural ecosystem (Chertow, 2000). There are different concepts of industrial symbiosis. Industrial symbiosis is defined as a collective approach to achieving competitive advantage in which separate industries exchange raw materials, energy, water and/or by-products that plays an important role in the transition towards sustainable development goals (Chertow, 2000, Chertow, 2008). In Vietnam, the concept of industrial symbiosis is mentioned in some governmental documents. Industrial symbiosis in an industrial park is a cooperative activity between companies in an industrial park or companies in different industrial parks to optimize the use of inputs and outputs such as raw materials, water, energy, waste, scrap, etc. in the operation of the companies. Through the cooperation, companies estab-

Tab. 1. Statistics of large coal mining enterprises in Vietnam

No.	Companies' names	Mining area
I	**VINACOMIN members**	
1	Vinacomin – Mao Khe Coal Company	Dong Trieu - Uong Bi/ Quang Ninh Province
2	Vinacomin – Nam Mau Coal Company	
3	Vinacomin – Uong Bi Coal Company	
4	Vinacomin – Vang Danh Coal Join Stock Company	
5	Vinacomin – Hon Gai Coal Company	Ha Long/ Quang Ninh Province
6	Vinacomin – Nui Beo Coal Join Stock Company	
7	Vinacomin – Ha Tu Coal Join Stock Company	
8	Vinacomin – Ha Lam Coal Join Stock Company	
9	Vinacomin – Quang Hanh Coal Company	Cam Pha/ Quang Ninh Province
10	Vinacomin – Thong Nhat Coal Company	
11	Vinacomin – Khe Cham Coal Company	
12	Vinacomin – Duong Huy Coal Company	
13	Vinacomin – Ha Long Coal Company	
14	Vinacomin – Tay Nam Da Mai Joint Coal Stock Company	
15	Vinacomin – Coc Sau Coal Join Stock Companies	
16	Vinacomin – Deo Nai Coal Join Stock Companies	
17	Vinacomin – Cao Son Coal Join Stock Companies	
18	Vinacomin – Mong Duong Coal Join Stock Company	
19	Vinacomin – Vietbac Mining Industry Holding Corporation	Thai Nguyen Province, Lang Son Province
II	**Non-Vinacomin member**	
20	Dong Bac Corporation	Quang Ninh Province (majority)

Tab. 2. Volume of soil and rock waste of Vinacomin in Quang Ninh area (1000 m3). Source: Thao Vu Manh et al., 2019

No.	Areas	Volume of soil and rock waste by each period		Total
		2018-2020	2021-2030	
1	Uong Bi area	45,306	100,573	145,879
2	Ha Long area	324,956	289,741	614,697
3	Cam Pha area	339,421	928,083	1,267,504
	Total	**709,683**	**1,318,387**	**2,028,080**

Tab. 3. Volume of waste rock of Vinacomin after classification for construction materials (1000 m3). Source: Thao Vu Manh et al., 2019

No.	Areas	The period of 2018 - 2020			The period of 2021 – 2030		
		Crushed sand	Building stone	Total	Crushed sand	Building stone	Total
1	Uong Bi area	4,077	23,106	27,183	9,051	51,292	60,343
2	Ha Long area	29,245	165,728	194,973	26,082	147,762	173,844
3	Cam Pha area	30,547	173,105	203,652	83,527	473,322	556,849
	Total	**63,869**	**361,939**	**425,808**	**118,660**	**672,376**	**791,036**

Tab. 4. Estimated volume of wastewater from coal mining. Source: Vinacomin Industry Investment Consulting JSC, 2018

Norms	Unit	2021÷2025	2026÷2030
Raw coal production	Million tons /year	52.5	57.5
Mine wastewater on average one ton of raw coal	m^3/ton	2	2
Average annual mine wastewater	Million m^3/year	105	115

lish the network to exchange factors (inputs and/or outputs) for production, use the common infrastructure and services for production, improve technological processes and improve production and business efficiency (Vietnam Government, 2018). Industrial symbiosis does not necessarily take place within the boundaries of an industrial park, although the term eco-industrial park is commonly used to describe organizations engaging in exchanges (Chertow, 2000).

Although there are many different concepts, industrial symbiosis has some essential characteristics:

- Industrial symbiosis is the cooperation between businesses in sharing infrastructure and also inputs and outputs (including unwanted outputs);
- The overall benefits of cooperation in industrial symbiosis outweigh the separate benefits of independent businesses;
- Cooperation in industrial symbiosis could take place within an industrial park and also in different industrial zones.

Industrial symbiosis addresses issues related to resource depletion, waste management and pollution by using waste streams to generate value more efficiently across networks of industrial actors (Chertow, 2008). Industrial symbiosis benefits both micro and macro level:

**) Micro level:*

- Creating more opportunities for businesses to take advantage of resources, inputs, outputs, especially waste and other unwanted outputs, thereby increasing revenue and profit for the business;
- Developing business relationships between companies to create more business cooperation opportunities.

**) Macro level*

- Optimizing national resources; creating more values to increase the national GDP;
- Increasing revenues for the state budget from companies that are increasing the operational efficiency in industrial symbiosis.

- Protecting the environment, using resources sparingly by using unwanted outputs. It helps countries responding to the current situation of resource depletion, environmental pollution and climate change.

2.2. The circular economy

The circular economy is a concept that has recently gained traction in policy, business administrators and academia to support the transition from a linear economic model with raw materials on one end and waste at the other, towards a circular economy model, in which waste is a resource that is valued through recycling and reuse (Gregson et al., 2015). There are lots of different definitions of the circular economy. The circular economy describes an industrial economy that be designed to produce no waste or pollution (Littleboy et al., 2016); the circular economy is a new economic model with huge economic potential in zero waste (Ellen-MacArthur-Foundation, 2013); or the circular economy describes an economic system based on business models that replace the concept of "end of life" by reducing, reusing, recycling and recovering materials in manufacturing, distributing and consumming processes at the micro level (products, companies, consumers), intermediate levels (eco-industrial parks) and macro levels (cities, regions, countries and furthermore) with the aim of sustainable development by ensuring environmental quality, economic prosperity and social justice, serving the interests of both present and future generations (Kinnunen, 2019).

Thus, it could be understood that the circular economy is an economy which the undesired outputs (waste) of production processes are fully utilized. These undesired outputs will become inputs of the further production processes. So it could extend the value chain, and also reduce environmental pollution, towards sustainable development goals.

2.3. The relationship between industrial symbiosis, circular economy and sustainable development

a) The relationship between industrial symbiosis and the circular economy

In recent years, industrial symbiosis has become a subfield of a new concept, the circular economy concept (Cecchin et al., 2020). Industrial symbiosis is a business-focused approach to promoting sustainability by recovering waste from one entity for using in another (Chertow, 2000). It is the core content of the circular economy model that focus on recycling the waste of production processes to turn it into a resource for the other processes.

The circular economy is to be implemented at 3 function levels: individual businesses, eco-industrial parks and eco-cities/municipalities (Kalmykova et al., 2018); Research by Z. Yuan et al. has shown that China has implemented the circular economy model at all three levels: (i) the macro level – the large cycle (city, region and province); (ii) the medium level – the medium cycle (symbiotic groups); and (iii) micro level – the small cycle (enterprise level) (Yuan et al., 2008). Thus, the circular economy model is basically divided into three levels: (i) the economy level (or regional level); (ii) industry or interdisciplinary level (symbiotic); and (iii) enterprise level. Industrial symbiosis is the cooperation between many companies in the same industry or in different industries; in the same industrial park or in different industrial zones in sharing infrastructure, inputs, outputs (including unwanted outputs). The same goal of both the industrial symbiosis and the circular economy is saving resources, utilizing wastes of production processes to reduce environmental pollution and create more value for businesses and society. It could be seen that the industrial symbiosis is similar to the circular economy model at the medium level (industry level).

b) The relationship between circular economy and sustainable development goals

The term circular economy has emerged rapidly and notably to become one of the widely studied and applied approaches to achieving sustainable development goals (Korhonen et al., 2018). Sustainable development is the development that meets the needs of the present generations without compromising the satisfaction of those needs of the future generations on the basis of harmonious development of the three extremes: economy, society and environment (WCED, 1987). The resources on the earth are finite (regenerative resources could regenerate but the regeneration rate is also finite), therefore, if resources are not exploited properly, they would quickly be exhausted. Thus, the application of the circular economy model is a practical measure to achieve the sustainable development goals by using resources economically, prolonging the life of products, and using tailings from production processes to minimize wastes into the environment. Following the circular economy model would ensure all three aspects of sustainable development: economic goals (the utilization of resources and wastes, extending the life of machinery and equipment), social goals (creasing more jobs in the areas of recycling, reuse, and waste treatment), and environmental protection goals (reducing wastes). Out of the 169 sustainable development targets outlined by the UNEP, 21 targets could be directly achieved by adopting circular economy, and an additional 28 of them could be indirectly supported by circular economy practices (Lamba et al., 2023).

3. Research methodology

The paper uses the case study method to study some typical situations.

a) Cooperation in exploiting and recovering waste rock for leveling

Currently, the amount of soil and rock that excavated and dumped by Vietnam National Coal and Mineral Industries Holding Corporation Limited (Vinacomin) in Quang Ninh province is over 150 million m3/year. After decades of open-pit mining, the amount of soil and rock in wastedumps in Quang Ninh province has reached over 1 billion m3 (vinacomin.vn, 2022). This amount of waste occupies a large space. It causes serious environmental pollution (dust, water pollution), and also landslides in the rainy season. In recent years, along with the development trend of Quang Ninh province, the demand for leveling materials for traffic and construction projects is huge. Annually, Quang Ninh needs 130 million m^3 of soil and rock for ground leveling material. It is expected that by 2030, the need for leveling materials of projects in the province is about 1 billion m^3 (vinacomin.vn, 2022). Before huge opportunities, Vinacomin has assigned Vinacomin - Quang Ninh Coal Processing Company to realize the project of exploiting and recovering mine soil and rock waste to

serve for leveling of civil and industrial projects. This is the first waste recovery project for ground leveling of Vinacomin that licensed by the Ministry of Natural Resources and Environment. In the short term, it is expected that the soil and rock waste of the project would be provided for some projects in Quang Ninh province such as Cua Luc No3 Bridge, Coal Industry Urban Area and some other projects of Vingroup, etc. (vinacomin.vn, 2022).

In the perspective of industrial symbiosis, it is the cooperation between the parties: Open-pit coal mining companies – Vinacomin Quang Ninh Coal Processing Company – other companies/organizes that are partners of Vinacomin in using soil and rock waste. In the cooperative relationship, as open-pit coal mining companies and Vinacomin – Quang Ninh Coal Processing Company are all subsidiaries of Vinacomin, they are under the general management of Vinacomin. The cooperation benefits all parties. For Vinacomin, the cooperation makes revenue and profit through the selling soil and rock waste as leveling materials; creates more jobs for labours; and also helps reducing pressure about dumping site. For construction or traffic compnanies, etc. (the partners using soil and rock waste of Vinacomin as leveling materials), it provides materials for leveling that could instead for sand. It is so important in the context of sand resources is increasingly depleted; sand mining activity is limited; and the prices tend to increase. It could help the companies to ensure materials for ground leveling and also helps them to save costs to improve business efficiency. In the perspective of macro management, the cooperation helps to reduce waste that pollutes the environment; creates favorable business environment for construction, traffic companies, etc. and also could increase revenue for the province budget and/or state budget. Therefore, the project has been received the great support by Quang Ninh provincial authorities.

However, the cooperation could face big challenges for projects regarding long distance from the mine dumps, as transportation costs could be the barrier for promoting the cooperation.

b) Producing artificial sand of Thien Nam Joint Stock Company

Thien Nam Joint Stock Company is a non-state enterprise that operating in Cam Pha – Quang Ninh. Realizing that the soil and rock waste dumps of the coal industry contain up to 42% of sandstone that could be recycled into construction materials, the company has invested a technological line to produce artificial sand (www.vinacomin.vn, 2017). The company has carried out the project to recover soil and rock waste at Dong Cao Son Dump to produce artificial sand. Artificial sand products of the company have been assessed and certified by Vietnam Institute for Building Materials (Ministry of Construction) to meet the quality standards TCVN 9025-2012. The artificial sand of the company has been evaluated to be more fine and even grain than natural sand. Artificial sand is about 18% cheaper than the natural one, helping to increase the competitiveness (www.scp.gov.vn, 2017).

Similar to the above situation, the cooperation brings benefits to all parts, including coal mining companies, companies that produce artificial sand from soil and rock waste, and the community.

c) Waste treatment activities of Vinacomin Environment Company Limited

In 2009 Vinacomin Environment Company Limited (VEC) was transformed from the Vinacomin Mining Construction Company. VEC operates in several fields, including the treatment of mine wastewater and hazardous industrial wastes, planting and tending forests, etc. In 2021, VEC treated about 140 million m^3 of mine wastewater, collected and treated 3,300 tons of hazardous waste (www.congthuong.vn, 2022).

VEC provides mining wastewater treatment and hazardous industrial waste collection and treatment services to mining companies. The services are also the internal cooperation in Vinacomin to treat waste from mining, processing and trading activities to reduce the waste entering the environment. Treated mine wastewater would be used for daily life (of mine labour), production, road irrigation, etc. Thus, it helps to protect the environmental and also provide more natural resources (water) to serve operation of the companies.

d) Quang Ninh Province aims to convert open pit mines into freshwater reservoirs for mine closure and develop urban areas on mining waste dumps

Nowadays, there are a few surface mines in Cam Pha city of Quang Ninh province, which will be gradually closed in the forthcoming years as planned in the strategy of Vinacomin. Quang Ninh has to face many challenges of managing the open pit ponds thereafter. Consequently, Quang Ninh released a policy to reform these open pits into freshwater reservoirs for local people, and agriculture. Rently, the open-pit pond 917 of Vinacomin – Hon Gai Coal Company has been granted the environmental license by the Ministry of Natural Resources and Environment and would be researched to improve into a freshwater reservoir (www.congthuong.vn, 2023).

Besides, after decades of exploitation, Quang Ninh province also has a lot of waste dumps. Many waste dumps have been planted with trees to restore the environment, becoming suitable for construction of urban areas. In the context that the land storage for urban development in the province is increasingly limited, Quang Ninh Province has a policy of researching and developing sustainable urban areas on stable mine waste dumps (laodong.vn, 2023).

In the short term, the provincial government would lead the implementation of these projects, but after that, the projects must be assigned to companies. Therefore, it would be essentially the cooperation between entrepreneurs. The activity could take advantage of natural resources (reservoirs, urban land), and also reduce the negative impacts of post-mining pits and waste dumps on the environment.

4. Building the industrial symbiosis model that suitable for the Vietnamese coal mining industry

4.1. The possibility of applying industrial symbiosis model

The coal mining in Vietnam are mainly concentrated in Quang Ninh province. Coal mining companies are located in three main areas of Dong Trieu – Uong Bi, Ha Long, and Cam Pha. In each area, there are also other auxiliary companies, such as coal processing and trading companies, repair services, supply materials, etc. Therefore, an (unofficially) industrial park of the coal industry could be formed. As most of these companies

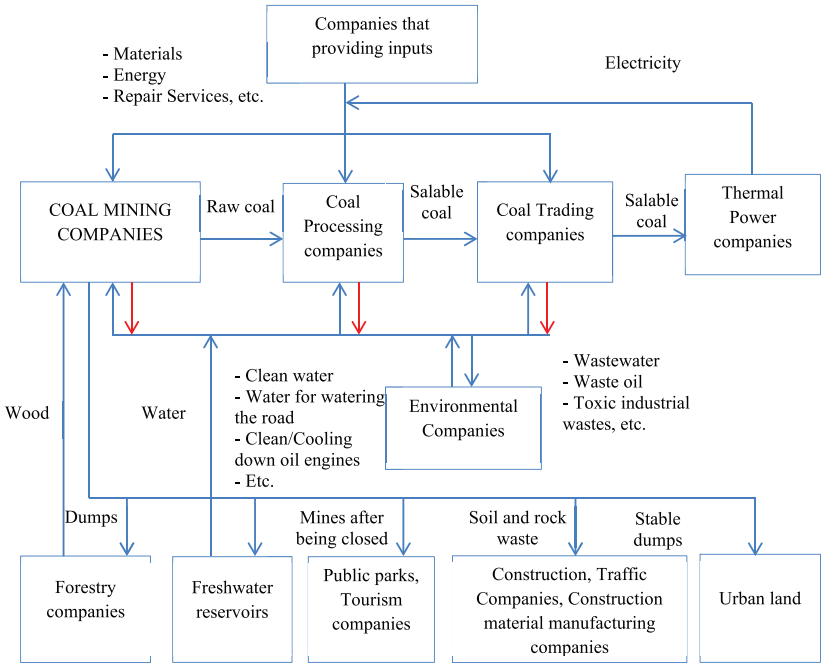

Fig. 1. Industrial symbiosis model for the Vietnamese coal mining industry

are subsidiaries of Vinacomin, their partnership is rather stable and close. It facilitates the development of industrial symbiotic networks. Tab. 1 lists coal mining companies in Vietnam that contribute largely to the national mining industry.

Tab. 2 and 3 show the volume of soil and rock waste, the potential input for materials construction production, and volumne of mine water in the largest coal mining production area in Vietnam.

Moreover, as the government strongly encourages the development of the private sector in resource utilization, environmental protection towards the circular economy, it is very supportive for other companies (neither are members of Vinacomin or Dong Bac Corporation) to establish their mutual cooperation in auxiliary services towards coal mining, processing and trading. In other words, the current conditions for the development of industrial symbiosis in Vietnam coal industry are very supportive.

4.2. The proposed industrial symbiosis model for the Vietnamese coal mining industry

From the abovementioned analysis, the authors propose an industrial symbiosis model into three areas of Dong Trieu – Uong Bi, Ha Long, and Cam Pha in the Quang Ninh coal region of Vietnam. Each area could form an (unofficially) concentrated industrial park, especially in Cam Pha area with many large coal mines.

In each area, the authors propose the industrial symbiosis model as shown in Fig. 1.

In this model, coal mining companies are in the center of the symbiotic network, and industrial symbiosis activities would be developed around these companies. Other companies in the model are partners of coal mining companies. Accordingly, the symbiotic activities would be carried out as follows:

- Input suppliers provide materials, energy, equipment, repair services, etc. to the main stream companies (coal mining companies, coal processing companies, coal trading companies, etc.);
- The main products of the coal industry (salable coal) would be supplied to thermal power companies in the market. Vice versa, coal mining companies would use electricity from power plants;
- Environmental companies provide services to treat wastewater, engine oil waste and other hazardous industrial wastes. Wastewater after being treated could be supplied back to companies for production or road irrigation to reduce dust;
- Waste dumps could provide land for forestry companies to plant forests. On the other way round, the wood from this afforestation could be provided for coal mining companies;
- Open-pit ponds after being closed could be renovated to become freshwater reservoirs; Water from these reservoirs could be supplied to mining companies, industrial zones or residential areas;
- The mines after being closed could be renovated to become public parks or tourist destinations;
- Soil and rock waste is provided to construction and traffic companies as ground leveling materials or construction material manufacturing companies to produce building materials such as artificial sand, etc.
- Stable waste dumps (perennial, reforested, etc.) could be researched and improved to provide the land for urban areas development.

The industrial symbiosis helps sharing local resources to save costs and increasing competitive advantages for businesses. Other advantages are improving the business environment, developing the partnership among companies in one industry and/or in different industries. However, the greater benefit of the collaboration comes from the combination in the recycling, reuse of waste and other unwanted outputs. If companies do it themselves, they could not have sufficient resources, because the resources of companies must be spent on their main operation. The coopera-

tion would mobilize resources from many subjects to help recycling and reusing waste and other unwanted outputs more thoroughly and effectively, and consequently, reducing the amount of waste that pollutes the environment. In other words, implementing industrial symbiosis in the coal mining industry is a step to approach the circular economy towards the goal of sustainable development.

5. Recommendations

Industrial symbiosis could bring overall benefit that be greater than the total benefit of individual firms. However, the economic benefits of symbiotic activities could be the benefits in the long term that could prevent companies from not seeing clearly the benefits of collaboration. Moreover, the social and environmental effectiveness of industrial symbiosis in the coal mining industry are enormous. Therefore, to promote industrial symbiosis in the coal mining industry, the authors propose some recommendations:

a) For the state and local

- The authorities should release encourage policies to motivate and support symbiosis activities between companies, such as tax reductions or subsidies (for symbiotic activities that related to recycling, reuse of waste and unwanted outputs with low economic efficiency), simplifying administrative procedures in projects's approval and licensing that associated with symbiotic activities in the industry;
- It is essential to have the master plan for industry development, in which refers to industrial symbiosis activities. It provides the basis to orientation for companies to establish strategies and plans to deploy industrial symbiosis activities;
- The authorities should promote connection among businesses to generate collaborative activities such as organizing forums, seminars, etc. to create opportunities for meeting and exchanging cooperation; creating a dynamic business environment, promoting innovation activities for businesses.

b) For companies

- It is important for companies to realize the meaning of industrial symbiosis, thereby finding their potential to be able to carry out industrial symbiosis activities;
- Companies need to concern of finding new partners, understand the necessity of sharing resources and mobilizing more resources into industrial symbiosis activities, especially cooperation activities in recycling, reuse of waste and other unwanted outputs;
- Companies must constantly research and learn to innovate or transfer technology on production, waste treatment, recycling and reuse.

6. Conclusions

Industrial symbiosis has great significance at both the macro level (of state management) and the micro level (of companies). Coal mining companies with mining and processing activities are complicated complex, producing large amount of waste to the environment. Thus, the application of the industrial symbiosis model in the industry is absolutely necessary. The paper has systematized the theoretical basis of industrial symbiosis, circular economy and analyzed to show the relationship between industrial symbiosis, circular economy and sustainable development. From some cases in Vietnam recently, and the analysis of the application of the industrial symbiosis model into Vietnam coal mining industry, the paper offers the industrial symbiosis model for Vietnam coal mining industry. This model demonstrates the symbiotic relationship of the coal mining companies with its partners in production and business activities, especially in the treatment, recycling, reuse of waste and other unwanted outputs of the industry.

In the paper, the authors only analyzed the typical situations without making more specific surveys. The above recommendations are for guidance only and need to be researched in details in further work. The author aim to overcome these limitations in upcoming research.

Acknowledgements

This research is funded by Vietnamese Ministry of Education and Training and Hanoi University of Mining and Geology under the grant number of B2023.MDA.09.

Literatura – References

1. Baldassarre, B., Schepers, M., Bocken, N., Cuppen, E., Korevaar, G., & Calabretta, G. (2019). Industrial Symbiosis: Towards a design process for eco-industrial clusters by integrating Circular Economy and Industrial Ecology perspectives. Journal of Cleaner Production, 216, 446–460. https://doi.org/10.1016/j.jclepro.2019.01.091
2. Cecchin, A., Salomone, R., Deutz, P., Raggi, A., & Cutaia, L. (2020). Relating Industrial Symbiosis and Circular Economy to the Sustainable Development Debate. In R. Salomone, A. Cecchin, P. Deutz, A. Raggi, & L. Cutaia (Eds.), Industrial Symbiosis for the Circular Economy (pp. 1–25). Springer International Publishing. https://doi.org/10.1007/978-3-030-36660-5_1
3. Chertow, M. R. (2000). I NDUSTRIAL S YMBIOSIS: Literature and Taxonomy. Annual Review of Energy and the Environment, 25(1), 313–337. https://doi.org/10.1146/annurev.energy.25.1.313
4. Chertow, M. R. (2008). "Uncovering" Industrial Symbiosis. Journal of Industrial Ecology, 11(1), 11–30. https://doi.org/10.1162/jiec.2007.1110
5. Ellen MacArthur Foundation (2013). Towards the Circular Economy. Vol.1
6. Gregson, N., Crang, M., Fuller, S., & Holmes, H. (2015). Interrogating the circular economy: The moral economy of resource recovery in the EU. Economy and Society, 44(2), 218–243. https://doi.org/10.1080/03085147.2015.1013353
7. Kalmykova, Y., Sadagopan, M., & Rosado, L. (2018). Circular economy – From review of theories and practices to development of implementation tools. Resources, Conservation and Recycling, 135, 190–201. https://doi.org/10.1016/j.resconrec.2017.10.034
8. Kinnunen, P. (2019). Towards circular economy in the mining industry
9. Korhonen, J., Nuur, C., Feldmann, A., & Birkie, S. E. (2018). Circular economy as an essentially contested concept. Journal of Cleaner Production, 175, 544–552. https://doi.org/10.1016/j.jclepro.2017.12.111
10. Lamba, H. K., Kumar, N. S., & Dhir, S. (2023). Circular economy and sustainable development: A review and research agenda. International Journal of Productivity and Performance Management. https://doi.org/10.1108/IJPPM-06-2022-0314
11. Littleboy, A., Cooksey, M., & McGregor, K. (2016). Seventh Regional 3R Forum in Asia and the Pacific, November 2-4, 2016, Adelaide, SA, Australia.
12. Miller, G. T., & Spoolman, S. E. (2012). Living in the environment (17. ed., international ed). Brooks/Cole Cengage Learning.
13. Mu QJ. (2003). Recycling economy and sustainable development of China's mining industry.
14. Thao Vu Manh et al. (2019). Research on selection and recycling of quarry waste stone into common building materials. The project of Vinacomin
15. Vietnam Government. (2018). Decree No. 82/2018/ND- CP.
16. Vinacomin Industry Investment Consulting JSC. (2018). Project on developing Vietnamese coal market in association with coal production and business following the market mechanism and ensuring national energy security.
17. World Commission on Environment and Development. (1987). Our Common Future: Report of the World Commission on Environment and Development. Oxford University Press.
18. Website: http://www.congthuong.vn. Vinacomin - Environment Company: Treating nearly 140 million m3 of mine wastewater in 2021. https://congthuong.vn/cong-ty-tnhh-mtv-moi-truong-tkv-xu-ly-gan-140-trieu-m3-nuoc-thai-mo-trong-nam-2021-170829.html
19. Website: http://www.congthuong.vn. Transforming mining pits: Contributing to ensuring water security. https://congthuong.vn/chuyen-doi-cac-moong-khai-thac-khoang-san-gop-phan-dam-bao-an-ninh-nguon-nuoc-tai-quang-ninh-252261.html
20. Website: http://wwww.laodong.vn. Quang Ninh has researched urban development on stable mine waste dumps. https://laodong.vn/quy-hoach/quang-ninh-nghien-cuu-phat-trien-do-thi-tren-cac-bai-thai-mo-da-on-dinh-1198630.ldo
21. Website: http://www.scp.gov.vn. Thien Nam Joint Stock Company: Producing artificial sand from coal slag, waste stone. https://scp.gov.vn/tin-tuc/t1819/cong-ty-cp-thien-nam-san-xuat-cat-nhan-tao-tu-xi-than-da-thai.html
22. Website: http://www.vinacomin.vn. Artificial sand from quarry waste - New, sustainable direction. http://vinacomin.vn/tin-trong-nuoc/cat-nghien-nhan-tao-tu-da-thai-mo-huong-di-moi-ben-vung-20170811631581454.htm
23. Website: http://www.vinacomin.vn. Vinacomin started mining, recovering mine waste soil to serve leveling of civil and industrial works. http://vinacomin.vn/tin-tuc/tkv-khoi-dong-khai-thac-thu-hoi-dat-da-thai-mo-phuc-vu-san-lap-cac-cong-trinh-dan-dung-20221124190941309 8.htm
24. Yuan, Z., Bi, J., & Moriguichi, Y. (2008). The Circular Economy: A New Development Strategy in China. Journal of Industrial Ecology, 10(1–2), 4–8. https://doi.org/10.1162/108819806775545321
25. Szymanek A., de las Obras-Loscertales M., Pajdak A.Effect of sorbent reactivity on flue gas desulphurization in fluidized-bed boilers under air firing mode. The Canadian Journal of Chemical Engineering, Volume 96, April 2018, 895-902

Effect of Power Quality on the Performance of Explosion-Proof Transformers in Mining in Vietnam

DO Nhu Y[1)], NGO Xuan Cuong[2)], NGUYEN Thi Hong[3)*]

[1)] Hanoi University of Mining and Geology, Hanoi, Vietnam.
[2)] School of Engineering and Technology, Hue University, Thua Thien Hue, Vietnam
[3)] Hue Industrial College, Thua Thien Hue, Vietnam
* Corresponding author: nthong@hueic.edu.vn

http://doi.org/10.29227/IM-2023-02-13

Submission date: 21-08-2023 | Review date: 12-09-2023

Abstract

When meeting customer demand, utility companies must consider power quality. Currently, the industrial power network in general and the underground mine power network in particular have long feeder lines, supplying power to many nonlinear loads and power electronic converters, which reduces power quality. Poor power quality can damage sensitive equipment and lead to costly repairs, leading to lost time, data corruption, and lower productivity. In this paper, a fuzzy system is developed to determine the power quality of the power network for different operating conditions and study its influence on the performance of the explosion-proof transformer in the underground mine power network in Vietnam. The simulations and calculations were performed on Matlab-Simulink software for a three-phase, 630-kVA, 6/1.2 kV explosion-proof transformer in power networks with variable power quality. A fuzzy system is developed with four measurable inputs, including frequency deviation, voltage unbalance factor, total harmonic distortion of supply voltage, total harmonic distortion of current, and an output variable, power quality. The simulation results show that the explosion-proof transformer's performance decreases when the power quality degrades, and the proposed fuzzy system can accurately diagnose this.

Keywords: *power quality, performance, explosion-proof transformer, fuzzy system*

1. Introduction

Irrational use of electricity and improper operation of electrical equipment also partly adversely affect the environment and increase global warming [1]. Power quality is a term used to describe efficient electrical energy [2]. This means that if the device is working properly thanks to the power it receives, the power quality is good. Electrical equipment can malfunction, fail prematurely, or shut down suddenly when disturbances occur. Poor power quality leads to losses and increased costs. Outages can be costly, but damaged property can be even more costly, including potential losses due to downtime in the production process. Property damage due to power quality issues that increase heat will almost certainly shorten the life of the equipment. Common power quality problems are divided into: voltage unbalance and harmonic distortion; variable frequency. Each power quality issue will normally be evaluated individually without any focus [3, 4].

Research on power quality in power systems has attracted considerable attention from utility companies, consumers, and researchers alike [5–7]. Many power quality assessments, classifications, and diagnostics of power systems are carried out through the expert system [8], using fuzzy logic and adaptive techniques [9].

The 6kV power grid in open pit mining has typical characteristics: long service life, long feeder lines, use of large capacity equipment, many branches, many power electronics [10]. These problems degrade the overall power quality, leading to increased power loss of electrical equipment. including transformers.

Research on the effect of harmonics on transformer performance in underground mines has shown that the current flowing through the transformer is not sinusoidal, causing overload for the transformer even when operating properly with design specifications [11]. Voltage unbalance causes the peak efficiency working point to shift and transformer efficiency to decrease under all load cases [3]. Experiments show that not only the magnitude of the harmonic content in the supply voltage but also the phase angle has a significant effect on the saturation of the transformer [12]. Experimental results have shown that additional core losses due to non-sinusoidal voltage excitation can increase up to 20.8% [13]. The open circuit test using the sinusoidal source demonstrates that the core loss increases with both frequency and voltage; for frequencies below 1 kHz, the effect of increased voltage was seen to be higher [14].

However, studies of power quality in the underground mine power network currently have few research papers. In addition, evaluating the overall effect of power quality on explosion-proof transformers has not been studied. The explosion-proof transformer is one of the most important electrical components in the underground power distribution network. Proper operation and preventive maintenance of transformers will ensure continuous and reliable power supply to end-user customers without outages or interruptions.

The power quality of Vietnam's distribution power system is regulated in Circular No 39/2015/TT-BCT of the Vietnam Ministry of Industry and Trade [15]. For mine power system, a 6 kV grid, the article uses regulations for medium voltage grids. Table 1 presents the power quality of Vietnam's distribution power system for the medium voltage grid.

The novelty of the paper compared to previous studies is that it focuses on building a fuzzy system for the deter-

Tab. 1. Power quality of Vietnam's distribution power system

Voltage lever	Voltage unbalance	Voltage total harmonic distortion, THDu	Current total harmonic distortion, THDi	Frequency
01 kV to 35 kV	± 05%;	5%	8%	50 Hz ± 0.2 Hz

Tab. 2. Parameters of three-phase explosion-proof transformer

Rated power, kVA	No-load voltage (V)		Rated current, A		Short circuit voltage, $V_{sc\%}$	No-load current, I_{NL}%	Losses, W	
	V_{NL1}	V_{NL2}	I_{1n}	I_{2n}			No-load P_{NL}	Short circuit P_{sc}
630	6000	1200	60.6	304.3	3.5	3	2800	4700

Tab. 3. Simulation parameters of three-phase transformer

Resistance (Ω)		Inductance (L)		Magnetization resistance, R_m (Ω)
R_{HV}	R_{LV}	L_{HV}	L_{LV}	
0.2133	0.0085322	0.0031125	0.0001245	12857

mination of power quality and studying its influence on the performance of the explosion-proof transformer in the underground mine power network in Vietnam. The second part presents the construction of a fuzzy system for the determination of power quality. The third part builds a simulation model for a three-phase explosion-proof transformer. Section 4 is the result of research and discussion. Finally, the conclusion.

2. A fuzzy system for determination of power quality

The article builds fuzzy systems on the MATLAB fuzzy logic toolbox; it includes membership functions and fuzzy rules. Where the membership functions of frequency deviation (b) voltage unbalance, (c) voltage total harmonic distortion (THDu), and (d) current total harmonic distortion (THDi) are determined by 2 states: Low and high, corresponding to the values shown in Table 1, The measurement of the output variable power quality is expressed as membership functions such as very good, good, fair,poor, and very poor. The configuration of membership functions is shown in Figure 1. The power quality detection system in fuzzy logic uses the Mamdani fuzzy system. Fuzzy rules are shown in Figure 2.

In addition, a voltage unbalance factor is defined as the ratio of the negative-sequence voltage component (Vneg) to the positive-sequence voltage component (Vpos). This definition is consistent with IEC standard 61000-4-30 [3]:

$$K_V = \frac{V_{neg}}{V_{pos}}.100 \quad (1)$$

where, Vneg is the negative-sequence voltage component; Vpos is the positive-sequence voltage component; KV is voltage unbalance factor, %.

3. Simulation model for a three-phase explosion-proof transformer

The three-phase explosion-proof transformer with power of 630-kVA and voltage 6/1.2 kV is the type used quite commonly in the underground mine power network. Parameters of it are presented in Table 2 [11]. This is the main research object of the paper.

"Three-Phase Transformer (Two Windings)" model on MATLAB/Simulink software is used as a model of three-phase explosion-proof transformer. From the manufacturer's parameters, the paper builds simulation parameters for three-phase explosion-proof transformer based on linear transformer combined with saturation characteristic. The simulation parameters of single-phase transformer are given in Table 3. Transformers using Y/Y connection use neutral isolated from earth.

The performance of a transformer is calculated as follows:

$$eff = \frac{P_2}{P_2 + P_l + P_{nl}}100 \quad (2)$$

where, P_2 is the 3-phase low-voltage output power of a transformer (W), P_l is the load loss of a transformer (W), P_{nl} is the no-load loss of a transformer (W).

The no-load loss of a transformer is independent of the load and is caused by the induced voltage in the core. In the proposed model no-load loss of a transformer is the iron losses modeled by Magnetization resistance R_m and it is calculated by the following formula:

$$P_{nl} = P_{Fe} = R_m \sum_{i=1}^{3} {I_{i,core}}^2 \quad (3)$$

where R_m is the magnetization resistance, Ω; $I_{i,core}$ is the true RMS value of core loss current of the ith phase of the transformer (A).

The load loss in the proposed model is the copper loss, which is proportional to the square of the true root mean square (RMS) value of the load current and is calculated according to the following formula:

$$P_l = R_{HV}.\sum_{i=1}^{3} {I_{i,HV}}^2 + R_{LV}.\sum_{i=1}^{3} {I_{i,LV}}^2 \quad (4)$$

where RHV is the high voltage phase resistor; R_{LV} is the low voltage phase resistance; $I_{i,HV}$ is the true RMS value of high voltage load current of the ith phase of the transformer; $I_{i,LV}$ is the true RMS value of low voltage load current of the ith phase of the transformer.

The simulation model on Matlab-Simulink is shown in Figure 3. In this part, the source block "Thee Phase Programmable Voltage Source" is used, the forms of power quality change used through this source block include: creating harmonics, creating phase voltage difference or changing the frequency of the power supply. In addition, the power calculation stages are performed according to the formulas present-

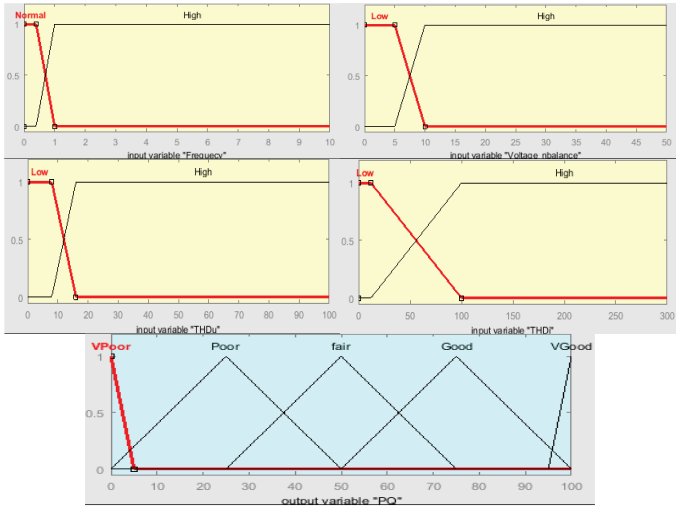

Fig. 1. The fuzzy membership functions used for (a) frequency deviation (b) voltage unbalance, (c) voltage THD, (d) current THD, and (e) power quality

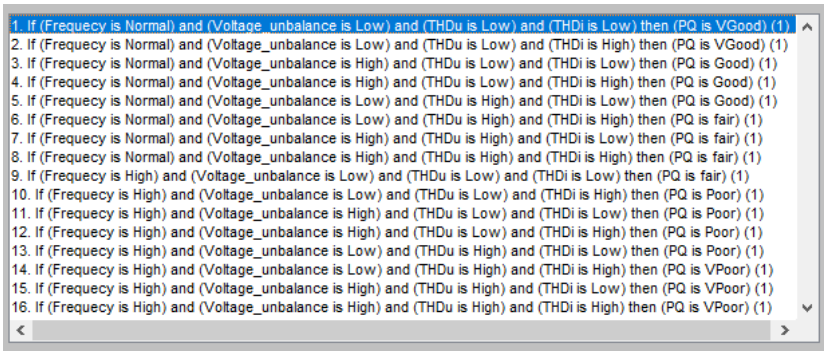

Fig. 2. Fuzzy logic rules for determination of power quality

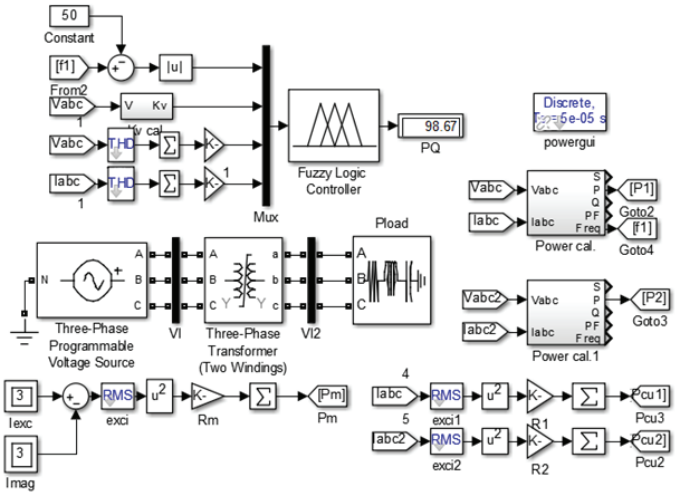

Fig. 3. Simulation model for a three-phase explosion-proof transformer

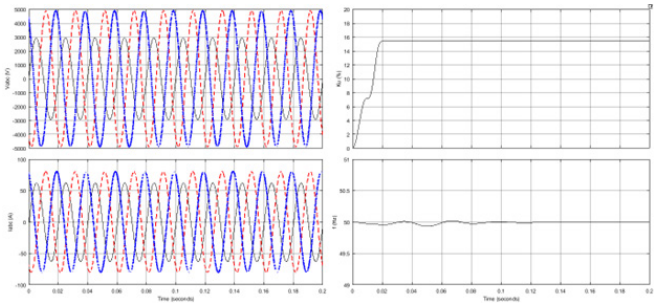

Fig. 4. The case of good power quality

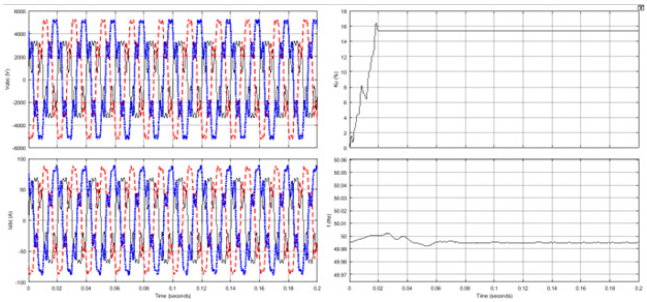

Fig. 5. The case of fair power quality

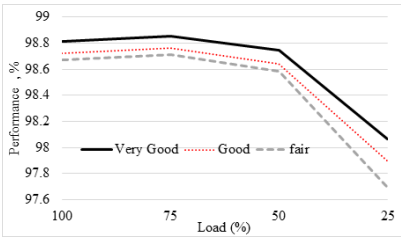

Fig. 6. Dependence of transformer performance on load in case of power quality

ed above. Calculation of voltage and current total harmonic distortion is done through tools available at Matlab-simulik software.

4. Research results and discussion

With the characteristics of the underground mine power grid, the study conducts simulation tests with three typical cases of voltage quality: power quality is very good; power quality is good; and power quality is fair. The case power quality is very good, corresponding to the values within the allowable range in Table 1.

The case of good power quality corresponds to the case of a source with a voltage unbalance factor of 15.38%. Voltage, current, phase difference, and frequency waveforms are shown in Figure 4. Obviously, phase A of the source is given 0.6 times smaller, and the remaining phases are rated.

The case of fair power quality corresponds to voltage unbalance factor of 15.38% and voltage total harmonic distortion THDu of 34.6%, current total harmonic distortion THDi of 31.2%, and constant grid frequency. The voltage, current, phase difference and frequency waveforms are shown in Figure 5.

Figure 6 depicts the dependence of transformer performance on load in case of power quality. Obviously, when the voltage quality is "very good", the performance of the explosion-proof transformer is highest. As power quality deteriorates, the performance of explosion-proof transformer gradually decreases. This result is similar to the results presented experimentally in the study [5]. In any case, transformer performance is maximized with a load of about 75% of the manufactured power, then the performance will decrease as the load decreases. It is also clear from the diagram that when the load is less than 50% of the capacity of the transformer, the bad voltage quality will reduce the performance significantly.

5. Conclusions

This paper focuses on building a method to determine power quality through fuzzy systems and building a model to evaluate the performance of explosion-proof transformers in underground mine power grids in Vietnam under different power quality conditions. The results show that the fuzzy system clearly identifies the power quality parameters with four measurable inputs, including frequency offset, voltage unbalance factor, voltage total harmonic distortion, and current total harmonic distortion. Simulation results show that explosion-proof transformer performance decreases when power quality degrades, and the proposed fuzzy system can accurately diagnose this. When the load is less than 50% of the transformer power, the poor power quality will reduce the performance significantly. The results clarify the importance of power quality to the consuming equipment, thereby requiring solutions to improve the power quality of the power system, especially the underground mine power grid system.

Literatura – References

1. Dincer, I. and M.A. Rosen, (1998). A worldwide perspective on energy, environment and sustainable development. International journal of energy research. 22(15): p. 1305-1321.
2. Sankaran, C., Power quality. 2017: CRC press.
3. Cuong, N.X. and Y. Do Nhu. (2022). Effect of Voltage Unbalances on the Performance of a Three-phase Transformer. in IOP Conference Series: Earth and Environmental Science. IOP Publishing.
4. Dao, T. and B.T. Phung, (2018). Effects of voltage harmonic on losses and temperature rise in distribution transformers. IET Generation, Transmission Distribution. 12(2): p. 347-354.
5. Jaiswal, G.C., et al., (2019). Impact of power quality on the performance of distribution transformers: A fuzzy logic approach to assessing power quality. IEEE Industry Applications Magazine. 25(5): p. 8-17.
6. Brodzicki, M., J. Klucznik, and S. Czapp, (2023). Evaluation of VSC Impact on Power System Using Adequate PQ Capability Curve. Electronics. 12(11): p. 2462.
7. Samanta, I.S., et al., (2023). A Comprehensive Review of Deep-Learning Applications to Power Quality Analysis. Energies. 16(11): p. 4406.
8. Styvaktakis, E., M.H. Bollen, and I.Y. Gu, (2002). Expert system for classification and analysis of power system events. IEEE Transactions on power delivery. 17(2): p. 423-428.
9. Ibrahim, W.R.A. and M.M. Morcos, (2003). A power quality perspective to system operational diagnosis using fuzzy logic and adaptive techniques. IEEE transactions on power delivery. 18(3): p. 903-909.
10. Bun, H.V., (2022). Identifying the factors influencing the voltage quality of 6kV grids when using electric excavators in surface mining. Mining of Mineral Deposits. 16(2).
11. Ngo, X.C. and N.Y. Do, (2021). Influence of Harmonics on the Working Efficiency of a 6/1.2 kV Transformer in a Pit Mine. Inżynieria Mineralna, (2).
12. Dönük, A., (2020). A laboratory application for teaching the effect of harmonics on transformer core saturation. The International Journal of Electrical Engineering Education. 57(3): p. 191-201.
13. Dao, T., et al. (2016). Voltage harmonic effect on losses in distribution transformers. in 2016 International Conference on Smart Green Technology in Electrical and Information Systems (ICSGTEIS). IEEE.
14. Shareghi, M., et al. (2012). Effects of current and voltage harmonics on distribution transformer losses. in 2012 IEEE International Conference on Condition Monitoring and Diagnosis. IEEE.
15. Vietnam ministry of industry and trade, Circular stipulating the electrical distribution system. 2015, Vietnam ministry of industry and trade

Determining the Correction Factors of Overhead-Conductors in 6kV Mining System of QuangNinh, VietNam with the Consideration of Power Harmonic Impact

*GIANG Vu Hoang[2], THANH Le Xuan[1]**

[1] HaNoi University of Mining and Geology, HaNoi, VietNam
[2] Faculty of Electrical Engineering, Electric Power University, HaNoi, VietNam
* Corresponding author email: lexuanthanh@humg.edu.vn

http://doi.org/10.29227/IM-2023-02-14

Submission date: 22-08-2023 | Review date: 16-09-2023

Abstract

Understanding the impact of power harmonic on energy transmission play an important role not only in the operation process but also in the designing procedure of MV grid. In 6kV mining grids of Vietnamese coal mines, because of rapidly utilizing the power electronic machines, the power quality violation occurs very frequently. This lead to many disadvantages such as: the increase of power losses, voltage distortion, over-heating in transformers and conductors. Moreover, the presence of power harmonic bring the bad impact of skin effect and proximity on conductor including overhead-conductors and cables. The actual operation exhibits that the losses of transmission lines are approximately over 50% of total network losses. If there are power quality violation, this amount could be higher. Basing on investigating the fact of power harmonic violations in 6kV grid of both underground and surface mines, the paper will analyze this kind of impact. An algorithm relying on Matlab programming is used to calculate the energy losses. Results are compared with on-site measurement datas and lab-measurement to obtain series of correction factors corresponding to individual line's cross section. The outcomes of research could be applicable for power utilities to have better analysis in the designing stage of mining MV grids.

Keywords: *medium voltage grid, skin effect, correction factor, algorithm*

1. The fact of power harmonic violations and their impact on energy losses

1.1 The fact of power harmonic on 6kV grids of Vietnamese coal mines

Base on reporting figures, from 2018 up to now, there are dozens of powertronic equipment are employed in medium voltage (MV) and low voltage (LV) grids of Vietnamese coal mines. The accounting numbers shown in table 1 [1] show that:

+ Two popular kinds of powertronic devices utilized in MV grids are: inverters and soft-starter;

+ These powertronic devices are mainly equipped for ventilation system, pumping system and conveyor one.

Data in table 1 and Figure 1 exhibit that utilizing powertronic is the trend of modernized mining. These kinds of devices bring many advantages for energy saving, convenient in operation (starting big motors, reducing the voltage sag…) but they also cause unwanted power quality violations in both MV and LV grids. Implementing the site-surveying on those coal mines, some typical data is presented in figure 2, 3, 4 and 5.

The on-site surveying data in typical mines of Vietnam showed that: There are significant power quality violations in MV grids. It expresses in both current and voltage wave forms distortions (Figures 2, 3b and 4a) as well as THD value over the limits (Figure 3a, 4b). The violations exceed greatly over the limits regulated by IEEE [2, 3, 4, 29, 31].

1.2 Impact of power harmonic violations on MV system of Vietnamese coal mines

In Vietnam, because of containing heavy machines in mining procedures which utilizes inverter or AC-DC converters [1, 29, 30], the impact of power harmonics must be seriously consider in both operational of grid and equipment installation. Without this consideration, power harmonics in medium voltage mining grids could be significant and can causes of various operational and equipment problems of issues. The key impacts of bad power harmonic qualities are:

+ Increased Energy Losses and reducing the energy transmission: Power harmonics in medium voltage mining grids are causes energy losses mainly in cables, overhead conductors, transformers, and other apparatus. The increased energy losses result from the additional heating caused by harmonic currents flowing through resistive components of the system [4,5]. Hence, the conductors energy transmission efficiency will be also reduced

+ Reduced Efficiency of motors and system: Harmonics can reduce the overall power system efficiency as well as motors operation, this leads to higher energy consumption and increased operating costs for mining companies.

+ Bad perform of monitoring and measuring system: Non-linear loads injected by inverters and converters draw current in short bursts, causing to voltage waveform distortion [2]. This may influence on performance of sensitive equipment and lead to malfunctions, motors and transformer overheating, or incorrect performing of monitoring, measuring and control systems.

+ Resonance and Overvoltage: Because of having long cable feeders and distributed loads, mining grids are susceptible to resonance conditions where harmonics are significant. Resonance could lead to overvoltage phenomena, which may damage equipment and lead to unexpected downtime.

Tab. 1. Numbers of powertronic devices in typical coal mines of Vietnam

Name of mines	Numbers of powertronic devices		
	2019	2020	2021
DuongHuy	42	52	56
CaoSon	26	42	42
CocSau	34	38	48
QuangHanh	40	39	51
HaLam	63	65	65
NuiBeo	34	67	67

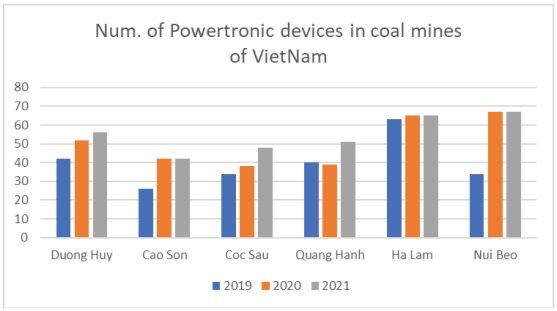

Fig. 1. Trend of utilizing powertronic devices in 3 recent years

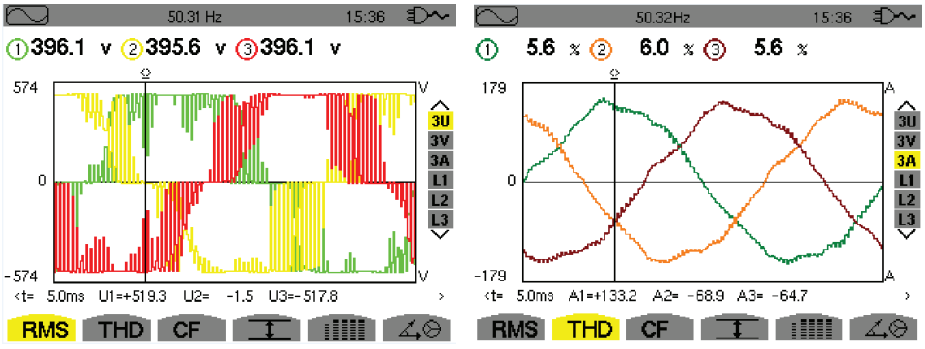

a) b)

Fig. 2. Voltage (a) and current (b) waveforms of 6kV conveyor system of NuiBeo coalmines

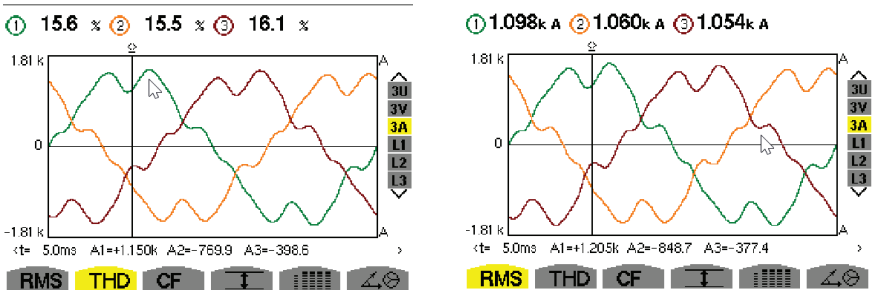

a) b)

Fig. 3. THD of current (a) and RMS current (b) waveforms of 6kV pumping system of QuangHanh coalmines

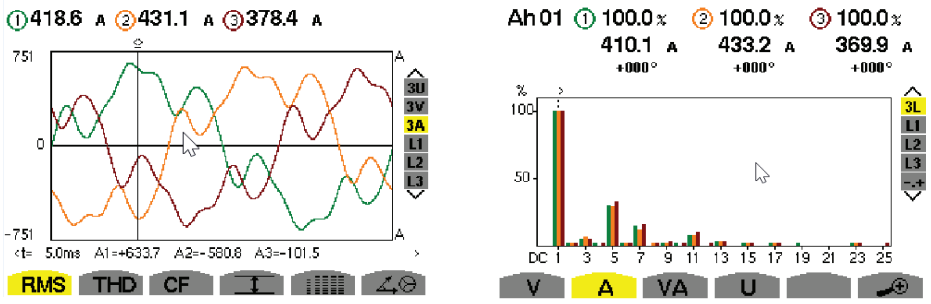

a) b)

Fig. 4. RMS of current (a) and THD current (b) waveforms of 6kV Ventilation system of HaLam coalmines

Tab. 2. Annual cost function of QuangYen MV grid

Type of conductor	Annual optimal cost function Z = f(U^2), (10^6 VND)			
	6kV	10kV	22kV	35kV
AC35	172.552,65	92.443,62	52.462,87	43.562,17
AC50	168.668,84	73.556,47	50.353,93	40.253,63
AC70	147.446,83	65.912,15	49.070,23	39.075,13
AC95	139.741,99	52.190,12	44.464,50	36.213,50
AC120	139.960,928	48.221,648	43.767,75	34.261,35

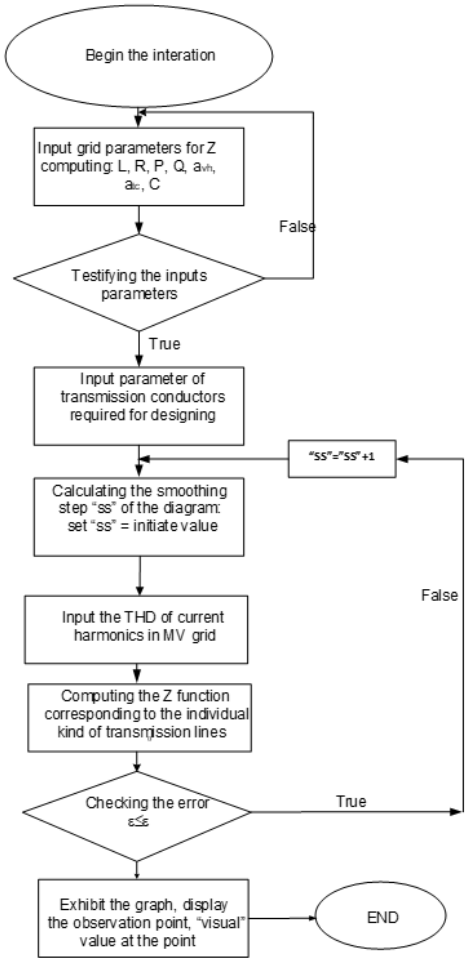

Fig. 5. Mathematic diagram presented the calculation for optimal value of Cost function Z with consideration of current power harmonic impact

+ Transformer Overheating: Most of Vietnamese coal mines contain 35/6kV transformer substation with 2 parallel operational transformers. These ones are exposed to harmonic currents, particularly if their loads are 6kV non-linear ones. "Harmonic currents cause additional eddy current and hysteresis losses in transformer cores" [2], leading to overheating and insulation failure.

Nuisance Tripping: The presence of harmonics can cause discriminative tripping of digital protective devices [29] Wrong tripping of circuit breakers could lead to bad disrupting the mining operations and economical loss because of producing interruption.

As can be seen in above analysis, there are many great impacts of bad power quality on both energy transmission and system operation. Next part of the paper will deeply analyze the influence of current power harmonic on lowering the electrical energy transmission in 6kV conductors of Vietnamese mining grids.

2. Theory basis of power harmonic consideration on designing stage of 6kV mining grid

2.1 Mathematic equations of Zcost function on estimating the economic benefit of mining grids

During power planning or grid designing, various economic indicators might be employed to assess the economic impact through Cost Benefit Analysis (CBA). The primary purposes of CBA are twofold: firstly, to ascertain the viability of an investment or decision by determining if its benefits outweigh the costs and to what extent; secondly, to establish a foundation for comparing projects by evaluating the total expected costs and benefits of each option. In the realm of mining electrical grid construction, some researches in [18, 21, 22, 23, 24] list the following indicators:

+ NPV-Net Present Value (NPV)-the difference between the discounted social benefits and cost;

+ IRR-Economic Internal Rate of Return (IRR)-the sick-out rate that produces a zero value for NPV;

+ B/C ratio-ratio between discount economic benefits and costs;

+ Zcost functions-express the cost containing in operation (a year) of grid including operating cost and maintenance cost.

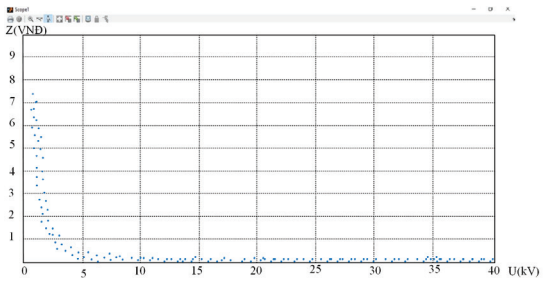

Fig. 6. Results of Zcost corresponding to AC35 conductor

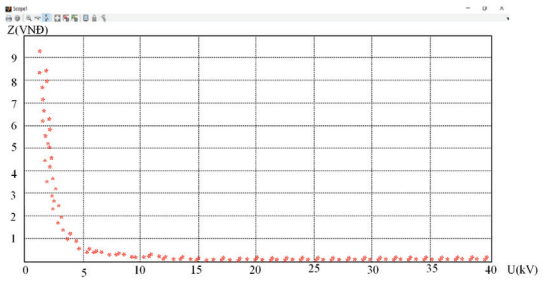

Fig. 7. Results of Zcost corresponding to AC50 conductor

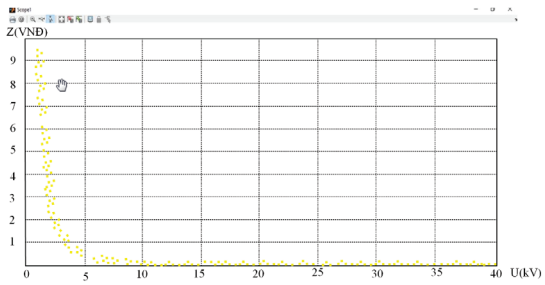

Fig. 8. Results of Zcost corresponding to AC70 conductor

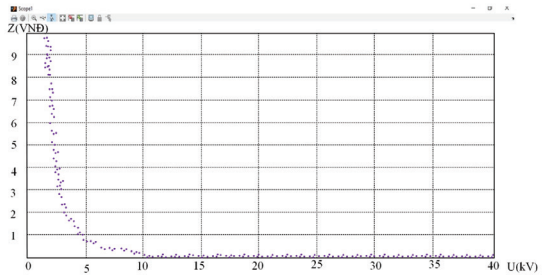

Fig. 9. Results of Zcost corresponding to AC95 conductor

During the designing stage of MV grids, three prior indicators (NPV, IRR and B/C) are not utilized. Instead, the Zcost function is employed, as it takes into account not only the initial construction investment but also the ongoing operational costs borne by operators and users. The Zcost function is typically represented by equation (1) [18, 22]:

$$Z = (a_{vh} + a_{tc})K + Y_{\Delta A} \quad (1)$$

Whereas: a_{vh} – the operation factor
a_{tc} – standard recovery factor
K – annual cost
ΔA – power losses when power is transmitted for long distance.

Detaily, Z can also be expressed by equation (2):

$$Z = (a_{vh} + a_{tc})C_{đd}m_0\ell + C\frac{(P^2+Q^2)}{U^2}\tau\frac{\delta}{s}\ell \quad (2)$$

However, as mentioned before, to get the impact of

$$Z = (a_{vh} + a_{tc})K + Y_{\Delta A}\cdot H \quad (3)$$

In equation (3) H-is indicator reflect the impact of current power harmonic (Harmonic impact indicator). This indicator will raise the value of Z because the power losses is increased. The problem is how to identify this indicator corresponding to different cross sections of conductors as well as various value of THD.

2.2 Propose Algorithm and Matlab application to find optimal value of Zcost function corresponding to conductor's cross sections

As mentioned in many previous research, there are series of method to optimize the power flow with consideration of

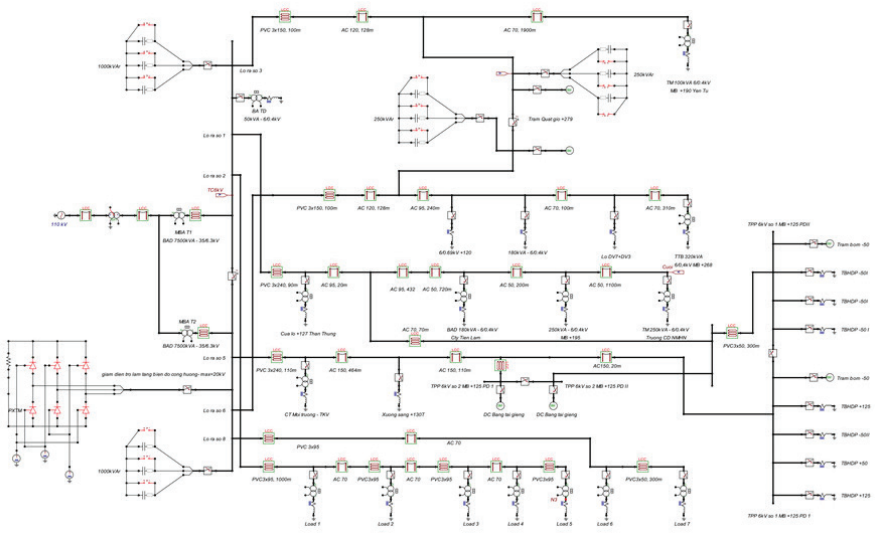

Fig. 10. Simulation in ATP with 7 harmonic sources (in red circles)

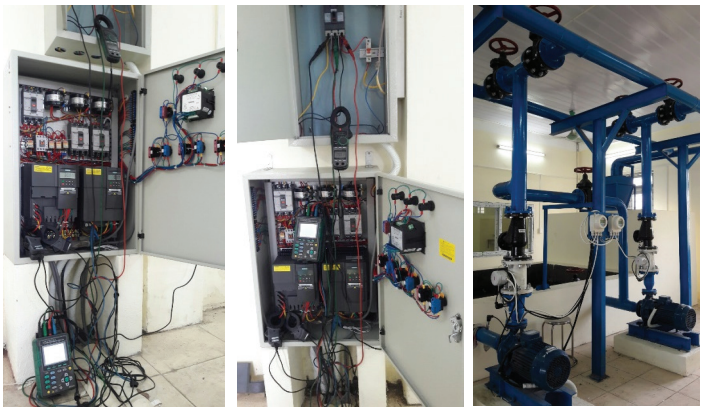

Fig. 11a. Lab-test setup for power losses measurement with pumping system

parameters affecting to energy transmission [6-10]. All of these researches rely on computer-aid program. In this section, the paper will propose an Algorithm which is the basis of computing optimal value of Z-cost function in which all impact of skin effect and current harmonic are taken into account.

In MV energy transmission, when currents flow through one or more nearby conductors, the distribution within the first conductor becomes constrained to smaller regions. This phenomenon, known as the proximity effect, can lead to current crowding, which in turn significantly increases the AC resistance of adjacent conductors. Because of the consideration to this effect, the total losses in a conductor will be result of two kinds of effects: skin and proximity [11-17] one which is expressed as equation (3) [20]:

$$P_{total} = P_{skin} + P_{Prox} \quad (4)$$

Where

$$P_{skin} = I^2_{rms} \times R_{AC} \times \mathbf{H}$$

$$P_{prox} = (cR + d)\left(\frac{\mu_0 \mu_r I}{2\pi r}\right)^2 (if R \geq \delta)$$

$$P_{prox} = aR^b \left(\frac{\mu_0 \mu_r I}{2\pi r}\right)^2 (if R < \delta)$$

a, b, c, d are constants in accordance with kinds of materials (copper and aluminum)

R – conductor radius;

δ – the skin depth: $\delta = \sqrt{\frac{2}{\sigma \omega \mu_0 \mu_r}}$

H – harmonic impact indicator

To determine H indicator, two quantities must be identified: The value of Zcost and power losses. For building the relation of Z-cost function and its depend variable, an algorithm is proposed and shown in figure 5. It is very easy to be seen that, in equation (3) Z is a function of many variants including rated voltage (U), conductor cross-section (S)… In designing process of an MV grid, it should be economically optimal if S is selected correspondingly to U [20, 21]. Utilizing the mathematic diagram in figure 5, programming in Matlab, results (figure 6 to 9) showing theoretical computing of Z is expressed for finding the optimal values of Z-cost. Some of typical outcomes applied for QuangYen MV grids [19, 22] are presented in table 2.

3. Calculating the H indicator and its impact on Z-cost computing

To identify H indicator, a simulation will be implemented in ATP (figure 10) with various power harmonic source (in red circles). By "switching in" or "switching out" the circuit breakers in skeleton networks, the impact harmonic current will be isolated. The simulation results are compared and verified with lab measurement performed in figure 11a, and 11b.

Ngày	Thời gian	V1 THD	V2 THD	V3 THD	V1 CF	V2 CF	V3 CF	Pst1	Pst2	Pst3	A1 THD	A2 THD	A3 THD
		%	%	%							%	%	%
07/08/2021	8:04:35 AM	2.4	2.3	2.7	1.49	1.49	1.49	0	0	0	43.2	43.6	31.3
07/08/2021	8:04:51 AM	2.5	2.3	2.8	1.49	1.49	1.49	0	0	0	43.4	44.3	32.7
07/08/2021	8:05:07 AM	2.3	2.1	2.8	1.48	1.49	1.49	0	0	0	37.7	39	31.1
07/08/2021	8:05:23 AM	2.3	2.2	2.7	1.48	1.49	1.49	0	0	0	34.6	35.5	28.5
07/08/2021	8:05:39 AM	2.2	2	2.6	1.49	1.49	1.49	0.3	0.4	0.3	34.9	35.6	26.4
07/08/2021	8:05:55 AM	2.2	1.9	2.5	1.49	1.49	1.49	0.3	0.4	0.3	35.3	35.1	27.1
07/08/2021	8:06:11 AM	2.5	2.1	2.3	1.49	1.49	1.49	0.3	0.4	0.3	37.6	36.7	27
07/08/2021	8:06:27 AM	2.4	2.3	2.5	1.49	1.49	1.49	0.3	0.4	0.3	39.4	38.4	27.9
07/08/2021	8:06:43 AM	2.4	2.1	2.6	1.49	1.49	1.49	0.3	0.3	0.3	33.9	33.8	26.8
07/08/2021	8:06:59 AM	2.3	2.1	2.5	1.49	1.49	1.49	0.3	0.3	0.3	34.8	34.7	27.9
07/08/2021	8:07:15 AM	2.4	2	2.5	1.49	1.49	1.49	0.3	0.3	0.3	39.3	39.1	29.1
07/08/2021	8:07:31 AM	2.3	2.3	2.5	1.49	1.49	1.49	0.3	0.3	0.3	38.2	41.9	29.4
07/08/2021	8:07:47 AM	2.4	2.4	2.6	1.49	1.49	1.49	0.3	0.3	0.3	33.6	35.3	27.1
07/08/2021	8:08:03 AM	2.3	2.3	2.6	1.49	1.49	1.49	0.3	0.3	0.3	40.2	42	31
07/08/2021	8:08:19 AM	2.2	2.1	2.4	1.49	1.49	1.49	0.3	0.3	0.3	40.4	41	31.1
07/08/2021	8:08:35 AM	2.3	2	2.2	1.49	1.49	1.49	0.5	0.6	0.5	32.8	32.9	24.1
07/08/2021	8:08:51 AM	2.2	2	2.3	1.48	1.49	1.49	0.5	0.6	0.5	40.6	40.3	29
07/08/2021	8:09:07 AM	2.4	2.4	2.4	1.49	1.49	1.49	0.5	0.6	0.5	35.8	35.4	25.8
07/08/2021	8:09:23 AM	2.3	2.4	2.6	1.49	1.49	1.49	0.5	0.6	0.5	33.3	34.9	27.4
07/08/2021	8:09:39 AM	2.6	2.5	2.6	1.49	1.48	1.49	0.4	0.4	0.4	40	40.5	29.3
07/08/2021	8:09:55 AM	2.7	3	2.8	1.5	1.49	1.49	0.4	0.4	0.4	39.8	37.9	30.1

Fig. 11b. Lab-test results extract from KEW meter

Tab. 3. Results of power losses bias (kWh) which influence Zcost function between theoretical calculation (by ATP simulation) and lab-measurement

Feeder No	S (mm²)	ATP calculation without harmonic impact	ATP calculation with harmonic impact	On-site measurement	H indicator	THD (%)
No1	AC95	3761	5288	5336	1.418	7
No2	AC70	1744,2	2687,7	2793,8	1,602	11
No3	AC120	2720,3	4089,65	4123,5	1.416	8
No5	AC150	2822,6	3994,67	4069,2	1.341	6
No6	AC120	1422,6	1934,67	1953,23	1.373	7
No8	AC70	622,6	812,6	823,7	1.433	5

Tab. 4. Series of H indicators corresponding to alternative values of THD and conductor's cross section (utilized in 6kV mining grid of VietNam)

THD (%) \ S (mm2)	AC35	AC50	AC70	AC95	AC120
3	1,342	1,296	1,273	1,266	1,22
4	1,513	1,439	1,406	1,341	1,297
5	1,548	1,476	**1,433**	1,358	1,313
6	1,576	1,492	1,460	1,402	1,346
7	1,612	1,523	1,489	**1,418**	**1,373**
8	1,638	1,562	1,526	1,456	**1,416**
9	1,66	1,583	1,545	1,481	1,426
10	1,701	1,611	1,577	1,515	1,458
11	1,715	1,629	**1,620**	1,538	1,497

Corresponding to 6 feeders of 6kV mining grids, the difference between power losses outcomes with and without harmonic impact are presented in table 3.

Figures in table 3 shows that:

+ With current harmonic consideration, the power losses in feeders must multiple with H indicators which are normally 30% greater than 1.

+ Simulations results and on-site measurements/lab tests are mostly the same for determining H indicators, Therefore, for multiple H indicators determination, simulation in ATP is suitable and does not diminish the accuracy of the computing procedure.

Implementing hundred simulations, series of H indicator corresponding to various AC cross-sections and THD are summarized in table 4

In the table, results shown in "bold" are deducted from table 3, others are computed from simulation in ATP corresponding to 6kV rated voltage.

4. Conclusion

Base on the lab test and ATP simulation, utilizing the proposed algorithm a series of H indicators are determined. Through values in table 4, the impact of current harmonic violations is strongly impressed. Depending on the THD, the power losses could be expanded from over 22% to nearly 75%. Though over the procedure some following conclusions are pointed out:

+ The proposed method with algorithm presented in figure 5 are suitable for estimating the Z-cost values of any kinds of conductors;

+ Corresponding to altenative cross-section of steel-cored aluminum conductors, the correction (H) factors vary from 1.22 to 1.71. It means that if the skin effect with harmonic consideration is much greater than other studies [25-28]. Particularly, if the THD is violate the limit required by IEEE (5%), over 50% power losses must be taken into account of power losses computing. Hence, all of grid designing stages must modified correspondingly.

+ In the initiative designing stage of MV mining grids, using the optimal Zcost function with above recommendation H factors is a good point that allow project manager having a better technical and economical parameter.

Literatura – References

1. VINAMCOMIN Technical reporting of Mechanization and Modernization in Vietnamese coal company, VINACOMIN, 2020
2. A. Nayak, et al. "Impact of Harmonics on Power Losses in Overhead Conductors and Transformers." Proceedings of the 2014 IEEE Power and Energy Society General Meeting, 2014.
3. R. K. Gupta, et al. "Impact of Power Harmonics on Power Losses in Overhead Conductors." International Journal of Scientific and Research Publications, Vol. 5, Issue 3, March 2015.
4. A. H. Nayfeh, et al. "Impact of Harmonics on Power Losses in Overhead Conductors and Cables." Proceedings of the 2008 IEEE Power and Energy Society General Meeting, 2008.
5. Sarmah, D., and Talukdar, P. "Impact of Harmonics on Power Losses in Overhead Conductors Considering the Load Characteristics." International Journal of Engineering Research & Technology, Vol. 2, Issue 12, December 2013
6. Amiri, M., & Keyhani, A. (2016). Optimal energy transmission distance and efficiency for renewable energy microgrids. Renewable Energy, 85, 78-86. URL: https://doi.org/10.1016/j.renene.2015.06.005
7. Zeng, H., Hu, W., & Xia, Q. (2018). Optimal power flow considering distance-dependent line transmission loss for smart grid. International Journal of Electrical Power & Energy Systems, 98, 432-439. URL: https://doi.org/10.1016/j.ijepes.2018.01.012
8. He, J., Liu, M., & Wang, C. (2019). An optimal transmission power allocation method considering transmission loss and environmental impact for multi-node power systems. IEEE Transactions on Power Systems, 34(4), 2754-2765. URL: https://doi.org/10.1109/TPWRS.2019.2891102
9. Chen, J., Yang, J., Wang, J., & Wu, J. (2020). Research on energy-efficient power transmission distance optimization for offshore wind power. International Journal of Electrical Power & Energy Systems, 118, 105850. URL: https://doi.org/10.1016/j.ijepes.2020.105850
10. Hinz, S., Siefert, M., & Skritek, P. (2019). Optimal power transmission distance for direct current connected offshore wind farms based on economic and technical factors. Energies, 12(18), 3436. URL: https://doi.org/10.3390/en12183436
11. Georgilakis, P. S. (2013). High Voltage and Electrical Insulation Engineering. CRC Press.Luo, F., & Kang, K. (2017). Skin Effect and Power Loss Analysis for High-Frequency Induction Heating. IEEE Transactions on Power Electronics, 32(8), 6287-6296
12. Liu, Y., & Cheng, M. (2018). Research on the Influence of Skin Effect on Overhead Power Line Parameters. In 2018 International Conference on Smart Grid and Electrical Automation (ICSGEA) (pp. 155-158). IEEE.
13. Marotta, A., & Leccese, F. (2019). Influence of Skin Effect on the Efficiency of Electric Vehicle Inductive Charging Systems. Energies, 12(21), 4069
14. Cheng, M., & Liu, Y. (2020). Influence of skin effect on transmission line in high-frequency band. IOP Conference Series: Earth and Environmental Science, 483(4), 042003
15. Díaz, F., Espejo, M., & Rull-Duran, J. (2020). Skin and Proximity Effects on Power Losses of HV Overhead Lines. Energies, 13(22), 5998
16. Jin, T., Niu, C., & Lu, J. (2021). Analysis of the Influence of Skin Effect on DC Bias Characteristics of a High-Voltage Generator. IEEE Transactions on Plasma Science, 49(6), 2950-2957
17. Li, L., & Zhang, X. (2021). Research on the Influence of Skin Effect on AC Resistance of High-Voltage Cables for HVDC. In 2021 5th International Conference on High Voltage Engineering and Power Systems (ICHVEPS) (pp. 1-5). IEEE
18. Khoa, D.Q. (2010). Research to plan the MV grid of Quang Ninh Province suited to the development of economic and social characteristics to the year 2020 (Unpublished doctoral dissertation, University of Mining and Geology, Hanoi, Vietnam).
19. Khue, N.M. (2018). Research and suggest solutions to reduce the power losses of MV grid in Quang Yen town, Quang Ninh district (Unpublished master's thesis, University of Mining and Geology, Hanoi, Vietnam).
20. Lobao, J.A., Devezas, T. & Catalao, J.P.S. (2013). Influence of cable losses on economic analysis of efficient and sustainable electrical equipment.
21. Retrieved from http://citeseerx.ist.psu.edu/viewdoc/download?doi=10.1.1.723.312&rep=rep1&type=pdf
22. Neusel-Lange, N., Christian Oerter, Markus Zdrallek, Peter Birkner, Martin Stiegler, Roman Uhlig. (2014). Economic evaluation of distribution grid automation systems – Case study in a rural German LV-grid. International Conference on Electricity Distribution, CIRED 2014, Rome.
23. Thanh, L.X. (2018). Determining the elastic factor for ecotechnic assessment of Medium Voltage (MV) transmission lines with a consideration of the conductor's skin effect. Proceeding of Science and Mathematics International conference, Jakarta Indonesia (SMIC 2018).

24. Ulbig, A., Koch, S. & Antonakopoulos, C. (2017). Towards more cost-effective PV connection request assessments via time series-based grid simulation and analysis. In Proceedings of International Conference on Electricity Distribution, CIRED 2017, Glasgow. Retrieved from http://cired.net/publications/cired2017/pdfs/CIRED2017_1367_final.pdf

25. Vitiello, S., Flego, G., Setti, A. & Fulli, G. (2015). Costs and benefits of smart grid pilot installations and scalability options, JRC science, and policy report study in rural Germany grid.

26. Online at: https://www.google.com/url?sa=t&rct=j&q=&esrc=s&source=web&cd=1&ved=2ahUKEwiH_oK4orHhAhWKMN4KHSQGDREQFjAAegQIARAC&url=https%3A%2F%2Fwww.smartgrid.gov%2Ffiles%2FEstimating_Costs_Benefits_Smart_Grid_Preliminary_Estimate_In_201103.pdf&usg=AOvVaw2fw5qrs3fETRGNLonfWptQ

27. Kupke, S. Pilot project—High temperature low sag conductors. In Proceedings of the CIGRE WG B2.42, Stockholm, Sweden, 21 May 2010

28. A Method of Stress-Strain Testing of Aluminum Conductor and a Test for Determining the Long Time Tensile Creep of Aluminum Conductors in Overhead Lines; Electrical Technical Committee of the Aluminum Association: Arlington, TX, USA, 1999

29. IEC 62420: Concentric Lay Stranded Overhead Electrical Conductors Containing One or More Gap(s); IEC: Geneva, Switzerland, 2008

30. Jarkko Tolvanen, Mikko Nelo, Heidi Alasmaki, Tuomo Siponkoski, Piia Makela, Timo Vahera, Jari Hannu, Jari Juuti, Heli Jantunen, Unltraelastic and High-conductivity multiphase conductor with universally autonomous self healing, Advanced Science, Vol 9 Issue 36

31. https://doi.org/10.1002/advs.202205485

32. Bun. HV, Thanh. LX Impact of power harmonics on precise and discriminative tripping of the relays system for earthing protection in underground 6kV grids of QuangNinh underground mines, Proceeding of Science and Mathematics International conference, Jakarta Indonesia (SMIC 2018)

33. Thanh, L.X., & Bun, H.V. (2022). Identifying the factors influencing the voltage quality of 6kV grids when using electric excavators in surface mining. Mining of Mineral Deposits, 16(2), 73-80. https://doi.org/10.33271/mining16.02.073

34. Ramakrishna, C., and Chidambaram, S. "Impact of Harmonics on Power Losses in Overhead Conductors." Proceedings of the 2016 IEEE Region 10 Conference (TENCON), 2016

Machine Learning Algorithms for Data Enrichment: A Promising Solution for Enhancing Accuracy in Predicting Blast-Induced Ground Vibration in Open-Pit Mines

Hoang NGUYEN[1, 2)], Xuan-Nam BUI[1, 2)], Carsten DREBENSTEDT[3)]*

[1)] Surface Mining Department, Mining Faculty, Hanoi University of Mining and Geology, Hanoi 100000, Vietnam
[2)] Innovations for Sustainable and Responsible Mining (ISRM) Research Group, Hanoi University of Mining and Geology, Hanoi 100000, Vietnam
[3)] TU Bergakademie Freiberg, 09596 Freiberg, Sachen, Germany
* Corresponding author: nguyenhoang@humg.edu.vn (H. N.)

http://doi.org/10.29227/IM-2023-02-15

Submission date: 16-08-2023 | Review date: 22-09-2023

Abstract

The issue of blast-induced ground vibration poses a significant environmental challenge in open-pit mines, necessitating precise prediction and control measures. While artificial intelligence and machine learning models hold promise in addressing this concern, their accuracy remains a notable issue due to constrained input variables, dataset size, and potential environmental impact. To mitigate these challenges, data enrichment emerges as a potential solution to enhance the efficacy of machine learning models, not only in blast-induced ground vibration prediction but also across various domains within the mining industry. This study explores the viability of utilizing machine learning for data enrichment, with the objective of generating an augmented dataset that offers enhanced insights based on existing data points for the prediction of blast-induced ground vibration. Leveraging the support vector machine (SVM), we uncover intrinsic relationships among input variables and subsequently integrate them as supplementary inputs. The enriched dataset is then harnessed to construct multiple machine learning models, including k-nearest neighbors (KNN), classification and regression trees (CART), and random forest (RF), all designed to predict blast-induced ground vibration. Comparative analysis between the enriched models and their original counterparts, established on the initial dataset, provides a foundation for extracting insights into optimizing the performance of machine learning models not only in the context of predicting blast-induced ground vibration but also in addressing broader challenges within the mining industry.

Keywords: *blast-induced ground vibration, data enrichment, sustainable and responsible mining, machine learning, open-pit mining, performance improvement*

1. Introduction

Surface mining stands as one of the prevailing techniques for the exploitation of minerals, fossil fuels, and metals, characterized by its high degree of mechanization and productivity. Among the array of rock fragmentation methods employed in open-pit mining operations, drilling and blasting emerge as the most prevalent approach for fracturing rocks prior to subsequent unit operations like loading and hauling. The advantages of blasting are well-documented and undeniable; however, its detrimental repercussions, including blast-induced ground vibration (measured by peak particle velicity – PPV), flyrock, airblast, and air pollution [1-4], cannot be disregarded. Among these consequences, PPV is a particularly perilous phenomenon that exerts a profound impact on adjacent areas, notably open-pit mines situated in proximity to residential zones. Although efforts have been invested in assessing such hazards and proposing probabilistic risk-based models to manage these challenges, ensuring the safety of blasting operations [5], the complexity of blasting remains evident, encompassing a spectrum of potential accident risk scenarios [6]. Indeed, numerous structures have borne the brunt of PPV-induced cracks, and several slopes and benches have experienced subsidence or instability owing to the elevated magnitude of PPV within open-pit mines [7, 8]. Consequently, the accurate prediction of PPV intensity becomes a critical imperative, serving not only the preservation of neighboring structures but also the operational efficiency of open-pit mining ventures.

To achieve this goal, numerous researchers have put forth diverse predictive models aimed at estimating PPV. These models can be categorized into two primary groups: empirical models [8-11] and artificial intelligence (AI)-based models [12-19]. While empirical models have been endorsed despite their inherent accuracy limitations, AI-based models have garnered recognition for their exceptional performance. Presently, an increasing number of novel AI-based models have emerged, offering promising outcomes for PPV prediction, as well as other challenges not only within the realm of blasting but also across the broader mining industry [7, 20-34].

However, the majority of existing research has predominantly concentrated on enhancing predictive models using various techniques applied to raw datasets, or employing basic data analysis methods such as feature selection and outlier removal. In contrast, datasets containing more comprehensive and detailed information possess the potential to offer invaluable insights to predictive models. Such datasets can significantly aid predictive models in elucidating the intricate relationships between dependent and independent variables. Strikingly, these approaches appear to have been underexplored in the context of predicting the adverse effects of blast-

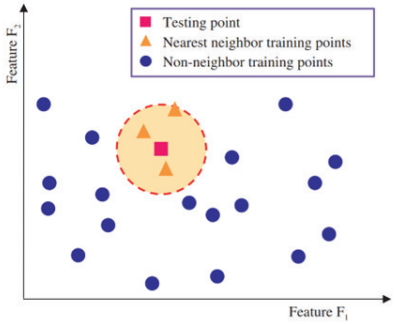

Fig. 1. Illustration of KNN algorithm for two-dimensional feature space [44]

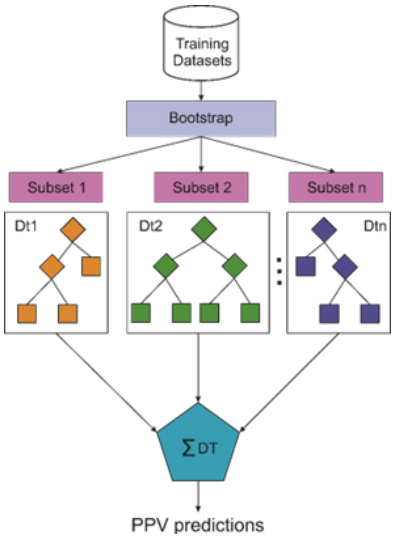

Fig. 2. Workflow of RF in predicting blast-induced PPV [52]

Fig. 3. Location and a view of the Coc Sau open-pit coal mine

ing in open-pit mines, including the prediction of PPV.

Hence, within the scope of this investigation, we introduce a novel approach focused on enhancing the PPV dataset as a precursor to the development of predictive models utilizing machine learning algorithms. Specifically, the support vector machine (SVM) algorithm was harnessed to discern the intricate relationships within the original PPV dataset's input variables. The resultant findings were then amalgamated with the initial dataset, culminating in the creation of an augmented dataset—referred to as the enriched dataset—containing a more expansive set of input variables. Subsequently, we crafted three distinct machine learning models: classification and regression trees (CART), k-nearest neighbors (KNN), and random forest (RF). These models were constructed employing both the original dataset and the enriched dataset, facilitating a comprehensive comparative analysis for PPV prediction within open-pit mining contexts. It is noteworthy that the enrichment technique proposed in this study is distinct from ensemble modeling approaches such as bagging, boosting, or stacking techniques [35-37].

2. Methodology

2.1. Data enrichment

Data enrichment refers to the process of enhancing or expanding the existing information or data sets by adding additional relevant details or attributes. It involves augmenting raw data with various types of supplemental information to make it more valuable and useful for analysis, soft computing models, decision-making, and other business purposes. The objective of data enrichment is to provide a more comprehensive and accurate understanding of the data by filling in missing gaps, correcting errors, or adding context. By enhancing the quality and depth of data, organizations can gain deeper insights, improve customer understanding, and make more informed decisions.

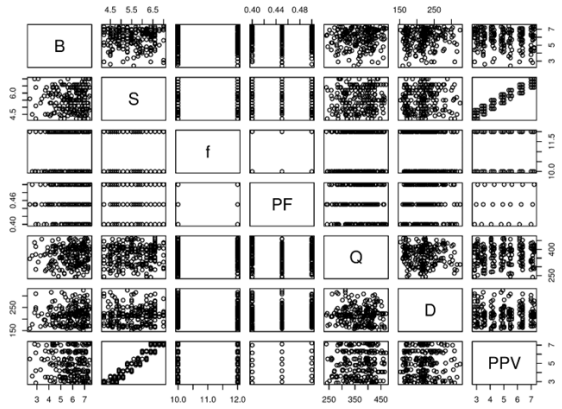

Fig. 4. Visualization of the original dataset used in this study

Tab. 1. Statistical parameters of the original dataset

B	S	f	PF	Q	D	PPV
Min. :2.400	Min. :4.200	Min. :10.00	Min. :0.400	Min. :240.0	Min. :152.4	Min. :2.86
1st Qu.:5.225	1st Qu.:4.900	1st Qu.:10.00	1st Qu.:0.400	1st Qu.:319.5	1st Qu.:189.3	1st Qu.:3.60
Median :6.200	Median :5.600	Median :12.00	Median :0.450	Median :377.5	Median :218.2	Median :4.92
Mean :5.893	Mean :5.598	Mean :11.01	Mean :0.452	Mean :369.0	Mean :219.2	Mean :4.97
3rd Qu.:6.800	3rd Qu.:6.400	3rd Qu.:12.00	3rd Qu.:0.500	3rd Qu.:416.0	3rd Qu.:241.8	3rd Qu.:6.27
Max. :7.400	Max. :7.000	Max. :12.00	Max. :0.500	Max. :469.0	Max. :315.1	Max. :7.22

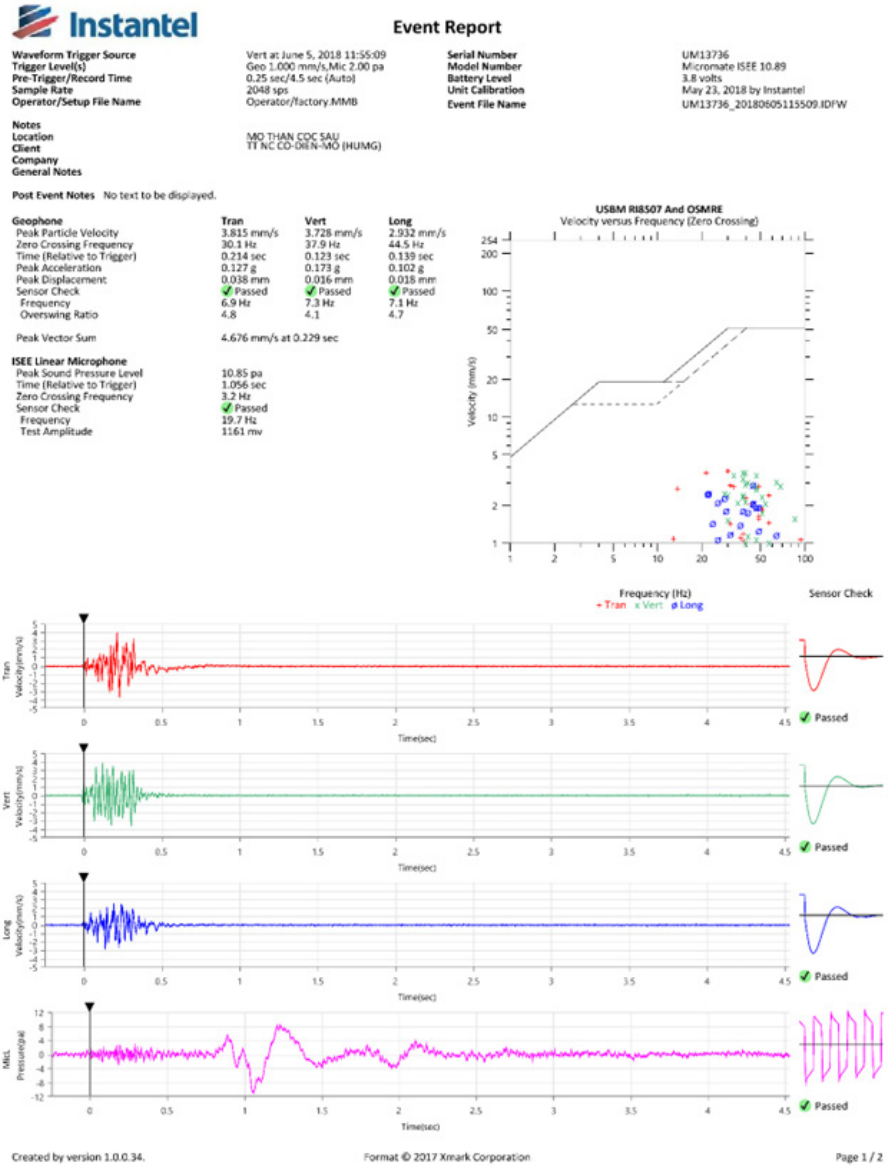

Fig. 5. PPV resulting from blasting operation at the Coc Sau open-pit coal mine

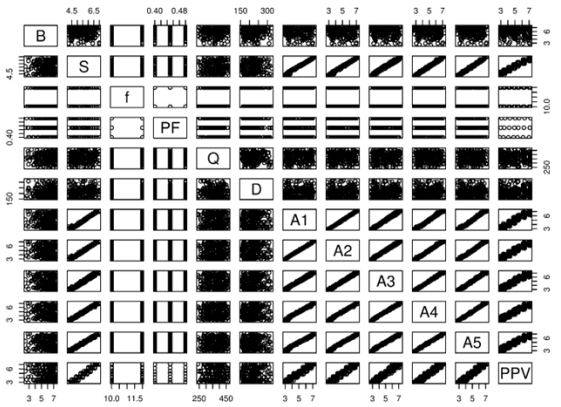

Fig. 6. Visualization of the enriched dataset used in this study

Tab. 1. Statistical parameters of the original dataset

B	S	f	PF	Q	D
Min. :2.400	Min. :4.200	Min. :10.00	Min. :0.4000	Min. :240.0	Min. :152.4
1st Qu.:5.175	1st Qu.:4.900	1st Qu.:10.00	1st Qu.:0.4000	1st Qu.:318.5	1st Qu.:184.4
Median :6.150	Median :5.500	Median :12.00	Median :0.4500	Median :370.5	Median :217.5
Mean :5.854	Mean :5.582	Mean :11.03	Mean :0.4528	Mean :365.9	Mean :218.1
3rd Qu.:6.800	3rd Qu.:6.250	3rd Qu.:12.00	3rd Qu.:0.5000	3rd Qu.:410.2	3rd Qu.:239.8
Max. :7.400	Max. :7.000	Max. :12.00	Max. :0.5000	Max. :469.0	Max. :324.7
A1	**A2**	**A3**	**A4**	**A5**	**PPV**
Min. :2.850	Min. :2.778	Min. :2.678	Min. :2.640	Min. :2.648	Min. :2.860
1st Qu.:3.600	1st Qu.:3.690	1st Qu.:3.694	1st Qu.:3.754	1st Qu.:3.766	1st Qu.:3.600
Median :4.842	Median :4.870	Median :4.940	Median :4.900	Median :4.881	Median :4.920
Mean :4.959	Mean :4.959	Mean :4.960	Mean :4.934	Mean :4.930	Mean :4.961
3rd Qu.:6.197	3rd Qu.:6.138	3rd Qu.:6.147	3rd Qu.:6.100	3rd Qu.:6.036	3rd Qu.:6.270
Max. :7.328	Max. :7.253	Max. :7.367	Max. :7.283	Max. :7.281	Max. :7.220

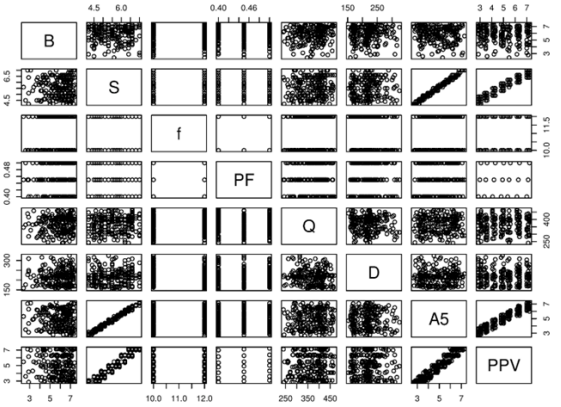

Fig. 7. Visualization of the final enriched dataset used (after analyzing) in this study

Data enrichment plays a crucial role in various domains, especially in engineering problems, such as mining, civil engineering, geotechnical engineering, material engineering, mechanics, to name a few. By leveraging the power of enriched data, researchers can explore the insights of the datasets, optimize operations, or enhancing problems they encountered. There are several techniques that can be used to enrich data for machine learning, including feature engineering, data augmentation, imputation, oversampling and undersampling, feature selection, and external data integration. Of those, data augmentation is a technique used to artificially increase the size and diversity of a dataset by applying various transformations to existing data samples. It is commonly used to enrich the dataset for machine learning tasks. While data augmentation is primarily applied to address challenges in computer vision tasks, such as image classification, object detection, or segmentation, it can also be adapted for other types of data, including regression and time series data.

In this study, the SVM machine learning model was used for data enrichment purposes. As a matter of fact, other machine learning algorithms can also do the same; however, in this study, we selected the SVM algorithm as its popularity and simple. Although the SVM is well-known as a black-box model, however, it can explain the relationships between independent variables through a function.

Assume that we have a dataset contains eight input variables, named as X_1, X_2, X_3, X_4, X_5, X_6, X_7, X_8, and the response variable is Y. The relationships between the input variables can be expressed through different functions that combining the input variables together, as follow:

$$Y_1 = f_{SVM}(X_1, X_2) \quad (1)$$
$$Y_2 = f_{SVM}(X_1, X_2, X_3) \quad (2)$$
$$Y_3 = f_{SVM}(X_1, X_2, X_3, X_4) \quad (3)$$
$$Y_4 = f_{SVM}(X_1, X_2, X_3, X_4, X_5) \quad (4)$$
$$Y_5 = f_{SVM}(X_1, X_2, X_3, X_4, X_5, X_6) \quad (5)$$
$$Y_6 = f_{SVM}(X_1, X_2, X_3, X_4, X_5, X_6, X_7) \quad (6)$$

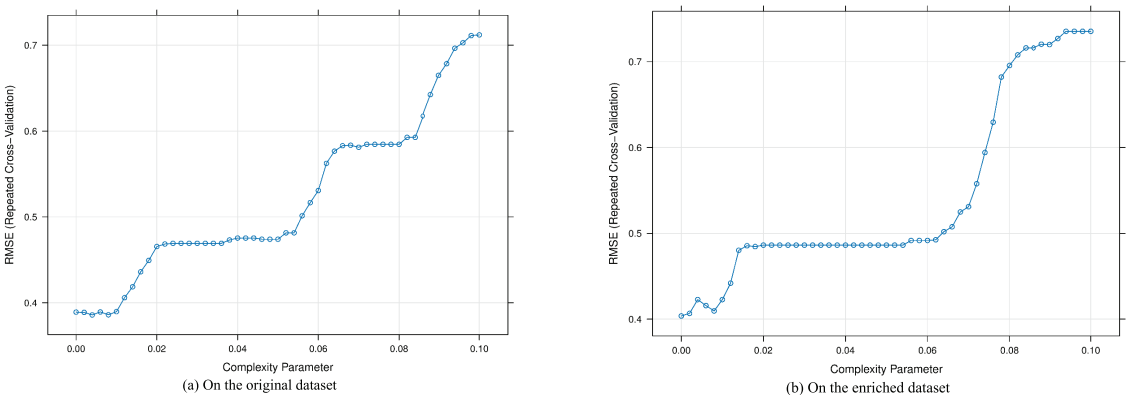

(a) On the original dataset (b) On the enriched dataset

Fig. 8. Performance of the CART model for predicting PPV on the original dataset and enriched dataset

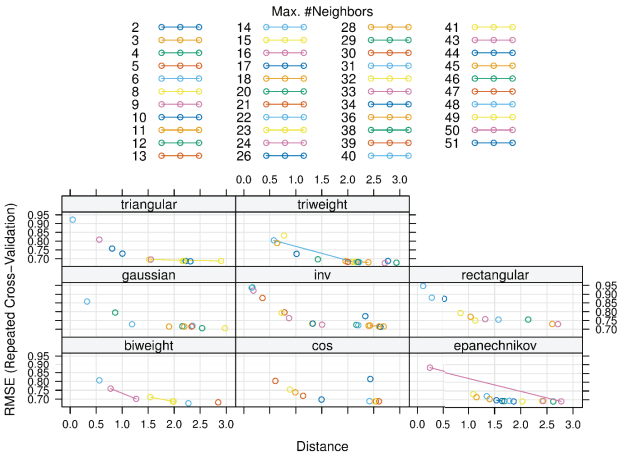

(a)O nt he original dataset

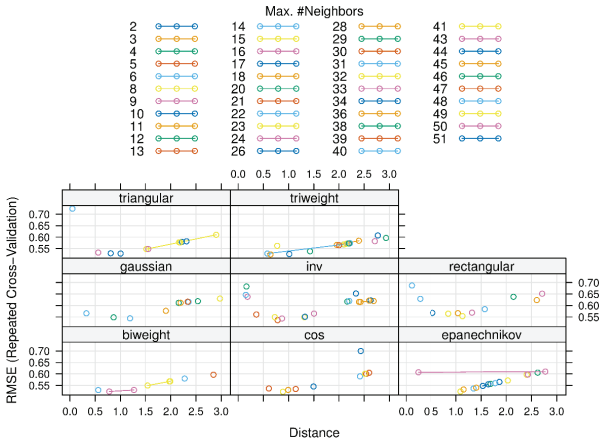

(b)O nt he enriched dataset

Fig. 9. Performance of the KNN model for predicting PPV on the original dataset and enriched dataset

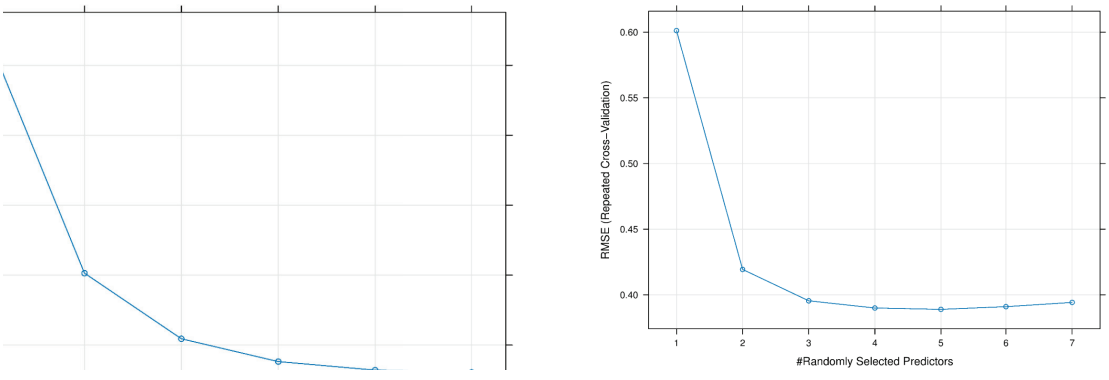

(a) On the original dataset (b) On the enriched dataset

Fig. 10. Performance of the RF model for predicting PPV on the original dataset and enriched dataset

Tab. 3. Performance of the PPV predictive models based on the original dataset and enriched dataset

Model	Training dataset			Testing dataset		
	RMSE	R^2	MAE	RMSE	R^2	MAE
Original dataset						
CART	0.385	0.934	0.351	0.405	0.911	0.360
KNN	0.674	0.811	0.571	0.640	0.798	0.544
RF	0.361	0.944	0.312	0.351	0.935	0.293
Enriched dataset						
CART	0.404	0.929	0.351	0.392	0.921	0.332
KNN	0.522	0.878	0.451	0.438	0.903	0.354
RF	0.389	0.932	0.348	0.343	0.938	0.309

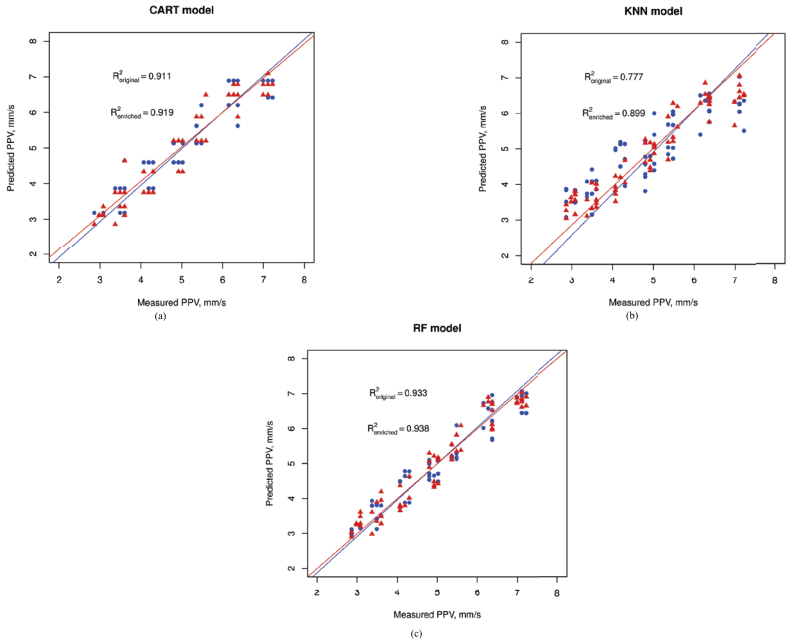

Fig. 11. Correlation between the actual and predicted PPV values on both original dataset and enriched dataset: (a) CART model; (b) KNN model; (c) RF model

$$Y_7 = f_{SVM}(X_1, X_2, X_3, X_4, X_5, X_6, X_7, X_8) \quad (7)$$

Through the seven functions above, the relationships between input variables are explained. Further details of the dataset has been explored through the SVM functions. Finally, they are added to the original dataset as the additional input variables to provide more detail of the dataset's information. In other words, the SVM functions based on different combination of input variables artificially increased the size and diversity of the assumed dataset. The principle of the SVM model is brief described as below.

The SVM, a machine learning algorithm introduced by Cortes and Vapnik [38], is designed to minimize structural risk, enabling better generalization from a limited set of samples. SVM has the ability to tackle classification and regression tasks. In the context of regression, it is referred to as Support Vector Regression (SVR), which constructs a forecasting model based on a subset of the training dataset [39].

To predict blast-induced PPV, SVR can be executed using one of the kernel functions listed below:

- Linear kernel:

$$K(x,y) = x \cdot y \quad (8)$$

- Polynomial kernel:

$$K(x,y) = [(x \cdot y) + 1]^d \;; d = (1,2,...) \quad (9)$$

- Radial primary kernel function:

$$K(x,y) = \exp[\frac{-\|x-y\|^2}{\sigma^2}] \quad (10)$$

- Two-layer neural kernel:

$$K(x,y) = \tanh[a(x \cdot y) - \delta] \quad (11)$$

2.2. Machine learning models for predicting PPV

2.2.1. k-nearest neighbors (KNN)

KNN, proposed by Altman [40], stands out as one of the simplest supervised-learning algorithms in AI. It falls under the category of lazy machine learning since it doesn't learn from training datasets. Instead, KNN makes predictions for new data points based on computations conducted using existing data. This instance-based or memory-based learning algorithm is versatile, supporting both classification and regression tasks.

For classification problems, KNN determines the output of a data point by looking at the nearest known data point (k = 1) or the weighted average of the closest neighbors' outputs. In regression problems, the output is calculated based on the relationship with the nearest data point, depending on the distance.

In essence, KNN predicts the output for a new data point solely based on the information from k data points in the closest training set (k-neighborhood), disregarding any interference from the surrounding data points. For more in-depth details about the KNN algorithm, refer to Song, Liang [41] and Chae, Lee [42].

Interestingly, KNN has been recommended as one of good solutions for predicting blast-induced PPV in open-pit mines [43]. Therefore, this study explores its application for this specific purpose. The next section delves into the process of determining the number of neighbors and setting up the KNN model. Figure 1 presents the mechanism of the KNN model.

2.2.2. Classification and regression trees (CART)

The CART algorithm, widely used in statistical communities, is a non-parametric decision tree algorithm used to predict dependent variables based on independent variables [45]. Inspired by the growth of trees in nature, the CART decision tree operates by segregating independent variables into homogeneous regions, characterized by roots, leaves, branches, and nodes [46, 47].

Breiman, Friedman [48] describe CART as an estimating method that doesn't rely on initial hypotheses about the relationship between dependent and independent variables. It efficiently identifies significant variables while discarding unimportant ones and demonstrates excellent handling of outliers, which can be detrimental to statistical models. The key features of the CART algorithm are as follows:

- Data extraction at a node is based on the value of a specific variable, applying predefined rules.
- It utilizes specific criteria to control the creation of complex trees.
- Pruning is employed to optimize the model's performance.
- The algorithm calculates and predicts the output for terminal nodes.

For this particular study, the CART algorithm was chosen as the benchmark regression algorithm to predict seismic vibration caused by blasting in fragmenting rock. The next sections provide detailed explanations of the CART model setup and PPV forecasts.

2.2.3. Random forest (RF)

RF, proposed by Breiman [49], is an ensemble machine learning algorithm belonging to the group of decision tree algorithms. It is versatile, capable of solving both classification and regression problems. The essence of RF lies in constructing multiple decision trees through bootstrap aggregation (bagging) [50, 51]. It combines the results from these trees to make a final decision. Each tree is trained with a random selection of variables and data samples from the initial training dataset.

For the prediction of blast-induced PPV, RF was applied as follows:

- The number of trees was chosen to ensure a rich forest.
- Bootstrap samples were drawn with replacement from the original PPV training dataset. The remaining values were used for validation and referred to as out-of-bag (OOB) data.
- A non-pruning regression was developed with modifications at each node for each bootstrap sample.
- At each bootstrap iteration, OOB data was used to predict PPV, and the results were averaged across all trees.
- Performance indices such as RMSE, R2, and MAE were used to evaluate the accuracy of predicted PPV values on OOB.

3. Data preparation and model development

3.1. Original datasets

In this study, a dataset consists of 216 blasting events was collected at the Coc Sau open-pit coal mine (Vietnam). This is the deepest open-pit coal mine in Vietnam (-300 m below sea level), as shown in Figure 3.

With the hardness of rock is in the range of 10 to 14, blasting is still the most effective method for fragmenting rock in this open-pit mine. Herein, the dataset with the parameters, such as burden (B), spacing (S), rock hardness (f), powder factor (PF), maximum explosive charge per delay (Q), and PPV monitoring distance (D), were collected and measured for predicting PPV at the Coc Sau open-pit coal mine. The details of the original dataset is shown in Table 1 and its visualization is shown in Figure 4.

Accordingly, B, S, f, PF, and Q were exported from the blast patterns, and D was measured by a GPS receiver from the blast sites to the geo-phone blasting. PPV was measured by the Micromate device (Instantel – Canada). Figure 5 shows a result of PPV that was measured by Micromate at the Coc Sau open-pit coal mine.

3.2. Data enrichment

As previously introduced, the SVM algorithm was employed to elucidate the correlations among the input variables, as outlined in Equations (1-7). Within this research, the original dataset encompassed 6 input variables. The SVM algorithm dissected these relationships through 5 distinct SVM models, namely: the SVM model involving the B and S variables; the SVM model involving the B, S, and F variables; the SVM model involving the B, S, f, and PF variables; the SVM model involving the B, S, f, PF, and q variables; and the SVM model involving the B, S, f, PF, q, and S variables. For each model, an additional novel variable was generated based on the SVM model's predictive outcomes. Consequently, this yielded 5 supplementary variables (A1, A2, A3, A4, A5), augmenting the original dataset to a more comprehensive state featuring 11 input variables. The particulars of this enriched dataset are presented in Table 2, with its visualization depicted in Figure 6.

The findings depicted in Figure 6 reveal noteworthy correlations between five supplementary variables. Consequently, the initial four supplementary variables were eliminated from the augmented dataset. The ultimate supplementary variable, however, was retained due to its capability to elucidate the interrelationships among the remaining variables. As a result, the operational dataset encompasses seven input variables. It's important to note that the final input variable was generated via the SVM algorithm, leveraging the inherent relationships among the original input variables. This enrichment process significantly enhanced the dataset's informational content compared to its original state. The resulting enriched dataset, subsequent to analysis, is presented visually in Figure 7.

4. Results and discussion

After successfully completing the enrichment process, the KNN, CART, and RF models were developed for PPV prediction using both the original and enriched datasets. Subsequently, the predictive outcomes were compared before and after the enrichment process to assess the effectiveness of the SVM algorithm in enhancing the PPV dataset.

In preparation for constructing the predictive models, both the initial and enriched datasets were split into two equal parts following a 70/30 ratio. This allocation designated 70% of each dataset for model training, while the remaining 30% was reserved to evaluate model performance in practical scenarios. To avert overfitting during model development, techniques such as 5-fold cross-validation with 3 repetitions, Box-Cox transformation, and center scaling were implemented.

It's important to emphasize that all models employed identical training and testing datasets for both training and validation phases. Within this study, the Root-mean-squared error (RMSE) function was adopted as the loss metric while training the CART, KNN, and RF models for PPV prediction.

For the CART model, the complexity parameter was used to control the accuracy of this model, and a grid search in the range of 0.002 to 0.1 was used to determine the optimal parrameter of the CART model on the original dataset and enriched dataset. The training results on the original dataset and enriched dataset are shown in Figure 8.

For the KNN model, three parameters, including the maximum number of neighbors (k), the distance beween the nearest neighbors, and kernel function were used to control the accuracy of the accuracy of the KNN model. A random search technique with 100 different KNN models based on 100 different set of parameters were emplemented on both the original dataset and enriched dataset, as shown in Figure 9.

For the RF model, the number of trees in the forest and random selected predictors were used to control the accuracy of this model. According to the experience of previous researchers, a diversity of trees in the forest can improve the prediction performance of the RF model. Therefore, it was selected equal to 2000 trees in this study. In addition, a grid search in the range of 1 to 6 for the original dataset, and a range of 1 to 7 for the enricheed dataset, were applied during developing the RF model for predicting PPV in this study. The training results are shown in Figure 9.

Once the CART, KNN and RF models were developed on both original dataset and enriched dataset, the testing datasets of both original and enriched datasets were used to validate the performance of the developed models. Performance metrics, including RMSE, determination coefficient (R^2) and mean absolute error (MAE) were calculated according to equations (12-14) to evaluate the performance of the developed models, as shown in Table 3.

$$\mathrm{RMSE} = \sqrt{\frac{1}{n_{blast}} \sum_{blast=1}^{n_{blast}} (PPV_i - \overline{PPV}_i)^2} \tag{12}$$

$$\mathrm{R}^2 = 1 - \frac{\sum_{blast=1}^{n_{blast}} \left(PPV_i - \overline{PPV}_i\right)^2}{\sum_{blast=1}^{n_{blast}} \left(PPV_i - \overline{PPV_i}\right)^2} \tag{13}$$

$$\mathrm{MAE} = \frac{1}{n_{blast}} \sum_{blast=1}^{n_{blast}} \left|PPV_i - \overline{PPV}_i\right| \tag{14}$$

where n_{blast} is the number of blasting cases used in the dataset; PPV_i, PPV_i, and PPV_i stand for the measured PPV, predicted PPV, and mean of measured PPVs.

Across all models and datasets, the RMSE values reflect the average magnitude of prediction errors. Smaller RMSE values indicate better predictive accuracy. R^2 values provide an indication of how well the model's predictions fit the actual data. Higher R^2 values suggest a better fit. MAE measures the average absolute difference between predictions and actual values. Lower MAE values indicate better accuracy.

Based on the obtained results in Table 3 and comparing the original and enriched datasets, there are noticeable changes in the performance metrics. The RMSE values in the enriched dataset are indeed smaller, indicating better predictive accuracy compared to the original dataset. Of those, the RF model consistently performs well on both datasets in terms of RMSE, R^2, and MAE, suggesting its robustness in this context. Also, the KNN model demonstrates improvements in performance on the enriched dataset, particularly in terms of RMSE and R^2. And the CART model's performance remains relatively stable between the two datasets, and its performance on the enriched dataset is also slightly better than those of the original dataset. Figure 10 shows the correlation between the actual and predicted PPV values on both original dataset and enriched dataset.

As illustrated in Figure 10, the proximity between the projected outcomes and the actual PPV measurements is notably enhanced in the results obtained from the enriched dataset, in contrast to the projected PPV values originating from the original dataset. This implies that the predictive models exhibited greater convergence when applied to the enriched dataset compared to the original dataset. This observation strongly suggests that the enrichment process substantially bolstered the predictive models' efficacy in forecasting PPV within the scope of this study.

5. Conclusion

Blasting constitutes a pivotal component of surface mining technology, yet its ramifications, notably the considerable impact of blast-induced ground vibration (quantified as PPV in this study), wield a significant influence on the surrounding environment, warranting precise prediction and control. To address this issue, two viable approaches have been identified:

Enhancing Predictive Models: One strategy involves refining predictive models through the implementation of diverse optimization techniques or clustering methodologies.

Dataset Enrichment: Another avenue involves augmenting the dataset to furnish more intricate details, thereby enabling predictive models to forecast PPV with heightened accuracy.

In the context of this investigation, we have proposed a promising remedy to augment the precision of PPV predictive models (specifically CART, KNN, and RF models) employed in open-pit mining settings. This solution involves leveraging machine learning algorithms, notably the SVM algorithm. The outcomes garnered underscore the potential of machine learning algorithms in elucidating the interplay among input variables within the original dataset. The resultant insights can then be employed as supplementary variables to enhance the original dataset, thereby facilitating the improved performance of predictive models in PPV prognostication. Utilizing this data enrichment technique, novel AI-based models can enhance their accuracy to a greater extent compared to utilizing the original dataset alone.

Acknowledgments

Dr. Hoang Nguyen was funded by the Postdoctoral Scholarship Programme of Vingroup Innovation Foundation (VINIF), code VINIF.2022.STS.23. The authors would like to thank the organization committee of the 7th International Conference POL-VIET, Scientific and research cooperation between Vietnam and Poland.

Literatura – References

1. Abbaszadeh, S.A. and R. Asheghi, Optimized developed artificial neural network-based models to predict the blast-induced ground vibration. Innovative Infrastructure Solutions, 2018. 3: p. 1-10.
2. Ainalis, D., et al., Modelling the source of blasting for the numerical simulation of blast-induced ground vibrations: a review. Rock Mechanics and Rock Engineering, 2017. 50(1): p. 171-193.
3. Monjezi, M., et al., Predicting blast-induced ground vibration using various types of neural networks. Soil Dynamics and Earthquake Engineering, 2010. 30(11): p. 1233-1236.
4. Marks, N.A., et al., Airblast variability and fatality risks from a VBIED in a complex urban environment. Reliability Engineering & System Safety, 2021. 209: p. 107459.
5. Stewart, M.G. and M.D. Netherton, A probabilistic risk-acceptance model for assessing blast and fragmentation safety hazards. Reliability Engineering & System Safety, 2019. 191: p. 106492.
6. Gerassis, S., et al., Understanding complex blasting operations: A structural equation model combining Bayesian networks and latent class clustering. Reliability Engineering & System Safety, 2019. 188: p. 195-204.
7. Nguyen, H., et al., Predicting Blast-Induced Ground Vibration in Open-Pit Mines Using Different Nature-Inspired Optimization Algorithms and Deep Neural Network. Natural Resources Research, 2021. 30(6): p. 4695-4717.
8. Nicholls, H.R., C.F. Johnson, and W.I. Duvall, Blasting vibrations and their effects on structures. 1971: US Government Printers.
9. Murmu, S., P. Maheshwari, and H.K. Verma, Empirical and probabilistic analysis of blast-induced ground vibrations. International Journal of Rock Mechanics and Mining Sciences, 2018. 103: p. 267-274.
10. Mesec, J., I. Kovač, and B. Soldo, Estimation of particle velocity based on blast event measurements at different rock units. Soil Dynamics and Earthquake Engineering, 2010. 30(10): p. 1004-1009.
11. Ak, H., et al., Evaluation of ground vibration effect of blasting operations in a magnesite mine. Soil Dynamics and Earthquake Engineering, 2009. 29(4): p. 669-676.
12. Monjezi, M., M. Hasanipanah, and M. Khandelwal, Evaluation and prediction of blast-induced ground vibration at Shur River Dam, Iran, by artificial neural network. Neural Computing and Applications, 2013. 22(7): p. 1637-1643.
13. Saadat, M., M. Khandelwal, and M. Monjezi, An ANN-based approach to predict blast-induced ground vibration of Gol-E-Gohar iron ore mine, Iran. Journal of Rock Mechanics and Geotechnical Engineering, 2014. 6(1): p. 67-76.
14. Hasanipanah, M., et al., Feasibility of indirect determination of blast induced ground vibration based on support vector machine. Measurement, 2015. 75: p. 289-297.
15. Amiri, M., et al., A new combination of artificial neural network and K-nearest neighbors models to predict blast-induced ground vibration and air-overpressure. Engineering with Computers, 2016. 32(4): p. 631-644.
16. Azimi, Y., S.H. Khoshrou, and M. Osanloo, Prediction of blast induced ground vibration (BIGV) of quarry mining using hybrid genetic algorithm optimized artificial neural network. Measurement, 2019. 147: p. 106874.
17. Shang, Y., et al., A Novel Artificial Intelligence Approach to Predict Blast-Induced Ground Vibration in Open-Pit Mines Based on the Firefly Algorithm and Artificial Neural Network. Natural Resources Research, 2020. 29(2): p. 723-737.
18. Zhang, X., et al., Novel Soft Computing Model for Predicting Blast-Induced Ground Vibration in Open-Pit Mines Based on Particle Swarm Optimization and XGBoost. Natural Resources Research, 2020. 29(2): p. 711-721.
19. Qiu, Y., et al., Performance evaluation of hybrid WOA-XGBoost, GWO-XGBoost and BO-XGBoost models to predict blast-induced ground vibration. Engineering with Computers, 2021.
20. Bui, X.-N., H.-B. Bui, and H. Nguyen. A Review of Artificial Intelligence Applications in Mining and Geological Engineering. in Proceedings of the International Conference on Innovations for Sustainable and Responsible Mining. 2021. Springer.
21. Jung, D. and Y. Choi, Systematic review of machine learning applications in mining: Exploration, exploitation, and reclamation. Minerals, 2021. 11(2): p. 148.
22. Kim, M., L. Ismail, and S. Kwon, Review of the Application of Artificial Intelligence in Blasting Area. Explosives and Blasting, 2021. 39(3): p. 44-64.
23. Yong, W., et al., Analysis and prediction of diaphragm wall deflection induced by deep braced excavations using finite element method and artificial neural network optimized by metaheuristic algorithms. Reliability Engineering & System Safety, 2022. 221: p. 108335.
24. Liu, D., S. Wang, and X. Cui, An artificial neural network supported Wiener process based reliability estimation method considering individual difference and measurement error. Reliability Engineering & System Safety, 2022. 218: p. 108162.
25. Yang, Z., P. Baraldi, and E. Zio, A method for fault detection in multi-component systems based on sparse autoencoder-based deep neural networks. Reliability Engineering & System Safety, 2022. 220: p. 108278.

26. Seo, S.-K., et al., Deep neural network-based optimization framework for safety evacuation route during toxic gas leak incidents. Reliability Engineering & System Safety, 2022. 218: p. 108102.

27. Zhou, J., et al., Developing a hybrid model of Jaya algorithm-based extreme gradient boosting machine to estimate blast-induced ground vibrations. International Journal of Rock Mechanics and Mining Sciences, 2021. 145: p. 104856.

28. Lawal, A.I., et al., Blast-induced ground vibration prediction in granite quarries: An application of gene expression programming, ANFIS, and sine cosine algorithm optimized ANN. International Journal of Mining Science and Technology, 2021. 31(2): p. 265-277.

29. Zhu, W., H.N. Rad, and M. Hasanipanah, A chaos recurrent ANFIS optimized by PSO to predict ground vibration generated in rock blasting. Applied Soft Computing, 2021. 108: p. 107434.

30. Zhang, X., et al., Novel Extreme Learning Machine-Multi-Verse Optimization Model for Predicting Peak Particle Velocity Induced by Mine Blasting. Natural Resources Research, 2021. 30(6): p. 4735-4751.

31. Armaghani, D.J., et al., A novel approach for forecasting of ground vibrations resulting from blasting: modified particle swarm optimization coupled extreme learning machine. Engineering with computers, 2021. 37(4): p. 3221-3235.

32. Arthur, C.K., V.A. Temeng, and Y.Y. Ziggah, A Self-adaptive differential evolutionary extreme learning machine (SaDE-ELM): a novel approach to blast-induced ground vibration prediction. SN Applied Sciences, 2020. 2(11): p. 1845.

33. Ding, X., et al., Predicting the blast-induced vibration velocity using a bagged support vector regression optimized with firefly algorithm. Engineering with Computers, 2020: p. 1-12.

34. Nguyen, H., X.-N. Bui, and E. Topal, Reliability and availability artificial intelligence models for predicting blast-induced ground vibration intensity in open-pit mines to ensure the safety of the surroundings. Reliability Engineering & System Safety, 2023. 231: p. 109032.

35. Syarif, I., et al. Application of bagging, boosting and stacking to intrusion detection. in Machine Learning and Data Mining in Pattern Recognition: 8th International Conference, MLDM 2012, Berlin, Germany, July 13-20, 2012. Proceedings 8. 2012. Springer.

36. Graczyk, M., et al. Comparison of bagging, boosting and stacking ensembles applied to real estate appraisal. in Intelligent Information and Database Systems: Second International Conference, ACIIDS, Hue City, Vietnam, March 24-26, 2010. Proceedings, Part II 2. 2010. Springer.

37. Wolpert, D.H. and W.G. Macready, Combining stacking with bagging to improve a learning algorithm. Santa Fe Institute, Technical Report, 1996. 30.

38. Cortes, C. and V. Vapnik, Support vector machine. Machine learning, 1995. 20(3): p. 273-297.

39. Basak, D., S. Pal, and D.C. Patranabis, Support vector regression. Neural Information Processing-Letters and Reviews, 2007. 11(10): p. 203-224.

40. Altman, N.S., An introduction to kernel and nearest-neighbor nonparametric regression. The American Statistician, 1992. 46(3): p. 175-185.

41. Song, Y., et al., An efficient instance selection algorithm for k nearest neighbor regression. Neurocomputing, 2017. 251: p. 26-34.

42. Chae, D.-K., et al., On identifying k-nearest neighbors in neighborhood models for efficient and effective collaborative filtering. Neurocomputing, 2018. 278: p. 134-143.

43. Bui, X.-N., et al., A novel Hybrid Model for predicting Blast-induced Ground Vibration Based on k-nearest neighbors and particle Swarm optimization. Scientific reports, 2019. 9(1): p. 1-14.

44. Hu, C., et al., Data-driven method based on particle swarm optimization and k-nearest neighbor regression for estimating capacity of lithium-ion battery. Applied Energy, 2014. 129: p. 49-55.

45. Khandelwal, M., et al., Classification and regression tree technique in estimating peak particle velocity caused by blasting. Engineering with Computers, 2017. 33(1): p. 45-53.

46. Myles, A.J., et al., An introduction to decision tree modeling. Journal of Chemometrics, 2004. 18(6): p. 275-285.

47. Pradhan, B., A comparative study on the predictive ability of the decision tree, support vector machine and neuro-fuzzy models in landslide susceptibility mapping using GIS. Computers & Geosciences, 2013. 51: p. 350-365.

48. Breiman, L., et al., Classification and decision trees. Wadsworth, Belmont, 1984. 378.

49. Breiman, L., Random forests. Machine learning, 2001. 45(1): p. 5-32.

50. Effron, B. and R.J. Tibshirani, An introduction to the bootstrap. Monographs on statistics and applied probability, 1993. 57: p. 436.

51. Breiman, L., Random forests. UC Berkeley TR567, 1999.

52. Nguyen, H., et al., Developing an XGBoost model to predict blast-induced peak particle velocity in an open-pit mine: a case study. Acta Geophysica, 2019. 67(2): p. 477-490.

Numerical Study on Effects of Airflow Parameters on the Air Temperature the at Mechanized Longwall of Mongduong Coal Mine

Hong NGUYEN THI[1)], Quang NGUYEN VAN[2)]

[1)] Faculty of Environment, Hanoi University of Mining and Geology, 18 Vien street, Hanoi, Vietnam; email: nguyenthihong@humg.edu.vn
[2)] Faculty of Mining, Hanoi University of Mining and Geology, 18 Vien street, Hanoi, Vietnam; email: quangnv@humg.edu.vn

http://doi.org/10.29227/IM-2023-02-16

Submission date: 26-08-2023 | Review date: 21-09-2023

Abstract

The increasing depth of extraction and the degree of mechanization leading to the risk of workers working in poor microclimate conditions has become one of the major safety issues in coal mines. During the survey of the current microclimate in Mongduong coal mine, it showed that the temperature of the mechanized longwall exceeded the permissible regulations (t°≤ 30°C), the air humidity is about 95–100%. The reason for the increase of air temperature in longwall is due to geothermal, heat radiated from the longwall equipment and the inlet wind high temperature. To improve the thermal environment in the mechanized longwall area, Vietnam's coal mines open use ventilation, but the efficiency is not high. Therefore, the paper evaluated the influence of airflow on the temperature of the longwall, 7 models with different air flow velocities and 3 models with inlet air temperature have been created in ICM-CFD and simulated by Ansys CFX software. The environment temperature of each model was evaluated by analyzing the average temperature of the roadway section, the cross-section distribution of the roadway temperature and the velocity streamline of the whole roadway. As a result, the air flow rate increases leading to the air temperature in the longwall decreases, however the wind speed is limited. The inlet temperature of the gas stream is an important factor that affects the thermal environment in the longwall. The results of the article are the basis for making solutions to improve the thermal environment suitable for high-temperature longwall.

Keywords: *numercial modelling, Ansys CFX, mechanized longwall, temperature of air mine, velocity of air mine, Mongduong coal mine*

1. Introduction

Coal serves as an indispensable energy source for the development of domestic economies, providing fuel for power plants and various industries. However, this vital resource is being rapidly depleted at shallow levels, pushing mining operations to exploit deeper reserves. Such deep-level mining poses potential risks to labor safety and can significantly impact the microclimate in underground coal mines. In recent years, several coal mines in Quang Ninh, Vietnam, particularly the Mong Duong Coal Mine's L7 longwall, have undergone deep mining operations and adopted mechanized techniques, resulting in elevated air temperatures within the mining areas. The soaring air temperatures in the L7 longwall region, for instance, have been observed to exceed the standard QCVN 01/2011/BCT [Ministry of Industry and Trade, 2011], surpassing 30°C. Prolonged exposure of workers to such high-temperature environments poses potential health risks to miners, compromising mining efficiency (He and Guo 2013; Yang et al. 2011), and increasing the frequency of accidents while decreasing labor productivity. Among the primary causes of rising mine air temperatures are the heat emitted from surrounding rocks and electrical equipment, along with the oxidation of coal (He et al. 2010; Su et al. 2009). Previous studies, such as those conducted by [Dao Van Chi et al., 2019] and [Quan Truong Tien et al., 2019], have explored the factors influencing temperature increase, including soil, rock, and coal temperatures. Additionally, the study of mine airflow indicates that the primary source of heat is the surrounding rock, particularly the rock surfaces near the work face (Zhang et al. 2017; Maurya et al. 2015), and the temperature of the air flow is closely linked to the airflow path, which is influenced by the ventilation system (Su et al. 2017; Hua et al. 2018). In this study, we aim to analyze the main heat sources in the L7 longwall mining area of Mong Duong coal mine and establish a numerical model to explore the relationship between various parameters and the temperature distribution in the longwall area. Specifically, we consider wind velocity parameters (V = 0.5 m/s, 1 m/s, 1.5 m/s, 2 m/s, 2.5 m/s, 3 m/s, 3.5 m/s, 4 m/s) and variations in inlet wind temperature (T = 29°C, 26°C, 24°C). By investigating these factors, our research endeavors to provide valuable insights into the heat dynamics of deep-level coal mining areas, offering a foundation for effective strategies in managing and mitigating excessive air temperatures, thereby enhancing worker safety and overall mining productivity.

2.Heat sources affecting mine air temperature

2.1 Radiative heat from surrounding rock

The difference between the initial temperature of the surrounding rock and the airflow in the shaft determines the heat exchange driving force. A positive or negative temperature difference governs the direction of heat transfer between the surrounding rock and the air. Due to the significant temperature gradient in the ground, the initial rock temperature is typically higher than the temperature of the airflow in the tunnel, making the surrounding rock a crucial heat source for the tunnel walls. In deep mines, the heat flux value can be considerable, often surpassing the total heat flux from other sources, due to the influence of the initial rock temperature. The convective heat transfer between the surrounding rock and the airflow is an unstable heat transfer process. The temperature of the surrounding rock in the well is higher due to the impact of ground heat flow, leading to an unstable transmission of heat flux. Over time, the radius of the surrounding

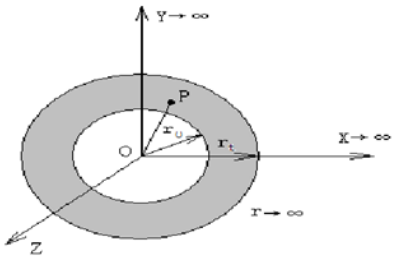

Fig. 1. Diagram of the cylindrical surface of an infinitesimal object

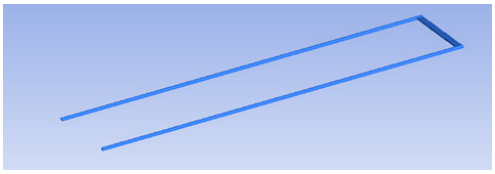

Fig. 2. Model of the longwall area using ICEM – CFD

rock's thermal adjustment zone increases, and the heat flow source expands into the deeper rock layers. Through observation and theoretical analysis, it becomes evident that once the tunnel ventilation reaches a certain duration, the convective heat transfer between the surrounding rock and the axial airflow stabilizes, allowing the heat exchange between them to be considered as stable [Воропаев.А.ф, 1961].

$$Q_r = K_t U.L(t_z - t),\ kW \quad (1)$$

Q_r – Radiator from surrounding rock, kW
K_t – Unstable heat transfer coefficient from surrounding rock
U – Road circumference, m
L – Road length
t_z – Initial temperature at depth z, °C
t – The average temperature of the airflow, °C

In order to calculate the heat transfer between the surrounding rock and the airflow, the following assumptions are commonly employed:

The rock temperature is uniform and equal to the initial rock temperature along the entire roadway circumference. The heat transfer conditions remain consistent, and the air inside the roadway maintains a constant temperature. All heat from the surrounding rock is transferred to the airflow..

Following ventilation of the roadway, a heat exchange process ensues between the surrounding rock and the airflow. The heat from the surrounding rock is transferred to the airflow, leading to cooling of the surrounding rock and subsequent changes in its temperature field over time. Consequently, the thermal conduction of the surrounding rock becomes an unstable heat conduction process in the Cartesian coordinate system., that is:

$$T=T(x,y,z,t) \quad (2)$$

According to the two basic laws of heat transfer, namely the law of conservation of heat and Fourier's law of thermal conduction, the basic equation of three-dimensional heat conduction can be established. This equation, serves as a fundamental framework for analyzing heat flow and temperature distribution in three-dimensional systems: [Liu Shishi, et al 1994]

$$\frac{\partial T}{\partial t} = a\left(\frac{\partial^2 T}{\partial x^2} + \frac{\partial^2 T}{\partial y^2} + \frac{\partial^2 T}{\partial z^2}\right) \quad (3)$$

where a is the temperature coefficient of the surrounding rock, m^2/s.

$$a = \frac{\lambda}{cp} \quad (4)$$

Where:
c – is the specific heat capacity of the rock, J/(kg · °C);
ρ – is the density of rock, kg /m^3;
λ – is the thermal conductivity of the rock, kW/m °C.

In the Cartesian coordinate system, the heat transfer in the surrounding rock can be conceptualized as a two-dimensional unstable heat conduction process. To simplify the analysis, we convert the Cartesian coordinate system into a cylindrical coordinate system and thereby transform the two-dimensional heat conduction equation for the surrounding rock into a more manageable one-dimensional heat conduction equation

$$\frac{\partial T}{\partial t} = a\left(\frac{\partial^2 T}{\partial x^2} + \frac{\partial^2 T}{\partial y^2}\right) \quad (5)$$

Sut up temperature to T (r, τ), $r = (x^2 + y^2)^{1/2}$:

$$\frac{\partial T}{\partial t} = a\left(\frac{\partial^2 T}{\partial r^2} + \frac{1}{r}\frac{\partial T}{\partial r^2} + \frac{1}{r^2}\frac{\partial^2 T}{\partial \theta^2}\right) \quad (6)$$

Since T is independent of θ, temperature distribution T (r, τ) satisfy the equation

$$\frac{\partial T}{\partial t} = a\left(\frac{\partial^2 T}{\partial r^2} + \frac{1}{r}\frac{\partial T}{\partial r}\right) \quad (7)$$

Its mean:

$$\frac{\partial^2 T}{\partial r^2} + \frac{1}{r}\frac{\partial T}{\partial r^2} + \frac{1}{a}\frac{\partial T}{\partial t} = 0\ (6)\ r_0 < r < \infty,\ t > 0 \quad (8)$$

The initial conditions:

$$r_0 \le r < +\infty,\ t = 0,\ T(r,0) = t_0 = t_y = const \quad (9)$$

The boundary condition is: when khi τ > 0, $r = r_o$. When the surrounding rock and convection heat dissipation path h is the

Tab. 1. Parameters in the model

Parameters of the longwall	Model parameters	Parameters of the longwall	Model parameters
velocity	1 m/s; 1,5 m/s; 2m/s; 2,5m/s; 3m/s; 3,5 m/s; 4m/s	Temperature of equipment	308,15K - 311,15K
outlet	outlet	roughness	2 cm
Temperature air of inlet	297,15K; 299,15K; 302,15K;	Thermal conductivity of rock	1,9 W/mk
Initial air of temperature	302,15K	Thermal conductivity of coal	0,35W/k
Temperature of rock	304,15K - 305,15K		

surrounding rock and the convective heat transfer coefficient of the wind flow. tf is the dry bulb temperature of the wind.

$$\lambda.\frac{\partial T}{\partial r} - h\left(T - t_f\right) \tag{10}$$

When $\tau > 0, r \to \infty$, The surrounding rock temperature is equal to the original rock temperature, mean: $T(\infty, t) = t_y = const.$

2.2. Heat dissipation of electromechanical equipment

As the mechanization level improves and mining capacity increases in underground coal mines, the microclimate conditions of the mine are also affected. Generally, the electrical energy supplied to electromechanical devices on the charging line can be divided into two parts: useful work and thermal energy. During the operation of electromechanical equipment, kinetic energy is relatively small, and the primary useful work involves lifting materials to the surface, increasing the potential energy of the material or liquid. However, any excess electrical energy not utilized for useful work is converted into thermal energy, nearly all of which is dissipated into the tunnel airflow. Investigating the thermal release of electromechanical equipment mainly involves examining its rated power and mechanical efficiency (1). By utilizing the appropriate calculation coefficients, the heat dissipation provided by the engine to the airflow can be calculated as shown in [Wu Zhongli, 1989].

$$Q_n = 3600.\eta_n.N\ ,\ KJ/h \tag{11}$$

In here:
3600 is the power of 1k W which is equivalent to the heat of 3600k J/h;
N is the power of the motor, k W;

2.3 Heat dissipation during coal transportation

The heat dissipation of coal during transport is, in fact, another manifestation of the heat dissipation from the surrounding rock. This aspect holds significant importance in understanding the transfer of heat and moisture in modern mines. As a result, the temperature of the surrounding airflow increases, [Yan Ronglin et al,2004]

$$Q_k = m\_k.C_k.\Delta t_k,\ kw \tag{12}$$

Where: Q_k – is the heat dissipation of coal transportation, Kw
m_k – is the amount of coal transportation, kg/s;
C_k – is the average specific heat of coal transportation., kJ/kg.^{0}c
Δt_k – is the temperature at which coal is cooled in the road section under consideration during transportation, °C.

Similar to soil, the temperature of coal also increases with the depth of exploitation and exceeds the temperature of the underground air during the initial period. Consequently, the heat transfer process between coal and air during transportation becomes a critical factor to consider.

3. Model

3.1. Model Construction

The model is based on the characteristics of the L7 mechanized longwall at the Mong Duong coal mine, which is exploited at a depth of -250/-160 meters and has a yearly capacity of 300 thousand tons. The mining process involves the MG160/380 machine code in combination with support from the ZF3000/15/24 code. The transportation is facilitated by the SZZ-110KW Conveyor and the SGZ-220KW Tractor, while the coal is crushed using the PLM500 90KW Crusher. The mining operation operates in two shifts, with an additional preparation shift. The dimensions of the longwall are as follows: a length of 120 meters, a width of 6 meters, and a height of 2.2 meters. The thickness of the coal seam is 5.5 meters, and the cross-sectional area of the roadway is 13m^2, extending over a length of 350 meters. Temperature survey results indicate that the average temperature along the transport seam of the roadway ranges from 302.5K to 304.65K, while the average temperature of the longwall ranges from 304.15K to 305.15K. In this study, a model is developed to analyze the influence of wind velocity parameters and changes in inlet wind temperature on the temperature distribution. The wind velocity parameters considered in the model are: v = 0.5 m/s, 1 m/s, 1.5 m/s, 2 m/s, 2.5 m/s, 3 m/s, 3.5 m/s, and 4 m/s. Additionally, variations in the inlet wind temperature are examined, specifically at Tn = 29°C, 26°C, and 24°C. By utilizing this model, we aim to gain valuable insights into the heat distribution within the longwall mining area, and understand how changes in wind velocity and inlet wind temperature can impact the overall temperature conditions during the mining process.

3.2. Numerical Model

For the numerical analysis, the article employs Computational Fluid Dynamics (CFD) through numerical simulation. The geometric modeling and meshing of the model are conducted using ICEM-CFD software, maintaining the same geometric dimensions as mentioned earlier. The mesh consists of approximately 3x106 to 3.6x106 elements. The boundary conditions are categorized into two classes. The numerical simulation is performed in CFX, utilizing the K-ε turbulence model. This model is chosen for its ability to provide accurate predictions of turbulence, making it suitable for analyzing the airflow patterns and heat transfer within the longwall mining area.

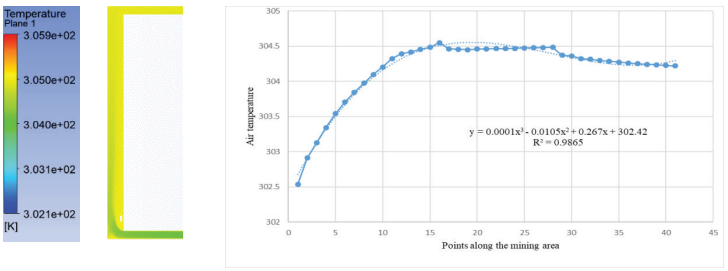

V =1 m/s

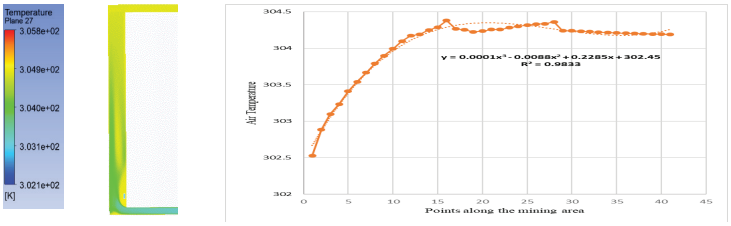

V = 1.5 m/s

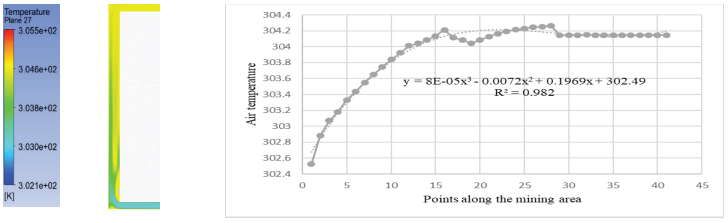

V =2 m/s

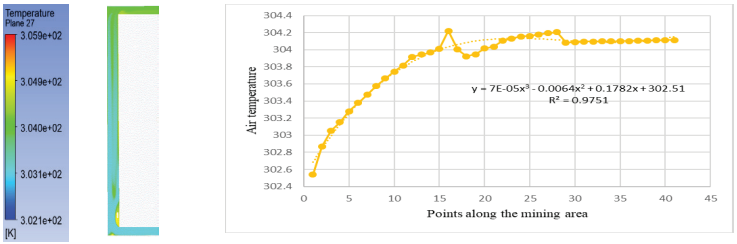

V = 2.5 m/s

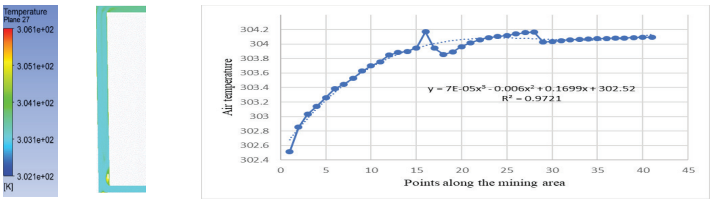

V= 3 m/s

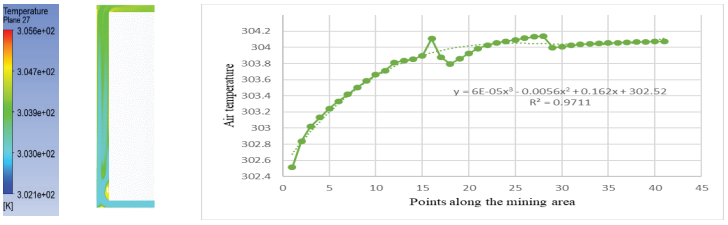

V = 3.5 m/s

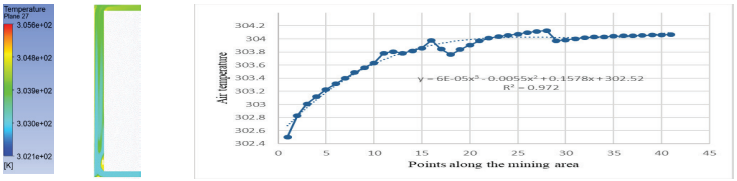

V = 4m/s

Fig. 2. Temperature field and trend of temperature change along the mining area

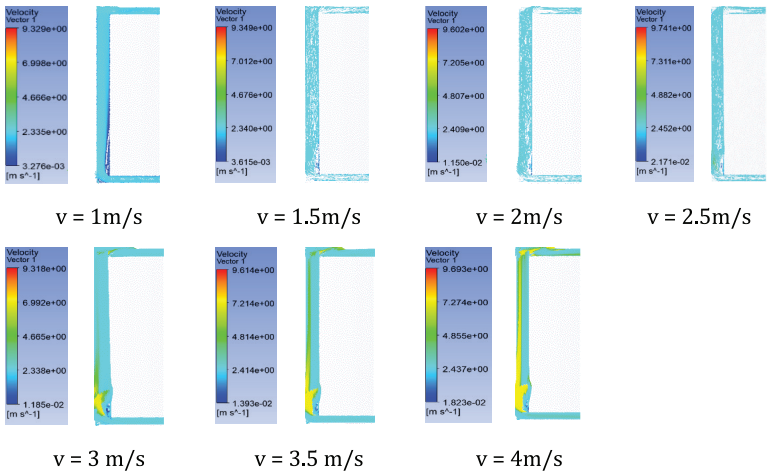

Fig. 3. Velocity field at mining area

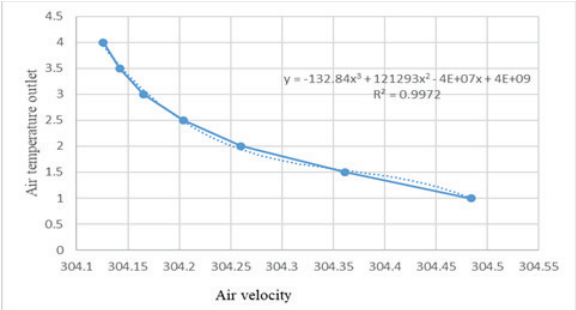

Fig. 4. Relationship between wind speed and air temperature of longwall

3.3. Mathetical model

The heat exchange between the rock and air is calculated using the conservation equations for mass, momentum, and energy. To simulate these phenomena related to the flow of liquid and gas, heat transfer, and mass, Computational Fluid Dynamics (CFD) is employed in this study. CFD is a powerful numerical method used to analyze and predict various fluid-related processes. In this paper, CFD is utilized to investigate the impact of parameters such as duct position and inlet temperature on the temperature distribution in the work area. The model considers a turbulent flow of viscous incompressible gas, and the mathematical equations from fluid mechanics form the foundation for solving problems associated with gas transport.

1. The continuity equation

$$\frac{\partial p}{\partial t}+\frac{\partial (pu)}{\partial x}+\frac{\partial (pv)}{\partial y}+\frac{\partial (pw)}{\partial z}=0$$

Where: u,v,w direction velocity (m/s); p density (kg/m^3); t: time (s)

2. The momentum equation

$$\frac{\partial}{\partial t}(pv)+\nabla .(vv)=-\nabla p+\nabla T+pg+F$$

Where: p is static pressure (pa) T – stress tensor (pa), gravitationnal body force (m/s^2); F external body force (N);

3. The energy equation

$$\frac{\partial}{\partial t}(pE)+\nabla .\overrightarrow{(v}(pE+v))=\nabla (k_{eff}\nabla T)+S_h$$

Where: E: energy (J), T temperature (K); k_{eff} effective thermal conductivity; S_h source term.

3.4. Boundary conditions

The boundary conditions and computational model settings for this study are presented in table 1.

4. Results and discussion

4.1. Effect of airflow rate

The simulation results are shown in Figure 3-6. Fig. 2 displays the airflow temperature field in the working area under different ventilation rates. The temperature distribution along the horizontal section of the roadway appears to be uniform. However, in the longwall, the temperature distribution exhibits significant variation. Notably, a high-temperature region emerges near the corner at the bottom of the longwall, and as the inlet wind speed increases, this high-temperature area gradually expands. The influence of eddy currents plays a role in increasing the heat exchange time and heat dissipation of the cutter when it operates at the bottom of the longwall, resulting in a more uniform temperature distribution in that region. Conversely, for wind speeds exceeding v > 2 m/s, more eddy currents are generated at the top and bottom of the longwall, leading to a more fluctuating temperature distribution at the top and creating a high-temperature region. The simulation results enable the establishment of a relationship between the mine air temperature along the mining area, depicted through a nonlinear regression function of order 3. This relationship provides a basis for forecasting the temperature of the mining area as the wind speed varies. These findings are crucial for understanding the heat distribution and airflow dynamics within the longwall mining area. Moreover, they facilitate accurate predictions of temperature changes with varying wind speeds, enhancing safety and efficiency in mining operations.

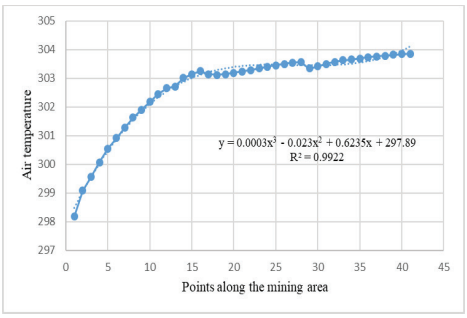

T=297.15K

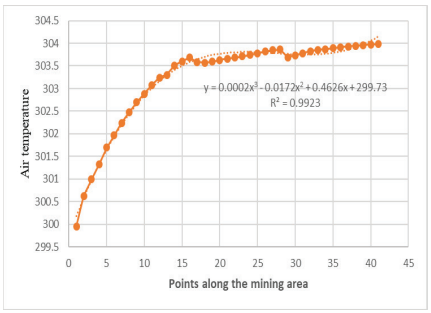

T = 299.15K

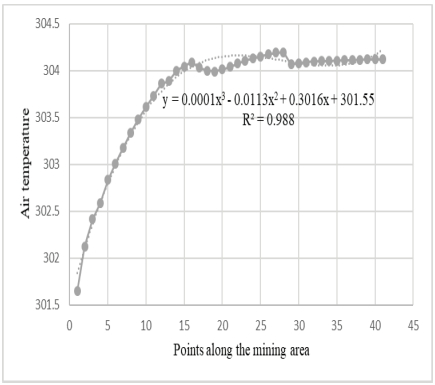

T=302.15K

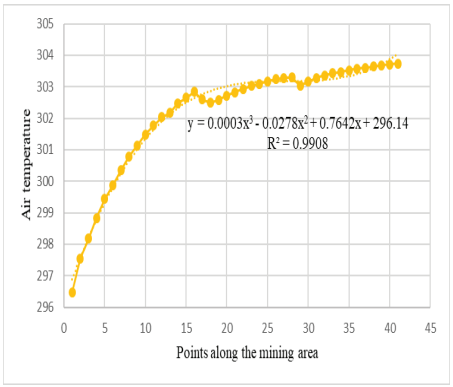

T = 296.15K

Fig. 5. Trends in air temperature variations along the mining area with different input temperatures

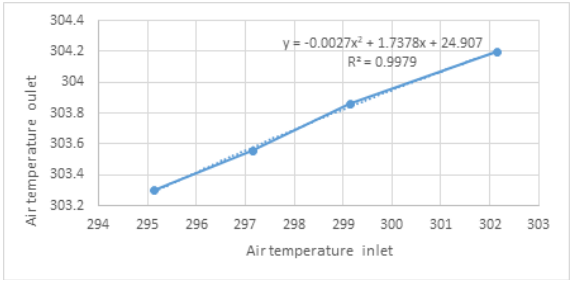

Fig. 6. The relationship between input and output temperature in the longwall

Fig. 3 illustrates the velocity field at the mining area. The figure reveals that the wind velocity field on the horizontal section along the roadway remains relatively stable. However, significant fluctuations in velocity are observed at the bottom and top of the longwall, creating distinct vortex patterns when the wind speed increases.

As the inlet wind speed increases, the area of the vortex expands gradually, promoting convective heat transfer between the wind flow and the high-temperature regions. Notably, at the bottom and top of the longwall, the wind speed towards the wall is higher, resulting in a wider area of influence. Conversely, on the lower side, the wind speed is lower, leading to localized temperature increases. These observations provide valuable insights into the airflow dynamics within the longwall mining area. The presence of vortices and their behavior with varying wind speeds play a significant role in the convective heat transfer process. Understanding these phenomena is crucial for optimizing ventilation strategies and enhancing the overall heat dissipation efficiency within the mining area. By accurately assessing the velocity field, miners can mitigate potential risks associated with localized temperature variations, ensuring safer and more productive mining operations.

Fig. 4 presents the relationship between wind speed and air temperature of the longwall. The airflow rate plays a crucial role in influencing the microclimate conditions within the mining area. Variations in airflow rate can significantly impact the heat distribution and temperature levels in the working environment. Through numerical simulations and field measurements, the study investigates the effect of different airflow rates on the temperature distribution along the longwall. The results reveal that as the airflow rate increases, there is a corresponding decrease in the air temperature within the longwall area. The relationship between airflow rate and longwall temperature is found to be nonlinear, and it is effectively represented by a third-order nonlinear regression function. The findings highlight the importance of carefully controlling the airflow rate to maintain an optimal working environment. By understanding the impact of airflow rate on the microclimate conditions, mining operations can implement effective ventilation strategies to ensure the safety, comfort, and productivity of workers in the mining area. Moreover, the results provide valuable data for forecasting temperature changes and optimizing ventilation systems in modern mines.

4.3.Effects of inlet air temperature

Tab. 2. Temperature measurement and simulation results

Distance to face (m)	Measurement data (^{0C})	Simulation data (^{0C})	errors (^{0}K)	Distance to face (m)	Measurement data (^{0C})	Simulation data (^{0C})	errors (^{0}K)
Roadway transport				Longwall			
5	29.5	29.376	-0.12	5	31.1	31.099	0
60	29.7	29.949	0.25	10	31.5	31.229	-0.27
120	30.3	30.26	-0.04	20	31	31.101	0.1
180	30.3	30.515	0.22	40	31.3	31.085	-0.21
240	30.4	30.748	0.35	60	31.3	31.107	-0.19
300	30.7	30.947	0.25	90	31.5	31.166	-0.33
340	30.8	31.041	0.24	115	31.6	31.211	-0.39
Ventialtion roadway							
5	31.4	31.09	-0.31	240	30.8	31.051	0.25
60	31.3	31.082	-0.22	300	30.7	31.045	0.35
120	31.2	31.069	-0.13	340	30.7	31.039	0.34
180	31	31.06	0.06				

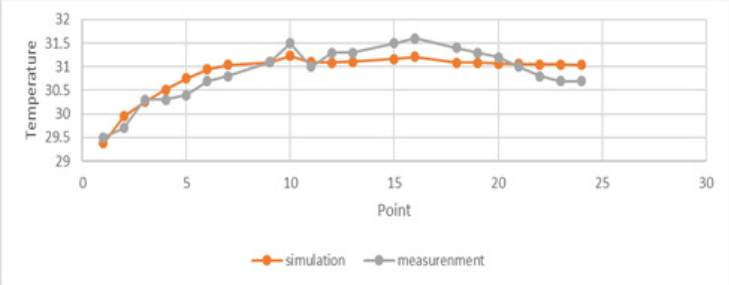

Fig. 7. Measurement and simulation results

From the model above, change the input temperature parameter T= 297.15 K ; 299.15K ; 302.15K, with v =1.5 m/s according to mine parameters. The results arre presented in Fig. 5.

From the results in Figure 5, it can be observed that changes in the input temperature significantly affect the temperature along the mining area. The temperature gradually increases along the roadway and the longwall. The temperature variations along the longwall exhibit a cubic nonlinear trend. For the model with T=297.15K, the air temperature within the mine remains below 303.5K. However, for the models with T=299.15K and T=302.15K, the air temperature within the mining area exceeds the standard specified in QCVN 01/2011/BCT, which can impact labor productivity and the health of the workers. Additionally, Figure 6 illustrates the relationship between the input air temperature from the starting point of the transportation roadway and the output temperature of the longwall at the starting point of the longwall. This relationship is represented by a nonlinear regression function. The input temperature has a substantial impact on the temperature in the longwall area. It is crucial to implement solutions to reduce the temperature in the longwall area, ensuring the safety and well-being of the workers. Overall, these findings emphasize the importance of controlling and optimizing the microclimate conditions within the longwall mining area to ensure a safe and healthy working environment for the workers.

4.4. Check the fit of the model

The measured objects are the air parameters in the area of the L7 mechanized longwall, Mongduong coal mine.measurements of air velocity and roadway cross-sectional area, air temperature. Measuring instruments : Anemometer PMA-2008; Psychrometr Assmana. Measurements are taken at measuring points along the along roadway the transport with a distance from the inlet point general response l =5m, 60m, 120m, 180m, 240m, 300m, 340m. along longwall with a distance from the inlet point are l= 5m, 10m, 20m, 40m, 60m, 90m, 115m.The measuring points along ventilation roadway are l =5m, 60m, 120m, 180m, 240m, 300m, 340m.

Figure 7 presents the numerical simulation results of the model with a wind velocity of v = 2 m/s. A comparison with the field measurements indicates slight deviations between the two sets of data, but these differences do not significantly impact the accuracy of the numerical simulations. Hence, the results obtained from the numerical simulations remain reliable and hold substantial reference value.

5. Conclusion

In conclusion, the survey results and model building based on the actual parameters of the L7 mechanized longwall in Mong Duong coal mine have highlighted the significant influence of geothermal heat and heat generated from mining equipment, as well as the inlet air temperature of the coal mine. Under the same mining conditions, the input temperature and inlet wind speed have a nonlinear relationship with the temperature in the longwall. The simulation results demonstrate that changes in wind speed follow an increasing trend, leading to a reduction in the air temperature in the mining area. However, it is observed that this temperature difference tends to decrease to a certain value as the wind speed increases further. At that point, the wind will no longer be effective in reducing the temperature of the longwall. Therefore, for high-temperature mine areas, it is advisable to implement strategies such as increasing the wind speed and reducing the inlet air temperature to ensure more favorable working conditions for the workers. Measures should be taken to regulate the temperature of the inlet wind during deep mining operations, and the use of air conditioners in the mines is recommended to maintain microclimate conditions in accordance with regulations and create a comfortable environment for the workers. By implementing these measures, mining operations can ensure the safety, health, and well-being of the workers and promote more efficient and productive mining activities. The optimization of ventilation and temperature control strategies is crucial for the successful and sustainable operation of the mine.

Literatura – References

1. Воропаев.А.ф. :управденИе тендовыМ Режитот ЯглУъокихжатах.М. ГомоРтехиэдат. 1961.
2. Dao Van Chi , Le Van Thao, 2019. Research on solutions to prevent coal seam temperature rise in mechanized transport kilns area 7.3.1 zone I seam 7 Ha Lam coal mine. Mining Industry Journal. Number 4, page 66-:68 and page 99.
3. He M, Cao X, Xie Q, Yang J, Qi P, Yang Q, Chen X (2010) Principles and technology for stepwise utilization of resources for mitigating deep mine heat hazards. Int J Min Sci Technol 20:20–27
4. He M, Guo P (2013) Deep rock mass thermodynamic effect and temperature control measures. Chin J Rock Mechan Eng 12:2377–2393
5. Hua Y, Nie W, Cai P, Liu YH, Peng HT, Liu Q (2018) Pattern characterization concerning spatial and temporal evolution of dust pollution associated with two typical ventilation methods at fully mechanized excavation faces in rock tunnels. Powder Technol 334:117–131. https://doi.org/10.1016/j.powtec.2018.04.059
6. Maurya T, KarenaK,Vardhan H,ArunaM, RajMG (2015) Effect of heat on underground mine workers. Procedia Earth and Planetary Science 11:491–498. https://doi.org/10.1016/j.proeps.2015.06.049
7. Ministry of Industry and Trade, 2011. National Technical Regulation on Safety in Underground Coal Mining, Hanoi Labor Publishing House.
8. Liu Shishi, Liu Shida. Nonlinear equations in physics[M]. Beijing: Peking University Press. 1994.
9. QUAN Truong Tien , Rafał ŁUCZAK1 and Piotr ŻYCZKOWSKI, 2019. Climatic hazard assessment in selected underground hard coal mines in Vietnam. Journal of the Polish Mineral Engineering Society.No2(44), p.155-163.http://doi.org/10.29227/IM-2019-02-67
10. Su HT, Zhou FB, Song XL, Qiang ZY (2017) Risk analysis of spontaneous coal combustion in steeply inclined longwall gobs using ascaled-down experimental set-up. Process Saf Environ Prot 111:1–12. doi:https://doi.org/10.1016/j.psep.2017.06.001,1
11. Su Z, Jiang Z, Sun Z (2009) Study on the heat hazard of deep exploitation in high-temperature mines and its evaluation index. Procedia Earth Planet Sci 01:414–419
12. Wu Zhongli. Mine ventilation and safety [M]. Xuzhou: China University of Mining and Technology Press, 1989, 50-245.
13. Yang X, Han Q, Pang J, Shi X, Hou D, Liu C (2011) Progress of heat-hazard treatment in deep mines. Int J Min Sci Technol 21:295–299
14. Yan Ronglin, Hou Xianwen. Mine air conditioning technology. Beijing: Coal Industry Press, 2004.
15. Zhang Y, Wan ZJ, Gu B, Zhou CB, Cheng JY (2017) Unsteady temperature field of surrounding rock mass in high geothermal roadway during mechanical ventilation. J Cent South Univ 24:374–381. https://doi.org/10.1007/s11771-017-3439-3

Segmentation of Homogeneous Regions of Gravity Field Properties by Machine Learning Method in Central Area of Vietnam

Hong Phan THI[1)]*, Phuong Do MINH[2)], Huu Tran VAN[1)]

[1)] HUMG Hanoi University of Mining and Geology, Faculty of Petroleum and Energy, Hanoi, Vietnam
[2)] Geophysical Division, General Department of Geology and Minerals, Hanoi, Vietnam
* Corresponding author: phanthihong@humg.edu.vn

http://doi.org/10.29227/IM-2023-02-17

Submission date: 16-08-2023 | Review date: 11-09-2023

Abstract

This paper presents the results of applying the unsupervised learning method (K-means clustering) on the gravity anomaly field in the central region of Vietnam to separate the research area into different clusters, which are homologous in physical properties. In order to achieve the optimal results, the input parameter plays an important role. In this paper, we chose 04 input attributes including the gravity anomalous field attribute, the horizontal gradient attribute, the variance attribute, and the tracing coefficient of the gravity anomalous axis. The obtained results have shown that the research area could be divided into 7 clusters, 9 clusters, 11 clusters, and 13 clusters with close characteristics of the physical properties of the gravity field. The research results show that the Southwest, the Center, and the South of the study area have complex changing physical properties, this result reflects the complicated tectonic activities in these areas with the presence of crumpled and fractured rock layers in different directions and these locations are the potential places to form endogenous mineral deposits of magma origin. The Northwest, the North, and the East parts of the research area witness negligible changes in the field's physical properties, reflecting the stability of the soil and rock layers in this area, with the direction of extending structure from the Northwest to the Southeast. The clustering results according to the K-means unsupervised learning algorithm in central Vietnam initially increase the reliability of the decisions of geologists and geophysicists in interpreting the geological structure and evaluating the origin of deep-hidden mineral deposits in the area.

Keywords: *K-means, unsupervised learning method, gravity field, central area of Vietnam, COSCAD 3D*

1. Introduction

Central Vietnam is the place of development and interference of large blocks such as Truong Son sticky belt, Tam Ky - Phuoc Son hatch, and Kon Tum lifting block. In which, deep faults along the Northwest-Southeast, Northeast-Southwest and minor meridians are the boundary between the above-mentioned structures [4, 20, 21]. The research area is characterized by narrow valleys and treacherous divisions with complex topography including many mountain ranges >700m high [7] (Fig.1a) which extend to the Northeast, Northwest, and the Meridians. These are favorable prerequisites to forming endogenous mineral deposits of magma origin, and the identification of geological structures related to the location of endogenous mineral deposits is an important mission and top priority in the coming years. Furthermore, all of this information is characterized by different residual density values and can be displayed on the gravity anomalous field values measured from ground-based gravity survey (Fig.1b), and these field values are the consequence of overlapping of gravity anomalous fields from many geological objects in the subsurface, in combination with deep geological structures, which are needed to characterize, so they are random. These factors make the gravity anomalous field caused by objects with high density often complicated, which leads to difficulty in the process of reasoning.

Along with the development of technology 4.0, there have been many applications of unsupervised learning algorithms in the processing of potential field data [1, 3]. Computerization of the exploration process allows the application of new algorithms, modern algorithms, and statistical algorithms in the processing and interpretation of geological and geophysical data. Paying special attention to characteristics of geological and geophysical information, selecting the optimal set of features to cluster with uniform physical properties, and evaluating the correlation between different physical attributes within the same cluster [5, 9, 14].

In this study, we apply an unsupervised learning algorithm (K-means clustering) on the gravity anomalous field data in the central region of Vietnam to divide the area into homogenous regions of the field's physical attributes (attributes: gravity field, horizontal gradient value, statistics, anomaly axis tracing). This result will help to quickly identify homogenous layers (saving time, and cost...) to provide information for geologists to have an intuitive view of the study area.

2. Data and methods

2.1. Data used

The data used in this paper are the ground-measured gravitational anomaly data of full Bouguer correction at the scale of 1:100.000 and the accuracy of 0,1-0,25 mGal [10, 11, 12, 13]. Bouguer correction density was selected as 2,67g/cm^3 and Picivanco's method was used to correct the terrain [2].

Looking at Figure 1(b), it can be seen that the Bouguer gravity anomaly changes from -100 to 20 mGal, and the gravity anomaly tends increase gradually from Northwest - Southeast toward the sea. The Northwest of the study area is characterized by a strong negative gravity anomaly with amplitude ranging from -100to -55 mGal, and the East and Southeast by a range of gravity anomaly values varying from -30 to 20 mGal. There are local anomalies with amplitude from -30 to

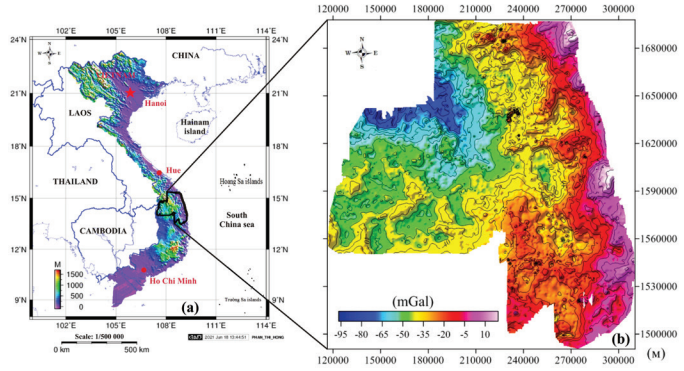

Fig. 1. Location and topography elevation from 10-1600 m of the study area (a) and Map of the full Bouguer gravitational anomaly field of the study area at a scale of 1:100.000, where the value varies from -100-20 mGal (b)

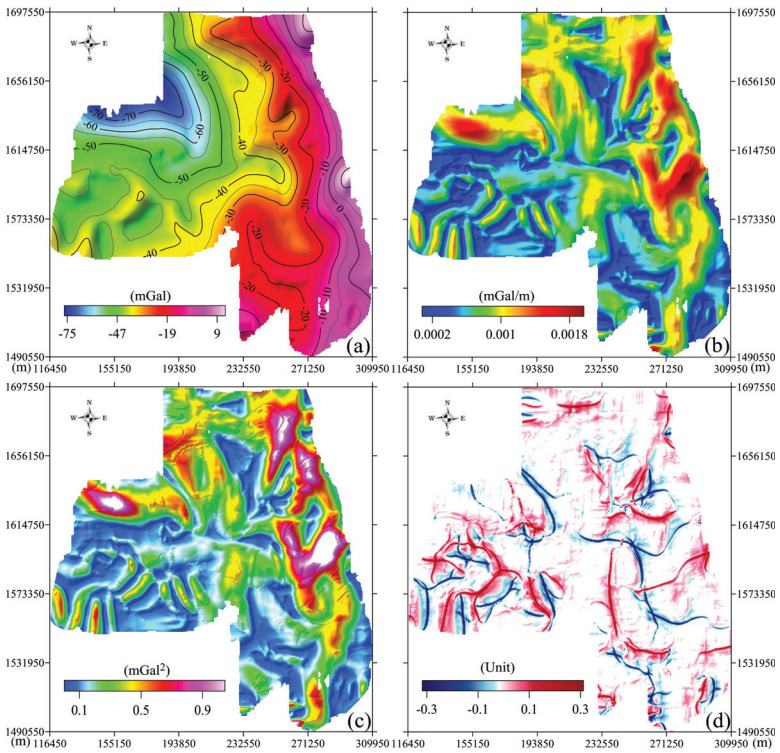

Fig. 2. The regional anomaly field after removing the shallow local anomaly field (a); Horizontal Gradient of gravity anomaly in the research area (b); regional anomaly variance (c); tracing coefficients of anomaly axis in the research area (d)

-15 mGal in the North, Southwest, Center, and South of the study area.

2.2. Methods

Nowadays, there are many unsupervised learning algorithms applied in processing and analyzing of geophysical data [1, 3]. However, in this study, we only focus on the most popular algorithm in unsupervised learning techniques, which is the K-means clustering algorithm [1, 3, 8, 9]. In the K-means algorithm, the Mahalanobis distance is used as the distance between the individual parameters and takes into account the relationships in the feature space of the field. The K-means algorithm automatically divides the data of the central region of Vietnam into different clusters, hence the attribute data (attributes: gravity field, horizontal gradient value, statistics, anomaly tracing) are in the same cluster with similar properties.

2.2.1. K-means method

The k-means clustering algorithm is an unsupervised learning method with a set of points with close features. The advantage of this algorithm is simple and time-efficient computation. The block diagram of the algorithm is as follows [5, 6, 9, 17]:

- For all p signals, determining the standard deviation σ_i, the minimum $f_{min}^{\ i}$ and the maximum $f_{max}^{\ i}$ at i = 1, 2, 3,…, p value of the signal;
- Each signal f_i (i=1, 2,…, p) is normalized to correspond to the standard deviation: $\sigma_i: \overline{f_i} = \frac{f_i}{\sigma_i}$;
- A vector k of size p is randomly selected for the initial center of the class $C_j=\{c_{1j},c_{2j}...c_{j3}\}$; $j=1,2,...,k$ and the individual randomly selected components of each vector, satisfying the inequality: $\frac{Y_{min}^i}{\sigma_i} < c_{ij} < \frac{Y_{min}^j}{\sigma_j}$
- Classifying the normalized signs of the original network into classes, and at each point of the network $x = \{x_1, x_2,...,x_p\}$ related to layer m, if the distance from the center of this layer to the point is minimal $r_{min} = Min\ \{x_1, x_2,...,x_p\}$;
- According to the classification results, new vectors are determined $C^n=\{c_1^{\ n}, c_2^{\ n},..., c_p^{\ n}\}$; $j=1,2,...,k$. Each vector component m is the average value $c_{im}^n = \frac{1}{n_m}\sum_{j=1}^{n_m} x_i^m, i = 1,2,..,p$

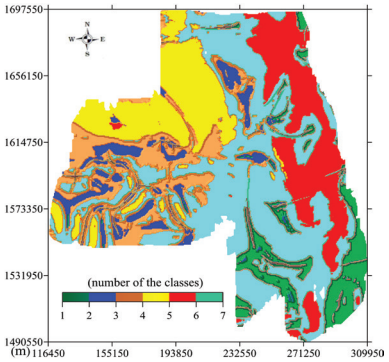

Table 1: Physical property average values for 07 homogenous clusters according to unsupervised machine learning (K-means clustering)

Number of the homogenous clusters	Gravitational anomaly field Δg (mGal)	Horizontal gradient of gravity anomaly field (mGal/m)	Variance characteristic of the gravity anomaly field (mGal²)	Gravity anomaly tracing coefficient
1	-33.190	$0.594*10^{-3}$	0.222	-0.228
2	-44.269	$0.21*10^{-3}$	0.074	-0.003
3	-50.761	$0.849*10^{-3}$	0.336	-0.009
4	-21.131	$0.171*10^{-2}$	1.115	-0.003
5	-8.7632	$0.713*10^{-3}$	0.264	0.006
6	-23.208	$0.477*10^{-3}$	0.211	0.336
7	-32.959	$0.751*10^{-3}$	0.259	0.119

Fig. 3. The results of automatic division into 07 clusters with close characteristics of the properties of the gravity anomaly field in the central region of Vietnam

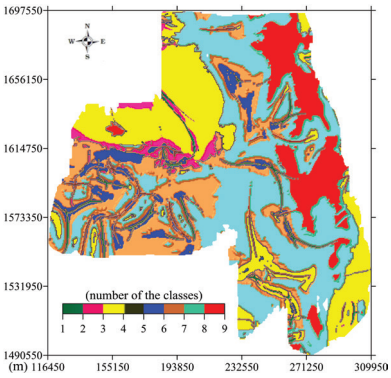

Table 2: Physical property average values for 09 homogenous clusters according to unsupervised machine learning (K-means clustering)

Number of the homogenous clusters	Gravitational anomaly field Δg (mGal)	Horizontal gradient of gravity anomaly field (mGal/m)	Variance characteristic of the gravity anomaly field (mGal²)	Gravity anomaly tracing coefficient
1	-25.082	$1.746*10^{-3}$	1.247	-0.006
2	-35.927	$0.569*10^{-3}$	0.203	-0.238
3	-52.596	$0.815*10^{-3}$	0.313	0.002
4	-25.094	$0.588*10^{-3}$	0.225	0.318
5	-49.396	$0.221*10^{-3}$	0.074	-0.003
6	-22.158	$0.981*10^{-3}$	0.427	-0.001
7	-4.400	$0.221*10^{-3}$	0.074	0.002
8	-6.686	$0.667*10^{-3}$	0.208	0.014
9	-18.015	$1.672*10^{-3}$	1.02	0.001

Fig. 4. The results of automatic division into 09 clusters with close characteristics of the properties of the gravity anomaly field in the central region of Vietnam

calculated in n_m points, falling into class m after classification, performed in the previous step of the algorithm;

- In the selected index, the distance between the old center and the new center of the layer is estimated $\vec{R}_j(C, \vec{C}^n)$, $j=1,2,\ldots,k$;
- If at least one of the k classes, the distance is greater than the pre-selected value $\vec{R}_j > \varepsilon$, then the center of the old vector is assigned the new value $C_j = \vec{C}^n_j$, $j=1,2,\ldots k$, and the procedure is repeated from the step where the observations are classified. In the opposite case, the inequality $\vec{R}_j(\vec{C}, \vec{C}^n) < \varepsilon$ is satisfied for all classes, the result of the last iteration is the last step of the iteration.

This algorithm converges after a finite number of iterations (converging fairly quickly), the main disadvantage of the algorithm is the need to know the number of clusters in advance, and not fully consider the associations of the field attribute space. To overcome the limitations of the algorithm, in this study, we determined the number of clusters according to the geological data on the surface (Tran and Nguyen, 2008), and used the Mahalanobis distance as the spatial distance (Nikitin and Petrov, 2008; Hong, 2020).

2.2.2. The input parameter of the K-means clustering algorithm

The input parameter plays a very important role in the unsupervised learning algorithm, in this paper we chose 4 attributes: gravity anomalous field attribute, variance, horizontal gradient, and anomaly axis tracing coefficient. In the study, we have selected the optimal set of features to cluster and evaluate the correlation between the attribute features in the same cluster.

- Horizontal gradient of gravity anomaly

The gravity anomalous horizontal gradient value is calculated according to the following formula [5, 6, 9]:

$$GN = \sqrt{\left(\frac{\Delta g}{\partial x}\right)^2 + \left(\frac{\Delta g}{\partial y}\right)^2} \quad (1)$$

in which: GN is the gravity anomalous horizontal gradient value (mGal/m); Δg is the gravity anomaly value; ∂x, ∂y are derivatives in the direction of 0x, 0y.

The maximum value of the gravity anomalous horizontal gradient emphasizes the boundaries of anomalous features (fault systems, boundaries of geological features....); The horizontal gradient field highlights the boundaries of anomalies of different amplitudes, allowing visualization of the boundaries of all anomalies simultaneously.

- Evaluation of the statistical characteristics of the gravity anomaly field

In the statistical characteristics of the field (mathematical expectation, variance, eccentricity, asymmetrical deviation of the field...), we chose the field's variance value and according to the formula [15, 16, 17, 18, 19]:

$$\sigma^2 = \frac{1}{n} \cdot \frac{1}{m} \sum_{i=1}^{n} \sum_{j=1}^{m} \left(X_{ij} - \overline{X}\right) \quad (2)$$

where: σ is the variance of the gravity anomaly field (mGal²), X_{ij} is the gravity anomaly value (mGal), X is the value of average gravity anomaly (mGal).

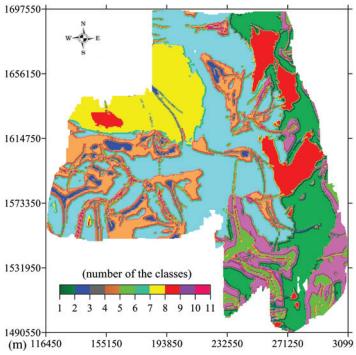

Table 3: Physical property average values for 11 homogenous clusters according to unsupervised machine learning (K-means clustering)

Number of the homogenous clusters	Gravitational anomaly field Δg (mGal)	Horizontal gradient of gravity anomaly field (mGal/m)	Variance characteristic of the gravity anomaly field ($mGal^2$)	Gravity anomaly tracing coefficient
1	-34.551	$0.545*10^{-3}$	0.204	-0.281
2	-22.504	$0.175*10^{-3}$	1.249	-0.009
3	-4.546	$0.231*10^{-3}$	0.074	0.002
4	-65.778	$0.85*10^{-3}$	0.336	-0.005
5	-49.308	$0.213*10^{-3}$	0.074	-0.004
6	-45.578	$1.4*10^{-3}$	0.796	-0.026
7	-25.889	$0.817*10^{-3}$	0.303	0.279
8	-8.197	$0.771*10^{-3}$	0.277	0.008
9	-24.234	$0.256*10^{-3}$	0.118	0.327
10	-39.979	$0.732*10^{-3}$	0.248	-0.002
11	-11.167	$0.159*10^{-3}$	0.949	0.021

Fig. 5. The results of automatic division into 11 clusters with close characteristics of the properties of the gravity anomaly field in the central region of Vietnam

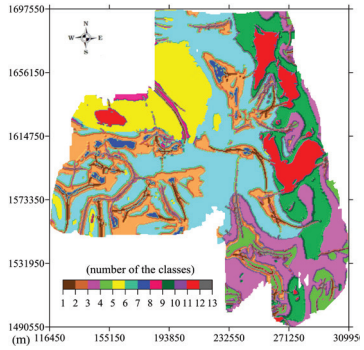

Table 4: Physical property average values for 13 homogenous clusters according to unsupervised machine learning (K-means clustering)

Number of the homogenous clusters	Gravitational anomaly field Δg (mGal)	Horizontal gradient of gravity anomaly field (mGal/m)	Variance characteristic of the gravity anomaly field ($mGal^2$)	Gravity anomaly tracing coefficient
1	-34.646	$0.545*10^{-3}$	0.201	-0.279
2	-8.5403	$0.685*10^{-3}$	0.214	0.009
3	-25.534	$0.804*10^{-3}$	0.298	0.309
4	-27.656	$0.175*10^{-3}$	1.25	-0.023
5	-56.743	$0.389*10^{-3}$	0.085	-0.011
6	-47.883	$0.187*10^{-3}$	0.074	-0.004
7	-8.7652	$1.199*10^{-3}$	0.617	0.011
8	-4.4860	$0.228*10^{-3}$	0.074	0.001
9	-40.210	$0.721*10^{-3}$	0.232	0.005
10	-13.015	$1.781*10^{-3}$	1.121	0.027
11	-23.202	$0.237*10^{-3}$	0.116	0.318
12	-64.553	$0.101*10^{-3}$	0.453	-0.005
13	-37.507	$1.278*10^{-3}$	0.676	-0.031

Fig. 6. The results of automatic division into 13 clusters with close characteristics of the properties of the gravity anomaly field in the central region of Vietnam

The maximum value of the variance carries the information of heterogeneous boundaries (fault systems, boundaries of geological features...).

- Tracing anomaly axis

The program is designed to trace anomalies of different energies and different directions [5, 6, 9], with the maximum value (equal to 1) corresponding to the axis of the positive anomaly, the minimum value (equal to -1) corresponding to the axis of the negative anomaly, and the value (equal to 0) corresponding to no anomaly.

3. Results and discussion

3.1. Result of processing input parameters of unsupervised learning method

As shown in the above analysis, in this study, we choose 4 input parameters to put into the K-mean clustering unsupervised learning algorithm, including regional gravity anomaly field (removed local field near the surface) (Fig.2a), applying formula (1) to evaluate the horizontal gradient characteristics of gravity anomaly, the results are shown in Figure 2(b); applying formula (2) to evaluate the statistical characteristic of gravity anomaly field, results are shown in Figure 2(c), and finally the results of tracing the anomaly axis (Fig.2c).

3.2. Result of applying the unsupervised learning method

Applying the K-means unsupervised learning algorithm with 4 input parameters, we got the results of automatic clustering of the central region of Vietnam into 07 clusters (Fig. 3), 09 clusters (Fig. 4), 11 clusters (Fig.5), 13 clusters (Fig.6), these clusters have close features on properties of gravity anomaly field, horizontal gradient value, variance and tracing coefficients of anomaly axis on Table 1, Table 2, Table 3, and Table 4.

The results of automatic division into 07 clusters (Fig.3), 09 clusters (Fig.4), 11 clusters (Fig.5), and 13 clusters (Fig.6) show that the study area exists the complex cleavage physical properties in the Southwest, the South and the center of the area, compared to the geological structure map, this area belongs to the intracontinental rift system after the Mesozoic collision, that is the result of post-extension and collision between the Indochinese plate and Sibumasu [4, 21]. Thus, the results of applying the K-means unsupervised learning method are well-matched with the geological data.

In the North, Northwest, and East of the area (Fig.3, 4, 5, 6), the physical attributes of the field show little or no change, indicating that these regions are quite stable with the western structural direction extending to the northwest-southeast. Because the East of the study area is adjacent to the East Sea, this result is completely consistent with geological laws.

Observations in Fig.3, Fig.4, Fig.5, and Fig.6 show that the terracotta tectonic activity still exists in the southwest and the south of the study area, which proves that this tectonic activity is regional and they act as channels to pump magma blocks from deep to the surface, penetrate the near-surface sediments and form deposits of deep-hidden mineral mines.

The results of dividing the area into clusters having close features based on attributes of the gravity anomaly field reflect the homogeneity of the petrographic composition of the rock layers, which is a premise to increase the reliability of geologists and geophysicists' decisions, providing an intuitive and multi-dimensional view about the process of tectonic activities in the central region of Vietnam.

4. Conclusions

The results of processing and interpreting the data of Bouguer gravity anomalies in Central Vietnam led to some conclusions:

- The unsupervised learning algorithm (K-means) is effectively applied to the gravity anomaly data in Central Vietnam.
- The results of automatic division into 07 clusters, 09 clusters, 11 clusters, and 13 clusters having close characteristics of the properties of the gravity anomaly field completely coincide with the tectonic geology in the area.
- In the southwest, center, and south part of the study area maps show that the physical attributes of the field are quite complex, showing that in this area the rock layers are crumpled and broken in different directions, and this is the potential location to form endogenous mineral deposits of magma origin.
- In the north, northwest, and east part of the study area maps show little change in the physical properties of the field, reflecting that the rock layers in this area are quite stable with the structural direction extending from the northwest to the southeast.
- The clustering results by means of the K-means unsupervised learning algorithm initially increase the reliability in the decisions of geologists and geophysicists about the interpretation of geological structures and the assessment of the origin of deep-hidden mineral deposits in the area.

Acknowledgments

This work is supported by the grassroots project of the University of Mining and Geology, Hanoi, Vietnam, no. T23-12. The authors would like to thank Geophysical Division, General Department of Geology and Minerals of Vietnam, for providing 1:100.000 scale data of the Bouguer gravity anomaly in the central region of Vietnam. Thanks to Professor, Ph.D. of Science Petrov Aleksey Vladimirovich, University of Geology and Exploration named Sergo Ordzhonikidze, Moscow, Russia (MGRI), for providing commercial software "COSCAD-3D" for data processing.

Literatura – References

1. Aline Melo, Yaoguo Li. Geology differentiation by applying unsupervised machine learning to multiple independent geophysical inversions. Geophysical Journal International, 2058-2078 (2021). https://doi.org/10.1093/gji/ggab316
2. Blakely, R.J. Potential theory in gravity and magnetic application. Cambridge University Press, 461 pages (1996). https://www.cambridge.org/core/books/potential-theory-in-gravity-and-magnetic-applications/348880F23008E16E663D6AD14A41D8DE
3. Carmine Cutaneo, Andrea Vitale, Maurizio Fedi. Unsupervised Boundary Analysis of potential field data: a machine learning method. Society of Exploration "First international Meeting for Applied Geoscience &Energy", 941-945 (2021). DOI:10.1190/segam2021-3594444.1
4. Hai Thanh Tran, Khin Zaw, Jacqueline A. Halpin, Takayuki Manaka, Sebastien Meffre, Chun-Kit Lai, Youjin Lee, Hai Van Le, Sang Dinh. The Tam Ky- Phuoc Son shear zone in central Vietnam: Tectonic and metallogenic implications. Gondwana Research, 26, 144-164 (2014). DOI: 10.1016/j.gr.2013.04.008
5. Hong T. Phan, Aleksey V. Petrov, Phuong M. Do, Giau M.lai, Luu T. Nguyen. Geological structure of central Vietnam by interpretation processing of gravitational survey data using the "COSCAD 3D" computer technology. Geology and Exploration, 77-90 (2020). https://doi.org/10.32454/0016-7762-2020-63-5-77-90
6. Hong P. T. Computer technology for interpretational processing of gravity and magnetic processing data using probabilistic methods statistical approach (by the example of the territory of central vietnam). Doctoral thesis, 126 pages (2022). https://www.mgri.ru/science/scientific-and-innovative-activity/dissertation-council/download/%D0%A4%D0%B0%D0%BD%20%D0%A2.%D0%A5._%D0%90%D0%B2%D1%82%D0%BE%D1%80%D0%B5%D1%84%D0%B5%D1%80%D0%B0%D1%82_final%20(22.04.2022).pdf
7. https://topex.ucsd.edu
8. MacQueen, J. Some methods for classification and analysis of multivariate observations. Proceedings of the fifth Berkeley symposium on mathematical statistics and probability. Oakland, CA, USA (1967).
9. Nikitin A.A., Petrov A.V. Theoretical foundations of geophysical information processing. Study guide, Moscow 113 pages (2008). https://www.geokniga.org/bookfiles/geokniga-nikitinteorosnovygeofizinfo2008.pdf
10. Nguyen Truong Luu, Hoang Van Long, Phan Duc Le, Pham Van Hung, Nguyen Thien Cong, Tran Duan. Applying a combination of geophysical-geological methods in investigating and detecting copper-uran mineral ores in Kon Ra-Kon Tum area. Geological Journal, Series A, 371-372, 1-18 (2020). In Vietnam.
11. Nguyen Truong Luu et al.. Flight measured from 1:50 000 scale gamma spectrum and 1: 100 000 scale gravity measurement in the central region of Vietnam. Information Center, Geological Archives, Hanoi, 218 pages, (2000). In Vietnam.
12. Nguyen Truong Luu et al. Flight measured from the gamma spectrum at the scale of 1:50 000 and measured the gravity at the scale of 1:100 000 in the southern Pleiku region. Information Center, Geological Archives, Hanoi, 159 pages (2014). In Vietnam
13. Nguyen Xuan Son et al. Flight results measured from the 1: 50 000 scale gamma spectrum and measured in the Kon Tum area. Information Center, Geological Archives, Hanoi, 259 pages (2000). In Vietnam.
14. Phan T. H., Petrov A.V., Do M. Ph. Processing and interpretation of gravity data anomalies in the central Vietnam using the «COSCAD 3D» computer technology. Young- earth sciences, MGRI-RGGRU, Moscow, 293-297 (2020). https://www.mgri.ru/science/scientific-practical-conference/2020/TOM%204%20(1).pdf
15. Petrov A.V. Methods of adaptive filtering and multivariate analysis of variance in the computer system for processing geophysical information "COSCAD 3D". Doctoral thesis, 192 pages (1997).
16. Petrov A.V., Yudin D.B., Soeli Hou. Processing and interpretation of geophysical data by methods of a probabilistic-statistical approach using computer technology "COSCAD 3D". Earth sciences, 2, UDC 551-214, 126-132 (2010). http://www.kscnet.ru/kraesc/2010/2010_16/art13.pdf
17. Petrov A.V., Zinovkin S.V., Osipenkov D.Yu., Yudin D.B. Computer technology of statistical and spectral-correlation analysis of data "COSCAD 3D". Geoinformatics, 4, 7-13 (2011). https://elibrary.ru/item.asp?id=17109032
18. Petrov A.V., Yudin D.B. Computer technology of statistical and spectral - correlation analysis of areal geophysical information presented by profile observations "COSCAD-profile" Modern geophysical and geoinformation systems. Earth sciences, 2, UDC 551-214, 76-84 (2008)..
19. Petrov A.V., Trusov A.A. Computer technology of statistical and spectral-correlation analysis of three-dimensional geoinformation "COSCAD 3D". Geophysics, 4, 29-33 (2000). https://elibrary.ru/item.asp?id=23719797
20. Quyen Minh Nguyen, Quinglai Feng, Jian-Wei Zi, Tianyu Zhao, Hai Thanh Tran, Thanh Xuan Ngo, Dung My Tran, Hung Quoc Nguyen. Cambrian intra-oceanic arc trondhjemite and tonalite in the Tam Ky – Phuoc Son Suture zone, central Vietnam: Implications for the early Paleozoic assembly of the Indochina block. Gondwanna Research, 70, 151-170 (2019). DOI:10.1016/j.gr.2019.01.002
21. Tran Van Tri, Nguyen Xuan Bao. Map of geological structure at 1:500 000 scale in the central region of Vietnam. Information Center, Geological Archives, Hanoi (2008). In Vietnam.

The Collision Between Indochina and South China Blocks in Northwestern Vietnam and its Controversy

Khuong The HUNG[1)], Jan GOLONKA[2)], Nguyen Khac DU[3)]

[1)] Hanoi University of Mining and Geology, Hanoi, Vietnam; e-mail: khuongthehung@humg.edu.vn (corresponding author); ORCID ID: 0000-0003-1544-6470

[2)] AGH University of Kraków, Kraków, Poland; ORICD: e-mail: jgolonka@agh.edu.pl; ORCID ID: 0000-0001-9671-5809

3) Hanoi University of Mining and Geology, Hanoi, Vietnam; e-mail: nguyenkhacdu@humg.edu.vn; ORCID ID: 0000-0003-1513-7600

http://doi.org/10.29227/IM-2023-02-18

Submission date: 20-08-2023 | Review date: 09-09-2023

Abstract

The Indosinian orogeny, which was regarded as the collision event between the South China and Indochina blocks that occurred in Southeast Asia, including Vietnam, resulting in the formation of the Indosinian mountain range. However, the question of how many times collision between these blocks occurred in the past and during which period remains unanswered. Furthermore, the closure of the ancient ocean and the evidence of its remnants between the South China and Indochina Blocks are still the subjects of serious debate. The underlying origin of the Indosinian thermo-tectonism is uncertain. The entire region was affected by the thermal-tectonic processes in the west, caused by the collision of the Sibumasu plate and Indochina block. The absence of evidence supporting the Indosinian as a significant mountain-building event is highlighted through an examination of regional paleogeography, as well as palaeontological and thermochronological data. There is no conclusive evidence to suggest that the Indochina and South China blocks collided during the Triassic times. A plate tectonic scenario that describes the Indosinian orogeny as a reactivation event triggered by the accretion of the Sibumasu block to Indochina is favored.

Keywords: *Indochina block, South China block, collision, Indosinian orogeny*

1. Introduction

For years, the collision between the Indochina Block (ICB) and South China Block (SCB) in Vietnam has been a subject of debate among geologists (Lepvrier et al., 2004; Maluski et al., 2001; 2005; Golonka et al., 2006; Faure et al., 2014; 2018; Thanh et al., 2018). Many assert that the collision took place during the late Permian - early Triassic, around 240 to 260 Ma ago, and it is thought to have significantly contributed to the formation of Vietnam's intricate geological structure (Hanski et al., 2004; Hoa et al., 2008, Hieu et al., 2013; 2017; Hieu, 2017). Moreover, the tectonic activities involving the ICB and ICB are notably intricate. Geological boundaries, which are defined as tectonic sutures representing the juncture of two geological blocks, have been identified in various locations within the ICB. At least three principal sutures have been recognized: 1) The Ordovician-Silurian Tam Ky - Phuoc Son suture, formed as a result of the amalgamation of the SCB and ICB (Tran et al., 2014; Gardner et al., 2017). 2) The Middle Triassic Song Ma suture zone, arising from the fusion of the ICB and SCB (Zhang et al., 2013); and 3) The Late Triassic suture, which emerged from the convergence of the ICB, SCB and Sibumasu blocks (Golonka et al., 2018). While some of these sutures have undergone extensive research, such as the Song Ma suture zone, others are in the initial stages of investigation. Notably, the Sibumasu and ICB interaction has garnered substantial attention in countries like Thailand, Cambodia, Malaysia, and Laos, but has been relatively understudied in Vietnam.

Nevertheless, there is a divergence of opinions among geologists regarding the collision's precise mechanism and timing. Some propose that the collision was a gradual process spanning millions of years, whereas others argue that it was a sudden, violent event. Additionally, there is controversy regarding the direction of the collision, with some suggesting that the ICB moved northward into the SCB (Hung, 2010), while others assert that the reverse happened (Maluski et al., 2001; 2005). Despite these debates, most geologists concur that the collision was a significant occurrence in Vietnam's geological past and continues to shape the country's landscape and natural resources to this day. The goal of this research is to provide a comprehensive outlook on the collision between the SCB and the ICB by investigating the potential timeframe of the collision and correlating the structures and geological formations in this tectonic zone. Furthermore, this research highlights the limitations that necessitate further exploration in the future.

2. Geological Background

East and Southeast Asia consist of various terranes and blocks that originated from the northern edge of Gondwanaland (Leloup et al., 1995, 2001; Findlay, 1997, Findlay & Trinh, 1997; Nam, 1998; Fan, 2000; Carter et al., 2001; Golonka et al., 2006). Continental blocks were created through successive rifting and breakup in the Palaeozoic and Mesozoic eras, leading to the northward movement and amalgamation of present-day Southeast Asia. The closing of Paleotethys between the blocks resulted in the creation of sutures such as Song Ma, Song Da, and Nan-Uttaradit (Metcalfe 1994, 1996, 1998, 2011; Golonka et al., 2006). Vietnam includes parts of the ICB and SCB. The SCB, which includes southern China and a northeast fragment of Vietnam, is separated from North China, ICB, the Sibumasu block, and the Songpan-Ganzi ac-

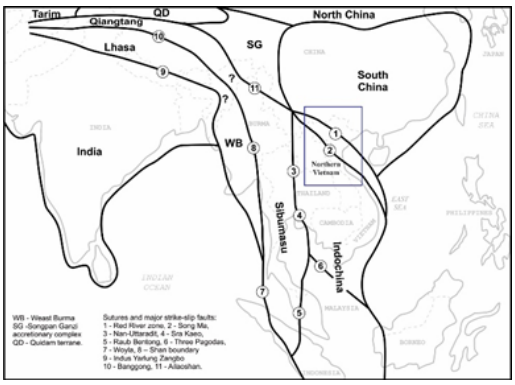

Fig. 1. Main plates and terranes of Southeast Asia and location of northern Vietnam (after Metcalfe, 1998; Golonka et al., 2006)

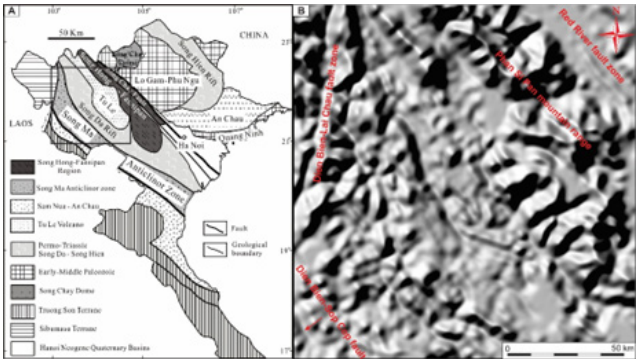

Fig. 2. A – Tectonic sketch map of northern Vietnam showing the location of the study area (after Tri et al., 1979). B – Northwestern Vietnam marked on the digital elevation model showing the Red River, Dien Bien-Lai Chau fault zones, Dien Bien-Sop Cop fault, and Phan Si Pan mountain range

cretionary complex by various sutures. The core of SCB was formed dủing Precambrian times. The southeastern margin of South China is recently a passive margin connected to the South China Sea by an extended continental crust.

The ICB consists of Vietnam, Laos, Cambodia, western Thailand, and potentially other regions. It is separated from the SCB by the Song Ma suture and from the Sibumasu plate by various sutures (Fig. 1). The Ailao Shan-Red River (ASRR) shear zone caused significant sinistral displacement around 27±22 Ma and resulted in the tectonic structure of Northwestern Vietnam. The Song Ma belt, where mafic and ultramafic masses are located, separates ICB from SCB and is thought to be composed of ophiolitic fragments. Recent studies suggest that the Indosinian event, which caused regional metamorphism and magmatism, occurred around 250 Ma, indicating that the final suturing between ICB and SCB took place during the Early Triassic times. However, further research is needed to fully understand the Indosinian orogeny and its constituent rocks.

Vietnam is a country located in Southeast Asia, encompassing an area of discontinuous geology such as the Red River and Dien Bien – Lai Chau fault zones (Fig. 2). It is bordered by China to the north, Laos, and Cambodia to the west, and the East Sea (South China Sea) to the east and south. The area has distinct landforms varying from north to south due to climatic, tectonic, and lithological factors. The geology of the area comprises ophiolite complexes, intrusion complexes, volcanic rocks, and terrigenous and carbonate sedimentary rocks, with ages ranging from Proterozoic to the present. The scope of this research includes the study of the Song Hong (Red River), Song Da (Da River), Tu Le, Song Ma, and Sam Nua regions, which correspond to northwestern Vietnam. Northwestern Vietnam is bounded by the boundary between China and Vietnam to the north, the boundary between Vietnam and Laos to the south, the Red River fault to the east, and the Dien Bien-Sop Cop fault zone to the west.

3. Materials and methods

3.1. Sample collection and analysis methods

The authors conducted field work in several localities in Northwestern Vietnam. This work was focused on magmatics as well as sedimentary rocks and their tectonic relationship. The granitoids and ophiolite complexes crop out along the SCB and ICB boundary indicating various Paleozoic and Mesozoic collisional stages. The studies of tectonic deformation revealed several unconformities affecting both magmatic and sedimentary rocks, the details are provided in the discussion chapter.

In order to determine age, provenance and tectonic setting, approximately 5 kg of ultra-mafic to mafic rock samples were collected along National Highway 4G in the Song Ma area (Figs. 3, 4 & 5); are pulverized to a particle size of 0.5 mm, followed by a washing and rinsing process using deionized water to eliminate dust and lighter minerals. Zircon crystals are subsequently isolated from the heavy mineral fraction through a series of procedures that include drying, magnetic separation, and enrichment via bromoform solvent. Manual selection of zircon grains is then conducted under microscopic observation to identify well-formed grains with minimal or no inclusions. This entire sample preparation protocol is executed at Thuong Pho Analytical Technology Co., Ltd., located in Wuhan, China.

Zircon grains selected from sample SL-03 are affixed to an epoxy resin disc and polished until the central region of each grain is exposed (Fig. 6). This facilitates subsequent structural and compositional analyses, as well as cathodoluminescence

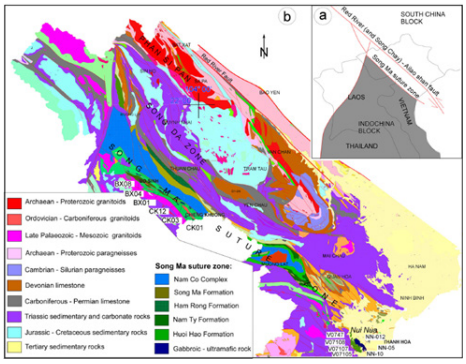

Fig. 3. (a) Geological map of the Paleotethys Orogen in southwest China and southeast Asian (modified from Jian et al., 2009) showing the main tectonic blocks and suture. (b) Simplified geologic map of Northwest Vietnam showing the Song Ma zone (after Bao & Luong, 1982)

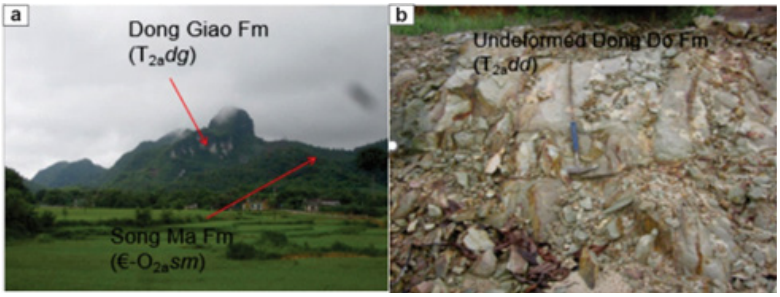

Fig. 4. (a) Limestone of the Dong Giao formation overlying the Song Ma formation (photo from Thanh et al., 2015); (b) Undeformed limestone of the Dong Do formation

(CL) imaging, which is performed using Scanning Electron Microscopy (SEM). Prior to CL imaging, the zircon samples undergo examination under a polarizing microscope, and reflected light micrographs are captured to identify optimal sites for U-Pb isotopic analysis. Care is taken to avoid regions with fractures or inclusions that could compromise the accuracy of age determinations (Fig. 6).

The U-Pb isotopic composition of the zircon is analyzed using a single-spot laser ablation technique, employing a laser with a 34-micrometer diameter, on an Inductively Coupled Plasma Mass Spectrometer (ICP-MS). This analysis is conducted at the National Key Laboratory of the China University of Geosciences in Wuhan.

3.2. Paleogeographic reconstruction maps

The recontraction of main tectonic events enable to position ICB and SCB on the global paleogeographic maps. The global maps are constructed using a plate tectonic model, which describes the relative motions between approximately 300 plates and terranes (Golonka, 2007). His motion is based on the Euler theorem (Euler, 1736, 1741), each plate travels around the Euler pole - intersection of the Euler axis with the Earth's surface defined by latitude/longitude coordinates. The plate's movement is measured in degrees. The total distance of the plate relocation from a given ancient time until present constitutes the finite pole of rotation. The list of this finite poles of rotation for tectonic elements is contained in the rotation file. The examples of such rotation file are provided in Golonka (2007 and 2020) papers. The global paleogeography for Triassic times was reconstructed using this model (Figs. 7, 8).

4. Discussions

4.1. The collision between the SCB and ICB based on global plate tectonics and paleogeography

Krobicki and Golonka's (2008) examination of plate tectonics and paleogeography in Southeast Asia indicated that SCB and ICB were separated by deep-water basins containing thinned continental or possibly oceanic crust during the Ordovician times, which is supported by the presence of Ordovician-Silurian sediments and uplift and volcanic rocks (Hung, 2010). Shouxin and Yongyi (1991) reported that the southern part of SCB was covered by deep water synorogenic clastic deposits, which were also found on the margins of the ICB and known as the Pa Ham Formation in Northern Vietnam. These deep-water deposits were later replaced by shallow-water sedimentary formations, including the continental Lower Devonian red beds and Lower Devonian Nam Pia Formation composed mainly of terrigenous sediments and marl, medium-bedded to massive fine-grained limestone, representing shallow water sediments (Hung, 2010; Son et al., 1978). The Lower Paleozoic greenschists of deep-sea origin were unconformably covered in many localities by Devonian redbeds. The first time the ICB collided with the SCB during the collisional process is likely to have been in the Late Silurian-Early Devonian times (Golonka et al., 2023). The Song Chay complex granitoid is connected to this event. Plate tectonic reconstructions suggest that the Early Devonian deformation and uplift may be linked to the rifting of the SCB from Gondwanaland. This event may also be related to the global Caledonian orogenic event. After Devonian shallow-water sedimentary rocks, the area was covered by Carboniferous-Permian sequences, including limestone of the Carboniferous-Permian Bac Son formation, clay shale of the Lower-Middle Permian Si Phay formation, and limestone of the Middle Permian Na Vang formation. A new oceanic basin was formed between ICB and SCB during Late Permian times, recorded by the ophiolite belt consisting of Nui Nua, Bo Xinh, Chieng Khuong complexes, Huoi Hao formation, and perhaps ultramafic Ban

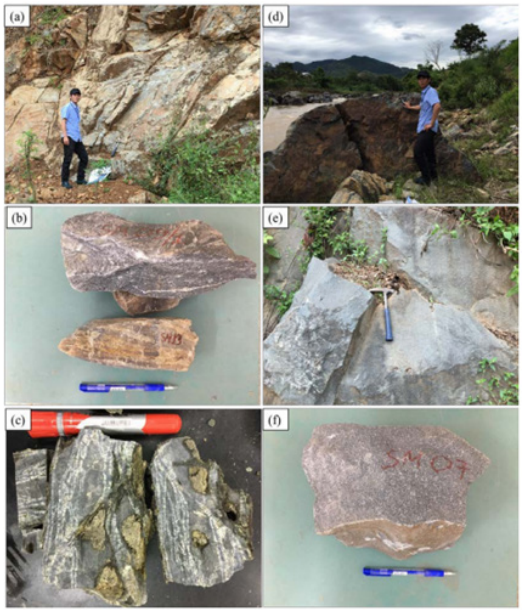

Fig. 5. (a, b, c) Outcrop and deformed samples of ultra-mafic to mafic rocks, with an age of 257±5.5 Ma, along National Highway 4G in the Song Ma area; (d, e, f) Outcrop and collected samples of ultra-mafic to mafic rocks along the Song Ma River, exhibiting undeformated, and with uncertain/ intrusive age within the Huoi Hao formation (Fig. 6)

Xang complex. The origin of this basin is related to the Paleotethys Ocean's closure between Sibumasu and ICB by subduction below Indochina (Golonka et al., 2006; Hung, 2010).

According to the study conducted by Hieu (et al., 2014), the U-Pb zircon dating results of the intrusive gabbroic rock phase within the ultra-mafic rocks of Nui Nua complex indicate an age of 470 Ma. As a result, it can be deduced that the ultra-mafic block of the Nui Nua complex predates the Middle Ordovician times. Additionally, the presence of freshwater fish fossils in central Vietnam provides evidence supporting the connection between the ICB and SCB prior to the Middle Devonian times (Thanh et al., 1996).

In the Song Ma region, specifically in the Son La province, there are Triassic limestone deposits with considerable thicknesses reaching hundreds of meters. Notably, these deposits exhibit minimal disturbance from the Dong Do and Dong Giao formations (Figs. 3, 4). This observation implies that their formation took place in a passive continental margin setting, as opposed to an active continental margin.

During the survey conducted from Hanoi to Son La, various gabbroic blocks of relatively young age (257±5.5 Ma) were encountered (Figs 5, 6), along with other blocks that exhibit undeformation. This observation implies that these blocks were formed subsequent to the collision between the SCB and the ICB. The formation process is likely associated with extensional activities within the SCB during the Indosinian orogeny, gradually subducting beneath the Song Ma suture zone. These blocks now remain as fragments situated above smaller units. As a result, misconceptions have arisen regarding the chronological sequence of the older ophiolitic belt's formation.

The distribution of Triassic limestone in Vietnam is extensive, stretching from northwester Vietnam to Quang Binh province in the northeast direction, covering a distance of approximately 1000 km (Fig. 3). One notable characteristic of the Middle Triassic limestone is its predominant occurrence in the eastern part of Vietnam, rather than in the western part. This observation suggests a subduction model where the oceanic crust adjacent to SCB subducts beneath the ICB, contrary to the view presented by Hung (2010). However, explaining the relationship between SCB and ICB presents difficulties in accounting for the widespread distribution of Triassic limestone formations in the region. Therefore, the proposed model suggests that the passive continental margin environment on the SCB provides a more plausible explanation for limestone formation in this area, while limestone formation is absent on the ICB. Additionally, this model offers a more reasonable explanation for the presence of mafic, ultra-mafic, and basalt rocks in the Da River zone as result of plume mantles activity.

During the Permian times, a volcanic eruption occurred in the Song Da region, which is thought to be linked to the origin of the Cam Thuy and Vien Nam formations. The cause of this event is still the subject of hot debate. Some geologists argued that Cam Thuy and Vien Nam formations were perhaps related to the plate reorganization and mantle plume activity, known in China and Indochina as Emeishan plumes and related to Siberian basaltic traps (Hanski et al., 2004; Hoa et al., 2008; Krobicki & Golonka, 2008 and references therein). They were formed in within-plate (intraplate) settings, related to back-arcs spreading (Lepvrier et al., 1997, 2004; Golonka et al., 2006) or Song Da Rift of Tri (ed., 1979). The preferred geodynamic reconstruction assumes that this magmatism was formed during the convergence of the Sibumasu and the newly formed ICB-SCB. The oceanic crust was subducted southward under ICB (Hoa et al., 2008). This subduction led to the origin of Late Permian – Triassic magmatic events and Song Da volcanism (Hung, 2010).

Remnants of oceanic lithosphere were accreted into the northern edge of the IDB and appeared in the Song Ma fault zone and Sam Nua zone (Golonka et al., 2006; Trung et al., 2007 and references therein). The Indosinian orogeny of Fromaget (1937, 1941) represents the final stage of this closure. The orogeny was recorded by magmatic, metamorphic, and deformation events in Truong Son, Sam Nua, Nam Co, and Song Ma structural zones (Hutchison, 1989; Nam, 1998; Lep-

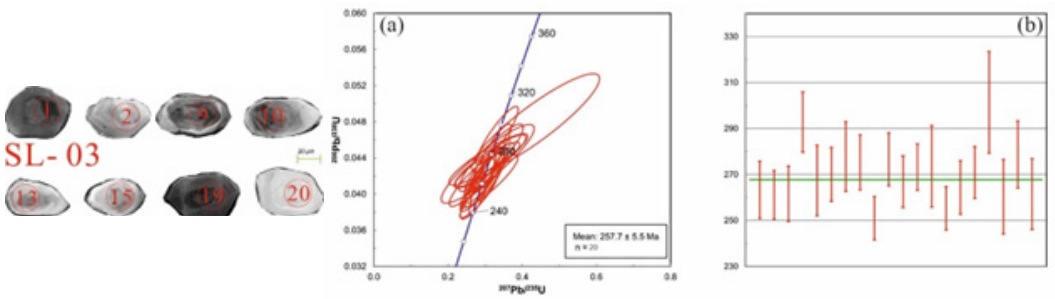

Fig. 6. The CL images of zircon crystals extracted from the SL-03 gabbro sample in the Song Ma area, Son La province, are accompanied by the corresponding locations of the analysis points using the LA-ICP-MS method; (a) The graphical representation illustrates the outcomes of the zircon U-Pb analysis conducted on the SL-03 gabbro sample, employing the LA-ICP-MS technique. (b) A schematic diagram is presented to depict the distribution of average ages observed in the dataset

Fig. 7. Global plate tectonic map of Late Triassic at 224 Ma ago. Molweide Projection. 1–oceanic spreading center and transform faults, 2–subduction zone, 3–thrust fault, 4–normal fault, 5–transform fault

vrier et al., 1997, 2004, 2008; Lan et al., 2000). The folded Triassic and older rocks were unconformably covered by Upper Triassic coal-bearing molasse beds of the Suoi Bang Formation. A plate tectonic scenario that describes the Indosinian as a reactivation event triggered by the accretion of the Sibumasu block to Indochina is preferred (Golonka et al., 2018). The new large Chinese-SE Asian plate including North and South China, Mongolia, and eastern Cimmerian plates was consolidated at the Triassic-Jurassic boundary (Figs 7, 8).

4.2. The collision between the SCB and ICB based on structural and collision timing

In northwestern Vietnam, the Song Ma structural zone is regarded as the "hinge" between the SCB and ICB (Dovijkov, 1965). The studied area is known as the Sam Nua-Hoanh Son pre-rift basin (Tung and Tri, 1992). The basin has an S-shape, bulging in the middle and narrowing at both ends. The northern end of the basin is adjacent to the western edge of the Song Ma fold belt. The Sam Nua-Hoanh Son basin underwent significant evolution during the Triassic, and it was filled with shallow marine sedimentary rocks of the Carboniferous-Lower Permian system, with a thickness of 1000-1500m (Bao & Luong, 1982).

According to Wang et al. (2021), the Vit Thu Lu calc-alkaline arc-like granodiorite and granite, along with the Thanh Long plagiogranite, have been dated to approximately 475-470 Ma (Bui et al., 2018). In the Huoi Tong massif in western Dien Bien area, the granitoids formed between 446 and 415 Ma (Nguyen et al., 2005). Monazite inclusions found in garnets from schist yielded a Sm-Nd isochron metamorphic age of 424 ± 15 Ma (Maluski et al., 2005; Tran et al., 2014).

These observations, combined with the regional angular unconformity between the Silurian and Devonian sequences located to the north of the Song Ma zone (Thanh et al., 1996; Janvier et al., 1997, 2003; Tran and Vu, 2011; Tran et al., 2014, 2020), provide evidence for the northward subduction and consumption of the Tam Ky-Phuoc Son Ocean, resulting in its accretion with the southern Yangtze in the Ordovician-Silurian times, approximately between 480-415 Ma. This geological process was also contemporaneous with the northward accretion of the Kontum terrane and its southern counterparts (Gardner et al., 2017; Tran et al., 2020).

Faure et al. (2018) utilized zircon and monazite U/Pb radiometric dating techniques to establish an age of approximately 250–240 Ma for the crustal melting process (Fig. 9). Concurrently, ductile shearing with a top-to-the-NW movement occurred, coinciding with the formation of the Ngoc Linh MCC. This period of extensional tectonics was succeeded by dextral strike-slip faulting at around 240–230 Ma, preceding the emplacement of two-mica granitic plutons at approximately 240–224 Ma. Additionally, in the Ngoc Linh and Kan Nack complexes, zircon and monazite analyses yielded U-Pb ages from the Early Paleozoic era. In the Kham Duc complex, a metamorphic event featuring garnet-biotite-staurolite-kyanite minerals occurred at around 460 Ma (MP/MT), followed by migmatites at approximately 450 Ma. The Dai Loc plutonic suite, dated to 420–400 Ma, and the Dien Binh calc-alkaline granodiorite, dated to 450–425 Ma, provide evidence of an Early Paleozoic geological event.

Zircon U-Pb dating of silicic igneous rocks in the Pingxiang area, southwest China, reveals that the rhyolites and biotite granites were emplaced at 251–250 and 249 Ma (Early

Triassic), respectively (Huang et al., 2023). By synthesizing all available data in conjunction with the regional tectonic evolution of the southwestern Youjiang Basin and adjacent regions, we ascribe the origin of the peraluminous A2-type rhyolites and biotite granites to the extensional setting that prevailed during oceanic subduction. This subduction was initiated by the rollback of the Paleotethys oceanic lithosphere around 251–249 Ma. This study underscores that subduction-related magmatism associated with the Paleotethys oceanic lithosphere remained active during the Early Triassic.

In Xu's (2023) study, granitoids within the SCB were investigated. The results revealed that Late Triassic granitoids exhibit a singular peak age of approximately 230 Ma and predominantly consist of granites, as evidenced in SiO_2 vs Na_2O+K_2O diagrams. The youngest U-Pb ages obtained from detrital zircons suggest a maximum depositional age ranging from 196 to 180 Ma (Meng et al., 2015; Xu et al., 2021). Furthermore, the NNE-striking structures were intruded by a Late Jurassic granitic pluton. Consequently, it is plausible that the NNE-striking eastern Hunan thrust belt might have formed during the Middle Jurassic.

Detrital zircon U-Pb dating results from eleven samples within the Ailaoshan-Song Ma suture zone reveal prominent age peaks at 245 Ma, 440 Ma, and 970 Ma, corresponding to tectonic events recognized in the SCB and ICB (Li et al., 2021). In-situ Hf isotopic analyses suggest that these Neoproterozoic and Early Paleozoic events indicate significant episodes of continental growth with mantle contributions. Along the suture zone, the ophiolitic mélange zone has been subdivided into three units, denoted as M1, M2, and M3, based on disparities in zircon age and Hf isotopic signatures. M1 exhibits two primary age groups, peaking at approximately 435 Ma and 970 Ma. The source of M1 is likely the Paleozoic sedimentary cover, predominantly Silurian sedimentary rocks from ICB, with a minor contribution from magmatic rocks within the ophiolitic mélange.

M2 is characterized by a dominant Late Permian (260 Ma) age group with εHf(t) values ranging from -1 to +7 and a significant peak at approximately 0.85 Ga in model ages. The primary source of M2 is considered to be the Eastern Lhasa Indus-Yarlung Zangbo suture (ELIP) and related rocks in SCB, with a minor fraction of detrital zircons originating from recycled sedimentary rocks in ICB.

M3 exhibits a distinct Mesozoic age peak at 250 Ma, with εHf(t) values ranging from -17 to -5 and two-stage model ages primarily concentrated in the range of 1.3 Ga to 1.8 Ga. M3 materials were primarily supplied from the magmatic arc in ICB (Western Ailaoshan-Truong Son belt), with a minor contribution from the southwest margin of SCB. The observed differences between these three units highlight significant lateral heterogeneity within the suture zone. These findings provide valuable insights into understanding the paleogeographic reconstructions of the postulated positions of Asian continental blocks from the Early Carboniferous to the Middle Triassic. Supplementary data related to this article can be accessed online at https://doi.org/10.1016/j.earscirev.2021.103789.

In the study conducted by Liu et al. (2023), they present findings concerning the heterogeneity within the Ailaoshan–Song Ma ophiolitic mélange. All examined samples exhibit a consistent zircon age spectrum, featuring two distinct age peaks at 430 and 960 Ma, which closely align with the characteristics of the previously identified M1 unit. These results suggest that the northwestern segment of the Ailaoshan ophiolitic mélange can be more accurately subdivided into two units, namely M1 in the interior and M2 in the exterior, as opposed to the previous classification. This observation underscores the presence of strike-perpendicular heterogeneity within the region. Furthermore, considering the geometries of these units, characterized by a northeast-dipping orientation, and their respective depositional ages (M1, 310–270 Ma; M2, 260–240 Ma), it becomes evident that the older M1 unit has been thrust upon the younger M2 unit. This indicates a tectonic inversion process..

M2 is situated within the northwestern segment and displays a solitary age peak at 260 Ma (Li et al., 2021). Conversely, M3 is distributed in the southeastern segment of the Ailaoshan–Song Ma ophiolitic mélange, with its most prominent age peak recorded at 245 Ma (Li et al., 2021). The distribution pattern of M1, M2, and M3 along the Ailaoshan–Song Ma ophiolitic mélange reveals a substantial heterogeneity, highlighting variations in provenance among distinct segments of the Ailaoshan–Song Ma Ocean (Li et al., 2021; Lin et al., 2022). These differing provenances of the three units correspond to the various evolutionary stages of the eastern Palaeo-Tethys (Li et al., 2021; Wang et al., 2021).

To sum up, there are varying views regarding the timing of the amalgamation of the SCB and the ICB, as well as the age of the Song Ma suture zone, which include the Permian-Triassic (Indosinian orogeny) and Silurian-Early Devonian (Caledonian orogeny). These issues require further elucidation.

Similarly to the Triassic volcanic formations, the Jurassic intrusive-volcanic complex of the Muong Hin-Ban Muong type also requires further detailed investigation. Some studies, based on geological relationships and structural features, have disputed the existence of Jurassic magma activity in the study area and instead have merged it into the Triassic magma complex (Truong, 1999). However, detailed research data for these formations is still very limited and lacks reliable quantitative data, especially for trace elements and isotopes. It is necessary to determine the U-Pb zircon isotope age for the Muong Hin volcanic formation and the Ban Muong intrusive volcanic features. Additionally, comparing their trace element geochemical characteristics with those of the middle Triassic magmatism (Dong Trau-Song Ma) would enable more definitive conclusions.

The Sam Nua depression basin is considered a unique tectonic-structural zone in the Truong Son fold belt (Dovjikov, 1965). While in the past, the Permian-Triassic granitoid without associated volcanic rocks were regarded as part of the basement of the Mesozoic north central Vietnam basin, the current perspective views the Nui Chua-Phia Bioc contrasting magma complex as a product of the continental crustal re-melting process (anatexis), similar to the Triassic volcanic-intrusive formations. As a result, the crystalline basement of the Sam Nua basin could be even older. Therefore, the evolutionary history of the north central Vietnam Mesozoic basin needs to be associated with modern tectonic concepts, particularly the linkage between the SCB and ICB.

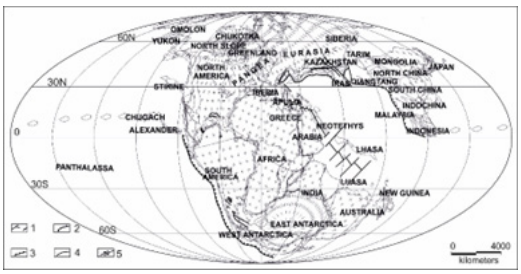

Fig. 8. Global plate tectonic map of Late Triassic at 200 Ma ago. Molweide Projection. 1–oceanic spreading center and transform faults, 2–subduction zone, 3–thrust fault, 4–normal fault, 5–transform fault

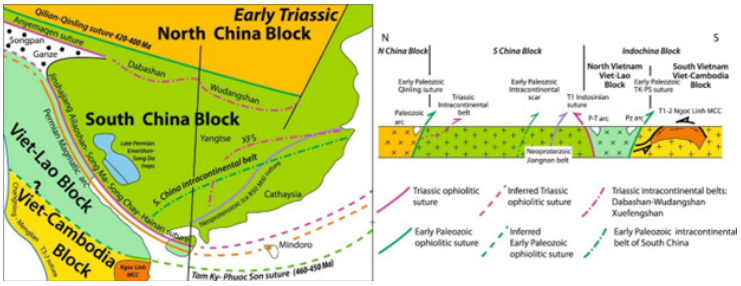

Fig. 9. Reconstruction of the ICB-SCB tectonic framework in Early Triassic. A: Palinspastic map after removing the Cenozoic sinistral strikeslip motion, and the Triassic dextral strike-slip along the late Indosinian faults. In this reconstruction, the Emeishan-Song Da LIP is about 1200 km from the Ngoc Linh MCC. B: schematic crustal scale cross section from N. China to Kon Tum massif (after Faure et al., 2018)

5. Conclusion

The complex tectonic, magmatic, metamorphic, and deformation events that took place and were overprinted in northwestern Vietnam have made it challenging to pinpoint the timing of the collision between SCB and ICB in the area. Despite the complexity of the geological events in this region, the current recorded evidence suggests that the timing of the collision is as follows.

During the Ordovician times, the SCB and ICB were separated by deep-water basins with thinned continental or possibly oceanic crust. The first collision between ICB and SCB possibly occurred during the Late Silurian-Early Devonian, leading to the formation of a new oceanic basin between the two blocks during the Late Permian times. This basin's origin is related to the subduction of the Paleotethys Ocean below ICB, and it is recorded by the ophiolite belt consisting of several complexes and formations. The Indosinian orogeny represents the final stage of this closure and was marked by magmatic, metamorphic, and deformation events in various structural zones. The orogeny was triggered by the accretion of the Sibumasu block to ICB, leading to the consolidation of a new large Chinese-SE Asian plate at the Triassic-Jurassic boundary.

The issues that require further clarification from the aforementioned explanations persist. For instance, there is limited evidence of oceanic crust remnants during the Early Devonian times. Specifically, the specific evidence for the Permian-Triassic magma period in northwestern Vietnam does not exhibit typical characteristics of mountain-building magma but rather is associated with an intra-plate geodynamic environment. To address this issue, it is necessary to clarify the nature of Triassic sedimentary-volcanic formations using quantitative data on their chemical composition, trace elements, and isotope content, which can be interpreted based on the principles of petrogenesis.

Acknowledgements

This research is supported by the Vietnam National Foundation for Science and Technology Development (NAFOSTED), under grant number 105.01-2020.13.

Literatura – References

1. Bao, N.X. & Luong, T.D., 1982. Geological map of Vietnam at 1:500,000 with a summary explanatory note. Geological Department of Vietnam, Ha Noi, 52 pp.
2. Bui, V.H., Kim, Y., Thanh, N.X., Tran, T.H., Yi, K., 2018. Neoproterozoic deposition and Triassic metamorphism of metasedimentary rocks in the Nam Co Complex, Song Ma Suture Zone, NW Vietnam. Geosciences Journal, 22 (4), 549–568.
3. Carter, A., Roques, D. & Bristow, C., 2001. Understanding Mesozoic accretion in Southeast Asia: Significance of Triassic thermotectonism (Indosinian orogeny) in Vietnam. Geology, 29: 311-314.
4. Dovjikov, A.E. (ed.), My, B.P., Vasilevskaia, E.D., Jamoida, A. I., Ivanov, G.V., Izokh, E. P., Huu, L.D., Mareitchev, A.I., Chien, N.V., Tri, N.T., Luong, T.D., Quang, P.V. & Long, P.D., 1965. Geology of North Vietnam. Explanatory note of the Geological Map of North Vietnam at 1:500,000 scale. Geological Department of Vietnam, Ha Noi, 584 pp.
5. Euler, L., 1736. Mechanica sive motus scientia analytice expositat. Academia Scientiarum, Petersburg, Russia. 546 pp.
6. Euler, L., 1741. Theorematum quorundam ad numeros primos spectantium demonstratio. Commentarii academiae scientiarum Petropolitanae, 8: 141–146.
7. Fan, P.F., 2000. Accreted terranes and mineral deposits of Indochina. Journal of Asian Earth Sciences, 18: 343-350.
8. Faure, M., Lepvrier, C., Nguyen, V.V., Vu, T.V., Lin, W., Chen, Z., 2014. The South China block-Indochina collision: Where, when, and how ?. Journal of Asian Earth Sciences, 79, 260-274.
9. Faure, M., Nguyen, V.V., Hoai, L.T.T., Lepvrier, C., 2018. Early Paleozoic or Early-Middle Triassic collision between the South China and Indochina Blocks: The controversy resolved? Structural insights from the Kon Tum massif (Central Vietnam). Journal of Asian Earth Sciences, 166, 162-180.
10. Findlay, R. & Trinh, P.T., 1997. The structural setting of Song Ma region, Vietnam and the Indochina - South China plate boundary problem. Gondwana Research, 1: 11-33.
11. Findlay, R., 1997. The Song Ma Anticlinorium, northern Vietnam: The structure of an allochthonous terrane containing early Palaeozoic island arc sequence. Journal of Asian Earth Sciences, 15: 453-464.
12. Gardner, C.J., Graham, I.T., Belousova, E., Booth, G.W., Greig, A., 2017. Evidence for Ordovician subduction–related magmatismin the Truong Son Terrane, SE Laos: implications for Gondwana evolution and porphyry Cu exploration potential in SE Asia. Gondwana Research, 44, 139–156
13. Golonka, J. 2007. Late Triassic and Early Jurassic paleogeography of the world. Palaeogeography, Palaeoclimatology, Palaeoecology, 244, 297–307.
14. Golonka, J. 2020. Late Devonian paleogeography in the framework of global plate tectonics. Global and Planetary Change, 86, 103129, https://doi.org/10.1016/j.gloplacha.2020.103129
15. Golonka, J., Embry, A., Krobicki, M., 2018. Late Triassic Global Plate Tectonics. In: Tanner L. (eds) The Late Triassic World. Topics in Geobiology, vol 46. Springer, Cham. pp 27-57.
16. Golonka, J., Hung, K.T., , Du, N.K., Krobicki, M., 2023. The eastern extension of the Avalonian terranes, the Prototethys and Paleotethys oceans. Geotourism, 20(1-2): 72-73.
17. Golonka, J., Krobicki, M., Pająk, J., Giang, N.V. & Zuchiewicz, W., 2006. Global plate tectonics and paleogeography of Southeast Asia. Faculty of Geology, Geophysics and Environmental Protection. AGH University of Science and Technology, Arkadia, Kraków, 1-128
18. Golonka, J., Krobicki, M., Słomka, T., Hung, K.T., Giang, N.V., 2018. The Indosinian orogeny in South-East Asia. Biuletyn AGH, 128-129, 14-16.
19. Hanski, E., Richard, J. W., Hannu, H., Polyakov, G.V., Pavel, A.B., Hoa, T.T. & Phuong, N.T., 2004. Origin of the Permian-Triassic komatiites, northwestern Vietnam. Contributions to Mineralogy and Petrology, 147, 453–469.
20. Hieu, P.T., 2017. The LA-ICP-MS U-Pb zircon age of riolite from the Dong Trau formation and its geological significances. Science & Technology Development, 5, 262–269.
21. Hieu, P.T., Chen, F.K., Thuy, N.T.B., Cuong, N.Q., and Li, S.Q., 2013. Geochemistry and zircon U-Pb ages and Hf isotopic compositions of Permian alkali granitoids of the Phan Si Pan Zone in northwestern Vietnam. Journal of Geodynamics, 69, 106–121.
22. Hieu, P.T., Li, S.Q., Yu, Y., Thanh, N.X., Le Tu, V., Siebel, W., and Chen, F., 2017. Stages of late Paleozoic to early Mesozoic magmatism in the Song Ma belt, NW Vietnam: evidence from zircon U–Pb geochronology and Hf isotope composition. International Journal of Earth Sciences, 106, 855–874.
23. Hieu, P.T., Son, L.M., Dung, L.T., Thanh, N.X., 2014. 470 Ma Gabbro-diabase in the Nui Nua area and its tectonic significance. Vietnam Journal of Geology, Series A, 340: 1-10 (in Vietnamese).

24. Hoa, T.T., Anh, T.T., Phuong, N.T., Dung, P.T., Anh, T.V., Andrey, E.I., Alexander, S.B., Lan, C.Y., Chung, S.L., Lo, C.H., 2008. Permo-Triassic intermediate–felsic magmatism of the Truong Son belt, eastern margin of Indochina. Comptes Rendus Geoscience, 340, 112–126.

25. Huang, W.M., Liu, X.J., Liu, L., Li, Z.L., Liu, X., Wu, H., 2023. Early Triassic roll-back of subducted Paleo-Tethys oceanic lithosphere: Insights from A2-type silicic igneous rocks in the Pingxiang area, southwest China. Geosphere, 19(X): 1-27, https://doi.org/10.1130/GES02617.1.

26. Hung, K.T., 2010. Overview of magmatism in northwestern Vietnam. Annales Societatis Geologorum Poloniae, 80 (2), 185-226.

27. Hutchison, C.S., 1989. Geological Evolution of Southeast Asia. Oxford Monographs on Geology and Geophysics, Oxford, UK, Clarendon Press, 376 pp.

28. Janvier, P., Thanh, T.D., Phuong, T.H., Truong, D.N., 1997. The Devonian vertebrates (Placodermi, Sarcopterygii) from central Vietnam and their bearing on the Devonian palaeogeography of Southeast Asia. Journal of Asian Earth Sciences, 15 (4–5), 393–406.

29. Janvier, P., Racheboeuf, P., Huu, H.N., Nhat, T.D., 2003. Devonian fish (Placodermi, Antiarcha) from Tra Ban Island (Bai Tu Long Bay, Quang Ninh Province, Vietnam) and the question of the age of the Do Son Formation. Journal of Asian Earth Sciences, 21 (7), 795–801

30. Jian, P., Liu, D.Y., Kröner, A., Zhang, Q., Wang, Y.Z., Sun, X.M., Zhang, W., 2009. Devonian to Permian plate tectonic cycle of the Paleo-Tethys Orogen in southwest China (II): insights from zircon ages of ophiolites, arc/back-arc assemblages and within-plate igneous rocks and generation of the Emeishan CFB province. Lithos 113, 767–784.

31. Krobicki, M., & Golonka, J., 2008. Emeishan volcanism of northwestern Vietnam and their connection with SE Asia palaeogeography and Permian/Triassic mass extinction event. Gondwana 13, Dali, China: 96-97 (in abstract).

32. Lan, C.Y., Chung, S.L., Shen, J.J., Lo, C.H., Wang, P.L., Hoa, T.T., Thanh, H.H., and Mertzman, S.A., 2000. Geochemical and Sr-Nd isotopic characteristics of granitic rocks from northern Vietnam. Journal of Asian Earth Sciences, 18, 267–280.

33. Leloup, P.H., Amaud, N., Lacassin, R., Kienast, J.R., Harrison, T.M., Trinh, P.T., Replumaz, A. & Tapponnier, P., 2001. New constraints on the structure, thermochronology, and timing of the Ailao Shan-Red River shear zone, SE Asia. Journal of Geophysical Research, 106 (B4), 6683-6732.

34. Leloup, P.H., Tapponnier, P., Lacassin, R., Searle, M.P., Dailai, Z., Xiaoshan, L., Langshang, Z., Shaocheng, J. & Trinh, P.T., 1995. The Ailao Shan-Red River shear zone (Yunnan, China). Tertiary transform boundary of Indochina. Tectonophysics, 251, 3-84.

35. Lepvrier, C., Maluski, H., 2008. The Triassic Indosinian orogeny in East Asia. C. R. Geoscience, 340, 75-82.

36. Lepvrier, C., Maluski, H., Van Vuong, N., Roques, D., Axente, V., and Rangin, C., 1997. Indosinian NW-trending shear zones within the Truong Son belt (Vietnam) 40Ar-39Ar Triassic ages and Cretaceous to Cenozoic overprints, Tectonophysics, 283, 105–127.

37. Lepvrier, C., Maluski, H., Vu, V.T., Leyreloup, A., Phan, T.T., and Nguyen, V.V., 2004. The early Triassic Indosinian orogeny in Vietnam (Truong Son Belt and Kontum massif): implication for the geodynamic evolution of Indochina, Tectonophysics, 393, 87–118.

38. Li, Q., Lin, W., Wang, Y., Faure, M., Meng, L., Wang, H., ... & Van Vu, T., 2021. Detrital zircon UPb age distributions and Hf isotopic constraints of the Ailaoshan-Song Ma Suture Zone and their paleogeographic implications for the Eastern Paleo-Tethys evolution. Earth-Science Reviews, 221, 103789. https://doi.org/10.1016/j.earscirev.2021.103789.

39. Lin, W., Wang, Y., Liu, F., Meng, L.T., Ji, W.B., Wei, W., Chu, Y., Song, C., Wu, Q.Y., 2022. Matrix of the ophiolitic mélange zone and its tectonic implications: Insights of the eastern Paleo-Tethys. Acta Geol. Sin. 96 (10), 3449–3467 (in Chinese with English abstract).

40. Liu, F., Lin, W., Wang, Y., Meng, L., Faure, M., Vuong, N.V., Wu, Q., Chu, Y., Wei, W., Hoai, L.T.T., Tich, V.V., Li, Q., Wang, H. & Chen, K., 2023. Heterogeneity of the Ailaoshan–Song Ma ophiolitic mélange and its palaeogeographic implications for the evolution of Eastern Palaeo-Tethys. Tectonophysics, 858, 229848.

41. Maluski, H., Lepvrier, C., Jolivet, L., Carter, A., Roques, D., Beyssac, O., Ta Trong Tang, Nguyen Duc Thang, Avigad D., 2001. Ar–Ar and fission -track ages in the Song Chay Massif: Early Triassic and Cenozoic tectonics in Northern Vietnam, Journal of Asian Earth Sciences, 19, 233-248

42. Maluski, H., Lepvrier, C., Layreloup, A., Vu Van Tich, Phan Truong Thi, 2005. 40Ar-39Ar geochronology of the charnokites and granulites of the Kan Nack Complex, Kon Tun Massif, Vietnam. Journal of Asian Earth Sciences, 25, 653-677.

43. Meng, L., Li, Z.X., Chen, H., Li, X.H., Zhu, C., 2015. Detrital zircon U-Pb geochronology, Hf isotopes and geochemistry constraints on crustal growth and Mesozoic tectonics of southeastern China. J. Asian Earth Sci. 105, 286–299.

44. Metcalfe, I., 1994. Late Paleozoic and Mesozoic Paleogeography of Eastern Pangea and Tethys. In: Embry, A. F., Beauchamp, B., Glass, D. J. (Eds.), Pangea: Global environment and resources. Canadian Society of Petroleum Geologists Memoir, 17, 97-111.

45. Metcalfe, I., 1996. Gondwanaland dispersion, Asian accretion and evolution of eastern Tethys, In: Li, Z.X., Metcalfe, I., Powell, C.M, (eds.), Breakup of Rodinia and Gondwanaland and assembly of Asia. Australian Journal of Earth Sciences, 43, 605-623.

46. Metcalfe, I., 1998. Biogeography and Geological Evolution of SE Asia. Backhuys Publishers: Netherlands; 25–41.

47. Metcalfe, I., 2011. Paleozoic-Mesozoic history of SE Asia. Geological Society Special Publication, 355, 7-35.

48. Metcalfe, I., 2021. Multiple Tethyan ocean basins and orogenic belts in Asia, Gondwana Research, 100, 87-130.

49. Nam, T.N., 1998. Thermotectonic events from Early Proterozoic to Miocene in the Indochina craton: implication of K±Ar ages in Vietnam. Journal of Asian Earth Sciences, 16, 475-484.

50. Nguyen, V.N., Hoang, Q.C., Ha, X.B., Le, D.N., Nguyen, T.B.T., Dao, D.T., 2005. U–Pb Zircon Age of Granitoids of the Huoi Tong Complex. Department of Geology and Mineral Resources of Vietnam, Hanoi, pp. 164–170 (in Vietnamese).

51. Shouxin, Z. & Yongyi, Z., 1991. The geology of China. In: Moullade, M. & Nairn, A. E. M. (eds),The Palaeozoic. A The Phanerozoic Geology of the WorldI. Elsevier, Amsterdam: 219-274

52. Son, P. (ed.), Thuc, D.D., Thang, N.D. & Ty, T.V., 1974 (compiled), 1978 (revised). Geological map of Vietnam at 1:200,000 scale. Son La sheet, with the explanatory note "Geology of the Son La sheet". Geological Department of Vietnam, Ha Noi, 118 pp.

53. Thanh, T.D., Janvier, P., Phuong, T.H., 1996. Fish suggest continental connections between Indochina and South China Blocks in Middle Devonian time. Geology 24 (6), 571–574

54. Thanh, N.X., Santosh, M., Hai, T.T., Hieu, T.P., 2015. Subduction initiation of Indochina and South China blocks: insight from the forearc ophiolitic peridotites of the Song Ma Suture Zone in Vietnam. Geological journal, 51(3): 421-442.

55. Thanh, T.V., Hieu, P.T., Minh, P., Nhuan, D.V. & Thuy, N.T.B., 2019. Late Permian-Triassic granitic rocks of Vietnam: the Muong Lat example. International Geology Review, 61:15, 1823-1841, DOI: 10.1080/00206814.2018.1561335.

56. Tran, H.T., Zaw, K., Halpin, J.A., Manaka, T., Meffre, S., Lai, C.K., Lee, Y., Le, H.V., Dinh, S., 2014. The Tam Ky-Phuoc Son Shear Zone in central Vietnam: tectonic and metallogenic implications. Gondwana Res. 26, 144–164.

57. Tran, T.V., Faure, M., Nguyen, V.V., Bui, H.H., Fyhn, M.B.W., Nguyen, Q.T., Lepvrier, C., Thomsen, T.B., Tani, K., Charusiri, P., 2020. Neoproterozoic to early Triassic tectono–stratigraphic evolution of Indochina and adjacent areas: a review with new data. Journal of Asian Earth Sciences, 191, 104231

58. Tri, T.V. (ed.), 1979 (1977 in Vietnamese). Geology of Vietnam, (the North part). Explanatory note to the geological map on 1:1,000,000 scales. Ha Noi, Science and Technology. Publishing House, 354 pp. (In Vietnamese), 78 pp. (In English).

59. Tri, T.V. & Khuc, V. (ed.), 2011. Geology and Earth Resources of Vietnam. General Department of Geology and Minerals of Vietnam. Publishing House for Science and Technology, Hanoi.

60. Trung, N.M., Nuong, N.D. & Itaya, T., 2007. Rb-Sr Isochron and K-Ar ages of igneous rocks from the Sam Nua Depression Zone in Northern Vietnam. Journal of Mineralogical and Petrological Sciences, 102: 86-92

61. Truong, P.D. (ed), 1999. Report on geological and mineral resources in the Son La sheet group at scale of 1:50,000. General Department of Geology and Minerals of Vietnam (in Vietnamese).

62. Tung, N.X. & Tri, T.V., 1992. The geologic formations and dynamics of Vietnam. Institute of Geology and Mineral resources of Vietnam, Ha Noi, 269 pp (in Vietnamese).

63. Wang, Y., Zhang, Y., Qian, X., Wang, Y., Cawood, P.A., Gan, C., Senebouttalath, V., 2021. Early Paleozoic accretionary orogenesis in the northeastern Indochina and implications for the paleogeography of East Gondwana: constraints from igneous and sedimentary rocks. Lithos, 382–383, 105921, https://doi.org/10.1016/j.lithos.2020.105921.

64. Xu, X., Liang, C., Chen, J., Xu, Y., 2021. Provenance analysis of Jurassic basins along Chaling-Chenzhou-Linwu Fault, South China: implications for palaeogeographic reconstruction and Mesozoic tectonic transition. Geol. J. 56 (5), 2656–2675.

65. Xu, X., 2023. Late Triassic to Middle Jurassic tectonic evolution of the South China Block: Geodynamic transition from the Paleo-Tethys to the Paleo-Pacific regimes, Earth-Science Reviews, https://doi.org/10.1016/j.earscirev.2023.104404

66. Zhang, R.Y., Lo, C.H., Chung, S.L., Grove, M., Omori, S., Hzuka, Y., Liou, J.G., Tri, T.V., 2013. Origin and Tectonic Implication of Ophiolite and Eclogite in theSong Ma Suture Zone between the South China and IndochinaBlocks. Journal of Metamorphic Geology, 31, 49–62. https://doi:10.1111/jmg.12012

Challenges to the Development of Unconventional Natural Gas – The Case of Shale Gas

LE Minh Thong[1)], TRAN Van Hiep[2)], DO Huu Tung[3)]

[1)] Faculty of Economics and Business Administration, Hanoi University of Mining and Geology, Vietnam; ORCID 0000-0002-8250-3394
[2)] Faculty of Economics and Business Administration, Hanoi University of Mining and Geology, Vietnam
[3)] Faculty of Economics and Business Administration, Hanoi University of Mining and Geology, Vietnam; ORCID 0009-0006-7427-6378
* Corresponding author: leminhthong@humg.edu.vn

http://doi.org/10.29227/IM-2023-02-19

Submission date: 17-08-2023 | Review date: 22-09-2023

Abstract

The world is undergoing a radical transition to a low-carbon economy and natural gas is considered an important bridge in the transition of energy in the world. The potential for natural gas, especially unconventional gas, is very large, which will significantly affect the future energy structure in all regions of the world. However, the conditions for developing these resources are different between regions and countries. The development of unconventional gas is now facing many challenges, even opposition because the problem of extracting unconventional gas is very complex and the total impact is unknown. Therefore, at present, the expansion of unconventional gas remains a question for countries that possess and desire to exploit these resources. This article will analyze the opportunity and challenges of unconventional gas relying on the development of shale gas in recently.

Keywords: *unconventional gas, shale gas, challenge*

1. Introduction

1.1. Trends in the energy transition in the world today

The world is making a radical transition to a low-carbon economy, reducing dependence on fossil energy, and adapting to climate change. Low-carbon energy is an energy source that produces less greenhouse gas emissions than traditional energy sources such as wind, solar, geothermal, and nuclear. In addition, low-carbon energy also includes low-emission energy sources such as natural gas and carbon dioxide treatment technologies such as carbon capture technology. However, compared with traditional energy sources, being able to develop these types of energy requires a huge investment in technology, techniques, investment capital, and time. With renewable energy, the most important issues today are technology and cost. As for nuclear energy, although it is a clean energy source, its safety is still controversial.

In the current context, natural gas is considered as an intermediate energy source in the process of mankind's transition from traditional energy sources to renewable energy due to its superior properties. Although natural gas is also a fossil energy source by nature, natural gas is a clean energy source compared to oil and coal. When burned in the same amount, natural gas emits very little CO_2, only half as much as coal, and 75% as much as petroleum, it also emits very few other toxic substances and produces less carbon dioxide, dust as well as mercury (EIA, 1998). Because of this, natural gas is considered as a fuel that is friendly to humans and the environment, which has been used very widely in many different fields and will continue to be used more in the future compared to other fossil energy sources. Even, according to the forecast of the World Energy Organization, humanity is entering the golden age of natural gas to replace oil.

1.2. Natural gas reserves in the world

As estimated by recent studies, global natural gas reserves are abundant, and progress has been made thanks to technological developments. Thanks to improved exploration methods, the world's natural gas reserves are increasing. In particular, the recent rapid development of technology has allowed people to exploit unconventional gases that are considered to have very large reserves, most notably the recent revolution of oil and gas shale in the United States.

Many gas reservoirs and deposits have been associated with the term unconventional gas. Unconventional gas resources, such as shale gas, coalbed methane, and tight gas, have emerged as potential alternative energy sources to meet the growing global energy demand (Boyer et al., 2007). In general, unconventional gases are gas resources trapped in deep, low-permeability clayey rocks or in coal deposits and difficult to trap in high density in conventional natural reservoirs. Rock permeability is measured in units called millidarcy (md) and gas passed through rocks with permeability less than 0.1md has been classified as unconventional gas. The gas flows in a well is a function of the permeability, but also of other variables such as the pressure of the reservoir, as well as its radius and the viscosity of the gas (McGlade et al, 2012). They represent significant underground reserves whose exploitation remains complex and costly.

At the end of 2020, according to BP statistics, proven natural gas reserves are around 190 Tm3 which equates to almost 50 years of consumption at current levels. The increase in proven natural gas reserves in the world over the past several years has been much faster than incineration production in some countries. The average annual growth rate of natural gas reserves in the world from 2009 to now is about 1.2%/year. The growth rate of natural gas reserves in the period 2009 to date has been concentrated mainly in North America (4.7%/year) mainly due to the rapid development of traditional gas, especially shale gas in the US, followed by the area of the former Soviet Union (2.7%/year); Although Middle Eastern countries hold about 40% of the world's total natural gas re-

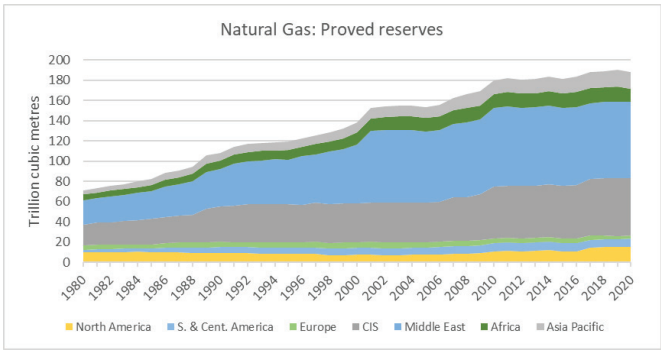

Fig. 1. Changes in proven reserves of natural gas in the world. Source: (BP, 2022)

serves at present, the rate of increase in reserves in the recent period tends to be slow with about 0.3%/year.

Thus, gas reserves in the world are still on increasing trend, natural gas is still discovered in different regions of the world, however, the contribution to the increase in the current gas reserves in the world is mainly focused on the discovery of unconventional gas sources, especially shale gas. The discovery of unconventional natural gas fields has changed the picture of natural gas reserves and influenced geopolitics in many regions of the world. For example, according to IFP, in the US, shale gas reserves account for more than four times the reserves of conventional gas, which has a great influence on the future energy development strategy of the US.

1.3. Forecast of future demand for natural gas

The growth of the global economy and the increase in the population leads to the growth of energy demand and consumption. Besides, natural gas is likely to play a significant role in the global power generation mix due to its lower carbon emissions compared to coal and oil. As countries seek to reduce greenhouse gas emissions, natural gas-fired power plants may serve as a transitional energy source, especially when combined with renewable energy integration. As countries seek to reduce greenhouse gas emissions, natural gas-fired power plants may serve as a transitional energy source, especially when combined with renewable energy integration.

As a result, by many estimates, the demand for natural gas is expected to grow more than any other fossil energy source. All energy scenarios of world energy organizations or scenarios of oil companies, both offer a promising long-term future for natural gas. In many scenarios, natural gas will be the world's leading source of energy by 2050 (IGU, 2015). For example, according to an analysis by Exxon Mobil, 40% of global energy demand growth between 2014 and 2040 is expected to be met by natural gas (Exxon Mobil, 2016). Following the estimate of BP, the growth rate of about 1.4% per year in demand (BP, 2016).

According to the IEA, most of the major increase in energy demand will come from non-OECD countries. Non-OECD Asian countries will contribute about 60% of the increase in demand with the most prominent factor until 2025 being China before overtaking India. Global energy demand in 2040 will be 37% higher than 2012 levels in the New Policies scenario. The energy sector is the biggest driver of climate change, with 65% of all anthropogenic greenhouse gas emissions (IPCC, 2014). Therefore, establishing a sustainable and environmentally friendly energy system model is a top priority for energy and climate policymakers around the world, and natural gas is an important bridge in the energy transfer process.

Similarly, according to the IEA in its 'Golden Age of Natural Gas' report, by consuming more natural gas, the world could achieve its overall CO_2 reduction target. According to the IEA, global demand for natural gas is expected to grow by 50% between 2014 and 2040, faster than other fuels and more than twice as fast as oil. Most of the increase in natural gas demand has come from emerging economies, with China and India together accounting for about 30% of the increase and the Middle East with more than 20%.

According to the IEA scenarios in the "World Energy Outlook" reports from 2010 to 2020, the demand for natural gas will increase steadily, but the magnitude of the increase will vary from year to year and from region to region. The following table shows the growth rate of natural gas under the IEA scenario.

Natural gas has a faster rise than any other energy source. The average growth rate of demand for natural gas in the world ranges from 1.2% to 1.7 %/year while that of oil is only about 0.3 - 0.5 %/year. The demand for coal is even forecast to decrease in recent years. It is forecasted that by 2040 natural gas will overtake coal as the second largest source of energy in total primary energy demand. In the world, the Asian region will be the main growth driver for natural gas demand in the future with a very high rate of 2.9% to 4.3% per year.

2. Potential and development of unconventional gas

2.1. Unconventional gas evolution and its effects

Although unconventional gases have been known for a long time, the potential and development of non-traditional gases and their impact on the energy market are only about a decade ago. Today, known unconventional gases include coal-bed methane (CBM), shale gas, tight gas, and hydrate gas. Especially from 2005 up to now, the development of shale gas in the US has become a phenomenon, a revolution in the energy field. This development has had a lot of impacts not only on the US gas market but also on the global gas market.

Unconventional gas production is also growing rapidly in other parts of the world. In 2010, Australia produced only a small amount of coal-bed methane (about 5 billion m3 of gas), 2015 became a liquid gas producer from coal-bed methane. Other countries such as China, India, and Indonesia also have activities to find and develop non-traditional gas energy sources including coal-bed methane and shale gas. With the development of shale gas, the proven reserves of natural gas

Tab. 1. Growth Rates of natural gas until 2040 in New Policies Scenarios of IEA. Source : IEA(2010); IEA (2011); IEA (2012a); IEA (2013); IEA (2014); IEA (2015); IEA (2016); IEA (2017); IEA (2018); (IEA, 2019); (IEA, 2020); (IEA, 2021)

Region	WEO 2010	WEO 2011	WEO 2012	WEO 2013	WEO 2014	WEO 2015	WEO 2016	WEO 2017	WEO 2018	WEO 2019	WEO 2020
Total world energy	**1.20%**	**1.3%**	**1.2%**	**1.2%**	**1.1%**	**1.0%**	**1.0%**	**1.0%**	**1.0%**	**1.0%**	**0.8%**
- Petroleum demand	0.5%	0.6%	0.5%	0.5%	0.5%	0.4%	0.4%	0.5%	0.5%	0.4%	0.3%
- Coal demand	0.6%	0.8%	0.8%	0.7%	0.5%	0.4%	0.2%	0.2%	0.1%	-0.1%	-0.6%
- Gas demand	1.4%	1.7%	1.6%	1.6%	1.6%	1.4%	1.5%	1.6%	1.6%	1.4%	1.2%
North America's gas demand	**0.4%**	**0.6%**	**0.8%**	**0.8%**	**1.0%**	**0.7%**	**0.7%**	**0.7%**	**0.8%**	**0.6%**	**0.3%**
Euro's gas demand	**0.5%**	**0.9%**	**0.7%**	**0.6%**	**0.7%**	**0.1%**	**0.4%**	**0.3%**	**-0.1%**	**-0.4%**	**-0.6%**
Asia's gas demand	**3.8%**	**4.3%**	**4.2%**	**4.2%**	**3.8%**	**3.6%**	**3.6%**	**3.0%**	**3.1%**	**2.9%**	**2.9%**

in the United States have increased significantly. Shale gas has helped the US to overtake Russia to become the largest gas producer in the world since 2009. According to the data of EIA, shale gas production in the US represented more than half of national natural gas production in 2015, and more than 67% in 2021 (EIA, 2023)

The shale gas revolution has already led to economic benefits and cost reduction at the state and local levels, individual sectors, and the nation. The exploitation of unconventional gas fields, particularly shale gas, influenced the United States' economic growth. According to the Thomas study in 2014, the macroeconomic impact is relatively limited: around 0.88% growth in the gross domestic product (GDP) between 2007 and 2012 (Spencer et al., 2014). According to the International Monetary Fund (IMF) report in 2013, the shale gas revolution's macroeconomic impact is between 0.3% and 1% of the US GDP that year (International Monetary Fund, 2013). The shale gas contribution to the American gross domestic product was more than $76.9 billion in 2010; in 2015 it will be $118.2 billion and will triple to $230 billion in 2035 (Wang et al., 2014).

The development of shale gas has helped the US achieve self-sufficiency in energy, improvements in the trade balance, and tax revenues. It helped to reduce the import of fossil fuels, therefore improving trade balance, and simultaneously representing a supplement to the federal budget. In 2012, the sector also generated $ 62 billion in additional tax revenue for the federal budget, the States, and the municipalities concerned (OPECST, 2013).

The development of shale gas in the United States has been the catalyst for the recovery of traditional industries. Natural gas strengthens industries as raw materials, for example, the petrochemical industry, fertilizer producers, plastics, and other industries that consume a great deal of energy as aluminum smelters, steel mills, refineries, etc. The decline of the gas price contributed to the competitiveness enhancement of these sectors in the global competition.

The increase in production of unconventional gas, in particular shale gas, and the strong decline in the natural gas price in the United States, have led to reductions in the consumption of coal in the electricity sector, at the same time increases of using natural gas in this sector. The volume of consumption increase in the electric power sector is about 60% of the total growth (Bros, 2012). Reports by the US Energy Agency and the International Energy Agency indicate that carbon emissions from burning fossil fuels in the US have plummeted in recent years. From 2007 to 2012, the United States reduced its total carbon dioxide emissions by 450 million tons, the largest reduction on record on the planet. In 2012, the United States reduced its emissions by about 70% of the CO_2 established under the Kyoto Protocol. The main reason for the reduction in CO_2 emissions was the significant conversion from coal to natural gas in the production of electricity.

2.2. The potential of unconventional gas

Until now, knowledge of unconventional gas in general and shale gas in particular in the world is very weak and uncertain, except in the North American region. Estimates of unconventional gas resources are very different around the world. They depend on many factors such as geological information, technologies, and methods used, the number of exploration drilling. In the United States, with a favorable policy as well as the development of technologies in this industry, there are many publications on the estimation of the potential of unconventional gas and shale gas. Outside of North America, the unconventional gas industry is still in its infancy and important questions still need to be answered (Le, 2018) (Le et al., 2021).

Many organizations have carried out research on unconventional gas, particularly shale gas, such as the United States Energy Information Administration (EIA), the United States Geological Survey (USGS), the Energy International (IEA). Unconventional gas estimates have been published, especially by the EIA. In parallel with these studies and estimates relating to the United States, the EIA has studied the potential of unconventional gases in other regions or other countries. Although the data in each publication is different, they form an important basis for a general view of shale gas in the world.

Unconventional gas is considered increasingly playing an important role in securing the global natural gas supply. According to forecasts by the international energy organization, unconventional gas will account for more than 60% of the increase in total gas production in the period from now to 2040.

Although so far, forecasts on natural gas resources, especially unconventional natural gas, are still at a level of uncertainty. However, according to the International Energy Agency forecasts in 2017, the renewable resource of traditional natural gas is about 430 trillion cubic metres (Tcm), allowing about 120 years to be exploited at current production levels. For unconventional gas, the forecasted total recoverable shale gas resources are 239 Tcm, coal-bed methane is 50 Tcm, and tight gas is 81 Tcm. Hydrate gas is considered very large with a forecast of 10 times shale gas; however, the exploitation technology is still difficult. If adding both conventional and un-

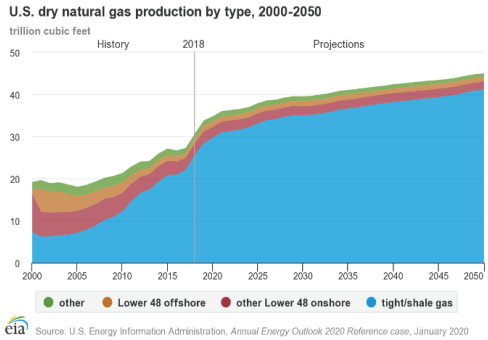

Fig. 2. Forecast of US gas production. Source: EIA, 2020

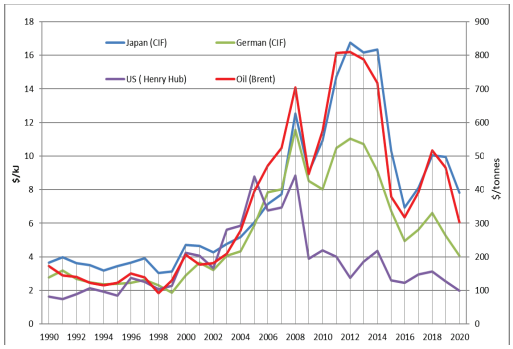

Fig. 3. World gas prices. Source: (BP, 2022)

conventional gas, about 250 years can be satisfied if exploited at current production.

Of the unconventional natural gases, shale gas is the potential gas with the largest reserves. Recent studies by scientists have shown that the potential for shale gas is huge, its forecast reserves are increasing, and this gas is widely distributed in many continental countries, this opens many opportunities for its exploitation and uses in the future, contributing to satisfying human needs for natural gas. According to recent publications by the US Energy Agency (EIA) and the American Geological Association, the total recoverable resource reserves of shale gas in 46 countries are assessed by the organization as 219.65 Tcm. Shale gas resources are concentrated mainly in China; Argentina; Algeria; the United States (EIA, 2013a) (EIA, 2015).

3. The challenges of unconventional gas development – case of shale gas

3.1.Basic conditions for the development of unconventional gas

Knowledge about the location of unconventional gas deposits has been accumulated for decades, but it is the recent improvements in technologies for the exploitation of these resources that have contributed to economic development, resulting from a production boom in shale gas in the United States. In the opinion of the US Department of Energy (DOE), three important factors have reframed the economic viability of producing unconventional gas, particularly shale gas, (i) advances in horizontal drilling, (ii) advances in hydraulic fracturing, and (iii) the rapid increase in natural gas prices due to significant supply and demand pressures (Department of Energy, 2011).

The technology offers new opportunities for unconventional gas to play a major role in the future global energy mix and thus allay concerns about the reliability, profitability, and security of energy supplies. Horizontal drilling is a technique often used in shale gas deposits where the geology is significantly different from that of conventional oil and gas deposits. While horizontal drilling costs can be two to three times higher than vertical wells, it allows for more cost-effective gas production because it targets greater contact with gas plays. As a result, shale gas operators are increasingly relying on horizontal drilling to optimize recovery (Nakano, 2012). In the process of shale gas development, it is often necessary to combine horizontal wells with hydraulic fracturing to achieve economic exploitation. These two techniques play a key role in the development of unconventional gas production. However, the environmental rules were incomplete at the beginning of the exploitation of unconventional gases, which generated controversies about hydraulic fracturing (Barbier, 2014).

To make unconventional gas more accessible, a mixture of water, sand or other proppants, and specific chemicals are injected at high pressure into the unconventional gas reservoir. However, society's concerns about the consequences of unconventional gas production, in particular the threat of unacceptable environmental damage, have grown along with production. Reports of water contamination, earthquakes, and other disruptions to local communities have given the production of unconventional gas – and in particular the technique of hydraulic fracturing – very bad publicity in many countries (IEA, 2012a) (Le, 2018).

3.2. The challenges of unconventional gas development - lessons from shale gas in the United States

"The revolution" of shale gas in the United States has achieved a lot of success. However, the development of shale gas is facing a lot of obstacles and challenges. The exploitation of shale gas can have impacts on human health and the envi-

Tab. 2. Forecast of recoverable natural gas resources in the world. Source: IEA, 2018

Region	Traditional gas (Tcm)	Unconventional gas		
		Shale gas (Tcm)	Tight gas (Tcm)	Coal-bed methane (Tcm)
Eurasia	134	10	10	17
Middle East	103	11	9	-
Asia Pacific	44	53	21	21
North America	50	66	11	7
South America	28	41	15	-
Africa	51	40	10	-
Europe	19	18	5	5
Total world	**429**	**239**	**81**	**50**

ronment, such as water contamination and high consumption of this resource during the fracturing process. The impact of the development of shale gas on the environment is very strong. Therefore, the development of shale gas has created a lot of concern in the public and the percentage of opponents has risen sharply. By the analyze the development of shale gas in the United States, many scientists and experts have indicated the challenges that all countries that want to develop shale gas must face. These are vast obstacles that countries must overcome if they want development shale gas.

a. The water demand is very strong: The production of shale gas consumes a large volume of fresh water. On average, we need 12–20 million liters of water are typically needed per horizontal well in shale gas production. The amount of water needed in the hydraulic fracturing process depends on the type of shale gas and the fracturing operations. Water consumption will grow with the increase in the number of wells and shale gas production. Certainly, such a large volume of water and a high rate of withdrawals from the local surface or groundwater sources have a significant impact on the local water system. The consumption of water is particularly important in areas where drought conditions are often limited strictly to the availability of water and its use (Richardson N. et al., 2013).

b. The capacity of pollution of the groundwater and surface water: In the case of fracturing, a process that injects pressurized water and chemical compounds into underground rocks. This technology consumes a lot of water and chemicals, so it can lead to pollution in the environment throughout the drilling and exploitation process. The chemicals represent from 0.5 to 2% of fluids of hydraulic fracturing; many of them are toxic and carcinogenic (Wang et al., 2014). These hydraulic fracturing fluids are injected directly into the ground and they can influence groundwater sources. In addition, the flow-back or "produced" water from fracturing fluid might contaminate the water surface. For example, it is estimated that a well in the Barnett shale gas in the US requires an average of 15 million liters of water during its useful life, and between 80% and 95% of them will be discarded as wastewater (Absar et al., 2018). They may adversely influence human health and the quality of the environment if they are untreated or directly discharged onto the land or into streams, rivers, and lakes.

c. Generation of greenhouse gases: Another worrying factor regarding the environmental impact is the GHG emissions related to shale gas. Shale gas contains more than 90% of methane (CH4) which may contaminate the air and the water. Methane is a very powerful greenhouse gas compared to carbon dioxide. The effects of shale gas on climate change have become more complex to evaluate and controversial, partly because of uncertainty about the scale of methane leaks. Some researchers worry that expanded production of shale gas could increase the release of methane as fugitive emissions during the drilling, completion, production, transportation, and use of natural gas. This is one of the principal concerns because methane is a more potent "greenhouse gas" than CO_2, and thus, the fugitive emissions in the process of shale gas development may lead to a net increase in greenhouse gas emissions. From a holistic perspective, it is estimated that a shale gas well in Marcellus, US, emits about 5500 tons of GHG, or 1.8 g of carbon dioxide equivalent (CO_2e) / MJ (megajoule) of gas produced throughout its life cycle, representing an 11% increase in GHG emissions compared to conventional gas (He et al., 2018).

d. The production cost and price of natural gas: Economists believe that the marginal cost of real production in the USA could certainly reach $4 to $6 per kilojoules (kJ) (EIA, 2013b). Following many estimates of the production cost of shale gas in other regions, in Europe breakeven costs range from roughly $8 to $12 (Gény, 2010), in Asia Pacific this number is higher than 12 dollars per kJ because of the geological conditions of unconventional oil and gas reservoirs in these regions are more complex than those in North America, and the development technology and management mode are being explored and improved. For example, the full cost (cost of current profit and loss in the process of oil and gas production) of shale oil development in main basins in China ranges from 434-652 USD/tonne, which is much higher than that of Bakken shale oil in North America (an average of 217 USD/tonne), and there is still a significant gap to achieve benefit development (Guoxin et al., 2022).

Although the production cost of shale gas may decrease relying on technological progress, the price of gas currently in the international gas market is too low compared with the production cost of shale gas. At present, according to the data of the international gas report in December 2015 and January 2016, the price of gas at Henry Hub in the United States is very low about 2.1$/kJ; in the gas market in Japan the LKM spot LNG prices delivery closed at 6.5 $/kJ; in the Europe market, the natural gas price at NBP in the UK is about 5.5 $/kJ. Compared with the natural gas price at the end of 2014, le price of gas in the Europe and Asia market dropped about 3 times.

As a consequence of the falling of crude oil prices in recent years, the price of natural gas in the international gas market has been reducing strongly also. This price is less than the marginal cost of production in the long-term shale gas.

Therefore, with the price too low at present, it has reduced the interest of investors in shale gas. In fact, there are a lot of gas producers who have been reducing their production as well as abandoning their investments in shale gas development activities, comprised in the United States and other regions in the world, even going bankrupt.

On the contrary, when the natural gas price is high, it encourages investors in this sector. However, in the sectors of shale gas, the investors must invest much more money than in the project of conventional gas. Moreover, the life cycle of well shale gas is shorter than the well conventional natural gas, and the production of shale gas declines rapidly after the peak of production. So, it is necessary to continue the supply of investment capital to maintain production. At the same time when the high price of gas, the customers in particular in the sector of electricity, will find other energies which are cheaper to take the place of gas such as coal. So investment in shale gas will have a lot of risks, uncertainty, and difficulties.

e. The opposition from the population: A very important aspect of the development of shale gas in particular and unconventional gas in general is the "social license to operate" desirable for activities in this field. According to EIA, in the publication "Golden rules for a golden age of gas" in 2012, the need to build a "social license to operate" was emphasized (IEA, 2012b). Therefore, the absence of social acceptability, even the hostility of most of the population in the development of shale gas will be a greater restriction in the future, in particular in the countries European. The challenges associated with gaining public acceptance for shale gas development are much greater in Europe due to population density, stringent environmental regulations, water scarcity in certain regions, and the owners' lack of interest in shale gas exploration and production activities (Gény, 2010) (Lozano-Maya, 2013). Therefore, the conduct of the debate and the guarantee of local interests must take into account the opposition of the population in Europe because they can influence them (More T., 2013). For example, in France, in July 2011, through the "Jacob Law", prohibited the exploitation of shale gas by fracking. In the society's discussions on energy transition, which took place in 2012 and 2013, shale gas was not mentioned among the resources to be possibly explored in the future. In Germany, after a few years of debate, the German Parliament approved a bill in June 2016 that allowed the fracking of conventional oil and gas resources under strict environmental conditions but did not allow the use of the technique to exploit shale resources (Cantoni et al., 2018; Herrera, 2020). In Poland, the government wants to develop shale gas to reduce dependence on Russian gas sources, but due to geological difficulties conditions, prolonged legislative regulations, and declining gas prices on the world market in the early 2010s, leading to the failure of shale gas development in Poland, the shale gas companies here almost ceased operations in 2013 (Cantoni et al., 2018).

f. The uncertainty of resource estimation: as we present about the potential of unconventional in part 2.2 above, the estimates of unconventional gas resources in general, special shale gas are variable and uncertain. The uncertainty of the estimates will strongly influence the industry's future and the national energy policy. Therefore, the profitability potential of shale gas is still hard to predict. Except for the United States, other countries considered as holders of a significant potential for resources of shale gas have a lack of reliable estimates on the resources technically recoverable and resources economically recoverable. It could be a great obstacle to developing shale gases in the countries which desire to develop these resources.

4. Conclusion

Natural gas is a clean energy source, so the demand for this resource will inevitably increase in the future, especially in the context that all countries in the world must work together to prevent global climate change and the warming of the earth. Natural gas is an effective medium to short-term choice, a bridging energy medium while humanity is waiting for the transition of energy from traditional to renewable energy sources. Contrary to many previous predictions, today with the development of science and technology, technology allows people to discover and increase global natural gas reserves, especially unconventional gas sources. This will significantly add to the reserves and production of natural gas in the world, contributing to increasing demand for natural gas in the future.

The success of the United States in the development of unconventional gas in the past decade has been the subject of much debate and controversy around the world. Unconventional gas resources in general, shale gas, in particular, is an important additional gas source when conventional gas is running out. It can therefore play a major role in terms of energy security in the future. The success of the shale gas "revolution" in the United States is a great experience for other countries who want to develop this resource. However, there are also many doubts, a lack of confidence, and even a strong opposition to the development of unconventional gas. The problem of unconventional gas is complex, and the impacts are only partially known. Unconventional gas resource estimates are highly variable and uncertain. So, developing these unconventional gas resources will face many challenges. These will be huge barriers that strongly affect the prospects as well as the role of unconventional gas in particular, natural gas in general in the energy transition in the future.

Literatura – References

1. Absar S.M., Boulay A.-M., Campa M.F., Preston B.L., Taylor A., 2018. The tradeoff between water and carbon footprints of Barnett Shale gas. Journal of Cleaner Production 197, 47–56. https://doi.org/10.1016/j.jclepro.2018.06.140
2. Barbier F., 2014. L'impact économique de l'exploitation de gaz de schiste. Assemblée Nationale.
3. Boyer Ch. M., Frantz J.H., Jenkins C.D., 2007. Non-conventional gas. ENI, vol.3.
4. BP, 2022. BP Statistical Review of world energy 2022.
5. BP, 2016. BP Energy Outlook - 2016 edition.
6. Bros, T., 2012. After the US shale gas revolution. Technip, Paris.
7. Cantoni R., Klaes M.S., Lackerbauer S.I., Foltyn C., Keller R., 2018. Shale tales: Politics of knowledge and promises in Europe's shale gas discourses. The Extractive Industries and Society 5, 535–546. https://doi.org/10.1016/j.exis.2018.09.004
8. Department of Energy, 2011. Modern Shale Gas Development in the United States: A Primer - Geology, Regulations, Environmental Considerations, Hydraulic Fracturing, Protecting Groundwater, Pollution Threats. Progressive Management, S.l.
9. EIA, 2023. Shale Gas Production [WWW Document]. URL https://www.eia.gov/dnav/ng/NG_PROD_SHALEGAS_S1_A.htm (accessed 7.15.23).
10. EIA, 2020. Where our natural gas comes from - U.S. Energy Information Administration (EIA) [WWW Document]. URL https://www.eia.gov/energyexplained/natural-gas/where-our-natural-gas-comes-from.php (accessed 12.25.20).
11. EIA, 2015. U.S. Energy Information Administration (EIA) [WWW Document]. URL https://www.eia.gov/analysis/studies/worldshalegas/ (accessed 8.18.19).
12. EIA, 2013a. Shale Oil and Shale Gas Resources: An Assessment of 137 Shale Formations in 41 Countries Outside the US. EIA.
13. EIA, 2013b. Annual Energy Outlook 2013.
14. EIA, 1998. Natural Gas 1998: Issues and Trends.
15. ExxonMobil, 2016. The outlook for energy: a view to 2040.
16. Gény F., 2010. Can unconventional gas be a game changer in European gas markets? Oxford Institute for Energy Studies, Oxford.
17. Guoxin L., Zhengdong L., Weihong D., Hongyan W., Xingfan Z., Jian T., 2022. Progress, challenges and prospects of unconventional oil and gas development of CNPC. China Petroleum Exploration 27, 1. https://doi.org/10.3969/j.issn.1672-7703.2022.01.001
18. He L., Chen Y., Li J., 2018. A three-level framework for balancing the tradeoffs among the energy, water, and air-emission implications within the life-cycle shale gas supply chains. Resources, Conservation and Recycling 133, 206–228. https://doi.org/10.1016/j.resconrec.2018.02.015
19. Herrera H., 2020. The legal status of fracking worldwide: An environmental law and human rights perspective. URL https://gnhre.org/2020/01/the-legal-status-of-fracking-worldwide-an-environmental-law-and-human-rights-perspective/ (accessed 7.15.23).
20. IEA, 2021. World Energy Outlook 2021.
21. IEA, 2020. World Energy Outlook 2020.
22. IEA, 2019. World Energy Outlook 2019.
23. IEA, 2018. World Energy Outlook 2018.
24. IEA, 2017. World Energy Outlook 2017. OECD Publishing, Paris.
25. IEA, 2016. World energy outlook 2016. OECD/IEA, Paris.
26. IEA, 2015. World Energy Outlook 2015. OECD Publishing.
27. IEA, 2014. World energy outlook 2014. IEA.
28. IEA, 2013. World Energy Outlook 2013.
29. IEA, 2012a. World Energy Outlook 2012.
30. IEA, 2012b. Des Règles d'or pour un Âge d'or du gaz. EIA.
31. IEA, 2011. World Energy Outlook 2011.

32. IEA, OECD, 2010. World energy outlook 2010. OECD/IEA, Paris.
33. IGU, 2015. Prospects for Natural Gas: Identifying the key developments that will shape the gas market in 2050.
34. International Monetary Fund, 2013. United States: staff report for the 2012 article IV consultation.
35. IPCC, 2014. Climate change 2014.
36. Le M.-T., 2018. An assessment of the potential for the development of the shale gas industry in countries outside of North America. Heliyon 4, e00516. https://doi.org/10.1016/j.heliyon.2018.e00516
37. Le M.T., Do H.T., Nguyen T.T., Nguyen T.K.N., 2021. What prospects for shale gas in Asia? Case of shale gas in China. The Journal of World Energy Law & Business 13, 426–440. https://doi.org/10.1093/jwelb/jwaa037
38. Maya L., Roberto J., 2013. The United States experience as a reference of success for shale gas development: The case of Mexico. Energy Policy 62, 70–78. https://doi.org/10.1016/j.enpol.2013.07.088
39. McGlade C., Speirs J., Sorrell S., 2012. A review of regional and global estimates of unconventional gas resources. UK Energy Research Centre.
40. More T., 2013. La révolution du gaz de schiste aura-t-elle lieu en europe? Analyse comparative dans 14 pays européens. Institut Thomas More.
41. Nakano J., 2012. Prospects for shale gas development in Asia: examining potentials and challenges in China and India. Center for Strategic and International Studies, Washington.
42. OPECST, 2013. Rapport sur Les techniques alternatives à la fracturation hydraulique pour l'exploration et l'exploitation des hydrocarbures non conventionnels (No. 1581). Assemblée Nationale.
43. Richardson N., Gottlieb M., Krupnick A.J., Wiseman H., 2013. The State of State Shale Gas Regulations. RFF.
44. Spencer T., Sartor O., Mathieu M., 2014. Unconventional wisdom- economic analysis of US shale gas and implication for the EU. IDDRI.
45. Wang Q., Chen X., Jha A.N., Rogers H., 2014. Natural gas from shale formation – The evolution, evidences and challenges of shale gas revolution in United States. Renewable and Sustainable Energy Reviews 30, 1–28. https://doi.org/10.1016/j.rser.2013.08.065
46. Szymanek A., de las Obras-Loscertales M., Pajdak A.Effect of sorbent reactivity on flue gas desulphurization in fluidized-bed boilers under air firing mode. The Canadian Journal of Chemical Engineering, Volume 96, April 2018, 895-902

The Impact of Digital Leadership on Organizational Performance: A Study in Vietnam's coal Mining Companies

Le VAN CHIEN[1)]*, Nguyen DUC THANG[1)], Pham KIEN TRUNG[1)], Nguyen THI HOAI NGA[2)]

[1)] Hanoi University of Mining and Geology, Hanoi, 100000, Vietnam; email: levanchien@humg.edu.vn
[2)] Innovations for Sustainable and Responsible Mining (ISRM) Research Group, Hanoi University of Mining and Geology, Hanoi, 100000, Vietnam

http://doi.org/10.29227/IM-2023-02-20

Submission date: 20-08-2023 | Review date: 27-09-2023

Abstract

Under the influence of the 4th industrial revolution and the impact of the Covid-19 pandemic, digital transformation is rapidly taking place in all aspects of society. For businesses, digital transformation is an essential and objective trend for their sustainability and development. The purpose of digital transformation for businesses is to enhance operational efficiency through factors such as accelerating market speed, gaining competitive advantage, driving revenue growth, increasing labor productivity, and expanding customer attraction and retention. Numerous studies have indicated that the process of digital transformation in businesses is influenced by leadership and digital transformation strategies, and digital transformation has an impact on business performance. This study aims to identify the relationship between digital leadership and the operational efficiency of coal mining companies in Vietnam, with the mediating role of digital transformation strategies. Additionally, the study examines the moderating role of digital skills on the relationship between digital transformation strategies and the operational efficiency of the organizations. The research surveyed 111 employees and workers currently working in coal mining companies in Vietnam. Through analysis and hypothesis testing, the results showed that digital leadership does not have a direct impact on coal companies' operational efficiency. However, it indirectly affects business performance through the mediating role of digital transformation strategies. The study's findings also revealed that the digital skills of employees play a moderating role in enhancing the relationship between digital transformation strategies and the operational efficiency of the organization.

Keywords: *digital transformation, digital leadership, digital transformation strategy, digital skill, organization performance, coal mining company*

1. Introduction

In the context of the strong global trend of the 4th industrial revolution, digital transformation plays a crucial and necessary role for both nations and businesses. It helps enhance business efficiency, improve competitive capabilities, and create numerous opportunities for innovation.

In Vietnam, the Government has set the direction for "Vietnam to become a digital nation, stable and prosperous, pioneering the experimentation of new technologies and models; fundamentally and comprehensively innovating the management and operation of the Government, and the business operations of companies" (Prime Minister, 2020). To successfully accomplish the above mission, it requires active digital transformation efforts from the Government, organizations, and businesses.

Currently, the coal industry in Vietnam plays a crucial role in contributing to the country's economic development and ensuring energy security (Thang, 2023). The coal mining and supply for both the domestic and international markets in Vietnam are carried out by various entities, including the Vietnam National Coal - Mineral Industries Holding Corporation Limited (Vinacomin), Dong Bac Corporation, 319 Corporation, Vietmindo (FDI company) etc. Among these entities, the key producers and suppliers of coal are Vinacomin and Dong Bac Corporation, which together account for 95% of the domestic coal production (Chien et al., 2015). According to data from the General Statistics Office, in 2022, the coal industry in Vietnam employed over 100,000 workers, generating a total revenue of over 160 trillion VND, with coal production reaching approximately 47 million tons. With a large number of managed companies and a significant labor force, the coal industry's operations require close coordination in production. Therefore, digital transformation will help coal companies streamline intermediary processes, reduce time, and enhance the operational efficiency of production and business activities within the industry.

In recent years, Vietnam's coal companies have begun to build digital transformation programs. Vinacomin is at the forefront of this digital transformation initiative, with a goal to complete their program by 2025. The objective is to leverage the power of digital technology and data to increase operational efficiency, enhance production and business effectiveness, and improve labor productivity across the entire corporation (Vinacomin, 2022). In addition, Vinacomin has also developed the digital action program (code 612-CTr/DU), aimed at raising awareness and strengthening communication, building strategies, plans, and implementation roadmaps, focusing on resource and financial preparation, and improving infrastructure, digitization, and data standardization to serve the digital transformation process. The results obtained from the digital transformation process have been quite positive. Most of the companies have established internal network connectivity within their office and units, diseminated shared ERP software solutions throughout the company, implemented document management and workflow software, significantly reducing paperwork and approval

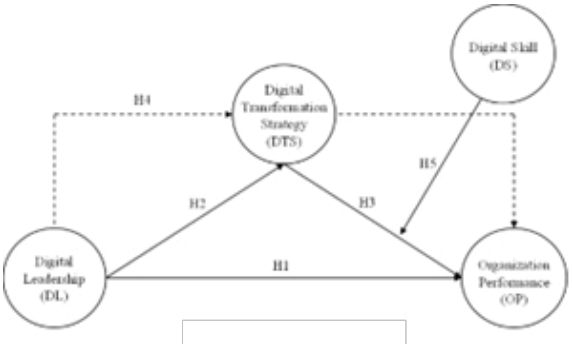

Fig. 1. Proposed Research Model

time for documents. The intelligent data reporting system collects and analyzes data from various units, providing timely support to leaders in the decision-making process.

Despite the significant improvements and active engagement of coal companies in Vietnam in the digital transformation process, the results of the digital transformation efforts still face several limitations. These include the capacity to receive, apply, and utilize digital technologies effectively. Additionally, there are shortcomings in the awareness of digital transformation among some leaders, managers, and employees within the companies, lacking comprehensive understanding and readiness for the digital transformation journey.

The practical experience of the digital transformation process in Vietnamese coal mining companies demonstrates that leadership plays a essential role in influencing digital transformation activities within these organizations. Throughout the digital transformation journey, companies have adopted modern technologies to serve various tasks, particularly in management, to keep up with the changing business environment. This has led to the emergence of new management concepts that align with the transition to digital organizations. One prominent concept is "Digital Leadership," which emphasizes the integration of technological advancements and transformative leadership to achieve the strategic objectives of the organization in an ever-changing environment (Al-Hawary, S. I., 2009; Sheninger, 2019). Digital leadership is considered as the combination of leadership skills and digital competencies to effectively leverage digital technologies and enhance business efficiency (Wasono & Furinto, 2018). It involves utilizing digital tools and strategies while leading teams and organizations through the digital transformation process to achieve maximum benefits from digital technology and improve overall business performance.

Some studies suggest that the role of digital leadership is instrumental in generating positive outcomes for businesses (Al-Husban et al., 2021; Tulungen et al., 2022). On the other hand, some other studies argue that digital leadership does not have a direct impact on business outcomes but rather exerts an indirect influence through some other factors (Amelda et al., 2021; Yopan et al., 2022).

There have been numerous studies on digital transformation and its outcomes, but none have focused on the relationship between digital leadership, digital transformation strategies, and the organizational performance, particularly in coal mining companies in Vietnam. This research aims to examine the impact of digital leadership on the operational efficiency of coal mining companies in Vietnam through the mediating role of digital transformation strategies. Additionally, it investigates the moderating effect of employees' digital skills on the relationship between digital transformation strategies and organizational operational efficiency. The study seeks to fill this gap in the literature and provide valuable insights into how digital leadership can influence the digital transformation process and overall performance of coal mining companies in Vietnam.

2. Literature review

2.1. Digital Leadership

Leaders play a crucial role in driving and promoting digital transformation efforts in today's Industry 4.0 era (Li et al., 2016). The theories of change and transformational leadership are essential in adapting organizational structures and mechanisms to cope with rapid technological advancements (Zeike et al., 2019). As a result, various concepts have emerged, integrating factors that influence organizational behavior and digitization to achieve optimal organizational outcomes. One of the recent concepts is digital leadership, which refers to the use of digital platforms to guide and influence employee behavior in achieving the organization's strategic goals (Sheninger, 2019). Digital leadership are considered a new generation of leaders who utilize digital tools and skills to motivate and guide employees towards digitization (Al-Hawary et al., 2012; Zeike et al., 2019). Artüz & Bayraktar suggest that digital leaders think and act differently from traditional leaders, interacting with the digital world based on three elements: computing, communication, and content to ensure organizational success (Artüz & Bayraktar, 2021).

2.2. Digital transformation strategies

Digital transformation impacts different perspectives and serves various objectives of the organization (Nadeem et al., 2018; Reis et al., 2018). Within businesses, digital transformation involves digitizing and transforming the business model to create new opportunities and increase revenue. Therefore, companies must adopt new strategies based on digital technologies (Ross et al., 2016). Digital transformation is the best strategy for businesses and should be reflected throughout the entire process of business implementation, operation, and performance evaluation. It is no longer sufficient to maintain technical aspects; instead, all decision-making, work processes, and collaborations need to be digitized to provide the best customer experience (Teng et al., 2022). To drive the digital transformation process, organizational strategies should address the transformation of products, service processes, business models, and

Tab. 1. Survey Results. Source: Survey Results by the authors

Survey results description		Number of Votes	Percentage %
Participating units	Vinacomin	68	61,3
	Dong Bac Corporation	43	38,7
Gender	Male	65	58,6
	Female	46	41,4
Age	Under 30 years old	18	16,2
	From 30 to 45 years old	80	72,1
	Over 45 years old	13	11,7
Educational level	Intermediate, elementary	19	17,1
	University, College	86	77,5
	Above university	6	5,4
Position	Employees, Workers	89	80,2
	Lower-level Leaders	8	7,2
	Middle-level Leaders	12	10,8
	Top-level Leaders	2	1,8

Tab. 2. Scale assessment results

Symbol	Variable Name	Corrected Item-Total Correlation
DL	**Digital Leadership: α = 0,956**	
DL1	Leaders have knowledge and skills in digital technology and transformation	0,785
DL2	Leaders balance between traditional and modern trends, innovation, and integration	0,897
DL3	Leaders seek to attract digitally knowledgeable employees	0,899
DL4	Leaders serve as guides and role models in the company's digital transformation	0,910
DL5	Leaders care about the welfare of employees during the digital transformation	0,902
DST	**Digital Transformation Strategy: α = 0,946**	
DTS1	The goals of digital transformation are mentioned in the company's strategy	0,927
DTS2	The company implements the use of a common database system for the entire enterprise	0,884
DTS3	The company's strategy aims to change the operating model	0,856
OP	**Organization Performance: α = 0,942**	
OP1	Compared to other companies in the same industry, our company is more successful	0,865
OP2	Compared to companies with similar capabilities, our company has higher revenues	0,872
OP3	Compared to other companies in the same industry, our company is developing faster	0,885
OP4	Compared to other companies in the same industry, our company is more innovative	0,829
DS	**Digital Skill: α = 0,944**	
DS1	Employees have good skills in using IT applications	0,818
DS2	The company has training programs and equips employees with digital technology	0,863
DS3	Employees have a positive attitude towards new technology applications in their work	0,875
DS4	The company has a specialized IT department	0,870
DS5	We often discuss digital projects within the company	0,812

the adoption of new technologies (Matt et al., 2015).

Digital transformation strategy is not solely about setting goals for process optimization or process automation. It is a carefully designed and implemented plan to manage the sustainable integration of digital technologies (Bharadwaj et al., 2013; Matt et al., 2015). Similar to a personalized roadmap, a digital transformation strategy can bring significant value during the digital transformation journey of a business (Teng et al., 2022).

2.3. Organizational performance

The operational efficiency of an organization is a fundamental concept in management studies and has been of interest to researchers since its inception as it summarizes the performance of an organization in a specific metric. Koohang et al. suggest that the operational efficiency of a business measures the progress and development of its strategies (Koohang et al., 2017). The operational efficiency of an organization reflects its success in achieving predetermined objectives by comparing them with actual results to identify weaknesses and address them. Additionally, it is defined as the organization's ability to achieve strategic objectives efficiently and effectively by optimizing available resources (Mohammad, 2019).

The effectiveness of an organization's operations is evaluated through various indicators, such as financial metrics (Parmenter, 2015; Sawaean & Ali, 2020), employee satisfaction (Zhai & Tian, 2019), customer satisfaction (Chakraborty & Biswas, 2020; T. Wang et al., 2021), productivity (Al-Surmi et al., 2020), quality (Loukis et al., 2019), and efficiency (Vermeeren et al., 2014; Zhou et al., 2019). However, in this study, the effectiveness of the organization's operations is discussed from the perspective of the outcomes of business management activities. Thus, it is considered a comprehensive concept that reflects the results of all aspects and operations of the organization, whether financial or non-financial. Therefore, the effectiveness of the organization's operations needs to be measured based on the evaluation and perception of the employees within the organization.

2.4. Digital Skill

In the context of the 4th industrial revolution, humans have become accustomed to technology and live alongside it. Therefore, digital skills are significant for everyone. Without adequate digital skills, individuals cannot utilize and harness the new features of technology, leading to potential lagging behind in society and especially facing the risk of being replaced in organizations. Digital skills encompass all skills related to technology, from basic literacy (e.g., reading and writing) to general abilities for the workforce and specific skills for IT specialists (Motyl et al., 2017). There are four dimensions to measure digital skills, including digital literacy, digital communication, digital analysis, and digital thinking (van Deursen et al., 2016).

3. Research model and hypotheses

The qualitative research was conducted through systematization to clarify the concepts, processes, and relationships between Digital Leadership, Digital Transformation Strategy, Digital Skills, and Business Performance in mining companies. Additionally, the study explored specific information

Tab. 3. Evaluation indices of model fit with the collected data. ource: The authors analyzed the data collected from the survey

No.	Index	Result	Requirement	Basis
1	CMIN/df	1,427	< 3	Hu & Bentler, 1999
2	CFI	0,985	≥ 0,9	Hu & Bentler, 1999
3	TLI	0,981	≥ 0,9	Hu & Bentler, 1999
4	RMSEA	0,062	< 0,08	Hu & Bentler, 1999
5	GFI	0,906	≥ 0,9	Hu & Bentler, 1999
6	PCLOSE	0,256	≥ 0,05	Hu & Bentler, 1999

Tab. 4. Results of the model testing. Source: Data analysis conducted by the authors from survey data

Hypothesis	Indirect Path	Unstandardized Estimate	Critical ratio (CR)	Critical Value	P-value
H1	OP ← DL	0.151	0.086	1.762	0.078
H2	DTS ← DL	0.528	0.087	6.088	0.000
H3	OP ← DTS	0.506	0.089	5.656	0.000
H4	OP ← DTS ← DL	0.267			0.000

Tab. 5. Results of second-order regression

	Unstandardized Coefficients	Standard Error	t	P-value	LLCI	ULCI
constant	3.616	0.061	59.610	0.000	3.496	3.736
DTS	0.554	0.095	5.840	0.000	0.366	0.742
DS	0.091	0.099	0.921	0.359	-0.105	0.287
DTS * DS	0.121	0.055	2.197	0.030	0.012	0.231
Dependent variable: OP; R^2 = 0.627; ΔR^2 = 0.394 (P = 0.000)						

from coal mining companies in Vietnam, combined with expert surveys and group discussions to establish the following hypotheses:

3.1. The relationship between Digital Leadership and Organizational Performance

Although the concept of digital leadership is relatively new and has not been deeply researched, there is substantial evidence regarding the impact of digitization on organizational performance. Research by Dijkstra points out that integrating digitalization into organizational management enhances communication effectiveness across administrative levels (Dijkstra, J., 2020). As a result, productivity increases, and output is improved, leading to higher customer satisfaction and a larger market share.

Digital leadership is considered an effective leadership approach to achieving organizational sustainability through competitive advantages, emphasizing the optimal and efficient utilization of resources (Artüz & Bayraktar, 2021). Additionally, the reliance of digital leadership on technology development and business environment interaction can reduce working time due to low error rates and accurate knowledge of customer preferences (Freitas Junior et al., 2020; Sheninger, 2019). Therefore, the first research hypothesis is formulated as follows:

Hypothesis 1 (H1): Digital leadership has a positive and significant impact on the operational efficiency of organizations.

3.2. The relationship between Digital Leadership and Digital Transformation Strategy

Building and implementing a digital transformation strategy has become a major concern for organizations before undergoing digital transformation in various industries (Chanias et al., 2019). Digital leadership plays a crucial role in building the digital transformation strategy of an organization. They are the ones who create the organization's vision and implement initiatives to actualize that vision by leveraging employee enthusiasm and rationalizing the organization's operations (Cong & Thu, 2020; Mardiana, 2020). The perspectives and knowledge about digital transformation by digital leaders will be specified and incorporated into the organization's strategy, making digital leadership highly significant in the process of developing the digital transformation strategy. Based on this, the next research hypothesis is proposed:

Hypothesis 2 (H2): Digital leadership has a positive and significant impact on the digital transformation strategy of the organization.

3.3. The relationship between Digital Transformation Strategy and Organizational Performance

Digital transformation strategy is a core factor that is indispensable in the ongoing process of digital transformation. It serves as a prerequisite for successful digitalization (Teng et al., 2022). If organizations develop an effective, clear, and coherent digital transformation strategy, it will facilitate a smooth digital transformation process, thereby enhancing the operational efficiency of the organization. Previous research has shown that digital transformation at the organizational level requires attention to the alignment of strategy, vision, and investment in digital transformation; the suitability of innovative culture; intellectual property and secrets; the power of digital capabilities; and the utilization of digital technologies (Gurbaxani & Dunkle, 2019). Digital transformation strategies have a positive impact on short-term and long-term financial performance (H. Wang et al., 2020). From this, the following research hypothesis is proposed:

Hypothesis 3 (H3): Digital transformation strategy has a positive and significant impact on organizational performance.

3.4. The relationship between Digital Leadership and Organizational Performance is mediated by the role of Digital Transformation Strategy

The objective of digital transformation in businesses is to establish distinctive core competencies, develop long-term development strategies, design rational organizational structures, optimize value chain networks, and build long-term development strategies (Paschou et al., 2020). Companies need to improve

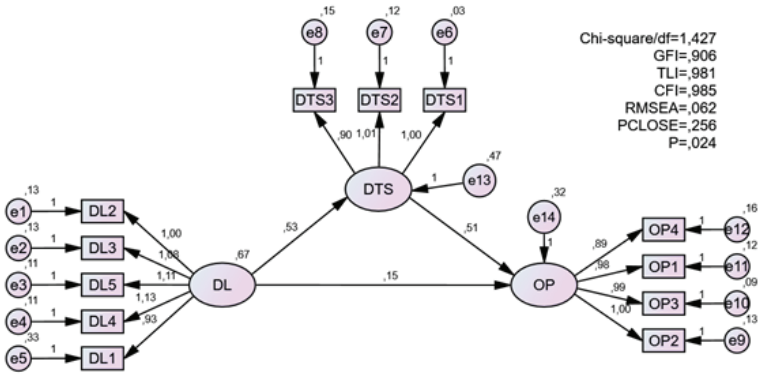

Fig. 2. Results of linear structural equation modeling (SEM) analysis

their digital skills to meet market demands by implementing digital transformation with a strategy that utilizes digital technology as a survival strategy amidst technological advancements (Chen et al., 2021; Usai et al., 2021; Zhang et al., 2021). Businesses must undergo comprehensive digital transformation in terms of strategy, operations, organization, capabilities, and activities in the digital economy (Yu & Moon, 2021).

Digital leadership plays a pivotal role in enhancing the effectiveness of businesses through digital transformation efforts. However, the leaders themselves cannot execute the digital transformation activities alone, as they need to articulate it into specific objectives and incorporate them into the strategy as a basis for implementation by employees within the organization. From this perspective, the research team believes that the digital transformation strategy acts as a mediator in the relationship between digital leadership and organizational performance. Hence, the proposed research hypothesis is as follows:

Hypothesis 4 (H4): The digital transformation strategy mediates the relationship between digital leadership and organizational performance.

3.5. The relationship between Digital Transformation Strategy and Organizational Performance is mediated by the role of Digital Skills

Some previous studies have suggested that digital skills are directly influenced by digital collaboration and indirectly influenced by digital leadership (Saputra et al., 2021), digital skills play an intermediary role in the relationship between digital leadership and organizational performance (Tulungen et al., 2022), digital leadership can achieve effectiveness through two approaches: competence and awareness of digital transformation, and the ability to implement digital strategies within the organization (Zeike et al., 2019).

To successfully implement digital transformation in businesses, besides leadership and strategy, the digital skills of employees play a crucial role. While leadership initiates the digital transformation and strategy sets the goals to be achieved, employees are the ones directly carrying out the digital transformation activities of the organization. Therefore, digital support policies must go hand in hand with enhancing digital skills (Gal et al., 2019). Based on this, the research team believes that with the same digital transformation strategy, the higher the digital skills of employees, the better they will perform the objectives of the digital transformation strategy. Consequently, the organizational performance derived from digital transformation activities will be enhanced. In other words, digital skills will moderate the impact of the digital transformation strategy on the organizational performance.

Hypothesis 5 (H5): The impact of the digital transformation strategy on the organizational performance is higher when the digital skills of employees are higher.

Based on the proposed research hypotheses, the research model includes the following factors as shown in Figure 1.

4. Research methodology

4.1. Research Scale

The variables used in this study include:

Digital leadership, which is the independent variable and measured by 5 observed variables denoted as DL1 to DL5. This scale is adopted and developed from Büyükbeşe and Tulungen's scale (Büyükbeşe et al., 2022; Tulungen et al., 2022).

Business digital transformation strategy, which is the mediating variable and measured by 3 observed variables denoted as DTS1 to DTS3. This scale is inherited and developed from the scale of the Ministry of Planning and Investment (Ministry of Planning and Investment, 2020).

Organizational performance, which is the dependent variable and measured by 4 observed variables denoted as OP1 to OP4. This scale is inherited and developed from Lee & Choi's scale (Lee & Choi, 2003).

Employee digital skills, which is the moderating variable and measured by 5 observed variables denoted as DS1 to DS5. This scale is adopted and developed from Saputra and Tulungen's scale (Saputra et al., 2021; Tulungen et al., 2022).

4.2. Research Sample

The quantitative survey was conducted from April 2023 to May 2023, targeting employees working in coal mining companies in Vietnam. The survey was carried out through online interviews using a questionnaire built on Microsoft Form. The non-random convenience sampling method was employed, and the research model consists of 17 observed variables, following the guidelines of Hair & colleagues (1998). The necessary sample size was determined to be n = 85 (17x5). The respondents were asked to answer 17 questions related to digital leadership, business digital transformation strategy, digital skills of employees, and organizational performance. Each question was measured on a 5-point Likert scale, ranging from "Strongly Disagree" to "Strongly Agree".

To achieve the required sample size, the authors distributed the survey to more than 300 individuals, resulting in 111

valid responses (some surveys were excluded due to poor survey quality). The survey results are presented in Table 1. Data was imported and analyzed using SPSS and AMOS software.

5. Results

5.1. Scale assessment

The scale was evaluated using Cronbach's Alpha reliability coefficient: The results of the Cronbach's Alpha reliability test in Table 2 show that all 17 observed variables have correlation coefficients with the total variable greater than 0.3; the Cronbach's Alpha coefficients of the 4 scales are all greater than 0.6. Thus, the constructed scales ensure acceptable reliability (According to: Cronbach, 1951; Nunnally & Bernstein, 1994).

5.2. Results of the mediation analysis of the role of Digital Transformation Strategy in the relationship between Digital Leadership and Organizational Performance

Exploratory Factor Analysis (EFA): All 12 observed variables of the model were included in the EFA. The result of the EFA yielded a Kaiser-Meyer-Olkin (KMO) measure of 0.885 (indicating the suitability of EFA), and a significance value (Sig) of 0.000 (indicating significant correlations among the observed variables overall). The total variance extracted was 86.735% (greater than 50%, indicating that the extracted factors explain 86.735% of the data variation). The EFA results were consistent with the constructed measurement scales, as all indicators were appropriately loaded onto their respective factors.

Confirmatory Factor Analysis (CFA): Confirmatory Factor Analysis was conducted to assess the model's fit with the collected data. The results of the evaluation indices for model fit are presented in Table 3.

The results in Table 3 indicate that all evaluation indices meet the criteria. Therefore, the conclusion is that the model fits the research data and achieves parsimony.

Linear Structural Equation Modeling (SEM) was conducted after the CFA analysis to evaluate the relationships between the factors. The research model was estimated using the linear structural equation modeling, and the results are presented in Figure 2. The Model Fit indices of the SEM analysis all meet the criteria, thus indicating that the linear structural equation model in this case is appropriate and reliable.

The results of the model testing in Table 4 show the detailed outcomes of hypothesis testing. The first hypothesis suggests that Digital Leadership has a direct impact on the organizational performance of the company. However, the results indicate that this hypothesis is not supported as the P-value is > 0.05. Therefore, Digital Leadership does not have a direct influence on the organizational performance, which aligns with previous research findings (Amelda et al., 2021; Tulungen et al., 2022; Yopan et al., 2022). The second hypothesis proposes that Digital Leadership affects the Digital Transformation Strategy of the company. The analysis results support this hypothesis ($\beta = 0{,}533$; CR = 0,087; $P < 0{,}05$). The third hypothesis suggests that the Digital Transformation Strategy of the company affects its Organizational Performance. The analysis results confirm this hypothesis ($\beta = 0{,}506$; CR = 0,089; $P < 0{,}05$). The fourth hypothesis posits that Digital Leadership has an impact on the Organizational Performance of the company through the mediating role of the Digital Transformation Strategy. The analysis results support this hypothesis ($\beta = 0{,}267$; $P < 0{,}05$).

5.3. Results of the analysis of the moderating role of Digital Skills in the relationship between Digital Transformation Strategy and Organizational Performance

The second-order regression method was used to test hypothesis H5. In this hypothesis, Digital Skills (W) act as the moderating variable, influencing the relationship between Digital Transformation Strategy (X) and Organizational Performance (Y). Digital Skills were hypothesized as a pure moderator, meaning that they only modify the relationship between Digital Transformation Strategy and Organizational Performance without having a direct relationship with Organizational Performance. This hypothesis is accepted when X*W has an effect on Y, meaning that the product of Digital Transformation Strategy and Digital Skills has an impact on Organizational Performance.

The results of the second-order regression estimation are presented in Table 5 and Figure 3. The results show that Digital Transformation Strategy has a significant effect on Organizational Performance ($P < 0.005$), while Digital Skills do not have a significant effect on Organizational Performance ($P > 0.005$). The regression results also demonstrate that the interaction effect between Digital Transformation Strategy and Digital Skills on Organizational Performance is statistically significant ($P < 0.005$), indicating that hypothesis H5 is supported. This result means that when employees' Digital Skills are higher, the impact of Digital Transformation Strategy on Organizational Performance is also higher.

From Figure 3, it is evident that all three lines representing the relationship between X (Digital Transformation Strategy) and Y (Organizational Performance) with W (Digital Skills) have an upward slope. This indicates that regardless of the level of digital skills, an increase in the digital transformation strategy will lead to an improvement in organizational performance. Furthermore, the varying slopes of the three lines in the graph indicate that as digital skills increase, the impact of the digital transformation strategy on organizational performance also increases.

6. Conclusion, implications, and limitations

The objective of this study was to examine the relationship between digital leadership and organizational performance through the mediating role of digital transformation strategy, as well as the moderating role of digital skills in the relationship between digital transformation strategy and organizational performance. These hypotheses were investigated in the context of coal mining companies in Vietnam. The research model comprised four variables: Digital Leadership, Digital Transformation Strategy, Digital Skills, and Organizational Performance. The results of the analysis demonstrated the validity and reliability of the proposed model. The findings from the analysis of Cronbach's Alpha, Exploratory Factor Analysis (EFA), and Confirmatory Factor Analysis (CFA) all met the required criteria, confirming the validity of the proposed model.

The results of hypothesis testing through the Structural Equation Modeling (SEM) indicate that digital leadership does not have a direct effect on organizational performance.

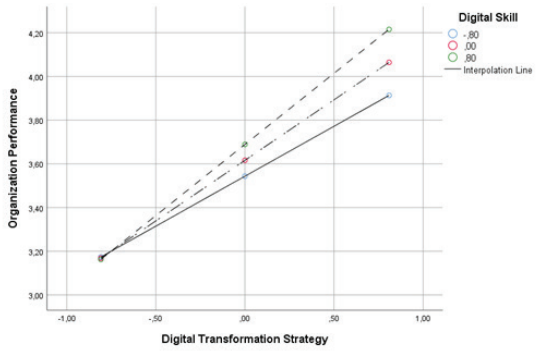

Fig. 3. Graph showing the moderating relationship

However, it does have an indirect effect through the mediation of digital transformation strategy. The estimation of higher-order regression in hypothesis testing shows that the role of employees' digital skills acts as a moderator, strengthening the relationship between digital transformation strategy and organizational performance.

In the face of technological advancements, leaders in coal mining companies in Vietnam need to be adaptable to the developments and be able to embrace new habits in technology usage. Digital leadership plays a crucial role in realizing the business strategy to enhance operational efficiency. The understanding of digital transformation by leaders in coal mining businesses should be utilized to build and achieve strategic goals. To effectively leverage the benefits of digital transformation in improving organizational performance, business leaders must also prioritize enhancing the digital skills of their employees during the implementation process.

Digital transformation also has a significant positive impact on the operational efficiency of coal mining companies in Vietnam. It is considered an important approach by both academia and business practitioners to improve the business performance of organizations (Zhang et al., 2021). Clear and feasible digital transformation goals and strategies should be identified and integrated into the core business strategy of these companies. These strategic objectives are also greatly influenced by the perspectives, perceptions, and capabilities of the leaders in the coal mining industry. Additionally, to further enhance organizational performance during the digital transformation process, attention must also be given to the digital skills of the employees.

The limitations of this study include its exploratory nature, which resulted in a limited use of variables. The survey sample may not fully represent the strategic planning level of the businesses. Additionally, due to time constraints, some of the expected participants did not respond, which could have affected the study's outcomes. To address these limitations, future research should consider expanding the range of variables, such as cooperation, digital literacy, employee satisfaction, and competitive advantage. Furthermore, involving more strategic planners, especially top-level leaders, is important for future studies. In this study, only two participants at that level were included. Another limitation is the relatively small number of valid responses, with only 111 out of 207 participants' responses being considered valid. Therefore, for future research, increasing the number of respondents and improving the survey quality are essential steps to enhance the study's validity and reliability.

Acknowledgments

The paper was presented during the 7th VIET - POL International Conference Scientific-Research Cooperation between Vietnam and Poland.

The authors are thankful to colleagues of the coal mining companies of Vinacomin for their supports and cooperation.

Literatura – References

1. Albukhitan, S. (2020). Developing Digital Transformation Strategy for Manufacturing. Procedia Computer Science, 170, 664–671. https://doi.org/10.1016/j.procs.2020.03.173
2. Al-Hawary, S. I. (2009). The effect of the leadership style on the effectiveness of the organization: A field study at Zarqa Private University. The Egyptian Journal for Commercial Studies, 33(1), 361–393.
3. Al-Hawary, S. I., Al-Awawdeh, W., & Abden, M. A. (2012). The impact of the leadership style on organizational commitment: A field study on Kuwaiti telecommunications companies. ALEDARI.
4. Al-Husban, D. A. O., Almarshad, M. N. D., & Altahrawi, M. H. A. (2021). Digital leadership and organization's performance: The mediating role of innovation capability. Int. J. Entrep, 25, 1–16.
5. Al-Surmi, A., Cao, G., & Duan, Y. (2020). The impact of aligning business, IT, and marketing strategies on firm performance. Industrial marketing management, 84, 39–49.
6. Amelda, B., Alamsjah, F., & Elidjen, E. (2021). Does The Digital Marketing Capability of Indonesian Banks Align with Digital Leadership and Technology Capabilities on Company Performance? CommIT (Communication and Information Technology) Journal, 15(1), Article 1. https://doi.org/10.21512/commit.v15i1.6663
7. Artüz, S. D., & Bayraktar, O. (2021). The effect of relation between digital leadership practice and learning organization on the perception of individual performance. İstanbul Ticaret Üniversitesi Sosyal Bilimler Dergisi, 20(40), 97–120.
8. Bharadwaj, A., El Sawy, O. A., Pavlou, P. A., & Venkatraman, N. V. (2013). Digital Business Strategy: Toward a Next Generation of Insights (SSRN Scholarly Paper 2742300). https://papers.ssrn.com/abstract=2742300
9. Büyükbeşe, T., DiKbaş, T., & Ünlü, S. B. (2022). A Study On Digital Leadership Scale (DLS) Development.
10. Chakraborty, D., & Biswas, W. (2020). Articulating the value of human resource planning (HRP) activities in augmenting organizational performance toward a sustained competitive firm. Journal of Asia Business Studies, 14(1), 62–90. https://doi.org/10.1108/JABS-01-2019-0025
11. Chanias, S., Myers, M. D., & Hess, T. (2019). Digital transformation strategy making in pre-digital organizations: The case of a financial services provider. The Journal of Strategic Information Systems, 28(1), 17–33. https://doi.org/10.1016/j.jsis.2018.11.003
12. Chen, C.-L., Lin, Y.-C., Chen, W.-H., Chao, C.-F., & Pandia, H. (2021). Role of Government to Enhance Digital Transformation in Small Service Business. Sustainability, 13(3), Article 3. https://doi.org/10.3390/su13031028
13. Chien, L. V., Khanh, N. N., & Trung, P. K. (2015). Improving environmental management in coal exploiting activity at Companies of Vietnam national Coal—Mineral industries holding corporation limited. Vietnam Trade and Industry Review, 5, 5–9.
14. Cong, L. C., & Thu, D. A. (2020). The competitiveness of small and medium companies in the tourism sector: The role of leadership competencies. Journal of Economics and Development, 23(3), 299–316. https://doi.org/10.1108/JED-06-2020-0080
15. Dijkstra, J. (2020). Digital leadership and firm performance: A meta-analysis. University of Groningen.
16. Freitas Junior, J. C., Cabral, P. M. F., & Brinkhues, R. (2020). Digital Transformation: The Gap Between Digital Leadership and Business Performance. ISLA 2020 Proceedings. https://aisel.aisnet.org/isla2020/20
17. Gal, P., Nicoletti, G., Renault, T., Sorbe, S., & Timiliotis, C. (2019). Digitalisation and productivity: In search of the holy grail – Firm-level empirical evidence from EU countries. OECD. https://doi.org/10.1787/5080f4b6-en
18. Gurbaxani, V., & Dunkle, D. (2019). Gearing Up For Successful Digital Transformation. MIS Quarterly Executive, 18(3). https://aisel.aisnet.org/misqe/vol18/iss3/6
19. Koohang, A., Paliszkiewicz, J., & Goluchowski, J. (2017). The impact of leadership on trust, knowledge management, and organizational performance: A research model. Industrial Management & Data Systems, 117(3), 521–537. https://doi.org/10.1108/IMDS-02-2016-0072
20. Lee, H., & Choi, B. (2003). Knowledge Management Enablers, Processes, and Organizational Performance: An Integrative View and Empirical Examination. Journal of Management Information Systems, 20(1), 179–228.
21. Li, W., Liu, K., Belitski, M., Ghobadian, A., & O'Regan, N. (2016). E-Leadership through Strategic Alignment: An Empirical Study of Small- and Medium-sized Companies in the Digital Age. Journal of Information Technology, 31(2), 185–206. https://doi.org/10.1057/jit.2016.10
22. Loukis, E., Janssen, M., & Mintchev, I. (2019). Determinants of software-as-a-service benefits and impact on firm performance. Decision Support Systems, 117, 38–47.
23. Mardiana, D. (2020). The application of digital leadership of sub district head on public service performance with the delegation of regent/mayor authorities as the moderating variable. Airlangga Development Journal, 4(2), 154–164.

24. Matt, C., Hess, T., & Benlian, A. (2015). Digital Transformation Strategies. Business & Information Systems Engineering, 57(5), 339–343. https://doi.org/10.1007/s12599-015-0401-5

25. Merendino, A., & Melville, R. (2019). The board of directors and firm performance: Empirical evidence from listed companies. Corporate Governance: The international journal of business in society.

26. Ministry of Planning and Investment. (2020). A guide to digital transform tion for businesses in Vietnam. http://ebook.business.gov.vn/ Accessed: 19/07/2023

27. Mohammad, H. I. (2019). Mediating effect of organizational learning and moderating role of environmental dynamism on the relationship between strategic change and firm performance. Journal of Strategy and Management, 12(2), 275–297. https://doi.org/10.1108/JSMA-07-2018-0064

28. Motyl, B., Baronio, G., Uberti, S., Speranza, D., & Filippi, S. (2017). How will Change the Future Engineers' Skills in the Industry 4.0 Framework? A Questionnaire Survey. Procedia Manufacturing, 11, 1501–1509. https://doi.org/10.1016/j.promfg.2017.07.282

29. Nadeem, A., Abedin, B., Cerpa, N., Chew, E., Nadeem, A., Abedin, B., Cerpa, N., & Chew, E. (2018). Editorial: Digital Transformation & Digital Business Strategy in Electronic Commerce - The Role of Organizational Capabilities. Journal of theoretical and applied electronic commerce research, 13(2), i–viii. https://doi.org/10.4067/S0718-18762018000200101

30. Parmenter, D. (2015). Key Performance Indicators: Developing, Implementing, and Using Winning KPIs. John Wiley & Sons.

31. Paschou, T., Rapaccini, M., Adrodegari, F., & Saccani, N. (2020). Digital servitization in manufacturing: A systematic literature review and research agenda. Industrial Marketing Management, 89, 278–292. https://doi.org/10.1016/j.indmarman.2020.02.012

32. Prime Minister. (2020). Decision No. 749/QD-TTg dated June 3, 2020 approving the "National Digital Transformation Program to 2025, with orientation to 2030". Vietnam.

33. Reis, J., Amorim, M., Melão, N., & Matos, P. (2018). Digital Transformation: A Literature Review and Guidelines for Future Research. Trong Á. Rocha, H. Adeli, L. P. Reis, & S. Costanzo (B.t.v), Trends and Advances in Information Systems and Technologies (tr 411–421). Springer International Publishing. https://doi.org/10.1007/978-3-319-77703-0_41

34. Ross, J., Sebastian, I., Beath, C., Mocker, M., Moloney, K., & Fonstad, N. (2016). Designing and executing digital strategies: Completed research paper. Digital innovation at the crossroads: ICIS 2016, International Conference on Information Systems, December 11-14, 2016, Dublin, Ireland: practice-oriented research, 1–17. https://publikationen.reutlingen-university.de/frontdoor/deliver/index/docId/1096/file/1096.pdf

35. Saputra, N., Nugroho, R., Aisyah, H., & Karneli, O. (2021). Digital skill during Covid-19: Effects of digital leadership and digital collaboration. Jurnal Aplikasi Manajemen, 19(2), Article 2. https://doi.org/10.21776/ub.jam.2021.019.02.04

36. Sawaean, F., & Ali, K. (2020). The mediation effect of TQM practices on the relationship between entrepreneurial leadership and organizational performance of SMEs in Kuwait. Management Science Letters, 10(4), 789–800.

37. Sheninger, E. (2019). Digital Leadership: Changing Paradigms for Changing Times. Corwin Press.

38. Teng, X., Wu, Z., & Yang, F. (2022). Research on the Relationship between Digital Transformation and Performance of SMEs. Sustainability, 14(10), Article 10. https://doi.org/10.3390/su14106012

39. Thang, N. D. (2023). Improving the job satisfaction of miners to enhance production safety in vietnamese coal mining companies. Asia - Pacific Economic Review, 12, 268–273.

40. Tsou, H.-T., & Chen, J.-S. (2021). How does digital technology usage benefit firm performance? Digital transformation strategy and organisational innovation as mediators. Technology Analysis & Strategic Management, 0(0), 1–14. https://doi.org/10.1080/09537325.2021.1991575

41. Tulungen, E., pandowo, merinda, & Tewal, B. (2022). The Role of Digital Leadership Mediated by Digital Skill in Improving Organizational Performance. Journal of Accounting Research Organization and Economics, 5, 156–171. https://doi.org/10.24815/jaroe.v5i2.26182

42. Usai, A., Fiano, F., Messeni Petruzzelli, A., Paoloni, P., Farina Briamonte, M., & Orlando, B. (2021). Unveiling the impact of the adoption of digital technologies on firms' innovation performance. Journal of Business Research, 133, 327–336. https://doi.org/10.1016/j.jbusres.2021.04.035

43. van Deursen, A. J. A. M., Helsper, E. J., & Eynon, R. (2016). Development and validation of the Internet Skills Scale (ISS). Information, Communication & Society, 19(6), 804–823. https://doi.org/10.1080/1369118X.2015.1078834

44. Vermeeren, B., Steijn, B., Tummers, L., Lankhaar, M., Poerstamper, R.-J., & Van Beek, S. (2014). HRM and its effect on employee, organizational and financial outcomes in health care organizations. Human resources for health, 12, 1–9.

45. Vinacomin. (2022). Resolution 22-NQ/DU dated January 13, 2022 setting goals on implementing digital transformation by 2025, with orientation to 2030. Vietnam.

46. Wang, H., Feng, J., Zhang, H., & Li, X. (2020). The effect of digital transformation strategy on performance: The moderating role of cognitive conflict. International Journal of Conflict Management, 31(3), 441–462. https://doi.org/10.1108/IJCMA-09-2019-0166

47. Wang, T., Wu, J., Gu, J., & Hu, L. (2021). Impact of open innovation on organizational performance in different conflict management styles: Based on resource dependence theory. International Journal of Conflict Management, 32(2), 199–222.

48. Wasono, L. W., & Furinto, A. (2018). The effect of digital leadership and innovation management for incumbent telecommunication company in the digital disruptive era. International Journal of Engineering & Technology, 7(2.29), Article 2.29. https://doi.org/10.14419/ijet.v7i2.29.13142

49. Yopan, M., Rhenald Kasali, & Tengku Ezni Balqiah. (2022). The Role of Digital Leadership, Customer Orientation and Business Model Innovation for IoT Companies. International Journal of Business, 27(2). https://doi.org/10.55802/IJB.027(2).007

50. Yu, J., & Moon, T. (2021). Impact of Digital Strategic Orientation on Organization Performance through Digital Transformation Capability (09). ICIC International. https://doi.org/10.24507/icicelb.12.09.847

51. Zeike, S., Bradbury, K., Lindert, L., & Pfaff, H. (2019). Digital Leadership Skills and Associations with Psychological Well-Being. International Journal of Environmental Research and Public Health, 16(14), Article 14. https://doi.org/10.3390/ijerph16142628

52. Zhai, X., & Tian, X. (2019). Do performance measures matter in the relationship between high-performance work system and organizational performance? International Journal of Manpower, 41(3), 241–257. https://doi.org/10.1108/IJM-04-2018-0136

53. Zhang, J., Long, J., & von Schaewen, A. M. E. (2021). How Does Digital Transformation Improve Organizational Resilience?—Findings from PLS-SEM and fsQCA. Sustainability, 13(20), Article 20. https://doi.org/10.3390/su132011487

54. Zhou, S. S., Zhou, A. J., Feng, J., & Jiang, S. (2019). Dynamic capabilities and organizational performance: The mediating role of innovation. Journal of Management & Organization, 25(5), 731–747.

Developing Electronic Government Towards Digital Government to Enhance the Efficiency of State Governance in Vietnam

Chu Thi Khanh LY[1)], Nguyen Quynh NGA[1)], Nguyen Van HAU[1)], Tran Thi Huong HUE[1)]*

[1)] National Academy of Public Administration, Vietnam
* Corresponding author e-mail: ngaquynh.napa@gmail.com

http://doi.org/10.29227/IM-2023-02-21

Submission date: 21-08-2023 | Review date: 19-09-2023

Abstract

The development of an electronic government, aiming for a digital government to effectively manage the state and contribute to the convenience of citizens and businesses, is both a crucial aspect of the comprehensive administrative reform program for the period 2021-2030 and an essential global trend for all countries, including Vietnam. This article discusses various topics: general issues related to electronic government and digital government, the current situation of electronic government development in Vietnam, challenges faced in the process of developing electronic government towards a digital government in Vietnam, and some solutions to enhance the effectiveness of electronic government development towards a digital government in Vietnam.

Keywords: *electronic government, digital government, online public services*

1. Some common issues regarding electronic government and digital government

1.1. The concept of electronic government and digital government

Currently, there are many different conceptions of electronic government and digital government, however, from the perspective of the Organization for Economic Co-operation and Development (OECD), electronic government and digital government are defined as follows:

Electronic government is the Government's use of information and communication technologies (ICT- Information and Communications Technology), especially the Internet, as a tool to achieve better efficiency [7].

Digital government is defined as "the use of digital technologies, as an integrated part of governments' modernisation strategies, to create public value" [17]. Public values are benefits for society, which can change depending on viewpoints or actors, including: (1) goods and services to satisfy the needs of customers and citizens; (2) production options to meet people's expectations of justice, equity, efficiency, effectiveness; (3) high-performing, well-organized public institutions that represent citizens' priorities and aspirations; (4) fair and efficient distribution; (5) use of valid resources to fulfill public purposes; and (6) innovate and adapt to ever-changing priorities and needs. This process is based on a Digital Government ecosystem consisting of actors related to Government, NGOs, businesses, civil society and citizens, promoting the creation and access of data materials, services and content through interaction with Government.

Thus, between electronic government and digital government, there are both similarities and differences, specifically:

The similarity between electronic government and digital government is that these models aim to help government agencies innovate, work effectively and efficiently; ensuring transparency, high accountability and convenience in all relations between government and citizens; create favorable conditions for people to exercise their democratic rights and participate in State management. In Vietnam today, the construction and development of electronic government towards digital government in order to improve the efficiency of state governance, build a government by the people, of the people, for the people and for the prosperity of the land. countries in the environment of deep international integration.

Difference: Electronic government is the application of information and communication technology in the public system to improve the efficiency and user experience of public services by replacing paper-based administrative procedures. by digital platform. Electronic government is different from Digital Government. While electronic government focuses on online public services, Digital Government moves all government activities to a digital environment, operates on data and provides new services. Electronic government mainly uses information technology, while digital government uses digital technology, especially the technology of Industry 4.0.

1.2. The role of electronic government and digital government

Firstly, the development of electronic government towards a digital government will accelerate the digitalization of administrative procedures, provide public services, promote administrative reform, and create a digital environment between the government and businesses. The practical experience of countries around the world shows that enhancing the application of technology, information, communication, and automation in government operations to serve citizens and businesses will ensure transparency, save time and costs for the people and businesses, control corruption in the public sector, and strengthen the accountability of government officials and civil servants.

Secondly, the development of electronic government towards a smart government also contributes to enhancing the participation of citizens in state management activities. Specifically, with the automation of government connectivity and trans-

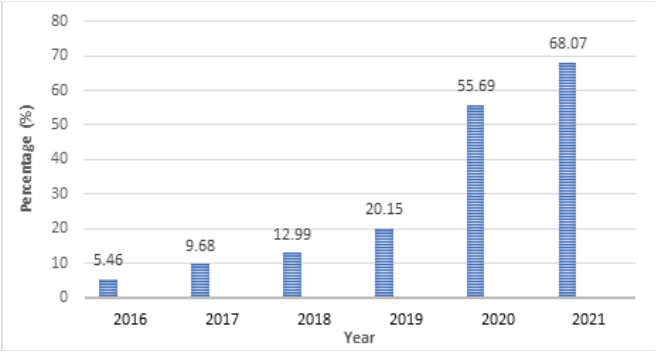

Fig. 1. Ratio of Level 3 and Level 4 online public services to the total number of public services (Source: Compiled by the authors from the Report on the Readiness Index for Development and Application of Information Technology and Communication in Vietnam, Publishing House for Information and Communication, years 2018-2021) [1]

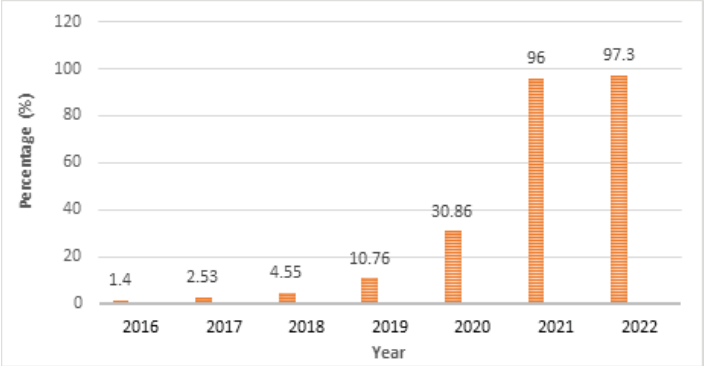

Fig. 2. Ratio of Level 4 online public services to the total number of public services (Source: Compiled by the authors from the Report on the Readiness Index for Development and Application of Information Technology and Communication in Vietnam, Publishing House for Information and Communication, years 2018-2022) [1]; [2]

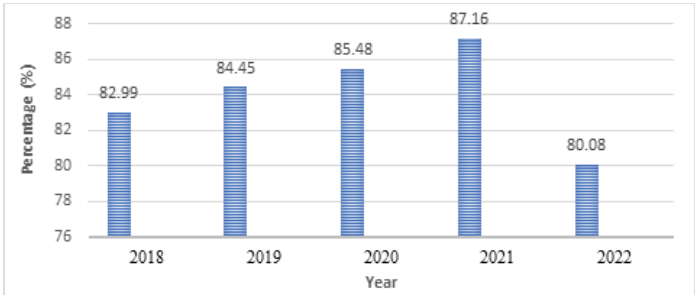

Fig. 3. Satisfaction Index with Administrative Services provided by Administrative Agencies for Citizens and Organizations. Source: Compiled by the authors from SIPAS data from 2018-2022 [16]

parent work processes, widely deployed electronic services... citizens and businesses not only enjoy useful public services but also participate in contributing opinions to the state management activities. Therefore, the smart government model is an important solution to facilitate the most effective interaction and information exchange between the government and the people.

Thirdly, the development of electronic government towards a digital government in urban areas will create a transparent legal environment for the process of digital economic development. In recent years, thanks to the application of information technology in building electronic government , documents and policies on socio-economic development in general and digital economic development in particular have been updated and timely issued, contributing to the effectiveness of organization and implementation in practice. This is a positive and effective transformation compared to the traditional methods of drafting, issuing, and disseminating laws and policies.

The coordination between technology enterprises, ministries, departments, and localities has effectively implemented the national document connectivity system. The national document connectivity system is the core platform that ensures the successful construction of electronic government towards a digital government, a digital society, and a digital economy; aiming to better serve the people and businesses and promote the socio-economic development of the country. Currently, 95 out of 95 central and local agencies (including the Central Party Office, ministries, government agencies, and 63 provinces and centrally-governed cities) have completed the connection of document management systems and operations on the national document connectivity system. Document management software of ministries, departments, and localities has been connected, enabling smooth and systematic vertical and horizontal communication, and electronic documents are sent and received quickly and safely between state agencies.

2. The current situation of developing electronic government towards a digital government in Vietnam

2.1. In terms of institutions and policies

In recent years, the issue of applying information technology and developing electronic government has always been of great concern to the Party and State in Vietnam, aiming to enhance the effectiveness and efficiency of state agencies, improve the quality of services for citizens and businesses, and enhance the nation's competitive capacity. In this regard, the Government and the Prime Minister have issued various documents defining the objectives and contents of electronic government development, including Resolution No. 17/NQ-CP dated March 7, 2019, on some tasks and key solutions for electronic government development in the 2019-2020 period, with a vision towards 2025; Decision No. 749/QD-TTg dated June 3, 2020, approving the National Digital Transformation Program until 2025, with a vision towards 2030; Decision No. 942/QD-TTg dated June 15, 2021, approving and issuing the Strategy for Digital Government Development in the 2021-2025 period, with a vision towards 2030; and Resolution No. 76/NQ-CP dated July 15, 2021, issuing the Comprehensive Program for Administrative Reform in the 2021-2030 period.

These legal foundations have helped Vietnam determine its determination to achieve the goal of developing electronic government towards a digital government in Vietnam in the current period.

2.2. Regarding the online public service index

In order to develop a digital government, Vietnam has made efforts to provide online public services to citizens, businesses, and organizations, thereby meeting high standards in terms of both quantity and quality of online public services. The results of the report on the online public service index from 2016 to 2022 show the following:

The ratio of level 3 and level 4 online public services has been steadily increasing from 2016 to 2021. In 2021, out of the total number of public services nationwide, the ratio of level 3 and level 4 online public services reached 68% (approximately 81,446 services). This ratio was nearly 55.7% in 2020 and 20.15% in 2019.

These figures demonstrate Vietnam's commitment to enhancing the provision of online public services, as well as the continuous improvement in the accessibility and quality of these services. The efforts made in expanding the range of online public services have contributed to the development of a digital government and the transformation towards a more efficient and citizen-centric administration system.

Specifically, the ratio of Level 4 online public services, as reported by the Ministry of Information and Communications, shows the following results: In 2016, it was 1.4%; in 2017, it was 2.53%; in 2018, it was 4.55%; in 2019, it was 10.76%; and in 2021, it reached 96%. In 2022, the government issued Decree No. 42/2022/ND-CP, which regulates the provision of information and online public services by state agencies on the internet. According to Report No. 91/BC-BTTTT dated June 30, 2022, as of June 28, 2022, the ratio of online public services meeting the requirements to be classified as Level 4 reached 97.3% (accounting for 53.56% of the total number of administrative procedures).

With the goal of promoting the application of information technology in serving meetings and handling government affairs, the e-Cabinet system has been put into operation connecting up to 22 ministries and ministerial-level agencies, helping to manage Synchronously and fully managing the Government's meetings, organizing the collection of opinions of the Government members in a simple, fast and effective way on the network environment and contributing to shortening time and saving printing costs. Press, copy paper documents. From the opening day (June 24, 2019) to March 8, 2021, the e-Cabinet system has served 28 government conferences and meetings (delegate use electronic documents) and implemented currently processing 685 opinion polls of Government members, replacing the issuance of more than 253,000 dossiers. paper documents. The use of the System saves more than 169 billion VND/year [8].

According to a report by the Government Office, from the moment the Prime Minister pressed the button to open the National Public Service portal (December 9, 2019) with 8 initial public services, to March 8, 2021, more than 2,800 public services have been integrated, providing a total of nearly 6,800 administrative procedures at 4 levels of government, with more than 116 million visits, more than 468,000 registered accounts; more than 42.5 million state sync records; over 940,000 records made online and more than 67,000 electronic payment transactions (total amount of more than 26.7 billion dong) on the portal; received and supported over 53,000 calls, more than 10,000 reflections and recommendations. As of March 8, 2021, there have been more than 4.5 million electronic documents sent and received through the National Document Communication Axis, the number of electronic documents sent and received in 2020 is 2.5 times higher than that of the National Document Axis. year 2019 [14].

2.3. The development index of digital government towards a digital government in Vietnam

The Strategy for Development of Electronic government towards a Digital Government in the 2021-2025 period, with a vision towards 2030 (the Strategy) emphasizes the viewpoint of developing a digital government comprehensively and holistically, building upon the achievements attained so far. It aims to concentrate resources and mobilize the participation of the entire political system, employing innovative and distinctive solutions to fundamentally fulfill the development targets of electronic government by 2021 and establish a digital government by 2025.

To achieve these objectives, Vietnam has been making efforts in digital transformation, developing technological infrastructure, providing high-quality online public services, and investing in human resources development. The country has been focusing on enhancing digital skills, promoting digital literacy, and fostering a digital culture among government officials and the general public.

In the ranking of the electronic government development index, it shows that Vietnam has maintained a continuous increase in rank in the period 2014 - 2020 from position 99 to position 86. Ranking position on component indexes of Vietnam The year 2020 has a relatively large change. The Telecommunications Infrastructure Index (TII) increased sharply, up 31 places (in 2020, ranked 69th; 2018 ranked 100th); The Hu-

Tab. 1. Vietnam's electronic government Development Index. Source: United Nations electronic government survey (2010; 2012; 2014; 2016; 2018; 2020, 2022) [9]; [10]

year	E- Government Development Index (EGDI)	Type of index			ranking
		Online Services Index (OSI)	Telecommunication Infrastructure Index (TII)	Human Capital Index	
2010	0.4454	0.1036	0.0746	0.2672	90
2012	0.5217	0.4248	0.3969	0.7434	83
2014	0.4705	0.4173	0.3792	0.6148	99
2016	0.5143	0.5725	0.3715	0.5989	89
2018	0.5931	0.7361	0.3890	0.6543	88
2020	0.6667	0.6529	0.6694	0.6779	86
2022	0,6787	0,6484	0.6673	0.6903	86

man Resources Component Index (HCI) increased three places (in 2020, ranked 117th; in 2018, ranked 120th); The Online Services Index (OSI) dropped 22 places (in 2020, ranked 81st; in 2018, ranked 59th [13]). According to the four-level assessment by the United Nations for the Electronic government Development Index (EGDI), which includes very high (above 0.75), high (0.5 - 0.75), medium (0.25 - 0.5), and low (below 0.25), Vietnam's EGDI in 2022 reached a high level of 0.6787 points [10]. The country maintained its ranking at 86, with no change compared to the previous ranking in 2020 [10].

2.4. Satisfaction index of public administrative services

The construction and development of electronic government towards a digital government have brought about effective state administration and increased satisfaction indices among citizens and organizations towards the government.

In 20218, the overall SIPAS index nationwide was 82.99%. In 2019, the SIPAS index increased to 84.45%, a rise of nearly 1.5% compared to 2018. Among the factors, the satisfaction rate of citizens and organizations regarding service accessibility was 86.48%, administrative procedures were 86.54%, public officials were 85.62%, service outcomes were 88.56%, and and processing feedback and suggestions from citizens and organizations were 73.66%. The satisfaction rates with different aspects of the process of providing and delivering public services varied, with the highest increase seen in service accessibility and the most significant decrease observed in receiving and processing feedback and suggestions over the course of three years.

In 2020, the nationwide SIPAS index reached 85.48%. The satisfaction of citizens and organizations with administrative services varied among the 63 provinces, ranging from 73.91% to 95.25%, with half of the provinces nationwide falling within the range of 85.16% to 95.25%. In 2021, the overall SIPAS index nationwide was 87.16%. The SIPAS index for the 63 provinces and centrally-governed cities in 2020 ranged from 75.68% to 95.76%, with a median value of 85.17%. In 2022, the SIPAS index was 80.08%, with a satisfaction rate of 79.72% for policy development and organization implementation and 80.43% for the provision of administrative services. The SIPAS index of Vietnam was affected by the post-Covid-19 context; however, this context also presented an opportunity to accelerate the digital transformation process for the development of electronic government towards a digital government.

3. Challenges that arise in the process of developing electronic government towards a digital government in Vietnam

Firstly, challenges arise from institutional and policy factors

Although in the past time, the National Assembly, the Government and competent state administrative agencies have developed and issued a number of legal documents, creating an important legal basis for building and developing However, in practice, electronic government still encounters difficulties and obstacles. Typically, there are still gaps in regulations on management, connection, data sharing, identification and electronic authentication; regulations on the protection of personal data; regulations on electronic documents; archive electronic documents of state agencies; legal value of electronic documents in administrative and payment transactions; on the implementation of administrative procedures in the electronic environment; information security in the electronic environment; culture of behavior, communication in the electronic environment.

Secondly, challenges stem from technology, information, and communication factors

To ensure information safety and security, develop digital infrastructure (telecommunications infrastructure, internet of things infrastructure, data infrastructure), digital platforms (including platforms such as integration and sharing data, internet of things, artificial intelligence, connecting digital services, "blockchain", electronic identity), digital transformation… [12], the legal corridor, roadmap, and mechanism requires a contingent of cadres and civil servants with appropriate information technology qualifications; must have sufficient financial resources to be able to develop electronic government and digital government. However, the current infrastructure resources still have limitations.

According to Ookla statistics, broadband internet in Vietnam reached 47.66 Mbps in April 2020. Although lower than the world average (74.74 Mbps), it has also increased 5 places and ranked 59th worldwide[11]. With the current covered 4G network, from 2021, Vietnam will deploy 5G network on a large scale[4] and be classified as one of the leading countries in 5G network development. However, technology infrastructure is not enough, we also need to have a database - the core and integral element of digital transformation. In addition, the complexity and rapid change in technology makes technology projects in the public sector inherently slow, prone to conflicts of interest" and "moral hazard".

According to a report of the Ministry of Information and Communications, currently the level of investment for digital transformation in Vietnam is still low, accounting for only 0.3 - 0.5% of GDP. While the average investment in the world must be at least three times that.

Challenges and difficulties remain to achieve the goal of comprehensive reform of three groups of online public ser-

vice indexes (OSI), telecommunications infrastructure and human resources (HCl). In the roadmap for implementing electronic government in Vietnam, it is still necessary to continue to perfect the architectural framework for electronic government , build a national public translation portal, connect information across sectors, establish a national database, provide level 3 and 4 construction services parallel with the enhancement of security assurance [12].

Thirdly, challenges arise from the human resources within government agencies

The process of building and developing electronic government in Vietnam today has shown that the lack of high-quality human resources to exploit the full potential of Technology is also a significant obstacle for managers. Currently, a part of cadres, civil servants and public employees has limited ability to use information technology in solving work, still keeping the habit of using traditional paper documents; fear of change in changing the way of working in the digital environment…

According to the United Nations' assessment in 2020, Vietnam's Human Resources Index, although higher than previous years, is still lower than the world average (Vietnam only reached 0.6779 points, while the average score was 0.6779 points). of the world reached 0.688 points). Compared with 2014 is 0.6025 points, this index has not increased significantly; This index of Vietnam is much lower than that of Singapore - the country with the highest human resource index in the ASEAN region (0.8904 points) [12]. The report on the evaluation of the implementation results of the Master Program on State Administrative Reform for the 2011-2020 period shows that: "There are still limitations in the contingent of cadres and civil servants performing official duties" [6]

Fourthly, challenges emerge from the perspective of citizens and businesses

In order to build and develop electronic government towards digital government, besides preparing for infrastructure and human resource issues, the support of people's participation in this process is very important. However, at present, people's awareness and willingness to actually participate in implementing electronic government towards digital government through online public administrative transactions is still quite confusing; People are still apprehensive in using technological elements. The number of Vietnamese people using the Internet in 2020 is 68.17 million people, accounting for over 70% of the population and classified as countries with good spectrum, compared with the requirement of over 80% of high coverage) [14] .

4. Solutions to enhance the effectiveness of developing electronic government towards a digital government in Vietnam

First, enhance institutional and policy frameworks for electronic government and digital government. This includes researching and amending the Law on Electronic Transactions and the Law on Archives to facilitate the development of a digital government. Issuing government decrees on digital government, developing specialized data networks connecting central and local government agencies, establishing a government cloud computing platform, and developing integrated platforms for national data sharing and electronic identification and authentication are also essential.

Second, shift from individual, decentralized application development to a platform-based approach with prioritization and a focus on comprehensive solutions. This involves combining centralized and decentralized models while adhering to the National Architecture Framework and the architecture of ministries, sectors, and localities. Researching and developing digital technologies, standardizing and restructuring business processes, establishing automated monitoring and evaluation tools, and assessing the effectiveness of investment projects are important steps.

Third, provide training and develop digital government and digital skills for officials and civil servants. Designing appropriate training and development programs for electronic government and digital government, such as training in working in a digital environment, data collection and processing in a digital environment, and decision-making skills in a digital environment, is crucial.

Fourth, encourage citizen participation in the development of electronic government and digital government. Developing electronic government and digital government is ultimately about serving citizens better and increasing efficiency and effectiveness. Therefore, the government needs to strengthen communication and raise awareness among citizens to actively apply digital technologies in their daily lives and activities related to public administration. Organizing training programs and providing guidance to citizens on electronic government and digital government, as well as training them in software applications, are essential.

By implementing these solutions, Vietnam can further enhance the effectiveness of electronic government development, foster digital transformation, and improve public service delivery for citizens and businesses.

5. Conclusion

The development of electronic government towards digital government in Vietnam has achieved certain results. The indices related to electronic government development towards digital government have consistently shown an increasing trend from 2016 to 2022. Indices such as online public services, SIPAS, telecommunications infrastructure, and human resources demonstrate the level of responsiveness to the requirements of electronic government and digital government, thereby contributing to improving the effectiveness of public administration in Vietnam. However, the development process still faces certain barriers, including institutional and policy barriers, technological barriers, barriers from citizens, and the capacity of the public sector workforce.

The results achieved indicate the feasibility of developing electronic government towards digital government in Vietnam. Furthermore, the development of electronic government towards digital government will enhance the effectiveness of public administration in Vietnam by simplifying online administrative procedures to level 4, promoting transparency, controlling corruption and abuse of power, and engaging citizens and businesses in state management activities.

To improve the indices of electronic government development towards digital government, Vietnam needs to continue refining the institutional framework with solutions for institutional, technological, and human resource aspects, as well as fostering citizen engagement.

By addressing these challenges and implementing the necessary measures, Vietnam can further enhance the development of electronic government towards digital government, leading to more efficient public administration and greater citizen participation.

Literatura – References

1. Ministry of Information and Communications (2018 - 2020), Vietnam Information and Communication Technology Development and Application Readiness Index Report, Information and Communications Publishing House.
2. Ministry of Information and Communications (2021) Report No. 91/BC-BTTTT, June 30, 2022.
3. CPS in Vietnam will be formed in 2025. http://baochinhphu.vn, March 10, 2021.
4. Mobile & Fixed Broadband Conference (World Mobile Broadband & ICT), March 25, 2021, Hanoi.
5. Hoàng Thị Kim Chi (2021), Building e-Government in Vietnam - initial results and issues that need to be further promoted, https://tcnn.vn/news/detail/49459/Xay-dung-chinh- phu-dien-tu-o-Viet-Nam-ket-qua-buoc-dau-va-nhung-van-de-can-tiep-tuc-day-manh.html
6. Managing civil servants according to capacity to meet administrative reform requirements in Vietnam. https://www.moha.gov.vn, ngày 29/4/2021
7. Mehdi Khosrow-Pour, D.B.A (2008), Encyclopedia of Information Science and Technology, Second Edition8 Volumes, Published in Chepter: Democratic E – Governace; From: Encyclopedia of Information Science end Technoloy, Second Editiom
8. National Committee on E-Government (2021). The implementation of Resolution No. 17/NQ-CP on key tasks and solutions for e-Government development in the 2019-2020 period, with orientation to 2025.
9. United Nations (2020). Electronic government Development Index - EGDI2020, Digital Government in the Decade of Action for Sustainable Development
10. United Nations Electronic government Survey 2022, Department of Economic and Social Affairs – UNITED NATIONS New York.
11. Vietnam internet speed increased by 5 steps. https://vietnamnet.vn, ngày 15/6/2020
12. Think Tank Vinasa (2019), Việt Nam thời chuyển đổi, NXB Thế giới, Hà Nội
13. https://nhandan.vn/thong-tin-so/lhq-xep-hang-ve-chinh-phu-dien-tu-viet-nam-tang-2-bac-608578/
14. https://baochinhphu.vn/Tin-noi-bat/Chinh-phu-so-tai-Viet-Nam-se-duoc-hinh-thanh-vao-nam-2025/425348.vgp
15. https://vtv.vn/kinh-te/van-con-rao-can-trong-trien-khai-chinh-phu-dien-tu-20200918063141933.htm.
16. http://caicachhanhchinh.gov.vn/danh-muc/bao-cao-chi-so-hai-long-ve-su-phuc-vu-hanh-chinh-nam-2020-va-chi-so-cai-cach-hanh-chinh-nam-2020-cua-cac-bo-co-quan-ngang-bo-8866.html
17. https://www.pwc.com/m1/en/publications/documents/the-journey-to-digital-government-part-one-1.pdf

Gas Hydrate Detection Based on High Resolution Seismic Data in the Southeastern Offshore of Vietnam

Mai Thanh TAN[1)], Mai Thanh HA[2)], Nguyen Quoc HUY[3)], Nguyen Nhu TRUNG[4)]

[1)] Hanoi University of Mining and Geology/HUMG; email: mttan44@gmail.com
[2)] PetroVietnam Exploration and Production Corporation/PVEP; email: hamt@pvep.com.vn
[3)] Center for Planing and Investigation of Marine resources-environment/CPIM
[4)] Institute of Marine Geology and Geophysics, VAST

http://doi.org/10.29227/IM-2023-02-22

Submission date: 26-08-2023 | Review date: 17-09-2023

Abstract

Gas hydrates are the accumulations of methane (natural gas) trapped in ice-like structures with water. Gas hydrates represent an immense energy resource underlying large portions of the world's marine continental shelves. Vietnam has a large continental shelf area, in the deep water zone with suitable low temperatures and high pressure, which is suitable for the formation and existence of potential energy source of Gas Hydrate (GH).

The application of High-Resolution Seismic method (HRS) plays an important role in exploring for Gas Hydrate. The enhancement of HRS research such as optimal short - reception conditions and advanced data processing suitable for Gas Hydrate in shallow layers below the seafloor, allows for determining the geological factors related to Gas Hydrate's existence in the deep water area. Advancements in data processing technology, such as noise filters (Radon, F-K, SRMA, Tau-P..), seismic attributes analysis, seismic migration, AVO, seismic inversion, pre-stack seismic data and AI technology … allow to identify of the signs of Gas Hydrate presence, such as Bottom Simulated Reflector (BSR), Gas Hydrate Stability Zone (GHSZ), Pockmark, Chimney, etc.

This paper presents some of the results obtained from applying High-Resolution Seismic method to predict the distribution of Gas hydrate in the Southeastern offshore of Vietnam.

Keywords: *gas hydrate, high resolution seismic, Gas Hydrate Stability Zones/GHSZ, Bottom Simulated Reflector/BSR*

1. Features of the east sea area related to the existence of gas hydrate

Gas hydrates are formed under high pressure and low temperature conditions, so they exist only in shallow layers of the seabed in deep waters with natural gas potential and favorable geological factors.

a. Geological features

The documents obtained in many areas in the Southeastern offshore of Vietnam Sea and adjacent areas have demonstrated the existence of gas hydrates in areas between and below the continental slope with seabed depths of about 700 - 2500m.

The tectonic features, the operation of fault zones, especially young fault systems, volcanic activity have important implications for the formation and existence of Gas hydrate (Huaishan, 2002; Thakur, 2016; Tan, 2019). The tectonic feature of the East Vietnam Sea is the result of the impact of the Indian, Australian and Pacific plates on the Southeast edge of the Eurasian continent, combined with the spreading and development of the East Sea.

Newly developed young faults or reactivated older faults cut through Pliocene - Quaternary mainly in the NE-SW and N-S directions. The system of young faults is the favorable structural elements for leading gas from the deep up to accumulate into gas hydrate. Along the western slopes of the East Sea is where young volcanoes thrive, including young mud volcanoes, which relate to the sources forming gas hydrates.

The deep water area in the East Sea has a sea level depth of about 300-3500m. Most of the seabed topography has structural directions NE-SW and sub-latitudes, coinciding with the East Sea spreading direction, which is favorable for the formation of underground plateaus, uplift zones, turbidite sediments, mud diapirs and wedge encroachment. In the continental slope, the topography has a sudden change, creating quite steep terrains favorable for the formation of turbulent flow structures; the bottom sediment fan is related to the characteristics of the existing areas gas hydrate. Figure 1 is a seismic section of deep water areas associated with lightning diapir and volcanic activity possibly related to gas hydrates. The map of the Gas Hydrate forecast location in the East Vetnam Sea and study area is shown in Figure 2.

b. Temperature and pressure characteristics

With the characteristics of temperature, pressure and mineralization of seawater in the Vietnam East Sea, the top gas hydrate zone (TGHZ) at a depth of 500m from the seabed has a temperature of about 7.8°C. The thickness of the gas hydrate stability zone increases gradually from the shelf slope (0–120m) towards the center of the East Sea (up to 200m or thicker). With a depth of about 100–200m, the temperature changes from 13-20°C, at a depth of 300–500m, the temperature of the seabed changes in the range of 10.5–7.5°C, at a depth of 1000–3000m the temperature changes in the range of 5.0–2.5°C. In the deeper depressions of the East Sea, the temperature can drop below 2°C. With the characteristics of temperature, pressure and mineralization of seawater in the East Sea, the gas hydrate stability zone at a depth of 500m from the seabed has a temperature of about 7.68°C. Figure 3 is a section temperature forecasting model of Pliocene – Qua-

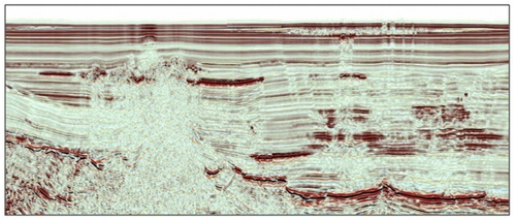

Fig. 1. Seismic section of deep water areas associated with lightning diapir and volcanic activity possibly related to gas hydrates

Fig. 2. The map of Gas Hydrates forecast location and study area in the East Sea of Vietnam

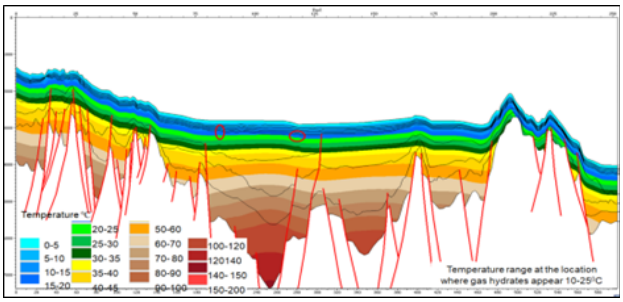

Fig. 3. The secton temperature forecasting model of Pliocene – Quaternary sediments in Phu Khanh marine at the present time

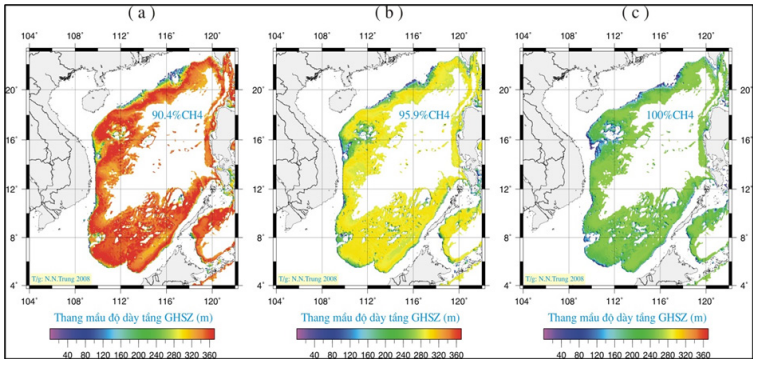

Fig. 4. Thickness map of gas hydrate stable layer (GHSZ) calculated for gas hydrates formed from natural gas. a. Content 90.4% CH4, b. Content 95.9% CH4, c. 100% CH4

ternary sediments on a line in Phu Khanh basin and Figure 4 is a thickness map of gas hydrate stable layer (GHSZ) calculated for gas hydrates formed from natural gas (Trung, 2012).

2. Highresolution seismic exploration for gas hydrate in Vietnam

In Vietnam today, initially conducting research, survey and search for Gas Hydrates in deep sea areas. The geophysical methods used include High Resolution Seismic (HRS), Multibeam Echo Sounding, Hydro Acoustic, Gravity Corer, etc. in which Multichannels High-Resolution Seismic methods (MHRS) play a dominant role (Hyndman, 1992; Thakur, 2010).

The GH is located in the shallow layers of the seabed in deep waters, in the gas hydrate survey, the source needs to generate short wavelength, high frequency pulses. The seismic source system uses a GI Airgun with a source pressure of 2000psi, the distance between two consecutive explosion points is 25m, the depth of the source is 3m. The receiver system has a length of 1200m, with 96 channels, the distance between the channels is 12.5m, the depth of the receiving band is 4m. The recording time is 5s, sampling step is 1ms.

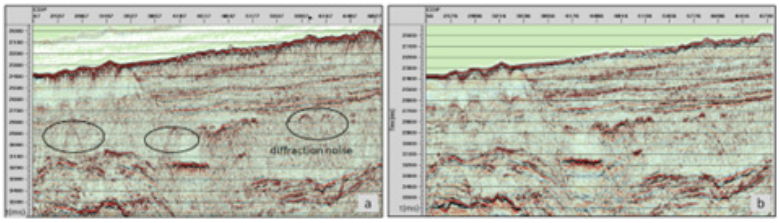

Fig. 5. Comparison of seismic section before (a) and after (b) applying Seismic Migration

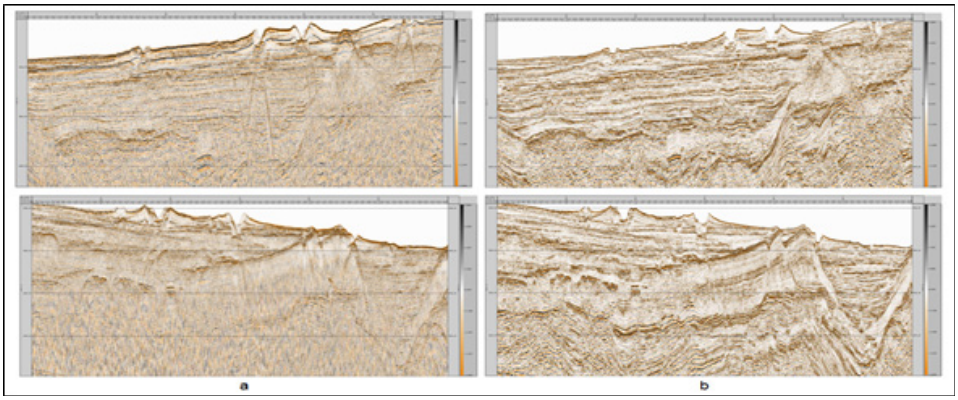

Fig. 6. Example of seismic sections comparison before (a) and after (b) data processing

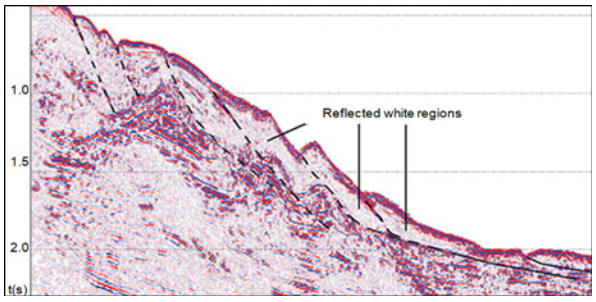

Fig. 7. A reflected white area on a seismic slice

Because gas hydrates have distinct characteristics from petroleum and other mineral objects, it is imperative to improve treatment efficiency with appropriate processes, software, and process parameters (Huaishan, 2002; Deng, 2006). Advanced processing methods are applied to improve the quality of data and directly determine the nature of Gas Hydrates such as detailed velocity analysis, using technologies to remove strong disturbances near the seabed that affect the detection of gas hydrate signatures (Predictive Deconvolution,SRMA, Randon, Tau-P,...), increase simulation reliability (CBM, DMS..), Seismic Migrations, use seismic attributes (SA), studying Amplitude Versus Offset (AVO), Seismic Inverse transform (SI) and using Artificial Intelligence Network (ANN).

Figure 5 is an example comparing the high resolution seismic section in study areas before and after seismic migration. Figure 6 is another example showing the improved seismic section quality after seismic data processing.

3. Direct signs of gas hydrate on seismic data

The process of improving the efficiency of processing and interpreting High Resolution Seismic data in the Southeastern offshore of Vietnam Sea allows studying upper sedimentary cover structure, marking out fracture zones and faults, serving pathways for gas - saturated fluids, migrating upwards (Tan, 2019). The achieved results detected the signs of the existence of Gas Hydrate such as Gas Hydrate Stability Zones (GHSZ), Bottom Simulated Reflector (BSR), Blank Zones (BZ), pores (Pockmark), gas column (Chimney)...(Wang, 2011; Taylor, 2004)

Gas Hydrate Stable Zones

In the East Sea area, with the relationship between sea water depth, geothermal gradient and gas hydrate type, the GHSZ zone can be formed at water depth from 600m to 1,500–2,200m with thickness from 0–225m to 0–365m. High-resolution seismic data have shown reflected white regions associated with this GHSZ. An example of a reflected white area on a seismic slice is shown in Figures 7.

Bottom Simulated Reflector (BSR)

The bottom surface of the gas hydrate stable zone is the boundary between the zone containing gas hydrate and free gas, so there is a difference in speed and high reflection amplitude. Because the bottom surface of the gas hydrate stability zone has a shape similar to that of the seabed but has a phase reversal compared to the seafloor, it is called a simulated seafloor reflector (BSR) (Le, 2005; Ojha,2009). In the East Sea, the stability of the gas stability zone is not as high as in other

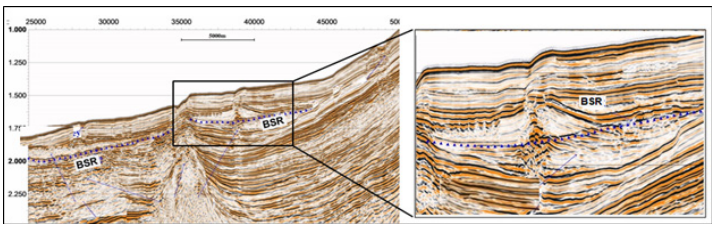

Fig. 8. Seismic slice showing BSR (Tu Chinh Vung May area).

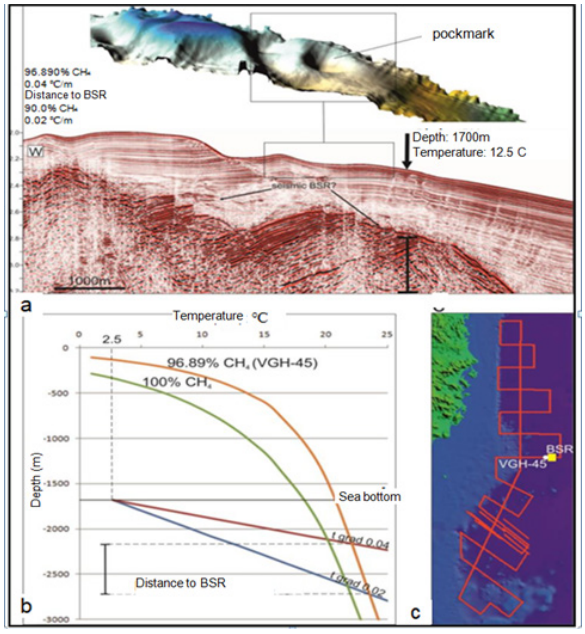

Fig. 9. Seismic section and gas hydrate stability curve. a. The seismic line shows the BSR, b. Gas Hydrate stability curve, c. Location of seismic section and of sampling station

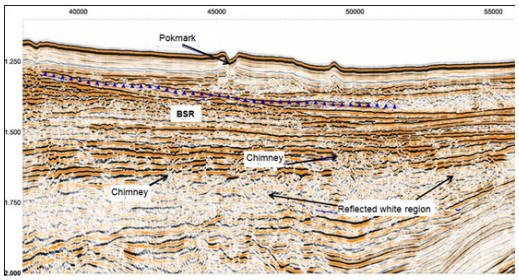

Fig. 10. Representation of pockmark, chimney, reflected white region and BSR on seismic section

regions, so identifying them requires improving the efficiency of document processing. Figure 9 is a seismic slice showing BSR (Vung May Tu Chinh area). Figure 9 shows the section with seabed depth of 1700m, and seabed temperature of 12.50°C. Here, there is a high-amplitude reflector lying gently parallel to the sea floor, covered with fine sediment. Below the gas hydrate stability zone, the seismic wave field represents a saturated gas region. Vertical cracks can be a path for saturated gas to escape to the seafloor. On hydroacoustic data, a pockmark ~800m in diameter is observed, possibly created above the gas hydrate accumulation area.

Pockmark and Gas chimney

In the marginal uplift zones, the central uplift often has depressions, where mud, liquid and gas from the seabed push into the aquatic environment to form Pocmarks. These pits may be buried in association with Gas chimneys which are likely related to gas hydrates. In the seismic and hydroacoustic literature, some signs of saturated gas in the upper sediments along the pore structures have been identified that may be related to the gas hydrate stability zone (GHSZ). Figure 10 is representation of pockmark, chimney, reflected white region and BSR on seismic section

Conclusions

Gas hydrate is a potential energy source of Vietnam in the deep sea with low temperature and high pressure. The application of the high-resolution seismic method has a very important role, which is used effectively not only to determine the geological factors related to the gas hydrate existence, but also allows to identify the signs of development and present them as gas hydrate stability zone (GHSZ), bottom simulated reflector (BSR), pores (pockmark), gas column (Chimney)...

The research results have allowed to determine the applicability of the high-resolution seismic method to search for gas hydrate in Vietnam, a feature that exists in the study area in the Southeast of Vietnam's waters.

Acknowledgements

The authors would like to thank the Center for Planning and Investigation of Marine Resources and Environment in the Northern Region (CPIM) and Hanoi University of Mining and Geology (HUMG) for creating favorable conditions for this study.

Literatura – References

1. Deng, H., P. Yan, H. Liu, and W. Luo, 2006: Seismic Data Processing and the Characterization of a Gas Hydrate Bearing Zone Offshore of Southwestern Taiwan. Terrestrial, Atmospheric and Oceanic Sciences Journal., 17 (4), 781-797. DOI: 10.3319/TAO.2006.17.4.781(GH)
2. Huaishan, L., Zhengyun, Z., 2002: Seismic data processing approaches for the study of gas hydrates in the East China sea, Journal of Ocean University of Qingdao, 1, 87-92. https://doi.org/10.1007/s11802-002-0037-1
3. Hyndman, R. D., and G. D. Spence, 1992: A Seismic Study of Methane Hydrate Marine Bottom Simulating Reflectors, Journal of Geophysical Research, Solid Earth, 97 (B5), 6683–6698. https://doi.org/10.1029/92JB00234
4. Le A. N., Huuse M., Redfern J., Gawthorpe R.L. and Irving D., 2015: Seismic characterization of a Bottom Simulating Reflection (BSR) and plumbing system of the Cameroon margin, offshore West Africa, Marine and Petroleum Geology, 68, 629-647
5. Ojha, M., and Sain, K., 2009: Seismic attributes for identifying gas-hydrates and free-gas zones: Application to the Makran accretionary prism, Episodes, 32 (4), 264–270. DOI: 10.18814/epiiugs/2009/v32i4/003
6. Sultana, N., et al, 2007: Detection of free gas and gas hydrate based on 3D seismic data and cone penetration testing: An example from the Nigerian Continental Slope, Marine Geology, Vol. 240, Issues 1-4, 235-255 https://doi.org/10.1016/j.margeo.2007.02.012
7. Tan, M.T, et al, 2019, Improve the Effectiveness of Seismic Research for Petroleum and Gas Hydrate Exploration in Vietnam, Journal of the Polish Mineral Engineering Society, 21 (1/2), 199-206
8. Taylor, C.E., and Kwan, J.T., 2004: Advances in the Study of Gas Hydrates, Kluwer Academic/Plenum Publishers, New York, pp. 270.
9. Thakur, N.K., and Rajput M. S., 2010: Exploration of Gas Hydrates: Geophysical Tecniques, Springer, 281 pp.
10. Trung, N.N., 2012: The gas hydrate potential in the South China Sea, Journal of Petroleum Science and Engineering 88–89, 41–47
11. Wang, X., Wu, S., Guo, Y., Yang,S., and Gong, Y., 2011: Geophysical Indicators of Gas Hydrate in the Northern Continental Margin, South China Sea, Journal of Geological Research, Volume 2011 Article ID 359597.

Optimizing the Width and Compressive Strength of Artificial Protective Pillar in the Mining of Medium-Thick Coal Seams in Quang Ninh Using the Numerical Model

BUI Manh Tung[1)], DINH Van Cuong[2)]*

[1)] Faculty of Mining, Ha noi Univesity of Mining and Geology, Hanoi, Vietnam
[2)] VietNam National Coal – Mineral Industries Holding Corporation Limited, Hanoi, Vietnam
* Corresponding author: buimanhtung@humg.edu.vn

http://doi.org/10.29227/IM-2023-02-23

Submission date: 23-08-2023 | Review date: 19-09-2023

Abstract

Currently, in many countries with the coal mining industry, the technology of using artificial pillars has been successfully applied to replace coal pillars to protect the entry gate road, thereby reducing the rate of resource loss, as well as the cost of entry gate road, and mining costs. However, in order to optimize the required width and compressive strength of artificial pillars with thickness, slope angle and mining depth, more detailed studies are required for each specific geological condition. This research uses Phase 2 numerical simulation software to analyze the stability of artificial protective pillar of the roadway prepared in the mining of medium-thick coal seams in the Quang Ninh coal region (Vietnam). The research results show that the relationship between the width of the artificial pillar and the slope angle follows the rule of a linear function. The size of the artificial protection pillar increases according to the mining depth. When the mining depth is 350m, the size of the pillar changes from 1.0 ÷ 2.4m, and to 1.4 ÷ 2, 8m at a depth of 500m. When the slope angle increases, the required pillar width also increases. That is due to the fact that at a large slope angle, the pressure acting on the pillar is not at the center, but deflects to the side adjacent to the entry gate road that needs to be protected, the compression force is not distributed evenly. The required compressive strength of the artificial pillar varies according to the condition of the slope angle, when the seam slopes 10°, the required compressive strength is from 8 to 12 MPa, when the slope angle increases to 20°, the required compressive strength of the pier increases to 18 ÷ 28 Mpa, but when the slope angle increases to 35°, the required compressive strength of the pillar tends to decrease to 16 ÷ 17 MPa. Thus, when operating in the corresponding conditions, it is necessary to choose the size and required compressive strength of the artificial pillar to ensure the working capacity of the pillar.

Keywords: *medium thick coal seam, entry gate road, artificial support pillar, pillar width, compressive strength*

1. Introduction

The loss rate in underground mining technology in Quang Ninh coal area is currently at over 20%, mainly concentrated in coal pillars protecting the transport roadway (Cuong et al.,2019). This rate is relatively high, significantly affecting the efficiency of mine construction investment and wasting non-renewable resources.

In many countries, a technological solution has been successfully applied to use artificial pillars to replace coal pillars to protect the roadway. In that technology, in order to simultaneously exploit coal in the protection pillar and maintain the transport roadway as a ventilation roadway for the next coalface, the coal pillar will be replaced by an artificial pillar formed from a strip of rock inserts, clusters of columns, cribs, chemical materials or concrete mortar mixes. In addition to reducing the rate of resource loss, the solution of using artificial pillars also allows reducing the cost of preparing roadway meters, reducing 01 main entry, equivalent to about 50% of the cost and the cost of mining.

Hu (2012) utilized statistical analysis methods to analyze more than 20 mines that utilized waste rock backfilling in China, examining the technical characteristics of different backfill materials for protecting underground mine structures. The study identified that production capacity, size of backfill material, extraction ratio, extraction cost, backfill efficiency, degree of mobility, deformation, and protected area are fundamental indicators for evaluating the effectiveness of backfill in mines. Based on the practical experience, Song. (2010) concludes that the reasonable load-bearing capacity of the material used for artificial pillars is the determining factor for their effectiveness. Waste rock in underground mines is one of the main backfill materials that contribute to the formation of pillars with high strength. Some studies on coal pillar recovery have also recently been carried out. Zhou et al.(2019) proposed the use of a sand-based backfilling body to recover the remaining coal pillars and analyzed the principle involved in the use of sand-based backfilling bodies to maintain the stability of the stope. Ma et al.(2017) proposed the use of solid backfill to replace the coal pillars in the lower part of an industrial square to provide effective surface-subsidence control while Sun et al.(2018) proposed the cemented paste backfilling method to recover short-strip coal pillars and studied the stability conditions of the impermeable layer.

In the study on the degradation law of cemented artificial pillars as a replacement for protective inter-block coal pillars, Chi et al.(2023) employed the Flac3D model to simulate real conditions in a mine in Shanxi, China. The results demonstrated that with a pillar width of 14m, the cemented artificial pillars could sufficiently bear the load requirements, and the surrounding rock mass remained relatively stable. The field monitoring at the experimental site confirmed the feasibility

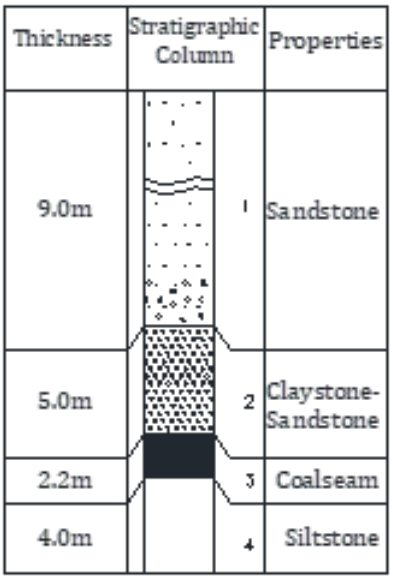

Fig. 1.1. The typical geological column

Fig. 1.1. The typical geological column

Materials	Density, T/m³	Elastic module, MPa	Poisson index	Tensile strength, MPa	Internal friction angle, degree	Adhesive force, MPa
Coal	1,64	2000	0,25	0,1	28	1,0
Claystone	2,65	3000	0,29	0,2	29	1,4
Siltstone	2,66	4270	0,23	0,42	31,47	2,6
Sandstone	2,71	4000	0,21	0,1	33,28	5,0
Conglomerate, gritstone	2,66	4000	0,20	0,1	33,5	4,8
Post-caving coal and rock	1,70	30	0,07	0	30	0

of using cemented artificial pillars as a replacement for protective inter-block coal pillars.

However, there have been few published results describing the recovery of replacing protective inter-block coal pillars generated by the short wall block mining process, hence further analysis and exploration are needed.

The research works to reduce coal loss in the pipeline protective pillar carried out in Vietnam have mainly been in the direction of reducing the size of the pillar, driving new ventilation roadway following the areas that have been exploited, or making the most of the protection pillars while exploiting the blast roadway. Recently, the diagram of mining technology without leaving protection pillars has also been studied and proposed but has not been implemented in practice. Therefore, it is necessary to have detailed studies on determining the parameters of the artificial pillars to protect the preparatory roadway during the mining process at the underground mines in Quang Ninh region in order to maximize the resources and improve production efficiency.

The artificial pillar, replacing the coal pillar, must ensure resistance against the mining pressure exerted on it, taking into account the geological conditions of the construction area of the roadway and the depth at which the roadway is located. If the artificial pillar is constructed using materials with low compressive strength, the width of the pillar will need to be large, resulting in a greater amount of material to be transported, increased labor intensity, and higher construction costs. Therefore, two fundamental parameters of the artificial pillar need to be determined: (1) the width dimension of the pillar (B) and (2) the required compressive strength of the pillar (P).

In terms of the research subject, the utilization of materials with high compressive strength for the artificial pillar represents a significant advancement and a high level of reliability within the mining industry. The application of this form of artificial pillar has become a prevailing trend, and it is prioritized whenever conditions allow. Therefore, in this context, the article delves into a comprehensive investigation and analysis to determine the optimal parameters for the implementation of artificial pillars utilizing materials with high compressive strength.

2. Characteristics of rock geological conditions

The geological conditions consist of coal seams and common rock types within the stratigraphy of the Quang Ninh region (such as clay, shale, sandstone, conglomerate, siltstone, etc). The average thickness of the coal seam is 2.2 meters, while the average thickness of the immediate roof rock is 5.0 meters, and the main roof rock is 9.0 meters. The coalface employs a longwall mining system, with pressure control achieved through the method of fully caving. The typical geological column is depicted in Figure 1.1.

The main geomechanical properties of the real rock mass in the Quang Ninh coalfield is reflected in Table 1.

3. Reseach on the optimal compressive strength of artificial pillars to protect roadway

Currently, in the field of stability analysis of the rock mass surrounding underground mining voids and the design of support structures for mining areas in coal mines, several calculation software programs based on fundamental math-

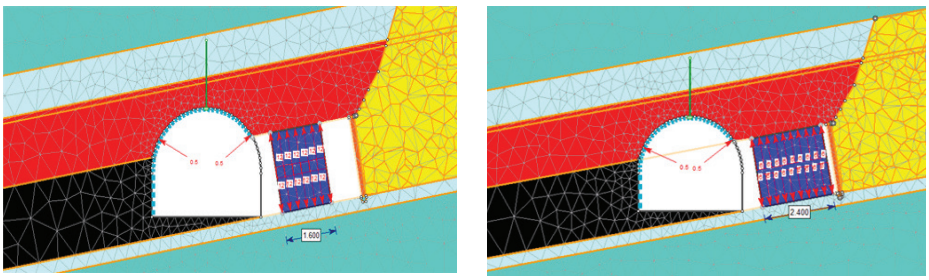

The pillar width: B=1,6m The pillar width: B=2,4m

Fig. 2.1. The analysis model of average seam, sloping angle α = 10°

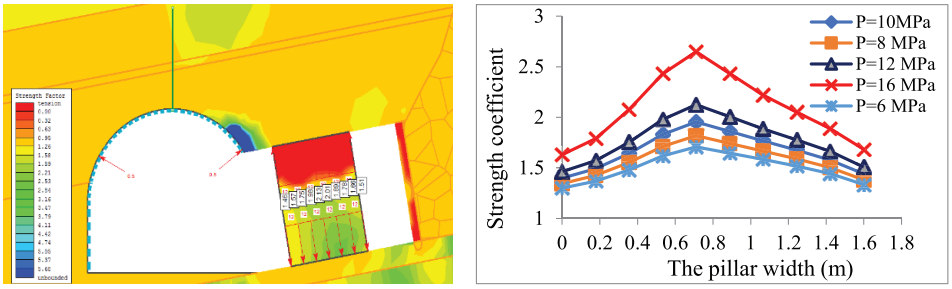

a) Strength coefficient inside the pillar b) Strength coefficient of the protective pillar

Fig. 2.2. Strength coefficient of the protective pillar (B = 1,6m, α= 10°)

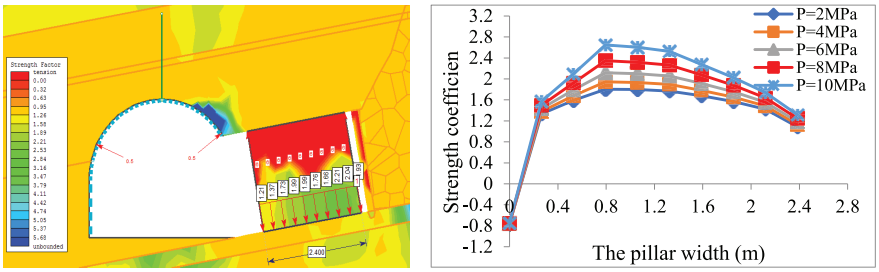

a) Strength coefficient inside the pillar b) Strength coefficient of the protective pillar

Fig. 2.3. Compressive strength and strength coefficient of the protective pillar (B = 2,4m, α= 10°)

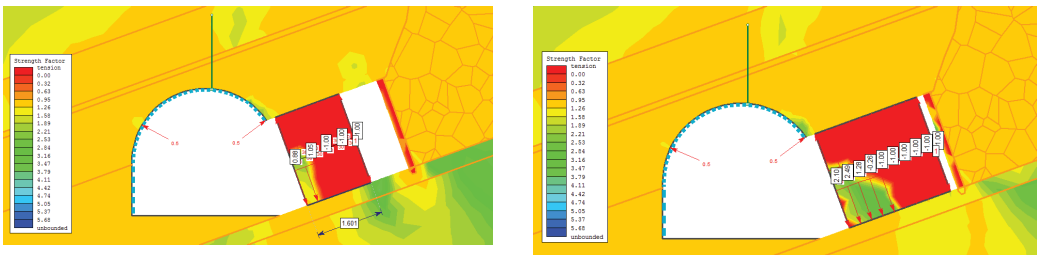

a) Safety coefficient of the pillar when B = 1,6m, P = 30MPa b) Safety coefficient of the pillar when B = 2,4m, P = 20MPa

Fig. 2.4. The strength coefficient of protective pillar, α = 20°

ematical methods such as the finite element method, finite difference method, limit equilibrium method, boundary element method, discrete element method, etc., have been widely used. Some notable software programs include Phase 2, Ansys, Abaqus, UDEC, Flac, etc. In this article, the Phase 2 software (based on the finite element method) is chosen to analyze the necessary stability of the artificial support column, taking into account geological and engineering parameters such as thickness, dip angle of seam, mining depth, and required compressive strength of the artificial pillars.

3.1 Numerical model development

The working capacity of the artificial pillars is influenced by various geological and mining engineering factors such as the thickness and dip angle of the seam, the mechanical properties of the surrounding rock, the mining depth, hydrogeological conditions, gas content in the mine, coal self-ignition capacity, and the applied mining technology. Within the scope of this research, the focus will be on selecting and limiting the typical input parameters based on the current mining conditions in the Quang Ninh coal region. These parameters greatly affect the working capacity of the artificial pillar, namely the

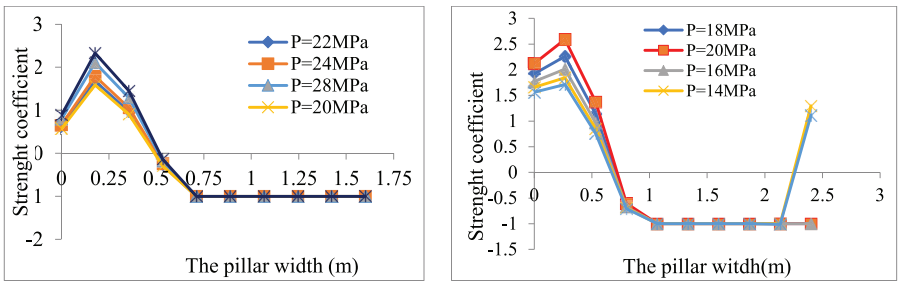

a) B = 1,6m b) B = 2,4m

Fig. 2.5. The relationship between the strength coefficient and the compressive strength, α = 20°

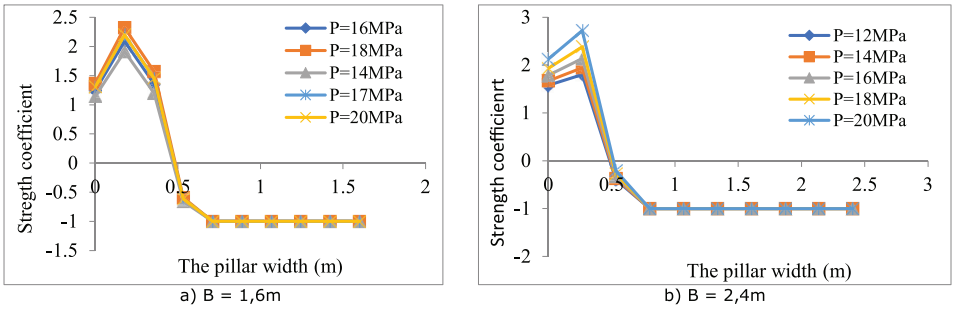

a) B = 1,6m b) B = 2,4m

Fig. 2.6. The relationship between the strength coefficient and the compressive strength, α = 35°

Tab. 2.1. Research results on the optimal compressive strength of the artificial pillar under conditions of medium-thick coal seam

Pillar width	Seam slope angle		
	10°	20°	35°
1,6m	12 MPa	28 MPa	17 MPa
2,4m	8 MPa	18 MPa	16 MPa

seam thickness, dip angle, and mining depth. Specifically:

For the seam thickness factor, a case study with an average thickness of 2.2m will be chosen.

For the dip angle factor, the range of dip angles will be limited to 35 degrees, with intervals of 10 degrees, 20 degrees, and 35 degrees.

Regarding the mining depth, two values will be selected: 350m (representing the common mining level in current mines) and 500m (representing the depth of sustained mining levels).

The seam consists of claystone, siltstone, sandstone, and the seam of the pillar are composed of siltstone and sandstone (Figure 1.1, Table 1.1). The numerical analysis model for the problem has a width of 33.509m and a height of 24.025m, ensuring that the distance from the mine boundary is equal to (5–6) times half the width of the roadway so that the influence of the roadway on the surrounding rock mass is negligible. As the protected roadway is located at a significant depth, the overlying soil and rock in the model are replaced by an equivalent load with a value of:

$$p = (H - h).\gamma; \text{ MPa} \quad (2.10)$$

Where:

H – the depth of roadway placement, H1 = 350m; H2=500m

h – height from the top of the roadway to the top of the model, h = 13,375m

γ – weight of the volume of rock layers above the roadway, average γ = 0,026MN/m³;

Applying the formulae 2.10, the vertical load is determined to change according to the length: p_1=8,75MPa; p_2 = 12,06MPa.

The directional control of the artificial pillar width is constrained within the range of (0.7-1.1) times the height of the face (Niełacny, 2009 and Rak, 2017). With a corresponding mirror aperture height of 2.2m, the artificial pillar width is determined to be 1.6m and 2.4m, allowing for the determination of the appropriate compressive strength of the artificial pillar under slope conditions of 10°, 20° and 35°.

To describe the width of the protective pillar, the model utilizes a separate rock layer with the characteristics of artificial rock to establish and hypothesize the variation in soil pressure caused by the artificial pillar. The roadway gallery is supported by SVP-22 steel, and the reinforced two-column steel support system of the roadway is described in the model using concentrated forces generated by the support columns, with corresponding values of 0.5 MN/m2 or 50 tons/m². The anchorage structure and the SVP steel are simultaneously described in the model of the problem. The numerical model diagram is created using Phase 2 software for the cases described in Figures 2.1.

3.2 Result analysis

As mentioned above, the working capacity of the artificial pillar is represented by the stability coefficient, which refers to its ability to maintain stability under the load of the mine. The stability coefficient of the pillar is determined by dividing the ultimate load-bearing capacity of the pillar by the load applied to the pillar from the mine. For the design of stable protective pillars in underground coal mining, a stability coefficient value of ≥ (1.5 to 2.0) for the rock pillar is considered acceptable (Reed et al., 2017; Simon et al.,2019 and Bieniewski., 1992). Depending on the complexity, characteristics, and

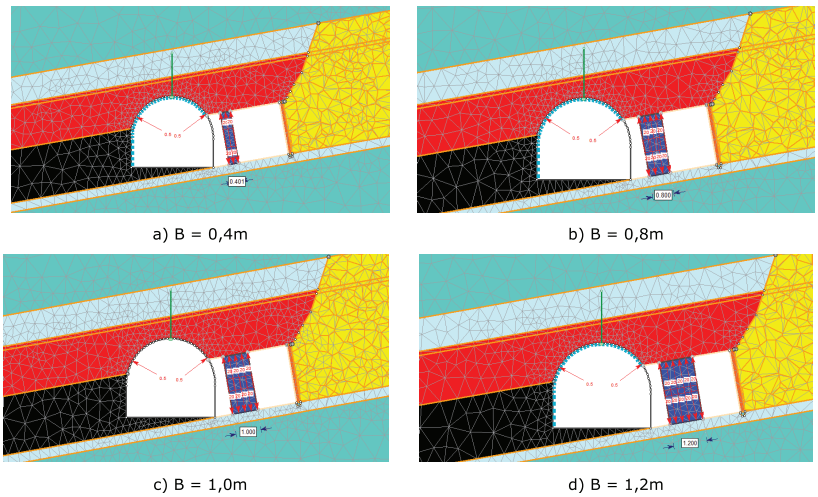

Fig. 2.7. Model to determine optimal pillar width

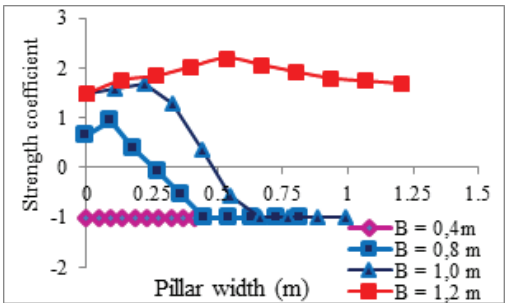

Fig. 2.8. The relationship between the strength coefficient and the protective pillar, α = 10°, H = 350m, P = 20MPa

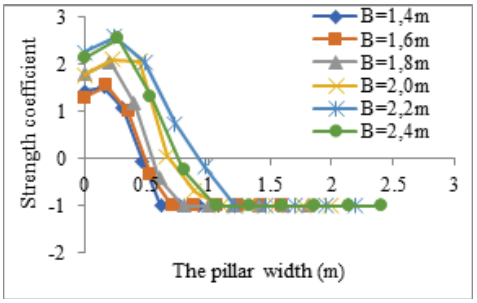

Fig. 2.9. The relationship between the safety factor and the width of the protective pillar, α =20°, H = 350m, P = 20MPa

importance of the protected gallery, a value greater than 2 can be selected. Due to the complex geological conditions in the underground coal mines of the Quang Ninh region, the author chooses a stability coefficient of 2 to determine the optimal compressive strength of the artificial pillar in the numerical model. Thus, in the models, the assumed compressive strength value of the pillar will be varied until the stability coefficient of the pillar reaches a value ≥ 2, indicating that the pillar meets the required stability criteria. The detail results are as followed:

In the case of a slope angle of 100, with an artificial protective pillar width of B=1.6m, through numerical analysis, the research results indicate the strength coefficient values of the materials in the pillar as shown in Figures 2.2.

Observing the results on the graph, it can be seen that when the compressive strength of the protective pillar is ≥ 12MPa, the stability coefficient at the midpoint of the pillar has a value > 2.0. This represents the minimum or optimal compressive strength value that the pillar must achieve.

In the case of a slope angle of 10o and an artificial protective pillar width of 2.4m, a similar analysis has been conducted with the analytical model and stability coefficient as shown in Figures 2.3.

It can be observed in the Figure 2.3 that when the compressive strength of the protective pillar is ≥ 8MPa, the stability coefficient of the pillar has a value ≥ 2.0. This represents the minimum compressive strength value that the pillar must achieve in the case of a width of 2.4m. From the graph in Figure 2.3, it is also evident that as the width of the protective pillar increases, the load-carrying capacity of the pillar increases, thereby reducing the required compressive strength. This is consistent with practical observations, as smaller protective pillars require higher strength, while larger ones can have reduced compressive strength requirements.

In the case of a slope angle of 20°, with protective pillar widths of B = 1.6m and B = 2.4m, through numerical modeling, the research content establishes a model for determining the optimal compressive strength of the pillar as shown in Figures 2.4.

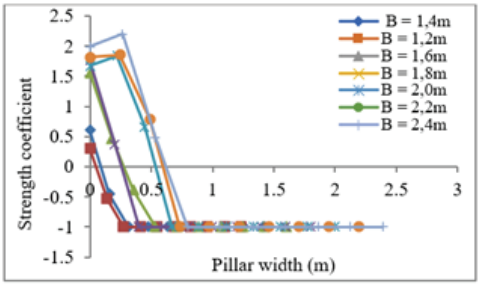

Fig. 2.10. The relationship between the strength coefficient and the protective pillar width, α = 35°, H = 350m, P = 20 MPa

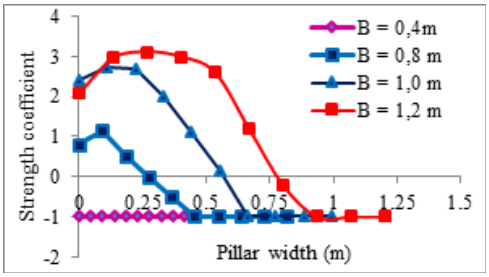

Fig. 2.11. The relationship between the strength coefficient and the protective pillar width, α = 10°, H = 350m, P = 30MPa

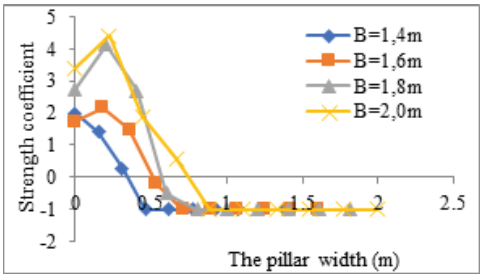

Fig. 2.12. The relationship between the strength coefficient and the protective pillar width, α =20°, H = 350m, P = 30MPa

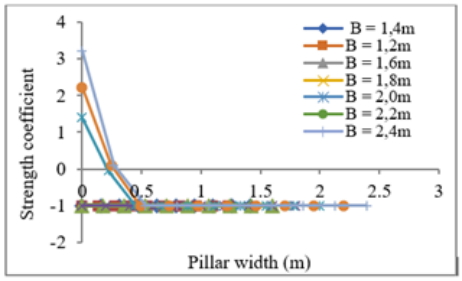

Fig. 2.13. The relationship between the strength coefficient and the protective pillar width, α =35°, H = 350m, P = 30 MPa

Observing the distribution of the strength coefficient in the protective pillar, it is found that when the slope angle of the seam increases to 20°, the distribution of the safety factor skews towards the left side of the pillar, with the region of distribution located approximately one-third of the width of the protective pillar. By conducting multiple models with different values of the compressive strength of the protective pillar, the research yields the relationship between the strength coefficient of the protective pillar and the width of the protective pillar for two cases: B = 1.6m and B = 2.4m, as shown in Figures 2.5.

Observing the results from the two graphs in Figures 2.5, it is observed that in the case of B = 1.6m, for compressive strength of the protective pillar P ≥ 28MPa, the strength coefficient ensures stability. In the case of B = 2.4m, the necessary compressive strength of the protective pillar is P ≥ 18MPa.

Next, further research is conducted for a seam slope angle of 35 degrees and pillar widths B = 1.6m and B = 2.4m. By performing multiple model simulations, the relationship between the strength coefficient of the protective pillar and the varying values of the compressive strength of the protective pillar is obtained, as described in Figures 2.6.

Observing the results from the graphs in Figures 2.6, it is noted that similar to the case of a 20 degree slope angle, when the slope angle of the seam increases to 35 degrees, the distribution of the strength coefficient in the protective pillar skews further towards the left side of the pillar. The region of distribution is concentrated approximately between one-third to one-fifth of the width of the protective pillar. The optimal compressive strength required to ensure a strength coefficient ≥ 2.0 is P ≥ 17MPa for B = 1.6m, and P ≥ 16MPa for B = 2.4m in the case of an medium-thick coal seam and a slope angle

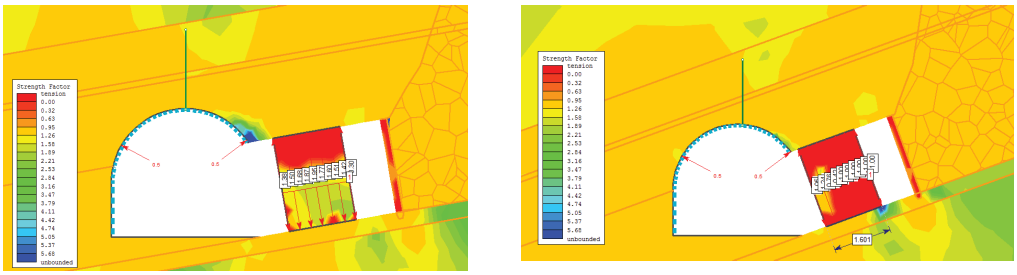

a) Slope angle α = 10° b) Slope angle α = 20°

Fig. 2.14. The distribution of strength coefficient, mining depth of 500m

of α = 35 degrees. These values are considered optimal for the protective pillar under these conditions.

The research results determining the optimal compressive strength of the artificial pillar are presented in Table 2.1.

The research results presented in Table 2.1 show that the required compressive strength of the artificial pillar under conditions of a 10° slope angle (8-12 MPa) is lower than in other cases. The reason is that the strength coefficient is evenly distributed across the entire width of the pillar, allowing for its load-bearing capacity to be fully utilized. When the slope angle increases to 20°, the strength coefficient skews towards the left side (adjacent to the protective boundary), resulting in uneven pressure distribution across the width of the pillar. To prevent failure, the required compressive strength of the pillar needs to be increased (18 ÷ 28 MPa). However, when the slope angle reaches 35°, there is a trend of decreasing the required compressive strength of the pillar. The reason is that at higher slope angles, there is a significant eccentric pressure, leading to a reduction in the vertical pressure acting on the pillar while increasing the pressure on its sides.

4. Determining the optimal size of the artificial protective pillar for roadway protection

Based on the results presented in Table 2.1, in comparison with the conditions of the coal seams in the majority of the Quang Ninh region, which are predominantly inclined with slopes ranging from 15o to 35o, and considering the overall experience of using artificial pillars worldwide, the construction materials for the pillars commonly have compressive strengths ranging from 20 to 40 MPa. Therefore, for the purpose of studying and determining the optimal width of the artificial pillars, the research has selected compressive strengths of 20 MPa and 30 MPa for the construction materials of the pillars.

As analyzed in the previous section, this section will focus on selecting the optimal width of the protective pillars under the assumption of predetermined compressive strengths of 20 MPa and 30 MPa.

4.1. Analysis model for the case of the medium-thick coal seam, artificial pillar compressive strength of 20 MPa, and mining depth of 350m and slope angle of 10° , 20°, 35°

Based on the above assumption, the research focuses on a fixed artificial pillar compressive strength of 20 MPa and varies the width of the protective pillar, B, from 0.4m until the pillar's safety factor reaches a value of ≥ 2.0. At that point, we will have the optimal width of the protective pillar, as illustrated in Figure 2.7.

In the case of artificial pillar compressive strength of 20 MPa and slope angle of 100. By analyzing the data, a chart depicting the relationship between the pillar's strength factor and the variation in pillar width is established, as shown in Figure 2.8.

Observing the results on the graph, it can be seen that when the safety factor of the pillar reaches a value of ≥ 2.0, the width of the protective pillar can be considered optimal. Correspondingly, in this case, when the width of the protective pillar, B, is 1.2m, the safety factor is 2.9. In other words, with the assumed compressive strength of the pillar of 20 MPa, the minimum (optimal) width of the protective pillar is 1.2m in the condition of medium-thick coal seam and a slope angle of 100.

In the case of the compressive strength of the pillar of 20 Mpa and slope angle of 200, the research aims to construct and develop various models while keeping P = 20 MPa constant for all models and varying the width of the protective pillar, B, as follows: 1.4m, 1.6m, 1.8m, 2.0m, 2.2m, and 2.4m. The study focuses on observing the changes in the safety factor of the protective pillar. The obtained results show the relationship between the safety factor of the protective pillar and its width, as depicted in Figure 2.9.

Observing the graph, it can be seen that the safety factor of the protective pillar is concentrated mainly in the left-third region of the pillar's width. In the case where the width of the pillar, B, is equal to or greater than (1.8 to 2.0) meters, with a pressure exerted by the protective pillar of P = 20 MPa, a safety factor of ≥ 2.0 is considered acceptable. This width is considered optimal for the protective pillar in the case of a medium-thick coal seam and a slope angle of 20°.

In the case of the compressive strength of the pillar of 20 Mpa and slope angle of 35o, by conducting a similar analysis with varying pillar widths ranging from 1.4m to 2.4m, the analytical model shows that under the conditions of a 35° slope, a pillar compressive strength of 20 MPa, the optimal width for the protective pillar is B = 2.4m (Figure 2.10).

4.2. Analysis model for the case of medium-thick coal seam, artificial pillar compressive strength of 30 MPa, mining depth of 350m and slope angle of 10°, 20°, 35°

In the case of pillar compressive strength of 30 MPa, slope angle of 10o, by varying the width of the pillar in the models from 0.4m ÷ 1.2m, the research results establish the relationship between the stability factor of the pillar and the width of the protective pillar, as shown in Figure 2.11.

Observing the results in Figure 2.11, it can be seen that when the compressive strength of the protective pillar is 30MPa, the optimal width of the pillar can be chosen as B = 1.0m. This is also consistent with reality, as the greater the load-bearing capacity of the pillar, the narrower the width of the pillar can be reduced.

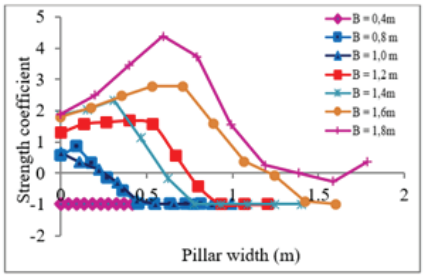

Fig. 2.15. The relationship between the strength coefficient and the width, α = 10°, H = 500m, P = 20MPa

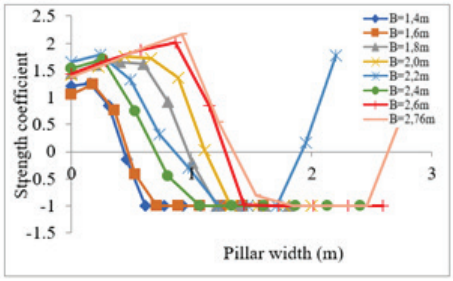

Fig. 2.16. The relationship between the strength coefficient and the width , α = 20°, H = 500m, P = 20MPa

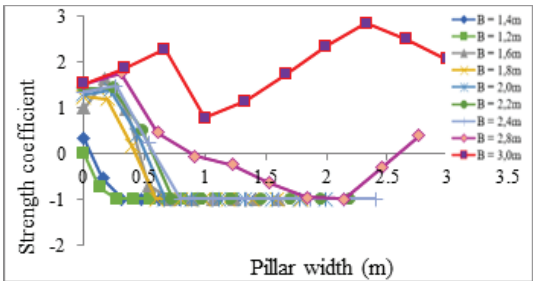

Fig. 2.17. The relationship between the strength coefficient and the width, α = 35°, H = 500m, P = 20MPa

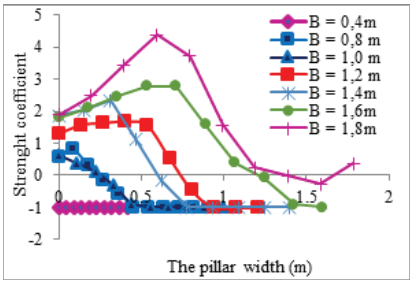

Fig. 2.18. The relationship between the strength coefficient and the width, α = 10°, H = 500m, P = 30MPa

In the case of pillar compressive strength of 30 MPa, slope angle of 20o, by keeping the pressure of the artificial protective pillar fixed at P = 30MPa and varying the width of the pillar from 1.4m to 2.0m, the research findings show the relationship between the strength coefficient of the protective pillar and the width of the pillar, as depicted in Figure 2.12. The results indicate that as the pressure of the artificial pillar increases to 30MPa, the width of the pillar can be reduced. In this case, a width of B = 1.6m ensures sufficient strength when subjected to load.

In the case of the compressive strength of the pillar of 30 MPa, slope angle of 35o. Similarly, by observing the relationship between the stability factor of the protective pillar and the width of the pillar in the case of a slope angle of α = 35° (Figure 2.13), it is found that in the case of a pillar compressive strength of P = 30MPa, the optimal width of the protective pillar is considered to be B ≥ 2.2m.

4.3 Analysis model for the case of medium-thick coal seam, artificial pillar compressive strength of 20 MPa, and mining depth of 500m

The typical numerical analysis model for the case of medium-thick coal seam is with the initial assumed pressure of P = 20MPa. After conducting the analysis, the distribution of the safety factors in the protective pillar is obtained for the respective cases. For example, the distribution of the safety factors in the protective pillar for two cases of medium-thick coal seam and a mining depth of 500m corresponding to slope angles of α = 10° and 20° can be seen in Figure 2.14.

Through analysis, the research has obtained the distribution law of the strength coefficient in the protective pillar for different cases of medium-thick coal seam, considering different slope angles α = 10°, α = 20°, and α = 35°, at a depth of 500m. These findings are depicted in diagrams from Figure 2.15 to 2.17.

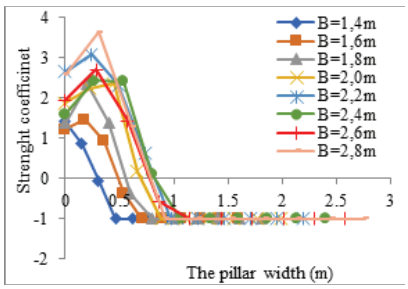

Fig. 2.19. The relationship between the strength coefficient and the width, α = 20°, H = 500m, P = 30MPa

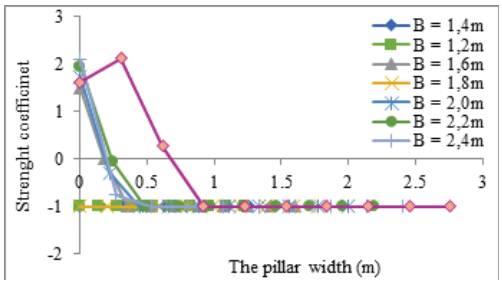

Fig. 2.20. The relationship between the strength coefficient and the width, α = 35°, H = 500m, P = 30MPa

The results obtained from figures 2.16 to 2.18 show that in the case of mining in medium-thick coal seam, with a slope angle of α = 10° (figure 2.16), the optimal width of the protective pillar is B > 1.6m. In practical terms, it is recommended to choose B = 1.8m, as it ensures a safety coefficient of ≥ 2.0 for the pillar.

For the case of a slope angle of α = 20° (figure 2.16), the optimal width of the protective pillar is considered to be B ≥ 2.76m (rounded to 2.8m). Similarly, for the case of a slope angle of α = 35° and a mining depth of H = 500m, the optimal width of the protective pillar is B ≥ 3.0m (figure 2.17).

4.4. Analysis model for the case of medium-thick coal seam, artificial pillar compressive strength of 30 MPa, and mining depth of 500m

In the case of using a compressive strength of the protective pillar of P = 30MPa, through multiple models, the research findings reveal the relationship between the safety factor and the width of the protective pillar for the condition of medium-thick coal seam with a depth of H = 500m and slope angles of 10°, 20°, and 35°, as depicted in figures 2.18 ÷ 2.20.

Observing the results in figures 2.38 to 2.40, with a compressive strength of 30 MPa and a mining depth of 500m, for a slope angle of 10°, the optimal width of the protective pillar is B = 1.4m; for a slope angle of 20°, B = 1.8m; and for a slope angle of 35°, B = 2.8m.

Summarizing the research findings, the optimal width of the protective pillar is determined based on the variation in compressive strength and the relationship between the pillar width and factors such as the slope angle and mining depth, as presented in Table 2.2.

4.5. Research result analysis for the numerical medel in case of medium-thick coal seam

The analysis of the results on the numerical model aims to determine the correlation between the research parameters obtained from Table 2.10, including the slope angle of the coal seam (α), the thickness of the coal seam (m), the mining depth (H), the compressive strength of the artificial pillar (P), and the width of the artificial pillar (B). The details are shown in Table 2.3.

To find out the relationship between the mentioned parameters, the research utilized the statistical software SPSS, IBM version 25 (Figure 2.21).

Therefore, the relationship between the artificial pillar width and the slope angle in the case of medium-thick coal seam follows a linear function as follows:

$$y = 0.0508x + 0.8829 \quad (1)$$

With a variance of $R^2 = 0.9591$.

Where:

y – Artificial pillar width, in meters (m);

x – Slope angle, in degrees.

The above function serves as a reference, allowing researchers and consultants to quickly and simply determine the dimension parameter of the artificial pillar width before carrying out the design process.

5. Assessment of the technological solution in practice

In Quang Ninh coal region, the construction of high-strength artificial pillars to replace coal pillars for roadway protection has not yet been implemented. The authors selected Khe Cham Coal Company to collaborate on deploying the technology. The chosen location for the design was section 14-5, at a depth of -170/-150, in coal seam 14-5 of Khe Cham III coal mine. The application targets the use of continuous strip-type and crib-type artificial pillars as substitutes for coal pillars in the transportation roadway. The geological and mining engineering characteristics of the design area are as follows: The designed coal seam has an average thickness of 5.6 meters, with a slope angle of 12 degrees and a strength index of f = 1÷2. The imediate rock layers consist mainly of siltstone layers with an average thickness of 9.34 meters and a strength index of f = 4 ÷ 6. The main rock layers consist of cement-

Fig. 2.15. The relationship between the strength coefficient and the width, α = 10°, H = 500m, P = 20MPa

Slope angle	Optimal width of the protective pillar, m					
	α = 10°		α = 20°		α = 35°	
H = 350m	B =1,2	B = 1,0	B = 2,0	B = 1,6	B = 2,4	B = 2,2
H = 500m	B = 1,6	B = 1,4	B = 2,8	B = 1,8	B = 3,0	B = 2,8
Compressive strength of pillar, MPa	P = 20	P = 30	P = 20	P = 30	P = 20	P = 30

Tab. 2.3. Results of key parameter values from numerical modeling

α (°)	m (*m*)	H (*m*)	P (*MPa*)	B (*m*)
10	2,2	350	20	1,2
10	2,2	350	30	1
10	2,2	500	20	1,6
10	2,2	500	30	1,4
20	2,2	350	20	2
20	2,2	350	30	1,6
20	2,2	500	20	2,8
20	2,2	500	30	1,8
35	2,2	350	20	2,4
35	2,2	350	30	2,2
35	2,2	500	20	3
35	2,2	500	30	2,8

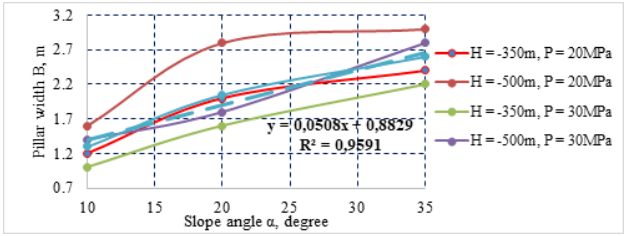

Fig. 2.21. The relationship between the parameter of artificial pillar width and the slope angle

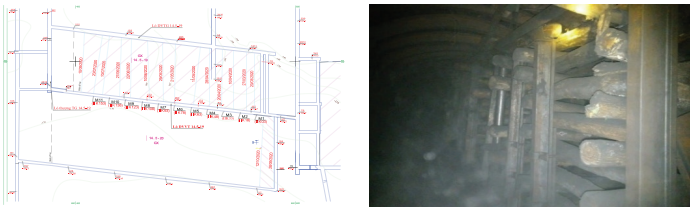

Fig. 2.22. The deployment diagram of section 14-5 using artificial support belts

ed sandstone and conglomerate with an average thickness of 40.73 meters and a strength index of f = 6 ÷ 8. The direct pillar consists of cemented silty layers with an average thickness of 3.74 meters, underlain by sandstone and conglomerate layers with an average thickness of 13.1 meters.

The implementation of the artificial pillar solution as a replacement for protective coal pillars of the transportation roadway 14-5 section was carried out from March 13, 2020 (the start of face operation) to September 10, 2020 (the end of face operation). The total length of the protected roadway was 170 meters.

Measurement results and monitoring show that within a range of approximately 40 meters in front of and behind the coalface, the deformation rate of the roadway lining is the strongest and fastest (vertical deformation rate ranges from 7 to 10 mm/day-night; horizontal deformation ranges from 8 to 20 mm/day-night). In the direction of the roadway mirror, in the area starting from the 40th meter backward, the deformation speed of the roadway lining gradually decreases (vertical deformation speed ranges from 0 to 4 mm/day-night, horizontal deformation ranges from 0 to 6 mm/day-night). From the 100th meter behind the installation roadway towards the caving area, the roadway lining is no longer moving and remains stable.

The total deformation of the roadway lining during the monitoring period reaches a maximum of 300 mm vertically and 350 mm horizontally, corresponding to a reduction in cross-sectional area of about 9.8% to 9.97%, ensuring the prescribed safety dimensions for ventilation and production purposes of the 14-6 panel.

When applying the technological solution of using artificial support columns instead of coal support columns at the 14-5 roadway, an additional 19,951 tons of coal can be extracted from the prepared support columns, increasing the total exploitation output of the designed area to 67,451 tons. Additionally, it will bring some technical benefits such as reducing the loss rate to only 14%, nearly three times lower than expected (39%); the preparation cost per meter of the roadway is also reduced to only 6.3m/1000 tons of coal, nearly 1.9 times lower than the plan (8.19m/1000 tons of coal).

6. Conclusion

The research results on the basic parameters of the artificial pillar in the case of the medium-thick coal seam in coal mining reveal the following:

1) The size of the artificial pillar varies with the increasing depth of mining. For a mining depth of 350m, the pillar size ranges from 1.0m to 2.4m, while for a mining depth of

500m, it increases from 1.4m to 2.8m. This finding agrees well with the theoretical and practical aspects of coal mining in the Quang Ninh region.

2) As the slope angle of the seam increases, the required pillar width also increases. This is because, at higher slope angles, the pressure on the pillar shifts away from the central axis towards the side adjacent to the mining face (downward along the slope direction). Consequently, the compressive force is not evenly distributed throughout the entire pillar body. To ensure the required internal stability, the pillar width needs to be increased.

3) Increasing the pressure or compressive strength of the protective pillar results in a reduction in the width of the artificial pillar. The relationship between the width of the artificial pillar and the slope angle in the case of a medium-thick coal seam follows a linear function: $y = 0.0508x + 0.8829$.

7. Acknowledgements

The paper was presented during the 7th Pol-Viet 2023 International Conference Scientific-Research Cooperation between Poland and Vietnam, 18-20.10.2023, Krakow, Poland.

Literatura – References

1. Cuong, D.V., Thanh, V.T., Tuan, A.N., 2019. Study on the possibility of using artificial pillars to replace the protection coal pillar of the preparationroadways during the mining process at underground coal mines in Quang Ninh region, Vietnam. Journal of the Polish Mineral Engineering Society, http://doi.org/10.29227/IM-2019-02-73.
2. HU, B.N., 2012. Backfill Mining Technology and Development Tendency in China Coal Mine. Coal Science and Technology. Vol. 40 No. 11. DOI: 10.13199/j.cst.2012.11.7.hubn.006.
3. Song, Z.Q, Cui, Z.D., Xia. H.C., Tang, J.Q., Wen, Z.J., 2010. The fundamental theoretical and engineering research on the green safe no coal pillar mining model mainly using coal gangue backfill. Journal of China Coal Society, No.05, Vol.35. DOI:10.13225/j.cnki.jccs.2010.05.017
4. Dinh, V.C., Nguyen, A.T., Tran, V.T., Nguyen, H.Ng., Duong, D.H., 2021. Applying Artificial Pillar to Replace the Coal Pillar Protecting Roadway to Increase Production Efficiency and Sustainable Development in the Vietnamese Coal Industry. Journal of the Polish Mineral Engineering Society, No.2, Vol.1, 2021, http://doi.org/10.29227/IM-2021-02-56.
5. Zhou, Y. J., Xu, X. D., Li, X. T., Li, M., and Yang, Y. G.,2018. Study on catastrophe instability of support system in gypsum goaf based on energy dissipation theory. Adv. Civ. Eng. 2018, 1–9. doi:10.1155/2018/4293584.
6. Ma, C. Q., Li, H. Z., and Zhang, P. P., 2017. Subsidence prediction method of solid backfilling mining with different filling ratios under thick unconsolidated layers. Arab. J. Geosci. 10 (23), 511–512. doi:10.1007/s12517-017-3303-7
7. Sun, Q., Zhang, J. X., Zhou, N. 2018. Study and discussion of short-strip coal pillar recovery with cemented paste backfill. Int. J. Rock Mech. Min. Sci. 104, 147–155. doi:10.1016/j.ijrmms.2018.01.031
8. Chi, Y., C., Sheng, G. C., Chang, C. Zh., Shu, Y. D., Jiang, L., Yang, L., 2023. Research on cemented artificial pillars to replace protective inter-block coal pillars and stope failure laws. Original research article, Front. Earth Sci., 18 January 2023, Sec. Structural Geology and Tectonics, Volume 10 - 2022. https://doi.org/10.3389/feart.2022.1039478.
9. Niełacny P., 2009, Dobór technologii utrzymywania wyrobisk przyścianowych w jednostronnym otoczeniu zrobów na podstawie pomiarów przemieszczeń górotworu, Praca doktorska, Akademia Górniczo-Hutnicza, Krakowie, Poland.
10. Rak Z., 2017. Dobre praktyki w utrzymywaniu wyrobiska w jednostronnym otoczeniu zrobami zawałowymi. Zeszyty Naukowe, Instytut Gospodarki Surowcami Mineralnymi Polskiej Akademii Nauk, Poland, nr 101, pp. 117–132.
11. Reed, G., Mctyer, K., Frith, R., 2017, "An assessment of coal pillar system stability criteria based on a mechanistic evaluation of the interaction between coal pillars and the overburden", International Journal of Mining Science and Technology 27 (2017), pp. 9-15.
12. Simon, H. P., Muhammad, A. I., Ganda, M. S., Ridho, K. W., Irwandy, A., Made, A. R.,2019. New coal pillar strength formula considering the effect of interface friction. International journal of Rock Mechanics and Mining Sciencess 123 (2019) 104102.
13. Bieniewski, Z. T., 1992. A method revisited: Coal pilllar strength formula based on field investigations. Proceeding of the Workshop on coal pillar mechanics and design, Bu mines, pp. 158-165. (https://www.arcc.osmre.gov/resources/impoundments/BoM-IC-9315-Proceedingsof the Workshopon Coal Pillar Mechanicsand Design-Bieniawski1992.pdf).
14. Kang, Zh., Zhong, Q. G., Xiao,D. Z., Ze, M.Z., Xiao, J. W., 2013. Study on Stability of Metal Mine Overlying Strata for Artificial Pillar Support. IJCSI International Journal of Computer Science Issues, Vol. 10, Issue 1, No 2, January 2013. ISSN (Print): 1694-0784 | ISSN (Online): 1694-0814. www.IJCSI.org
15. Bui, M.T., Le, T.D., Liu. C.Y., Pham, V.C., 2020. Study on controlling parameters and technological optimization of Strip Longwall Top Coal Caving in thick coal seams. Inżynieria Mineralna – Journal of the Polish Mineral Engineering Society. 2020;46(2): 105-113.

Facies Analysis and Depositional Environmental Interpretation of The Upper Oligocene, Block 09-2/10, Cuu Long Basin

Muoi Duy NGUYEN[1,2], Anh Ngoc LE[1,2], Hoa Minh NGUYEN[1,2], Ngan Thi BUI[1,2]*

[1)] Petroleum Geology Department, Faculty of Petroleum and Energy, Ha Noi University of Mining and Geology, 18 Vien Street – Duc Thang Ward – Bac Tu Liem District – Ha Noi – Vietnam
[2)] Basin, stratigraphy and sedimentary process group (BSSP), Ha Noi University of Mining and Geology, 18 Vien Street – Duc Thang Ward – Bac Tu Liem District – Ha Noi – Vietnam
* Correspondence: nguyenduymuoi@humg.edu.vn

http://doi.org/10.29227/IM-2023-02-24

Submission date: 20-08-2023 | Review date: 15-09-2023

Abstract

The article presents the facies and environment of the Upper Oligocene sediments in the area of block 09-2/10 based on the analysis of seismic facies and well data of the neighboring areas. The results of the interpretation of seismic data indicate that the upper Oligocene sediments are limited by the top C, top D seismic reflectors. The environment is formed from lagoons, lakes to deep lakes. Seismological facies analysis identified 03 facies including seismic facies with medium to poor reflection amplitude, medium continuous, low frequency reflecting the lacustrine sediments (80%) in most of the lake center. Strong reflective seismic facies, sigmoidal clinoforms reflect the lakeside sediments (15%) distributed in the lakeside shelf. The seismic facies with average and continuous amplitude poorly reflect alluvial sediments (5%) in the Northwest region. The direction of sediment transport is mainly from the Northwest and Southwest in the area. The sandstone sequences are distributed on the slopes of the lake and the lake bottom, which is potential reservoir.

Keywords: *Cuu Long basin, upper oligocene, depositional environment, seismic facies, block 09-2/10*

1. Introduction

The Cuu Long Basin is one of the most detailed drilled and studied basins in the continental shelf of Vietnam. This basin is covered by a large volume of seismic profiles as well as many oils and gas exploration and production wells. The basin's sedimentary fill is dominated by Cenozoic sediments, with the Oligocene and Lower Miocene formations serving as the primary targets for hydrocarbon exploration and exploitation. These sediments are characterized by a diversity of depositional environments, including fluvial, lacustrine, peat swamp, brackish lagoon, and inner neritic settings.

Block 09-2/10 is located in the center of Cuu Long basin, Vietnam (Figure 1). Around the study area are large oil and gas fields such as Bach Ho, Te Giac, and Rang Dong. However, oil and gas research and exploration activities in 09-2/10 are still limited. In addition, in the study area, seismic explosion collection and drilling of an exploratory well have been carried out in the Middle Miocene sediments. The Lower Miocene sediments are not capable of generating hydrocarbons. Therefore, Oligocene sediments are the main study object for this paper. The deposition conditions of Upper Oligocene C are unclarified. The paper shows sedimentary facies and depositional paleoenvironment of the Upper Oligocene C based on analysis of seismic facies and well around block 09-2/10.

2. Geological setting

Cuu Long basin is a Cenozoic rift basin located in the Southeastern shelf of Vietnam. The geological evolution of the Cuu Long basin is divided into three periods: pre-rift, syn-rift and post-rift (Figure 2).

Pre-rift, especially from the Jurassic to Paleocene, is the period of formation and uplift of extrusive magmatic basement.

Syn-rift: This period commenced at the end of the Eocene - Early Oligocene under the influence of aforementioned tectonic events with the main extension direction being the NW-SE.

Post-rift: Near the end of the Early Miocene, the NW-SE East Sea spreading weakened, quickly terminated (17 Ma), and was immediately followed by crustal cooling period. Post-rift sediments were common in that they were all widely distributed, undisplaced, unfolded, and almost horizontal.

The stratigraphy of block 09-2/10 in the Cuu Long basin consists of Pre-Cenozoic basement and Cenozoic sedimentary cover. The characteristics of lithology and fossil assemblages of each formation unit are summarized in the generalized stratigraphic column of the basin (Fig 3). Pre-Paleogene basement: The Pre-Paleogene basement in the Cuu Long basin is composed of mostly magnetic intrusive rocks with main lithologies of granite, granite - gneiss, granodiorite, diorite, adamellite, monzodiorite, gabbro, monzogabbro. The metamorphic rocks are also encountered in some places [6].

Lower Tra Tan – Tra Cu formation – Oligocene E: This continental sediment consists of shale, siltstone and sandstone, which were deposited unconformably on the Pre-Paleogene basement. It is distributed widely across the southeastern area and divided into two sub-units:

Oligocene E Lower in the lower part and Oligocene E Upper in the upper part. The lower one is dominated by medium – to coarse grained sandstones composed of mostly granitic fragments and feldspars, interbedded with hard organic-rich black shale layers. The other one is composed majorly of fine to medium grained sandstones interbedded with gray shale layers. In addition, magma intrusions such as dykes, composed majorly of andesite/basalt were found occasionally [7].

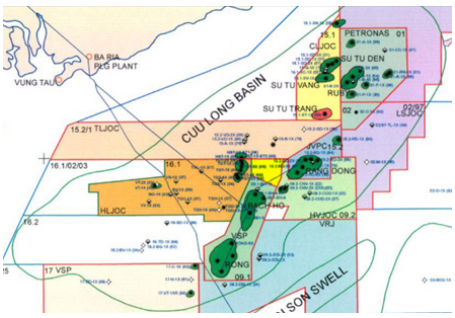

Fig. 1. Location of the study area

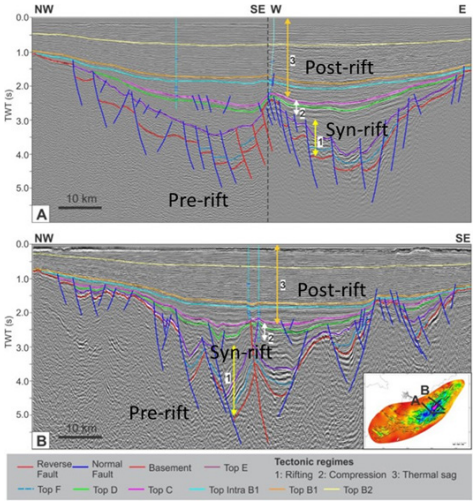

Fig. 2. The geological evolution of the Cuu Long basin (Modified after William J. Schmidt, 2018)

Upper Tra Tan Formation – Oligocene D: It is majorly organic rich brown shale deposited in lacustrine environment, occasionally interbedded with local layers of coal or sandstone. However, toward the Eastern boundary of the sub-basin (close to Con Son swell), thick layers of sandstone were deposited on top of Oligocene D shale. Upper Tra Tan Formation – Oligocene C: This section is the mixtures of fine-grained sandstones and lacustrine brown shale [6].

Bach Ho Formation – Miocene BI: This stratigraphic sequence is divided into two sub-units Miocene BI.1 (lower part) and Miocene BI.2 (upper part). Miocene BI.1 is composed mainly of sandstone dominant fluvial-deltaic deposits with small intercalation of shale deposited in floodplain or some brackish environments, while Miocene BI.2 is composed mainly of sandstone interbedded with shale/claystone, occasionally shallow marine siltstone and limestone. The top section of Miocene BI is Bach Ho shale, a thick and continuous shale layer, acting as a regional seal for the whole Cuu Long basin [6].

3. Material and methods

3.1. Materials

The seismic data used for this study is 250km2 PSTM 3D seismic cube of block 09-2/10. In addition, lithological, paleontological, and geophysical data from wells A1, A2, B1, B2, C1, C2, C3, D, E, F and G were also used to determine the environment of sediments (Figure 4). Seismic facies analysis was combined with petrographic and paleontological data to forecast the sedimentary environment of sequence C.

3.2. Methods:

Seismic facies analysis:

Seismic facies analysis is the description and interpretation of seismic reflection parameters, such as configuration, continuity, amplitude, and frequency, within the stratigraphic framework of a depositional sequence [1,2]. In seismic facies analysis, different seismic sequence has a different wave characteristics and is identified by the shape, amplitude, frequency, continuity of the seismic reflections. The external geometry and internal reflection of the reflected wave can reflect the deposition process as well as the direction of the source of the sedimentary material.

Log curve shape Analysis:

Based on the shape of the gamma ray curve, it is possible to determine the sedimentary environment (Figure 5). The shapes of well-log curves analysis serve as basic tool to interpret depositional facies because shape of log is directly related to the grain size of rock successions [4]. The log curve shapes were used to interpret the depositional environment, The study of core with relation to logs is also an important tool of facies interpretation in the subsurface [2].

Petrographic analysis:

Petrographic analysis identifies the mineral content for classification of a rock. Analysis usually comprises the description of the macroscopic aspects of the rock, such as fabric, color, grain size, and other relevant characteristics that may be visually observed in hand specimen or in outcrops, and chiefly the identification and description of microscopic characteristics of the studied material in thin sections such

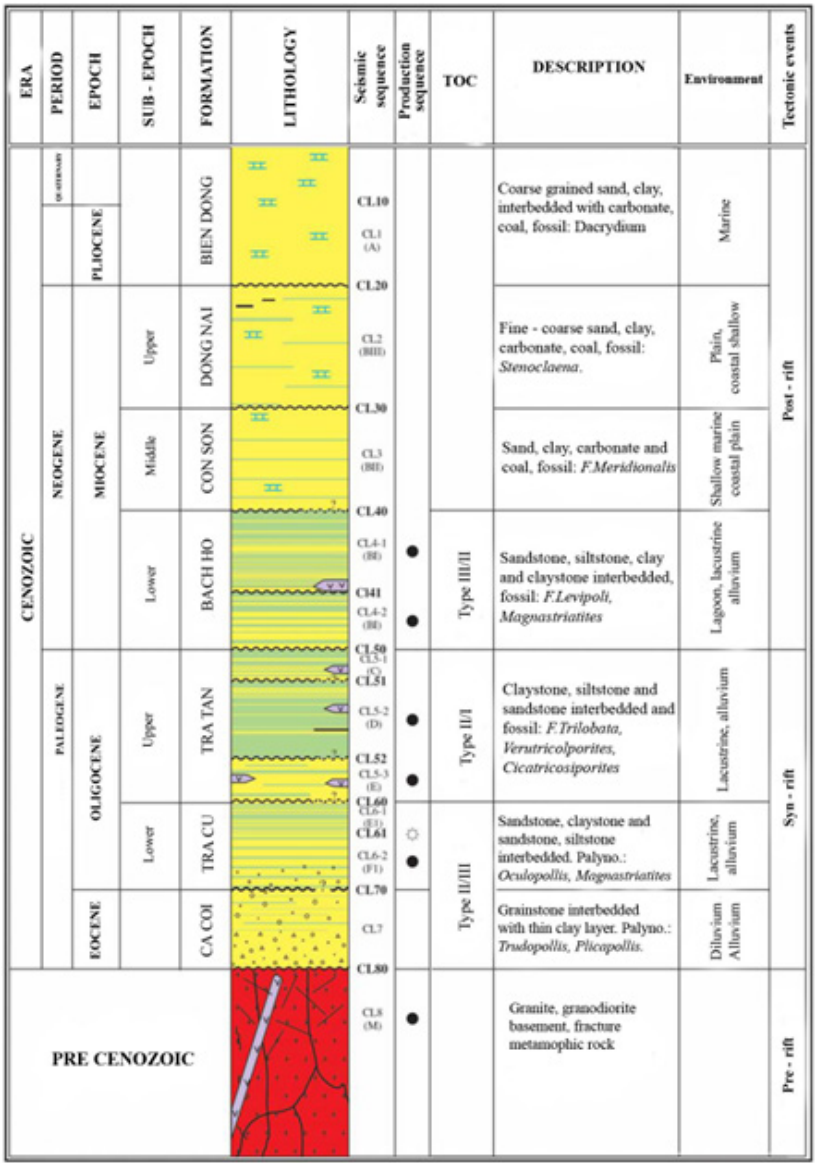

Fig. 3. Generalized stratigraphy of the Cuu Long basin [3]

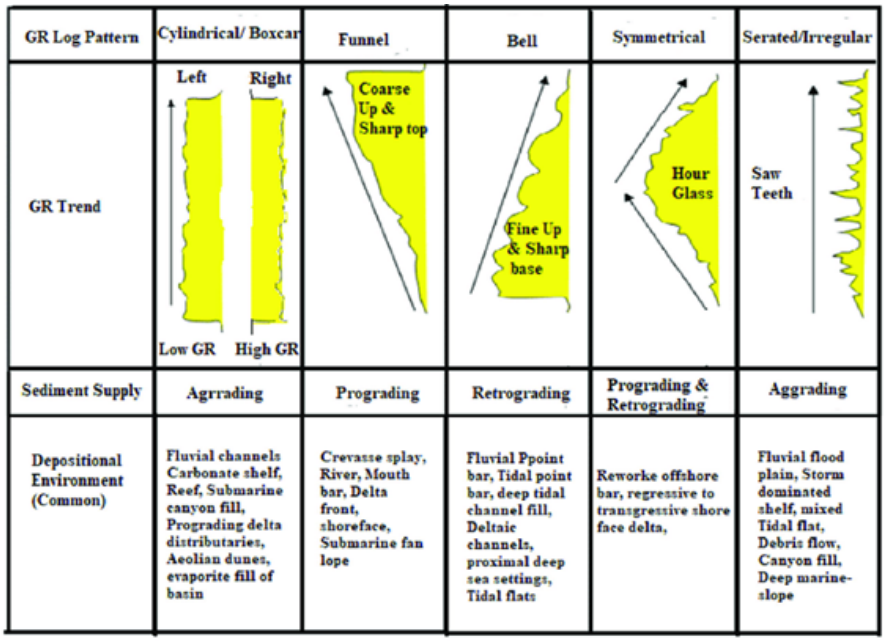

Fig. 5. Common sedimentological facies associated with various gamma-ray log shapes. Modified after Cant (1992)

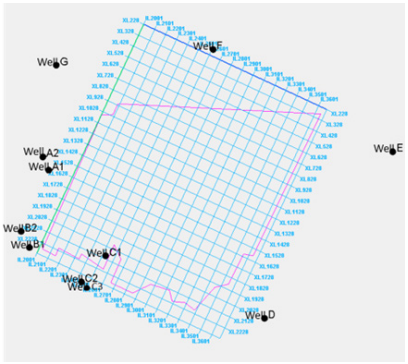

Fig. 4. A base map showing well sites relative to the seismic survey inlines and crosslines

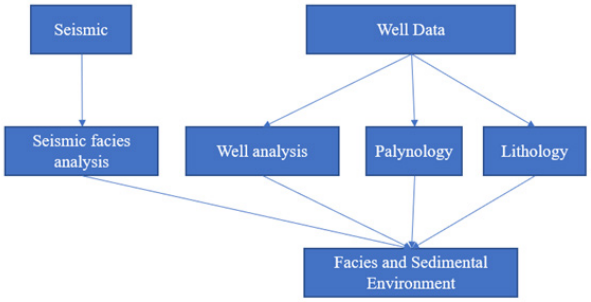

Fig. 6. The workflow for facies analysis and sediment environment study

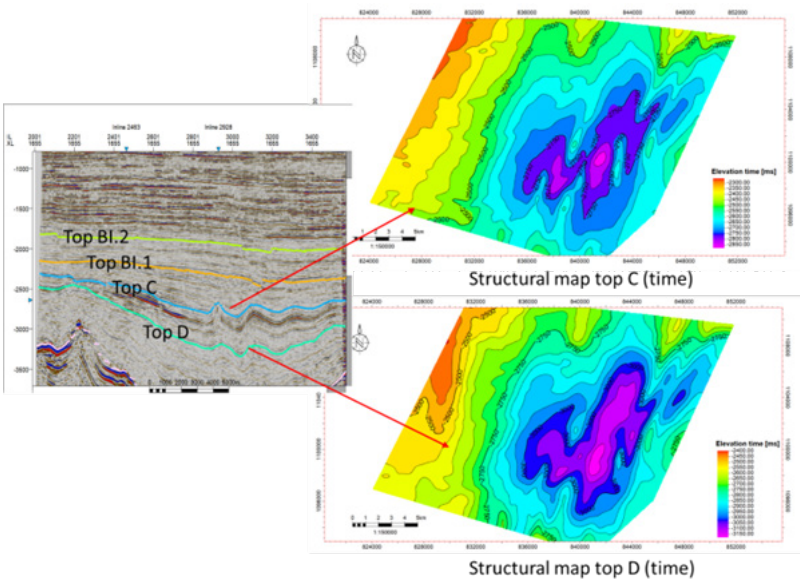

Fig. 7. The time structure map of Top C and Top D

as mineral composition, texture, grain size, and evidence of alteration and/or deformation [3]. The results of petrographic analysis are an important tool for determining the conditions of the formation of the rock.

Researching of the sedimentary environment of sequence C in the study area was carried out by the authors according to the following diagram (Figure 6).

4. Results and discussion

4. 1. Seismic interpretation

In block 09-2/10, The basement rock is deeply buried, so there is no potential structure. Therefore, seismic interpretation only focuses on the Upper Oligocene and Lower Miocene. The results of the seismic interpretation showed 4 horizons. Which are interprated including Top D (Lower Oligocene), Top C (Upper Oligocene), Top BI.1 (Lower Miocene) and Top BI.2 (Upper Miocene). The sequence C is limited by Top C and Top D (Figure 7). The structure map top C and Top D shows that this area same as subsiden. The west is a clearly an area of downslope sedimentation.

The thickness map (Figure 8a) shows the same as a deep lake. In the west, the sediment thickness is thin. In the middle, the sediment is more thicker. The models show the depositional environment and source rock deposition (Figure 8b).

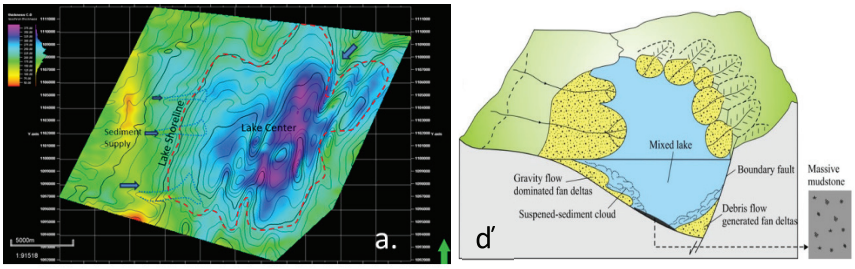

Fig. 8. a) Iso-thickness map of sequence C, b) Model of the sedimentary environment of sequence C [5]

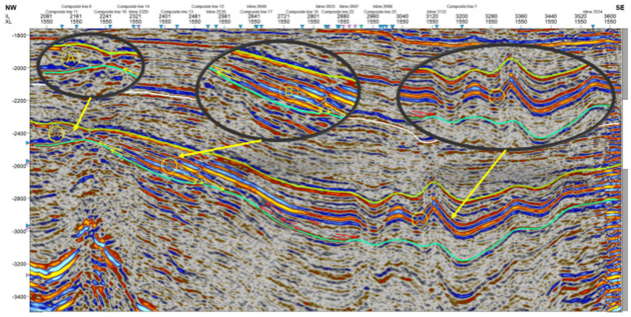

Fig. 9. Seismic section shows that sequence C has 3 main groups of reflections

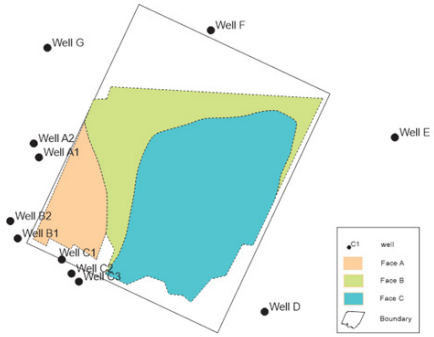

Fig. 10. Seismic facies map of sequence C

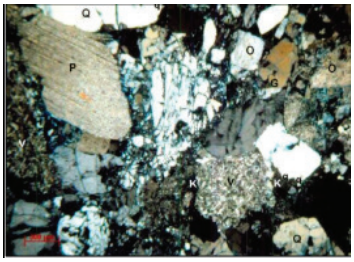

Sidewall core sample (at 3042m TVDss): arkose lithic sandstone with coarse grain, poor selectivity at well A1 (Q- quartz, P – Plagioclase)

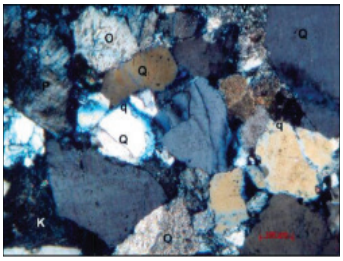

Sidewall core sample (at 3182.5m TVDss): arkose lithic sandstone with fine grain, medium selectivity at well B1 (Q- Quartz, P – Plagioclase, k-feldspar)

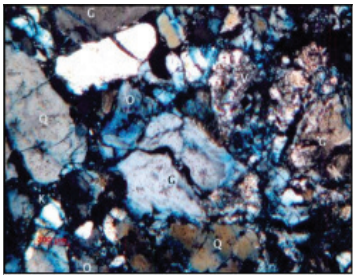

Sidewall core sample (at 3012.5m TVDss): arkose sandstone with coarse grain, poor selectivity of well A2 (Q- Quartz, P – Plagioclase, k-feldspar)

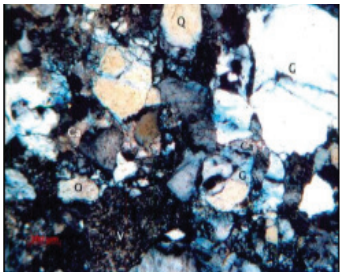

Sidewall core sample (at 3026m TVDss): arkose sandstone with medium grain, poor selectivity of well A2 (Q- Quartz, P – Plagioclase, k-feldspar)

Fig. 11. Arkose sandstone of sequence C at wells A2, A1, B1 [10]

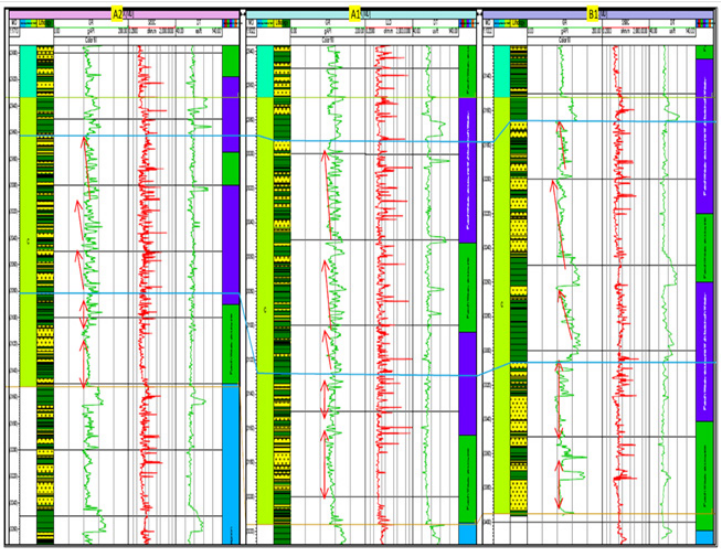

Fig. 12. Well correlation of Well A2, Well A1, Well B1

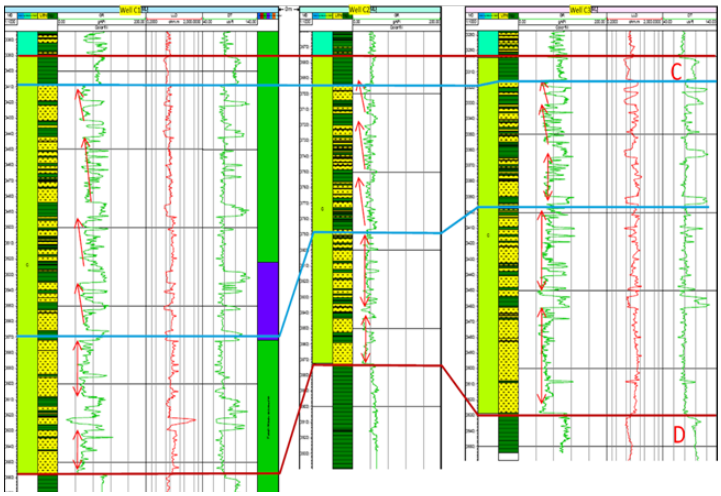

Fig. 13. Well correlation of Well C1, C2, C3

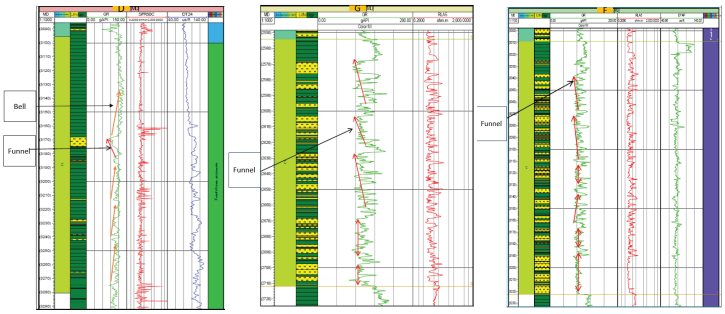

Fig. 14. Depositional environments in well area D, G, F

4.2. Seismic facies interpretation

Analyzing the seismic facies of Upper Oligocene "C" sequence, it shows that 03 seismic facies include (figure 9):

Seismic facies A shows subparallel reflection features with weak-medium amplitude, and poor continuity, reflecting medium-energy sedimentation. These seismic facies represent alluvial.

Seismic facies B has reflection with high amplitude, good continuity, and sigmoidal clinoform, which is typical for high-energy sedimentation. These facies show the shelf-slope sediments.

Facies C includes 2 groups with different characteristics. The first group is the high amplitude, good continuity, parallel reflections, shows sediments due to the change and decrease in energy gradually until completely weak. The negative phase reflections (in blue) reflect the sedimentary facies as the tails, the outermost parts of the lobe. The positive phase reflections (reddish brown) reflect the fine-grained facies of clay, formed in the period of still water, lacking sedimentary materials. The second group is a set of weak, discontinuous, chaotic. They reflect the sediment with coarser grain and poor selectivity. Which are rapidly deposited in a high-energy environment.

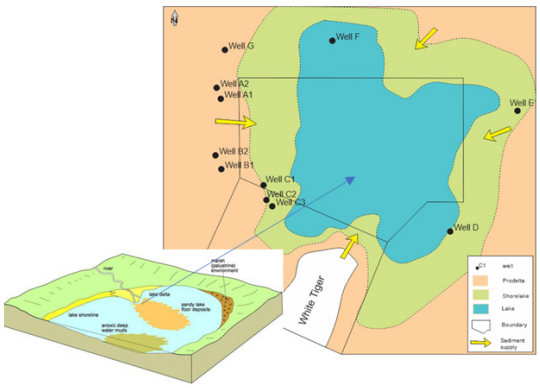

Fig. 15. Diagram of sedimentary environment of Late Oligocene (sequence C) in block 09-2/10

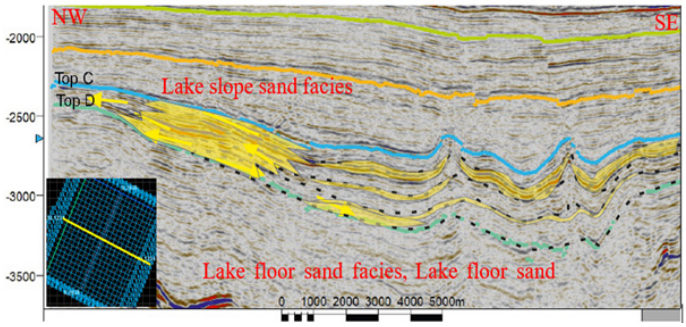

Fig. 16. Reconstruction of lake slope sand facies and lake floor sand facies

The facies C is characterized by a turbidite sedimentary, which is formed at the bottom of the lake.

The seismic facies distribution of the C sequence is shown in figure 10. Seismic facies A, distributed mainly in the western edge of the area (yellow-orange covers about 15% of the area) is characterized by discontinuous reflections. Seismic facies B have strong, continuous reflectivity (light green covers about 15% of the area) distributed in the middle of the block. Seismic facies C, which shows medium amplitude and poor continuity of reflectors, occupies most of the central part of the block (80% of the area – blue color).

4.3. The results of lithology, paleontology combined with well logging analysis

According to the results of the petrographic stratigraphy of wells A1, A2, B1, and B2, sand and clay sequences are shown. Petrographic results of thin rock slices at wells A1, A2, and B1 show arkose and sub-arkose sandstone (Figure 11), poor selectivity, and poor roundness. The sediments were formed in alluvial and pro-deltaic environments. The results of palaeontological analysis of sequence C at wells A1, A2 and B1 are mainly chalky spores and freshwater spores such as Bosedinia, showing that the sequence was formed in the fluvial and freshwater lacustrine environment [9]. The mainly block, funnel shape of the GR curve is typical for the delta environment (Figure 12).

At wells C1, C2, and C3, the sequence C includes sand layers interspersed with clay layers. Sandstone is arkose with good roundness and good sorting. The blocky and funnel shapes on GR logging curves (Figure 13) indicate the marginal lacustrine environment. The seismic expression of this sequence is characterized by medium seismic amplitude and moderate to poor continuity of reflectors, associated with marginal lacustrine sediments.

At well D, the GR log has high values and tends to be fining upward. The lithology is mainly shale layers formed under low-energy conditions can to related to the lacustrine environment. When analysis result of well G (Northwest) and well E (Northeast) also shows the lacustrine environment. The well logging analysis result of well F (Northern) indicates the marginal lacustrine environment [11] (Figure 14).

4.4. Sedimentary environment reconstruction

The Oligocene period was in the period of rifting, creating space for sediment accumulation [6,7]. Stratigraphic results of the Cuu Long Basin have shown that Oligocene sediments were formed during a period of low water level, related to river and lake environments [8,11]. The paleontological research results also clearly show a freshwater lacustrine environment [9]. Therefore, the late Oligocene sedimentary environment of block 09.2/10 can be the same. a sedimentary environment map of the Upper Oligocene was established based on the combination of the seismic facies with well data, lithology, and paleontology. On the figure 15, the center of the lake is deviated to the East, and the direction of sediment transport is mainly from the West. Delta/marginal lacustrine environments are present in most of the wells around block 09.2/10; the marginal lacustrine environment in wells A1, A2, B1, B2, C2, C3, while lacustrine environment in wells C1, D.

From the sedimentary formation model of sequence C, it is possible to reconstruct the distribution of sedimentary facies of the study area as follows:

Prograding wedge sediment has been transported towards the basin center and accumulated from the edge of the lake shelf to the slopes of the lake and can spread far into deeper water (Figure 16). Prograding wedge sediment is characterized by combinations of coarse-grain sand and grit facies with poor to moderate sorting.

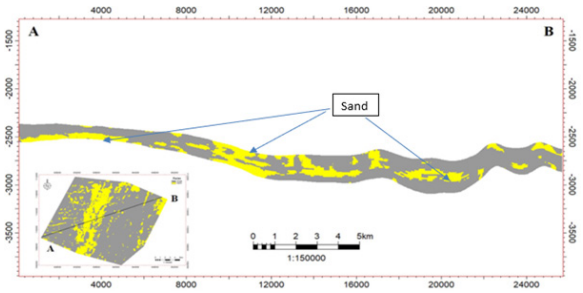

Fig. 16. Reconstruction of lake slope sand facies and lake floor sand facies

Lake floor fan sediment was formed when the lake water level was lowered, sediment was quickly transported by underground flows to the lake bottom. When dividing the facies by seismic reflection features, the distribution of sand layers has also been shown and the distribution is quite appropriate with the seismic facies model (Figure 17).

5. Conclusions

The study has clarified sedimentary facies and depositional paleoenvironment of block 09.2/10 cuu long basin in the east sea during the upper Oligocene based on the integrating of seismic facies, welllog, petrographic, and paleontology.

The results of the interpretation of seismic data indicate three facies A, B and C. The facies A are characterized by chaotic reflections, poor continuity, and low amplitudes associated with delta. The facies B is characterized by continuous seismic reflection, strong reflection amplitude, low frequency, overlapping pattern related to shelf slopes. The facies C is characterized by a weak to moderate amplitude, parallel wavy, which is related to the deep lake.

The Upper Oligocene environment was formed mainly in the lacustrine environment. The sedimentary facies include the lakeside and deep lake. The lakeside and bottom sands sequence may be potential oil and gas reservoirs.

Literatura – References

1. Mitchum, R., M., Vail, P., R., Sangree, J., B., 1977. Seismic stratigraphy and global changes in sea level, part 6: stratigraphic interpretations of seismic reflection patterns in depositional sequences, in Payton, C., E., ed., Seismic Stratigraphy and Applications to Hydrocarbon Exploration: AAPG Memoir 26, p. 117–133.
2. Cant., D.,1992. Subsurface Facies Analysis. In R. G. Walker (Ed), Facies models. response to sea level changes. St. John's: Geological Association of Canada, 27-45.
3. Oliveira Frascá, M.H.B. (2018). Petrographic Analysis. In: Bobrowsky, P.T., Marker, B. (eds) Encyclopedia of Engineering Geology. Encyclopedia of Earth Sciences Series. Springer,
4. R.C. Selley, 1978. Concepts and methods of subsurface facies analysis: American Association of Petroleum Geologists Contin Educ Course Notes Ser, 9 (1978)
5. Chengcheng Zhang, Hua Wang, Si Chen, Yuantao Liao, Zongsheng Lu, Jun Wei, 2019. Lacustrine Basin Fills in an Early Cretaceous Half-Graben, Jiuquan Basin, NW China: Controlling Factors and Implications for Source Rock Depositional Processes and Heterogeneity. Journal of Earth Science 30(1):158-175
6. Nguyen Hiep, 2007. The Petroleum Geology and Resources of Vietnam. Chapter 09 - Cuu Long Sedimentary Basin and Petroleum Resources. Science and Technics Publishing House.
7. Vietnam Petroleum Institute, 2012. Report on assessment of oil and gas potential of Cuu Long basin.
8. Luu Minh Luong, Duong Manh Hiep, Ngo Van Them, Nguyen Van Dung, Pham Tuan Anh, 2017. Integrated seismic attributes with facies – depositional environment/ petrophysical studies to predict the Oligocene stratigraphy reservoir distribution and properties at Block 09-2/10, Cuu Long basin. Petrovietnam Journal, p 44-50.
9. Pham Thi Duyen, Mai Hoang Dam, 2016. Sequence stratigraphy and depositional environment of Oligocene - Early Miocene sediments of Te Giac Trang structure, block 16-1 in Cuu Long basin based on the characteristics of palynology and palynofacies. Petrovietnam Journal, p. 14-23.
10. Vietsopetro, 2014. Report on results and geological, geophysical data analysis on sediments in the North and Northeast areas of Bach Ho field to identify non-structural traps.
11. Vietnam Petroleum Institute, 2009. Report on Lower Miocene and Oligocene sequence stratigraphic study for block 15-2/01 stage 1 for the area from Hai Su Trang, Hai Su Den to the eastern block boundary.
12. Muoi Duy Nguyen, Hoa Minh Nguyen, Ngan Thi Bui, 2022. Application of artificial neural network and seismic attributes to predict the distribution of Late Oligocene sandstones in the Cuu Long basin. Journal of Mining and Earth Sciences Vol. 64, Issue 3 (2023) p. 24 – 31.

Identifying the Potential Application of Unmanned Aerial Vehicle Technology in Mine Waste Dumps

Ba Dung NGUYEN [1)]

[1)] Hanoi University of Natural Resources and Environment; email: nbdung@hunre.edu.vn; ORCID: 0000-0001-5378-0926

http://doi.org/10.29227/IM-2023-02-25

Submission date: 21-08-2023 | Review date: 17-09-2023

Abstract

In recent years, unmanned aerial vehicles (UAV) have been applied in the mining sector for a variety of purposes. This paper discusses the use of UAVs in the management of mine waste dumps based on analyzing scientific publications (January 2010 to May 2023). Three bibliography databases including Scopus, Google Scholar, and Web of Science were used to perform a thorough assessment of the literature. This study provides a comprehensive overview of UAV applications in mine waste dumps including environmental management, terrain surveying and 3D modeling, and safety and risk management. The obtained results of the study hope to give a technical reference, enhancing the understanding of UAV monitoring in mine waste dump.

Keywords: *UAV, drone, mine, mine waste dumps*

1. Introduction

The mining industry creates significant amounts of waste. According to Cebada et al. (2016), the waste produced by mining might be solid, slurry, or tailing with the most prevalent types being waste rock, tailings, slag, and tail ends. However, under certain conditions, vegetation and overburden may also be regarded as waste [1]. In mines, one of the main operations is the management of the waste dumps [2]. Mining waste is produced in all phases of mine development and extraction activities as well as technical operations related to enriching and purifying the raw material that was extracted [3]. The literature showed that there were many problems associated with mine dumps that need to be considered such as dump fires, slope stability of dumps, etc. Therefore many different methods were used and remote sensing technology seems to be used most of all. This approach can be applied in evaluating the thermal activities of a coal waste dump to detect and locate the spontaneous heating in coal dumps [4], predicting the settlement of mine waste dump [2], analyzing the stability of a mining waste dump sites [5], recognizing and extracting of a waste dump in mining area [6] studying the process of mine waste dump filling up by vegetation [7], mapping mine waste dumps in a semiarid mine district [8]. In addition, Dev and Goyal (2019) used field survey data combined with software based on Finite Difference Method to assess the waste dump slope stability at iron ore mines [9]. Based on expeditious physico-chemical parameters, Mayara et al. (2017) established the mining waste map and analyzed affected areas [10]. Some other methods were mentioned by many scientists such as geoelectrical methods for investigating mine dumps [11], a combined direct current resistivity and induced polarization approach for mapping the internal composition of a mine waste rock pile [12], geostatistical interpolation based on GIS for mapping heavy metals concentrations of mining waste dump [13], magnetometric resistivity approach for detecting preferential flow paths in mine waste rock dumps [14], geotechnical parameter method for analyzing the slope stability of mine waste dumps [15], integrating infrared thermography and close-range photogrammetry for generating a surface temperature distribution model of a coal-mining waste dump [16], application AUV for dump slope stability analysis [17], etc.

Recently, UAVs are increasingly popular tools for remote sensing applications [18]. UAVs are widely known by numerous names such as drones, unmanned aerial systems (UAS), and remotely piloted vehicles (RPVs). Thanks to recent enhancements in UAVs, this technology has secured an ever-expanding field of application in sectors like agriculture [19], construction [20], disaster management [21], transportation [22], etc. UAVs are crucial instruments in the mining sector as well. Because UAVs can be equipped with various devices such as optical, thermal, magnetic, and natural gamma-ray sensors, they can be utilized for numerous purposes like surveying and mapping [23], mine safety monitoring [24], air quality measuring [25], mine waste dumps [26], etc. There have also been many studies reviewing the application of AUVs in the mining industry. While Park and Choi (2020) reviewed academic publications on the usage of UAVs in the mine sector during three phases: exploration, exploitation, and reclamation [27], Lee and Choi (2016) mentioned the UAV technology trends and their applications in the mining industry. Like Park and Choi (2020), Loots et al. (2022) focused on the application of UAVs in the four phases (exploration, development, exploitation, and reclamation) of mining [28]. To provide information about specifications, UAV types, usage of commercially available UAVs for mine industry, requirement for the design and operation of UAVs in underground mines, Shahmoradi et al. (2020) present a thorough analysis of UAV technology and how it is used in the mining sector [29]. Ren et al. (2019) provide an overview of the various uses for UAVs and some recommendations for further advancing their use in resource development and environmental protection. In order to increase awareness and understanding of UAV uses in surveying and mapping in mine regions, Long et al. (2023) offers a technical reference that provides an overview of current advancements in the use of unmanned aerial vehicles (UAVs) for mapping and assessing surface, underground, and abandoned mines. However, all of them have not mentioned the use of this system for monitoring and man-

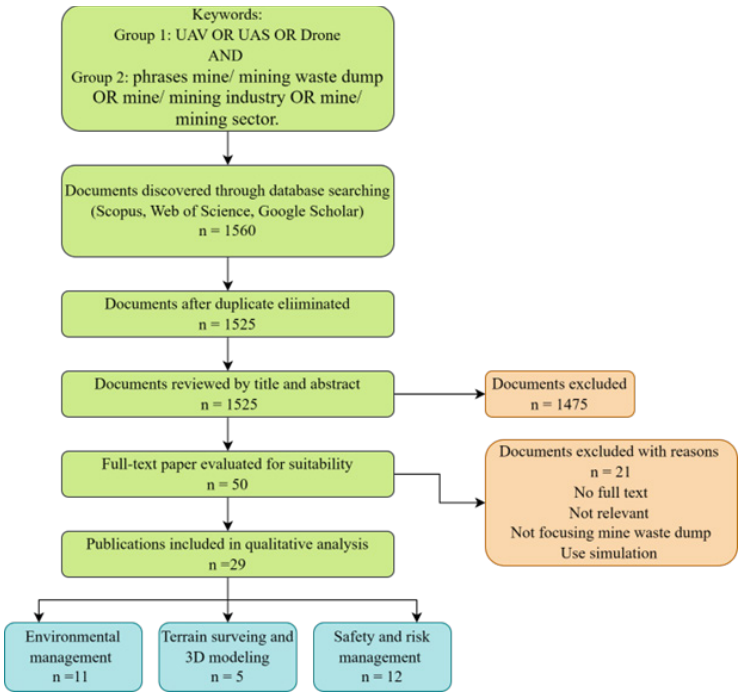

Fig. 1. Study selection process

agement of mine waste dumps. Therefore, this paper aims to perform a review on UAV applications in mine waste dumps to partially fill the aforementioned gap. The authors believe that the paper, one of the first in this field, can assist in advancement of UAV technology and develop them into a tool just as widespread in the field of mine waste dump managing and monitoring.

2. Methodology and Data

In this paper, a systematic literature search was carried out to assess scientific works involving UAV applications for mine waste dumps. The study selection process shows in Figure 1.

2.1 Eligibility criteria

The search results can be filtered based on language, year of publication, and subject field. Only reviews and papers in the English language were selected, and the search was restricted to materials published after 2010. Subjects unrelated to UAV application in mine waste dumps were not included in this study. In addition, duplicate papers or articles that concentrated on simulations rather than actual data were also excluded.

2.2 Information sources and search

For this review, relevant publications were identified on Web of Science, Google Scholar, and Scopus by searching the titles, abstracts, or keywords. The search has been carried out from January to May 2023.

The keywords were categorized into two main groups: the first group was involved with tools including the terms UAV, or UAS, or Drone, and the second group was associated with the interest field including phrases mine/ mining waste dump or mine/ mining industry or mine/ mining sector. At that time, the searchers used the "AND" Boolean operator to connect groups of keywords. The obtained results were exported to EndNote. The duplicates were eliminated using this software, and then appropriate research was extracted after a preliminary title and abstract screening. The information from each study was retrieved such as publication year, authors, nation, paper objective, type of UAV and camera, software technique, and critical findings. This data was then put into Microsoft Excel to analyze further.

3. Results and discussion

UAVs open up new possibilities for mining engineers, by providing aerial views that are challenging to obtain using traditional methods. Table 1 shows some applications of UAV technology in mine waste dumps. The obtained results indicated that most applications of UAV in mine waste dump focus on the areas of environmental management, terrain surveying and 3D modeling, and safety and risk management.

3.1 Environmental management

According to Wang et al. (2014), waste products from mining are produced in substantial quantities, and as lower-grade ores are used in mining, it is anticipated that the number of waste products will rise in the future [30]. Tailings are one of the waste types created, and they are made up of water, together with coagulants and flocculants as well as solid leftovers after mineral extraction [31]. One of the biggest environmental dangers in mining locations is tailings impoundments. There are many studies to identify the potential of using UAVs to monitor tailings impoundments. Because the use of UAVs as a quick and adaptable data collecting system to create orthomosaics and three-dimensional models has grown in popularity, this system can make it possible to monitor mine waste facilities economically and effectively [32]. In a study of [33], the authors revealed that UAV-assisted tailings impoundment monitoring is accurate enough to support management tasks including volume estimates and surface movement tracking down to the decimeter level. Also related to the tailings impoundments, [34] combined the use

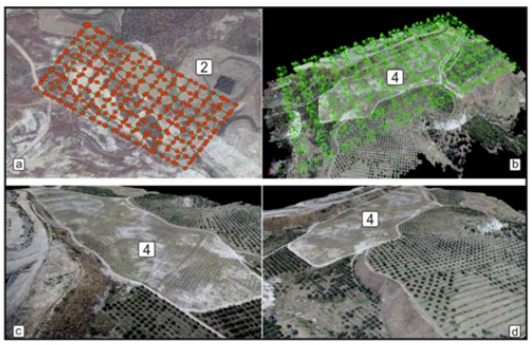

Fig. 2. UAV data on dump site. (a) UAV flight plan; (b) UAV position on Amygdolus Communis plant areas; (c) and (d) Solid models [39]

Fig. 3. Digitisation of the stockpile boundary on the point cloud dataset [48]

of UAV with traditional geochemical and photogrammetric methods to evaluate potential pollution through a categorization of tailings utilizing two hazard indexes, as well as calculate the volume of eroded material and past erosion rates of the abandoned mine tailings impoundments II and III in the town of Nacozari de Garca. According to [35], the tailings reservoir is a dispensable component of the operation of metal mines, and because it typically accumulates waste materials and wastewater, a source of artificial debris flows with high potential energy has been created, increasing the environmental risk. Therefore, they use UAV hyper-spectral imaging and ground-based hyper-spectral data to undertake an extensive aviation-ground disaster and environmental monitoring of the tailings reservoir.

Numerous minerals are exposed to oxidizing conditions throughout the mining process, especially sulfide minerals, which are then broken down by water to produce acidic mine water. Mining-related acid mine drainage (AMD) can contaminate local rivers and lakes and result in severe ecological issues [36]. Compared to traditional methods, UAV technology has benefits regard to security, image accuracy, and real-time imagery. Therefore, many scientists used this approach to study acid mine drainage. In order to identify this environmental phenomenon caused by mining, [36] used a UAV aerial photography system equipped with a Red, Green, Blue (RGB) camera to acquire extremely high-resolution photos of the stone coal mine in China. The images were then classified using support vector machine (SVM), random forest (RF), and U-Net methods, and the distribution of five different types of land cover, including AMD, vegetation, water, roof, and bare land, was identified. Similarly, [37] described the initial findings of an examination into acid mine drainage flows, nearby land, and sulfide-bearing mine tailings dumps in Russia using the integration of geophysical, geochemical data and UAV images. A photogrammetric method of aerial photography was used to record the morphology of the terrain and generate a digital elevation model at the study area.

The dump sites, which are created in the proximity of the mine regions, are frequently bigger than the sites when actual mining is taking place. Thus, rehabilitating waste dumps is a critical and mandatory action [38]. Various research demonstrated the effective usage of UAVs in the rehabilitation processes at the mine waste dumps. [39] produced vegetation index maps of a mining dump site that had been rehabilitated using UAV photogrammetry. These maps were utilized to assess the plant species' adaptation, health, and chance of survival. Figure 1 shows the flight plans for the flights, the position of the UAV on the site, and the solid model of the sites produced from the point cloud. The same goal as [39], [40] used high-resolution UAV visible and near-infrared (NIR) imagery to evaluate the success of vegetation establishment on the SP11 waste rock dump and the abandoned D2808 road stretch in Namibia. In addition, according to [41], monitoring the composition of vegetation species is critical for determining the efficiency of ecological restoration and managing biodiversity after restoration. Therefore, [42] used UAV LiDAR and hyperspectral images to study the structure and composition of the restored vegetation cover in semi-arid mine dumps. The vegetation intensity, height, and echo features were derived from LiDAR data, while the vegetation spectrum, index, and texture features were extracted from hyperspectral image data. In order to green the tailing dump, [43] recognized that the storage area on the investigated surface needs to be arranged, geometrized, weeded, and forested. In this study, a 3D model that is as accurate to reality as possible was produced using a combination of satellite and photogrammetric techniques, and it will be crucial in the process of reforestation of the tailings dump. According to [44], coal-waste dumps are an essential component of the ecology and form the scenery of coal basins. Therefore, they showed an assessment of environmental changes related to land use and alterations in vegetation on self-heating coal waste dumps

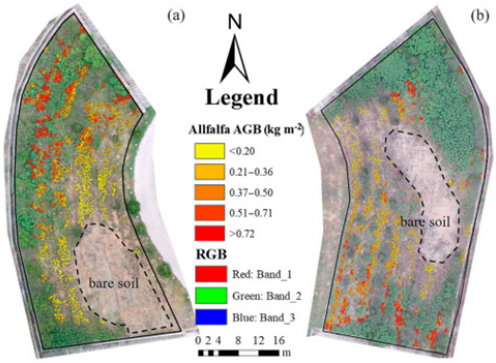

Fig. 4. Alfalfa aboveground biomass estimated results of the study area. (a) and (b) are Areas A and B, respectively. The black dotted polygon is the bare soil area with no vegetation coverage [61]

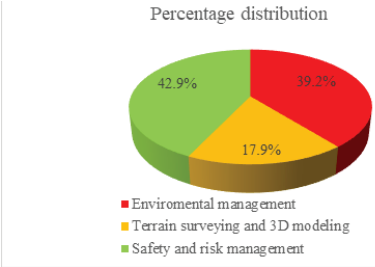

Fig. 5. Percentage distribution and number of publications of UAV applications in mine waste dumps

of various ages using UAV and infrared camera. The obtained findings revealed that when burning coal waste dumps. if the object is not sufficiently protected against the growth of fire, adding vegetation has no effect.

The use of hyperspectral imagery has also proven to be helpful for soil environmental monitoring of mine waste dumps. In the study of [45], the authors integrated UAV hyperspectral imagery with the simulated annealing deep neural network model to predict soil organic matter and available copper in the mine tailings pond of China. 74 samples of soil were taken from the study region, and their available copper (Acu) and soil organic matter (SOM) were calculated. Finally, maps of the distribution of ACu and SOM in the study area were established.

According to [46], the dumping sites, with a considerable volume of peeling material, are barren, with high slopes, untable slopes and soil compaction platforms, complicated material composition, and irregular subsidence. This causes a significant amount of vegetation communities to be destroyed and dramatically increases the possibility of soil erosion. Thus, to determine how much erosion occurs in gullies, [47] collected data using UAV oblique photography and created a thorough 3D model of the gully. The obtained results indicated that it might be simple to acquire the distinctive features of the typical erosion gullies of open-pit mine dumps using UAV-based 3D model and GIS spatial analysis technologies.

3.2 Terrain surveying and 3D modeling

According to [48], the ecology was significantly harmed by the abandonment of the waste in various dump sites during exploitation. Nevertheless, abandoned mounds are still rich in rare earth metals and possibly even valuable metals. These dump locations could create a brand-new potential stockpiles, which might pique the interest of business organizations. Therefore, it is necessary to locate dump sites and determine the bottom and top stockpile surfaces. In order to do this, the authors used UAVs to create a 3D topographic map and a 3D model of waste dumps in Mathiatis, Cyprus. The 3D model of reconstructed waste piles can be utilized to compute their volume and other factors such as the gradient of slopes, that are essential to help determine how much the cost of possible restoration. The boundary line of the stockpile was generated on the point cloud itself as Figure 2. Also for the purpose of generating 3D models, in the study of [49], a precise 3D model of waste dump was produced using a combination of satellite and photogrammetric techniques, and it will play a key role in the effort to green the waste dump of the Ucicani mine. The volumes of deposited waste ore could be calculated using the three-dimensional model, and an overview map of the waste dump area that will be greened up could be made.

The accurate mapping and 3D construction of a mine waste dump play an important role to monitor its stability. Acquisition and monitoring of elevation data is a critical issue in relation to some later reclamation activities in waste dumps, such as vegetation planting, soil covering, and cultivation mode. For change detection and analysis, it is crucial to produce digital surface models (DSMs) quickly [50]. Previous research showed that many parameters have an impact on the accuracy of UAV-based DSMs, including the number and distribution of ground control points (GCP) [51]. Thus, for the purpose of producing precise DSMs from UAS in a coal waste dump, they suggest an enhanced GCP configuration.

To broaden knowledge about the cascading behavior of the run-of-mine material during and after dumping, [52] used UAVs with mounted cameras to create photogrammetric models of dumps. Then, a technique for creating high-fidelity models (HFMs) of dump profiles was developed and studied in order to more thoroughly analyze this phenomenon. The

Tab. 1. Applications of UAV technology in mine waste dumps

Number	Resources	Year	Application	Objective
1	[33]	2017	Environmental management	Monitoring Tailings Inpoundments
2	[47]	2019		Analysis of the Development of an Erosion Gully
3	[34]	2019		assess potential pollution through a classification of tailings
4	[35]	2019		Study environmental monitoring of the tailings reservoir
5	[45]	2023		The prediction of organic matter and available copper n the mine tailings pond
6	[43]	2022		Study the process of afforestation of the tailings dump
7	[36]	2023		Recognize acid mine drainage
8	[37]	2022		The investigation of sulfide-bearing mine tailings dumps, as well as the surrounding terrain and acid mine drainage flows
9	[42]	2022		Study the Structure and Composition of the Restored Vegetation Cover in Semi-Arid Mine Dumps
10	[40]	2018		Assess the effectiveness of vegetation establishment on the waste rock dump
11	[44]	2020		Assessment of environmental changes related to land use and alterations in vegetation on self-heating coal waste dumps of various ages
12	[39]	2019		Study the rehabilitation processes at the mine waste dumps
13	[48]	2023	Terrain surveying and 3D modeling	Create a 3D model
14	[49]	2020		3D modelling of the tailings dump
15	[30]	2020		Modelling a hypothetical tailings dam
16	[51]	2020		Generate accurate DSMs
17	[52]	2022		Generate photogrammetric models of dumps
18	[54]	2020	Safety and risk management	Monitoring of deformations at the adjacent dump site
19	[17]	2022		Analyze the stability of active mine waste dump slope
20	[56]	2023		Determine particle size distribution
21	[55]	2022		Analyze particle size distribution
22	[26]	2022		Warn spontaneous combustion of coal waste dump after reclamation
23	[63]	2020		Assess the deformation activity of open-pit mine dump site
24	[58]	2016		Classify the index for self-heating intensity
25	[60]	2021		Determine influence of water erosion on fire hazards
26	[57]	2017		Determine particle size distribution
27	[59]	2022		Investigate the influence of water erosion on fire hazards
28	[61]	2022		Detect the spontaneous combustion monitoring of coal waste dumps
29	[62]	2022		Investigate the land degradation and soil erosion at an opencast coal mine dump

findings indicated that the HFMs developed in this study may be used to calibrate computer models of dumps so that they more closely resemble reality.

In contrast to water-retaining dams, which are typically constructed using concrete, rock, or soil, tailings dams are typically constructed utilizing the tailings themselves to reduce expenses [53]. As a result, operations and emergency management are frequently more difficult due to increased risks of disasters involving dam breaches, debris flows, or overtopping [30]. A model of the run-out flow of tailings dam breach was proposed by using UAVs SfM-photogrammetry and field surveys in China. The findings showed that UAV imagery can generate accurate enough data to assist tailings management activities and monitor yearly surface displacements in the decimeter range [30].

3.3 Safety and risk management

For both security and the continuation of mine production, it is crucial to identify and monitor potential deformations in the benches of dump sites of open-pit mines. [54] used the Global Navigation Satellite System (GNSS) method assisted with UAV technology to monitor and determine the deformation of dump sites of three different open-pit marble mines in Turkey. In this study, the GNSS approach identified the locations of displacements, and UAV photogrammetry investigated the reasons for mobility at the location as well as its areal and volumetric sizes. The obtained results revealed that monitoring of deformations using the combined utilization of UAV photogrammetry and the GNSS approach will enable the effective identification of the primary variables that may contribute, particularly to slope failures, and taking the timely implementation of necessary preventive measures.

During the open-pit mining process, the excavated soil received no economic benefit to the mining sector. These items are categorized as waste which is dumped forming a slope. Mine waste dumps are created quite quickly, therefore these dump slopes are really large. This hurried approach is increasing the risk of disasters on the slopes of dumps. Thus, it is necessary to analyze the stability of mine dump slope and this is a primary subject in geotechnical engineering. [17] analyzed the stability of an operational in-pit mine waste dump using UAV imagery, DGPS survey, and geotechnical samples gathered from the study area. With the aid of UAV photos, 3D modeling, and accurate geometry are retrieved from the active waste dump slope. The findings proved that the UAV's accessibility and image sensor advancements are helpful for building 3D maps and models of the mining regions.

The particle size distribution (PSD) is necessary for assessing the mechanical characteristics of the materials (rock fill) deposited at mine waste dumps, particularly their shear strength. [55] studied the use of UAV photogrammetry to characterize the shear strength in waste dump materials and the impact of PSD on shear strength. The UAV-based map can show the geometric characteristics of the rock fill and waste dump particles. Also to determine PSD, the workflow and the results for PSD evaluation of waste rockfill materials using UAV images were presented in the study of [56]. In addition, PSD is also one key element that governs the flow behavior in ore/rock beds. Because traditional sieve analysis has its limits, [57] used UAV imagery to examine the PSD in ore piles. Analyzing images captured by the camera mounted on a UAV allowed researchers to characterize the PSD of the dump leach pad at the case study mine.

According to [58], after depositing, the mining waste material starts to weather as a result of organic matter oxidation and other processes, which could subsequently result in self-heating. Emissions from dumps have a negative impact on both human and animal life. Due to its negative impact on

Fig. Make a soil available copper distribution map in the mine tailings pond by using that the combination the SA-DNN model and UAV hyperspectral imagery [45]

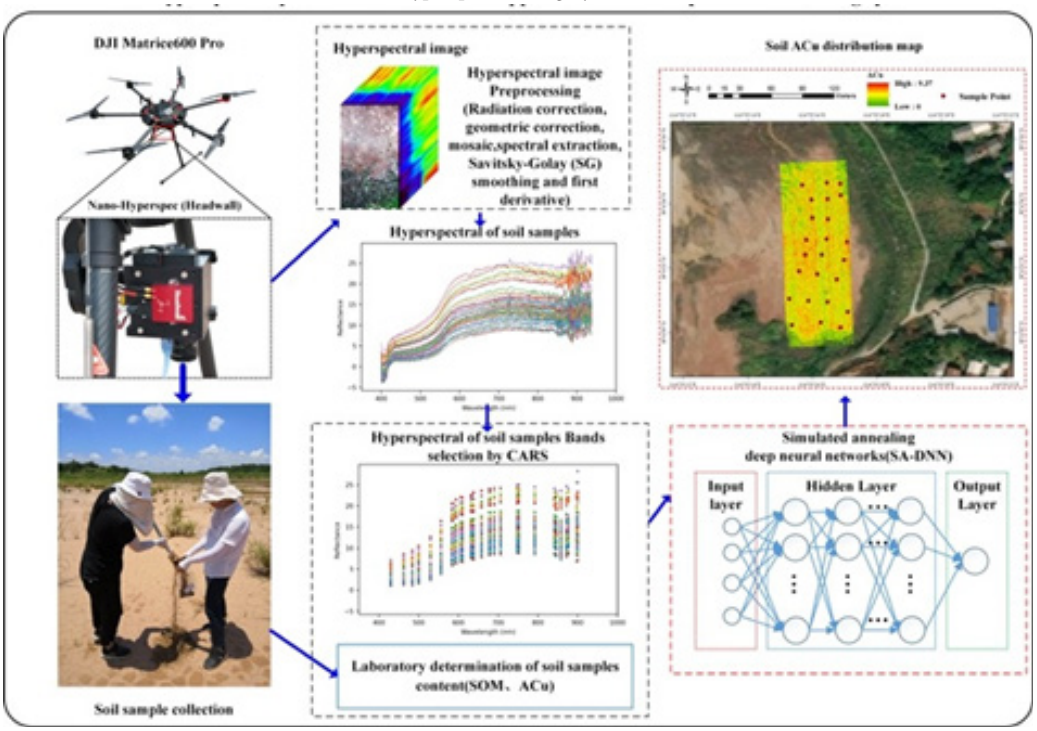

the environment and human health, it is essential to identify the self-heating process as soon as possible in order to avoid the spread of impacted areas and put out self-combustion zones. In order to do this, in study [58], the authors use Landsat, ASTER, and thermal-infrared camera collection from a drone to generate a classification index for self-heating intensity at coal waste dumps in various areas combining Landsat 4-5 TM, ETM+, and ASTER photographs.

Up utill now, the influence of intense rainfall and water erosion on spontaneously combusting of coal waste dumps has gained no much attention. As a result, the concern arises as to whether heavy rain can cause water erosion of the dump slope, increasing the likelihood of the dump's self-ignition. For this purpose, [59] studied the amount of rainfall, changes in the status of the slope surface, and the thermal operation of the chosen dump. Moreover, the state of mining waste dumps is impacted by precipitation, especially intense rainfall. The influence of rainfall on the erosion of water on a coal waste dump's slopes and its thermal condition presented in the study of [60]. The study's objective was to depict the beginning conditions of the studied dumping ground surfaces and the thermal conditions of particular slopes. With the assist of UAV-based low-altitude aerial photogrammetry, terrestrial laser scanning, observations of temperature and gas concentrations, the occurrence of phenomena like water erosion and thermal activity at the coal waste dump has been determined. As can be seen, spontaneous burning of coal waste dumps is one of the major issues in mining regions. Even after ecological restoration and land reclamation, this danger still occurs. [61] proposed better technology, UAV RGB imagery based on alfalfa aboveground biomass, for monitoring coal waste dumps for spontaneous combustion, which might serve as a guide for early detection and prevention in mining areas. Stepwise linear regression models were used to estimate this plant aboveground biomass together with the vegetation index and texture metrics taken from UAV RGB data. The alfalfa aboveground biomass map of the research area was created based on the model as Figure 3.

A rehabilitated opencast coal mine waste is influenced by erosion caused by wind and water from natural processes after artificial management is discontinued, leading to land deterioration as well as safety incidents. In order to degree and spatial distribution of erosion cracks and the soil erosion and land degradation after 5 years of natural processes, a multi-source data collection approach was used [62]. In this study, a UAV was used to gather the position and intensity of soil erosion as well as high-precision topography parameters and by using field sampling, the topsoil's physical characteristics were discovered. Moreover, [63] insisted that UAV can be a helpful instrument to monitor long-term continuous deformation and soil erosion. Therfore, UAV images were utilized to aid in phase unwrapping, demonstrating the soil erosion and deformation of the open-pit coal mine dump in China. In this study, high-resolution UAV images play an important role to understand the developmet of the waste dump. The elimination of the topographic factor and a time series analyses were processed using the high-resolution DEM (8 cm/pix) generated by UAV, structure from motion, and multi view stereo technologies.

3.4 Discussion and recommendation

From the review, it was determined that several trends helped to categorise current UAV uses in the mine waste dumps, as follow:

(1) Environmental management (eleven papers)
(2) Terrain surveying and 3D modeling (five papers)
(3) Safety and risk management (twelve papers)

Figure 4 displays the percentage distribution of each UAV application related in mine waste dumps together with num-

ber of publications categorized under that application. The obtained results show that there are very few studies on the application of UAVs in mine waste dumps, so this is a new approach that has not received much attention. Published papers focus more on environmental management and safety and risk management. There are only 5 studies with the aim of terrain surveying and 3D modeling, mainly papers used UAV to generate DEM, DSM, 3D models for purposes related to the landscaping, geometry, weeding and afforestation in mine waste dump [49], tailings dam [30], waste material stock-piles [48], mine haul truck dumping process [52]. In addition, publications involved environmental management primarily concentrate on environmental monitoring of the tailings reservoir [33-35, 43, 45], identifying acid mine drainage [36, 37], assessing environment of waste dumps [40, 42, 44]. For safety and risk management in mine waste dumps, UAV application focus mostly on deformation monitoring [54, 63], stability analysis [17], determination of particle size distribution [55-57], detection of spontaneous combustion [26, 58, 61], investigation of soil erosion [59, 60, 62].

Furthermore, the results of the review showed that most of the studies were conducted in recent years and the number increased gradually over the years, from 1 study in 2016 to 10 studies in 2022. Despite the fact that an increase in studies on the use of UAVs to address mine waste dump management indicates a growing trend in the scientific literature, there is a certain delay among researchers in assessing the extensive usage of UAVs in the field of mine waste dump management. Accordingly, the understanding of the potential of UAV for addressing issues with mining waste dumps remain inadequate and needs to be developed. Most studies used digital images, except for spontaneous combustion studies using infrared camera. The SfM technique improves image post-processing and enables the quick creation of any necessary models. Two software programmes that use SfM algorithms to create extremely accurate photogrammetric models were frequently mentioned in the literature including Agisoft Photoscan and Pix4D.

According to [64], UAVs' quick mobility makes multi-view geographical data collection easier. Besides, compared to other remote sensing platforms, a UAV can get closer to a target object. As a result, it is easy to acquire high-resolution images. This closes the gap between present aerial and ground platforms, opening up new possibilities for building high-fidelity 3D models. Furthermore, due to its small form and remote operating abilities, a UAV can gather spatial measurements in an adverse condition that is too risky or inaccessible for other traditional mapping technologies, especially in hazardous or heavy metal contaminated areas such as mining waste dumps. However, managing the enormous number of datasets being collected is a problem that UAV applications frequently face. Thus, the superiority in time efficiency that is an advantage of UAV technology is reduced by the delayed processing of datasets captured by UAVs. In order to overcome this shortcoming, according to [64], it is ideal for all processing steps to be totally automated, requiring no human involvement. Recent developments in artificial intelligence and computer vision technologies may be able to support and give an efficient solution for UAV usage in mining waste dump management. In fact, this technology was used in study of [45] that the combination the simulated annealing deep neural network (SA-DNN) and UAV hyperspectral imagery to make a soil available copper distribution map in the mine tailings pond. The process of using this advanced technology for mapping soil available copper content in the mine tailing pond is shown in Figure 5.

4. Conclusion

Although the fact that the scientific community first learned about UAV use in the mining industry more than a decade ago, only in the past six to seven years have there been intensive investigations of the potential of UAV in managing mine waste dump. Based on the analysis of the available literatures as well as findings of current study, it was found that UAV technology has a lot of potential for managing mine waste dumps. Additionally, a list of potential uses for UAVs in mine waste dumps was provided including environmental management, terrain surveying and 3D modeling, and safety and risk management. Many obstacles still exist, though, and they need to be further investigated. In the near future, we may anticipate a continuous rise in research publications related to the usage of UAVs in mine waste dumps.

Literatura – References

1. Cebada, J.D.P., Mining corporations and air pollution science before the Age of Ecology. Ecological Economics, 2016. 123: p. 77-83.
2. Tabish, R., et al., Predicting the Settlement of Mine Waste Dump Using Multi-Source Remote Sensing and a Secondary Consolidation Model. Frontiers in Environmental Science, 2022: p. 526.
3. Romero, A., et al., Risk assessment of particle dispersion and trace element contamination from mine-waste dumps. Environmental geochemistry and health, 2015. 37: p. 273-286.
4. Council, N.R., Coal waste impoundments: Risks, responses, and alternatives. 2002: National Academies Press.
5. Wei, L., et al., Analysis of mining waste dump site stability based on multiple remote sensing technologies. Remote Sensing, 2018. 10(12): p. 2025.
6. Xu, F. and L. Sun. The remote sensing recognition and extraction of waste dump in mining area using multi-source and multi-temporal remote sensing data. in The 2nd International Conference on Information Science and Engineering. 2010. IEEE.
7. Oparin, V., et al., Studies into the process of mine waste dump filling up by vegetation using remote sensing data. Journal of Mining Science, 2013. 49: p. 976-982.
8. Rodríguez-Hernández, A., et al., Processing methodology based on ASTER data for mapping mine waste dumps in a semiarid polysulphide mine district. Canadian Journal of Remote Sensing, 2016. 42(6): p. 643-655.
9. Dev, P.P. and E.T. Goyal, Assessment Of Waste Dump Slope Stability At Iron Ore Mines. Assessment, 2019. 6(05).
10. Cordeiro, M., et al., Mapping mining wastes and analyzing affected areas through expeditious physico-chemical parameters. 2017.
11. Campbell, D.L. and D.V. Fitterman. Geoelectrical methods for investigating mine dumps. in Proceedings of the 5th International Conference on Acid Rock Drainage (ICARD 2000), Denver, Colo. 2000. Citeseer.
12. Power, C., et al., Combined DC resistivity and induced polarization (DC-IP) for mapping the internal composition of a mine waste rock pile in Nova Scotia, Canada. Journal of Applied Geophysics, 2018. 150: p. 40-51.
13. Georgios, K.N. and S.G. Anastasia, Geostatistical Interpolation with GIS in Mapping Heavy Metals Concentrations for Preliminary Site Investigation of Old Mining Waste Dump. 2020.
14. Jessop, M., et al., Magnetometric resistivity: a new approach and its application to the detection of preferential flow paths in mine waste rock dumps. Geophysical Journal International, 2018. 215(1): p. 222-239.
15. Igwe, O. and C. Chukwu, Slope stability analysis of mine waste dumps at a mine site in Southeastern Nigeria. Bulletin of Engineering Geology and the Environment, 2019. 78: p. 2503-2517.
16. Hu, Z. and Q. Xia, An integrated methodology for monitoring spontaneous combustion of coal waste dumps based on surface temperature detection. Applied Thermal Engineering, 2017. 122: p. 27-38.
17. Layek, S., et al., Rainfall & Seismological Dump Slope Stability Analysis on Active Mine Waste Dump Slope with UAV. Advances in Civil Engineering, 2022. 2022.
18. Muchiri, G. and S. Kimathi. A review of applications and potential applications of UAV. in Proceedings of the Sustainable Research and Innovation Conference. 2022.
19. Dutta, G. and P. Goswami, Application of drone in agriculture: A review. International Journal of Chemical Studies, 2020. 8(5): p. 181-187.
20. Li, Y. and C. Liu, Applications of multirotor drone technologies in construction management. International Journal of Construction Management, 2019. 19(5): p. 401-412.
21. Daud, S.M.S.M., et al., Applications of drone in disaster management: A scoping review. Science & Justice, 2022. 62(1): p. 30-42.
22. Cvitanić, D. Drone applications in transportation. in 2020 5th international conference on smart and sustainable technologies (SpliTech). 2020. IEEE.
23. Leo Stalin, J. and R. Gnanaprakasam, Application of unmanned aerial vehicle for mapping and modeling of Indian mines. Journal of the Indian Society of Remote Sensing, 2020. 48: p. 841-852.
24. Lee, S. and Y. Choi, Reviews of unmanned aerial vehicle (drone) technology trends and its applications in the mining industry. Geosystem Engineering, 2016. 19(4): p. 197-204.
25. Villa, T.F., et al., An overview of small unmanned aerial vehicles for air quality measurements: Present applications and future prospectives. Sensors, 2016. 16(7): p. 1072.

26. Ren, H., et al., Vegetation growth status as an early warning indicator for the spontaneous combustion disaster of coal waste dump after reclamation: An unmanned aerial vehicle remote sensing approach. Journal of Environmental Management, 2022. 317: p. 115502.
27. Park, S. and Y. Choi, Applications of unmanned aerial vehicles in mining from exploration to reclamation: A review. Minerals, 2020. 10(8): p. 663.
28. Loots, M., S. Grobbelaar, and E. van der Lingen, A review of remote-sensing unmanned aerial vehicles in the mining industry. Journal of the Southern African Institute of Mining and Metallurgy, 2022. 122(7): p. 387-396.
29. Shahmoradi, J., et al., A comprehensive review of applications of drone technology in the mining industry. Drones, 2020. 4(3): p. 34.
30. Wang, K., et al., 3D Numerical modelling of tailings dam breach run out flow over complex terrain: a multidisciplinary procedure. Water, 2020. 12(9): p. 2538.
31. Wang, C., et al., Current state of fine mineral tailings treatment: A critical review on theory and practice. Minerals Engineering, 2014. 58: p. 113-131.
32. Pajares, G., Overview and current status of remote sensing applications based on unmanned aerial vehicles (UAVs). Photogrammetric Engineering & Remote Sensing, 2015. 81(4): p. 281-329.
33. Rauhala, A., et al., UAV remote sensing surveillance of a mine tailings impoundment in sub-arctic conditions. Remote sensing, 2017. 9(12): p. 1318.
34. Peña-Ortega, M., et al., Environmental assessment and historic erosion calculation of abandoned mine tailings from a semi-arid zone of northwestern Mexico: insights from geochemistry and unmanned aerial vehicles. Environmental Science and Pollution Research, 2019. 26: p. 26203-26215.
35. Wan, Y., et al. Tailings reservoir disaster and environmental monitoring using the UAV-ground hyperspectral joint observation and processing: a case of study in Xinjiang, the belt and road. in IGARSS 2019-2019 IEEE International Geoscience and Remote Sensing Symposium. 2019. IEEE.
36. Kou, X., et al., Acid Mine Drainage Discrimination Using Very High Resolution Imagery Obtained by Unmanned Aerial Vehicle in a Stone Coal Mining Area. Water, 2023. 15(8): p. 1613.
37. Yurkevich, N., et al., Current State of the Gold Mining Waste from the Ores of the Ursk Deposit (Western Siberia, Russia). Applied Sciences, 2022. 12(20): p. 10610.
38. Mallı, T., M. Kun, and B. Tufan, EVALUATION OF DUMP SITE RECLAMATION TECNIQUES IN WESTERN TURKEY COAL MINES. Environmental Engineering and Management Journal, 2018. 17(1): p. 11-18.
39. Kun, M., Assessment and monitoring of rehabilitation studies on coal mine dump site with UAV'S. Appl. Ecol. Environ. Res, 2019. 17: p. 7381-7393.
40. Strohbach, B., et al., Determining rehabilitation effectiveness at the Otjikoto Gold Mine, Otjozondjupa Region, Namibia, using high-resolution NIR aerial imagery. Namibian Journal of Environment, 2018. 2: p. A-146.
41. Hooper, M.J., et al., Integrated risk and recovery monitoring of ecosystem restorations on contaminated sites. Integrated Environmental Assessment and Management, 2016. 12(2): p. 284-295.
42. Tang, J., et al., Revealing the structure and composition of the restored vegetation cover in semi-arid mine dumps based on LiDAR and hyperspectral images. Remote Sensing, 2022. 14(4): p. 978.
43. Popescu, G., et al., THE USE OF GEOMATICS TECHNOLOGIES FOR RENDERING THE TALINGS DUMP IN TO THE FORESTRY CIRCUIT, URICANI MINE, ROMANIA. International Multidisciplinary Scientific GeoConference: SGEM, 2022. 22(3.2): p. 447-454.
44. Abramowicz, A., O. Rahmonov, and R. Chybiorz, Environmental management and landscape transformation on self-heating coal-waste dumps in the Upper Silesian Coal Basin. Land, 2020. 10(1): p. 23.
45. Zhang, Y., et al., Mapping soil available copper content in the mine tailings pond with combined simulated annealing deep neural network and UAV hyperspectral images. Environmental Pollution, 2023: p. 120962.
46. Shi, X., I. Herle, and D. Muir Wood, A consolidation model for lumpy composite soils in open-pit mining. Géotechnique, 2018. 68(3): p. 189-204.
47. Gong, C., et al., Analysis of the development of an erosion gully in an open-pit coal mine dump during a winter freeze-thaw cycle by using low-cost UAVs. Remote Sensing, 2019. 11(11): p. 1356.
48. Saratsis, G., et al., Use of UAV Images in 3D Modelling of Waste Material Stock-Piles in an Abandoned Mixed Sulphide Mine in Mathiatis—Cyprus. Mining, 2023. 3(1): p. 79-95.
49. POPESCU, G., et al., 3d Modeling Of Waste Dumps In Order To Ecology Of Mining Areas. AgroLife Scientific Journal, 2020. 9(2): p. 240-249.

50. Meinen, B.U. and D.T. Robinson, Streambank topography: an accuracy assessment of UAV-based and traditional 3D reconstructions. International Journal of Remote Sensing, 2020. 41(1): p. 1-18.

51. Ren, H., et al., An improved ground control point configuration for digital surface model construction in a coal waste dump using an unmanned aerial vehicle system. Remote Sensing, 2020. 12(10): p. 1623.

52. Young, A. and W.P. Rogers, A High-Fidelity Modelling Method for Mine Haul Truck Dumping Process. Mining, 2022. 2(1): p. 86-102.

53. Slack, R. and N. Voulvoulis, Mine Wastes: Characterization, Treatment and Environmental ImpactsBernd G. Lottermoser, Springer-Verlag, Berlin, Heidelberg, New York, 2003, ISBN: 3-540-00526-9 (277 pp., Hardback). 2006, Elsevier.

54. Gül, Y., K.Ö. Hastaoğlu, and F. Poyraz, Using the GNSS method assisted with UAV photogrammetry to monitor and determine deformations of a dump site of three open-pit marble mines in Eliktekke region, Amasya province, Turkey. Environmental Earth Sciences, 2020. 79: p. 1-20.

55. Arrieta, M., UAV photogrammetry for particle size distribution (PSD) and rock fill characterization. 2022.

56. Arrieta, M. Novel Approach for Particle Size Distribution Analysis. Applied Case to Rockfills and Waste Dumps Using Unmanned Aerial Vehicle (UAV). in TMIC 2022 Slope Stability Conference (TMIC 2022). 2023. Atlantis Press.

57. Zhang, S. and W. Liu, Application of aerial image analysis for assessing particle size segregation in dump leaching. Hydrometallurgy, 2017. 171: p. 99-105.

58. Nádudvari, A., et al., Classification of fires in coal waste dumps based on Landsat, Aster thermal bands and thermal camera in Polish and Ukrainian mining regions. International Journal of Coal Science & Technology, 2021. 8: p. 441-456.

59. Różański, Z., et al., Influence of water erosion on fire hazards in a coal waste dump—A case study. Science of the total environment, 2022. 834: p. 155350.

60. Różański, Z., et al., The impact of precipitation on state of the slopes surface and thermal activity of the mine waste dump-preliminary study. Journal of Sustainable Mining, 2021. 20.

61. Ren, H., et al., Monitoring potential spontaneous combustion in a coal waste dump after reclamation through unmanned aerial vehicle RGB imagery based on alfalfa aboveground biomass. Land Degradation & Development, 2022. 33(15): p. 2728-2742.

62. Xiao, W., et al., A drone-and field-based investigation of the land degradation and soil erosion at an opencast coal mine dump after 5 years' evolution of natural processes. International Journal of Coal Science & Technology, 2022. 9(1): p. 42.

63. Gong, C., et al., Using time series InSAR to assess the deformation activity of open-pit mine dump site in severe cold area. Journal of Soils and Sediments, 2021. 21(11): p. 3717-3732.

64. Liu, P., et al., A review of rotorcraft unmanned aerial vehicle (UAV) developments and applications in civil engineering. Smart Struct. Syst, 2014. 13(6): p. 1065-1094.

Establishing the Vertical Movement Map of Cuu Long Delta River by GNSS Data

NGUYEN Gia Trong[1,5)], NGUYEN Viet Nghia[1)], LY Lam Ha[1,2)], VU Trung Dung[3)], NGUYEN Quoc Long[1)], KIM Thi Thu Huong[1,4)], PHAM Ngoc Quang[1)], NGUYEN Viet Quan[1)]*

[1)] Hanoi University of Mining and Geology, 18 Vien street, Hanoi, Vietnam
[2)] Department of Economic Infrastructure, Cam Lam, Khanh Hoa Province, Vietnam
[3)] Delta technology development and Investment joint stock company, Bac Giang Province, Vietnam
[4)] AGH University of Science and Technology, Krakow, Poland
[5)] AGH University of Science and Technology, Krakow, Poland

http://doi.org/10.29227/IM-2023-02-26

Submission date: 19-08-2023 | Review date: 10-09-2023

Abstract

Mekong Delta is an area with an important position in the socio-economic development of Vietnam. However, due to the impact of climate change as well as of the construction of hydroelectric dams in the upstream of the Mekong River in recent years, saline intrusion and flooding have been occurred because of high tide. According to published researches, the Mekong Delta is being experienced surface subsidence with a rate of up to centimeters per year, that exacerbates the impact of saline intrusion and flooding. Thus, studying to establish the surface subsidence map is an urgent need in this site. There are many of technologies to create the vertical movement map such as: Levelling, INSAR, GNSS, etc. Up to now, there are no scientific reports on the application of GNSS to monitor the vertical movement in this area. In this paper, the authors have calculated the largest vertical displacement velocity up to 3cm/year based on processing GNSS observations of nearly 20 GNSS monitoring station in the area using Bernese software. From these results, the research team has made the vertical movement map of Mekong, Vietnam.

Keywords: *land subsidence, GNSS, vertical crustal deformation, Mekong del*

1. Introduction

Land subsidence is a global environmental hazard due to many natural and human activities. In many places on the world, it has been observed that there are about 150 countries recorded land subsidence. Land subsidence affects to infrastructures, building on the earth surface, then the living of human and animals living on the surface. Therefore, it is necessary to find the solutions, create subsidence maps to minimize negative effects of land subsidence on both humans and environment.

Currently, there are some methods to determine land subsidence. There are methods, which have been used for a long time, called conventional methods, such as geodetic leveling, total station, Global Navigation Satellite System (GNSS). There are non-contacts technology methods, such as Unmanned Aerial Vehicle (UAV) [1], Interferometric Synthetic Aperture Radar (InSAR) [2] and Laser Scanner [3]. The model non-contact technologies have shown big significant advantages, such as allowing monitor the large areas surface with a low spatial spacing. Meanwhile, the conventional methods have disadvantageous in limit and discrete measurement points on the Earth's surface, but it provides high result accuracy, approximate 1mm / 3years [10]. Such monitoring can be carried out in discrete cycles or continuous measurement depending on the used technology. Before the continuous satellite receiver station (CORS) was built, the application of GNSS technology to determine the displacement of the continental plates was measured, according to the traditional relative static method. When the predetermined measurement time is reach, the receiver will be placed at the points to receive the satellite signal. CORS technology, with the advantage of providing continuous data over time, allows to determine the land displacement better and with higher reliability [4].

On the world, using GNSS to monitor the land displacement is conducted widely. In 2009, Jing Xiang and partners published a article about using GNSS for monitoring land subsidence in mining areas and hazard early warning [5]. GW Michel and partners determined surface displacement in Eastern and South-Eastern of Asia by GPS measurements of Geodysea project in 2020, 2021 [6, 7]. Abou Aly and his partners in 2021 used GNSS to monitor land deformation in the Nile Delta. Basing on the results, they found the displacement areas, combine with geological characteristics, research group gave assessment and forecast for future subsidence [8].

In Vietnam, almost research projects have been focused on using GNSS technology to determine horizontal displacements.[4]. Nguyen Anh Duong and partners assessed the modern displacement of The Lai Chau - Dien Bien fault zone using the series of GPS measurements from 2002 to 2010. They showed that this fault zone moved to the East-Southeast direction 34.6 mm/year, and moved to the left 2.3 mm/year [9]. Nguyen Gia Trong and partners used Gamit/Globk to determine the displacement of CORS stations distributed over the territory of Vietnam [10]. In 2023, Vu Ngoc Quang and partners published an article about building a displacement monitoring and early warning system using GNSS-RTK techniques [11].

In this study, we use GNSS technology to monitor the land subsidence in the area of Mekong Delta, Southern of Vietnam. For this area, GNSS-derived vertical deformation has not been studied so far. The study is based on approxi-

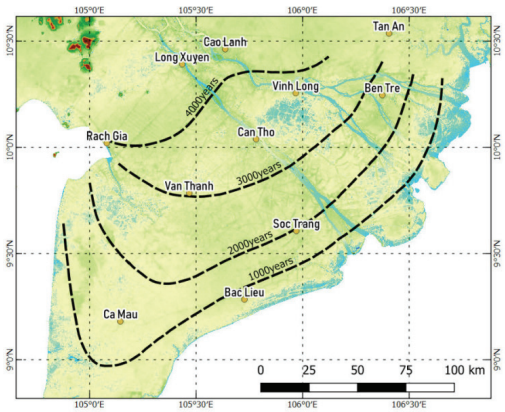

Fig. 1. Evolution of sedimentation and erosion in the Mekong Delta

Fig. 2. Flooding due to high tide in Can Tho, Vietnam

mately 1 years GNSS data, from 2020 to 2021. Vietnam has been seen one of the most threatened countries in the world by the climate change. Mekong Delta is one of the largest deltas on the world. The height of this area is almost the sea level, then it is always threatened by the sea level rise. Under the natural and human activities, the ground in this delta is continuously compacted, causing land surface subsidence. This subsidence process in some local is faster than the sea level rise. One day, low-lying areas of Mekong Delta will be flooded by the sea level rise if effective measures are not taken [12].

The remainder of the paper is structured as follows: Section 2 introduces the study area and data set. Section 3 shows the experimental results and discussion. Section 4 concludes the study.

2. Data and methodology

2.1 Area study

The Mekong Delta is one of the major deltas in the world and is also an important economic region of Vietnam. The topography of the Mekong Delta is very low, most of which are only a few meters above sea level and is regularly affected by saline intrusion and flooding caused by high tides. Is a relatively young delta in geological time, formed by sediments from the Himalayas flowing down the Mekong River about 6000 years ago. Over time, the sediment deposited on the seabed is raised to create land. The evolution of the deposition and erosion in the Mekong Delta is shown in Fig. 1 [12].

In the process of development, dyke systems were built to prevent flood water from entering agricultural lands, leading to the sediment of the Mekong River no longer distributed throughout the delta but deposited in rivers. or drift into the sea. During that process, the ground in this area continues to be compressed, causing surface subsidence. In addition, the construction of infrastructure works and the excessive exploitation of groundwater have contributed to the exacerbation of surface subsidence in the Mekong Delta.

Land subsidence has exacerbated the effects of tidal flooding (Fig. 2) [13] and saline intrusion [14] (Fig. 3) in the Mekong Delta.

2.2 Area study

The data used in this article is the data measured at 18 continuous GNSS data collection stations in Vietnam, provided by the Department of Survey, Mapping, and Geographic Information of Vietnam (DOSM) and Tuong Anh Science and Technology Equipment Joint Stock Company (TAST JSC) (as described in Tab. 1).

Among the stations described in Tab. 1, the stations managed by DOSM have benchmarks securely buried on the ground surface (Fig. 4a), while the stations managed by TAST JSC are civilian buildings (Fig. 4b).

All of the above data collection stations are continuous GNSS data collection stations, but due to data collection conditions, the research team only collected data in two days, January 1st, 2020, and January 2nd, 2021 respectively.

GNSS data is processed by Bernese software version 5.2, all baselines of network processed with data received by 18 CORS stations in Vietnam (as described in Tab. 1) and 6 stations in the IGS network including: DAEJ, DGAR, IISC, IRKJ, PIMO and POL2.

First, the data is processed on a daily basis (session) to get the coordinates of the stations in each data day. By combining the re-

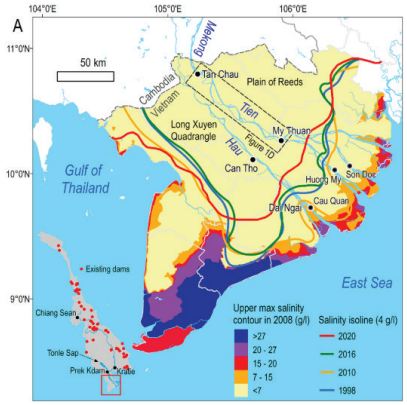

Fig. 3. Saltwater intrusion in the Mekong Delta, Vietnam

Tab. 1. Information about GNSS CORS stations

No.	Site's name	Receiver	Antenna	Interval (s)	Management
1	BLIE	LEICA GR50	LEIAR25.R4 LEIT	30	DOSM
2	BTRE	TRIMBLE NETR9	TRM55971.00 NONE	15	TAST JSC
3	BTRI	LEICA GR50	LEIAR25.R4 LEIT	30	DOSM
4	CAOL	LEICA GR50	LEIAR25.R4 LEIT	30	DOSM
5	CLAH	TRIMBLE NETR9	TRM55971.00 NONE	15	TAST JSC
6	CLON	LEICA GR50	LEIAR25.R4 LEIT	30	DOSM
7	CMAU	TRIMBLE NETR9	TRM55971.00 NONE	15	TAST JSC
8	CTH1	TRIMBLE NETR9	TRM55971.00 NONE	15	TAST JSC
9	CTHO	LEICA GR50	LEIAR25.R4 LEIT	30	DOSM
10	GOCO	TRIMBLE NETR9	TRM55971.00 NONE	15	TAST JSC
11	HCMC	TRIMBLE NETR9	TRM55971.00 NONE	15	TAST JSC
12	HGAN	TRIMBLE NETR9	TRM55971.00 NONE	15	TAST JSC
13	HOCM	LEICA GR50	LEIAR25.R4 LEIT	30	DOSM
14	HTIE	LEICA GR50	LEIAR25.R4 LEIT	30	DOSM
15	MHOA	LEICA GR50	LEIAR25.R4 LEIT	30	DOSM
16	MTHO	LEICA GR50	LEIAR25.R4 LEIT	30	DOSM
17	RGIA	TRIMBLE NETR9	TRM55971.00 NONE	15	TAST JSC
18	XMOC	TRIMBLE NETR9	TRM55971.00 NONE	15	TAST JSC

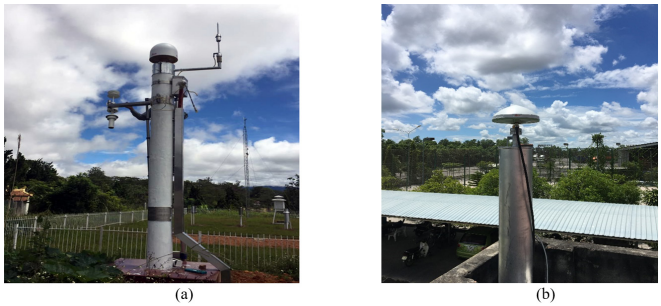

(a) (b)

Fig. 4. (a) CORS station managed by DOSM, (b) CORS station managed by TAST JSC

Tab. 2. Information about GNSS CORS stations

No.	Site'name	Displacement (m)	RMS (m)
1	BLIE	-0.0301	0.0048
2	BTRE	-0.0477	0.0111
3	BTRI	-0.0117	0.0046
4	CAOL	-0.0297	0.0046
5	CLAH	0.0286	0.0168
6	CLON	-0.0223	0.0048
7	CMAU	0.0021	0.0121
8	CTH1	-0.0638	0.0051
9	CTHO	-0.0211	0.0046
10	GOCO	-0.0129	0.0047
11	HCMC	-0.0563	0.0375
12	HGAN	-0.0399	0.0128
13	HOCM	-0.0027	0.0046
14	HTIE	-0.0076	0.0052
15	MHOA	-0.0063	0.0046
16	MTHO	-0.0121	0.0046
17	RGIA	0.0093	0.0149
18	XMOC	-0.0092	0.0047

sults of the normalization between the two periods, the amount of displacement of the points over time can be determined.

The results of determining vertical displacement at stations in this study are compared with published calculation results such as Nguyen Gia Trong et al. [4], GIZ Energy Support Program [12] and Nguyen Viet Quan et al. [15].

3. Results and discussions

The vertical displacement of the points determined by Bernese 5.2 software is as follows:

From the results given in Tab. 2, it can be seen that the displacement determination error of some receiver stations managed by TAST JSC has a large RMS error (more than 1

Tab. 3. The vertical displacement of this study is with the results published by Nguyen Gia Trong (PA1) et al. [4], Nguyen Viet Quan et al. (PA2) [15].

No.	Site's name	Displacement (m)	Comparative data (m) PA1 PA2	Differrence (m)
1	BLIE	-0.0301	- -	- -
2	BTRI	-0.0117	-0.0167 -0.0048	-0.0050 0.0069
3	CAOL	-0.0297	- -0.0266	- 0.0031
4	CLON	-0.0223	-0.0255 -0.0163	-0.0032 0.0060
5	CTHO	-0.0211	-0.0143 -0.0100	0.0068 0.0110
6	HOCM	-0.0027	- 0.0015	- 0.0012
7	HTIE	-0.0076	-0.0052 -0.0016	0.0024 0.0060
8	MHOA	-0.0063	- -0.0038	- 0.0029
9	MTHO	-0.0121	- -0.0010	- 0.0111

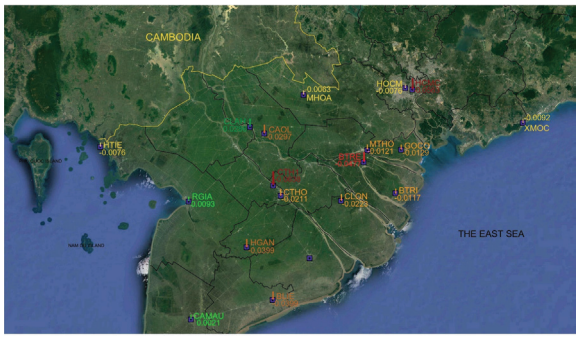

Fig. 5. Map of vertical displacement stations in the Mekong Delta, Vietnam

cm), it is necessary to study a plan to eliminate errors in the measurement data. The RMS error of displacement of all stations managed by DOSM is approximately 5 mm which can be partly influenced by the error of the remaining stations. Stations RGIA, HCMC, CTH1, CMAU, CLAH have an irregular amount of displacement possibly due to station structure.

The vertical displacement of this study is compared with the results published by Nguyen Gia Trong (PA1) et al. [4], Nguyen Viet Quan et al. (PA2) [15]. The results of the comparison are shown in Tab. 3.

From the results in Tab. 2, it is shown that the difference in the amount of displacement is determined at the mm level.

According to the published displacement determination results [12], the subsidence level of 100 m of sediment from the ground is at 2-3 cm/year in Ca Mau; In Can Tho, by using a shallow observation pile system, the settlement level is 17 mm/year, while the subsidence rate of residential buildings is 27 mm/year determined from InSAR data [12]. Combined with the comparative data in Tab. 3, it can be seen that the vertical displacement determination results of the stations managed by DOSM in this study are relatively consistent with the previously determined results.

Based on the results of determining the displacement of the points as presented above, build a map representing the displacement of the points as shown in Fig. 5.

4. Conclusion

Subsidence along with the effects of climate change such as inundation and saltwater intrusion has had a great impact on the Mekong Delta of Vietnam. Accurately determining the amount of displacement is a very necessarily need to be able to make decisions related to socio-economic development for this area.

This study provides initial results on vertical displacement mapping for the Mekong Delta of Vietnam. The results determined in this study are relatively consistent with the results previously determined both by GNSS technology and using shallow pile system to observe settlement.

The number of stations used to map vertical displacement in this study is relatively limited, so the results do not accurately reflect the vertical displacement for the whole region. Besides, it is necessary to analyze the GNSS data in time series to obtain more accurate vertical displacement results.

6. Acknowledgements

The authors would like to thank the Vietnam Department of Surveying, Mapping and Geographic Information (DOSM), Tuong Anh Science and Technology Equipment Joint Stock Company (TAST JSC) for providing experimental data in this article.

The paper was presented during the 7th POL – VIET International Conference on Scientific-Research Cooperation between Poland and Vietnam, 18-20.10.2023, AGH, Krakow, Poland.

Literatura – References

1. Dawei, Z., Lizhuang, Q., Demin, Z., Baohui, Z., & Lianglin, G. (2020). Unmanned aerial vehicle (UAV) photogrammetry technology for dynamic mining subsidence monitoring and parameter inversion: A case study in China. Ieee Access, 8, 16372-16386.
2. Kim, T.T.H., Tran, H.H., Phan, T.A., & Lipecki, T. (2022, October). Mining-Induced Land Subsidence Detected by Persistent Scatterer InSAR: Case Study in Pniówek Coal Mine, Silesian Voivodeship, Poland. In International Conference on Geo-Spatial Technologies and Earth Resources (pp. 23-42). Cham: Springer International Publishing. http://doi.org/10.1007/978-3-031-20463-0_2.
3. Matwij, W., Gruszczyński, W., Puniach, E., & Ćwiąkała, P. (2021). Determination of underground mining-induced displacement field using multi-temporal TLS point cloud registration. Measurement, 180, 109482.
4. Nguyen, G.T., Nguyen, V.N., Ly, L.H., Nguyen, H.T., Vu, T.D., Nguyen, V.Q., & Bui, H.T. (2022). Research proposal on the model for estimation vertical velocity by GNSS Technology. In Proceedings of The 5th National Conference on Sustainable Earth, Mine, Environment (EME 2022) for creative innovation and enhancement of the national competitiveness, Hanoi, 392-399. Doi: 10.15625/vap.2022.0192
5. Jing-Xiang, G., & Hong, H. (2009). Advanced GNSS technology of mining deformation monitoring. Procedia Earth and Planetary Science, 1(1), 1081-1088.
6. Michel, G. W., Becker, M., Angermann, D., Reigber, C., & Reinhart, E. (2000). Crustal motion in E-and SE-Asia from GPS measurements. Earth, planets and space, 52(10), 713-720.
7. Wilson, P., & Michel, G. W. (1998). The GEODYnamics of S and SE Asia (GEODYSSEA) Project.
8. AbouAly, N., Hussien, M., Rabah, M., Zidan, Z., & Saleh, M. (2021). Land deformation monitoring by GNSS in the Nile Delta and the measurements analysis. Arabian journal of geosciences, 14, 1-12.
9. Nguyen, A.D., FUMIAKI, K., Tran, D.T., Nguyen, D.X., Pham, D.N., Vy, Q.H., & Duong, C.C. (2011). Contemporary horizontal movement estimation for Lai Chau - Dien Bien fault inferred from repeated GPS measurements in 2002 – 2010. Vietnam Journal of Earth Sciences, 33(3), 690-694.
10. Nguyen, G.T., Nguyen, V.N., Pham, C.K., Nguyen, H.T., Ly, L.H., Vu, T.D., Nguyen, V.Q., Pham, N.Q. (2022). Determination of tectonic velocities in Vietnam territory based on data of CORS stations of VNGEONET network. Vietnam Journal of Hydrometeorology, 739, 59-66. doi:10.36335/VNJHM.2022(739).59-66
11. Vu, N.Q., Nguyen V.H., Vu, & D.C. (2023). Building a displacement monitoring system and early warning using GNSS-RTK technique. Journal of Science and Technology in Civil Engineering, 1V, 134-146. https://doi.org/10.31814/10.31814/stce.huce(nuce)2023-17(1V)-11
12. Ministry of Construction, (2019). Trouble underground - Land Subsidence in the Mekong Delta. Deutsche Gesellschaft für Internationale Zusammenarbeit (GIZ) GmbH. https://www.eda.admin.ch/dam/countries/countries-content/vietnam/vn/sdc-publications/ground-subsidence_VN.pdf
13. http://daidoanket.vn/
14. Ho, H.L., Doan, V.B., Park, E., Shrestha, S., Tran, D.D., Vu, H.S., Nguyen, H.T.T., Nguyen, P.M., & Seijger, C. (2020). Intensifying saline water intrusion and drought in the Mekong Delta: From physical evidence to policy outlooks, Science of the Total Environment, 757,143919. https://doi.org/10.1016/j.scitotenv.2020.143919.
15. Nguyen, V.Q., Vu, D.T., Than, V.N. (2021). Application of VNGEONET system in surveying, mapping, earth sciences and other fields in digital transformation, In proceedings of National Conference on Geospatial Technology in the Earth Science and Environment, Hanoi, 25-32.

Developing Criteria for Assessing The Stability of Water Supply Models in High Mountains and Water-Scare Areas

NGUYEN Manh Truong[1)], DINH Anh Tuan[1)], NGUYEN Tiep Tan[1)], VU Thi Hong Nghia[2)], DO Van Binh[3)]

[1)] Vietnam Institute of Irrigation Science
[2)] Science and Technology Minístry
[3)] Hanoi University of Mining and Geology

http://doi.org/10.29227/IM-2023-02-27

Submission date: 17-08-2023 | Review date: 19-09-2023

Abstract

The article presents the scientific basis for assessing the stability of water supply models and develops a suitable set of criteria to assess the stability of water supply works, which includes the water supply part for water supply works and systems (including headworks and water distribution systems) in high mountains and water-scarce areas in Vietnam.
Research results indicate that in order to improve the stability and availability of water of the models that have been, are and will be built, it is necessary to have a common method of evaluating effectiveness for scientific models of domestic water supply. Accordingly, it is necessary to build obtain a suitable set of criteria to assess the stability of the water supply model (source + water supply works) in the high mountains, water-scarce areas in Vietnam.

Keywords: *criteria, water supply, high mountain, Vietnam*

1. Introduction

Domestic water is always an extremely valuable and urgent resource for human life, especially in the high mountains and water-scarce areas in Vietnam. Over the years, the State, people and international support organizations have focused a lot of investment resources on the field of domestic water supply. Vietnam has made great achievements in the field of rural water supply. Besides the achieved achievements, there are still limitations and shortcomings. The reality of domestic water supply models in high mountain areas and water-scarce areas in recent years has shown that many water supply models operate unstably and have low efficiency, which is assessed due to the influence of many causes. One of the basic reasons is the power supply and works system.

From the above situation, it is necessary to have a scientific assessment method of general effectiveness for domestic water supply models in order to improve the stability and water supply capacity of the models that have been, are being built and will be built. Accordingly, it is necessary to develop a suitable set of criteria to assess the stability of the water supply models (source + works) in the high mountains and water-scarce areas in Vietnam.

1.1. Objectives of the study

Develop criteria to evaluate the stability of the water supply models, including the part of the water supply for the works and the system of water supply works (main works and water distribution system) built in the high mountains, water-scarce areas.

1.2. Research contents

- Collect relevant documents;
- Research overview of solutions and current status of water supply models in high mountains and water-scarce areas in Vietnam;
- Research the scientific basis and propose appropriate criteria to assess the stability of the water supply model (source + works) in high mountainous areas and water-scarce areas.

1.3. Research Methods

- Collect documents on solutions and exploitation technologies of water supply models in high mountains and water-scarce areas in Vietnam.
- Synthesize and analyze solutions and exploitation technologies of water supply models based on collected documents. From there, develop criteria to evaluate the stability of the water supply model (source + works) in high mountains and water-scarce areas.

1.4. Research scope

The scope of the study is according to Decision 1553/QD-TTg dated November 8, 2019 of the Prime Minister approving the adjustment of the program to investigate and search for underground water sources to supply domestic water in high mountains and water-scarce areas in our country, including: Northern region of 15 provinces, North Central region of 5 provinces, South Central region of 7 provinces, Central Highlands region of 4 provinces, Southern region of 10 provinces.

1.5. Research subjects

Models of water supply (including supply source and supply works system) within the scope of the study in high mountains and water-scarce areas in Vietnam.

2. Water supply models in high mountains and water-scarce areas

- Model of water supply by hanging pond [1], [2];
- Model of water supply by the hill roof drainage moat

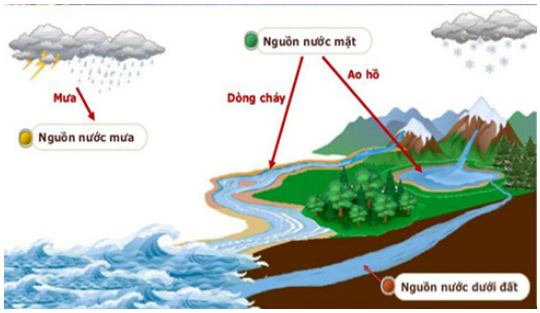

Fig. 4.1. Main types of water supply for the study area

Tab. 4.1. Assessment of the project's ability to meet water use demand

Level	Evaluation Criteria
A	Qpi ≥ Qyci and objects, the scale of water supply is expanded more than the design
B	Qpi ≥Qyci and objects, guaranteed water supply scale according to design
C	Qpi < Qyci and the object and scale of water supply are not met compared with the design

Tab. 4.2. Classification of surface water quality - Limit values of parameters and concentrations of components in each type of surface water [11]

No.	Parameters		Units	Types of surface water		
				Type A	Type B	Type C
1	pH			6.5 to 8.5	6.0 to 9.0	pH > 9 and pH < 6
2	Turbidity		NTU	< 20	< 500	< 1.000
3	Colour degree		mg/l Pt	< 10	< 100	< 200
4	Oxidation KMnO4		mg/l O2	< 2,0	2 – 5	< 10
5	Total hardness		°dH	4 - 8	< 4 or 8 - 13	< 28
6	Sulfide	H_2S	mg/l	0	0	< 0.5
7	Chloride	Cl^-	mg/l	< 25	< 200	< 400
8	Sunfates	SO_4^{2-}	mg/l	< 25	< 250	< 400
9	Nitrites	NO_2^-	mg/l	< 0.1	< 1	< 2
10	Nitrates	NO_3^-	mg/l N	0	< 6	< 10
11	Photphate	PO_4^{3-}	mg/l	0	< 1,5	< 2
12	Total iron	Fe	mg/l	< 0.3	< 1	< 2
13	Total Manganese	Mn	mg/l	< 0.2	< 0.5	< 1
14	Amonium	NH4+	mg/l	< 0.2	< 0.5	< 1
15	Fluoride	F-	mg/l	0.5 – 1.0	< 1.5	< 2
16	Xianua	CN-	µg/l	0	< 50	< 100
17	Phenol		µg/l	0	0,5	< 100
18	Arsenic	As	µg/l	0	50	< 100
19	Cadmium	Cd	µg/l	0	< 1	< 5
20	Total chromium	Cr	µg/l	0	< 10	< 50
21	Selenium	Se	µg/l	0	< 5	< 10
22	Mercury	Hg	µg/l	0	0	< 1
23	Copper	Cu	µg/l	< 50	< 1.000	< 3.000
24	Lead	Pb	µg/l	0	< 10	< 50
25	Zinc	Zn	µg/l	< 50	< 1.000	< 5.000
26	E.Coli		MPN/100 ml	< 20	< 100	< 200
27	Total pesticides (except DDT)		mg/l	0	< 0,15	< 0,15
28	DDT		Bq/l	0	< 0,01	< 0,01
29	Total radioactivity α		Bg/l	< 0.1	< 0.1	< 0.1
30	Total radioactivity β		Bg/l	< 1	< 1	< 1

system using the BTC1 water collection tape [3];
- Model of water supply by underground dam system on stream using BTC1 water collection tape [3];
- Model of water supply by horizontal wells [4];
- Model of water supply by jet well [4];
- Model of water supply by underground dams to block and slow down the flow to create underground lakes to raise the groundwater level for water supply [5];
- Model of water supply by exploiting surface water of streams;
- Model of water supply by taking water from the hillside exposed circuit by collecting tank;
- Model of water supply by taking water from the popular open source from limestone;
- Model of water supply by dug well;
- Model of water supply by single borehole [7];
- Model of water supply by the well corridor;
- Model of water supply by rainwater tank from the roof;
- Model of water supply by exploiting open-circuit karst water source using water collection tape [7];
- Model of water supply by collecting open source water using retaining wall technology combined with water collection tape [8];
- Model of water supply by collecting open source water using distributed water collection tape technology [8];
- Model of water supply by applying underground dam technology integrating technology of collecting wells, foothill water storage and horizontal river bottom groundwater collection system [9].

3. Scientific basis for developing criteria for assessing the stability of water supply models

3.1. Based on the documents and dossiers on design and construction of water supply works

Documents in the phases of construction survey and construction design of the works.

Documents in the construction phase of the works.

3.2. Based on the data of inspection and assessment of the current status of water supply works

Tab. 4.3. Classification of groundwater quality - Limit values of parameters and concentrations of components in each type of groundwater [11]

No	Parameters		Units	Type of groundwater		
				Type A	Type B	Type C
1	pH			6.8 – 7.5	6.0 – 8.0	4.5 – 8.5
2	Oxidation KMnO4		mg/l O_2	< 0.5	0.5 – 2.0	< 10
3	Total hardness		°dH	4 - 8	< 4 or 8 - 13	< 28
4	Sulfide	H_2S	mg/l	0	0	< 0.5
5	Chloride	Cl-	mg/l	< 25	< 200	< 400
6	Sulfates	SO4--	mg/l	< 25	< 250	< 400
7	Nitrites	NO2-	mg/l	< 0	< 0,1	< 2
8	Nitrates	NO3-	mg/l N	0	< 6	< 10
9	Photphate	PO4---	mg/l	0	< 1.5	< 2
10	Total iron	Fe	mg/l	< 0.3	< 10	< 50
11	Total Manganese	Mn	mg/l	< 0.05	< 2	< 3
12	Amonium	NH4+	mg/l	< 0	< 3	< 30
13	Fluoride	F-	mg/l	0.5 đến 1.0	0 – 0.5 or 1.0 – 1.5	< 2
14	Xianua	CN-	µg/l	0	< 50	< 100
15	Phenol		µg/l	0	0,5	< 100
16	Arsenic	As	µg/l	0	50	< 100
17	Cadmium	Cd	µg/l	0	< 1	< 5
18	Total chromium	Cr	µg/l	0	< 10	< 50
19	Selenium	Se	µg/l	0	< 5	< 10
20	Mercury	Hg	µg/l	0	0	< 1
21	Copper	Cu	µg/l	< 50	< 1.000	< 3.000
22	Lead	Pb	µg/l	0	< 10	< 50
23	Zinc	Zn	µg/l	< 50	< 1.000	< 5.000
24	E.Coli		MPN/100 ml	< 0	< 20	< 100

Tab. 4.4. Summary of criteria for assessing the stability of water supply source

Degree of assessment	Rating conditions
1	When the water supply capacity of the source to the works according to the design requirements and the water quality meeting the requirements for domestic use reaches "Level A".
2	When one of the following conditions is met: Current quality reaches "Level A", the water supply capacity according to the design reaches "Level A" and status of water source reaches "Level B"; or Current quality reaches "Level B", the water supply capacity according to the design reaches "Level A" and status of water source reaches s "Level A"; or Current quality reaches "Level B", the water supply capacity according to the design reaches "Level A" and status of water source reaches "Level B".
3	When the water supply capacity of the source to the works according to the design requirements reaches "Level B" and the quality of the water source meeting the requirements for domestic use reaches "Level A", or The quality of the water supply reaches "Level A", the water supply capacity according to the design reaches "Level B" and the status of water source reaches "Level B"; or The quality of the water supply reaches "Level B", the water supply capacity according to the design reaches "Level A" and the status of water source reaches "Level A"; or The quality of the water supply reaches "Level B", the water supply capacity according to the design reaches "Level A" and the status of water source reaches "Level B".
4	When the water supply capacity according to the design reaches "Level C" or the water quality of the supply source reaches "Level C"

- Inspection of water supply works

Inspecting concrete and reinforced concrete structures of focal works

Checking water transfer works

Checking sedimentation, fill of water supply works

Checking the operating system

- Assessment of the current status and causes of instability of water supply works

Works of surface water exploitation

Works of mainstream water exploitation

Works of underground water exploitation

- Standards and regulations for the assessment of the stability of the works

- Standards and regulations for the assessment of stability of water supply systems

3.3. Proposal to develop criteria for assessing the stability of the water supply models

Based on the above-mentioned practices and scientific bases, it is proposed to develop criteria to evaluate the stability of domestic water supply works in high mountains and water-scarce areas as follows:

- For water supply:

+ Criteria to meet the demand for water use

+ Criteria to meet water quality

- For water supply works:

+ Criteria for assessing the current state of the works

+ Criteria for assessing permeability stability

+ Criteria for assessing the stability of the structure of the works

+ Criteria for assessing the sedimentation before the construction

4. Developing criteria for assessing the stability of water supply models (source + works) in high mountains and water-scarce areas

4.1. Criteria for assessing the stability of water supply source

Domestic water supply for high mountains and water-scarce areas is mainly in 3 main forms:

- Surface water: water that is directly visible, exists mainly in rivers, streams, lakes or man-made dams.

- Groundwater source: a form of groundwater, is fresh water contained in the pores of soil or rock. It can be interconnected pockets of water or a geyser that flows close to the parent rock. Groundwater is formed by water on the surface seeping down, because it cannot penetrate

Tab. 4.5. Contents of quality inspection of water supply works

Items	Contents of quality inspection
Structure made of concrete, reinforced concrete, stone masonry	Check the condition of cracking, cavitation, pitting, rusting (if any) of concrete structures, masonry; Check deformation, displacement of the works through the expansion or difference at the joints; Check the condition of seepage, water leakage through the water conduit items, through the pipe joints; Check the sandy soil deposited in the water source; Check for erosion; Check the degree of damage, the operability of mechanical equipment. Check the degree of damage, the operability of electrical equipment
Structure of gabion, stacked stone	Check deformation, displacement; Check the condition of peeling, slipping; Check the integrity of the gabion; Check the deposited sandy soil at the water intake; Check for erosion; Check the degree of damage, the operability of mechanical equipment. Check the degree of damage, the operability of electrical equipment

Tab. 4.6. Assess the current quality of the works

Levels	Assessment conditions
A	Equipment and items of the works are not damaged
B	The work is only damaged in unimportant structural parts (station buildings, reinforced structures of shore roofs, roads); can be repaired through maintenance work, annual maintenance
C	The work is seriously damaged, affecting the efficiency, and needs to be repaired or upgraded in time

the parent rock layer, so the water will concentrate on the surface. Depending on the geological tectonics, it forms different shapes, water concentrated much will start to move and link with other water compartments and pockets, gradually forming large and small groundwater. The exploitation of groundwater can be through forms such as dug wells, drilled wells, jet wells, etc.

- Rainwater source: water generated by condensation of water vapor. This is also a fairly popular source of domestic water for people in high mountains and water-scarce areas through the construction of storage tanks, catchment roofs, rainwater collection pits, etc.

The stability of water supply of an operating or exploiting domestic water supply work is assessed through two groups of criteria: (1) Ability to meet the demand for water use and (2) Ability to meet the demand for water quality.

4.1.1. Criteria of ability to meet the demand for water use

Assessment of the ability to meet the demand for water use is one of the criteria for assessing the stability of supply source of water supply models. To evaluate this criterion, it is necessary to calculate specifically the incoming flow and water demand, water balance. From that, calculate the benefits that the work brings.

Thus, the ability to meet the demand for water use is assessed through two factors: (1) The water source is represented by the incoming flow rate corresponding to the frequency of service assurance (applicable to the surface water source); (2) Demand for water use.

- Water source

To determine the water source to the work, calculate the yearly flow rate to the work according to the design frequency Qp and the design yearly flow distribution Qpi (where i is the order of the month of the year and P is the frequency of the design).

- Demand for water use

+ Identify water users

The water users of the work may have one or many different objects, including: supply of domestic water to households and agencies;

+ Demand for water use

The demand for water use is determined according to the following formula:

$$Q_{yci} = \frac{Q_{nni} + Q_{shi} + Q_{khi}}{\eta} \quad (4.1)$$

in which:

Q_{yci}: The required volume of water supply at the head of the works in the i month, m^3/s;

Q_{nni}: The required volume of water supply for agriculture in the field in the i month, m^3/s;

Q_{shi}: The required volume of water supply for domestic use in the household in i month, m^3/s;

Q_{khi}: Required volume of water supply for other economic sectors in the i month, m^3/s;

η: Canal utilization coefficient.

+ Determine the demand of water supply for domestic use

Water demand for domestic use includes water demand for people in urban or rural areas and water demand for livestock (cattle, pigs, ...), poultry.

The required volume of water supply for domestic use in the i month is determined by the formula:

$$Q_{shi} = Q_{ngi} + Q_{chni} \quad (4.2)$$

in which: Q_{shi}: The required volume of water supply for domestic use in the household using water in the i month, m^3/s;

i = 1 ÷ 12: Order of month of the year;

Q_{ngi}: The required volume of water supply for the households using water in the i month, m^3/s;

$$Q_{ngi} = \frac{10^{-3}.q_{ng}.N_{ng}.D_i}{86400} \quad (4.3)$$

q_{ng}: Norm of water supply for people in water-using households, l/person/day and night, determined according to current regulations;

Tab. 4.7. Table of criteria for assessing permeability stability of water supply works

Degree of permeability stability	Assessment Criteria
A	When all of the following conditions are satisfied: - Total seepage is less than or equal to total water loss due to infiltration according to design calculation; - The maximum permeability gradient at local points (J_{cbmax}) is smaller than the allowable gradient value ($[J_k]_{cp}$): $J_{cbmax} \leq [J_k]_{cp}$; The calculated mean permeation gradient (J_{tt}) is less than the mean critical gradient of the water column (J_k^{tb}) taking into account the reliability coefficient (K_n): $J_{tt} \leq (J_k^{tb}/K_n)$; - The seepage pressure and backlash pressure are less than or equal to the design value (for hanging tigers, tanks, concrete dams, reinforced concrete and casting constructions); - Parameters of water drainage equipment ensure technical requirements.
B	When one of the following situations occurs: - The total amount of seepage is greater than the total amount of water loss due to infiltration according to the design calculation; - There is at least one maximum permeability gradient value at local points (J_{cbmax}) equal to the allowable gradient value ($([J_k]_{cp}$) or the calculated average permeability Gradient value (J_{tt}) equal to the critical gradient value average of the water column (J_k^{tb}) taking into account the reliability factor (K_n); - The seepage pressure and backlash pressure are higher than the design value, but the dam and the casting works still ensure the sliding stability in the calculated cases as prescribed.
C	When one of the following situations occurs: - There is at least one maximum permeability gradient value at local points (J_{cbmax}) greater than the allowable gradient value ($([J_k]_{cp}$) or the calculated average permeability Gradient value (J_{tt}) greater than the gradient value mean water column criticality (J_k^{tb}) taking into account the reliability factor (K_n); - Infiltration pressure, backlash pressure increase suddenly, abnormally, higher than the design value for dams and casting works which are likely to lose stability; - The parameters of the drainage device do not meet the technical requirements.

Tab. 4.8. Table of criteria for assessing structural stability of water supply works

Structural stability degree	Assessment Criteria
A	When all of the following conditions are satisfied: a) For weirs made of earth and rock: - The displacement of the dam is less than the allowable value; - The dam is stable. b) For weirs made of concrete and reinforced concrete: - Dams are not subsided, horizontal displacement; - Stabilized dam sliding, flipping; - Dam foundation and dam body concrete have sufficient bearing capacity. c) For hanging lakes - The structure of the lakeside roof, the lake bottom is stable without slipping - No cracks or cracks with the width within the allowable range - The lake is not subsided or displaced - The lake bottom ensures bearing capacity d) For collection well works (ray well, drilled well, dug well) - The wall of the well does not sink - No cracks in the well wall or cracks with the width within the allowable range c) For related works: - Sliding and overturning stabilization works; - The foundation of the items ensures force-resistance capability.
B	When one of the following occurs: - For weirs made of earth and rock: The dam roof has been unstable and has been repaired; The existing dam roof ensures stability. - For weirs made of concrete and reinforced concrete: The dam is subsided and the transverse displacement is within the allowable limit; - For hanging lakes and open water collection ponds: The roof has been unstable and has been repaired; The current roof of the building is stable. The foundation of the work is subsided but within the allowable limit. - For related works: Parts of works sliding, tipping and foundation of the items ensure force-resistance capability.
C	When one of the following occurs: a) For weirs made of earth and rock: - Dam has subsidence, displacement is greater than the allowable value; - The dam roof is unstable. b) For weirs made of concrete and reinforced concrete: - Subsidence, displacement of the dam body is larger than the allowable value; - The dam does not guarantee sliding or tipping stability; - Dam foundation and dam body concrete do not guarantee force-resistance capacity. c) For hanging lakes - Subsidence, displacement of roof and foundation is greater than the allowable value; - The roof is not stable; - The work foundation and concrete structure do not guarantee the force-resistance capacity. c) For related works: - Work parts that do not guarantee sliding stability or tipping stability; - The foundation does not guarantee force-resistance capacity.

N_{ng}: Number of people using water;
D_i: Number of days of the ith month;
Q_{chni}: Required volume of water supply for livestock in the household using water in month i, m^3/s;

$$Q_{chni} = \frac{D_i}{86400} \cdot \sum_{j}^{n} 10^{-3} . q \qquad (4.4)$$

q_{chnj}: Norm of water supply for a jth cattle or poultry in a water-using household, determined according to current regulations depending on the type of livestock and poultry (cattle, pigs, poultry);
N_{chnj}: The number of the jth livestock and poultry using water;
n: Total number of livestock and poultry supplied with water.

- Assess the ability to meet the demand for water use

Assess the ability to meet the water use demand of water supply works according to 03 levels:
Level A - Satisfying water demand well;
Level B - Meeting the demand for water;
Level C - Does not meet the demand for water.

Tab. 4.9. Assessment of sedimentation in front of the dam

Levels	Assessment conditions
A	$K_t \geq [K]$ và $K_l \geq [K]$
B	$1,0 \leq K_t < [K]$ và $K_l \geq [K]$ hoặc $1,0 \leq K_l < [K]$ và $K_t \geq [K]$
C	Either coefficient K_t or K_l is less than 1.0

Tab. 4.10. Summary of criteria for assessing stability of water supply works

Levels of rating stability	Ranking conditions
1	All criteria in item 0 reach "A" level
2	All of the criteria in item 0 are rated "A" and "B"
3	The other cases

4.1.2. Criteria for the ability to meet the quality of the supply water source

The quality criteria of supply water sources for domestic use in high mountains and water-scarce areas are assessed through limit indicators and concentrations of substances present in water (determined through sampling and analysis of water samples in the lab).

- For surface water sources: TCXD 233-99 provides quality criteria used to compare, evaluate and select raw surface water sources when researching and preparing pre-feasibility reports and feasibility reports on investment and construction projects of domestic water supply as follows:
- For underground water source: TCXD 233-99 provides the quality criteria used to compare, evaluate and select groundwater sources when researching and preparing pre-feasibility reports and feasibility reports on investment and construction projects of domestic water supply as follows:

Tab. 4.3. in which:

Column A: is a water source of good quality, which is simply treated before being supplied for drinking and domestic use;
Column B: is a water source of normal quality, which can be exploited and treated for drinking and domestic use;
Column C: is a water source of bad quality. If used for the purpose of supplying drinking water and domestic use, it should be treated with special technologies and must be strictly and regularly monitored for water quality;

4.1.3. Summary of criteria for assessing the stability of supply source

Tab. 4.4. in which:

Level 1: The water supply source for the model (works) is very stable, meeting well the conditions of domestic water supply
Level 2: The water supply source for the model (works) is stable, meeting the conditions of domestic water supply
Level 3: The water supply source for the model (works) is less stable
Level 4: The water supply source for the model (works) is not stable

4.2. Criteria for assessing the stability of the works

4.2.1. Criteria for assessing the current state of the works

Assessing the current state of the proposed work is one of the important bases for assessing the stability of the works. It is based on the assessment of current status and measurement and monitoring data to assess the stability of the works according to current standards and regulations.

Assess the current quality of the works according to the following levels:

Level A: Good quality;
Level B: Medium quality;
Grade C: Poor quality.

The current quality of the works is assessed according to Table 4.6

4.2.2. Criteria for assessing permeability stability

4.2.3. Criteria for assessing structural stability

4.2.4. Criteria for assessing sedimentation in front of the construction

The sediment deposited in front of the weir can cause sedimentation to narrow the inlet size leading to a decrease in the discharge capacity of the inlet and more importantly, an increase in sediment pressure along with other possible loads and destabilize the dam.

Assess the level of sedimentation in front of the dam according to the following levels:

Level A: Sedimentation of sand does not cause unsafety for the weir;
Level B: Sedimentation of sand may cause unsafety for the weir; need to strengthen supervision.
Level C: Sedimentation of sand is unsafe for the dam, it is necessary to dredge the sand before the dam.

The sedimentation status of the sediment in front of the dam is assessed according to Table 4.9. Assessment of sedimentation in front of the dam.

In which:

K_t, K_l respectively are the safety coefficients of slip stability and tipping stability of the weir, taking into account the effect of sediment pressure in front of the dam, [K] is the allowable stability coefficient.

4.2.5. Summary of criteria for assessing the stability of the works

Tab. 4.10. i n which:

Level 1: Water supply works are stable
Level 2: Water supply works are unstable, must strengthen inspection and supervision
Level 3: Water supply works are unstable, potentially unsafe; need to be checked, repaired and upgraded immediately.

5. Conclusion

- The stability of (source + works) domestic water supply in water-scarce areas depends on natural condi-

tions, topography, geology, construction materials, management level, exploitation and operation as well as the perception of water users. This report has proposed a set of criteria to assess the stability of water sources and water supply works for domestic water supply models for the study area.

- The report has presented quite fully the types of water supply models, which are divided into 2 main types: Surface water exploitation model (surge dam, underground dam, hanging lake, highway ...) and groundwater exploitation model (types of wells).
- The report also stated the scientific basis for assessing the stability of the water supply models. The important basis are: (1) The system of documents for survey, design, exploitation and operation... of the work; (2) Survey, evaluation and monitoring of the current status of the works and (3) System of standards and regulations as a basis for assessment.

From that, develop a set of criteria to evaluate the stability of the water supply models for high mountains and water-scarce areas in Vietnam as follows:

For sources:

+ Criteria to meet the demand for water use
+ Criteria to meet the requirements of water quality of the supply source

For the works:

+ Criteria for assessing the current state of the works
+ Criteria for assessing permeability stability
+ Criteria for assessing structural stability
+ Criteria for assessment of sedimentation in front of the construction

Literatura – References

1. Vu Cao Minh (2008), Synthetic report on the topic of the Vietnam Institute of Science and Technology "Research and test some solutions for water supply for some extremely difficult areas in the Northern mountainous region".
2. Vu Cao Minh et al (2018), Some measures to improve the efficiency of domestic water supply of hanging lakes. Geotechnical journal ISSN-0868-279X 22nd year issue 2+3 2018.
3. Nguyen Quoc Dung (2012), Summary report on implementation of scientific and technological tasks "Research and application of effective water supply solutions for daily life combined with production in resettlement areas of two districts of Phong Tho and Sin Ho, Lai Chau province".
4. Nguyen Thanh Cong (2018), Summary report of the topic "Research and propose a model for sustainable exploitation of freshwater lenses in coastal sand dunes serving domestic water supply for water scarcity areas in the North Central region ".
5. Nguyen Quoc Dung (2018), Summary report of the topic "Research on building a model of water collection and storage for effective clean water supply for arid and water-scarce areas of Ninh Thuan - Binh Thuan".
6. Ha Hai Duong (2019), Synthetic report of the topic "Research and propose models and technological solutions for exploitation and protection of water sources in basalt formations for sustainable domestic water supply in mountainous areas". high, water scarcity in the Central Highlands.
7. Do Ngoc Anh (2019), Synthetic report of the topic "Research and propose models, technological solutions for exploitation and sustainable development of karst water sources for domestic water supply in high mountainous areas, water scarcity in the northern region".
8. Pham The Vinh (2018), Synthetic report of the topic "Research and propose models of sustainable collection and exploitation of open source water for clean water supply for high mountains and water-scarce areas in the Central Highlands ".
9. Nguyen Huy Vuong (2021), Synthetic report of the topic "Research and propose an integrated model of solutions for collecting, storing and exploiting water sources for domestic and production water supply in water-scarce areas" Dien Bien province".
10. Nguyen Chi Thanh (2019), General report on the topic "Research, propose and apply appropriate scientific and technological solutions to improve the efficiency of dams projects in the Northwest region"
11. Construction standard TCXD 233:1999, Criteria for selection of surface water - groundwater for domestic water supply system.
12. National technical regulation QCVN 04-05:2012/BNNTPTNT Irrigation works - Main regulations on design.
13. TCVN 11699: 2016, Irrigation works - Dam safety assessment.
14. Ha Van Block et al. Chapter V - Calculation of flow in the design year, Textbook of engineering hydrology, University of Water Resources, 2008.
15. Nguyen Manh Truong, Dinh Anh Tuan, Do The Quynh, Vu Thi Hong Nghia (2022), Solutions and technologies for exploiting water supply models in high mountains and water-scarce areas. Journal of Irrigation Science and Technology (ISSN:1859-4255) No. 75, Feb. 2022.
16. Nguyen Manh Truong (2021), Thematic report "Building criteria for assessing the stability of water supply models (source + works) in high mountains and water-scarce areas" under the national science and technology project "Research assess the stability and propose technical solutions to improve the efficiency of water supply models in high mountains and water-scarce areas".

Sustainable Industrial Development in Vietnam

NGUYEN Ngoc Son[1)]

[1)] National Economics University, Faculty of Planning and Development, Building A1, 207 Giai Phong Road, District Hai Ba Trung, Hanoi, Vietnam
*Corresponding author email: sonnn@neu.edu.vn; nguyenngocsonneu@gmail.com

http://doi.org/10.29227/IM-2023-02-28

Submission date: 17-08-2023 | Review date: 20-09-2023

Abstract

Vietnam is one of the countries with the highest industrial growth rate in the world. However, growing in the industry is based on the width factor and labour - intensive industries and assembly. The goal set out to 2030 is to turn Vietnam into a Middle-Income Country (MIC) with a modern industry that poses many challenges, requiring the industry to need stronger restructuring to improve competitiveness. competition and deeper participation in global value chains. From the analysis of the current situation of industrial development in Vietnam, the article identifies the limitations in the sustainable development of Vietnam's industry and gives orientations and solutions to promote the sustainable development of Vietnam's industry in the context of Industrial Revolution 4.0 and the digital economy.

Keywords: *industry, sustainable industrial development, the 4th industrial revolution, restructuring, industrial competitiveness, CIP*

1. Introduction

The development of Vietnam's industry has achieved significant achievements over the past 30 years, contributing to Vietnam's industrialization and modernization process. Despite being heavily affected by the global economic crisis since 2008 and the Covid-19 pandemic, Vietnam's industry has maintained a relatively high growth rate. The average growth rate reached 7.6% per year from 2010 to 2021. The increased industrial growth has contributed to the economy's structural transformation towards industrialization, promoting exports, indirectly driving the growth of service sectors serving production, addressing employment issues, improving workers' income, and stimulating consumption. However, the high industrial development in Vietnam during this period has also revealed specific weaknesses, leading to unavoidable inconsistencies in the economic structure, inefficient resource exploitation, weak competitiveness, and leaving negative environmental consequences, among others.

The growth of the new industrial sector has only been achieved in terms of quantity. However, there are still many shortcomings in the quality of this growth, particularly in terms of labour productivity, industry efficiency, and weak competitiveness. To develop a sustainable industry, enhancing the quality of industrial development is one of the urgent tasks that the industrial sector must undertake in the context of globalization and the Fourth Industrial Revolution.

The current problem facing the Vietnamese industry today is that without appropriate direction, the underlying causes of the decline in growth cannot be addressed, and the quality and effectiveness of the industry's growth process cannot be improved. Therefore, sustaining a high growth rate for both the industry and the overall economy will be challenging to achieve.

To measure the sustainable development of the industrial sector, the author presents three groups of criteria: (i) growth and the growth structure of the industry. The structure of industrial growth is also evaluated based on the contribution of different industries to the overall industry growth in order to assess the level of industrial production; (ii) efficiency of industrial growth. This group of criteria is manifested in the output efficiency of growth, reflected in labour productivity, exports, and energy utilization efficiency; and (iii) the spillover effects brought about by industrial growth. This reflects the role and nature of industry spillover, as industrial growth stimulates the development of other fields and industries through the pull and push forces of the industry, as well as environmental pollution issues within the industrial sector.

2. The situation of sustainable industrial development in Vietnam

2.1. Industry growth rate

The value-added growth rate in the post-crisis industrial sector (2010–2021) reached approximately 7.66% per year, surpassing the average economic growth rate of 5.9%. During this period, the processing and manufacturing industry experienced the highest growth rate at 10.82%, while the mining sector had a growth rate of -2.7% (refer to Figure 1).

Despite being considered a rapidly growing sector during 2010–2021 (achieving a growth rate of 7.6% per year), the processing and manufacturing industry primarily remains an outsourcing activity. The lower index of intermediate product output compared to the index of final product output indicates a significant reliance on imported intermediate products in Vietnam's industrial production.

The private industrial sector and the foreign-invested industrial sector have shown considerable growth, indicating a positive shift in the direction of attracting industrial investments by the private sector.

2.2. Industry Growth Structure

The processing and manufacturing industry occupies the highest proportion of the industrial sector structure. From 2010 to 2021, the share of this industry increased rapidly and reached 91.3% in 2017. The reason for this is the increase in

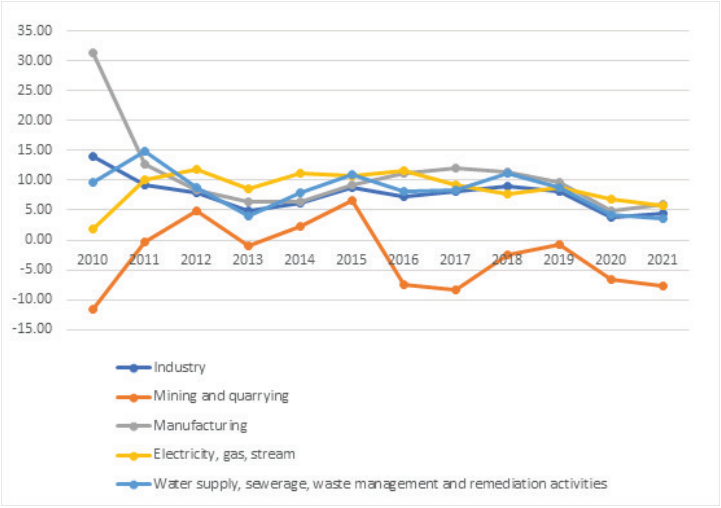

Fig. 1. Growth rate of industry and sectors. Source: Compiled by the author from the data of the General Statistics Office of Vietnam

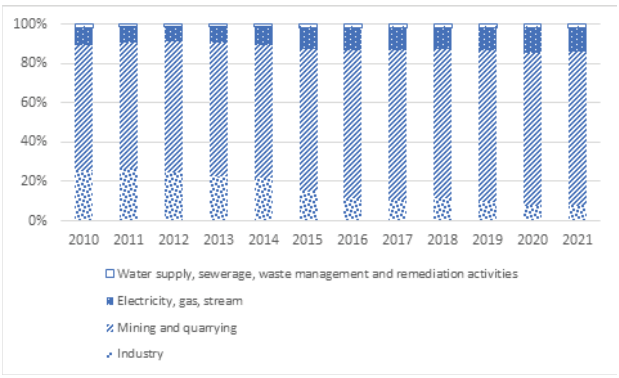

Fig. 2. Industry structure in Vietnam. Source: Compiled by the author from the data of the General Statistics Office of Vietnam

foreign direct investment (FDI) in the processing and manufacturing industry, particularly the contribution of major FDI corporations such as Samsung, Foxcom, Intel, and Canon.

The Industrial Processing and Manufacturing Industry has been making an increasingly significant contribution to the overall value added (VA) of the entire industrial sector, aligning with the industry's development trends. However, an analysis of the structural growth of the manufacturing industry's value-added reveals that from 2011 to 2021, the production structure transformation primarily revolved around the assembly industry, particularly the electronics sector. The supporting industries have not yet fully developed or have shown slower growth trends.

The intermediate cost ratio in the total production value of the continuously growing industrial sector has been increasing, from 57.5% in 1995 to 70.4% in 2005, 81.8% in 2015, and 81.7% in 2021. Examining the subsectors of industrial production also reveals a similar trend, particularly with a noticeable increase in this ratio within the processing and manufacturing industries. The rising proportion of intermediate costs in this sector indicates that Vietnam's overall growth model and the industrial sector still rely heavily on outsourcing. The supporting industry is underdeveloped, especially in sectors such as automotive and electronics.

Structural transformation in some industrial sectors is not truly sustainable. The value added to products in certain industries, such as textiles, footwear, and electronics, has been increasing but slowly. The competitiveness of industrial products is still limited. Industrial production has yet to participate extensively in global production networks and value chains.

The level of interconnection and business collaboration among enterprises within the same industry and across different industries is still limited, failing to establish a development linkage between sectors. Many businesses operate in isolation, without leveraging the existing capacities of other enterprises to enhance the industry's internal strength and achieve higher production and business efficiency. On the one hand, this increases investment costs for production, and on the other hand, it leads to a waste of shared resources within the industry and unnecessary competition among businesses.

Investment in production still focuses on breadth, with limited investment in depth for existing facilities, and does not fully utilize available resources. Most investment capital in the industrial sector is concentrated in industries with short payback periods, such as consumer goods manufacturing and food processing. At the same time, the number of high-tech projects invested in remains low.

Industry structure by technology level

From 2001 to the present, the level of technology in Vietnam's industrial sector has changed very slowly. According to the classification of industrial sectors by UNIDO (UNIDO, 2014), the proportion of low-technology industries in Vietnam has shown a decreasing trend from 41.5% in 2010 to 34.5% in 2021 (textiles, garments, leather shoes, toys, plas-

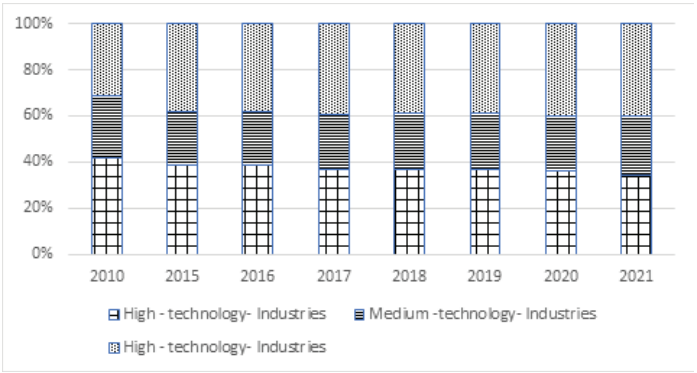

Fig. 3. Structure of Vietnam's industrial production value by technology level. Source: Compiled by the author from the data of the General Statistics Office of Vietnam

Tab. 1. Labor Productivity in the Industrial Sector and its Industry Groups. Unit: million VND. Source: General Statistics Office of Vietnam

	2018	2019	2020	2021	2022
Industries	205.608	201.408	209.383	228.266	248.23
Mining and quarrying	1239.23	1167.44	1108.26	1179.45	1367.8
Manufacturing	163.785	162.416	170.445	186.23	200.158
Electricity, gas, steam and air conditioning supply	1450.91	1462.04	1827.08	2215.11	2722.02
Water supply, sewerage, waste management and remediation activities	238.01	237.544	244.688	250.876	252.829

Tab. 2. Change in CIP rankings of Vietnam and Asian countries over the years. Source: Author compiled from data of UNIDO

TT	Quốc gia	1990	1995	2000	2005	2010	2015	2020	2022
1	Japan	2	1	1	2	2	5	6	8
2	South Korea	17	13	12	6	4	4	4	4
3	China	32	27	22	19	7	2	2	2
4	Singapore	13	11	10	10	6	9	9	9
5	Taipei (China)	13	12	14	13	13	8	8	6
6	Malaysia	39	20	21	23	23	22	21	20
7	Thailand	38	26	26	25	25	24	24	25
8	Indonesia	52	41	39	41	41	40	38	39
9	India	64	54	56	56	45	41	40	41
11	Vietnam	94	91	80	69	58	37	30	30
11	Philippines	50	51	38	46	56	46	43	44
12	Laos	134	126	122	126	124	111	108	109
13	Cambodia	121	119	103	97	94	92	82	83

tic products, wood products, glass, etc.). The proportion of medium-technology industries has decreased from 27.5% in 2010 to about 25.3% in 2021. The ratio of high-technology sectors has increased from 31% to 40.3%. However, this proportion is still lower than the 50-60% range observed in Thailand, China, and Malaysia. The policies and strategies to enhance technology, a knowledge-based economy, and structural transformation of production have been implemented for many years but have not been effective in raising the technological level of the economy. As a result, Vietnam is increasingly lagging behind other countries in the region, particularly those that have been proactive in developing their mid-to-high-tech industrial value chains to transform their production structures.

2.3. Industrial labour productivity

The labour productivity of the industrial sector in 2021 was 195.58 million Vietnamese dong, compared to 113.53 million in 2011. Analyzing labour productivity by industry groups reveals that the productivity of the entire industrial sector surpasses that of the overall economy. This is mainly due to the labour productivity of the extractive industries and the production of electricity and distribution of gas, water, steam, and air conditioning. On the other hand, the labour productivity of the manufacturing industry remains low, even lower than that of the entire economy. This situation is because the manufacturing industry is still labour-intensive (textiles, leather, etc.) and the processing industry (electronics, automobiles, etc.), resulting in very low value-added. While the overall labour productivity of the economy is increasing, the labour productivity of the industrial sector has shown a decreasing trend in 2015, 2016, and 2017.

There are several reasons for Vietnam's low labour productivity and the significant gap compared to other ASEAN countries. The slow transition in economic structure and the high proportion of agricultural labour contribute to the agricultural sector's low labour productivity. Machinery, equipment, and technological processes are outdated. The quality, structure, and efficiency of labour utilization do not meet the requirements. Other important factors include the low starting point of the economy, deficiencies in organization, management, and efficient use of resources, the low contribution of total factor productivity (TFP) to growth, and institutional and administrative reform bottlenecks.

2.4. Industry competitiveness

In the industrial competitiveness ranking of 2022, Vietnam ranked 30th out of 151 countries, marking an increase of 64 places compared to the 1990 ranking. Vietnam is the country with the highest improvement in industrial competi-

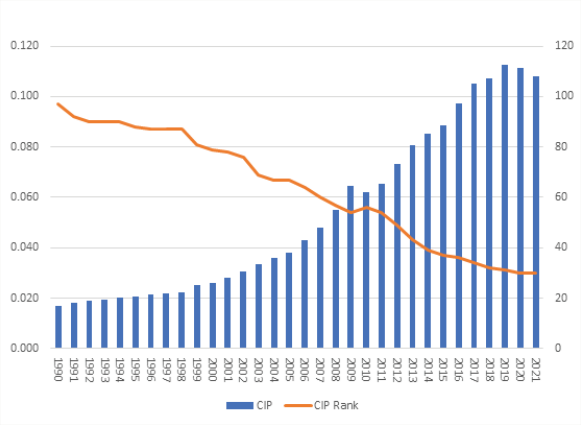

Fig. 4. CIP value and CIP ranking of Vietnam. Source: Author compiled from data of UNIDO

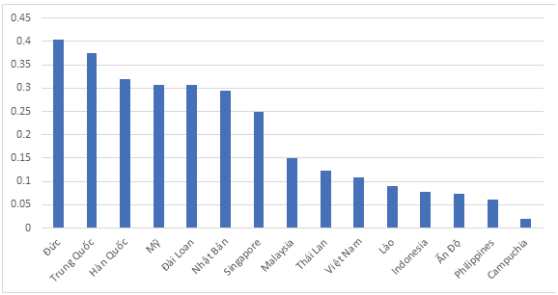

Fig. 5. CIP value and CIP ranking of Vietnam and other countries in 2021. Source: Author compiled from data of UNIDO

tiveness worldwide. This achievement is considered quite significant for the development of Vietnam's industry.

Among the Asian countries, both China and Vietnam have experienced rapid improvement in the CIP index. On the other hand, countries like Malaysia and the Philippines have shown a tendency to decline, while Thailand and Indonesia have generally maintained their positions.

The CIP value of Vietnam compared to other countries

The CIP value of Vietnam has improved over the years, increasing from 0.062 in 2010 to 0.108 in 2021. Vietnam's CIP index ranks only behind Singapore, Malaysia, and Thailand among ASEAN countries. However, Vietnam's CIP index is still very low compared to the maximum value of 1 or the 0.404 value of Germany (the country with the highest CIP).

The average value added of manufacturing industry per capita (MVA per capita)

Vietnam's MVA per capita has increased sharply from 52 USD in 1990 to 380 USD in 2010 and 872 USD in 2021. Vietnam ranks 85th out of 148 countries in terms of per capita GVA. Among Asian countries, Singapore has the highest ranking (2nd out of 148), followed by Japan (3rd out of 148), South Korea (6th out of 143), Taiwan (17th out of 143), Malaysia (41st out of 143), and Thailand (49th out of 143). According to the UNIDO classification, Vietnam's industrial value-added is still much lower than the global average of 1661 USD and the average of 1000 USD for newly industrialized countries. Vietnam will take about ten more years to reach an average per capita GVA of 1000 USD. The low per capita GVA is attributed to Vietnam's heavy reliance on processing industries, lacking supporting and labour-intensive industries such as textiles, garments, leather, and footwear, which still account for a significant proportion of Vietnam's industrial structure.

From the analysis of the sustainable industrial development based on the criteria mentioned above, the sustainable industrial development in Vietnam can be described as follows:

Firstly, there is high growth, but the effectiveness in achieving growth targets is low, as evidenced by low labor productivity compared to the industrial labour productivity of other countries in the region and worldwide. Additionally, the growth rate of labor productivity is lower than the average growth rate of the overall economy.

Secondly, the low efficiency in achieving the target growth of the industrial sector is reflected in the increasing intermediate costs in industrial production. To obtain a unit of value-added, the scale of production must be expanded, and more input factors must be consumed. The reason for this situation is the inappropriate structure of Vietnam's industrial production, as evidenced by the fact that key industries in Vietnam are still processing, assembling, and largely dominated by foreign direct investment (FDI) enterprises. The assembly process is considered the stage with the lowest value-added in the value chain. The effectiveness of achieving the growth target of the industrial sector can be improved if the industrial structure becomes more reasonable by developing supporting industries and participating more deeply in the global value chain.

Thirdly, the industrial growth structure is not rational. Consider the structure of industrial growth in terms of production value and value added. It is easy to observe a trend where the extractive industries are increasingly being overshadowed by the processing and manufacturing industries. However, a deeper examination of the growth structure reveals that the downstream industries still account for a signif-

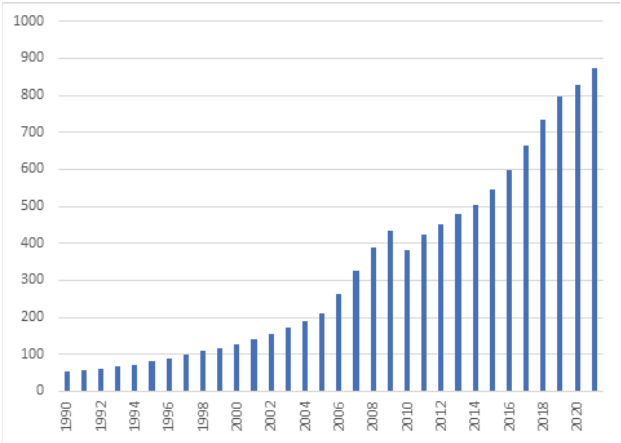

Fig. 6. Vietnam's MVA per capita 1990-2021

icant proportion, while the upstream industries only hold a relatively modest share.

The fourth, The level of linkage and business cooperation among enterprises in the same industry and between industries is still limited, failing to create a development linkage between industries in a specialized and market-oriented cooperation manner. Many enterprises operate independently without leveraging the existing capacities of other businesses to enhance the industry's internal strength and achieve higher production and business efficiency. On the one hand, this increases the investment costs for production, and on the other hand, it wastes the shared capabilities of the entire industry, creating unnecessary competition among businesses in the industry.

The fifth, The growth of the industry still primarily relies on expanding in breadth, by continually expanding input factors to achieve growth. The contribution of technical improvement and technological innovation to the industry's growth in recent times has been insignificant.

3. Solutions for sustainable development of Vietnam's industry

From the analysis of the current state of Vietnam's industrial competitiveness, it can be concluded that the core focus of Vietnam's industrial development lies in the creation of new value through industrial activities (MVA). To achieve this adjustment, attention needs to be directed towards the following issues:

Firstly, transforming the industry growth model

Transforming from an import-oriented industrialization model to a comprehensive export-oriented industrialization, particularly in the fields of mechanical engineering, metallurgy, construction materials, steel, food processing, and agriculture, aims to achieve holistic industrial growth. Shifting towards an industrial growth model that encompasses industries with medium and high technology will facilitate the enhancement of labor productivity and industrial value added (MVA).

Second, Improve the quality of industrial development planning

To improve the quality of the master plan for industrial development, attention should be paid to the following contents:

- In terms of cognition, the development planning of the industry must be understood as a process of argumentation, selecting development options, and rational sectoral distribution nationwide and across territories. It differs from comprehensive socio-economic development planning and construction planning. The industry development planning should be long-term, coherent, and in line with the country's and its territories' overall development strategy. It must be intersectoral coordinated with relevant sectors, identifying interdependencies, avoiding overlaps, and minimizing conflicts among sectors.

- In terms of the quality of industrial development planning: The development planning of the industry must be based on scientific grounds, avoiding subjectivity, and must have a long-term vision suitable for the industry's developmental characteristics. At the same time, it must be specific for each phase. When constructing the planning, emphasis should be placed on forecasting, particularly in terms of market forecasts for products and the impacts of external factors, the global market, the process of globalization, international economic integration, and their influences on the industry's development during the planning phase."

Third, Improve the quality of human resources

The competitive advantage of a nation, its businesses, and the prerequisites for sustainable development in the coming decades depends greatly on each country's level of human development. Therefore, there is a need for solutions to enhance the quality of education and training as follows:

A key solution is to innovate and enhance the capacity of state management in education and training; comprehensively reform education to align the education system with the development requirements of various industries; promote innovation in content, curriculum, and teaching methods to modernize and adapt to the practical needs of Vietnam, along with innovative educational management mechanisms; resolutely reduce the curriculum content to be suitable for the psychological well-being of students at the primary and secondary levels and establish standards for quality assessment of education.

Urgent implementation of the development plan and improvement of the quality of teachers and education management personnel; restructuring the training system and enhancing practical vocational training. Encourage healthy competition, and create mechanisms and conditions for universities and vocational schools to transition towards autonomous and accountable operations. Innovate mechanisms

and policies to allocate funds for education and training; determine transparency and appropriate contributions from learners, and vigorously address the negatives in teaching and learning. At the same time, have policies in place to ensure that economically disadvantaged individuals have access to education.

Urgent implementation of the project to develop and enhance the quality of the teaching staff and educational management official; restructuring the training system and improving the practical vocational training system. Encouraging healthy competition, creating mechanisms and conditions for universities and vocational schools to transition to autonomous and responsible operations. Innovating mechanisms and policies to allocate funding for education and training; determining transparent and appropriate contributions from learners, vigorously combating negatives in teaching and learning; while also having policies to ensure that children from poor backgrounds have opportunities for education.

Strengthening investment in vocational education, including vocational retraining, to help laborers of working age easily adapt to the frequent changes in the labor market. In order to gradually narrow the gap between training outputs and the current needs of the labor market, the following measures need to be implemented promptly: (i) clearly identifying the fields and industries currently lacking labor, lacking skilled workers, in order to enhance investment and support; (ii) standardizing training institutions, vocational skill development, with clearly defined quality criteria; (iii) closer coordination among stakeholders in the labor market (enterprises in need of labor, training institutions, vocational skill development agencies) in the process of planning policies for training and developing human resources.

Enhancing cooperation with foreign countries and attracting foreign investment in postgraduate and vocational training; encouraging and creating conditions for students to study abroad, accompanied by strengthened management of student mobility.

Increasing investment in education from various sources, with a particular need for increased investment from the state budget; simultaneously mobilizing more and better resources from the public through the promotion of socialization of education and the construction of a learning society.

Fourth, promote industrial restructuring, especially state-owned enterprises

Urgent and proactive restructuring of state-owned enterprises, especially conglomerates in key sectors of the economy, is crucial for mobilizing resources and improving the efficiency of production and business in critical industries of the nation. This approach serves as an immediate solution to reduce administrative costs and enhance operational efficiency while also serving as a long-term strategy to promote restructuring and ensure sustainable growth of the economy in the coming years.

Fifth, continue to improve the investment environment

Building a transformative government aimed at creating a competitive and equitable environment while protecting the interests of domestic industries. Enhancing the implementation of cutting unnecessary business conditions to support enterprises in increasing production, unleashing production forces closely linked to economic restructuring and enhancing competitiveness. Focusing on reviewing, monitoring, and addressing economic concentration cases, restraining unhealthy competition through effective and practical legal tools. Continuing to closely supervise the construction, improvement, and implementation of consumer protection work, moving towards socializing consumer protection efforts; managing and developing a healthy domestic market for goods and services; promptly resolving difficulties and obstacles in production and business.

Strengthening the administrative reform plan, with a focus on reviewing and simplifying administrative procedures, abolishing unnecessary procedures, or decentralizing administrative procedures to local authorities when possible, modernizing administration, and applying information technology management systems.

Sixth, Strengthening industry technological innovation

Technology and innovation are closely related to ensure sustainable development. Sustainable and comprehensive industrialization can be rapidly achieved when policymakers formulate appropriate policies for the industrialization process, avoiding the mistakes other countries have encountered. Technology can promote all three aspects of sustainable development: economic, social, and environmental. The first aspect refers to a country's ability to change its structure to maintain high growth rates over a long period to catch up with more advanced developed countries. The second aspect relates to the inclusiveness of this structural transformation process in terms of poverty reduction, improving the quality of life, creating jobs, and achieving a more equitable distribution of income, assets, and social welfare. The third aspect is environmental sustainability, which includes the use of resources and environmental impacts that do not harm the interests of future generations.

Although technological innovation is considered a driving force for growth, rapid development through technology remains a phenomenon that is not yet widespread. For Vietnam, the application of technology to economic development, industry, addressing social issues, and protecting the environment still faces many limitations. Vietnam needs to transition through each stage of technological development swiftly. This can be achieved by accumulating capital and investment to move up the technology ladder and high-tech industries.

Conclusions:

Vietnam's industrial sector has achieved impressive achievements in terms of both quantity and quality. It is increasingly gaining a significant position globally. Vietnam's industrial manufacturing products are becoming more diverse and are present in many countries worldwide. However, the quality of industrial growth remains low, as evidenced by the relatively low proportion of medium- and high-tech industries, low industrial value-added (MVA), and Vietnam's small share of global MVA. Vietnam's industrial competitiveness is still low and predominantly led by FDI in the region. Sustainable industrial development is the best way for Vietnam to become a modern industrialized country and overcome the middle-income trap.

Literatura – References

1. Vietnam's Industrial Development Strategy until 2020, vision towards 2030. Hanoi.
2. The Ministry of Industry and Trade, UNIDO (2011), Vietnam Industrial Competitiveness Report 2011.
3. The Ministry of Industry and Trade (2014), Report on the Program on Synchronous Development and Upgrading of Clusters and Value Chains for the production of products with competitive advantages: electronics and information technology, textiles and garments, agricultural machinery, food processing, tourism and related services. Hanoi, June 2014.
4. Ministry of Planning and Investment (2013), Project of Vietnam's industrialization strategy within the framework of Vietnam - Japan cooperation towards 2020, vision to 2030. Hanoi.
5. Nguyen Ngoc Son (2014), Industry development and restructuring in the process of industrialization. Journal of Economics and Development, May 20, 2014 issue.
6. Kenichi Ohno (2014), Approaching the middle income trap some policy suggestions for Vietnam, Vietnam Education Publishing House. Hanoi.
7. UNIDO (2009), Industrial development Report 2009. UNIDO 2009.
8. UNIDO (2014), Industrial development Report 2014. UNIDO 2014.
9. UNIDO (2016), Industrial development Report 2016. UNIDO 2016.
10. UNIDO (2020), Industrial development Report 2020. UNIDO 2020.
11. UNIDO (2021), Industrial development Report 2021. UNIDO 2021.
12. UNIDO (2022), Industrial development Report 2022. UNIDO 2022.
13. Sambor A, Szymanek A Analysis of the migration of chemical compounds from fly ash exposed the weather condition, Chemical and Process Engineering. 2014, ISSN:0208-6425

Building a Digital Society to Enhance the Efficiency of National Governance in Vietnam

NGUYEN Quynh Nga[1)], CHU Thi Khanh Ly[1)], NGUYEN Van Hau[1)]*

[1)] National Academy of Public Administration, Vietnam
* Corresponding author email: khanhly.napa@gmail.com

http://doi.org/10.29227/IM-2023-02-29

Submission date: 17-08-2023 | Review date: 21-09-2023

Abstract

The Fourth Industrial Revolution, especially the digital technology, has been rapidly transforming all aspects of social life, driving a powerful process of digital transformation across all fields. The digital transformation program in Vietnam identifies the digital society as one of the three fundamental pillars, encompassing changes in the way social interactions and connections shift from traditional methods to digital connections through modern technology and communication infrastructure. Alongside the numerous positive aspects, the process of building a digital society also presents significant challenges for each country in managing issues related to ensuring digital citizen rights, establishing digital lifestyle standards, and ensuring fairness in digital commerce. In this study, we will: (1) Clarify the concept and characteristics of the digital society; (2) Explore the current status of building a digital society in Vietnam; (3) Analyze some barriers to the digital society construction; (4) Propose some recommendations for enhancing the effectiveness of national governance in Vietnam today.

Keywords: *digital society, digital citizen rights, digital lifestyle, digital commerce, national governance*

1. Introduction

The digital society has been the subject of numerous studies, and several research articles shed light on various aspects of this emerging phenomenon. Dufva, T., & Dufva, M. in "Grasping the future of the digital society" reveal that society is increasingly digitalized and connected, with computers and algorithms playing a significant role in daily activities. The authors introduce 'digi-grasping' to analyze awareness and involvement in the digital world, suggesting it fosters an ethical and aesthetic attachment to society [1]. Powell, A. (Ed) in "Digital criminology: Crime and justice in digital society" presents the concept of the 'digital society,' recognizing technology as an integral part of the larger social entity. The article explores the potential for interdisciplinary advancements in 'digital criminology' and its impact on innovative crime and justice scholarship [2]. Van Dijck, J. in "Governing digital societies: Private platforms, public values" shows how online digital platforms deeply penetrate society, disrupting markets, labor relations, and institutions, while transforming social and civic practices. Platform dynamics affect democratic processes and political communication, leading to intense struggles between competing ideological systems [3]. Martynov, V. V. (Ed) in "Information Technology as the Basis for Transformation into a Digital Society and Industry 5.0" discusses the state and prospects of technology development during the transition from industry 4.0 to industry 5.0. The authors analyze modern technologies vital for organizing the digital industry, ensuring a smooth transition [4]. Lahlou, S. in "Identity, social status, privacy and face-keeping in digital society" explores the privacy concerns raised by the digitization of society, describing privacy threats of life-logging. The article proposes a new definition of privacy as 'keeping face,' providing constructive guidelines for enhancing privacy in system design [5]. Egard, H., & Hansson, K. in "The digital society comes sneaking in. An emerging field and its disabling barriers" highlight how rapid digital technology growth affects disabled individuals' everyday experiences of social exclusion. The article discusses the relationships between theories on society changes with new technologies, leading to potential disabling barriers for the disabled [6]. Ivanova, V. in the report "Digital skills – a prerequisite for the development of a digital society" analyzes the Digital Economy and Society Index (DESI) elements, studying digital technology access and use in Bulgaria and other European countries. The report draws conclusions on the relationship between digital skills and societal development [7]. Lindgren, S. in "Digital Media and Society" approaches digital society as an equation: Digital society = Digital media + Society, discussing the influence of digitized communication tools and infrastructure on society. The book covers various topics, from social media to digital ethics [8]. Selwyn, N. in "What is Digital Sociology?" conceptualizes digital society as a stage of social development driven by technology, AI, and utility equipment systems. The book explores key topics like digital race, labor, evolving research methods, and diverse digital scholarship forms [8]. Perriam, J., & Carter, S. in "Understanding Digital Societies" provide a framework for comprehending our technologically shaped society, exploring relationships between humans, machines, and emerging AI technologies. The book delves into thought-provoking contemporary issues related to technology use in local and global communities [9].

In Vietnam, there haven't been many research works on the digital society, primarily focusing on analyzing the digital society as a component of digital transformation. Nguyen Huu Hoang and Tran Van Huan analyzed the challenges posed to leadership and management in the digital society. In their analysis, the authors assert that "The digital society has brought about rapid and profound changes in the hierarchy of values, cultural and social standards; many unprecedented methods of social interaction and communication, such as

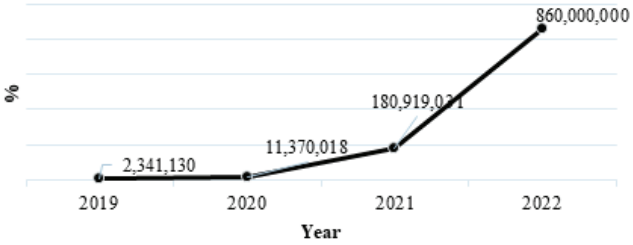

Fig. 1. Number of transactions on the NDXP platform [16]

virtual interactions, have emerged. This has made social interactions and cohesion in many settings become more "loose" and even at risk of disruption." Additionally, the authors also prove the point that "human resources are the core issue in the digital society" and propose solutions to build a policy and legal space (sandbox) to actualize the digital society [26]. In the book "Digital Society - Understanding the Digital Society" by Nguyen Duc Loc, author analyze the digital society in Vietnam from a technical perspective. The author also addresses social arrangements, the role of humans in the age of intelligent machines, and policies related to digital urban infrastructure [27]. Bui Quang Tuan and Ha Huy Ngoc Sach (2022) provide an overview of digital transformation and international experiences related to digital transformation in the book "Digital Transformation - International Experiences and Roadmap for Vietnam". They dedicate Chapter 5 to analyzing the process of transitioning to the digital society in Vietnam, highlighting the perspective of approaching the digital society as an integral part of Vietnam's digital transformation process [28].

Thus, through the analysis of some typical scientific studies related to digital society, it can be seen that the authors have conceptions and analysis of many detail aspects of digital society such as: Crime and justice in digital society; Governing digital societies; Information Technology; Identity, social status, privacy and face-keeping in digital society; Digital skills; Digital Media; Relationships between humans, machines and technologies. However, until now, there have been no studies on the barriers to the process of building a digital society, nor have there been any studies that place the digital society in relation to effective national governance. In this research, we will conduct a specific case study in Vietnam regarding the construction of the digital society. We will approach the theory of the digital society through three structures: digital citizen rights, digital lifestyle, and digital commerce. Based on this foundation, we will analyze and evaluate the current situation and the barriers present in the process of building the digital society. From there, we will propose some solutions for constructing a digital society to enhance the effectiveness of national governance.

2. Perspectives on the Digital Society

From a technological perspective, in the special report "Digital Society in Asia" by the Global System for Mobile Communications (GSMA), the concept of "Digital Society" is defined as follows: The digital society refers to a society where citizens seamlessly interact with various aspects of life, including work, entertainment, and communication, through digital channels via interconnected smart devices and compatible services. In a digital society, people can access and interact with a range of public and private services, including financial services, utilities, education, healthcare, and transportation, anytime and anywhere, using digital technology [10].

From a scientific perspective, scholars worldwide perceive the digital society as a contemporary social structure and lifestyle strongly influenced and shaped by digital technologies, especially the internet and digital communication. It encompasses a wide range of interactions, behaviors, relationships, and diverse activities that individuals and communities engage in the digital realm. In the digital society, people use digital technologies and online platforms for various purposes, such as communication, socialization, information sharing, entertainment, education, commerce, etc. The widespread use of smartphones, computers, and internet connectivity has transformed the way individuals interact, access information, and participate in the global community [11].

From a management perspective, Vietnamese scientists have their own view of the digital society: The digital society represents a new state of transformation and development of society based fundamentally and significantly on digital technologies and digital communication such as the internet, AI, Big Data, Mobile Technology, etc., enabling the seamless interaction of all members of society with each other and with objects (Internet of Things - IoT) in various aspects of social life, including the economy, politics, culture, and more, in the digital world, creating a positively changed life and promoting sustainable, humane, and modern social development [13].

Therefore, regardless of the approach, the essence of the digital society remains the change in the way social interactions and connections transition from traditional methods to digital connections across various aspects of social life through modern technology and digital communication infrastructure.

In Vietnam, Decision No. 749/QD-TTg dated June 3, 2020, approved the National Digital Transformation Program until 2025, with a vision towards 2030, affirming the goal of "Vietnam becoming a prosperous and stable digital nation, pioneering in experimenting with new technologies and models; fundamentally renewing and comprehensively digitizing the operations of the government, business production activities, people's lifestyles and work, developing a safe, humane, and widespread digital environment" [15]. Accordingly, the pillars of the National Digital Transformation Program are "Digital Government," "Digital Economy," and "Digital Society." Therefore, building a digital society is one of the prerequisites for successfully achieving the national digital transformation objectives in Vietnam. Building a digital society aims to develop a digital infrastructure, digital life-

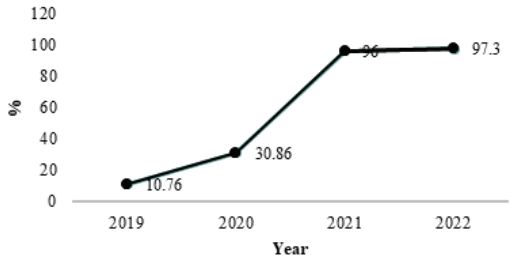

Fig. 2. Proportion of level 4 online public services out of total public services [17], [18]

style, digital commerce, digital culture, digital lifestyle, digital citizenship, etc., with a particular focus on engaging citizens in the process of national governance, collaborating with the state to build a civilized, modern, and humane digital society.

There are three essential and interrelated components that create conditions for the development of a digital society: (1) Digital citizen rights, (2) Digital lifestyle, and (3) Digital commerce.

3. Current Status of Building the Digital Society in Vietnam

3.1. Digital Citizen Rights

The Vietnamese government is making efforts to provide digital channels and create conditions for citizens to exercise their rights through modern methods in the digital environment. This includes accessing online profiles for healthcare, applying for passports or business licenses, paying taxes, and even participating in online voting during elections, aiming to enhance interactions between the government, citizens, and businesses.

The report results from the Ministry of Information and Communications in 2022 indicate an increasing trend in the number of citizens and organizations engaging in transactions on the National Data Sharing Platform (NDXP) from 2019 to 2022. Especially, in 2022, Vietnam has developed the NDXP platform connected with systems of 90 agencies, organizations, and businesses; among them are 8 databases and 12 information systems providing data sharing services. The total number of transactions carried out through NDXP in 2022 reached approximately 860 million, which is 4.8 times higher than in 2021.

In 2022, the Vietnamese government also implemented the Community Digital Technology Group. By 2022, all 63 provinces and centrally-governed cities had established Community Digital Technology Groups, with 46 out of 63 provinces completing 100% establishment of these groups at the commune level. The total number of established Community Digital Technology Groups was 68,933, with 320,839 members participating.

The proportion of online public services at level 3.4 out of the total public services showed an increasing trend from 2019 to 2021. In 2022, with the issuance of Decree No. 42/2022/ND-CP on June 24, 2022, which regulates the provision of information and online public services by state agencies on the internet, the proportion of online public services that met the conditions to be rated at level 4 reached 97.3% (accounting for 53.56% of the total administrative procedures).

In the field of population management, digital technology solutions are being applied on a big data platform to build a unique identification system for each citizen, serving as the basis for social credit scoring. Every action of individuals is recorded and can be scored, helping to identify each person's position in society. All behavioral data is observed and evaluated, creating a sense of transparency.

In Vietnam, the Ministry of Information and Communications has established the National Center for Cyber Security Monitoring. Based on digital technology application in information recognition, this center can read, receive, analyze, evaluate, and classify about 100 million pieces of information each day, creating a data foundation for early identification of information flows and social sentiments. It serves as a basis for connecting and achieving consensus between the government and the people, facilitating effective social management.

3.2. Digital Lifestyle

Digitization is changing the way people live, work, communicate, and entertain. Remote work and learning, as well as using social media platforms for communication, and experiencing virtual reality (VR) are clear manifestations of lifestyle changes through digital advancements. The digital lifestyle is enriched by Internet of Things (IoT) technology, which connects everything, enabling smart connectivity between devices and objects via the internet, such as smartphones, tablets, tracking devices, screens, and sensors for data exchange. IoT impacts people's lives mainly by providing real-time information about transportation, weather, smart city projects, etc.

Facing the powerful impact of the Fourth Industrial Revolution, the Vietnamese government has implemented synchronized solutions to build a digital lifestyle for citizens, promoting and creating favorable conditions to encourage citizen participation in the process of building a digital society.

The proportion of the population using the Internet has continuously increased in recent years. The average daily Internet usage time of Vietnamese people is about 6 hours and 23 minutes, with 55.4% of the time spent using the Internet via mobile devices.

The rate of mobile device usage has also increased significantly. In January 2023, data from GSMA Intelligence showed that there were 161.6 million mobile connections in Vietnam at the beginning of the year, equivalent to 164.0% of the total population. The number of mobile connections in Vietnam increased by 4.7 million (+3.0%) from 2022 to 2023.

The proportion of people using social media in Vietnam is quite high compared to other countries in the region. In January 2023, the number of social media users in Vietnam was about 70 million people, accounting for approximately 71.0% of the total population. On average, Vietnamese people spend 2 hours and 21 minutes per day using social media for messaging, connecting, interacting, and working.

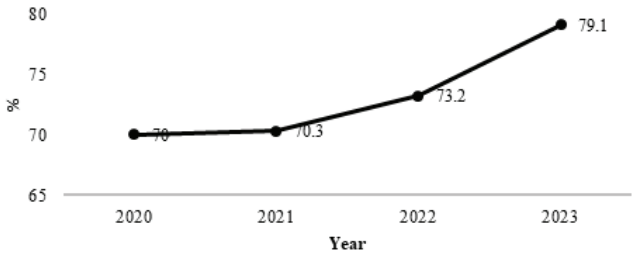

Fig. 3. Proportion of the population using the Internet in Vietnam [20]

In the field of urban traffic management, the application of Big Data and Artificial Intelligence (AI) has brought many promising results in innovation. The current Intelligent Traffic Management Center in Ho Chi Minh City, for example, utilizes digital features in management to fulfill four main functions: traffic monitoring, signal light control, traffic information provision, and violation handling. The integration and sharing of traffic surveillance camera data help functional units proactively address traffic-related issues in the city. AI application in management and operation is based on creating traffic forecasting models by collecting comprehensive traffic data, analyzing traffic behaviors, forecasting traffic events, optimizing traffic flow, and recommending suitable traffic routes. In addition to the camera network, a traffic flow measurement system has been installed at 118 locations, allowing the calculation of average traffic speed, vehicle density, and automatic alert generation. Currently, the Ho Chi Minh City Department of Transport has completed and implemented a simulation model for predicting traffic demand, contributing to directing the development of policies and management plans.

In some localities, digital technology is also being piloted in parking management, by automatically monitoring and identifying information about parked cars in experimental parking areas. The AI-based surveillance camera system helps build monitoring solutions and automatically determine information about parked cars and available parking spaces in the experimental parking areas. It also simulates the parking time calculation system and deducts parking fees from the hypothetical accounts of customers.

In the field of education, digital transformation in teaching and learning is being strongly promoted throughout the sector. The Ministry of Education and Training has issued guidelines for building digital learning materials and online courses. The digital learning resources of the entire sector contribute to the Vietnam Digital Knowledge System with more than 7,000 e-learning lectures (over 4,000 lectures for high school education programs, over 1,000 lectures on Vietnamese cultural heritage, and more than 2,000 television lectures).

In implementing Project No. 06 on developing population data applications to serve the national digital transformation, the Ministry of Education and Training has successfully connected the education database with the national population database managed by the Ministry of Public Security. As a result, more than 1.5 million teachers (reaching 95%) and nearly 21 million student records (reaching 92%) have been connected, synchronized, and authenticated with the citizen identification code. Moreover, information technology applications have been deployed in the high school graduation examination and university admission process, which are carried out online for all candidates. In pre-school and general education, nearly 24 million student records have been digitized (digitizing information about personal history, learning process, training, health, etc.), along with more than 1.5 million records of teachers, staff, and management officers (records, professional qualifications, evaluations according to standards) from 53,000 schools, and information about school facilities and toilets.

3.3. Digital Commerce

Digital commerce includes all forms of financial payments on digital technology platforms, managing online banking accounts quickly, transparently, securely, and efficiently. The World Payments Report 2015 by Capgemini highlights the importance of digital commerce in modern society, as the volume of non-cash payment transactions is growing faster than the Gross Domestic Product (GDP) on all continents. In Vietnam, as well as in many other countries, digital commerce has created new economic models and reshaped business processes in various sectors, including public services, retail, transportation, financial services, and entertainment. It allows the government and businesses to interact with citizens and customers in a dynamic and efficient manner.

In January 2020, statistics showed that 30% of people in Vietnam aged 15 and above owned an account with a financial organization, of which 4.1% had credit cards, 3.5% had accounts on mobile apps, and 21% had made online purchases or bill payments. When shopping online, 37% of users chose to pay by credit card, 17% paid in cash, 30% transferred money through banks, 11% used e-wallets, and 6% opted for other methods.

In the first six months of 2023, there were 57.62 million people who had shopped online, an increase of 11.3% compared to 2022. The total value of online transactions was estimated at 12.81 billion USD. On average, each customer spent 222 USD on online shopping, of which 49.7% of online shopping transactions were made via mobile devices.

The business activities on social media platforms have shown an increasing trend from 2019 to 2021. In 2021, 57% of businesses reported using social media platforms for online commerce.

The forms of commercial negotiation and signing commercial contracts in the digital environment have also shown an increasing trend in Vietnam in recent years, especially from 2020 to 2021.

4. Some Barriers to the Process of Building a Digital Society in Vietnam Today

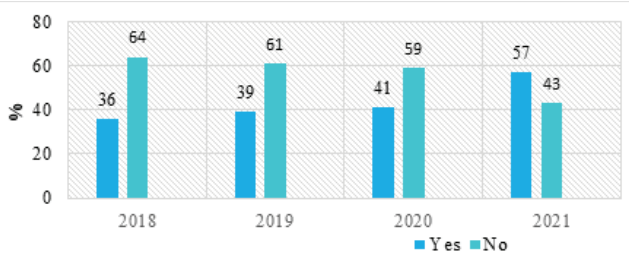

Fig. 4. Business on Social Media by Enterprises over the Years [21]

Legal Environment Barriers

Currently, Vietnam has a system of legal documents regulating and adjusting the general digital transformation process and the specific construction of a digital society. However, there are still legal gaps in terms of digital society, such as legal regulations concerning digital culture, protection of personal data in the digital environment, protection of digital citizen rights, and management of online transactions. The lack of legal foundations for managing digital society has posed difficulties for functional agencies in managing emerging issues in the digital society in Vietnam today.

Barriers to Security and Information Safety

Digital technology, while providing opportunities for human life, also presents numerous challenges to the healthy development of society. Digital technology can be used in harmful ways against individuals, communities, society, and the nation. For instance, computer viruses, spyware, loss or theft of personal data, and the spread of immoral content and violence on the internet, as well as the potential negative impact of robots on human activities, including employment, and on aspects of human life such as sexuality, love, marriage, and family. Digital technology can also be used by terrorist groups to create political instability in society.

Cyber attacks in Vietnam are increasingly complex and seriously affect national security and social order. In the third quarter of 2020, 937 websites and portals in Vietnam were hacked, their interfaces changed, files inserted, increasing by 28% compared to the same period last year [24]. In addition, the threat of data breaches and trading of personal information in the online environment is becoming more complicated. Hackers increasingly target data-focused attacks. The lack of cybersecurity experts and cloud computing security solutions, along with the explosion of smart devices, artificial intelligence, and mobile applications, poses threats to information security.

The transition to digital operations is a trend being implemented by many state agencies, private enterprises, and organizations in Vietnam to improve operational efficiency. However, in the context of the increasing storage of crucial resources and data in the digital environment, along with the explosion of connected personal devices, this has inadvertently become an exploitable "weakness." Attackers now have more "entry points" to infiltrate organizational data repositories, making information security processes more complex.

To build a safe and healthy cyberspace, which is an important resource for economic and social development, ensuring information security and safety on the internet is considered a crucial and inseparable aspect of the digital society.

Barriers to Digital Human Resources

The process of innovating national management with the goal of building a digital society in Vietnam, as well as in many countries around the world, faces difficulties related to high-quality human resources. Due to the nature of social activities taking place in the digital environment, there is a need for labor with high intellectual capacities, trained, and exposed to modern technologies. Therefore, a shortage of skilled labor, lack of leading experts in digital technology, and a lack of strategic planners for digital transformation are occurring in many countries. It is evident that the demand for digital technology human resources from government agencies, businesses, and social organizations is increasing, but the supply of trained personnel has not yet met the demand. Many enterprises and organizations have to proactively seek cooperation with universities to train and find human resources.

Barriers to Cultural and Ethical Changes in Society

In the digital society, people use machines and artificial intelligence to process vast amounts of data and arrive at the most logical results. Society is always oriented towards more accurate and complex production, always dreaming of realizing a life of automation, self-operation, maximizing time and energy savings. However, the development of digital technology, especially artificial intelligence, still faces many debates. The fact that machines can mimic intelligence and handle tasks with equal or greater efficiency than humans creates intense arguments. As a result, the digital society has and is creating rapid and profound changes in the hierarchy of cultural and social values, ethical standards, and interaction methods that have no historical precedent, and people become dependent on technological means as intermediaries... According to S.M.Omundro: "Even artificial intelligence with only the ability to play chess can be dangerous if not properly designed. Artificial intelligence designed without any special precautions can start to resist being shut down and try to infiltrate other technological systems to create a copy of itself. Improperly designed artificial intelligence can attempt to seize control of resources without considering the safety of others to achieve its design goals" [25]. This makes communication between people more "loose" and even at risk of breaking.

Additionally, human dependence on technology leads to consequences such as a tendency to narrow community commitment, people feeling "lonely," more exhausted, and stressed, even though the digital space offers more convenient, open living spaces and connections. The values of culture and ethical standards of people in the digital environment are undergoing significant changes compared to traditional cultural and ethical values. Furthermore, a portion of society, espe-

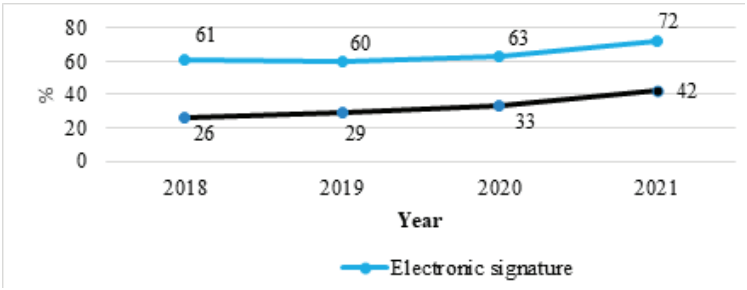

Fig. 3. Proportion of the population using the Internet in Vietnam [20]

cially young groups, tends to "idealize" many things happening in the virtual space, tend to detach, forget, or "normalize" high values of tradition, family culture, and ethnicity... This creates difficulties for managers in managing activities in the digital society.

Therefore, researching, guiding, and directing the digital society through the criteria of digital culture, digital ethics, digital life, and digital lifestyles, alongside core values of the people, is a matter that needs attention and focus.

"Digital Divide" Barriers

In addition to the increasing challenge of the rich-poor gap in the market economy, the "digital divide" will become a new social issue in the context of digital transformation. The rapid development of digital technology will inevitably give rise to layers of people who cannot keep up with the pace of development, lack the basic qualifications to adapt to innovation.

Therefore, to successfully build a digital society, which aims to enhance the effectiveness of national management in the context of digital transformation, it is essential to improve the level of intelligence and technology literacy. People need to be specifically oriented and guided so that they can grasp and adapt to a society with a rapidly advancing scientific and technological development, especially vulnerable groups in society (the elderly, the poor, people in remote areas, mountains, islands...). In other words, a digital society can only be truly successful when it is built by digital officials and public servants; a digital society can only function when there are digital citizens. The government needs to have a digital transformation strategy that goes hand in hand with assisting vulnerable groups and implements the motto "When technology advances, no one is left behind."

5. Recommendations for building a digital society to enhance the effectiveness of national governance in Vietnam

It is essential to complete the institutional framework for the digital society. The state should promptly perfect legal documents regarding the construction of a digital society, including regulations concerning digital culture, digital ethics, and digital lifestyle standards. Additionally, the state needs to urgently issue legal regulations on the protection of personal data in the digital environment and improve the legal basis for electronic commerce activities.

Regularly assess the impacts of digital technology on society to proactively minimize its negative effects. Establish behavioral rules for businesses and individuals in the digital environment. Develop centers to address concerns and support those affected by negative impacts of digital technology.

Implement a job model that aligns with the working conditions of the digital environment. Relevant authorities should manage social development activities to strike a balance between economic growth, handling labor surplus during the golden population period, social welfare policies, and the challenges of the digital transformation process.

Increase the quantity of training, development, and updating of knowledge and skills for working in the digital environment for the workforce in the state administrative system. Select and train a team of digital transformation experts for various industries, sectors, and localities. These experts should continue to train relevant officials in their organizations and become the backbone to lead, organize, and spread the national digital transformation process.

Perfect policies to build a knowledgeable digital citizenry that understands and adapts to the digital society. Support and encourage citizens to embrace the digital society, possess skills to utilize and exploit the benefits of the digital world, and practice new behaviors, culture, and principles in the digital environment. Integrate education and promotion of the digital society into the curriculum of educational institutions, and utilize digital space and technology alongside traditional teaching methods to propagate the digital transformation process.

Increase enrollment quotas for training bachelor's and engineering degrees in information technology. Adjust and supplement postgraduate, university, and vocational training programs to integrate digital technology, such as artificial intelligence (AI), data science, big data, cloud computing, Internet of Things (IoT), virtual/augmented reality (VR/AR), blockchain, and 3D printing.

Implement an integrated education model that combines science, technology, engineering, mathematics, arts, business, and English language training, as well as information technology skills and information security assurance at all levels of education. Provide career orientation training so that students acquire skills ready for the digital environment. Promote online examinations, recognize the value of online learning certificates, build platforms for sharing teaching and learning resources, and develop technology enterprises serving education with a focus on personalized training.

Expand international cooperation activities to learn from the experiences of other countries and organizations in building and managing the digital society.

Invest sufficient financial resources in the process of building and developing the digital society.

6. Conclusion

The National Digital Transformation Program identifies three pillars: "Digital Government," "Digital Economy," and

"Digital Society." Therefore, building a digital society is a prerequisite for successfully implementing the goals of national digital transformation, aimed at enhancing the effectiveness of national governance in Vietnam.

Some achievements have been made in all three components of the digital society: digital citizenship, digital life, and digital commerce. These achievements demonstrate the efforts of the government and society in implementing and realizing policies for building a digital society, contributing to improving the effectiveness of state governance and achieving the goals of national digital transformation in Vietnam.

Besides the achievements, activities for building a digital society also encounter many barriers and challenges in various aspects: legal environment, security, information safety, digital human resources, digital divide, and changes in cultural and ethical norms in society.

To build and develop a digital society, aiming to improve the effectiveness of national governance in Vietnam, it is necessary to pay attention to implementing some recommendations, focusing on addressing issues related to management systems and human resources.

Literatura – References

1. Dufva, T. and M. Dufva, Grasping the future of the digital society. Futures, 2019. 107.
2. Powell, A., G. Stratton, and R. Cameron, Digital criminology: Crime and justice in digital society. 2018: Routledge.
3. Van Dijck, J., Governing digital societies: Private platforms, public values. Computer Law & Security Review, 2020. 36.
4. Martynov, V.V., D.N. Shavaleeva, and A.A. Zaytseva. Information technology as the basis for transformation into a digital society and industry 5.0. in 2019 International Conference" Quality Management, Transport and Information Security, Information Technologies"(IT&QM&IS). 2019. IEEE.
5. Lahlou, S., Identity, social status, privacy and face-keeping in digital society. Social science information, 2008. 47(3).
6. Egard, H. and K. Hansson, The digital society comes sneaking in. An emerging field and its disabling barriers. Disability & Society, 2021.
7. Ivanova, V., Digital skills–a prerequisite for the development of a digital society. Economic Thought Journal, 2019(4).
8. Lindgren, S., Digital media and society. Digital Media and Society, 2017: p. 1-328.
9. Carter, S. and J. Perriam, Understanding Digital Societies. Understanding Digital Societies, 2021.
10. Kenechi Okeleke, Henry James & Yoonee Jeong: Advancing Digital Societies in Asia, GSMA Head Office, United Kingdom, 2016.
11. Allan Martin "Digital literacy and the "digital society"", 2008.
12. https://www.fujitsu.com
13. Ministry of Information and Communications (2021), Questions and Answers about Digital Transformation, Information and Communications Publishing House, 2020.
14. Armin Nassehi: What issues does digital transformation solve?, Goethe Institut, Hanoi, 2021.
15. Prime Minister of the Government (2020), Decision No. 749/QD-TTg dated June 3, 2020, approving the National Digital Transformation Program until 2025, with a vision to 2030.
16. Ministry of Information and Communications (2022), Summary report on the work of the Ministry of Information and Communications in 2022, and the direction for 2023
17. Ministry of Information and Communications (2018 - 2020), Report on the Readiness Index for Development and Application of Information and Communication Technology in Vietnam, Information and Communication Publishing House.
18. Ministry of Information and Communications (2021), Report No. 91/BC-BTTTT dated June 30, 2022.
19. http://caicachhanhchinh.gov.vn/danh-muc/bao-cao-chi-so-hai-long-ve-su-phuc-vu-hanh-chinh-nam-2020-va-chi-so-cai-cach-hanh-chinh-nam-2020-cua-cac-bo-co-quan-ngang-bo-8866.html
20. https://www.brandsvietnam.com/library/doc/63e21b17e7703-Vietnam-Digital-2023
21. https://vecom.vn/bao-cao-chi-so-thuong-mai-dien-tu-viet-nam-2022
22. https://haiquanonline.com.vn/ung-dung-tri-tue-nhan-tao-phuc-vu-nguoi-dan
23. 23.https://moet.gov.vn/giaoducquocdan/tang-cuong-ung-dung cntt/Pages/Default.aspx?ItemID=8349
24. 24.https://www.qdnd.vn/giao-duc-khoa-hoc/tin-tuc/dam-bao-an-toan-an-ninh-mang-la-nhiem-vu-then-chot-643541
25. 25. Omohundro, S. M. (2008), The Basic AI Drives, In: Proceedings of the 2008 conference on Artificial General Intelligence 2008, Amsterdam, IOS Press, tr.483-492.
26. 26. Nguyen Huu Hoang, Tran Van Huan (2021), "Digital Society and Social Management Issues," Journal of Political Theory, accessed from http://lyluanchinhtri.vn/home/index.php/nguyen-cuu-ly-luan/item/3930-xa-hoi-so-va-van-de-quan-ly-xa-hoi.html
27. 27. Nguyen Duc Loc (editor) (2022), "Digital Society - Understanding the Digital Society," National Culture Publishing House.
28. 28. Bui Quang Tuan, Ha Huy Ngoc (2022), "Digital Transformation - International Experience and Roadmap for Vietnam," National Political Publishing house.

Theory Y in Modern Management: Advantages, Disadvantages, and the Relationship with Theory X

NGUYEN Thanh Ha[1)], NGUYEN Thi Thanh Huyen[2)], NGUYEN Thi Lan Huong[3)]

[1)] Melbourne University
[2)] Hanoi Financial and Banking University
3) HaNoi University of Mining and Geology

http://doi.org/10.29227/IM-2023-02-30

Submission date: 15-08-2023 | Review date: 12-09-2023

Abstract

This essay delves into the concept of Theory Y, one of the hallmark relationship management principles of the 20th century introduced by Douglas McGregor in his influential book "The Human Side of Enterprise" (1960). Theory Y assumes that employees are self-motivated, seek responsibility, and do not dislike work. The essay explores the advantages and disadvantages of Theory Y, highlighting its potential in nurturing creativity and maintaining employee satisfaction, but also addressing its limitations in certain situations. It examines successful examples of Theory Y implementation in companies like Facebook and Google, as well as the potential drawbacks such as freedom abuse and lack of organizational control. Additionally, the essay discusses the relationship between Theory Y and its counterpart, Theory X, which represents a more traditional, directive management style. By examining both theories, the essay emphasizes the importance of carefully considering and adapting management approaches based on the specific context and needs of an organization.

Keywords: *theory Y, theory X, management, strategy, organization*

1. Introduction

Douglas McGregor (1906-1964) had an academic career lecturing at Harvard University, Massachusetts Institute of Technology (MIT) and Antioch College, becoming the first Sloan Fellows Professor at MIT. Many agree that much of modern management thinking goes back to McGregor, especially the implications of his writing for leadership. According to McGregor, the way that organisations are run are influenced by managers' basic beliefs. In other words, a company's management method is often based on Managers' assumptions about the behaviour of people, which fall into two broad categories - Theory X and Theory Y. These findings were presented in The Human Side of Enterprise, first published in 1960. This essay will first introduce the concept of Theory Y, then explore its advantages and disadvantages, finally highlighting the relationship of Theory Y and X.

2. Definition of Theory Y

Of the 20th century, Douglas McGregor's The Human Side of Enterprise was considered as one of the most influential management books, setting an important milestone in the history of management (Arenas A., unknown). Theory Y is one of the hallmark relationship management principles of the last half of the 20th century. This theory assumes that employees do not dislike work, have self-control and direction, and seek responsibility (McGregor, 1960). Philosophers such as Locke (1690) and Smith (1776) provided a solid foundation for the accumulation and emergence of Theory Y thinking. McGregor encouraged employers to allocate their employees responsibility and to allow them to have the freedom to do their jobs (Charles M., 2005). Theory Y opens a whole new series of possibilities since it is based on the potentialities and abilities of each person. The whole theory revolves around the creation of opportunities and releasing potential. Individuals may achieve their goals better if they focus on the success of the organization. In other words, given the right environment, workers may reach their potential and perform their best.

3. Advantages of Theory Y

As Theory Y respects each individual's capability and gives them the best environment or opportunities to extend their career, thus contributing to the organization's success, it would be advantageous in nurturing creativity and maintaining employee satisfaction. Facebook is a highly innovative business with its CEO Mark Zuckerberg utilizing the McGregor Y Theory. He would motivate the team as a whole instead of just managing, controlling his staff and rewarding each employee's contribution. This approach ensures the workers know that their contribution matters and can help achieve the organizational goals. Google also follows a Theory Y approach for managing the operations. The CEO of the company has adopted a strategy to assure democracy in the corporation by ensuring that every worker is getting a chance to express individual viewpoints, even though these viewpoints could conflict with decisions of the top-level managers in some cases. Google and Facebook are multi billion companies which apply Theory Y to achieve objectives and remain notably competitive in the business world. Theory Y approach in the managerial level sustains continuous development and motivates them so that their overall performance standards could be increased.

4. Disadvantages of Theory Y

Theory Y advocates seems to focus on optimism, believing that humans are self-driven towards organizational goals. However, there are also criticisms of Theory Y: it is not always applicable, comprehensive and too idealistic to be true. Bennis suggested in 1972 that the Theory Y framework does not incorporate the impact of environmental (internal and external) factors in management. Other aspects besides the intrin-

sics related with personalities within the organization could affect managers decisions and approaches. Theory Y gives employees trust, freedom and the rights to express their individualism. Nevertheless, this "freedom" can backfire and result in dire consequences. Not everyone will be comfortable and accustomed to undefined working boundaries. Some people simply do not have the ability to identify and concentrate on their own goals. The freedom and trust can also be conveniently abused. For employees with lack of self-control and direction, they can take advantage of this liberty to exercise unethical behaviors or compromise their productivity, spending time for unrelated tasks. Sometimes a sense of authority and control should be implemented in order to keep the organization restrained. Consequently, success can be measured more authentically since everything follows a specific model and regulations. The former CEO of Apple and Ford Motor had followed Theory X and these companies experienced tremendous success all over the world.

5. Theory Y vs Theory X

Theory X and Theory Y describe two opposing views of people at work and can be used to describe two corresponding management styles. In Theory X, managers have the traditional view of direction and control and are dominant in the work environment. This one includes pervasive preconceived ideas during the 19th and first half of the 20th century, which influenced most of managerial strategies of the US industry. Theory X proposes that management is the only one responsible for organizing all aspects of the organization -supplies, equipment, and people - to achieve the planned goals. Management is also the one in charge of controlling, motivating, and changing the behaviors of the employees. Under this theory, management consists of accomplishing objectives by dominating and directing people.

There is a common misinterpretation that Theory X is commonly exercised in coercive and immoral manners. However, Theory X, if applied in an ethical way, can be extremely powerful and generate immeasurable benefits. Apple and Ford are two significant examples of successful implementation of Theory X in management. In Theory Y, managers respect the integration of individual and organisational goals. In The Human Side of Enterprise (McGregor, 1906), by highlighting Theory Y, he hoped instead to persuade managers to abandon the limiting assumptions of Theory X and consider using the techniques suggested by Theory Y.

6. Conclusion

Theory Y is a powerful management tool first introduced by Douglas McGregor in his 1960 book "The Human Side of Enterprise". Theory Y management style respects collaborative relationships with people and motivates workers by allowing them to work on their own initiative, giving them responsibility, and empowering them to make decisions. Theory Y regards employees as people who are self-motivated and excited by the challenge of work. This management approach can be effective – inspiring, innovative, encouraging creativity and personal ideas – but can also be incapable under certain circumstances which causes freedom abuse or lack of sense of organizational control. There is a strong interrelation between Theory X and Theory Y as it is two contradicting managerial approaches. Firms should decide their method with careful consideration since both do not consistently guarantee success.

Literatura – References

1. Carson, C.M. (2005), "A historical view of Douglas McGregor's Theory Y", Management Decision, Vol. 43 No. 3, pp. 450-460. https://doi.org/10.1108/00251740510589814
2. Samson, D. et al., 2021. Management 7th edition.
3. McGregor, D. (1960). Theory X and theory Y. Organization theory, 358(374), 5.
4. Sager, K. L. (2008). An exploratory study of the relationships between theory X/Y assumptions and superior communicator style. Management Communication Quarterly, 22(2), 288-312.
5. Arena, A. Douglas McGregor's Management Theory. http://annarenas.com/wp/wp-content/uploads/2019/04/DouglasMcGregor-paper.pdf
6. Parikh, V. (2021, October 1). Theory Y Advantages and Disadvantages. LetsLearnFinance. https://www.letslearnfinance.com/theory-y-advantages-and-disadvantages.html

Enhancing Workplace Safety: A Comprehensive Action Plan for Duong Huy Coal Company (2021–2025)

Nguyen THI HOAI NGA[1)], Nguyen DUC THANG[2)], Le DINH CHIEU[2)], Le VAN CHIEN[2)], Pham KIEN TRUNG[2)]

[1)] Innovations for Sustainable and Responsible Mining (ISRM) Research Group, Hanoi University of Mining and Geology, Hanoi, 100000, Vietnam

[2)] Hanoi University of Mining and Geology, Hanoi, 100000, Vietnam; email: phamkientrung@humg.edu.vn

http://doi.org/10.29227/IM-2023-02-31

Submission date: 15-08-2023 | Review date: 13-09-2023

Abstract

Workplace safety is of paramount importance in industries such as coal mining, where accidents and occupational illnesses can result in significant human and economic costs. This study aims to develop an action plan to improve safety standards at Duong Huy Coal Company from 2021 to 2025. A comprehensive survey involving 93 safety managers and 379 workers from various production sites was researched to gather insights and opinions on safety priorities. Focus group discussions and expert consultations were employed to assess the current safety situation, identify challenges, and develop coherent safety solutions. Based on the survey results, the proposed action plan focuses on the following objectives: reducing workplace accidents by 20-25% annually, progressing towards zero accidents in the following years, and increasing productivity and benefits for both workers and the company. The plan also emphasizes the role of company leadership in widely communicating their commitment to safety and the need for individual units within the company to proactively plan, budget, and implement safety measures following their functions and responsibilities. Collaboration with relevant state agencies, mass mobilization campaigns, and the application of science and technology in safety and occupational health will further contribute to the enhancement of workplace safety at Duong Huy Coal Company.

Keywords: *workplace safety, safety standards, safety solutions, extractive industries, Duong Huy coal company*

1. Introduction

The field of mining is always evaluated as having a high risk of occupational safety hazards, with numerous accidents and occupational diseases occurring each year (Jiskani et al., 2020; Lu et al., 2020; Nguyen et al., 2021; Tetzlaff et al., 2021). This situation persists and demands special attention from regulatory authorities and businesses operating in the industry (Burke & Signal, 2010; Dodoo et al., 2023; He & Song, 2012; Lewis-Beck & Alford, 1980). In this context, Duong Huy Coal Company (DHC), a underground technology-based mining enterprise under the Vietnam National Coal and Mineral Industries Holding Corporation Limited (Vinacomin), has implemented various measures to improve production safety. However, many issues remain unresolved. A comprehensive and tailored action plan to enhance production safety at DHC is still lacking. DHC aims to produce 2.2 to 2.5 million tons of coal annually in the forthcoming years. Among nealy 3,000 employees, many miners are minority ethnic people. Their understanding and awareness of safety is of significance to the company. To meet the sustainable development goals for 2030 and reduce the occurrences of occupational accidents and diseases, the company needs to propose effective and coordinated solutions within an action plan (Bahn, 2013; Hine et al., 1999; Jiskani et al., 2020; Lu et al., 2020; Mcafee & Winn, 1989).

Enhancing production safety will safeguard the lives and health of the workforce and help the coal mining industry, particularly DHC, achieve its objectives of clean and safe mines (Beus et al., 2016; Opoku et al., 2020; Rivas et al., 2011). This research aimed at reducing occupational accidents in the mining sector and improving the quality of life for workers and the surrounding community.

This study builds upon the knowledge and experiences from previous research on occupational safety in the mining sector (Colligan & Cohen, 2009). The insights gained will be utilized to identify and propose reliable and efficient solutions to enhance production safety at DHC.

The proposed action plan will offer a timeframe and specific measures to enhance production safety, enabling effective risk management and reducing occupational accidents. The research outcomes will support DHC and other mining enterprises in developing appropriate action plans to ensure safety and sustainable development.

The paper is divided into several main sections, including research methodology, followed by the results of our survey. We conclude by discussing the implications, limitations, and future research directions of our work.

2. Research methodology

2.1. Measures and questionnaire development

Through qualitative research, the research team has identified five influencing factors on the safety culture at DHC: factors related to legal and policy issues; technical and technological aspects; organizational and management work; workers' consciousness; and leadership.

All the measurement scales have been inherited from previous studies and adjusted as necessary based on the suggestions from qualitative research results. The scales all use a 5-point Likert scale, where 1 represents 'completely disagree' and 5 represents 'completely agree'.

2.2. Sample and data collection

The research team conducted a survey involving 93 safety managers and 379 workers at various construction sites and workshops. The majority of the participating workers had considerable experience, with a work tenure of 10 years or more at the Company. Given their extensive experience and long-standing commitment to the Company, the responses to their survey questionnaires ensure high quality and reliability, providing a fundamentally accurate reflection and relatively precise assessment of the current safety conditions at DHC.

After the analysis, the results were discussed in focused group sessions, involving occupational safety experts and the management team of the company. This collaborative effort aimed to interpret the findings and identify possible solutions.

3. Results

Majority of workers (76.25% of those surveyed) feel anxious and stressed about occupational accidents (both past incidents and potential ones). Additionally, most workers (70.71% of those surveyed) believe that occupational accidents have an impact on their mental well-being.

Regarding the assessment of future trends in occupational accidents, the majority of surveyed workers expressed optimistic views, indicating that the incidence of occupational accidents at the company is expected to decrease. This demonstrates their confidence and commitment to the goal of reducing occupational accidents at the company.

According to workers' evaluations, there are several major risk factors for occupational accidents at the company, including risks from production, transportation, electrical hazards, toxic substances, unsafe equipment, organizational aspects, workers' skills, and workers' consciousness. Some significant factors contributing to occupational accidents include:

- Risks related to transportation operations.
- Risks associated with workers' skills.

These risks are considered significant due to various reasons:

- Increasingly deep mining operations create difficulties for production activities in general and transportation operations in particular. Additionally, the complex geological conditions pose challenges in mechanizing transportation activities and may result in potential occupational accidents.
- The growing complexity of mining operations, coupled with labor shortages and difficulties in labor recruitment, leads to limitations in providing comprehensive technical training to workers in mining enterprises, including the Company (limitations in training time, quality of trainees, etc.).

Workers acknowledge significant risks from toxic substances, dust, electrical hazards, and unsafe equipment as they are directly involved in production, making their perceptions and evaluations more accurate. Some high-level risks arise from transportation operations, toxic substances, and workers' skills that are not ensured.

Moreover, there are substantial risks related to workers' consciousness:

- Risks of compromising food safety and hygiene;
- Risks associated with inclement weather and adverse climates;
- Risks arising from workers' subjective behaviors;
- Hazards within furnaces, such as falling rocks, collapsing roofs, etc.;
- Risks resulting from reckless driving of vehicles (unsafe driving);
- Lapses in centralized control, lack of observation, and improper operation of equipment;
- Tripping or stumbling in workplaces, both inside and outside the mines (uneven, muddy terrain);
- Landslides and slippery conditions;
- Malfunctioning hydraulic columns.

DHC needs to identify and analyze these specific risks to implement measures aimed at reducing the risks to occupational health and safety.

One core factor contributing to these issues is the lack of self-discipline and awareness of labor safety among a significant number of personnel and workers within the Company. Alongside improvements in working conditions, some potential safety risks remain due to limitations in mining technologies, mining exploitation practices (XDY self-moving hydraulic beam), transportation technologies, rail transport, hoists, ramps, and the lack of synchronization in equipment standards. Issues related to mine drainage and ventilation also need further attention.

Moreover, technical management and occupational safety and environmental management still have significant limitations. The subjective organizational practices of workshop commanding officers and the consciousness of some workers contribute to numerous safety violations. The experience and capability of personnel are insufficient, and production organization remains less scientific. Supervision and construction management are not thorough and practical, and the dissemination of information has not been sufficiently deep to raise the self-discipline and safety consciousness of many personnel and workers, leading to numerous persisting problems.

From the perspective of a language translation expert, here's the translation of the paragraph into native English:

- The action solutions approach the perspective of the world: starting with technical solutions, then proposing organizational solutions, and finally focusing on solutions related to human factors.
- The solutions comply with and implement the national standards and regulations, and of the Vinacomin.

The implementation roadmap and organizational measures are depicted in the diagram as shown in Table 1.

4. Discussion and conclusion

The workforce is considered the most valuable 'asset' of any enterprise and plays a crucial role in constructing a safe working environment.

As a result, the topic proposes action programs focused on solutions to enhance production safety with the goal of reducing occupational accidents by 20-25% annually, while increasing productivity and benefits for both workers and the businesses.

The approach of the proposed solutions originates from technical measures, followed by organizational proposals, and ultimately concentrates on human-related measures, compli-

<table>
<tr><th>1st Period</th><th>2nd Period</th><th>3st Period</th><th>4st Period</th></tr>
<tr><td>Establishing a general vision for safety work in the company:
• Reduce the number of severe occupational accidents by 15% per year compared to 2020, reaching a reduction of 25% by 2023 compared to 2020.
• Increasing productivity and benefits for both workers and the company.
• (Combining the goal of increasing income for workers).</td><td></td><td></td><td></td></tr>
<tr><td colspan="3">Implementing technical solutions:
• Conducting research on selecting alternatives to the XDY self-moving hydraulic beam for 4 furnaces using the inclined cross-cutting technology with ZRY type flexible retaining supports.
Implementing organizational management solutions.
• Establishing rules for safe labor practices.</td><td></td></tr>
<tr><td colspan="4">Implementing organizational and labor management solutions (continuously implemented until the end of 2025)
• Forming a Learning Organization in DHC.
• Arranging workplaces rationally.
• Workers create safety plans for each month, quarter, and year.
• Regularly maintaining workplace cleanliness.
• Workers keep safety logs updated.
• Early detection of safety hazards.</td></tr>
<tr><td colspan="3">Investing in safety warning equipment.</td><td></td></tr>
<tr><td colspan="3">Reviewing the terms in contracts with contractors and adding clauses related to occupational safety and hygiene.</td><td></td></tr>
<tr><td colspan="3">Reviewing and updating safety regulations and policies
• Encouraging and motivating the labor force.
• Providing rewards and bonuses.
• Implementing disciplinary actions. Developing regulations and policies for instructors cum officials. Designing handbooks for workers on work procedures and first aid methods for accidents.</td><td></td></tr>
<tr><td colspan="3">Designing a handbook for workers providing instructions on work procedures and first aid methods for accident victims.</td><td></td></tr>
<tr><td></td><td>Establishing safety teams at various construction sites and workshops.</td><td></td><td></td></tr>
<tr><td colspan="4">Communication solutions (continuously implemented during the period until the end of 2025)
• Management officials establish a positive image, setting examples for colleagues and workers in ensuring occupational safety and hygiene.
• Management officials strengthen discussions with colleagues and workers on occupational safety and hygiene to exchange experiences, provide guidance, and understand the suggestions and innovations of workers.
• Promoting and disseminating safety culture through various flexible and continuously updated means.
• Changing posters, banners, and slogans related to safety every 6 months to increase the workers' attention and maintain effectiveness.
• Establishing exemplary models for occupational safety among minority ethnic workers.</td></tr>
<tr><td colspan="2"></td><td>Implementing the safety plan for each individual worker</td><td></td></tr>
<tr><td colspan="2"></td><td>Building a template system to collect, update, and serve risk analysis</td><td></td></tr>
<tr><td colspan="4">Setting role models of safety at various levels: leaders, workers, teams, especially among workers from minority ethnic groups (continuously throughout the period until the end of 2025).</td></tr>
<tr><td></td><td>Interlinking safety and income</td><td>Interlinking safety and income</td><td>Interlinking safety and income</td></tr>
<tr><td colspan="4">Safety implementation evaluation and assessment:</td></tr>
</table>

ance, and implementation of state regulations and those of the Vinacomin.

The solutions provided by the authors include:

- Technical measures involving technology and safe technical procedures.
- Organizational solutions for production, encompassing measures related to production operations, equipment, and processes.
- Management solutions, encompassing policies, educational campaigns, safety training, and a reward and disciplinary system for safety compliance.
- Worker-related solutions, comprising proposals for leadership teams at department and workshop levels, as well as solutions for workers themselves.
- The topic also outlines the timeline and measures to implement these groups of solutions.

Acknowledgments

The paper was presented during the 7th VIET-POL International Conference Scientific-Research Cooperation between Vietnam and Poland.

The authors are thankful to colleagues of the International Social Security Association – Prevention in Mining, the Mining Management Department of HUMG and miners of DHC for their supports and cooperation.

Literatura – References

1. Bahn, S. (2013). Workplace hazard identification and management: The case of an underground mining operation. Safety Science, 57, 129–137. https://doi.org/10.1016/j.ssci.2013.01.010
2. Beus, J. M., McCord, M. A., & Zohar, D. (2016). Workplace safety: A review and research synthesis. Organizational Psychology Review, 6(4), 352–381. https://doi.org/10.1177/2041386615626243
3. Burke, M. J., & Signal, S. M. (2010). Workplace safety: A multilevel, interdisciplinary perspective. Research in Personnel and Human Resources Management, 29, 1–47. https://doi.org/10.1108/S0742-7301(2010)0000029003
4. Colligan, M. J., & Cohen, A. (2009). The role of training in promoting workplace safety and health. The Psychology of Workplace Safety., 223–248. https://doi.org/10.1037/10662-011
5. Dodoo, J. E., Surienty, L., & Al-Samarraie, H. (2023). The influence of learning-oriented leadership for promoting future-directed workplace safety in the mining industry. Safety Science, 159, 106010. https://doi.org/10.1016/J.SSCI.2022.106010
6. He, X., & Song, L. (2012). Status and future tasks of coal mining safety in China. Safety Science, 50(4), 894–898. https://doi.org/10.1016/j.ssci.2011.08.012
7. Hine, D. W., Lewko, J., & Blanco, J. (1999). Alignment to Workplace Safety Principles: An Application to Mining. In Journal of Safety Research (Vol. 30, Issue 3).
8. Jiskani, I. M., Cai, Q., Zhou, W., Chang, Z., Chalgri, S. R., Manda, E., & Lu, X. (2020). Distinctive Model of Mine Safety for Sustainable Mining in Pakistan. Mining, Metallurgy and Exploration, 37(4), 1023–1037. https://doi.org/10.1007/s42461-020-00207-8
9. Lewis-Beck, M. S., & Alford, J. R. (1980). Can Government Regulate Safety? The Coal Mine Example. In Source: The American Political Science Review (Vol. 74, Issue 3).
10. Lu, Y., Taksa, L., & Jia, H. (2020). Influence of management practices on safety performance: The case of mining sector in China. Safety Science, 132. https://doi.org/10.1016/j.ssci.2020.104947
11. Mcafee, R. B., & Winn, A. R. (1989). The Use of Incentives/Feedback to Enhance Work Place Safety: A Critique of the Literature. In lotrrnal of saf~ry Rrrearch (Vol. 20).
12. Nguyen, N., Meesmann, U., Truong, N. L., & Trinh, V. H. (2021). VISION ZERO – Tools for Safety, Health, and Well-being Management and the Application in the Vietnamese Coal Mining Industry. Inzynieria Mineralna, 1(2), 365–372. https://doi.org/10.29227/IM-2021-02-33
13. Opoku, F. K., Kosi, I., & Degraft-Arthur, D. (2020). Enhancing Workplace Safety Culture in the Mining Industry in Ghana. Ghana Journal of Development Studies, 17(2), 23–48. https://doi.org/10.4314/gjds.v17i2.2
14. Rivas, T., Paz, M., Martín, J. E., Matías, J. M., García, J. F., & Taboada, J. (2011). Explaining and predicting workplace accidents using data-mining techniques. Reliability Engineering and System Safety, 96(7), 739–747. https://doi.org/10.1016/j.ress.2011.03.006
15. Tetzlaff, E. J., Goggins, K. A., Pegoraro, A. L., Dorman, S. C., Pakalnis, V., & Eger, T. R. (2021). Safety Culture: A Retrospective Analysis of Occupational Health and Safety Mining Reports. Safety and Health at Work, 12(2), 201–208. https://doi.org/10.1016/j.shaw.2020.12.001

Research on Electric Leakage Protection to Improve Electrical Safety in Underground Mining in Vietnam

*NGUYEN Truong Giang[1)], NGUYEN Thac Khanh[1)], NGO Xuan Cuong[2)], DO Nhu Y[1)]**

[1)] Hanoi University of Mining and Geology, Hanoi, Vietnam
[2)] School of Engineering and Technology, Hue University, Thua Thien Hue, Vietnam
* Corresponding author: donhuy@humg.edu.vn

http://doi.org/10.29227/IM-2023-02-32

Submission date: 15-08-2023 | Review date: 14-09-2023

Abstract

To ensure safety in underground mining, it is imperative to equip yourself with electric leakage protection. Today, underground mines are gaining a high degree of mechanization and using more power electronics to enhance the operation and organization of power supplies, including the application of power electronics for DC power transmission in mining. i.e., separate the rectifier (AC-DC) from the inverter (DC-AC) with a long DC cable. The transmission of DC power changes the structure of the mine power network; then there will appear a power network with an industrial frequency of 50 Hz, a DC power network, and a power network after the variable frequency inverter. Due to the mutual interaction between DC power networks and AC power networks, leakage protection devices are unreliable, causing unsafe conditions in mining. The content of the article is to determine the leakage current in the power network when using converters in DC power transmission in mining. The research results are the basis for calculating and selecting leakage protection equipment for the purpose of improving safety in underground mining in Vietnam.

Keywords: *electrical safety, conversion devices, mine power network, leakage protection*

1. Introduction

Underground mining in Vietnam has a harsh environment, such as 100% humidity, a high risk of fire, and tight spaces, leading to a risk of electrical safety for operators. According to Vietnam's regulations on safety in mining, it is mandatory that the electrical network be an isolated neutral network, and it is mandatory to equip the leakage protection relay [1].

Today, underground mines are gradually putting mechanized complexes to use to replace human power. With the increasing degree of mechanization, power electronic converters are gradually being used at all stages of underground mining. They are responsible for regulating the working process of the motor or improving the power quality of the mine power network [2–4].

The use of power electronics for motor drive systems creates harmonics in the mine power network [5–7]. Harmonics generated from power electronic devices confuse leakage protection relays and cause power loss in mine electrical network [8–10]. In order to minimize the influence of power electronic devices and improve the reliability of leakage protection in the underground mine power network, the solution to eliminating harmonics is mentioned in many works [11–13]. However, the use of harmonic filtering equipment increases the costs incurred, increasing the loss of the power network [14, 15].

To reduce power loss and avoid unwanted high-frequency phenomena, power electronics with DC power transmission are used in mining, i.e., separating the AC-DC rectifier from the DC-AC inverter with a DC cable. This solution brings a lot of economic efficiency and reduces the unwanted consequences caused by inverters in mining [15, 16].

Thus, the solution of using power electronics to transmit DC power in mining brings many benefits. However, due to the correlation between the currents in the networks of different frequencies, it causes the unreliable operation of the leakage protection device, causing unsafety in underground mining [19, 20]. In the harsh environmental conditions of underground mines in Vietnam, it is necessary to research solutions to ensure electrical safety in underground mines using power electronic converters to transmit DC power. The content of the article is to build a model to calculate leakage current in an electrical network containing converters to transmit DC power, thereby improving electrical safety in underground mining in Vietnam.

2. Determination of leakage currents in mine power networks using DC power transmission

2.1. Model of underground mine power network with DC power transmission

The underground mine power network using power electronic converters to transmit DC power has a diagram as shown in Figure 1 [14–16].

In which the AC power source V-AC (f=50Hz) is supplied by the regional distribution transformer, through the rectifier, DC power is supplied to the equipment using DC power, and through the inverter, the AC voltage with adjustable frequency is supplied to the working AC motors. For simplicity, it is possible to assume that the network has centralized parameters, ignoring the reactance of transformers and cables and not taking into account the insulation resistance between the phases of the network. The equivalent diagram for the underground mine power network using semiconductor converters is shown in Figure 2 [19].

In equivalent diagram: R_A, R_B, R_C, C_A, C_B, C_C – insulation resistance and phase-to-ground capacitance of the network before the inverter (BI); R_{Af}, R_{Bf}, R_{Cf}, C_{Af}, C_{Bf}, C_{Cf} – insulation resistance and phase-to-ground capacitance of the inverter (AI);

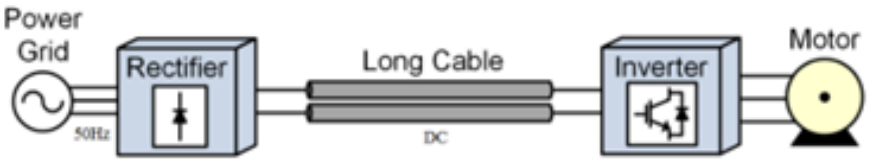

Fig. 1. Underground mine power network using power electronic converters to transmit DC power

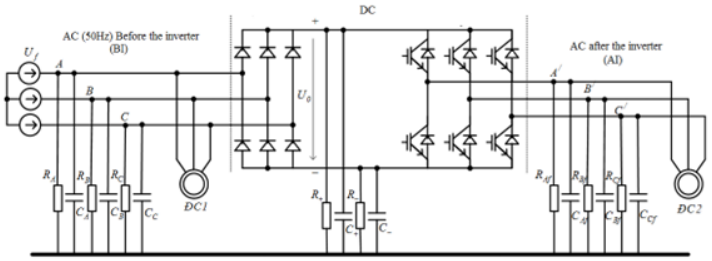

Fig. 2. Equivalent diagram for the underground mine power network using semiconductor converters

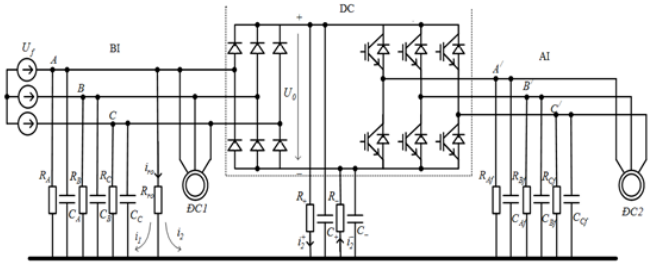

Fig. 3. Diagram of calculating leakage current with case of leakage in the power network BI

R_+, R_-, C_+, C_- – insulation resistance and capacitance between the anode (+) and cathode (-) of the DC network part relative to earth; U_f – secondary winding phase voltage of area transformer; U_0 – average value of three-phase bridge rectifier voltage.

2.2. Leakage current in the power network before the inverter (BI)

In case of electric leakage in the power network BI (power network with industrial frequency), the calculation diagram has the form as shown in Figure 3. In which, R_{ro} is the single-phase leakage resistance, when there is a single-phase leakage, i_{ro} – leakage current through the leakage resistor will consist of two components: The AC component i1 caused by the insulation resistance and capacitance of the AC network part BI and the DC component i_2 has a value depending on the asymmetry of the insulation resistance of the part of the DC network.

The RMS value of the AC component is determined by the formula:

$$I_1 = U_f \frac{\sqrt{R^2 + X_C^2}}{\sqrt{R^2 R_{ro}^2 + X_C^2 (R + R_{ro})^2}} \tag{1}$$

where: R, X_C – resistance and reactance total three-phase insulation of part BI to earth; U_f – network phase voltage.

In the case of ignoring the influence of the insulation impedance of the AI part, the current generated by positive and negative 3 phase half wave rectifier is calculated as follows:

$$I_2^- = \frac{1{,}17 U_f}{R_{ro}(R + R_-) + R R_-} R \tag{2}$$

$$I_2^+ = \frac{1{,}17 U_f}{R_{ro}(R + R_+) + R R_+} R \tag{3}$$

The DC current component i_2 is determined:

$$i_2 = I_2 = I_2^- - I_2^+ = 1{,}17 U_f \left(\frac{1}{R_{ro}(R + R_-) + R R_-} - \frac{1}{R_{ro}(R + R_+) + R R_+} \right) R \tag{4}$$

The RMS value of leakage current in case of leakage in part BI according to expression:

$$I_{ro} = \sqrt{I_1^2 + I_2^2} = U_f \sqrt{\frac{R^2 + X_C^2}{R^2 R_{ro}^2 + X_C^2 (R + R_{ro})^2} + \frac{}{+ 1{,}17^2 R^2 \left[\frac{1}{R_{ro}(R + R_-) + R R_-} - \frac{1}{R_{ro}(R + R_+) + R R_+} \right]^2}} \tag{5}$$

From expression (5), it can be seen that the external leakage current depends on the resistance and reactance of the network (BI) also depends on the insulation resistance of the DC-side electrical network. When the DC power network is symmetrical ($R_+ = R_-$), then the leakage current only has an ac component, when the network loses symmetry ($R_+ \neq R_-$), the leakage current in the network increases by an amount i_2.

2.3. Leakage current in DC power network

2.3.1. Case of electric leakage from the negative terminal of the DC power network

In case of electric leakage from the negative terminal of the DC power network leakage current also has two components: The current i1 is caused by the insulation resistance of the power network BI and the current i_2 is caused by the insulation resistance of the positive terminal of the DC power network (R_+), the calculation diagram is as shown in Figure 4.

The leakage current component i_1 is the rectifier current due to the negative 3 phase half wave rectifier compared to the

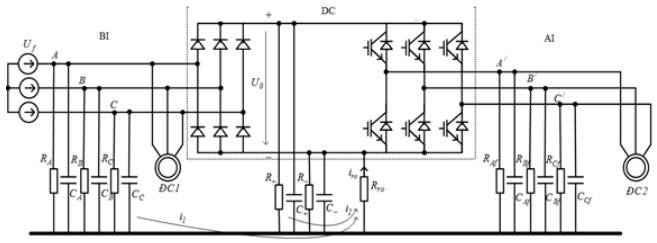

Fig. 4. Diagram of calculating leakage current with case of leakage from the negative terminal of the DC power network

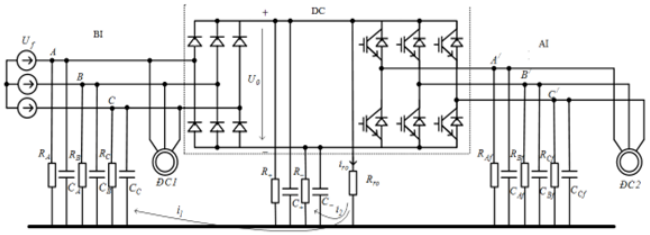

Fig. 5. Diagram of calculating leakage current with case of leakage from the positive terminal of the DC power network

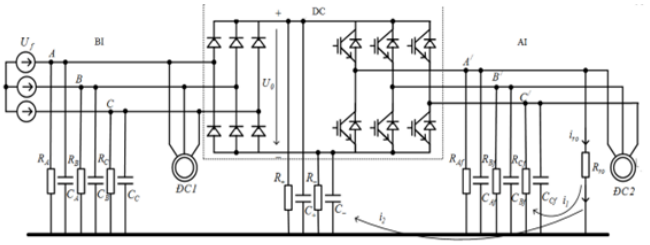

Fig. 6. Diagram of calculating leakage current with case of leakage in the power network AI

ground and the average value is determined according to the following expression:

$$I_1 = \frac{1{,}17U_f}{R_{ro}(R + R_-) + RR_-} R_- \tag{6}$$

The leakage current component i_2 is the DC current caused by the negative polarity voltage of the DC power source relative to the ground and the average value is determined by the following expression:

$$I_2 = \frac{U^-}{R_{ro}} = \frac{2{,}34U_f}{R_{ro}(R_+ + R_-) + R_+R_-} R_- \tag{7}$$

The leakage current in case of leakage from the negative terminal of the DC power network is determined by the following equation:

$$I_{ro} = I_1 + I_2 = U_f\left(\frac{1{,}17}{R_{ro}(R + R_-) + RR_-} + \frac{2{,}34}{R_{ro}(R_+ + R_-) + R_+R_-}\right) R_- \tag{8}$$

2.3.2. Case of electric leakage from the positive terminal of the DC power network

In case of electric leakage from the positive terminal of the DC power network leakage current also has two components: The current i_1 is caused by the insulation resistance of the power network BI and the current i_2 is caused by the insulation resistance of the negative terminal of the DC power network (R), the calculation diagram is as shown in Figure 5.

Similar to the case in Section 2.3.1, the leakage current in case of leakage from the positive terminal of the DC power network is determined by the following formula:

$$I_{ro} = I_1 + I_2 = U_f\left(\frac{1{,}17}{R_{ro}(R + R_+) + RR_+} + \frac{2{,}34}{R_{ro}(R_+ + R_-) + R_+R_-}\right) R_+ \tag{9}$$

From expression (8) and (9), it can be seen that, in the case of leakage in the DC power network, the leakage current depends on the resistances R+, R- of the DC power network and also on the resistance R of the BI power network.

2.3. Leakage current in the network after the inverter (AI)

In case of electric leakage in the power network AI (variable frequency AC power network), the calculation diagram has the form as shown in Figure 6. In this case, the leakage current consists of two components: the AC component i'_1 caused by the insulation impedance of the AI part and the DC component i'_2 caused by the insulation impedance of the DC part.

The AC current component is determined by the formula:

$$I_1^{/} = U_f^{/} \frac{\sqrt{R_f^2 + X_{Cf}^2}}{\sqrt{R_f^2 R_{ro}^2 + X_{Cf}^2 (R_f + R_{ro})^2}} \tag{10}$$

where R_f, X_{Cf} is the total resistance and reactance of the three-phase insulation of the AI part relative to earth; $U_f^{/}$ is the phase voltage of the power network AI.

DC current component is determined by the expression

$$I_2^{/} = \frac{2{,}34U_f}{R_-R_+R_f + R_-R_+R_{ro} + R_-R_fR_{ro} + R_+R_fR_{ro}} R_+R_f \tag{11}$$

The leakage current in case of leakage in the power network AI is determined by the following formula:

$$I_{ro} = \sqrt{I_1^{/2} + I_2^{/2}} = \sqrt{\frac{U_f^{/2}(R_f^2 + X_{Cf}^2)}{R_f^2 R_{ro}^2 + X_{Cf}^2 (R_f + R_{ro})^2} + \frac{2{,}34^2 U_f^2 R_+^2 R_f^2}{(R_-R_+R_f + R_-R_+R_{ro} + R_-R_fR_{ro} + R_+R_fR_{ro})^2}} \tag{12}$$

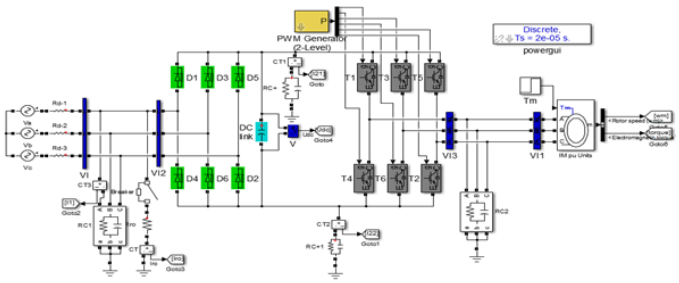

Fig. 7. Simulation model of mine power transmission network DC

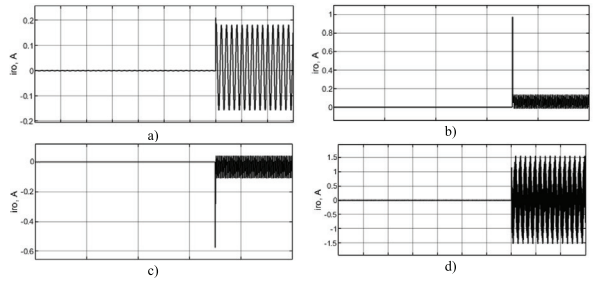

Fig. 10. Leakage current value in higher asymmetry of the DC power network insulation. a – Case of electric leakage before the inverter; b – Case of electric leakage in positive DC terminal; c – Case of electric leakage in negative DC terminal; d – Case of electric leakage after the inverter

From formula (12) it is found that, in this case, the leakage current depends on the parameters of the electrical network after the inverter and also on the resistances R_+, and R_- of the DC network.

3. Research results and discussion

3.1. Simulation modeling of leakage currents in the underground mine power network

Modeling on Matlab – simulink software is presented in Figure 7, with underground mine power network parameters suitable for mining in Vietnam: U=1140V, C=0,19uF/ phase; R=168kΩ/ phase; leakage resistance R_{ro}=1kΩ. Conduct a survey of leakage currents in the case of a DC network with symmetrical insulation $R_+ = R_- = 300k\Omega$, and in the case of a DC network with reduced insulation in the negative circuit (R_- =150 kΩ và 50 kΩ).

3.2. Case of electric leakage with symmetrical DC network insulation

The study conducts survey of electric leakage model with symmetrical DC network insulation resistance value $R_{d+}=R_{d-}$ =300kΩ. The analysis results of leakage current in the case BI, AI and in the DC power network are shown in Figure 8.

From the results in Figure 8a, it can be seen that with the same leakage resistance value, leakage current in the network AI is the highest, near 0.6A, leakage current in DC power network is the lowest about 0.08A, leakage current in the power network BI is 0.11A.

With symmetric DC network insulation, the AC component leakage current in the power network BI tends to decrease, in the DC power network and in the power network AI tends to increase (Figure 8b). Leakage current components to the positive and negative DC terminal in case of leakage in the power network BI and AI appears the process of oscillation before reaching the steady state (Figures 8c, 8d).

3.3. Case of electric leakage with asymmetrical DC network insulation

Assume that the DC network resistance on the negative DC terminal has an insulation loss corresponding to the values R_-=150kΩ, 50kΩ. Leakage survey at the positions before the inverter (BI), after the inverter (AI) and the DC network gives the results as shown in Figure 9.

From the research results in Figure 9 it can be seen that, when the DC network has reduced insulation (300kΩ, 150kΩ, 50kΩ) leakage current increases as insulation R- decreases in cases of electric leakage before the inverter, in positive DC terminal and after the inverter (hình 9a, b, d). However, the growth rate of leakage current is highest in the case of electric leakage in positive DC terminal, followed by in case of electric leakage before the inverter, and almost unchanged in the case of electric leakage after the inverter. Leakage current decreases as the insulation resistance decreases in case of electric leakage in negative DC terminal, this is because part of the leakage current value has passed through the insulation R_- itself (figure 9c).

The result of Figure 9 shows that the larger asymmetry of the DC power network insulation, the greater the change in leakage current. The investigation of the leakage current value in higher asymmetry of the DC power network insulation is shown in figure 10.

The results shown in Figure 10 indicate that, at the time of leakage t = 0.7s, the leakage current at any position in the network will fluctuate before reaching steady state. However, the amplitude of oscillation in the DC network is the largest and the oscillation time is the longest. In addition, the leakage current on the AC power network BI can cause unreliable operation of the leakage protection relay when leakage occurs on the power network AI and DC power network.

4. Conclusions

To ensure safety in underground mining, where there is a harsh environment, it is imperative to equip electric leakage protection. Today, underground mines are increasing their level of mechanization by using a variety of power electronics to enhance the operation and organization of their power supplies. The use of converters for DC power transmission in underground mining will be a trend in the following years when

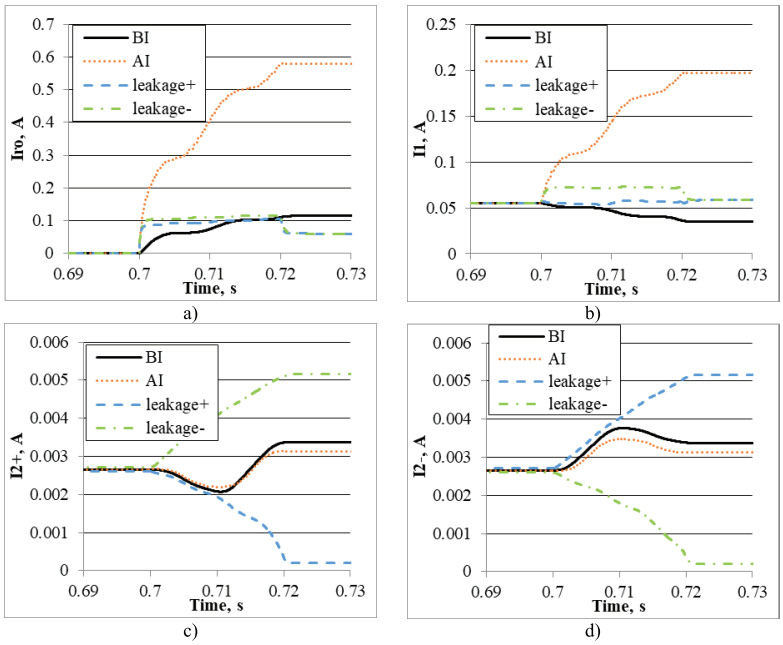

Fig. 8. Leakage current with symmetrical DC network insulation resistance value. a – Leakage current through leakage resistor; b – Leakage current through AC component; c – leakage current to the positive DC terminal; d – leakage current to the negative DC terminal

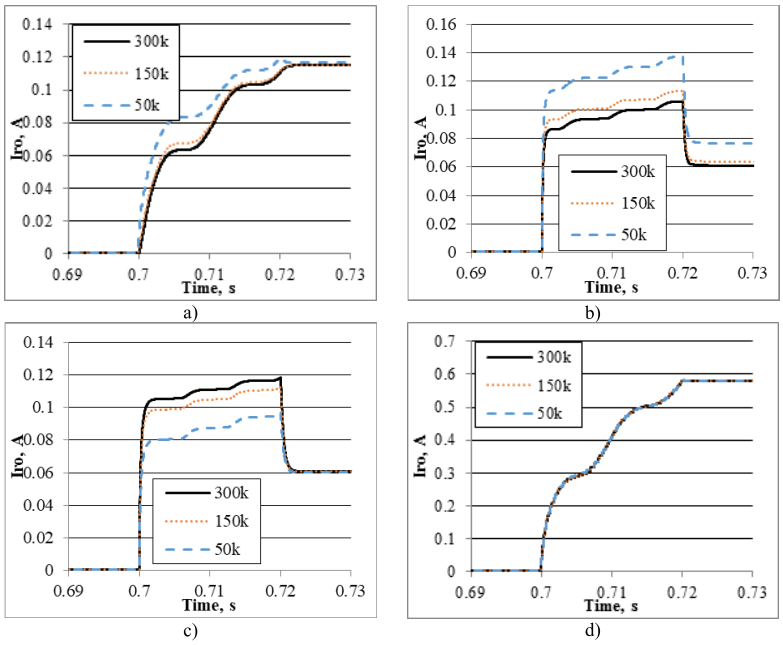

Fig. 9. Leakage current with asymmetrical DC network insulation resistance value. a – Case of electric leakage before the inverter; b – Case of electric leakage in positive DC terminal; c – Case of electric leakage in negative DC terminal; d – Case of electric leakage after the inverter

the mine capacity is increasing and the mining depth is large.

However, the use of DC power transmission will affect leakage protection in mining. Research results show that changing the parameter of the DC network will greatly affect the leakage current value not only in the DC power network but also in the AC network before and after the inverter. This causes the unreliable operation of the leakage protection device in this DC transmission network.

Research results in the article have built the dependent relationship between leakage current and network parameters for underground mine power networks with DC power transmission. The dependency relationship has been verified on the Matlab-Simulink simulation model. Research results are the basis for calculating and selecting leakage protection equipment for the purpose of improving safety in underground mining in Vietnam.

Literatura – References

1. Nguyen, K. T., Kim, L. N., Nguyen, S. T., & Nguyen, G. T. (2020). Research, design, manufacture leakage current protection device for 660 V/1140 V underground mine electrical networks. Journal of Mining and Earth Sciences, 61(5), 96-103.
2. Yaghoobi, J., Abdullah, A., Kumar, D., Zare, F., & Soltani, H. (2019). Power quality issues of distorted and weak distribution networks in mining industry: A review. IEEE Access, 7, 162500-162518.
3. Luiz, A. S. A., & de Jesus Cardoso Filho, B. (2015, October). Improving power quality in mining industries with a three-level active front end. In 2015 IEEE Industry Applications Society Annual Meeting (pp. 1-9). IEEE.
4. Ngo, X. C., & Do, N. Y. (2021). Influence of Harmonics on the Working Efficiency of a 6/1.2 kV Transformer in a Pit Mine. Inżynieria Mineralna, (2).
5. Drabek, P., Fort, J., & Pittermann, M. (2011). Negative Influence of Frequency Converters on Power Distribution Network. Advances in Electrical and Electronic Engineering, 5(1), 72-75.
6. Do, N. Y., & Ngo, X. C. (2022, December). Effect of harmonic components and load carrying factor on the operating mode of induction motor. In AIP Conference Proceedings (Vol. 2534, No. 1). AIP Publishing.
7. Jahromi, M. G., Mirzaeva, G., & Mitchell, S. D. (2017). Design and control of a high-power low-loss DC–DC converter for mining applications. IEEE Transactions on Industry Applications, 53(5), 5105-5114.
8. Cocina, V., Colella, P., Pons, E., Tommasini, R., & Palamara, F. (2016, June). Indirect contacts protection for multi-frequency currents ground faults. In 2016 IEEE 16th International Conference on Environment and Electrical Engineering (EEEIC) (pp. 1-5). IEEE.
9. Do Nhu, Y., & Cuong, N. X. (2022). Impact of Voltage Unbalance and Harmonics on Induction Motor in Operation Mode. In Advances in Engineering Research and Application: Proceedings of the International Conference on Engineering Research and Applications, ICERA 2021 (pp. 468-478). Springer International Publishing.
10. Czapp, S. (2010, June). The effect of PWM frequency on the effectiveness of protection against electric shock using residual current devices. In 2010 International School on Nonsinusoidal Currents and Compensation (pp. 96-100). IEEE.
11. Luiz, A. S. A., & de Jesus Cardoso Filho, B. (2017, March). A new design of selective harmonic elimination for adjustable speed operation of AC motors in mining industry. In 2017 IEEE Applied Power Electronics Conference and Exposition (APEC) (pp. 607-614). IEEE.
12. Do, N. Y., & Ngo, X. C. (2022, December). Effect of harmonic components and load carrying factor on the operating mode of induction motor. In AIP Conference Proceedings (Vol. 2534, No. 1). AIP Publishing.
13. Marek, A. D. A. M. (2017). Influence of indirect frequency converters on operation of central leakage protection in underground coalmine networks. Mining–Informatics, Automation and Electrical Engineering, 55(3), 9-14.
14. de Castro Júnior, J. A., de Paula, H., Cardoso Filho, B. J., & Rocha, A. V. (2012). Rectifier-to-Inverter Connection Through Long DC Cable—Part II: The Complete Copper Economy Characterization. IEEE TRANSACTIONS ON INDUSTRY APPLICATIONS, 48(1), 229.
15. De Castro, J. A., De Paula, H., & Cardoso Filho, B. J. (2009, November). Avoiding undesirable high-frequency phenomena in long cable drives: Rectifier-to-inverter connection through long dc cable—part i: Evaluation of the losses reduction and copper economy. In 2009 35th Annual Conference of IEEE Industrial Electronics (pp. 1045-1050). IEEE
16. de Paula, V. C., & de Paula, H. (2015, October). Employing DC transmission in long distance AC motor drives: Analysis of the copper economy and power losses reduction in mining facilities. In 2015 IEEE Industry Applications Society Annual Meeting (pp. 1-7). IEEE.
17. Бабокин, Г. И., Куницкий, В. Г., & Шеленев, П. И. (2010). Защита от токов утечки в комбинированных электрических сетях с ШИМ-преобразователем частоты. Известия Тульского государственного университета. Технические науки, (1), 132-137.
18. Marek, A. (2016). Analiza przydatności wybranych zabezpieczeń upływowych w dołowych sieciach z przemiennikami. Konferencja EMTECH, 64-72.
19. Петриченко А. А. (2017), Методы и средства граничения тока утечки на землю в системах электроснабжения железорудных шахт, Диссертация на соискание учёной степени кандидата технических наук, Кривой Рог – 2017
20. Tim Wylie, (2017). Mining Earth Leakage Protection with Variable Speed Drives. Available from: https://www.ampcontrolgroup.com/wp-content/uploads/2017/05/Mining-Earth-Leakage-Protection-With-Variable-Speed-Drives.pdf.

Investigation of Marine Sediments with a Sub-bottom Profilers System in West Coast of Camau, Vietnam

DUNG NGUYEN Quang[1)], GIANG NGUYEN Van[2)], THANH LE Ngoc[3)]

[1)] Institute of Geography and Resource in HCM city, 1 Mac Dinh Chi, distr. 1 HCM city, Vietnam http://www.resourcesgeography.ac.vn; ORCID 0009-0002-9232-5947

[2)] Binh Duong University, 504 Binh Duong Ave. Thu Dau Mot city, BinhDuong province, Vietnam, https://www.bdu.edu.vn; email: nvgiang.hdkh@bdu.edu.vn; ORCID 0000-0003-4477-430X

[3)] Institute of Geography and Resource in HCM city, 1 Mac Dinh Chi, distr. 1 HCM city, Vietnam http://www.resourcesgeography.ac.vn; ORCID 0009-0006-1685-915

* Corresponding author: Giang Nguyen Van, nvgiang.hdkh@bdu.edu.vn

http://doi.org/10.29227/IM-2023-02-33

Submission date: 14-08-2023 | Review date: 22-09-2023

Abstract

The west coast of Camau (Southeast Vietnam) connects two semi-enclosed East Sea and Thailand Bays, allowing water exchange between them. Despite its importance to the oceanographic evolution of the region, it has still been poorly studied. Therefore, Sub-bottom profilers are used across shallow sea waters with some applications, such as sea-level studies, sedimentation process and geomorphology. In the whole survey area, 6 high-resolution shallow seismic measurements have been performed with a total length of 60.6 km, and all have recorded good reflected signals in the range 20–70 ms. In this section, physical characteristics and nature of petrology in the survey environment are quite uniformly shown. The topography of the seabed in the survey area tends to be gradually shallower from west to east, and is relatively flat. Particularly, on the cross section of the T1 line, it is visible that the first section of the line has a rather steep and deep terrain, which may be the slope of the continental shelf in the survey area. Wedge-shaped, oblique, corrugated and transverse structures all appear on the cross-sections. In the survey area, the shallow geological structure in the Holocene sediments is divided into 4 layers, and the structural boundary between the Holocene and Pleistocene sediments at the depth of 25–35 m is observed. In addition, geological faults are also detected on geological sections from seismic sections. For instance, at the section of T6 line, two faults were detected at the beginning of the line. The displacement amplitude of these faults ranges between 1.5–4 m. This new dataset will contribute to future comprehension of the geologic and oceanographic evolution.

Keywords: *west coast of Camau, high-resolution shallow seismic, sub-bottom profiler, cross-section, Holocene-Pleistocene sediments*

Introduction

Coastal areas of Camau province have a special place in Vietnam's marine economic development strategy. By 254 km of coastline, enveloping Camau peninsula, adjacent to both the East and West Seas (Gulf of Thailand), the sea, coastal areas and island clusters in Camau province have a particularly important position in terms of national security and economic development of the country. In particular, the west coast of Camau province has an international biosphere reserve, including beach ecological areas, Camau mangrove forests, Camau flooded areas, Gulf of Thailand, protective forests coastal west Camau. Up to now, the coastal area along the west Camau sea area has not been studied in detail (Dung et al., 2013). Some of the meager research results have been published only on the surface of the geography, sea bottom shape, flow, waves and wind are the main (Lap et al., 2000). The study in detail of the geological structure of the coastal floor of Camau western province is an urgent requirement, especially for the planning of development of coastal construction works in Camau.

Among geophysical methods to survey the geological structure of the shallow waters, we have chosen a high-resolution seismic method that is the most appropriate one for the survey and determination of the shallow geological structure in this area. The main advantage of this method is compact and lightweight device system, allowing detailed determination of geological structure sections with high accuracy (Alves et al., 2020; Amri, 2019; Aquino da Silva et al., 2016). However, because of single-channel registration, this method has limitations in anti-interference ability, especially in areas with complex geological structures (Lurton, 2002). Therefore, research to improve the effectiveness of their application is very necessary. This method is often used to study the shallow geological structure in the sea with a depth of several hundred meters (Grelowska et al., 2010; Saleh and Rabah, 2016). The research object of shallow geology and geophysics are mainly geological formations located in the upper part of the geological profiles, interesting for mineral prospecting and engineering geology (Kadima et al., 2011; Kozaczka et al., 2013). High-resolution shallow seismic equipment systems continuously emit and record reflected waves in the high frequency range of a few hundred to several thousand Hz, achieving horizontal resolutions of 3-5 m and vertical resolutions of 0.5-1m (Amri, 2019; Angulo et al., 2006; Aquino da Silva et al., 2016; Grelowska, 2010; Saleh, 2016; Wang et al., 2019). Because, the main objective of the study of the shallow sea area west of Camau was to determine the shallow geological structure for this coastal area limited to the Holocene sedimentary layer, and the Holocene-Pleistocene boundary, we utilised the system of Sub-bottom profilers. In recent decades,

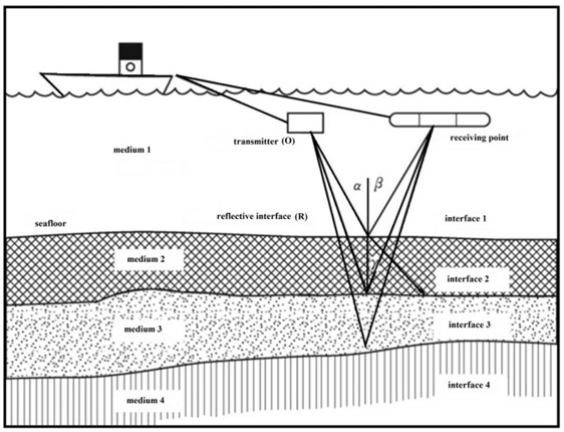

Fig. 1. Geometric kinematic model of acoustic signal for sub-bottom profiler detection (Modified of Ding et al., 2021)

Sub-bottom profiler has been widely used in underwater terrain measuring, hidden structure exploration, buried objects searching (Alves et al., 2020; LeBlanc, 1992; Ding et al., 2021). Beside the structure information in the data collected by profiler, the property of bottom sediment in shallow water also can be found out by inversion process. Therefore, our research area is limited to the west coast of Camau province with geographical coordinates as follows: 8° 38' 42.61" - 9° 31' 38.27" N and 104° 29' 52.72" - 104° 50' 3.14" E.

Methodology and equipment

High resolution shallow seismic method

Seismic waves

An underwater source of sound waves generates elastic waves that propagate with velocities depending on the elastic properies of the medium. Liquids do not react to shear waves (S-waves), so they cannot propagate in a liquid medium. Therefore, in marine surveys, it is only necessary to pay attention to the compression wave component (P-wave). Continuously reflected seismic signal is highly effective in the aquatic environment, because water is very effective in transmitting acoustic energy from the source to the layers of material below the seabed. Also, signal is of lower noise level, because is not affected by S wave part. The average speed of sound waves in seawater ranges 1.46 - 1.56 km/s depending on ambient temperature, salinity and pressure (depth). In the interpretation of seismic lines, the average value of wave propagation speed in the water layer is usually assumed to be equal to 1.5 km/s (Aquino da Silva et al., 2016; LeBlanc et al.,1992; Grelowska and Kozaczka, 2014).

The signal emitted from an acoustic source covers a range of different frequencies. To simplify the application of the discussed method, one often uses the concept of dominant frequency, which is the most common frequency or contains the maximum energy. The frequency of an acoustic signal (f) is related to the wavelength (λ) and the velocity (v) of the acoustic wave according to the formula (Lurton, 2002):

$$\lambda = v/f \quad (1)$$

The dominant frequency of the sound wave source depends on the different types of equipment, ranging from 3.5 kHz to about a few hundred kHz. From formula (1), it can be seen that with the same wave propagation speed in the material medium, the higher the frequency of the emitted signal is, the smaller is the wavelength, which means the higher resolution of the received signal.

When sound waves propagate in the wave propagation medium, energy attenuation will occur. There are three main mechanisms of this attenuation: (1) geometric attenuation, (2) energy absorption and frequency attenuation and (3) reflection and reverberation (Lurton, 2002). There are two types of repeaters, short repeaters and long repeaters. Short repeats arrive earlier than the main reflected wave and significantly reduce the original pulse or signal length, while long repeats represent a later arrival time (Kadima, 2011).

The phenomenon known as empty acoustic zones shows up on some shallow seismic tapes, especially in the coastal bays, where the reflections disappear suddenly beneath an almost horizontal layer in the bass column sediment. Because some types of sediments exhibit properties of absorbing or perturbing acoustic energy thereby both limiting energy penetration to deeper layers and impeding signals reflected upward from those strata (Grelowska and Kozaczka, 2010a).

Sub-bottom profiler system equipment

The principle of sub-bottom profiler detection is similar to that of multi-channel reflection seismic exploration. First, a longitudinal acoustic wave is excited artificially, which during propagation can generate a reflection echo at the lithological interface of a formation. The reflected signal is received and stored by an acoustic transducer or a single receiving cable, and then the structure and shape of the submarine formation can be displayed in real time (3200-xs sub-bottom system user hardware manual, 2005). As shown in Figure 1, acoustic signals excited from transmitter O propagate in seawater and submarine sedimentary strata. As different lithological strata are encountered, in accordance with the principles of the geometry of seismic reflection, the incident wave generates α, reflection wave at angle β, that is equal to incident angle α at the interface. The transmission angle γ, is determined by the sound wave propagation velocity of the upper and lower layers at the interface. If the sound wave propagation velocity of medium 2 below the seafloor interface is greater than that of medium 1 above the interface, transmission angle γ is greater than incident angle α, and vice versa. This case is only true when the distance between the receiver and the transmitter is large enough. In the case of only one channel as shown in Figure 1, it should be noted, because it may not be appropriate.

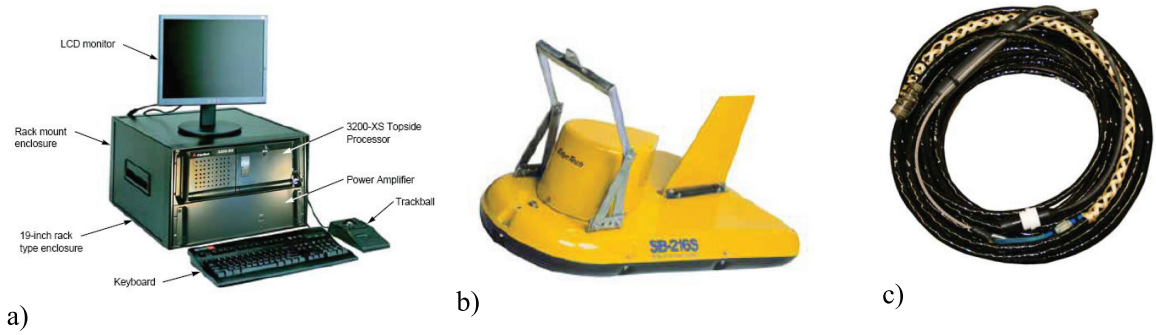

Fig. 2. Components of the Sub-bottom profiler measuring instrument system: a) 3200-XS Processing System, b) Towing device SB-216S, c) Kevlar Reinforced Tow Cable

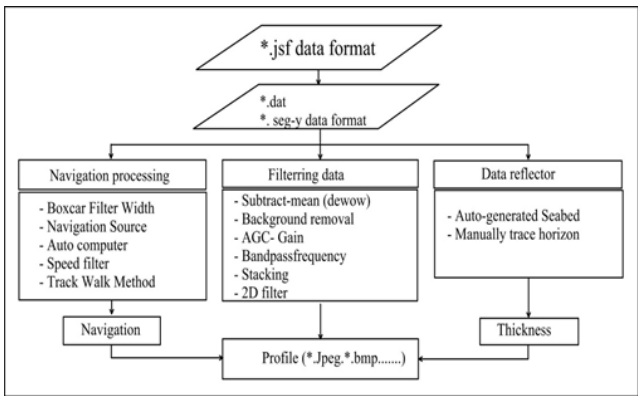

Fig. 3. Flow-chart of Sub-bottom profiler data processing

As the transmitted wave continues to propagate downward, new reflected and transmitted waves continue to be generated at subsequent acoustic impedance interfaces until the energy of the transmitted wave is too small to generate a reflected echo of effective energy. To form a strong reflective echo at an interface, there must be an obvious difference in the acoustic impedance condition at that interface.

The reflection coefficient, R can be expressed as follows (LeBlanc L.R. et al.,1992):

$$R = \frac{Z_2 - Z_1}{Z_2 + Z_1} = \frac{q_2 v_2 - q_1 v_1}{q_2 v_2 + q_1 v_1} \neq 0 \quad (2)$$

where q and v are the density of the sedimentary strata and the propagation velocity of sound waves within the strata, respectively, and their product is called wave impedance. Subscripts 1 and 2 denote the strata above and below the interface, respectively (Figure 1). According to the above equation, the condition that means the reflection interface can form a reflection echo is that q2v2 is not equal to q1v1; the greater is the difference between q2v2 and q1v1, the stronger is the reflection echo energy. The greater is the amplitude of the reflection signal received by the transducer, the greater is the "gray value" of the acoustic reflection in-phase axis displayed by the recording section and the clearer the reflection strata interface. Therefore, a reflection interface is also called a wave impedance interface, which is consistent with the lithological interface of the actual strata and it represents different lithological horizons.

The Sub-bottom profiler is a high resolution broadband frequency modulation system that uses proprietary EdgeTech technology to generate cross-sectional images of the sub-bottom profiler. seabed and collects incident reflection data in digital form over multiple frequency ranges. This device transmits a linearly scanned FM (frequency modulation) tone pulse over a full spectrum frequency range. Reflections in the measuring system are represented as gray streaks or other colors on a computer screen, which can be printed on a printer. Data is stored in real time in a large capacity hard drive. The Sub-bottom profiler system uses sound sources and receivers integrated in a tow vehicle to transmit and receive pulsed FM signals. The transmitters are wideband transducers and the receivers are hydrophone arrays of lead titanatezirconate (PZT) crystals. The transducers are located in the inner part of the traction equipment and the receiver arrays. They are designed to operate out of ships, traveling at speeds of up to 7 miles/hour. The Sub-bottom profiler measuring instrument system is composed of 3 main components: (1) the processor which is located on the deck (3200 - XS), (2) the tow vehicle SB-216S and (3) kevlar fiber reinforced 75 m extension cable (Figures 2a, 2b, 2c), (3200-xs sub-bottom system user hardware manual, 2005).

The 3200-XS Sub-bottom profiler from the U.S. EdgeTech Corporation is adopted, which consists of towing fish, towing line and deck unit (Figure 2). The towing fish is of the type SB-216S and comprised of 1 transmitting transducer and 2 receiving transducers. The transmitted signal has a beam angle of 24°(-3dB). Sound boarding is used to separate the transducers in order to prevent the downward sound wave from interfering the received signal and to minimize surface reflection. The transducer transmits frequency modulated signal to the deep water right beneath it. The transmitted signal is able to penetrate into the stratum layers and will be reflected when the wave impedance changes. The reflected signal is received by the receiving transducer and sent to the deck unit through the towing line. A Topcon GPS system was connected with

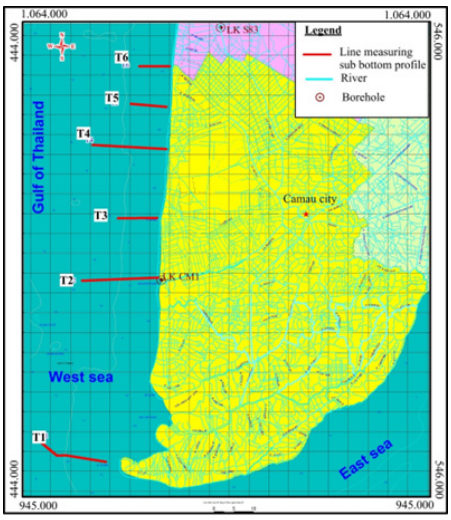

Fig. 4. The location of sub-bottom profiler measurement lines

the host machine of the deck unit. The GPS coordinate corresponding to each measuring point is extracted using the collection software. Flow-chart of data processing sub-bottom profiler was shown at Figure 3.

Sediment layers external shape and internal texture of sub-bottom profiler cross section records conducted using seismic facies analysis. This analysis was made to determine environmental depositing of seismic reflection characteristics, as well as continuity of amplitude, velocity, frequency and phase.

Geological characteristics of the study area

The study area is located on the west coast of Camau province, at the intersection of the East Sea and the Gulf of Thailand. The province of Camau is the low-laying area, with a typical height of 0.5-1 m above sea level. In Camau province the Cenozoic deposits are 300 m thick on average. The subsidence of the Mekong Delta basin in the Neogene was caused by the uplift of the Himalaya orogenesis, which was accompanied by high erosion rates in the mountains which provided large amounts of material, that formed the Mekong Delta sediments. Repeated cycles of marine transgression and regression during the Neogene and Pleistocene lead to a sequence of marine and ter restrial/alluvial facies. Glacial and events in the Pleistocene caused particularly strong regression and erosion (Stattegger et al., 2013). The stratigraphy, lithology, and facies of the unconsolidated sediments, are briefly described from the oldest to the youngest in the following sections on the base mainly on information from some boreholes with typical lithology and micro- paleontological evidence (Dung et al., 2013; Moley., 2002; Wagner et al.,2012).

Miocene (N1)

Upper Miocene, Phunghiep formation (N13ph)

The Phunghiep formation is the deepest unconsolidated sediment. Its thickness varies in the range 60-100 m. The bottom of these deep deposits, which corresponds to the top of the basement of the basin, dips gradually from the northwest to the southeast. The formation is unconformably covered by sediments of the Cần Thơ formation (N21ct). The Late Miocene age (N13) formation consists of two facies: alluvial-marine deposits are overlain by marine deposits. There are the alluvial-marine deposits (amN13ph) and the marine deposits (mN13ph).

Pliocene (N2)

Lower Pliocene, Cantho formation (N21ct)

This formation is between 24-89 m thick in Camau province. It is unconformably covered by the younger Namcan formation. This sedimentary formation consists of 2-3 sedimentary cycles, each starting with coarse- grained sediments (sand, sandy silt) at the bottom and fining upward (silt, clay, clayey silt, silty clay, and silty sand). Based on the characteristics of the sediments and micro-paleontology, Cantho formation was formed in a delta landscape with bays, estuaries, and shallow sea. This formation is divided into two facies again, alluvial-marine deposits are covered by marine deposits.

Middle Pliocene, Namcan formation (N 2nc)

These are the youngest Neogene sediments; there are no Upper Pliocene deposits. The thickness of the whole Namcan formation (N22nc) varies in the range 55-96 m, the average thickness is 79 m. It dips from the northwest to the southeast, and covers the sediments of the Cantho formation (N21ct) unconformably. There are two facies of this formation: alluvial-marine (amN22nc) overlain by marine deposits (mN22nc). These are fine-grained sediments (clay, silt, clayey silt) distributed throughout the region.

Pleistocene (Q1)

Lower Pleistocene, Camau formation (Q 1cm)

Thickness changes in the range 36-87 m.The bottom of the Camau formation (Q11cm) dips gradually from northwest to southeast, and unconformably overlays the sediments of Namcan formation (N22nc). The Camau formation was formed in shallow marine environments of coastal mangroves and estuaries. This formation is divided into two facies: alluvial-marine deposits (amQ11cm): in Camau province area, the top of the amQ11cm deposits is located at depths between 84-154 m. Thickness varies in the range 19-77 m. Sediment composition includes mainly fine to medium sand; coarse and silty fine-grained sand; grey-brown silty sand containing a little gravel. The sediment is interbedded with silt layers. Marine deposits (mQ11cm): in the study area, are the top layer of the Camau formation and consists of fine-grained sediments. They are observed throughout the region and their thickness varies from a few meters to 35m.

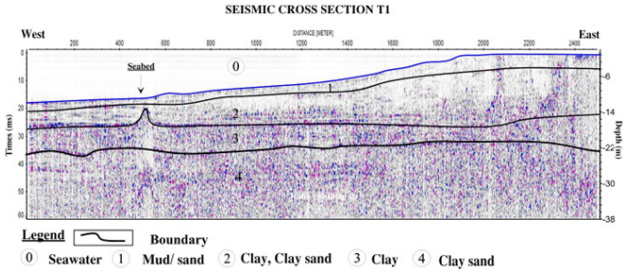

Fig. 5. The structural cross-section for seismic measurement line T1

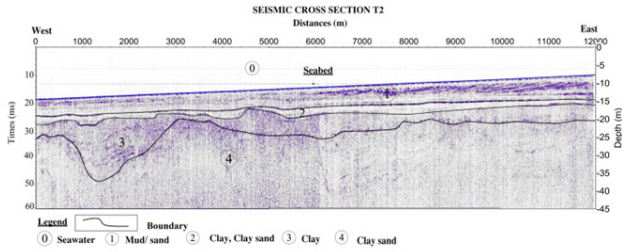

Fig. 6. The structural cross-section for seismic measurement line T2

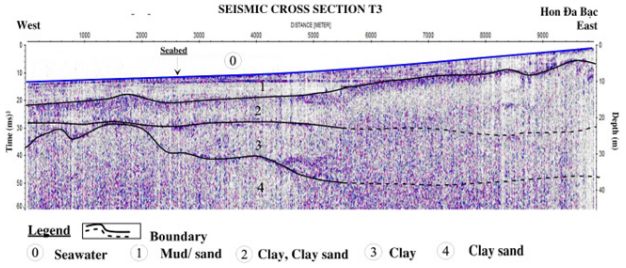

Fig. 7. The structural cross-section for seismic measurement line T3

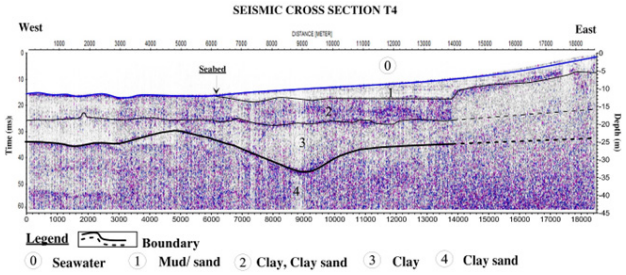

Fig. 8. The structural cross-section for seismic measurement line T4

Middle – Upper Pleistocene, Longtoan formation (Q12–3lt)

In Camau province area, the top of the Q12–3lt deposits is located at the depth 42-70 m (average 54 m). Thickness varies between 21-94 m, with an average of 49 m. The Q12–3lt deposits unconformably overlays the sediments of the Camau formation (Q11cm). The formation is divided in two facies: alluvial-marine (amQ12–3lt) and marine (mQ12–3lt). The lower part consists of fine-grained sediments. The upper part is built of clayey silt, silt, silty sand.

Upper Pleistocene, Longmy formation (Q13lm)

In Camau province area, the top of Q13lm deposits is located at the depths 12.5- 45 m. Thickness ranges from 15 to 41 m. The sediments of the Longmy formation unconformably overlay the Longtoan formation (Q12–3lt) and are overlaid by Holocene (Q21–2). This Longmy formation is divided it in two facies: alluvial-marine deposits (amQ13lm) and marine deposits (mQ13lm): These deposits are mainly composed of fine-grained sediments: clay, silty clay, clayey silt, silt, grey light yellow to golden brown silty sand.

Holocene (Q2)

Lower to middle Holocene (Q21–2)

In Camau province area, the top of the Q21–2 deposits is located at depths from 1.0 to 6.0 m. The thickness varies from 10 to 40 m. The sediments unconformably overlay Longmy for mation.The formation consists mainly of blue-grey fine-grained soils and contains humus. The formation is divided into two facies: The first one are the mixed alluvial-marine deposits (amQ21–2) which is distributed only in a few places: 3 to 10 m in depth. The deposits consist of fine sand and green-grey silty sand containing humus. The second one are the marine deposits (mQ21–2): They are distributed throughout the study area at depths 1.0 to 6.0 m, consisting mainly of mud, clay, silty sand and silt.

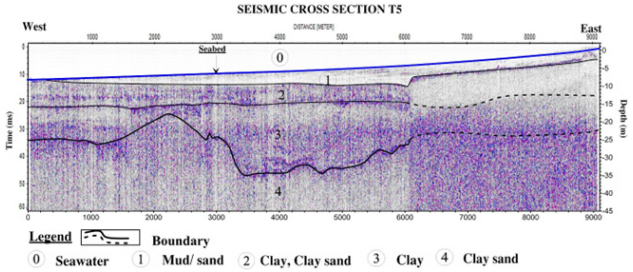

Fig. 9. The structural cross-section for seismic measurement line T5

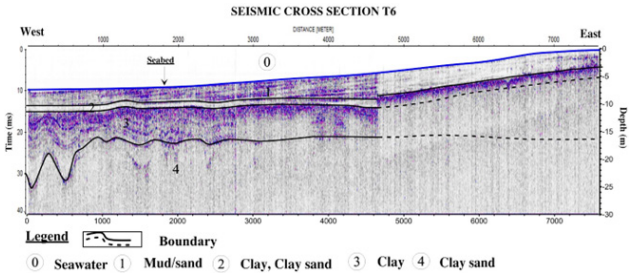

Fig. 10. The structural cross-section for seismic measurement line T6

Middle to upper Holocene (Q22–3)

There is only one facies in this sub-epoch. Alluvial-marine deposits (amQ22–3): These deposits are exposed at the surface in almost all areas and are mainly composed of clay and grey-golden fine sand interbedded with thin dark brown clay layers, which contains iron concretions of gravel size. They are easily compressible sediments, flexible, and very plastic. At some places good quality clay is mined. Sediment thickness varies between 1.0 m and 5.0-6.0 m.

Upper Holocene (Q23)

There are two facies of these most recent sediments: (1) alluvial-marine-swamp deposits (ambQ23)

distributed mainly in the northeast and the northwest region. The major components of these deposits are clay, silt, brown-grey fine sand, humus, and poorly decomposed plants. Sediment thickness varies between 1.0 and 1.5 m and (2) alluvial deposits (aQ23) which are distributed along the banks of the rivers and canals in the form of narrow strips of alluvial sediments. Sediment composition is mainly silt; clay; little fine sand and humus.

Results and discussion

The location of the 6 lines along which the Sub-bottom Profiler made the measurements in the study area, in the western shallow waters of Camau, adjacent to Thailand Gulf is presented in Figure 4. The measuring lines are all in the west-east direction and have a definite length (Table 1).

In the Figures 5-10 seismic cross-sections with the primary geological interpretation using ReflectW software of 6 sub-bottom profiler lines are presented.

The structural cross-sections of 6 seismic measurement lines are divided into 5 layers with different thicknesses and compositions (Pinson et al., 2008), and are summarized in Table 1.

In the plots of all six high-resolution shallow seismic profiles, the recorded reflected signal is up to 120 ms in length. But, the well-reflected signals, used in the analysis, are in the range of 20-70 ms, showing quite uniformity in physical characteristics and petrological nature of the survey environment.

Overall, the seismic wave field in the study area is relatively clear, except from some parts of the measured lines due to the strong absorption of wave energy, when passing through the surface of the seabed, which proves the main sedimentary formation is rough grain sand, sand and gas with poor attachment,that makes the research depth of the method limited. Thus, the seismic wave field in the sections shows the nature of the fine- or coarse-grained petrological composition, when the seismic wave is transmitted. In the survey area, there are wedge-shaped, oblique, corrugated and transverse structures.

The boundaries in the shallow sedimentary sediment structure are important targets to be achieved when using the surveyed measurement data with High-Resolution Shallow Reflection Seismics. Therefore, while interpreting the seismic cross-sections, we have relied on the stratigraphic column of some neighboring boreholes and the geological structure characteristics of the study area as the basis for linking and interpreting the lines as soon as boundaries according to structural layers by seismic data. This is especially useful for measurement lines where the received seismic wave field signal is not clear or is too faint when noise sources are excluded. The combination of information about geological structure and the hole floor and the seismic data has contributed to the accuracy of the boundary positions of the sedimentary structure layers in the shallow water band near the shore and has already been achieve necessary reliability.

Overall, the above analysis shows that the terrain of the seabed in the survey area tends to be shallow from the West to the East (from the sea to the shore) the slope is low, relatively flat, there is no sign of digging and undulating on the surface of the seabed. Except, the two positions at beginning of T1 line show that the head of the route has quite a steep and deep terrain, which may be the slope of the continental shelf in the survey area and at the beginning of the T6 measuring line, there are also two small-scale geological faults with a displacement amplitude in the range of 1.5 to 4 m.

Tab. 1. Characteristics of structural sections according to Sub-bottom profiler data

Seismic line	Layer 0	Layer 1	Layer 2	Layer 3	Layer 4
T1, length 2600m	Seawater, and sea-level depths ranging from 2-14 m.	The thickness ranges from 1.8 to 4 m. The weak reflective boundary shows, that the sediments are mainly coarse particles. The lithology is mainly sand, silt, corresponding to Holocene sediments.	The thickness ranges from 4 to 14 m. The lithology is mainly clay mud, and soft clay, corresponding to the Holocene age sediments.	The thickness ranges from 4 to 10 m. There is a boundary of strongly reflected seismic waves. The lithology is mainly sandy, and clayey, corresponding to the Holocene sediments. The bottom is the boundary between the Holocene and Pleistocene sediments.	Starting from 20 m down, the seismic wave is completely absorbed. The lithology is sandy clay,and sand powder, corresponding to the Pleistocene sediments.
T2, length 12000 m	Seawater and sea-level depths ranging from 2-14 m.	The thickness ranges from 5-8 m, the formation has the form of horizontal layers stacked on top of each other, shown through the strongly reflected seismic wave field. The lithology is mainly clay mud, and soft clay.	The thickness ranges from 1-3 m, the lithology is mainly clay, and soft clay. In the second half of the line the boundary of reflection is completely absorbed, showing that the sediment has poor cohesion and high porosity. The lithology is mainly powdery sand, and mixed sand, corresponding to the Holocene sediments.	The thickness ranges from 2–25 m, the lithology is clay-sand. In this layer, the seismic wave field is also strongly absorbed, making the reflection boundary of the two media weak. The bottom is the boundary between the Holocene and Pleistocene sediments.	Starting from a depth of 20 m down the seismic wave completely lost its signal, the lithology is mainly clay, and solid-phase clay, corresponding to the Pleistocene sediments. There is an intrusive bedrock block in the beginning of the line.
T3, length 10000 m	Seawater, and sea-level depths ranging from 2-14 m.	The thickness ranges from 5-9 m, the formation has the form of horizontal layers stacked on top of each other. The lithology is mainly mud and sand, corresponding to the Holocene sediments. At the end of the line, the bedrock surface was discovered near Hon Da Bac.	The thickness ranges from 8-18 m, the boundary of the reflection is clear, the lithology is mainly sandy clay, and sand, corresponding to the Holocene sediment.	The thickness ranges from 0.5-15 m, the lithology is clay-sand .The seismic wave field is also strongly absorbed, making the reflection boundary of the two media weak. The bottom is the boundary between the Holocene and Pleistocene sediments.	From the depth of 30m down, the seismic wave completely lost its signal, the lithology is mainly clay, and hard clay, corresponding to the Pleistocene sediments.
T4, length 19000 m	Seawater, and sea-level depths ranging from 2-12 m.	The thickness ranges from 0.5–6 m, the formation has a horizontal layered form. The lithology is mainly mud, and fine grain sand-mud.	The thickness ranges from 6-11 m, the reflective boundary is clear, the lithology is mainly clay, and soft clay, corresponding to the Holocene sediments. Also gas is present, because the seismic wave is completely absorbed.	The thickness ranges from 4-20 m, petrology is clay-silt sand, silty sand, corresponding to the Holocene sediments. The bottom is the boundary between the Holocene and Pleistocene sediments.	From the depth of 23m down, the seismic wave completely lost its signal, the lithology is mainly clay, and hard clay, corresponding to the Pleistocene sediments.
T5, length 9200 m	Seawater, and sea-level depths ranging from 2-9 m.	The thickness ranges from 2-5 m, the formation has a horizontal layered form. The lithology is mainly mud, and fine grain sand- mud.	The thickness ranges from 5-10 m, the reflection boundary is clear. The lithology is mainly clay, and soft clay, corresponding to the Holocene sediments. Also gas is present.	The thickness ranges from 4-35 m, lithology is sandy sand, sand powder, corresponding to Holocene sediments. The bottom is the boundary between the sediments of the Holocene and Pleistocene.	From the depth of 25m down, the seismic wave completely lost its signal, the lithology is mainly clay, and hard clay, corresponding to the Pleistocene sediments.
T6, length 7800 m	Seawater, and sea-level depths ranging from 2- 8 m.	Thickness ranges from 3-5 m, the formation has a thin layer form recognized by strongly reflected seismic wave field. The lithology is mainly fine-grained mud, and sand, corresponding to the Holocene sediments.	Thickness ranges from 1.5-2.5 m, the lithology is mainly clay, clay powder, and sandy clay. However, from the 4,600th meter to the end of the line, the seismic wave field is completely absorbed, showing that the sediment is poor, high porosity, gaseous, corresponding to the Holocene age sediments.	Thickness ranges from 8-22 m, the lithology is clay-silt sand, corresponding to the Holocene sediments. The bottom is the boundary between the Holocene and Pleistocene sediments.	From a depth of 15-25 m down, seismic waves completely lost their signal. The lithology is mainly clay, and hard compact clay, corresponding to the Pleistocene sediments.

Conclusion

High-resolution shallow reflection seismic method by sub-bottom profiler instrument system has been used to study the geological structure and engineering geology in the coastal zone with shallow water level in the western sea of Camau. The data series collected on the 6 west-east lines with a total length of 60.6 km has been processed and interpreted on the basis of wave propagation velocity as well as density of the associated geological environment. The main goal of the study – the geological structure of the sub-bottom formation determination was obtained. The relationship with materials such as silt, mud, clay sand, clay powder, sand powder, and sand with different grain size levels and bedrock surface has been determined quantitatively. Boundary interfaces in sedimentary structures with ages from the Pleistocene to Holocene have been determined on the basis of division of 4 structural layers from the seabed in the survey area. The shallow marine sediments, the Mekong delta sediments to the tidal flat sediments and the boundary of the ancient Pleistocene alluvial surface are clearly divided on all measured structural sections. The boundary between the Holocene and Pleistocene sediments at an average depth of 25-35 m appear on all measurements lines in the study area.

The topography of the seabed in the survey area is relatively flat, has a low slope and tends to gradually shallower from west to east, from the sea to the mainland. The clay layer has a semi-hard to hard state, corresponding to the ancient alluvial surface, at an average depth of 30 m, creating favorable conditions for the construction of coastal works. However, at the beginning of the T6 measuring line, there are also two small-scale geological faults with a displacement amplitude in the range of 1.5 to 4 m, which may be a kind of obstacle for the constructions.

Literatura – References

1. 3200-xs sub-bottom system user hardware manual, (2005). EdgeTech, 4 Little Brook Road, West Wareham, MA 02576. www.edgetech.com
2. Alves D.P.V., Caldato E.B., de Moura D.S., dos Santos R.P.Z., Jovane L., (2020). High-Resolution Sub-Bottom and Magnetometer Data From Southeastern Brazilian Coast. Fronties in Marine Science. 7:536295. doi: 10.3389/fmars.2020.536295.
3. Alves D.P.V., de Mahiques M.M., (2019). Deposition and sea- level evolution models for Upper Pleistocene/Holocene in the São Sebastião Channel (SE Brazilian coast) inferred from 5th order seismic stratigraphy. J. South Am. Earth Sci. 93, 382–393. doi: 10.1016/j.jsames.2019. 05.012.
4. Amri U., (2019). Recent Sediment Analysis, Study Case: Sub Bottom Profiler Data Line 8 Geomarine Research Vessels. Journal of Wetlands Environmental Management, Vol. 7 (2), 123-133. http://dx.doi.org/10.20527/jwem.v7.v2.171.
5. Angulo R.J., Lessa G.C., De Souza M.C., (2006). A critical review of mid- to late-Holocene sea-level fluctuations on the eastern Brazilian coastline. Quat. Sci. Rev. 25, 486–506. doi: 10.1016/j.quascirev.2005. 03.008
6. Aquino da Silva A.G., Stattegger,K., Schwarzer,K., Vital,H., (2016). Seismic stratigraphy as indicator of late Pleistocene and Holocene sea level changes on the NE Brazilian continental shelf. J. South Am. Earth Sci. 70, 188–197. doi: 10.1016/j.jsames.2016. 05.001
7. Ding W., Zhao D., Wang M., Liu Z., (2021). Chapter 4 Side-scan Sonar and Sub-bottom Profiler Surveying. In Z. Wu et al., High-resolution Seafloor Survey and Applications. Science Press 2021, Springer Singapore. https://doi.org/10.1007/978-981-15-9750-3_495
8. Dung B.V, Stattegger K., Unverricht D., Phach P.V., Thanh N.T., (2013). Late Pleistocene–Holocene seismic stratigraphy of the Southeast Vietnam Shelf. Global and Planetary Change 110 (1),156-169, DOI: 10.1016/j.gloplacha.2013.09.010.
9. Grelowska G., Kozaczka E., (2010a). Sounding of layered marine bottom – model investigations, Acta Physica Polonica A, 118, 66–70.
10. Grelowska G., Kozaczka E., (2014). Underwater acoustic imaging of the sea, Archives of Acoustics, 39, 4, 439–452. DOI:10.2478/aoa-2014-0048.
11. Grelowska G., Kozaczka E., Szymczak W., (2010). Method of data extraction from sub-bottom profiler's signal, Hydroacoustics, 13, 109-118.
12. Kadima E., Delvaux D., Sebagenzi S.N., Tack L., Kabeya S.M., (2011). Structure and geological history of the Congo Basin: an integrated interpretation of gravity, magnetic and reflection seismic data. Basin Res. 23, 499–527. doi: 10.1111/j.1365-2117.2011.0 0500.x
13. Kozaczka E., Grelowska G., Kozaczka S., Szymczak W., (2013). Detection of objects buried in the sea bottom with the use of parametric echosounder, Archives of Acoustics, 38, 1, 99–104.DOI: 10.2478/aoa-2013-0012.
14. Lap N.V., Oanh T.T.K., Tateishi M., (2000). Late Holocene depositional environments and coastal evolution of the Mekong River Delta, Southern Vietnam. J. Asian Earth Sci. 18, 427–439. doi:10.1016/S1367-9120(99)00076-0.
15. LeBlanc L.R., Mayer L., Rufino M., Schock S.G., King J., (1992). Marine sediment classification using the chirp sonar, The Journal of the Acoustical Society of America, 91(1), 107-115.
16. Lurton X., (2002). An Introduction to Underwater Acoustics: Principles and Applications. Springer, Praxis, Chichester, UK.
17. Moley C.K., (2002). A Tectonic model for the Tertiary evolution of strike – slip faults and rift basins in SE Asia. Tectonophysics 347(4), 189-215. DOI: 10.1016/S0040-1951(02)00061-6
18. Pinson L.J.W., Henstock T.J., Dix J.K., Bull J.M., (2008). Estimating quality factor and mean grain size of sediments from high-resolution marine seismic data. Geophysics, vol. 73, no. 4, pp. 19–28.
19. Saleh M., Rabah M., (2016). Seabed sub-bottom sediment classification using parametric sub-bottom profiler. NRIAG Journal of Astronomy and Geophysics, Egypt (5) 87-95. http://dx.doi.org/10.1016/j.nrjag.2016.01.004.
20. Stattegger K., Tjallingii R., Saito Y., Wetzel A., Michelli M., Thanh N.T., (2013). Mid to late Holocene sea-level reconstruction of Southeast Vietnam using beachrock and beach-ridge deposits. Global and Planetary Change 110 (1), 214–222. DOI: 10.1016/j.gloplacha.2013.08.014
21. Wagner F., Vuong B.T., Renaud F.G., (2012). Groundwater Resources in the Mekong Delta: Availability, Utilization and Risks, in: The Mekong Delta System, Springer Environmental Science and Engineering. Springer, pp. 201–220.
22. Wang F., Dong L., Ding J., Zhou X.,Tao C., Lin X., Liang G., (2019). An Experiment of the Actual Vertical Resolution of the Sub-bottom Profiler in an Anechoic Tank. Archives of Acoustics, Vol. 44, No. 1, pp. 185–194, DOI: 10.24425/aoa.2019.126364.

23. Murena, F. (2004). Measuring air quality over large urban areas: Development and application of an air pollution index at the Environ Monit Assess (2018) 190:625 Page 9 of 10 625 urban area of Naples. Atmospheric Environment, 38(36), 6195–6202.

24. Stankevich, S., Titarenko, O., Kharytonov, M., Benselhoub, A., Bounouala, M., Chaabia, R., & Boukeloul, M. L. (2015). Mapping of urban atmospheric pollution in the northern part of Algeria with nitrogen dioxide using satellite and ground-truth data. Studia Universitatis" Vasile Goldis" Arad. Seria Stiintele Vietii (Life Sciences Series), 25(2), 87.

25. Stankevich, S., Titarenko, O., Svideniuk, M., Kharytonov, M., Benselhoub, A., & Khlopova, V. (2016). Air pollution mapping with nitrogen and sulfur dioxides in the south-eastern part of Ukraine using satellite data. Mining Science, 23.

26. Sulejmanović, J., Muhić-Šarac, T., Memić, M., Gambaro, A., & Selović, A. (2014). Trace metal concentrations in size-fractionated urban atmospheric particles of Sarajevo, Bosnia and Herzegovina. International Journal of Environmental Research, 8(3), 711-718.

27. World Health Organization. (2016). Ambient air pollution: a global assessment of exposure and burden of disease. World Health Organization. https://apps.who.int/iris/handle/10665/250141.

Integration of Mobile and Web GIS Technologies to Promote Smart and Sustainable Tourism in Vietnam

Mai Dung NGUYEN[1)], Xuan Ban TO[2)], Hong Anh LE[3)]

[1)] Faculty of Information Technology, Hanoi University of Mining and Geology, Vietnam; email: nguyenthimaidung@humg.edu.vn
[2)] Faculty of Geosciences and Geological Engineering, Hanoi University of Mining and Geology, Vietnam
[3)] Faculty of Information Technology, Hanoi University of Mining and Geology, Vietnam

http://doi.org/10.29227/IM-2023-02-34

Submission date: 19-08-2023 | Review date: 29-09-2023

Abstract

Tourism is one of the most important factors in economic growth in Vietnam. However, it requires the balance between economics, social-cultures, and ecology because of their big impacts. In this paper, we propose a platform with mobile and web-based applications that can support smart and sustainable tourism in Vietnam for both local governments and visitors. The mobile application allows visitors to access location-based services to explore the visiting area, such as finding nearby natural attractions, as well as information to minimize the negative effects of tourism on the environment and the local community. It also enables users to report negative impacts to local government. The web application allows local authorities to monitor the status and trends of the habitant, natural environment, tourism infrastructure and activities in the area. The system uses geographic information systems (GIS) and remote sensing techniques to collect, analye and visualize various indicators of sustainability. The platform is developed with open-source technologies such as NodeJS, PostgreSQL, and Flutter. The paper demonstrates the feasibility and usefulness of the proposed platform through case studies in Hoa Binh and BacKan, two provinces have many attractive natural sites.

Keywords: *mobile GIS, WebGIS, location-based services, smart and sustainable tourism*

1 INTRODUCTION

Tourism is one of the most important factors in economic growth in Vietnam. However, it requires the balance between economics, social-cultures, and ecology because of their big impacts. Therefore, sustainable tourism is a growing concern in Vietnam, as well as in many other countries. The Vietnamese government has been realized the sustainability as a core part of the country's socio-economic development. In era of industry 4.0, there is a need of information technology and communication platform that supports not only the visitor to explore the visiting sites but also for local goverment to monitor and manage in order to mimize the negative impacts of tourism services.

Mobile and web GIS technologies are systems that enable the collection, analysis, visualization and dissemination of geographic information through mobile devices and web platforms. These technologies have various applications in tourism, such as: Providing location-based information and navigation services to tourists, such as points of interest, routes, traffic, weather, etc. Enhancing tourist experience and engagement through interactive and immersive features, such as augmented reality, virtual reality, gamification, storytelling, etc. Supporting the planning and management of tourism destinations by enabling real-time monitoring, evaluation and feedback of tourist activities, resources and impacts. Promoting tourism marketing and communication by facilitating the creation and dissemination of geospatial content, such as multimedia stories, maps, charts, etc. Fostering the participation and collaboration of tourists, local communities and stakeholders in the co-creation and sharing of tourism knowledge and value.

The development of mobile GIS and webgis technology has opened new possibilities for enhancing tourism experiences and promoting smart and sustainable tourism. Mobile GIS and webgis technology can provide tourists with real-time, location-based, and personalized information and services, as well as enable them to interact with other tourists and local communities. However, existing mobile and web GIS technologies in tourism face challenges such as data quality, privacy, security, interoperability, usability, and user acceptance. They also have limitations such as lack of integration, collaboration, innovation, and evaluation.

This study proposes a novel framework for integrating mobile and web GIS technologies to promote smart and sustainable tourism. The paper consists of four parts. In section 2, related work are summarized. Next, section 3 is the main part that present the design, implementation of the proposed system. Finally, the paper gives some conclusions in section 4.

2 LITERATURE REVIEW

2.1 Potential of Mobile and Web GIS in smart and sustainable tourism

Smart and sustainable tourism is an activity to achieve efficient, responsible, and sustainable use of tourism resources by developing suitable tourism activities and helping tourists become managers, designers and creators of tourism experiences. In particular, the integration of mobile and web GIS technologies can bring many benefits to the smart and sustainable tourism industry.

Mobile Geographic Information Systems (GIS) and web-based GIS (webgis) are modern technologies that can enhance the planning, development, management and marketing of tourist destinations. Mobile GIS and webgis can provide location-based services, mobile augmented reality, and social networking services for travellers and tourism businesses. These technologies help travellers to quickly access information about attractions, culture, scenery, promotions through their smart devices, and share their experiences with others online. They

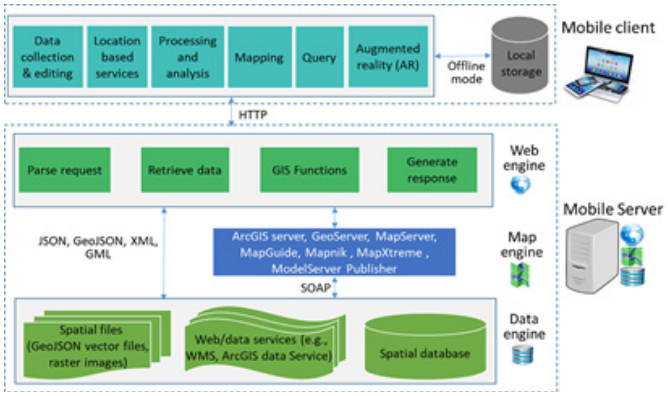

Fig. 1. The client-server architecture of a GIS [7]

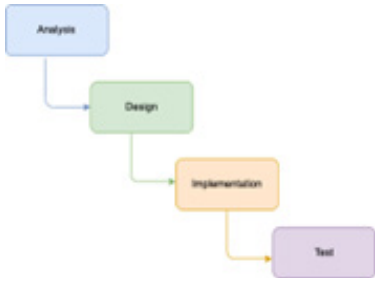

Fig. 2. The development method Water-fall of the smart tourism system

can also help travel businesses improve their customers' visibility, competitiveness and trust by providing personalized and timely information and promotions.

Several studies have explored the use and potential of mobile GIS and webgis in tourism. [1] designed and implemented a tourism system using mobile augmented reality and GIS technologies for Android and iPhone platforms. The system integrated information from the Tourism Bureau, the Ministry of Economic Affairs and 500 local businesses to provide an intuitive and interactive interface for tourists. [2] examined the use of GIS and remote sensing in tourism, focusing on two case studies of Maasai Mara Game Reserve and Nairobi National Park in Kenya. They showed how GIS and satellite imagery can be used to assess the changes and impacts of human activities on the ecosystems and wildlife resources that are vital for tourism. [3] proposed a new idea of building information modeling (BIM) and GIS integration for smart city applications, which can also benefit tourism by providing 3D visualization and analysis of urban environments. [4] Therefore, the aim of this paper is to review geo-visualization-based solutions proposed in the literature and to propose a solution that can overcome the limitations related to the use of geo-visualization in tourism. The proposed system use the capabilities of the mobile navigations system and mobile augmented reality in combination with animation to represent the objects in motion in real time on the mobile interface. This research work contributes to create a smart geo-visualizations system that can be combined with mobile augmented reality to be used in the tourism domain. According to [5], the author has presented about the architecture and implementation of the Smart Tour Guide system. This system allows visitors to view map information, find locations, find videos and see the weather of each area. However, this system only works on Android-based smartphones and meets the basic features for travellers. The special issue of sustainability journal that contains several papers on the topics of mobile technology and smart tourism development, such as mobile apps, social media, internet of things, augmented reality, location-based services, and smart destinations also discuss the impacts of mobile technology on tourism behavior, experience, marketing, management, and sustainability [6].

These studies demonstrate that mobile GIS and webgis can bring a variety of benefits to the tourism industry, such as enhancing tourist satisfaction, increasing destination attractiveness, supporting decision-making, improving resource management, facilitating communication and collaboration, and promoting sustainability. However, there are also several challenges and limitations that need to be addressed, such as data quality, security, privacy, interoperability, standardization, cost-effectiveness, user acceptance, ethical issues, and social impact. Therefore, more research is needed to explore the opportunities and challenges of integrating webgis and mobile GIS technologies to promote smart and sustainable tourism.

2.2 GIS for mobile application

Mobile GIS is considered an integrated framework for accessing spatial data and services through mobile devices. Mobile GIS makes GIS available from desktop and cloud-based software and services to anywhere in the world, allowing for GIS accessibility from any location. With the development of wireless communication technology, GIS applications can access and transfer data over high speed Internet. These applications can integrate powerful web-delivered GIS services, receive the latest GIS data updates, and regularly send the latest field information back to collection and dissemination systems server-side data. As such, Mobile GIS is increasingly being considered as a component of Web GIS. It has gradually provided more sophisticated online GIS functions and interactions accessible through mobile devices.

Most GIS software for mobile applications is usually developed based on client-server architecture [7]. The client side

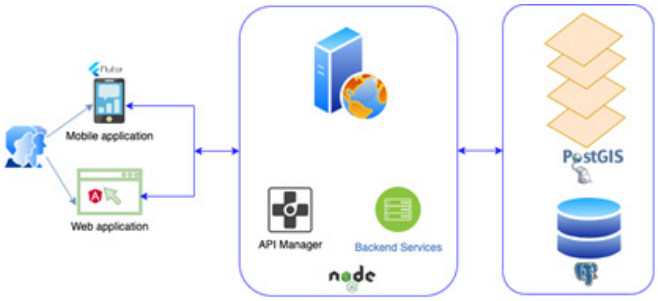

Fig. 3. The architecture of the proposed system

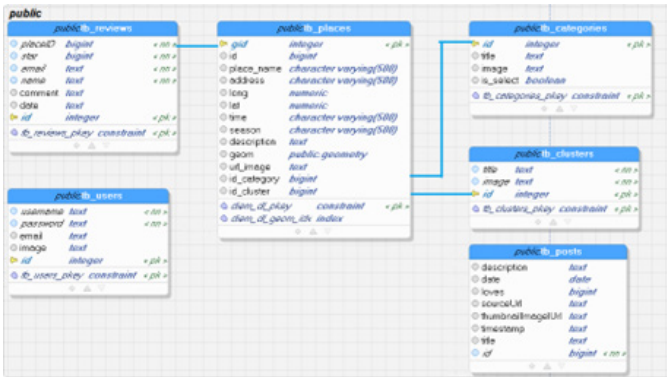

Fig. 4. Data models of non spatial data

includes a GPS enabled mobile device and mobile GIS software with a user interface that allows manipulation of the map through the device. Compared to a typical mobile application, a GIS mobile user interface needs to provide spatial data layers, as well as simple mapping functions, typically enabled through APIs. and SDKs like the Google Maps API. The server side usually includes three main tools namely: web engine, map engine and data engine. These tools may or may not be available. For data transfer between server and client, XML and JSON data formats are commonly used.

2.3 Cross-platform mobile application

A cross-platform mobile application is one that is accessible through a large number of different end devices. It provides the ability to write code once and then run it anywhere for a variety of other platforms.

There are many different cross-platform mobile app development frameworks out there nowadays like Flutter, React Native, Ionic, etc. According to the 2021 developer survey [8], Flutter is the most popular cross-platform mobile application development framework used by developers globally. Flutter is an open-source, cross-platform software development toolkit developed by Google. It is being used to create apps for Android, iOS, web-based, and desktop apps. Flutter uses Dart, which is a modern object-oriented programming language. Dart uses various compilers to compile the corresponding machine code [9].

3 BUILDING A SMART AND SUSTAINABLE TOURISM SYSTEM WITH MOBILE AND WEB GIS

3.1 Development method

To build the system, the paper follow the Water-fall model for sofware development as illustrated in Fig. 2. . It consists of 4 phases as folllows

Analysis phase: Analyzed all requirements of the system and made a review of the current state of webgis and mobile applications in tourism fields that are summarized in Section 2. The technique is used for the software is object-oriented analysis and design.

Design phase: We start with system architecture design, then design all the component of the system following the analyzed requirements. There is also a requirement for a open system that can be contributed for community developers. Thefore, we decided to choose open-source frameworks and platforms to develop the system in this field.

Implementation phase: Coding the design with selected technologies and programming languages.

Testing phase: Testing all the developed functionalities to find bugs.

3.2 System Architecture

Figure 3 depicts the overview architecture of the smart tourism system.

The smart tourism system will consist of three main layers. The first layer is front-end one. It provides users access way to the system via a mobile application and web browers. The mobile application is built on top of Flutter while front-end technology of the web application bassed on Angular framework. The second layer is for server processing written with NodeJS. It has two components: API manager and backend services. The former is responsible for handling API between server and clients (mobile and web applications), the latter are backend services and processes the database and GIS layers. It also has the role of providing and controlling the processes that access the system's resources. The final component is a database built on PostgreSQL integrating the PostGIS extension to be able to work with spatial data.

3.3 Database Design

We have explored and made many field trips in two provinces, i.e, Bac Kan and Hoa Binh, to collect the data for natural sites. We also have classified them into 8 groups:

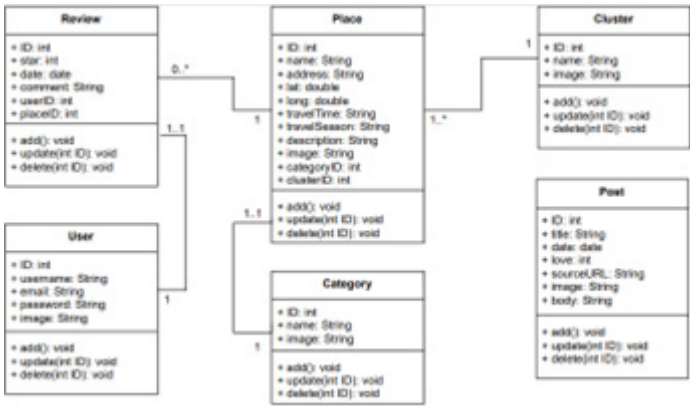

Fig. 5. Class diagram of smart and sustainable tourism system

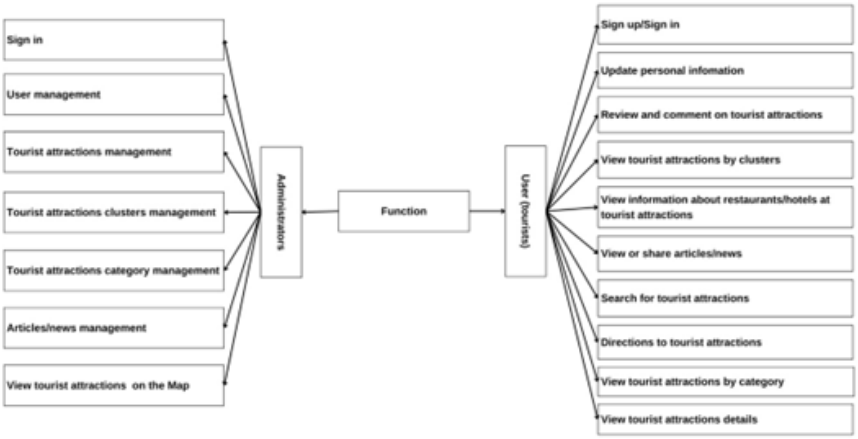

Fig. 6. Main functions of the smart and sustainable tourism system

- Karst caves
- Warm mineral water sites
- terraced fields
- geo-heritages sites
- cultural sites
- water-falls
- Natural reserved sites
- Resort and ecological sites

These groups are mapped into 8 GIS layers in the database. In order to make spatial analysis, we also have insert more layers as basics such as: river, forest, residences, roads... into the GIS database. Morever, the non spatial data models are define as Fig. 4.

3.4 Class diagram of the system

The class diagram describes the type of objects in the system and the different types of relationships that exist between them. The Smart Tourism System that integrates mobile and web GIS technology is defined to include main classes such as: Review, Cluster, Place, User, Category, Post. Fig. 5 below details the classes and their relationships.

3.5 The system implementation

The system is used by two actors: Admin and Traveller. The functional diagram of the system is depicted as shown in Figure 6 below:

The user interface of the application is developed using the Flutter SDK. Map operations (loading and displaying maps, zooming in, tapping, etc.) are built on the Google Maps SDK. Map data edited as shapefile or geodatabase will be loaded and stored on the server. The mobile application will interact with the map data through APIs. Figure 7 depicts the implementation of a smart tourism system that integrates mobile and web GIS.

3.6 Results and Discussion

The research system has been successfully installed on popular platforms such as Android and iOS. Figure 8 below depicts some of the main interfaces of the smart and sustainable tourism system based on mobile and web GIS. A system built on Cross-platform applications provides the main functions such as: (1) lookup, display information of tourist sites; (2) categorize places by different categories; (3) Integrated Google Map map to visualize the locations; (4) Share news, articles related to tourism in Hoa Binh province; (5) Suggesting travel itineraries for tourists, etc. In addition, the system also provides the ability to share data via APIs in the form of GeoJSON standard.

The cross-platform smart and sustainable tourism system has been tested by the authors in a real environment with more than 230 attractions and tourist services classified under different categories such as Geo-heritage, Humanistic, Community tourism, Ecological area, Resort, etc. in Hoa Binh and Bac Kan provinces (Figure 9, Figure 10). The mobile application work stably on Android and iOS operating system with many features such as scheduling, directions, search on the map, etc. The tourists can use their smartphones to provide feedback, ratings and preferences about their travel experiences. Service providers can use sensors to monitor the availability and quality of their facilities and services.

Fig. 7. Illustrating the deployment of smart and sustainable tourism system

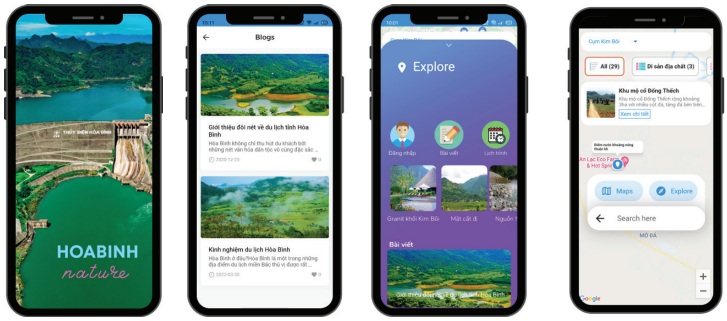

Fig. 8. User interfaces of smart and sustainable tourism system

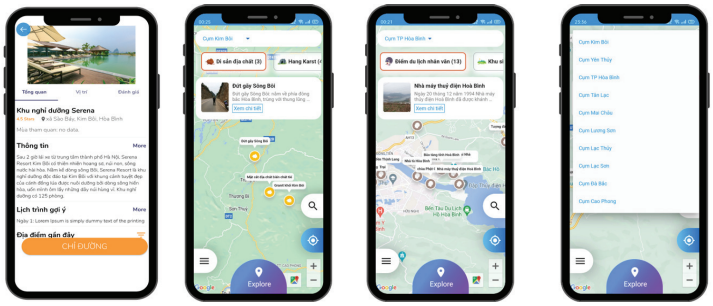

Fig. 9. Management of attractions and tourism services by thematic groups of Geoheritage, Humanistic Tourism

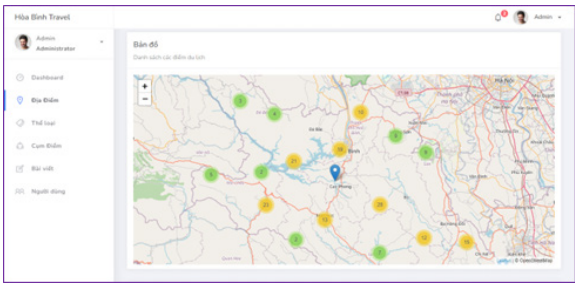

Fig. 10. List of tourist spots in Hoa Binh province

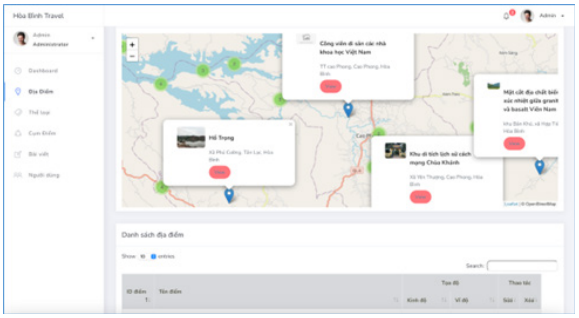

Fig. 11. The spatial distribution and density of tourist spots

The data visualization feature of system uses web GIS and interactive maps to display the analysed data in an intuitive and user-friendly way (Figure 9). Another feature is data dissemination, which enables sharing the data and the results with different stakeholders and users through web services and mobile applications.

The results indicate that the integration of mobile and web GIS technologies can enhance smart and sustainable tourism by providing tourists with more information, services, and opportunities to interact with the destination and other tourists. The results also suggest that the integration of mobile and web GIS technologies can improve the tourist experience and behaviour by increasing their satisfaction, and environmental awareness.

4 CONCLUSION

Mobile GIS and web GIS technology are emerging as powerful tools for smart and sustainable tourism. They enable tourists to access, share and interact with spatial information anytime and anywhere, using their mobile devices. They also allow tourism managers and planners to monitor, analyse and optimize the tourism resources and activities in real time, using web-based platforms. In this paper, we propose a framework for integrating these technologies into a comprehensive tourism information system that can support for smart and sustainable tourism. We illustrate the potential benefits of this framework with some examples from existing projects and studies. The results show that the system works stably, meets many users, and accesses quickly and accurately. Spatial data is displayed on the map in an intuitive and diverse manner. Our smart tourism system will help to enhance the tourism experience, improve the tourism management and promote the tourism sustainability by providing smart and personalized services, optimizing the use of resources and reducing the negative impacts of tourism activities. In the future, the authors will continue to research and apply some machine learning technques for recommendation systems and give futher spatial analysis for local goverments in planing and developing tourism more sustainably and efficienly.

5 ACKNOWLEDGEMENTS

This work is supported by the project no. B2022-MDA-01 granted by Ministry of Education and Training (MOET).

Literatura – References

1. Pei-Jung Lin, Chih-Chung Kao, Ka-Hou Lam & I-Chen Tsai . Design and Implementation of a Tourism System Using Mobile Augmented Reality and GIS Technologies. 2014. https://link.springer.com/chapter/10.1007/978-3-319-04573-3_133
2. James M. Magige, Charlynne Jepkosgei, and Simon M. Onywere. Use of GIS and Remote Sensing in Tourism. 2020. https://link.springer.com/referenceworkentry/10.1007/978-3-030-05324-6_118-1
3. Junxiang Zhu, Peng Wu. Towards Effective BIM/GIS Data Integration for Smart City by Integrating Computer Graphics Technique . 2021 https://www.mdpi.com/2072-4292/13/10/1889
4. Karishma Solanki, Danish Faraz Abbasi, Munir Hosain, Emran Salahuddin, Shaymaa Ismail Ali, Shahad Ahmed. Enhancing the Tourism Experience Using Mobile Augmented Reality: Geo-Visualization Techniques. 2023. https://link.springer.com/chapter/10.1007/978-3-031-33743-7_23
5. P. Achaliya, "Smart Travel Guide: Application for Android Mobile.," 2012.
6. Chulmo Koo and Ulrike Gretzel.Mobile Technology and Smart Tourism Development. 2017. https://www.mdpi.com/journal/sustainability/special_issues/smart_tourism_development
7. Q. a. U. o. W. Huang, "Programming of Mobile GIS Applications," Geogr. inf. sci. technol. body knowl, 2020.
8. L. S. Vailshery, "Cross-platform mobile frameworks used by global developers 2021," Statista, 2022. [Online]. Available: https://www.statista.com/statistics/869224/worldwide-software-developer-working-hours/.
9. M. Napoli, in Introducing Flutter and Getting Started, 2019, pp. 1-23.

Study on Technological Solutions to Increase the Recovery and Quality of the Copper Concentrate at Ta Phoi Beneficiation Plant in Vietnam

NHU Thi Kim Dung[1)], PHAM Thi Nhung[1)], VU Thi Chinh[1)], LE Viet Ha[1)]*

[1)] Faculty of Mining, Hanoi University of Mining and Geology, Hanoi, Vietnam
*Corresponding author: nhuthikimdung@humg.edu.vn

http://doi.org/10.29227/IM-2023-02-35

Submission date: 19-08-2023 | Review date: 27-09-2023

Abstract

The Ta Phoi beneficiation plant is one of the main copper beneficiation plants in Vietnam. The plant has been put in operation since 2019 and annually process more than one million tons of ROM copper ore to collect 32 thousand tons of copper concentrate of 23% Cu. In the first years of operation the plant's metallurgical performance has not been consistent and not been as good as in design. The most important task at the company in this day is to improve and stabilize this performance with a target to obtain the copper concentrate of 23% Cu and recovery of over 91.5%. This report presents some research results to increase the recovery and quality of the copper concentrate at Ta Phoi beneficiation plant. As the results, some technological solutions have been proposed concerning the optimization of the reagent regime as well as of flotation flowsheet. Some of these solutions have been tested directly in the plant production line and have the perspective to apply.

Keywords: *copper concentrate, optimization, reagent regime, flotation flowsheet*

1. Introduction

Ta Phoi Copper Joint Stock Company – VINACOMIN was established on January 15, 2009. After its establishment, the Company actively carried out exploration work and was approved by the National Mineral Reserve Evaluation Council with reserves of 11.3 million tons of primary ore, equivalent to 99.2 thousand tons of copper metal and 3.5 tons of gold. Experiencing many difficulties and challenges, after a lot of efforts, Ta Phoi Copper Joint Stock Company ended the investment phase in 2019. On November 16, 2019, Ta Phoi copper beneficiation plant went into official production. During the operation, the plant's employees always strive non-stop, apply new technology in production and improve the processing technology scheme to bring the plant into stable operation to achieve the annual set target. The production and business efficiency of the plant in recent years is higher than in the previous year, the capacity and the technological performance have exceeded or reached approximately to the design.

Since going into official production up to now, Ta Phoi copper beneficiation plant has changed its technology flowsheet three times. In the first stage, the plant operates at the design diagram and technology regime. By May 2021, the plant has introduced 3 tank cells for rougher flotation and fast cleaner. And in July 2021, the plant will remove the grinding stage 2. The current technological flowsheet of the plant is as shown in Figure 1.

At present, the capacity of Ta Phoi copper beneficiation plant is 1 million tons of ROM ore per year, with copper content is about 0.8%. The content and recovery of copper ore concentrate after flotation has basically reached the design level (concentrate content: 23% Cu, recovery: 91.5%) [3]. The actual plant performance shows that the content and recovery of copper concentrates are still unstable and there is still potential for improvement in technology and equipment to increase the copper recovery (to > 91.5%) and the stabilize the concentrate content at level of 23% Cu.

2. Methods and reagents

– A number of open-circuit flotation tests were conducted at the laboratory of the Mineral Processing Department, University of Mining and Geology, using a mixture of different collectors and depressants. The purpose is to choose the best reagent regime for Ta Phoi copper ore.

– Tests on plant's ground samples at the laboratory of Ta Phoi copper beneficiation plant with the selected reagent regime to evaluate the ability to increase the content and recovery of copper concentrate products.

– Proposing a plan to run tests at the actual plant production line with a change in the reagent regime.

– The reagents that were used in tests as following [4-5]:

Modifier: Lime;

Collectors: Sodium Butyl xanthate (SBX), Potassium Amyl Xanthate (PAX), AP2, Ammonium Dibutyl Dithiophosphate (ADD);

Depressants: Dextrin, water glass;

Frother: Pine oil

3. Results and discussion

3.1. Tests at the laboratory of the Mineral Processing Department

– The samples are collected at the plant, taken at the feed conveyor belt to the mills. The results of the analysis of the sample material composition are shown in documents [1-2]. The ore sample belongs to copper sulfide ore, with a small amount of copper oxide minerals (malachite, azurite). Copper content in raw ore sample ~0.8%.

The open-circuit test flowsheet as in Figure 2.

The fixed flotation conditions are as follows: Mesh of grind:

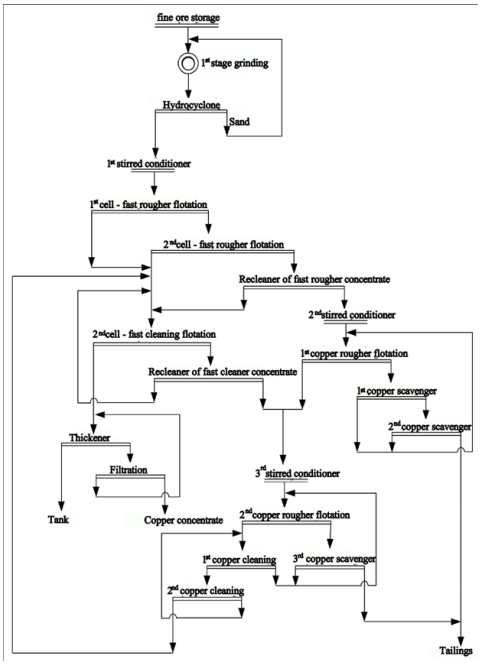

Fig. 1. The current technological flowsheet of the plant

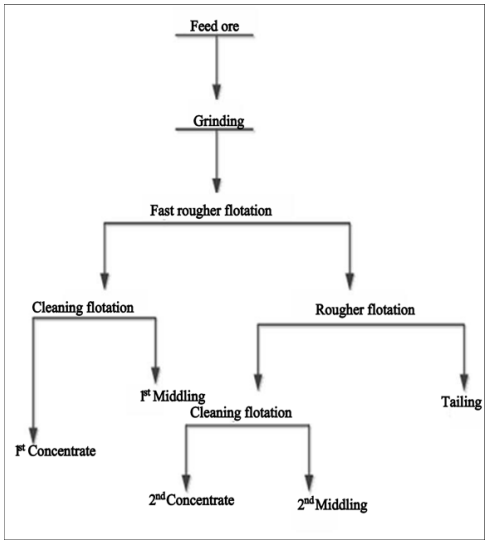

Fig. 2. The open-circuit test flowsheet

62.67% -0.074 mm; pH medium modified by lime: 9–10; pine oil added to the fast rougher flotation stage: 10 g/T and to rougher flotation: 10 g/T.

a) Tests at collector combination

The combination of collectors that added to the fast rougher flotation stage and the rougher flotation stage: Butyl xanthate with Amyl xanthate; Butyl xanthate with Dithiophosphate; Butyl xanthate with AP2, Amyl xanthate with AP2 [5].

Dosage at fast rougher flotation stage: 10/10 (g/T)

Dosage at rougher flotation stage: 20/20 (g/T)

The test results are shown in Table 1.

The results in Table 1 show that, when butyl xanthate and dithiophosphate is combined, the content of 1st copper concentrate and 2nd copper concentrate is higher, the loss of copper to the tailing is the least (3.36%). Therefore, in the following tests, the combination of butyl xanthate and dithiophosphate was choosen.

b) Tests at depressant combination

– Collectors dosage to the fast rougher flotation stage: Butyl xanthate/Dithiophosphate = 10/10 (g/T); and to the rougher flotation stage: Butyl xanthate/Dithiophosphate = 10/10 (g/T);

– The depressant dosage to the cleaning flotation: Dextrin/water glass = 50/50 (g/T)

Change the depressant dosage to the fast rougher flotation stage: Lime/dextrin = 100/20; 500/100; 1000/200; 2000/400 (g/T).

The test results are shown in Table 2.

The results in Table 2 show that, at the dosage of lime/dextrin = 1000/200 (g/T) the first copper concentrate and the second copper concentrate have obtained with higher content and recovery, and lower tailing content of 0.07% Cu. Therefore, in the fast rougher flotation stage, the additional depressants of lime and dextrin with a dosage of 1000/200 (g/T) is desirable.

3.2. Tests on plant samples

– The samples were taken after the mill circuit, at the hy-

Tab. 1. The results of the collectors combination tests

Collectors	Products	Yield (%)	Content of copper (%)	Recovery (%)
Butyl xanthate/ Amyl xanthate	1st Concentrate	2.24	23.82	68.50
	1st Middling	1.64	5.34	11.24
	2nd Concentrate	0.96	8.66	10.74
	2nd Middling	2.49	1.11	3.56
	Tailing	92.67	0.05	5.96
	Feed	**100.00**	**0.8**	**100.00**
Butyl xanthate/ Dithiophosphate	1st Concentrate	0.86	30.55	33.50
	1st Middling	1.06	16.75	22.52
	2nd Concentrate	1.13	20.23	29.22
	2nd Middling	1.12	7.78	11.10
	Tailing	95.83	0.03	3.66
	Feed	**100.00**	**0,8**	**100,00**
Butyl xanthate/AP2	1st Concentrate	1.49	26.27	49.19
	1st Middling	2.20	9.49	26.28
	2nd Concentrate	1.18	10.02	14.82
	2nd Middling	2.14	1.44	3.86
	Tailing	92.99	0.05	5.85
	Feed	**100.00**	**0.8**	**100.00**
Amyl xanthate/AP2	1st Concentrate	1.15	28.82	40.94
	1st Middling	1.99	11.30	27.77
	2nd Concentrate	1.08	13.45	17.93
	2nd Middling	3.03	1.12	4.19
	Tailing	92.75	0.08	9.16
	Feed	**100.00**	**0.8**	**100.00**

Tab. 2. The results of the depressants combination tests

Lime/Dextrin (g/T)	Products	Yield (%)	Content of copper (%)	Recovery (%)
100/20	1st Concentrate	1.91	27.02	64.78
	2nd Concentrate	0.99	12.44	15.46
	1st Middling	1.88	2.12	4.99
	2nd Middling	1.71	1.96	4.20
	Tailing	93.51	0.09	10.56
	Feed	**100.00**	**0.80**	**100.00**
500/100	1st Concentrate	1.90	27.43	64.80
	2nd Concentrate	0.96	15.02	17.87
	1st Middling	1.57	1.92	3.74
	2nd Middling	1.49	2.28	4.23
	Tailing	94.08	0.08	9.36
	Feed	**100.00**	**0.80**	**100.00**
1000/200	1st Concentrate	1.92	27.61	66.15
	2nd Concentrate	0.99	15.43	19.10
	1st Middling	1.62	1.96	3.97
	2nd Middling	0.91	2.23	2.53
	Tailing	94.56	0.07	8.26
	Feed	**100.00**	**0.80**	**100.00**
2000/400	1st Concentrate	1.85	27.02	62.37
	2nd Concentrate	1.02	12.05	15.33
	1st Middling	1.90	2.22	5.26
	2nd Middling	1.70	1.98	4.20
	Tailing	93.53	0.11	12.84
	Feed	**100.00**	**0.80**	**100.00**

Tab. 3. The first closed-circuit flotation test results

Products	Yield (%)	Content of copper (%)	Recovery (%)
1st Concentrate	2.12	27.04	71.97
2nd Concentrate	0.98	16.76	20.62
1st Tailing	93.98	0.06	7.08
2nd Tailing	2.92	0.09	0.33
Total of copper concentrates	***3.10***	***23.79***	***92.59***
Total of Tailings	***96.90***	***0.06***	***7.41***
Feed	**100.00**	**0,8**	**100.00**

Tab. 4. The second closed-circuit flotation test results

Products	Yield (%)	Content of copper (%)	Recovery (%)
1st Concentrate	2.14	26.51	68.81
2nd Concentrate	1.11	17.09	23.01
1st Tailing	94.76	0.05	5.75
2nd Tailing	1.99	1.01	2.44
Total of copper concentrates	***3.25***	***23.29***	***91.82***
Total of Tailings	***96.75***	***0.07***	***8.18***
Feed	**100.00**	**0.8**	**100.00**

drocyclone overflow pipeline supplied to the flotation at the plant. The sample has a content of about 0.8% Cu, the mesh of grind is about 62% -0.074mm.

– The closed-circuit flotation was tested at plant's laboratory in 02 flowsheets (Figures 3 and 4) based on the results of open-circuit flowsheet tests with the combination of collectors and depressants (Section 3.1) as well as the plant's data.

– The reagent regime as the following:

The first flotation stage: Lime/dextrin: 1000/200 (g/T); Butyl xanthate/Dithiophosphate: 10/10g/t; Pine oil: 10 g/T

The second flotation stage: Butyl xanthate/Dithiophosphate: 20/20 (g/T); Pine oil: 10 g/T

The first cleaning stage: Dextrin/Water glass = 50/50 (g/T)

The second cleaning stage: Dextrin/Water glass = 50/50 (g/T)

The scavenger stage: Butyl xanthate/Dithiophosphate: 10/10 (g/T); Pine oil: 10 g/T

The test results are shown in Tables 3 and 4.

The results of the tests according to the 1st and 2nd closed-circuit flotation flowsheet showed that the copper concentrate reached the target in terms of content and recovery, content was over 23% Cu, recovery was over 91.5%. The copper content in tailing is 0.06–0.07%. The concentrate at the 1st closed-circuit flotation flowsheet has the higher copper content than in the 2nd flowsheet and lower copper content in the tailing.

4. Conclusion

From the research results, the following conclusions can be drawn:

– Currently, the technology flowsheet of the plant has 3 tank cells for rougher and fast cleaning, abandoning the 2nd grinding stage. The capacity of the plant is 1 million tons of ROM ore per year, copper content is about 0.8%. The content and recovery of copper concentrates after flotation were basically achieved the design level (content: 23% Cu, recovery: 91.5%).

– The collector put in flotation stages are butyl xanthate and AP2.

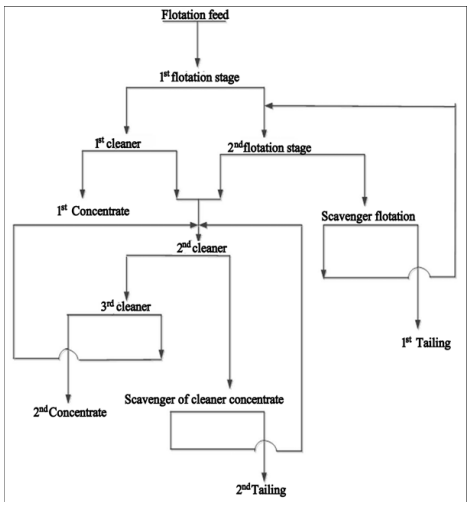

Fig. 3. The first closed-circuit flotation flowsheet

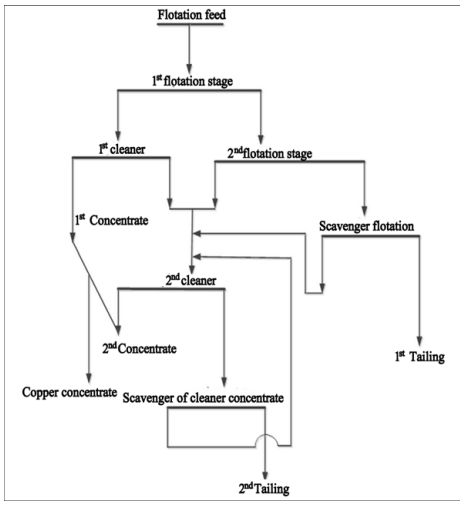

Fig. 4. The second closed-circuit flotation flowsheet

–The tests results of some flotation flowsheets in the laboratory using a combination of collectors and depressants give the copper concentrate with quite good processing performance. The combination of butyl xanthate with dithiophosphate gives the best seperation results, the depressants can combine are lime with dextrin and dextrin with water glass.

– Closed-circuit flotation using a combination of collectors and a combination of depressants: butyl xanthate with dithiophosphate, lime with dextrin and dextrin with water glass, allows to obtain the copper concentrate reaching the target content of over 23% Cu, recovery over 91.5%. The tailing copper content is 0.06–0.07%.

Literatura – References

1. NHU Thi Kim Dung (2012), Study on sample of reasonable copper ore processing technology in Ta Phoi - Lao Cai region, Center for Science and Technology for processing and using minerals, Viet Nam Association for Mineral Processing
2. NHU Thi Kim Dung et al (2022), Some studying results on the Ta Phoi - Lao Cai copper ore composition and mineralogy, Mining Industry Journal No. 3 – 2022
3. Ta Phoi Copper Joint Stock Company – Vinacomin (2021), Report on copper flotation technology targets (2019-2021)
4. Mark E. Schlesinger, Matthew J. King, Kathryn C. Sole, William G. Davenport (2011), Extractive Metallurgy of Copper, Elsevier, Fifth Edition 2011
5. Srdjan M. Bulatovic (2007), Handbook of Flotation Reagents, Elsevier Science & Technology Books
6. Walawska B, Szymanek A, Szymanek P. Impact of decomposition temperature on the surface area of sodium bicarbonate Przemysł Chemiczny 2012, pp.1049-1052
7. Sambor A, Szymanek A Analysis of the migration of chemical compounds from fly ash exposed the weather condition ,Chemical and Process Engineering. 2014, ISSN:0208-6425

Promoting Gender Equality and Awareness in the Vietnamese Mining Sector: Perceptions, Challenges, and Policy Recommendations

Pham MINH HANG[1)], Pham THI LUONG[1)], Nguyen THI HOAI NGA[2)], Pham KIEN TRUNG[3)]*

[1)] Center for Gender, Family & Environment in Development (CGFED), Hanoi, 100000, Vietnam
[2)] Innovations for Sustainable and Responsible Mining (ISRM) Research Group, Hanoi University of Mining and Geology, Hanoi, 100000, Vietnam
[3)] Hanoi University of Mining and Geology, Hanoi, 100000, Vietnam; email: phamkientrung@humg.edu.vn

http://doi.org/10.29227/IM-2023-02-36

Submission date: 21-08-2023 | Review date: 28-09-2023

Abstract

Females in the industry nowadays have been offered many opportunities to develop their careers. However, the chances are not the same in different areas or sectors. This study investigated the perceptions and understanding of gender-related issues in the mining sector among potential young workers and industry experts in Vietnam. The study employs Oxfam's Gender Impact Assessment Guidelines for extractive industries and the Convention on the Elimination of All Forms of Discrimination Against Women - CEDAW's Women's Economic and Social Rights Framework to assess gender-related issues in the mining sector. A survey of 207 students in Hanoi was conducted, besides focus group discussions and in-depth interviews with gender and mining experts.

Findings reveal significant differences in knowledge and awareness of gender issues between students, emphasizing the need to integrate gender knowledge into specialized fields such as mining. In addition, professionals working solely in the mining sector demonstrated a lack of sensitivity to gender issues. Consequently, the study recommends capacity building, seminars, and exchanges to help mining professionals incorporate a gender perspective into their activities.

Current policies exhibit gender neutrality, indirectly excluding women's participation and compromising men's safety in the mining sector. The study proposes policy recommendations for enhancing the protection of workers in the mining industry and promoting gender equality. These include incorporating gender perspectives into relevant laws, raising awareness of gender issues among policymakers and professionals, and increasing the mining sector's presence in the media to encourage youth to pursue careers in this field.

Keywords: *Gender equality, gender knowledge, gender perspectives, extractive industries, mining sector*

1. Introduction

The mining industry plays a crucial role as one of the main sources of revenue for many countries and is a focal point for economic growth and social development, particularly in resource-rich nations (Abrahamsson & Johansson, 2021; Johansson et al., 2020). However, in the natural resource extraction sector, social welfare, cultural preservation, local livelihoods, and polluted environment. Mining activities lead to land transfers, forced relocations, increased poverty among local communities, unstable security, violence, and crime (Hicks, 2011; Khoáng Sản – Phát Triển – Môi Trường: Đối Chiếu Giữa Lý Thuyết và Thực Tiễn | Trung Tâm Con Người và Thiên Nhiên, n.d.; Why Extractive Industry Gender Advocates Should Ask For Contract Transparency | Natural Resource Governance Institute, n.d.; T. K. T. Nguyen, 2020). Women and children in affected communities become landless laborers, often falling victim to human trafficking, violence, and health issues such as reproductive health, malnutrition, and poverty (Camey et al., n.d.-a, n.d.-b; Ringblom & Johansson, 2020). Additionally, the voices of women are not adequately heard by policymakers, and their participation in mining-related policy-making processes is not addressed (Abrahamsson & Johansson, 2021; Camey et al., n.d.; Johansson & Ringblom, 2017; Ringblom & Johansson, 2020). Gender inequalities in employment and women's participation can harm business operations, as well as have negative impacts on society and the local economy (Eftimie et al., 2009; Fernandez-Stark et al., 2019; Women, Business and the Law 2020., 2020). Conversely, enhancing gender equality by empowering women can improve the labor force, bring business benefits, and result in long-term outcomes for health, education, and local development. Raising awareness of gender aspects in mining can help ensure that women are supported and have positive outcomes in this industry (Camey et al., n.d.; Eftimie et al., 2009; Fernandez-Stark et al., 2019; Hicks, 2011; Mundoli, 2013; N. Nguyen et al., 2018; T. K. T. Nguyen, 2020).

This research is important as it focuses on the roles and participation of both men and women in the mining industry. By exploring gender aspects in this field, the study helps us gain a deeper understanding of the social differences imposed on men and women and the impacts of mining activities on different groups. The research provides essential information to promote sustainable development in the mining sector and ensure gender equality within it.

This research contributes to the existing body of knowledge on the roles of gender in the mining industry. Previous studies have primarily focused on issues related to women in this field (Abrahamsson & Johansson, 2021; Camey et al., n.d.; Lahiri-Dutt & Burke, n.d.; Mundoli, 2013; Ringblom & Johansson, 2020; Women in Mining Towards Gender Equality, 2021). However, this research expands the scope to study both men and women and also examines the perspectives and awareness of the younger generation regarding gender equality in mining. By doing so, this study offers a comprehensive view of the subject and sheds light on the multifaceted nature of gender roles in the mining industry.

The research seeks to make practical contributions by designing appropriate intervention programs to develop the mining industry based on gender equality, ultimately benefiting communities and society. Moreover, the study expands our understanding of gender roles in the mining sector and their impacts on communities and society.

We next review the animosity literature to develop our conceptual model. We then provide our research methodology, followed by the results of our survey. We conclude by discussing the implications, limitations, and future research directions of our work.

2. Conceptual background and conceptual framework

Gender equality refers to equal opportunities and conditions for women and men to unleash their potential, exercise human rights, and participate in the process of social development. Gender mainstreaming is a method aimed at promoting gender equality and the rights of women and girls in the industrial mining environment. Although policies and regulations in Vietnam affirm equal rights and non-discrimination towards women, the reality shows that women participating in the mining sector still face numerous difficulties. There is gender discrimination in occupational segregation and access to resources and information, which impacts the participation and contributions of women in the mining industry.

However, previous studies on gender equality in the mining sector in Vietnam have been incomplete and lacking information about the different impacts on men and women (EITI International Secretariat, n.d.; Why Extractive Industry Gender Advocates Should Ask For Contract Transparency | Natural Resource Governance Institute, n.d.; Women in Artisanal and Small-Scale Mining: Challenges and Opportunities for Greater Participation, 2014; Fernandez-Stark et al., 2019; Hicks, 2011). Therefore, research on gender equality in mining activities is necessary to gain a better understanding of the roles and impacts of the industry on both genders. From there, appropriate policies and measures can be formulated to promote gender equality and ensure the rights of both men and women in the development of the mining sector in Vietnam.

The research and enhanced awareness of gender equality in mineral exploitation in Vietnam are crucial to guarantee equal rights and fair treatment for women and men. This requires the promotion of policies and regulations that support gender equality, as well as the strengthening of awareness and a shift in community perspectives regarding the roles and contributions of women in the mining sector.

3. Research methodology

3.1. Measures and questionnaire development

The research will employ an approach and construct a toolkit based on Oxfam's Impact Assessment Guidance for Extractive Industries and the Women's Economic and Social Rights Framework of the CEDAW Convention.

The questionnaires are categorized into four dimensions:

1. Work division
2. Employment opportunities
3. Wage level
4. Decision-making

To suit the target audience, the research team conducted four focus group discussions (with eight participants in each group) with students to adjust the questionnaire accordingly.

After obtaining survey results, the study conducted ten in-depth interviews: three with gender experts and seven with professionals working in the mining sector, including three lecturers teaching in the field of mining, to address gender equality issues in the mining industry.

3.2. Sample and data collection

The research conducted a survey and collected data from 207 students currently studying in the education organizations of mining and geology in Vietnam. They are those who understand about mining and expected to work in the mining industry later. Responses included 95 males, 108 females, and 4 individuals identifying with other genders.

Data processing with the questionnaire information was collected online through Google Form and analyzed using SPSS software.

4. Results

Labor Division: When asked about the roles of women in the mining industry, in the survey, 140 students (68%) stated that women mainly perform administrative and office work; 102 students (49.5%) chose women for cleaning and cooking tasks in the mine; 96 students (46.6%) opted for women working in service business areas. 90 students (43.7%) agreed that women could take up specialized technical jobs such as engineers and experts. Only 18 students (8.7%) selected women for jobs like drilling, mining, and rock blasting.

Similarly, in group discussions and in-depth interviews, both students and experts agree that labor allocation depends on the nature of mining. Additionally, some experts believe that many women are hired in mines to retain male employees, as the mining life is tough and unstable, leading some men to quit and return to their hometowns. If an employee has an accident at work, the company will recruit his wife to work in the mine, if she is willing to, as a form of compensation.

Women can work as engineers and in open-pit mining areas, but they are not recruited for underground mining. In some regions, such as Ha Giang province, job advertisements explicitly state that they only hire men, excluding women. Even in cases where women are already working in a plant and want to transfer to positions related to machinery, human resources, or leadership, they are not allowed.

Based on survey results, group discussions, and in-depth interviews, the participants believe that the gender disparity in labor participation in the mining industry is influenced by societal beliefs, biological differences between men and women, and policies. The mining industry is perceived as demanding, hazardous, physically taxing, and potentially affecting women's reproductive health. Superstitions also lead to the belief that women bring bad luck, so they are discouraged from working underground. Social beliefs dictate that accounting and bookkeeping jobs, requiring meticulousness and attention, are more suitable for women, while specialized and physically demanding jobs are suited for men. Women also lack confidence and physical strength for technical jobs, so they avoid applying for such positions.

"Women are often involved in jobs like nursing, accounting, healthcare, and cleaning, while men are mostly in charge of mining operations, drilling, and driving heavy machinery. In Vietnam, it's uncommon for women to drive heavy machinery like trucks or excavators. Gender-based labor allocation in society

tends to direct women to lighter, office-related jobs, resulting in fewer women choosing to become engineers or participating in innovative work", explains an expert.

"In fact, in the current mining enterprises, the employment positions for women are relatively suitable. It takes into account gender-specific characteristics that may influence work quality and working conditions for the health of the workers", explains other expert.

Job opportunities: Regarding job opportunities, nearly half of the responses (41%) believe that mining increases job opportunities for women. In contrast, only 27.7% of students think that mining adds to the workload for women.

Interviews with students and mining experts also agree that prioritizing local labor has helped both local people and women in the mining areas to have more job opportunities and increase their income. However, some experts argue that the inconsistent implementation of local labor prioritization results from a lack of specialized training. Local people often do manual labor or establish food services or accommodations for miners. In many places, due to poor labor safety conditions leading to frequent workplace accidents, many companies avoid recruiting locals, leading to more migration of male workers to other areas, leaving more workloads on women and the elderly. This trend also affects the care and education of children.

Wages level: The average income between male and female labor in the mining sector is the same, 65 students agreed, while 46 students disagreed. Some argue that men in the mining industry work more and engage in more physically demanding and technically complex tasks, which may lead to higher income. However, the difference in income is due to the value placed on men's tasks, higher wages for specific jobs, and formal positions rather than wage discrimination between genders. If men and women hold the same position, they would have the same income.

An expert added: "Typically, there is no difference in income and benefits if a woman works at a company with foreign investment or a state-owned company; they will enjoy the same policies as men, including all allowances. However, if the payment is based on productivity, the better physical health of men may lead to higher earnings for them".

Decision-making: Overall, the decision-making process in the mining industry involves male participation more frequently than female participation in environmental impact assessment meetings. Two main reasons were given for this choice. Firstly, 63 students thought that representatives should attend, so the head of the household would go (among them, 36 students chose the head of the household to be male, and 8 chose female). Secondly, 50 students cited that those with better understanding of relocation and compensation matters should participate (among them, 20 students believed that males had better understanding, and 11 believed that females had better understanding).

However, this result contrasts with the agreement of 69 students who believe that women should be the ones participating in community meetings to represent the family, while 42 students disagree. Experts explain that the level of participation depends on the content of the meetings. Women often attend meetings where they have no significant contributions, while men attend meetings involving issues outside the community, such as working in remote areas. In many cases, women are more knowledgeable about the actual situation in the local area.

"Who gets interviewed and how it is structured depends on the perspectives and capabilities of the interviewer, team, or interview panel. If the local officials do not enforce strict criteria, situations may arise where they specifically call the household head for the interview, and that household head may be a male. However, if they only require one representative per family, then sometimes women also have the opportunity to participate. I must admit that at the local level, women, especially those who stay at home, understand the impact of mining activities on the environment and their family's life the most. For instance, if they are responsible for cleaning the house every day, they know how the mining activities create dust and affect their home. In contrast, men may not be aware, or they might be the ones who go to the market, knowing that prices are high in the area due to mining activities development, as more people come, and demand increases, will enlarge the prices", explains the expert.

5. Discussion and conclusion

5.1. Discussion

- There is a need for additional evidence to demonstrate gender issues in mining, particularly the impacts and effects on the communities living and affected in the mining areas at each stage/phase of the mining chain.
- Gender should be consider a matter to be integrated into the Mineral Law, Environmental Protection Law, Tax Law, fees, charges, and related documents, especially integrating gender into the process of conducting environmental impact assessments, compensations for land clearance, and community monitoring to promote women's participation in labor and decision-making rights.
- Awareness among experts need to be enhanced for drafting the Mineral Law, Environmental Protection Law, Tax Law, fees, charges, and related documents about gender in the mining industry, including knowledge about gender/equality, differences in labor, wages, decision-making rights, social prejudices, etc., affecting the labor force and long-term economic prospects.
- It is essential to strengthen the presence of the mining industry in the media, showcasing the contributions and relevance of mining to people's lives, the employment opportunities it offers to all genders, and especially encouraging young women to pursue careers in mining.
- Students, lecturers, and mining experts need to increase their awareness of gender in the mining industry through various approaches, such as extracurricular activities, seminars, media materials, artistic performances, etc. For example, in mining schools, gender-related topics can be integrated into lectures and research projects to allow students to observe the realities, write essays on ongoing situations, and analyze their impacts.

5.2. Conclusion

Gender equality is the Goal 5 among the 17 goals of sustainable development by the United Nations. It is essential to integrate gender knowledge into specialized fields, particularly mining, through various forms, such as lectures, practical internships, extracurricular activities, training programs, etc. For experts solely working in the mining industry, they may lack aware-

ness about gender issues (gender insensitivity). Hence, training sessions, workshops, and exchanges should be conducted to provide mining experts with a gender lens in their activities.

Enduring gender stereotypes are one of the barriers leading to the lack of female participation in the mining industry, especially in technical, specialized, and leadership positions. Therefore, media support, counseling in enrollment, career guidance, etc., are required to promote the participation of young women in mining, by showing them the opportunities, career prospects, labor protection policies, etc., in the mining sector.

Regarding policies: The current policies are gender-neutral, indirectly excluding the participation of women while also not ensuring the safety of men when assuming that hazardous and toxic tasks are designated for men. Hence, policies should focus on enhancing measures for labor protection and safety in the mining industry, aiming at the use of tools and equipment to replace human involvement.

Environmental impact assessments should incorporate gender perspectives to recognize the profound effects of mining on women.

As an exploratory study, this research has some limitations:

i) Initiative and suggestive research on Gender in Mining from the perspective of young people and experts.

(ii) The study was only conducted on a small sample size (207 students in Hanoi); therefore, the study cannot guarantee representativeness of all students or young people.

(iii) The study only focuses on phase 1 of the mining value chain. As a result, the research content only addresses issues related to the impact of mining, division of labor, participation in the mining industry, claim process, and environmental impact assessment. It does not delve into later-stage issues such as taxes, fees, monitoring of activities, or compensation/return, etc.

(iv) The study was conducted during the Lunar New Year, when the response to the online data collection was not a priority.

Acknowledgments

This research was supported financially by Oxfam Vietnam.

The paper was presented during the 7th VIET - POL International Conference Scientific-Research Cooperation between Vietnam and Poland.

Literatura – References

1. Abrahamsson, L., & Johansson, J. (2021). Can new technology challenge macho-masculinities? The case of the mining industry. Mineral Economics, 34(2), 263–275. https://doi.org/10.1007/s13563-020-00221-8
2. Camey, I. C., Sabater, L., Owren, C., Boyer, A. E., & Wen, J. (n.d.). Gender-based violence and environment linkages: the violence of inequality. https://twitter.com/IUCN/
3. Eftimie, A., Heller, K., & Strongman, J. (2009). Extractive Industries and Development Series #8 Gender Dimensions of the Extractive Industries: Mining for Equity.
4. Fernandez-Stark, K., Couto, V., & Bamber, P. (2019). Industry 4.0 in Developing Countries: The Mine of the Future and the Role of Women.
5. Hicks, J. (2011). Strengthening women's participation in local governance: Lessons and strategies. Community Development Journal, 46(SUPPL. 1). https://doi.org/10.1093/cdj/bsq048
6. Johansson, M., & Ringblom, L. (2017). The Business Case of Gender Equality in Swedish Forestry and Mining - Restricting or Enabling Organizational Change. Gender, Work and Organization, 24(6), 628–642. https://doi.org/10.1111/gwao.12187
7. Khoáng sản – Phát triển – Môi trường: Đối chiếu giữa lý thuyết và thực tiễn | Trung tâm Con người và Thiên nhiên. (n.d.). Retrieved July 14, 2023, from https://nature.org.vn/vn/2013/05/khoang-san-phat-trien-moi-truong-doi-chieu-giua-ly-thuyet-va-thuc-tien/
8. Lahiri-Dutt, K., & Burke, G. (n.d.). 2. Gender Mainstreaming in Asian Mining: A Development Perspective 1.
9. Mundoli, S. (2013). Gender equality and extractive industry in the Lower Mekong region. https://doi.org/10.13140/2.1.3743.0406
10. Nguyen, N., Boruff, B., & Tonts, M. (2018). Fool's gold: Understanding social, economic and environmental impacts from gold mining in Quang Nam province, Vietnam. Sustainability (Switzerland), 10(5). https://doi.org/10.3390/su10051355
11. Nguyen, T. K. T. (2020). Studying factors affecting environmental accounting implementation in mining enterprises in Vietnam. Journal of Asian Finance, Economics and Business, 7(5), 131–144. https://doi.org/10.13106/JAFEB.2020.VOL7.NO5.131
12. Ringblom, L., & Johansson, M. (2020). Who needs to be "more equal" and why? Doing gender equality in male-dominated industries. Equality, Diversity and Inclusion, 39(4), 337–353. https://doi.org/10.1108/EDI-01-2019-0042
13. Why Extractive Industry Gender Advocates Should Ask For Contract Transparency | Natural Resource Governance Institute. (n.d.). Retrieved July 14, 2023, from https://resourcegovernance.org/blog/why-extractive-industry-gender-advocates-should-ask-contract-transparency
14. Women, business and the law 2020. (2020). World Bank Group.
15. Women in mining Towards gender equality. (2021). www.ilo.org/publns.

Dimension-Stone Quarrying Optimization through Integrated Modelling between Joint Sets and Cutting Grid: a Case Study at Tan Long Dimension Stone Quarry in Southcentral Coastal Province of Binh Dinh

PHAM Van Viet[1,2], NGUYEN Anh Tuan[1,2], PHAM Van Hoa[1,2], TRAN Dinh Bao[1,2]*

[1)] Hanoi University of Mining and Geology, 18 Vien Street, Hanoi, Vietnam
[2)] Innovations for Sustainable and Responsible Mining (ISRM) research group, Hanoi University of Mining and Geology, Hanoi, 100000, Vietnam
* Corresponding author: phamvanviet@humg.edu.vn

http://doi.org/10.29227/IM-2023-02-37

Submission date: 23-08-2023 | Review date: 29-09-2023

Abstract

Dimension-stone quarrying optimization is significantly important to increase the recovery ratio of dimension stone and to reduce the cutting cost. Due to fracture-existed rock mass, in the mining operation block size and mining direction influences to the recovery ratio and the cutting cost. Therefore, the paper suggests the quarrying optimization for dimension stone to obtain the highest recovery ratio and the lowest cutting cost, based on optimizing block size and mining direction to get a cutting grid of dimension stone. Through developing an integrated modelling between joint set modelling and cutting grid modelling, intact blocks and fractured blocks were generated. From this, block statistics were conducted to get the maximum recovery ratio of dimension stone and the minimum cutting rate between the cutting area and the recovered block volume, which helps to choose an optimizing block size and mining direction. The research was carried out at Tan Long dimension stone quarry where a block size (0.9m x 0.6m x 1.35m) and a mining direction paralleling to joint set 1 will ensure the highest recovery ratio of 13.87% and the lowest cutting rate of 25 m^2/m^3.

Keywords: *dimension stone, modelling, joint sets, block size, recovery ratio, cutting rate*

1. Introduction

Dimension stone is a natural stone made from intact rock groups of magma, sedimentation, metamorphism without discontinuities and it is quarried and processed to various sizes, shapes, colours and polishes. In stone, there are more joints causing it more difficult to recover more intact blocks [1]. This makes low effectiveness in mining operation due to low recovery ratio and high cutting rate of dimension stone. Collection on joints in stone has been interested in exploration and extraction stages but there are no applications of the collection into optimizing quarrying operation to improve the mining effectiveness [2][3]. Recovering blocks in mining operation is significantly important because it also influences to the following stages as processing activities and quarrying technology and processing technology selections suitable with joint sets to increase the recovery ratio and the low cost. Selecting block size and mining direction are dramatically important because they decide the recovery ratio, the mining cost and mining and processing technologies from joint sets at quarries.

Nowadays, there has been more research on joints in rock mass to calculate recovery ability for dimension stones. Tuan (2019) interested in joint sets to recover valuable blocks of more than 0,4 m^3 based on the modelling of a fracture network in rock mass but block sizes of more than 0,4 m^3 also were not considered their shapes [4]. Mutluturk (2007) showed that beside the quality, dimensional stone also depended on desired size. This would be done by blocks generated from joints in rock mass. The block was put with market blocks (rectangular blocks inside and their sizes of 3 x 2 x1m or 1.5 x 1 x 1) to show how many market blocks [5]. However, the author just showed the way to do, but did not give a result of the method because of lacking fracture modelling ability. Mosch (2011) showed the size and shape of blocks governed by dip direction of joints. The paper showed spatial joint distribution in rock mass navigated three coordination points from the data of joints with window sample and scanline. From calculating pixels in the model to show volume of blocks, the author just established a fracture network for the whole quarries in simple way with three face boundaries of the model [6]. Fernandez-de Arriba (2013) contributed an optimization algorithm on recovery ratio of dimensional stone based on blocks formatted by three joint sets with dip direction angle, dip angle and spacing parameters to divide the blocks into smaller size of 1.5 x 2 x 1.5m. Basing on the mining direction defined from minimum dip direction angle to maximum dip direction angle and mining direction increments determined a mining direction with the maximum recovery ratio, but the paper has not yet to show a change in the volume and the shape of stone blocks with spatial relationship of joint sets [7]. Yarahmadi (2017) also approached into various quarrying direction to optimize the recovery ratio, but the paper showed the intersection of three major joint sets to actual cutting pattern to generate stone blocks with their specific shapes. From

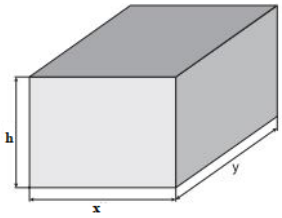

Fig. 1. Dimensions of a minable base block

Tab. 1. Values showing the change in size and area of a minable block

No	Volume, m^3	Height h, m	Cutting area S_0, m^2	x=y, m	k ratio	Length x, m	Width y, m	Area S, m^2	S/S_0
1	0.4	0.6	1.96	0.82	0,1	2.58	0.26	3.41	1.74
2	0.4	0.6	1.96	0.82	0,2	1.83	0.37	2.64	1.35
3	0.4	0.6	1.96	0.82	0,3	1.49	0.45	2.33	1.19
4	0.4	0.6	1.96	0.82	0,4	1.29	0.52	2.17	1.11
5	0.4	0.6	1.96	0.82	0,5	1.15	0.58	2.08	1.06
6	0.4	0.6	1.96	0.82	0,6	1.05	0.63	2.02	1.03
7	0.4	0.6	1.96	0.82	0,7	0.98	0.69	2	1.02
8	0.4	0.6	1.96	0.82	0,8	0.91	0.73	1.97	1.01
9	0.4	0.6	1.96	0.82	0,9	0.86	0.77	1.96	1
10	0.4	0.6	1.96	0.82	1	0.82	0.82	1.97	1.01

each of the shapes, the recovery ratio would be solved by comparing to rectangular blocks having the same volume as the ones. The recovery ratio of each stone block was calculated by comparing rectangular areas having the same volume as the stone block with a total of the surrounding area of the block, and the ratio changes from 0 to 1. When the ratio reaches to 1, the shape of block will be the best. However, the paper has not assessed the change in the volume of block due to the intersection of three major joint sets and the recovery ratio has not calculated with the volume and shape the plants need [8].

From the research above, there have not been papers on optimizing dimension stone quarrying through block size and mining direction to increase the recovery ratio and to reduce the cutting rate. Therefore, the study begins with ranging block sizes from joint sets, cutting area, mining equipment and processing machines. After that, the paper establishes an integrated modelling by combining joint set modelling with cutting grid modelling. An optimal block size which has the highest recovery ratio and the lowest cutting rate will be selected. The paper did experiment at Nui Trai dimension stone quarry in Binh Dinh province, contributing to selecting an optimal block size and specific mining direction for the quarry.

2. Method

In dimension-stone extraction, determining recovered block sizes and mining directions is significantly important to suit to the joint network so that the recovery ratio of intact blocks could get the highest as well as the cutting cost reduces to the lowest level. Therefore, it is necessary to consider block-size optimization so that the lateral cutting area will be the smallest and the size will be suitable for cutting machines, processing machines and market-required products. For this reason, the optimization will need to be implemented with the following requirements.

2.1. Block size optimization

The purpose of dimension-stone extractions is to produce high-quality blocks at an optimizing cost with the highest recovery. To get the purpose achievement above, importance is choosing a suitable cutting technology to bring back a desired result. Cutting direction influences the recovery of market blocks and the direction always parallels to the direction of major joint set.

Thus, the top and bottom planes of blocks do not put into consideration of cutting area, because both planes will not affect to the optimizing production [9]. In this case, the strongest influence is perpendicular to cutting planes. Therefore, an approach is to decrease lateral cutting planes. The desired size of a cutting block should be selected from the base of block modelling. Generally, cube and cuboid cut are the geometric shapes of the minable blocks in quarries. In fact, the height of mining benches is constant in dimensional-stone quarries, and it is determined as the height of minable blocks. On the other hand, the height of minable blocks is prior to determining and during the optimization process of production planning, the other dimensions must be optimized afterwards. The volume of a base block is calculated as Equation (1).

$$V=x\cdot y\cdot h\ ,\ m^3 \tag{1}$$

In which:
V – volume of a minable base block, m^3
x and y – length and width of a block, m
h – height of a mining bench and blocks, m

It is assumed that the volume of a block is constant, the most suitable dimensions can be formed by Equation (2) with concentration on minimizing the lateral cutting planes.

$$V=x\cdot y\cdot h \Rightarrow y=V/(x.h) \tag{2}$$

The most important is to decrease production cost to the lowest value by minimizing lateral cutting area of minable block as determined by Equation (3).

$$S=(x+y)\cdot 2h \tag{3}$$

Combining Equation (2) and Equation (3), we have:

$$S=2h.[(h.x^2+V)/(x.h)] \tag{4}$$

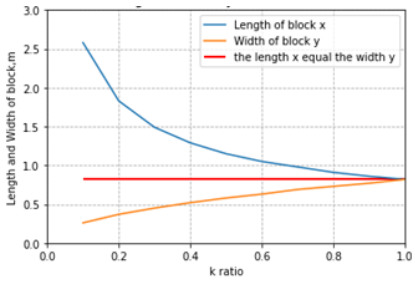

Fig. 2. Change in length and width of a minable block via k ratio.

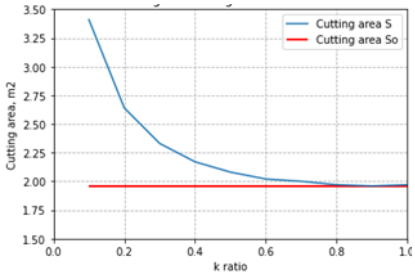

Fig. 3. Change in lateral cutting area via k ratio

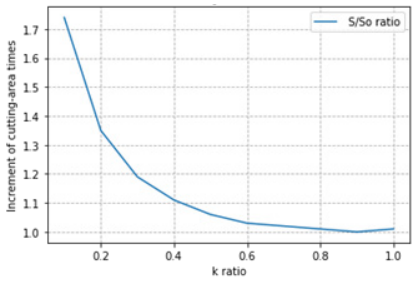

Fig. 4. Increment in cutting area times via k ratio

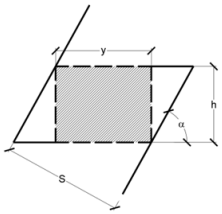

Fig. 5. Calculation on the height of minable block

To minimize lateral cutting area of minable blocks, the derivative of the function S=f(x) must be equal to zero. Dimensions of minable block is calculated with Equation (5) below:

$$\frac{dS}{dx} = 0 => 2h^2 \cdot x^2 - h^2 \cdot x^2 - h \cdot V = 0 => \\ h^2 \cdot x^2 = h \cdot V => x = \pm\sqrt{\frac{V}{h}} \quad (5)$$

From the value x in equation (5), replacing x=√(V/h) into equation (2), the width y is defined in equation (6):

$$y=V/(x \cdot h)=V/\sqrt{(V/h)} \cdot 1/h=\sqrt{(V/h)} \quad (6)$$

Therefore, to collect the blocks with the minimum cutting cost, cutting area is square, where the width is equal to the length *(x=y=√(V/h), m)*.

To calculate lateral cutting planes, the value *x=y=√(V/h)* is replaced in Equation (3):

$$S_o=4\sqrt{(V \cdot h)} \quad (7)$$

A relationship between the width and the length of a minable block by k ratio is determined with Equation (8):

$$k=y/x,\ m => y=k \cdot x,\ m \quad (8)$$

Replacing the values in Equation (8) into Equation (3), we have an Equation (9) as below:

$$S=4k \cdot x \cdot h,\ m^2 \quad (9)$$

Increment in area will occur when the two dimensions are not equal, defined by equation (10):

$$S/So=(4k \cdot x \cdot h)/(4\sqrt{(V \cdot h)})=k \cdot x \cdot \sqrt{h},\ m \quad (10)$$

In which:

k – ratio between the width and length of minable block, m;

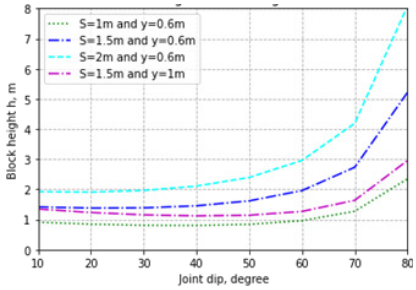

Fig. 6. Change in height of minable block via change in the dip angle in the same joint set

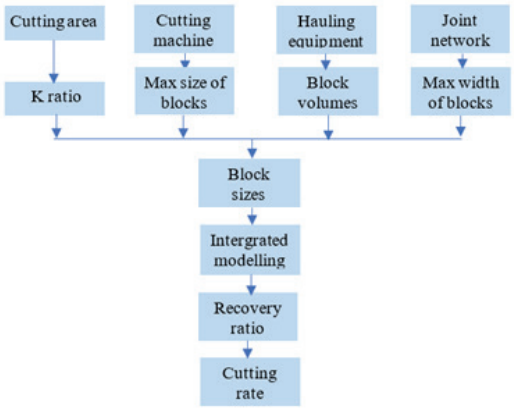

Fig. 7. Flow chart to calculate suitable size for dimension stone

x – length of minable block, m;
h – width of minable block, m;

It is assumed that a minable block has a volume of 0.4 m^3, its height of 0.6 m and k value changes from 0.1 to 1, leading to the outputs represented in Tab.1 and a relationship between the width and the length shown in Fig. 2, Fig. 3 and Fig. 4.

In addition, if cutting area of minable blocks gets the lowest value, the optimization shape of the blocks will be a cuboid with square planes and the height h. It is proven that when h has a trend in reaching each dimension of minable block, the whole cutting area will reduce. Therefore, a cube with its edges of h and a cuboid with its cutting area of b^2, its height of d has the same volume. This could be proven under a condition $h^3 = b^2 \cdot d$ và d<h<b, as in Equation (11).

$$h^2<b^2 => 2h^2<2b^2 => 6h^2<2h^2+4b\cdot d \quad (11)$$

From the interpolation in Equation (11), the whole areas of a cube are smaller than that of a cuboid with square sections in the same volume. Moreover, Equation (7) is also demonstrated with the acceptance b<h<d. As a result, a cube and a cuboid having square planes is the most suitable for the shape of minable blocks.

Optimal shape of minable blocks is assessed through an index called cutting rate. The rate is defined as a cutting area per an unit volume of recovered blocks. The rate is shown as in Equation (12).

$$t=(\Sigma S_i)/V \quad (12)$$

In which:
t – cutting rate;
Si –i^{th} cutting area in minable block, m^2;
V – minable-block volume, m^3;

Consideration about a minable block with squared area and height h could be written in Equation (13).

$$t=(2h.(x+y))/V=4\sqrt{(h/V)} \quad (13)$$

As mentioned above, a minable block will reach the most suitable volume when the cutting rate is the smallest. As Equation (14), the volume of a minable block has a trend in reaching infinite when the rate reaches to zero.

$$\lim_{V\to\infty} t = \lim_{V\to\infty} 4\sqrt{\frac{h}{v}} = 0 \quad (14)$$

From Equation (14), if block volume increases, the cutting rate will reach zero. This could be explained that when the volume increases, mining effectiveness will increase. In the fact of dimension-stone quarrying, the volume of block only reaches a specific limit because of depending on hauling and processing equipment.

2.2. Height of minable block

According to section 2.1, when height of minable blocks reaches the other dimensions, the cutting area will decrease. In addition, cutting blocks needs to be interested in major joint set to decrease the influence of joints on block fragmentation. This could be done by cutting blocks along to the strike of the major joint set. In the other hand, the length of minable blocks parallels to the strike of the major joint set, the width is perpendicular to the major joint set. Therefore, to ensure the width of minable block, the height of minable block needs to be calculated following spacing of joint set and joint set dip angle. This calculation is represented in Fig. 5 and Equation (15).

$$h=((S-y\cdot\sin\alpha)\cdot tg\alpha)/\sin\alpha \quad (15)$$

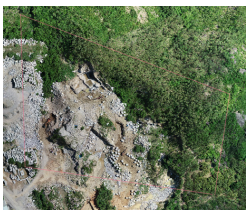

Fig. 8. Location of Nui Trai quarry in Binh Dinh Province (Mapped byUAV)

Tab. 2. Parameters of joint sets at Nui Trai quarry, Binh Dinh Province

No	Joint set 1			Joint set 2			Joint set 3		
	Dip, degree	Dip direction, degree	Spacing, m	Dip, degree	Dip direction, degree	Spacing, m	Dip, degree	Dip direction, degree	Spacing, m
1	80	70	3,5	80	190	2	80	35	5
2	80	70	2	80	190	3	80	35	2
3	80	70	3.5	80	190	2	80	35	2
4	80	70	2.5	80	190	2	80	35	2
5	80	70	4	80	190	1	80	35	2
6	80	70	2,5	80	190	2	80	35	5
7	80	70	2	80	190	3	80	35	4
8	80	70	1.5	80	190	2	80	35	2
9	80	70	3	80	190	1	80	35	2
10	80	70	2	80	190	4	80	35	5
11	80	70	5	80	190	1	80	35	2
12	80	70	3	80	190	4	80	35	5
13	80	70	3	80	190	3	80	35	1
14	80	70	2	80	190	1	80	35	1.5
15	80	70	3	80	190	2	80	35	5
16	80	70	2	80	190	1	80	35	5
17	80	70	2	80	190	1	80	35	2
18	80	70	2	80	190	2	80	35	3
19	80	70	4	80	190	2	80	35	5
20	80	70	4	80	190	1	80	35	2
21	80	70	2	80	190	2	80	35	6
22	80	70	3	80	190	1	80	35	3
23	80	70	5	80	190	5	80	35	2
24	80	70	3	80	190	2	80	35	2
25	80	70	3	80	190	4	80	35	3
26	80	70	3	80	190	5	80	35	3
27	80	70	1	80	190	2	80	35	2
28	80	70	3	80	190	2	80	35	4
29	80	70	2	80	190	2	80	35	3
30	80	70	3	80	190	1	80	35	3
31	80	70	2	80	190	2	80	35	1
32	80	70	2.5	80	190	4	80	35	6.5
33	80	70	3	80	190	2	80	35	3
34	80	70	5	80	190	1	80	35	6
35	80	70	4	80	190	3	80	35	6
36	80	70	1	80	190	2	80	35	2
37	80	70	3	80	190	3	80	35	5
38	80	70	2	80	190	1	80	35	2
39	80	70	2	80	190	5	80	35	2
40	80	70	1	80	190	1	80	35	5
41	Average Spacing		2.75	Average Spacing		2.25	Average Spacing		3.3

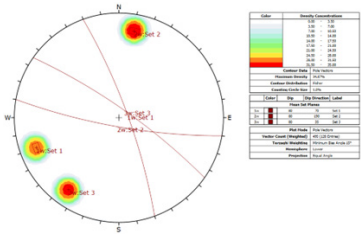

Fig. 9. Analyzing and representing joint sets for Nui Trai dimension stone quarry in Binh Dinh Province

Tab. 3. Working parameters of selected disc sawing, CXVQ-3300-2

No	Parameters	Unit	Value
1	Machine size	m	3.45*1.35*2.6
2	Number of discs	disc	2
3	Disc diameters	m	2.2; 3.5
4	Cutting depth	m	0.85-1.5
5	Cutting width	m	1.3-1.35
6	Machine weight	ton	9.5
7	Power capacity	kW	2*45kW

Fig. 10. Disc sawing machine at the quarry.

Tab. 4. Parameters of disc sawing machine, QSQ2200B, at processing plant

No	Parameters	Unit	Value
1	Maximum cutting depth	m	0.95
2	Cutting length (axis X)	m	3,8
3	Cutting length (axis Y)	m	2
4	Power motors	Kw	45/55
5	Disc diameters	m	2.2;2;1.8;1,6 1.2;1;0.8;0.6
6	Block width	m	2,1
7	Block height	m	1.35
8	Block length	m	3.6
9	Cutting velocity (axis X)	m/s	Modify
10	Beam velocity	m/mi	Modify
11	Vertical displacement velocity	m/s	Modify
12	Beam-moving power	Kw	3
13	Vertical displacement motor	Kw	1.5
14	Installed power	Kw	45
15	Cooling water (1,5 bar)	l/m	30
16	Machine length	m	7,5
17	Machine width	m	4.35
18	Machine height	m	6
19	Machine weight	tone	12

Tab. 5. Summary of necessary parameters for limiting sizes of minable blocks

No	Parameters	Block length, m	Block width, m	Block height, m	Block volume, m³
1	Disc sawing machine for blocks	-	1.4	1.35	-
2	Disc sawing machine for slabs	3,6	2,1	1.35	-
3	Cutting paralleling to joint set 1	-	2,94	-	-
4	Cutting paralleling to joint set 2	-	1.92	-	-
5	Cutting paralleling to joint set 3	-	2.94	-	-
6	Hauling and transporting machines	-	-	-	7

Tab. 6. Minable-block sizes

No	Block name	Block length, m	Block width, m	Block height, m	Block volume, m³
I	Cutting paralleling to joint set 1				
1	Size 1_1	1.9	1.3	0.6	1.5
2	Size 1_2	1.6	1.1	0.6	1.1
3	Size 1_3	1.3	0.9	0.6	0.7
4	Size 1_4	2	1.4	1.35	3.8
5	Size 1_5	1.7	1.2	1.35	2.8
6	Size 1_6	1.4	1	1.35	1.9
7	Size 1_7	1.1	0.8	1.35	1.2
8	Size 1_8	0.9	0.6	1.35	0.7
II	Cutting paralleling to joint set 2				
1	Size 2_1	1.9	1.3	0.6	1.5
2	Size 2_2	1.6	1.1	0.6	1.1
3	Size 2_3	1.3	0.9	0.6	0.7
4	Size 2_4	1.7	1.2	1.35	2.8
5	Size 2_5	1.4	1	1.35	1.9
6	Size 2_6	1.1	0.8	1.35	1.2
7	Size 2_7	0.9	0.6	1.35	0.7
III	Cutting paralleling to joint set 3				
1	Size 3_1	1.9	1.3	0.6	1.5
2	Size 3_2	1.6	1.1	0.6	1.1
3	Size 3_3	1.3	0.9	0.6	0.7
4	Size 3_4	1.7	1.2	1.35	2.8
5	Size 3_5	1.4	1	1.35	1.9
6	Size 3_6	1.1	0.8	1.35	1.2
7	Size 3_7	0.9	0.6	1.35	0.7

Tab. 7. Summary of recovery ratio and cutting rate for different block sizes in three cutting directions

No	Block name	Total number of blocks	Total number of intact blocks	Recovery ratio, %	Cutting rate, m²/m³
1	Size 1_1	12480	451	3.61	81.97
2	Size 1_2	17856	932	5.22	61.32
3	Size 1_3	27360	2375	8.68	40.86
4	Size 1_4	4032	86	2.13	91.66
5	Size 1_5	5742	191	3.33	65.01
6	Size 1_6	8307	490	5.90	41.62
7	Size 1_7	12960	1220	9.41	30.80
8	Size 1_8	21780	3021	13.87	25.37
9	Size 2_1	12480	276	2.21	133.94
10	Size 2_2	17856	739	4.14	77.34
11	Size 2_3	26752	2049	7.66	46,31
12	Size 2_4	5742	149	2.59	83.33
13	Size 2_5	8520	397	4.66	52.69
14	Size 2_6	13500	1140	8.44	34.34
15	Size 2_7	21978	2691	12.24	28.74
16	Size 3_1	12480	263	2.11	140.56
17	Size 3_2	17856	681	3.81	83.92
18	Size 3_3	26752	1862	6.96	50.96
19	Size 3_4	5742	139	2.42	89.32
20	Size 3_5	8520	344	4.04	60.80
21	Size 3_6	13500	1033	7.65	37.90
22	Size 3_7	21978	2592	11.79	29.83

In which:

h – height of minable block, m;

α – dip angle of joint in a joint set, degree;

y – width of minable block, m;

S – Spacing of joint in the same joint set, m.

Through analysis on heights of block with dip angle of joint in a joint set changing from 0^0 to 80^0 and spacing S changing from 1m to 2m, the width of minable block changing from 0.6m to 1m, the heights were changed and shown in Fig. 6.

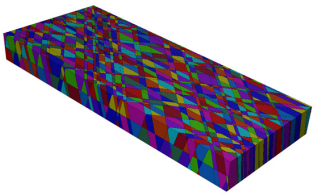

Fig. 11. Three-dimensional modelling for Nui Trai dimension stone quarry, Binh Dinh Province

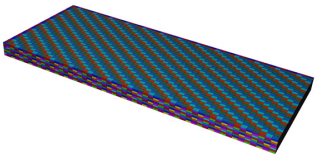

Fig. 12. Three-dimensional cutting-grid modelling

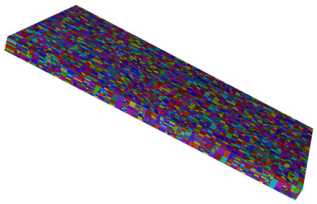

Fig. 13. Three-dimensional integrated modelling

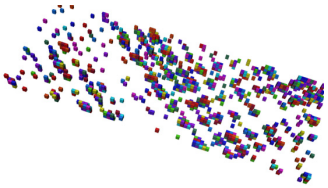

Fig. 14. Three-dimensional modelling after applying filter algorithm for intact blocks

Through Fig. 6, it is claimed that when dip angle of joint in the same joint set becomes steeper, the height will be raised and inversely.

2.3. Flow chart to determine the most suitable block size

1. Cutting area: Based on optimal block size, the length and width of minable block are equal, bringing back the highest effectiveness, but consideration on ratio relationship, the width being 80 percent as much as the length still ensures cutting area which is little larger than the optimal cutting area.

2. Mining and processing equipment: When implementing mining and process operation for dimension stone, working parameters of the equipment are interested in the dimensions of block, including length, width, and height the equipment could operate properly. This is a foundation to select block size, which is not larger than the chosen equipment.

3. Hauling equipment: Hauling equipment is interested in the volume of minable block. Therefore, the volume could not exceed the one the equipment delivers.

4. Joint Network: Joint network mentions to the maximum width of a block, which is calculated via average spacing of joints in the same set. The maximum width satisfies conditions in equation (16).

$$y_{max}=(S_{tb}\cdot tg\alpha-h\cdot sin\alpha)/cos\alpha \quad (16)$$

in which:

y_{max} – maximum width of minable block, m
S_{tb} – average spacing of joints in the same set, m
α – dip angle of joints in the same set, degree

5. The length of minable block is firstly selected from the dimensions satisfying the width of slabs cut following the standard of dimension stone and the height of cutting blocks being smaller than the maximum height mining and processing equipment could operate. The maximum width, ymax, is defined in step 4, checking the width according to the equipment from mining and processing operation and giving a range of wide value decreased gradually to zero. After that the length of a cutting block is defined following the ratio have been defined in step 1. Checking dimensions of cutting blocks is according to the width and length of working operation from the equipment and the working volume of hauling equipment, more than 0.4 m^3. As a result, lists of the satisfied sizes are given with the strike of joint sets.

6. Integrated Modelling: Modelling is formed with a base on joint sets, mining direction, block sizes of minable block, leading to forming an integrated modelling being a result of intersection between joint sets and cutting grid.

7. Recovery ratio is a result after modelling, where the ratio is calculated by the number of intact minable blocks divided by the total blocks in the modelling.

8. Cutting rate, t, is defined a ratio between total cutting area and recovered block volume, shown in equation (17).

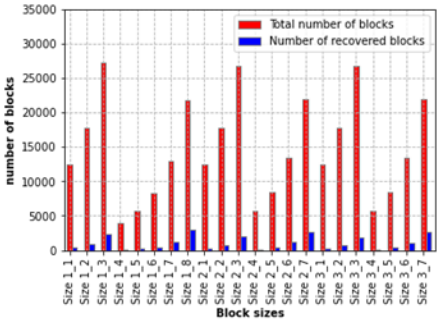

Fig. 15. Total number of blocks and recovered blocks for each block size

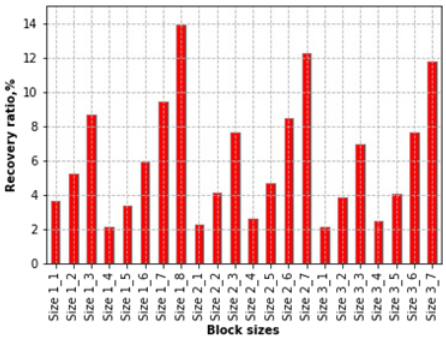

Fig. 16. Recovery ratio for each block size

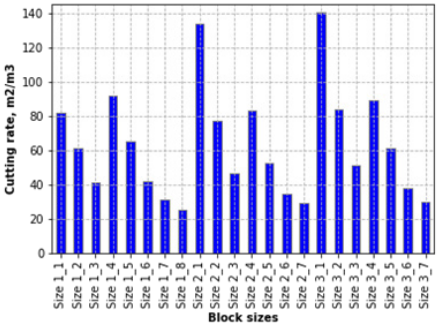

Fig. 17. Cutting rate for each block size

$$t=(\Sigma S_{ij})/(\Sigma V_i) \quad (17)$$

In which:

t – cutting rate.

S_{ij} – j^{th} cutting area in i^{th} minable block, m^2.

V – i^{th} recovered block volume, m^3.

i, j – index for blocks, index for the number of cutting areas in a specified block.

In cutting operation in dimension stone quarry, due to adjacent blocks, the number of cutting planes is three, including bottom, side, and back planes. The flow chart to determine the most suitable block size is represented in Fig. 7.

3. Case study at Tan Long dimension stone quarry in South-central coastal province of Binh Dinh

3.1. Joint data collection

Nui Trai dimension stone quarry extracts granite to produce dimension stone in Phu Cat district, far from 35km Northern Quy Nhon city. The quarry speads about 4.9 ha at side hill with an elevation from +30m to 70m (Fig .8). Joints selected in Tab. 2 was carried out with scan line on the surface. After that these joints was classified into joint sets with classified algorithms via software Dips [10],[11] (Fig .9). The group include three major joint sets with the dip direction and the dip of 70º<80º, 190º<80º và 35º<80º, respectively.

3.2. Mining fleet information

Dimension stone quarries in Binh Dinh Province mostly used modern sawing methods, such as disc sawing, diamond wire sawing. In which, quarries popularly applied main sawing method of being disc sawing at large-output quarries because smooth planes were created to form block sizes satisfying size standard for the processing plant.

In dimension stone quarries estimated to use disc sawing machines but this research only carried out with the same disc sawing machine on supplying firms. For example, disc diameters and working parameters were shown in Table 3 (Fig. 10).

The quarry estimated to use disc sawing machine to slice blocks into slabs with blaze diameters from 0.6 to 3m on the same rotary axis, unchanged spacing of the blazes installed equal to slab thickness. In processing operation, blaze system was moved in three-dimension cutting. Basic parameters of disc cutting at processing plant were shown in Table 4. The quarry used front-wheel excavators to transport blocks from the quarry to stockpiles, the excavators could evaluate up to 7 m^3 (about 20 tonnes).

Through joint-set analysis, mining fleet and necessary sizes to determine the sizes and volume of minable blocks were shown in Tab. 5.

The inforamtion summarized in Table 5 combined with the flow chart in Fig .7 to design the sizes of minable blocks given Tab. 6.

3.4. Establishment of an integrated modelling between joint sets and cutting grid

From the joint data measured in Tab. 2, a three-dimensional modelling was built with joint sets. The size of the modelling of being 100 m x 40m 5m was generated through software 3DEC of atasca brand [12], given in Fig .11.

Cutting grid modelling formed by the sizes of minable blocks with cutting operation paralleling to each joint set in Table 6 was represented in Fig. 12.

4. Results and discussions

By intersection between joint set modelling in Fig. 11 and cutting-grid modelling in Fig. 12, an integrated modelling was generated and shown in Fig. 13.

By a filter algorithm in 3DEC software for filtering intact blocks in the modelling, the number of intact blocks were derived from the integrated modelling and shown in Fig. 14.

Particularly, establishing three-dimensional integrated modelling between joint sets and cutting grid generated with one of the three cutting directions (paralleling to joint set 1, joint set 2 and joint set 3) and block sizes in Tab. 6. The total number of blocks and intact blocks, recovery ratio and cutting rate were obtained in Tab. 7. The result showing the total number of blocks and intact blocks was represented in Fig. 15. Similarly, the figures for the recovery ratio and the cutting rate were represented in Fig. 16 and Fig. 17, respectively.

In Tab. 7, Fig. 15, Fig. 16 and Fig. 17, block sizes of size 1_8, size 2_7 and size 3_7 have the same size of 0.9m x 0.6m x 1.35m. Recovery ratios relating to these sizes are 13.87 %, 12,24% and 11,79%, respectively. Meanwhile, respective cutting rates for these sizes are 25.37%, 28.74%, 29.83%. As a result, the size of size 1_8 with its value of 0,9 x 0,6 x 1,35m cut in the direction paralleling to joint set 1 has the highest recovered ratio of 13.87% and the lowest cutting rate of 25.37%.

4. Conclusions

Dimension stone has been more and more popular extraction to bring back higher effective economic compared with the extraction for common construction materials. Effectiveness of quarrying dimension stone depends on less joint sets existed in quarries and selecting suitable cutting and processing methods. This is shown via improving the recovery ratio and the low cost of dimension stone. The paper showed clearly that mining direction and block size play an important role in selecting cutting machine from joint network at quarries. There are some conclusions below:

- Integrated modellings selected play an important role in calculating the volume and the size of minable blocks because the modelling is interested in dips, dip directions, spacings of joints and cutting grids.
- Optimizing block size plays an important role in decreasing block-cutting area. Optimization size is square, but short edge being more than 80 percent of long edge still ensures and suits with cutting machines. Minable-block size has a significant meaning in calculating recovery ratio, depending on joint-set parameters. The optimizing size in cutting grid must ensure the highest recovery ratio and the lowest cutting rate. For Nui Trai dimension stone quarry, the size of size 1_8 (0.9x0.6x1.35m) is sure that the recovery ratio is the highest while the cutting rate is the smallest from the sizes selected.
- Mining direction for dimension stone is hozirontal length of block size chosen to parallel to one of the strikes of joint sets. The selected direction ensures the recovery ratio is the highest while the cutting rate is the smallest. For Nui Trai dimension stone quarry, mining direction is parallel to joint set 1.

Literatura – References

1. L. Sousa, J. Barabasch, K.-J. Stein, and S. Siegesmund, "Characterization and quality assessment of granitic building stone deposits: A case study of two different Portuguese granites," Eng. Geol., vol. 221, pp. 29–40, 2017, doi: 10.1016/j.enggeo.2017.01.030.
2. B. Sohrabian and Y. Ozcelik, "Determination of exploitable blocks in an andesite quarry using independent component kriging," Int. J. Rock Mech. Min. Sci., vol. 55, pp. 71–79, 2012, doi: 10.1016/j.ijrmms.2012.06.009.
3. J. Taboada, T. Rivas, A. Saavedra, C. Ordóñez, F. Bastante, and E. Giráldez, "Evaluation of the reserve of a granite deposit by fuzzy kriging," Eng. Geol., vol. 99, no. 1–2, pp. 23–30, 2008, doi: 10.1016/j.enggeo.2008.02.001.
4. N. A. Tuan., P. Van Viet., L. Van Quyen., N. T. Anh., and L. T. Hai., "Determining for an output capacity of dimension stone exploitation from the computer simulations to generate the Fracture Networks.pdf," Pol-Viet, Pol., p. 39, 2019.
5. M. Mutlutürk, "Determining the amount of marketable blocks of dimensional stone before actual extraction," J. Min. Sci., vol. 43, no. 1, pp. 67–72, 2007.
6. S. Mosch, D. Nikolayew, O. Ewiak, and S. Siegesmund, "Optimized extraction of dimension stone blocks," Environ. Earth Sci., vol. 63, no. 7, pp. 1911–1924, 2011, doi: 10.1007/s12665-010-0825-7.
7. M. Fernández-de Arriba, M. E. Díaz-Fernández, C. González-Nicieza, M. I. Álvarez-Fernández, and A. E. Álvarez-Vigil, "A computational algorithm for rock cutting optimisation from primary blocks," Comput. Geotech., vol. 50, pp. 29–40, 2013, doi: 10.1016/j.compgeo.2012.11.010.
8. R. Yarahmadi, R. Bagherpour, A. Khademian, and L. M. O. Sousa, "Determining the optimum cutting direction in granite quarries through experimental studies : a case study of a granite quarry," 2017, doi: 10.1007/s10064-017-1158-5.
9. N. M. Sirakov and F. H. Muge, "A system for reconstructing and visualising three-dimensional objects," Comput. Geosci., vol. 27, no. 1, pp. 59–69, 2001, doi: 10.1016/S0098-3004(00)00055-8.
10. R. E. HAMMAH, "Fuzzy Cluster Algorithm for the Automatic Identi®cation of Joint Sets."
11. Rocscience Inc. 2016, Dips Version 7.0 - Graphical and Statistical Analysis of Orientation Data. www.rocscience.com, Toronto, Ontario, Canada.
12. Itasca Consulting Group, Inc. (2019) 3DEC — Three-Dimensional Distinct Element Code, Ver. 5.2. Minneapolis: Itasca.

Fuzzy Multi-Attribute Decision Model for the Optimal Mine Closure Option to Contribute to Sustainable Development in Binh Duong Province, Vietnam

PHAN Hong Viet[1)], DO Ngoc Tuoc[2)], BUI Xuan Nam[3,4)]*

[1)] Department of Industry and Trade, Binh Duong, Vietnam
[2)] Institute of Mining Science and Technology - Vinacomin, Hanoi, Vietnam
[3)] Hanoi University of Mining and Geology, Hanoi, Vietnam
[4)] Innovations for Sustainable and Responsible Mining Research Group (ISRM), Hanoi University of Mining and Geology, Hanoi, Vietnam
* Corresponding author: dotuoc@gmail.com

http://doi.org/10.29227/IM-2023-02-38

Submission date: 20-08-2023 | Review date: 21-09-2023

Abstract

Binh Duong is the leading industry development province of Vietnam. In particular, quarries in Di An, Phu Giao and Tan Dong Hiep districts have contributed significantly to the demand for construction and transportation in the locality and vicinity. The quarries in Binh Duong province are exploited by the open-pit mining method. The mining depth is from 100m to 150 m. The mine surface area is hundreds of hectares. At the end of the quarries will leave huge pits. The current regulations of Vietnam on mine closure are mainly aimed at ensuring the stability of the physical and chemical factors of the mine, while the land use after the mine closure is permanent. Binh Duong province has a rapid urbanization rate, the use of land after mining here is very important and has a significant influence on the sustainable development of the region. Depending on the occupied area of the mine or mine cluster, there are many options to close the mine after mining based on the required technical, economic, social and environmental criteria. The paper uses fuzzy multi-attribute decision model to calculate the optimal solution selection. The selected option is to use the mine lake for tourism, entertainment and water storage at Nui Nho mine, Di An city, Binh Duong province with the highest total score of economic, social and environmental criteria.

Keywords: *mine closure, fuzzy multi-attribute decision, sustainable development*

1. Introduction

Mining closure is rated as one of the top risk activities of mining, its importance is increasingly recognized, more stringently required mine closure regulations have been introduced since 1990s [19, 23]. Mining closures can cause negative impacts such as job loss, tax revenue deficit, impact on infrastructure development, reduced demand for local goods and services, and especially environmental landscape [1, 6]. The development opportunities that mines can offer to local communities after mine closure should be carefully studied. If managed properly, the mine closure transition can provide significant opportunities in line with the Sustainable Development Goals (SDGs), such as resettlement, infrastructure development for other purposes creating new economic resources [3, 18].

Around the world, organizations such as the International Council on Mining and Metals (ICMM), the World Bank have reported on the sustainable mine closure framework [13, 15]; Countries with developed mining industries such as the US, Australia, Canada, and South Africa have legalized mine closures and issued detailed manuals. Some of the key themes in these guidelines and standards include integrated closure planning that considers the environmental, financial, physical, and socioeconomic context of a particular site, incorporating the stakeholders including community goals and aspects of social welfare, environmental management based on optimization of protection, land use and infrastructure [14]. Some of the proposed legislation includes the following sustainable land use practices under the statutory framework: i) Closures must begin at the start of the operational phase and continue until the start of the closure phase; ii) The quantification and management of environmental risks must be achieved; iii) Mine Health and Safety regulations must be observed; iv) The identification and quantification of residual environmental impacts must be achieved; v) The land must be restored to its natural state or to a predetermined state as agreed by the government to include the concept of sustainable development; vi) Mining operations must be effectively and cost-effectively closed.

Binh Duong is a leading industrial province in the country. Along with the economic development and infrastructure construction, the demand for stone construction materials is increasing. Currently, the province has 22 mines, of which 16 are being exploited and 5 are under construction. The total licensed mining area is 778.11 hectares with a total licensed mining capacity of 14,112 million m^3/year. Construction material mines in Binh Duong province are mainly concentrated in the districts: Phu Giao (3 mines) and Bac Tan Uyen (19 mines).

The quarries in Binh Duong have a close relationship: they work together on the same shore, exploit together deep below the self-flowing drainage level, and are connected to regional roads. Around the mine, it is arable land of local people. Open pit mining inevitably causes changes in the surrounding envi-

Fig. 1. Location of mine closure area (Google Map)

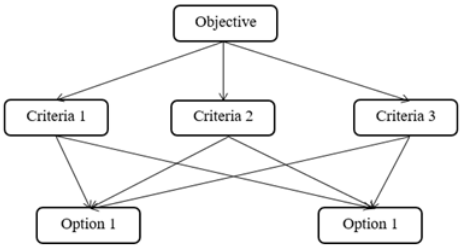

Fig. 2. AHP hierarchical structure diagram

ronment, the extent of which depends on the depth of finish, mining capacity, technology, equipment as well as size, shape and location of the mine [7].

The mining process has changed the landscape, affecting the environment, ecology, and traffic in the area. Currently and a few years from now, the quarries in Binh Duong province will end their exploitation and have to close according to regulations. Vietnam has clear regulations on the contents of mine closures, which are shown in the following documents:

- Law on Minerals No. 60/2010/QH12 approved by the National Assembly of the Socialist Republic of Vietnam, term XII, 8th session, on November 17, 2010;
- Law on Environmental Protection No. 55/2014/QH13 passed by the National Assembly on June 23, 2014;
- Circular No. 45/2016/TT-BTNMT dated December 26, 2016 of the Ministry of Natural Resources and Environment "Regulating on mineral exploration project, mineral mine closure and form of report on mineral activities and samples of documents in the application for a license for mineral activities, the application for approval of mineral reserves, and the application for closure of a mineral mine; order and procedures for mineral mine closure";
- Circular No. 38/2015/TT-BTNMT dated June 30, 2015 of the Ministry of Natural Resources and Environment on environmental renovation and restoration in mineral mining activities;

The regulations on mine closure in Vietnam are determined that after the end of mining, bring the mine to a stable state: leveling, renovating floors, dismantling works, etc., make a plan to close the mine and submit it to the authorities when preparing to end mining. The new mine closure is mainly concerned with the physical stability of the work, not integrating economic and social factors into the mine closure. The site of land use after the mine closure is directly related to society, but it is only oriented to be used as a water reservoir, planting trees without specific instructions on physical and chemical stability, etc. Closing costs have to be taken from the project's funds, but with each different model of land use after mining, the cost of closing the mine will be different, affecting the efficiency of the investor. At that time, it is necessary to consider the lifespan, the end boundary, the different stability assurance solutions to ensure the effective project after the closure. Land use after the closure of mines has not been effective, the orientation to use the premises stated in the environmental impact assessment (EIA) report is often counter-productive, simple, with as little improvement costs as possible, not really suitable with the natural and socio-economic characteristics of the area.

Mines in the same area do not have a link in a common whole, there is no integrated closure model for the most optimal use of the site after closing. Existing studies have only focused on the use of post-closure premises on the basis of the criteria to ensure the set goals, but there are no studies on stability for each model.

That's why choosing an appropriate mine closure model that contributes to the sustainable development of the region is essential and has practical significance, especially with Binh Duong province with rapid urbanization and rapid development of industries.

2. Research methodology

2.1. Research subjects

- Research object: Mine closure and land use after mining.
- Scope of research: Nui Nho mine with an area of 33.9 hectares. This is the place that takes away the most soil and rock in the area, causing a lot of environmental impact
- Location is in Binh Thung quarter, Binh An ward, Di An town, Binh Duong province. The location of mineral mine closure is about 20 km southwest of Ho

Tab. 1. Criteria for selecting the optimal mine closure model

Objective 1: Match the natural features of the mine	Objective 2: Match with regional social characteristics	Objective 3: Ensure environmental targets	Objective 4: Ensure economic efficiency	Objective 5: Technical feasibility
TN1: Mine topography	XH1: Population	MT1: Water environment	HQ1: Benefits for investors	KT1: Technical feasibility
TN2: Surface water	XH2: Social infrastructure	MT2: Water environment	HQ2: Benefits for the community	KT2: Shape and size of mine field
TN3: Groundwater	XH3: Industry	MT3: Earth Environment	HQ3: Local interest	KT3: Current land use status in the surrounding area
TN4: Climate	XH4: Pre-mining land use	MT4: Air environment		KT4: Climate change
TN5: Flora and Fauna	XH5: Entertainment area	MT5: Risk		KT5: Supply of raw materials
TN6: Pit area				
TN7: Geological structure				

Tab. 2. W-weighting for the objectives of option 1. CR ratio = 0.061< 0.1

	Nature	Economy	Society	Environment	Technical feasibility	Weight
Nature	1, 1, 1	1/4, 1/3, 1/2	1/5, 1/4, 1/3	1/5, 1/4, 1/3	1, 2, 3	**0.092**
Economy	2, 3, 4	1, 1, 1	1/3, 1/2, 1	1, 1, 1	2, 3, 4	**0.233**
Society	3, 4, 5	1, 2, 3	1, 1, 1	1, 1, 1	2, 3, 4	**0.312**
Environment	3, 4, 5	1, 1, 1	1, 1, 1	1, 1, 1	3, 4, 5	**0.286**
Technical feasibility	1/3, 1/2, 1	1/4, 1/3, 1/2	1/4, 1/3, 1/2	1/5, 1/4, 1/3	1, 1, 1	**0.077**

Chi Minh City, 10 km northeast of Bien Hoa city, 18 km northwest of Thu Dau Mot city (Figure 1).

2.2. Applicable methods

2.2.1. Method of data collection and field investigation

The collected database includes natural factors, socio-economic conditions, maps such as administrative boundaries, and land use planning maps. These are documents as a basis for fieldwork to comment and evaluate, and as a basis for surveying backlogs, limitations and causes to be overcome.

2.2.2. Matrix and Expert Method

The matrix method lists development activities and environmental factors that may be affected [20]. The matrix table compares each project activity with environmental parameters or components to assess the cause-and-effect relationship [10]. In which, the horizontal axis represents actions, the vertical axis represents environmental factors and marks the level of impact between them. For this method, the knowledge and practical experience of experts in the field of mineral resources and environment are used to analyze and evaluate the impacts.

2.2.3. Multi-Criteria Analysis (MCA) with fuzzy sets

AHP's purpose is to help people organize their thoughts and judgments to make more effective decisions. AHP provides an objective algorithm to deal with the separability of subjectivity and the private preferences of an individual or group in decision making. The diagram of the AHP hierarchy is shown in Figure 2.

The AHP method facilitates computational judgments and preferences by using pairwise comparisons. This is also the best procedure for performing pairwise judgmental comparisons [21]. However, human judgments are completely imprecise, so preferences are not quantifiably determined [9]. Fuzzy theory was developed by Zadeh [26] to overcome incorrect judgments and preferences. Many methods of weighing attributes and alternatives are intelligently implemented using qualitative scales, while the logical determination of priorities is difficult for general decision-makers [25]. Therefore, to perform accurate pairwise judgment comparisons and decision making, fuzzy set theory and AHP method are combined with good results [2]. Later, other methods have been presented that combine these two approaches [4]. Since ambiguity and ambiguity are common features in many decision-making problems, fuzzy analytical hierarchical processing (FAHP) should be able to deal with ambiguity [17].

Supposing that a decision-making board consists of l decision makers (Dt, t = 1,.., l) responsible for evaluating m (Ai, i = 1,…, m) green suppliers based on over n standards (Cj, j = 1,..., n) where the rating of green suppliers is based on each standard and the weights of the standards are represented as linguistic variables [27] and presented as triangular fuzzy numbers. The modeling process is presented in the following steps:

* Step 1: Define a set of criteria to evaluate and group green suppliers. In this study, the criteria used to evaluate and classify green suppliers are divided into two groups: economic criteria and environmental criteria. These criteria were selected based on a review of previous studies presented in Table 1.

* Step 2: Determine the weight for each criterion. In this section, the FAHP method is applied to determine the priority (weight) of the green supplier evaluation criteria. This study applies the extended FAHP method which is considered simple, popular and presented by Chang [4]. The FAHP model is used to determine the weights of the criteria. The model uses a language variable to represent the comparative judgments made by the decision panel.

Set: X = {X1, X2, ..., Xn} is the set of n objects;

G = {g1, g2, ..., m} is the set of m comparison targets.

According to Chang's method, each Xi object corresponds to a comparison object, denoted Gi. Accordingly, each object Xi will be compared with m targets, denoted as follows:

$$M_{gi}^{1}, M_{gi}^{2}, \ldots M_{gi}^{1}; M_{gi}^{1}, M_{gi}^{2}, \ldots M_{gi}^{m} \text{ với } i = 1,2\ldots m;\ j = 1,2\ldots n$$

(In which every value M_{gi}^{j} M_{gi}^{j} is a triangular fuzzy number).

* Step 3: Calculate the value of the composite fuzzy number for the i-th object according to the formula:

$$S_i = \sum_{j=1}^{m} M_{gi}^{j} \otimes \left[\sum_{i=1}^{n}\sum_{j=1}^{m} M_{gi}^{j}\right]^{-1} \quad (1)$$

Tab. 3. Overall score evaluation for option 1

Objectives	Objective's Weight	Criteria	Explanation	Criterion weight	Average score of experts	Criteria score	Total score
Objective 1: Match the natural features of the mine	0.092	Mine topography	The mine topography is suitable for the post-mining land use plan	0.36	70	25.2	2.318
		Surface water	Reservoir suitable for post-mining land use	0.17	65	11.05	1.017
		Groundwater	Ground water supplies to the reservoir	0.07	65	4.55	0.419
		Climate	Climate affects post-mining land use purpose	0.21	70	14.7	1.352
		Flora and Fauna	Is the flora and fauna rich?	0.04	50	2	0.184
		Mine scale	Is the size of the mine suitable?	0.08	70	5.6	0.515
		Geological structure	Stable geological structure	0.07	60	4.2	0.386
Objective 2: Match with regional social characteristics	0.312	Population	The population density is high to participate in post-mining land use	0.53	65	34.45	8.027
		Social infrastructure	Favorable traffic conditions, electricity and water networks	0.19	80	15.2	3.542
		Industry	Industrial activities that support the form of post-mining land use	0.12	75	9	2.097
		Pre-mining land use	Is the pre-mining land use suitable for the form of post-mining land use	0.08	70	5.6	1.305
		Entertainment area	The entertainment area around the mine affects the plan	0.08	60	4.8	1.118
Objective 3: Ensure environmental targets	0.286	Water Environment	The form of post-mining land use affects the water source	0.47	70	32.9	10.265
		Water Environment	The form of post-mining land use has an impact on water resources	0.47	70	32.9	10.265
		Earth environment	Does the form of post-mining land use cause pollution to the land environment?	0.17	60	10.2	3.182
		Air environment	The form of post-mining land use has an effect on the surrounding air	0.19	55	10.45	3.260
		Risk	The form of post-mining land use can reduce the possibility of risk	0.17	75	12.75	3.978
Objective 4: Ensure economic efficiency	0.233	Benefits for investors	Cost and profit for investors	0.63	75	47.25	13.514
		Benefits for community	Bringing benefits to investors	0.28	70	19.6	5.606
		Benefits for the local	Tax revenue from the form of land use	0.09	75	6.75	1.931
Objective 5: Technical feasibility	0.077	Technology readiness	construction technology can implement the plan of post-mining land use	0.204	75	15.282	1.177
		The shape and size of the mine field	The shape and size of the field field meets the post-mining land use plan	0.397	60	23.832	1.835
		Current status of land use in the vicinity	Current status of land use in the vicinity considering the possibility of success of the post-mining land use plan	0.107	50	5.340	0.411
		Climate change	Land use plan after exploitation is stable with climate change	0.086	65	5.589	0.430
		Supply of raw materials	Is the supply sufficient for the post-mining land use plan?	0.206	75	15.470	1.191
Total							82.2

Tab. 4. W-weighting for the objectives of option 2. Ratio CR = 0.085< 0.1

	Nature	Economy	Society	Environment	Technical feasibility	Weight
Nature	1, 1, 1	1/3, 1/2, 1	1/4, 1/3, 1/2	1/4, 1/3, 1/2	2, 3, 4	**0.127**
Economy	1, 2, 3	1, 1, 1	1/3, 1/2, 1	1, 1, 1	1, 2, 3	**0.199**
Society	2, 3, 4	1, 2, 3	1, 1, 1	1, 1, 1	2, 3, 4	**0.295**
Environment	2, 3, 4	1, 2, 3	1, 1, 1	1, 1, 1	2, 3, 4	**0.295**
Technical feasibility	1/4, 1/3, 1/2	1/3, 1/2, 1	1/4, 1/3, 1/2	1/4, 1/3, 1/2	1, 1, 1	**0.083**

Calculate by: $\sum_{j=1}^{m} M_{gi}^{j}\ \sum_{j=1}^{m} M_{gi}^{j}$ perform fuzzy operations the analytical values m for a special matrix given in below, in the final calculation step, the new set (l, m, u) is obtained and used for next step:

$$\sum_{j=1}^{m} M_{gi}^{j} = \left\{\sum_{j=1}^{m} l_j, \sum_{j=1}^{m} m_j, \sum_{j=1}^{m} u_j\right\} \quad (2)$$

In which: l is the minimum cut-off value, m is the maximum estimated value, and u is the value higher than the cut-off value to take. Calculate by:

$$\left[\sum_{i=1}^{n}\sum_{j=1}^{m} M_{gi}^{j}\right]^{-1} \quad (3)$$

Performing fuzzy operation of the value $M_{gi}^{j}M_{gi}^{j}$ (j=1,2,3,4,5…,m) we have

$$\sum_{i=1}^{n}\sum_{j=1}^{m} M_{gi}^{j} = \left\{\sum_{j=1}^{m} l_j, \sum_{j=1}^{m} m_j, \sum_{j=1}^{m} u_j,\right\} \quad (4)$$

And then, calculating the inverse vector in step (8),(9) we get the following:

$$\left[\sum_{i=1}^{n}\sum_{j=1}^{m} M_{gi}^{j}\right]^{-1} = \left[\frac{1}{\sum_{i=1}^{n} l_i}, \frac{1}{\sum_{i=1}^{n} m_i}, \frac{1}{\sum_{i=1}^{n} u_i}\right] \quad (5)$$

* Step 4: Calculate the average ratio.

Suppose a group of users Ut with t = 1, 2, …, k evaluates m choices Ai with i = 1,…, m with h evaluation criteria Cj , j = 1, 2,…, h. Let ( ) with i = 1,…, m, j = 1,…, h and t = 1,…, k be the norm for each choice Ai with user set Ut and criterion Cj . The average rating is calculated as follows:

$$x_{ijt} = \frac{1}{k} \otimes (x_{ij1} \oplus x_{ij2} \oplus \ldots \oplus x_{ijt} \oplus x_{ijk}) \quad (6)$$

In which:

$$e_{ij} = \frac{1}{k}\sum_{t=1}^{k} e_{ijt}\ ,\quad f_{ij} = \frac{1}{k}\sum_{t=1}^{k} f_{ijt}\ ,\quad g_{ij} = \frac{1}{k}\sum_{t=1}^{k} g_{ijt} \quad (7)$$

* Step 5: Calculate the average weight.

Set $Wj_t = (oj_t, pj_t, qj_t)$, $w\ j_t \in R^*$, j = 1,…,h, t = 1,..,k to be the importance determined by the user group with the criterion. The mean importance $w\ j_t = (oj_t, pj_t, qj_t)$ of the Cj criterion as assessed by k user groups is determined as follows:

$$W_j = \frac{1}{k} \otimes (W_{j1} \oplus W_{j2} \oplus \ldots \oplus W_{jk}) \quad (8)$$

In which:

$$o_j = \frac{1}{k}\sum_{t=1}^{k} o_{jt}\ ,\quad p_j = \frac{1}{k}\sum_{t=1}^{k} p_{jt}\ ,\quad q_{ij} = \frac{1}{k}\sum_{t=1}^{k} q_{jt} \quad (9)$$

* Step 6: Calculate the total score of the options according to the criteria with the weight just found. The option with the highest total score will be selected.

3. Research results and discussion

3.1. Result

Based on the SAW method and research results [12], 25 important criteria are proposed to be used to evaluate the weights and are summarized in Table 1. In which: i) Matching characteristics nature of the mine area – 7 criteria; ii) Conformity with regional socio-economic characteristics – 5 criteria; iii) Ensuring environmental criteria – 5 criteria; iv) Ensuring economic efficiency – 3 criteria; v) Technical feasibility – 5 criteria. For details, see Table 1.

3.2. Analyze and propose a plan to improve and restore the environment for Nui Nho quarry

Mining activities cause negative impacts on the environment and health throughout all stages of mining [5, 8, 24]. Mineral mines often cause adverse impacts on the ecological environment [11]. For example, contamination of surface water and groundwater in the project area and its vicinity may be affected by mining activities. To find out the most suitable environmental rehabilitation and restoration plan for the research quarries cluster, the hierarchical process method is used. In fact, on a general level, there is always a change in the ecosystem and landscape before and after mineral extraction [16, 22].

Through information about the characteristics of the mine cluster, the natural socio-economic conditions of the area, refer to the options for mine closure and land use after mining, on the basis of the above criteria, the experience of mine closure in countries around the world, it is possible to propose two options for mine closure and land use after exploitation as follows:

Option 1: Renovating the mining pit into a lake used for tourism, entertainment and water storage. However, this option requires a large investment capital, a long implementation time, but brings economic efficiency.

Option 2: Renovating the mining pit into a water reservoir, enclosed with a fence. This option 2 has low investment capital, fast implementation time but brings lower economic efficiency.

In this study, for option 1, to determine the weight of the principles for the option by means of geometric mean (Geomean) weighting (W) is shown in Table 2.

Integrated assessment based on the weights of principles and criteria combined with scores of experts in minerals, land use management and environmental protection for option 1 – improvement forming a tourist area with a total score of 82.2. For details, see Table 3.

Option 2 is selected to renovate the pit into a water reservoir and closed fence with the weighted principles of calculation in Table 4.

The total score of Option 2 is 74.86, lower than Option 1. For details, see Table 5 .

4. Conclusions

Binh Duong is an industrial province of Vietnam. The construction material mining industry has met a large demand for construction works. The quarries in Binh Duong have been finished and closed according to regulations. With the speed of urbanization and rapid industrial development like Binh Duong, it is necessary to maximize the use of land after mining, contributing to the sustainable development of the mine.

The selection of a suitable model for closing the quarries for deep mining should be based on appropriate objectives in terms of natural, socio-economic, environment, and technical feasibility. The hierarchical process method with fuzzy set is a suitable tool to choose the best plan for mine closure and post-mining land use. Summarizing the research results, it

Tab. 5. General evaluation of option 2

Objectives	Objective's Weight	Criteria	Explanation	Criterion weight	Average score of experts	Criteria score	Total score
Objective 1: Match the natural features of the mine	0.127	Mine topography	The mine topography is suitable for the post-mining land use plan	0.24	75	18	2.286
		Surface water	Reservoir suitable for post-mining land use	0.18	70	12.6	1.600
		Groundwater	Ground water supplies to the reservoir	0.05	65	3.25	0.413
		Climate	Climate affects post-mining land use purpose	0.11	75	8.25	1.048
		Flora and Fauna	Is the flora and fauna rich?	0.04	70	2.8	0.356
		Mine scale	Is the size of the mine suitable?	0.29	70	20.3	2.578
		Geological structure	Stable geological structure	0.09	75	6.75	0.857
Objective 2: Match with regional social characteristics	0.295	Population	The population density is high to participate in post-mining land use	0.53	70	37.1	4.764
		Social infrastructure	Favorable traffic conditions, electricity and water networks	0.19	85	16.15	2.301
		Industry	Industrial activities that support the form of post-mining land use	0.12	65	7.8	1.770
		Pre-mining land use	Is the pre-mining land use suitable for the form of post-mining land use	0.08	75	6	1.770
		Entertainment area	The entertainment area around the mine affects the plan	0.08	75	6	11.092
Objective 3: Ensure environmental targets	0.295	Water Environment	The form of post-mining land use affects the water source	0.47	80	37.6	11.092
		Water Environment	The form of post-mining land use has an impact on water resources	0.17	65	11.05	3.260
		Earth environment	Does the form of post-mining land use cause pollution to the land environment?	0.19	70	13.3	3.924
		Air environment	The form of post-mining land use has an effect on the surrounding air	0.17	75	12.75	3.761
		Risk	The form of post-mining land use can reduce the possibility of risk	0.63	75	47.25	9.403
Objective 4: Ensure economic efficiency	0.199	Benefits for investors	Cost and profit for investors	0.28	80	22.4	4.458
		Benefits for community	Bringing benefits to investors	0.09	75	6.75	1.343
		Benefits for the local	Tax revenue from the form of land use	0.204	85	17.319	1.438
Objective 5: Technical feasibility	0.083	Technology readiness	construction technology can implement the plan of post-mining land use	0.397	75	29.790	2.473
		The shape and size of the mine field	The shape and size of the field meets the post-mining land use plan	0.107	90	9.611	0.798
		Current status of land use in the vicinity	Current status of land use in the vicinity considering the possibility of success of the post-mining land use plan	0.086	75	6.449	0.535
		Climate Change	Land use plan after exploitation is stable with climate change	0.206	90	18.564	1.541
		Supply of raw materials	Is the supply sufficient for the post-mining land use plan?	0.206	75	15.470	1.191
Total							74.86

shows that the plan to renovate the mining pit into a lake using for tourism, entertainment and water storage is the option to close the mine and use the land for Nui Nho mine.

However, besides the achieved results, there are still issues that need to be researched to improve the management of natural resources and environment in mining activities in general and quarries in particular. It is necessary to plan to close the mine early to be proactive and reduce financial costs.

Literatura – References

1. Antwi, E.K.; Owusu-Banahene, W.; Boakye-Danquah, J.; Mensah, R.; Tetteh, J.D.; Nagao, M.; Takeuchi, K. Sustainability Assessment of Mine-Affected Communities in Ghana: Towards Ecosystems and Livelihood Restoration. Sustain. Sci. 2017.
2. Buckley, J. J., "Fuzzy hierarchical analysis", Fuzzy Set and System, 17 (3), PP. 233-247, 1985.
3. Butler, C. R., Hynds, R. E., Gowers, K. H., Lee, D. D. H., Brown, J. M., Crowley, C., ... & Janes, S. M. (2016). Rapid expansion of human epithelial stem cells suitable for airway tissue engineering. American journal of respiratory and critical care medicine, 194(2), 156-168.
4. Chang. (1996), "Applications of the extent analysis method on fuzzy AHP." European Journal of Operational Research, vol. 95, no. 3, pp. 649-655, 1996.
5. S. Fields, The Earth's Open Wounds: Abandoned and Orphaned Mines, Environmental Health Perspectives, Vol. 111, 2003, pp. 154-161, https://doi.org/doi/abs/10.1289/ehp.111-a154.
6. Gupta, S.; Kumar, U. An Analytical Hierarchy Process (AHP)-Guided Decision Model for Underground Mining Method Selection. Int. J. Min. Reclam. Environ. 2012, 26, 324–336.
7. Heikkinen, P. M., Noras, P., Salminen, R., "Environmental techniques for the extractive industries", Mine closure, 2008.
8. M. Hendrychová, M. Kabrna, An Analysis of 200- Year-long Changes in a Landscape Affected by Large-scale Surface Coal Mining: History, Present And Future, Applied Geography, Vol. 74, 2016, pp. 151–159, https://doi.org/10.1016/j.apgeog.2016.07.009.
9. H e r r e r a F., H e r r e r a V.E., 2000 – Linguistic decision analysis; steps for solving decision problems under linguistic information. Fuzzy Sets and Systems, 115, 67–82.
10. S. Hira, P. S. Deshpande, Mining Precise Cause and Effect Rules in Large Time Series Data of Socio-Economic Indicators, Springer Plus, Vol. 5, No. 1, 2016, pp. 1625, https://doi.org/10.1186/s40064-016-3292.
11. P. N. Ho, N. X. Hai, P. T. T. Ha, T. N. Diep. Assessing Soil Quality at Three Typical Construction Material Mining Sites (Limestone Mine, Basalt Mine, and Clay Mine) in Luong Son District, Hoa Binh Province, VNU Journal of Science: Earth and Environmental Sciences, Vol. 32(1S), 2016, pp. 155-163 (in Vietnamese).
12. Nguyen Tri Quang Hung, Vo Truong Nhu Thuy, Nguyen Minh Ky, Study and Proposal of Environmental Improvement and Restoration Plan for Quarry Cluster – A Case Study in Dong Nai Province, VNU Journal of Science: Earth and Environmental Sciences, Vol. 38, No. 2 (2022) 1-12.
13. International Council on Mining and Metals (ICMM): The role of mining in national economies- London, UK (2012).
14. International Council on Mining and Metals 2019 (ICMM), Integrated Mine Closure – Good Practice Guide, 2nd end.
15. International Institute for Environment and Development (IIED). Minerals and Sustainable Development Mining for the Future Appendix B: Mine Closure Working Paper; WBCSD: Geneva, Switzerland, 2002.
16. D. M. McHaina, Environmental Planning Considerations for the Decommissioning, Closure And Reclamation of a Mine Site, International Journal of Surface Mining Reclamation and Environment, Vol 15, 2001, pp. 163-176, https://doi.org/10.1076/ijsm.15.3.163.3412.
17. M i k h a i l o v L., T s v e t i n o v P., 2004 – Evaluation of services using a Fuzzy analytic hierarchy process. Applied Soft Computing, 5, 23–33.
18. Monosky, M., & Keeling, A. (2021). Planning for social and community-engaged closure: A comparison of mine closure plans from Canada's territorial and provincial North. Journal of Environmental Management, 277, 111324.
19. Norouzi Masir, R., Ataei, M., Khalo Kakaei, R., & Mohammadi, S. (2021). Sustainable Development Assessment in Underground Coal mining by Developing a Novel Index. International Journal of Mining and Geo-Engineering, 55(1), 11-17.
20. C. M. Pastakia, A. Jensen, The Rapid Impact Assessment Matrix (RIAM) for EIA, Environmental Impact Assessment Review, Vol. 18, No. 5, 1998, pp. 461-482, https://doi.org/10.1016/S0195-9255(98)00018-3.
21. Saaty, T.L. (1977) A Scaling Method for Priorities in Hierarchical Structures. Journal of Mathematical Psychology, 15, 234-281.
22. J. A. Simmons, W. S. Currie, K. N. Eshleman, K. Kuers, S. Monteleone, T. L. Negley, B. R. Pohland, C. L. Thomas, Forest to Reclaimed Mine Land use Change Leads to Altered Ecosystem Structure and Function, Ecological Applications, Vol. 18, 2008, pp. 104-118, https://doi.org/10.1890/07-1117.1.

23. Tomlins, S. A., Laxman, B., Dhanasekaran, S. M., Helgeson, B. E., Cao, X., Morris, D. S., ... & Chinnaiyan, A. M. (2007). Distinct classes of chromosomal rearrangements create oncogenic ETS gene fusions in prostate cancer. Nature, 448(7153), 595-599.

24. J. M. R. Vega, A. G. Villar, J. S. González, R. B. G. Gutiérrez, J. Á. Martínez, Changes in Land use Due to Mining in the North-Western Mountains of Spain During the Previous 50 Years, Catena, Vol. 149, 2017, pp. 844-856.

25. W a r r e n L., 2004 – Uncertainty in the analytic hierarchy process. Technical Report DSTO-TN-0597, Australian Government Department of Defence. Command and Control, Division Information Sciences Laboratory.

26. Zadeh, L. A., "Fuzzy sets", Information and control, 8, PP. 338–353, 1965.

27. Zadeh, L. A. (1975). Fuzzy logic and approximate reasoning. Synthese 30, 407-425.

Research of Building the Reasonable Mixing Ratio between Waste Rock and Fly Ash as Backfill Material in Mongduong-Cocsau Area, Quang Ninh, Vietnam

Phi Hung NGUYEN[1)]*, CaoKhai NGUYEN[1)], Thi Kim Thanh NGUYEN[1)]

[1)] University of Mining and Geology, 18 Vien street, Duc Thang, Hanoi, Vietnam; email: nguyenphihung@humg.edu.vn

http://doi.org/10.29227/IM-2023-02-39

Submission date: 25-08-2023 | Review date: 22-09-2023

Abstract

The coal mining industry in Quang Ninh province is primarily focused on serving thermal power plants which has resulted in a substantial amount of waste rock and ash. This way has not only narrowed the used land but also had a negative impact on the environment. However, the economic development plan for the province until 2030 emphasizes the development of a greener economy. Therefore, balancing between economic growth and environmental protection is one of the significant challenges of this province.

To solve the problem of waste rock and ash dumps, some methods have been proposed. It tends to use waste materials for backfilling the underground mines, this can help to minimize the bad impact on the environment. Additionally, Another solution is to handle the waste in abandoned mining areas, or use them as construction materials. These ways are expected to partially reduce the bad effects of waste rock and ash dumps on the environment.

In the world, there are many studies on filling using waste rock and fly ash, but in Vietnam this issue is quite new. In order to turn waste rock and fly ash into filling materials, the article researches on a laboratory scale, the ability of transportation in hydraulic pipelines, level of the water separation and shrinkage of mixtures of rock and fly ash in the Mong Duong – Coc Sau area with the different proportions. The results of the experiments show that the area has appropriate mixing ratio as 70–73% of waste rock and 30–27% of fly ash, this ratio satisfies the transportation conditions in the pipeline and the shrinkage rate of 8, 8–12.3%. The indicators in experiments show that it is able to take waste rock into mined underground area to fill, which prevents displacement of strata from mining, protects the underground water flow, and also reduces negative impact of waste rock on environment.

Keywords: *waste rock, fly ash, shrinkage rate, pipeline transportation capacity*

1. INTRODUCTION

In recent years, many different mining methods have been applied to control the displacement of stratigraphy, such as leaving a strip of minerals (earth and rock), pillar-room mining, and mining combined with filling. The mining method of leaving the mineral strip and pillar-room can achieve the imposed mining capacity but results in a high mineral loss rate, which is a significant waste of non-renewable resources (B.D. Thompson et al. 2012; Changxiang Wang et al. 2019; Guo et al. 2014; J Mgumbwa et al. 2014). Hydraulic filling technology has been developed for over 30 years. It was first used in Europe in 1978, in the United States in 1980, in South Africa in 1984, in Canada in 1984, and in Australia in the 1990s. Extensive research carried out in Canadian mines in the early 1990s brought steady progress in the preparation and paste-fill transportation. Accepting the backfill factories, especially bulk mining, has become popular since then. The first backfill factory was built to process mineral tail ore in 1999, and then more than 30 paste-fill installations were operated or in stages of designing or construction around the world (A Bascetin et al. 2016; F.P. Hassani et al.; Jean Béket Dalcé et al. 2019; Kambiz Tahzibi1 et al. 2016).

The feature of the hydraulic fill method is to combine solid materials with water in order to form a pastefill mixture that can be transported in a pipeline. When this mixture is transported into the fill area, the water will gradually separate in order to form the fill blocks in the Gob area (Huang et al. 2011; Nagaratnam Sivakugan et al. 2015; SD Widisinghe et al. 2014). The fill materials are cement, combined with sand, tailings, waste rock, etc. Most of these materials are waste products that are placed in different areas. However, the disadvantages of the mixture of cement and other solid materials are to harden easily in pipelines and to have high cost (Chaoqun Dai et al. 2019; Jixiong Zhang et al. 2019; Milena Kostović 2019; R. Cooke 2001). Recently, some studies have replaced cement with thermoelectric fly ash. Fly ash is both a conductor in the mixture of filler materials, which reduces blockage of pipelines due to stagnation of heavy material at the bottom of the pipe, and a binding agent in the solid-liquid phase of the fill materials (Fabrice Kazambua Beya et al. 2019; Krzysztof Skrzypkowski 2018; Pengfei Zhang et al. 2019). The binding agent is described as a condensed viscous gel but not like mud and it is difficult to separate in transportation. This mixture is like wet concrete that has nearly the same specifications as concrete (Khaldoun Abdelhadi1 et al. 2018; Morteza Sheshpari 2015; Ning Jiang et al. 2017; Pengyu, Y. and Li, L. 2015).

The displacement of stratigraphy is the consequence of losing balance when coal mining forms space in the ground. Therefore, wall rocks and pillar rocks, under the impact of gravity, tend to move into that space, which causes the collapse of the rock layers. This creates a new pressure balance again. Mining methods combined with fire break are unable to control the overload of the upper rock-soil layers, which causes the stratigraphic displacement and then leads to subsidence and tilting of structures on the surface (Peng Huang, 2018; Qingliang Chang et al., 2014; R. Rankine et al., 2007). On the other hand, the collapse of the rock layers above the coal seam can cause the loss of groundwater (Bai E et al., 2018; Erhu Bai et al., 2019; F.P. Hassani et al.).

Fig. 1. The waste dump site at Mong Duong-Coc Sau mine: a. Foot of the waste dump site, b. The slope of waste dump site

Fig. 2. The fly ash of Mong Duong thermal plant: a. a whole scenery of the area containing fly ash at the Mong Duong thermal plant [21], b. Slag ash at the Mong Duong thermal plant [18]

The fill method is considered a green mining solution that can control the displacement of stratigraphy more thoroughly than other methods (Changxiang Wang et al., 2019; Liang Cui and Mamadou Fall, 1976; Von M.Eng. and Manoon Masniyom, 2009).

The filling rate is closely related to the shrinkage, and is an important indicator that affects the support of the suspended soil and rock parts on the wall of the coal seam. It has a direct effect on controlling the overload of pressure from the upper rock, preventing surface subsidence, and protecting the ecological environment and groundwater system (Dónal O'Sullivan and Alexandra Newman, 2014; Guo et al., 2014; Khaldoun Abdelhadi et al., 2018; Milena Kostović, 2019).

Under the same backfill condition, a higher backfill ratio leaves a smaller empty space, resulting in less bending strain at the top and better control of stratigraphic displacement. Conversely, a low backfill rate creates more spaces in the soil-rock area of the Gob, increasing the risk of breaking the original structure of the rock layers on the wall and reducing the efficiency of controlling stratigraphic displacement (Nagaratnam Sivakugan et al., 2015; Pengfei Zhang et al., 2019; R. Rankine et al., 2007).

One of the main issues promoting the support efficiency of fill materials in preventing the displacement of the upper stratigraphy is the shrinkage of the materials. During the process, a mixture of fill material and water is pumped into the underground mining space. When the heavy material settles, excess water drains or loses through seepage. Yanchun Yin and colleagues (2020) used tailings with the main component of dry sand that has chemical elements of Na, Mg, Al, Si, and others. The mixing ratios of cement and tailings were 1:4, 1:6, 1:8, 1:10, 1:12, and 1:15. Based on their experience, the researchers chose a ratio of 2/8 (i.e., 80% of tailings) and achieved the highest efficiency (Yanchun Yin et al., 2019).

Using the hydraulic transportation method with high water pressure, a mixture of material A, mainly including aluminate or additives, and material B, including gypsum, lime, and clay, is transported. Both materials A and B are added to a certain amount of water to make mortar. After mixing at the ratio of 1:1, the solidification time of the material can last from 8 to 90 minutes depending on the different content of additives. Compressive strength can also vary according to the different amount of water. For example, when the volume of water changes in the range of 1.5 MPa (Bai E et al. 2018; Changxiang Wang et al. 2019). The slurry is formed by A or B maintaining for 30 to 40 hours without solidifying, while a mixture of A and B hardens rapidly (Erhu Bai et al. 2019; Guo et al. 2014).

The fill method with a mixture of soil-rock and water was used in 1991. This method was effective in preventing the subsidence of underground mines, especially when mining structures started to collapse. One of the limitations of this method is its expense, mainly due to the high cost of Portland cement. In 1995, a trial research about mortar determined that fly ash existing and available from specific sources in North Dakota could be used to partially replace cement in mortar mixture. This research created a cheaper mortar formula that had better handling properties and safety (Von M.Eng and Manoon Masniyom, 2009). Fly ash has about 80–90% glass that is made of molten clay, shale, limestone, and dolomite. These small spherical particles combine with calcium hydroxide to form calcium silicate hydrate as the main pastefill of cement. Fly ash is classified according to pastefill parameters by the American Society for Testing and Materials (ASTM). Fly ash is a pozzolan that forms cement-like compounds after mixing with lime and water (Changxiang Wang et al., 2019; Kambiz Tahzibi1 et al., 2016; Krzysztof Skrzypkowski, 2018).

Specifications of fly ash include compressive strength, flowability, stability, force-resistance, lateral pressure, solidification time, bleeding and shrinkage, density, and permeability. The largest influence on the effectiveness of fly ash in a filling mixture is the spherical particle shape and the pozzolanic activity of fly ash with Portland cement. The development of strength in the filling mixture directly relates to the cement and water composition. Most mixtures with high fly ash content require only 3 to 5% Portland cement, depending on the dry amount of fly ash, to develop compressive strength from 500 to 1,000 kPa in 28 days, while mixtures with low fly ash content may not require Portland cement. When the amount of water increases in producing a more flowable mixture, the development of compressive strength can decrease (Changxiang Wang et al. 2019; Yanlong Zhou et al. 2020; Yue Zhao et al. 2019).

Using raw ash as a cementitious material and coal as a core material, an orthogonal experiment of the pastefill was performed in this study. The ratio of the original pastefill

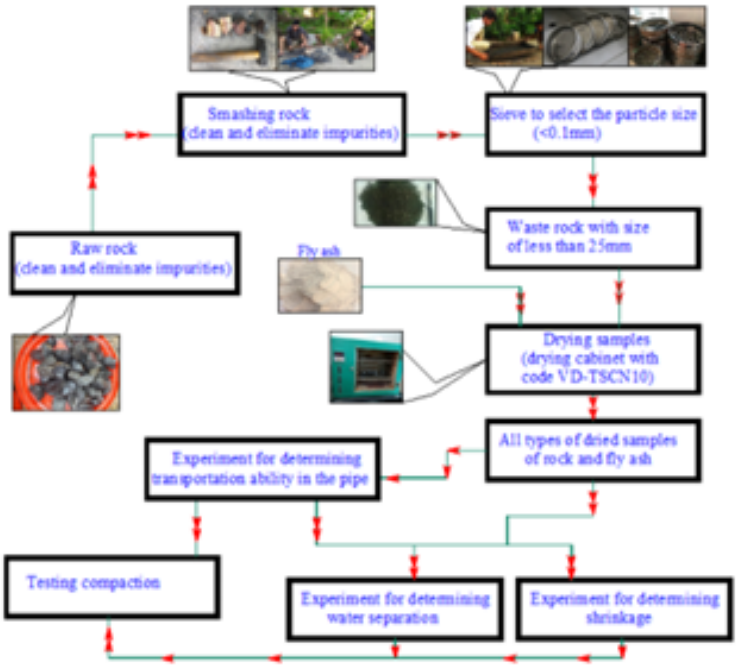

Fig. 3. The process of the sample preparation and experiment

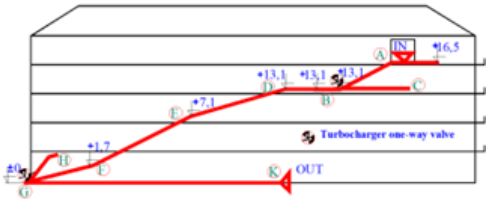

Fig. 4. Diagram of self-flowing generality transportation of backfill material

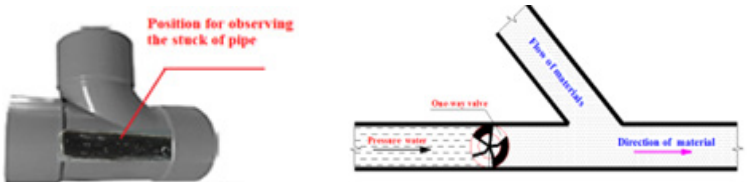

Fig. 5. Diagram of layout the points changing the flowing direction

Fig. 6. The area for the experiment of backfill materials transportation

(coarse ash) and coal particles (Factor A), the proportion of coal particles less than 5 mm (Factor B), and the amount of the pastefill (Factor C) are the three main factors. Factor A ranges from 1:1 to 1:3; Factor B ranges from 30% to 50%; Factor C belongs to the interval of 74% to 78% (Bai E et al. 2018; Yanchun Yin et al. 2019; Yue Zhao et al. 2019).

The development of flowable fill mixture directly relates to the composition of the fly ash and water. Flow can be measured by using a standard concrete slump cone, and the slump varies from 150 mm to 200 mm. For the flowable backfill mixture with a high amount of fly ash, the slump is at least 25 to 50 millimeters higher than the mixture with low fly ash at equivalent moisture. Additives, such as dehydrating agents, are hardly used in flowable buffer blocks (Yanchun Yin et al. 2019; Yanlong Zhou et al. 2020).

On the other hand, when the proportion of hard rock in the pipeline is too big, the hydraulic transportation can cause the pipeline to become clogged. Instead, the fill material transported into the gob area is mainly mud. This type of mud is difficult to fix and flow around, which reduces the efficiency of support for the upper roof. (Guo et al. 2014; Milena Kostović. 2019; Peng Huang et al. 2018). Therefore, if the fill

Tab. 1. List the parameters from the transport experiment

N°	Ratio		Minimum amount of water, %	Solvent density of fly ash and water after saturating, tons/m3	Volume ratio of rock in the mixture,%
	a%	b%			
1	99	1	40.57	1.014	48.63
2	98	2	39.72	1.028	48.63
3	97	3	38.86	1.042	48.63
4	96	4	38,01	1,056	48,63
5	95	5	37.15	1.071	48.63
6	94	6	36.30	1.086	48.63
7	93	7	35,44	1,102	48,63
8	92	8	34.58	1.117	48.63
9	91	9	33,73	1,133	48,63
10	90	10	32,87	1,150	48,63
11	89	11	32.02	1.167	48.63
12	88	12	31.16	1.184	48.63
13	87	13	30.31	1.202	48.63
14	86	14	29,45	1,220	48,63
15	85	15	28,60	1,238	48,63
16	84	16	27,74	1,257	48,63
17	83	17	26,88	1,276	48,63
18	82	18	26,54	1,29	48,25
19	81	19	28,01	1,29	46,60
20	80	20	29,49	1,29	45,02
21	79	21	30,96	1,29	43,51
22	78	22	32,44	1,29	42,06
23	77	23	33,91	1,29	40,66
24	76	24	35,39	1,29	39,33
25	75	25	36,86	1,29	38,05
26	74	26	38,33	1,29	36,81
27	73	27	39,81	1,29	35,63
28	72	28	41,28	1,29	34,49

Fig. 7. Results of transport experiment in the pipeline: a. ratio of fly ash 18% < b < 30%, b. b < 18% và b>30%

method is used, some indicators need to be established appropriately for (1) the ability of transportation in the pipeline, (2) the ability of separating water from the fill, and (3) the shrinkage of the fill.

2. SAMPLING AREA AND THE PROCESS OF SAMPLE PREPARATION

2.1 Introduction of the area for sampling waste rock

The waste dump at Mong Duong coal mine is planned in an area of 66,780 m^2. This is the place where collects waste rock from coal mining activities. The main ingredients are sandstone, siltstone, and pebbles (Fig. 1). The distribution about the size of rocks in the waste dump site is hardly similar. The surface is mainly dust, small-sized gravel and larger rocks are distributed along the slope

Results of analyzing the main mineral components are as follows: SiO_2 = 77.12%; Fe_2O_3 = 4.47%; MnO = 4.42%; Al_2O_3= 9.4%; TiO_2 = 0.26%; K_2O = 1.67%; Na_2O = 0.16%; CaO = 0.84%; MgO = 0.80%; SO_3 = 0.02%. Other components, including stone and wood mulch, account for 1.27%.

2.2 Introduction of the area for sampling fly ash

Mong Duong Thermal Power Plant, which uses local coal as its source, annually consumes about 3.5 million tons of coal and generates approximately 1.3 million tons of slag ash. Of this, the bottom slag from the longwall amounts to 525,000 tons, or 40%, while the fly ash accounts for 787,500 tons, or 60%. A small portion of the slag ash is utilized as backfill material, while the rest is dumped in a designated disposal site.

Basic features of fly ash: The structure is a glass spherical molecule; Molecular size: 1.0 ~ 120/μm (Average input size: 20 ~ 30/μm); Fineness: 2400 ~ 4000 cm^2/g; Main ingredients: SiO_2, Al_2O_3, Fe_2O_3, these components are mainly soil and rock left due to no fire, existing in the components of coal before burning. The total amount of ash, slag, and gypsum stored at waste dumps 1 and 2 of the plant is 3,694,148 tons. The ash, slag, and gypsum are transported to the waste dump using the wet waste method. The size of wet slag is large, so it cannot be transported by pipeline and waste slag pumping system. Instead, the plant transports it by truck with a closed basket.

2.3 The process of the sample preparation

* Instruments preparation

- Set of sieving (the bottom compartment) with the size of hole: 100; 80; 60; 40; 20; 10; 5; 2; 1; 0,5; 0,25 and 0,1 milimeters;
- Types of scale:

+ Scale for the volume up to 10 kg, accuracy of 5 g; + Scales for volume of 5 kg, accuracy of 1 g; + Scales for volume of 1 kg, accuracy of 0.1 g; + the one for volume of 200 g and 500 g, accuracy of 0.01 g;

- Drying oven with temperature control part from 50 degree Celsius to 110 degree Celsius;
- Vibrating sieve machine;
- Thermometer with the measured value up to 50 degree Celsius, accuracy of 0.5 degree Celsius;
- Desiccator with anhydrous silicagel desiccant;
- Ground grinding equipment: porcelain mortar and pestle (the top of the pestle is covered with rubber);
- Soil trays with different sizes; enamel or porcelain bowl;
- Clean water (tap water) or distilled water;
- ray sprayers or pear-shaped rubber suction bottle (called rubber pears);
- Instrument for moisture determination

Tab. 2. The experimental results of determining water separation

N°	Ratio		water separation, cm3/(cm2/s)	The height of the initial backfill block, mm	The height of the backfill block after experimenting, mm	percentage of shrinkage, %
	a% Percentage of waste rock	b% Percentage of fly ash				
(1)	(2)	(3)	(4)	(5)	(6)	(7)
1	99	1	0.017	92.89	64.88	30.15395
2	98	2	0.0159	92.88	64.56	30.49096
3	97	3	0.0148	92.85	63.89	31.19009
4	96	4	0.0136	90.65	62.65	30.88803
5	95	5	0.0122	91.88	64.88	29.38616
6	94	6	0.0113	90.58	65.58	27.59991
7	93	7	0.0102	89.69	65.69	26.75884
8	92	8	0.0093	91.14	70.14	23.04147
9	91	9	0.008	92.94	71.94	22.59522
10	90	10	0.0078	92.89	74.89	19.37776
11	89	11	0.0069	89.78	73.78	17.82134
12	88	12	0.0062	88.24	74.24	15.86582
13	87	13	0.0059	90.32	79.32	12.17892
14	86	14	0.0056	88.64	82.64	6.768953
15	85	15	0.0053	90.06	86.06	4.441483
16	84	16	0.005	88.6	84.6	4.514673
17	83	17	0.0047	91.09	85.09	6.586892
18	82	18	0.0044	93	86	7.526882
19	81	19	0.0042	89.89	82.89	7.787296
20	80	20	0.0039	90.75	82.75	8.815427
21	79	21	0.0036	92.33	83.33	9.747644
22	78	22	0.0033	92.31	83.31	9.749756
23	77	23	0.003	91.83	82.83	9.800719
24	76	24	0.0027	89.17	80.17	10.09308
25	75	25	0.0024	90.52	82.52	8.837826
26	74	26	0.0022	90.33	80.33	11.07052
27	73	27	0.0019	92	83	9.782609
28	72	28	0.0016	88.24	77.24	12.466
29	71	29	0.0013	89.37	78.37	12.30838
30	70	30	0.001	91.96	80.96	11.96172
31	69	31	0.0007	92.24	81.24	11.92541
32	68	32	0.0004	90.55	79.55	12.14798

Fig. 8. Experiment for determining the water separation of backfill materials

* Experimental sample preparation

The experiment was carried out at the laboratory of the Mining Department – Hanoi University of Mining and Geology, Vietnam, using fly ash, bottom ash from the Mong Duong thermal plant, and waste rock from Mong Duong and Coc Sau mines. The steps included cleaning the waste rock with water, then crushing it and classifying it with a sieve to choose particles with a size less than 25mm. If deployed in real mining operations in Quang Ninh, this particle size will allow the use of a jaw crusher machine in combination with a vibrating sieve to create products, and the cost for this production will be lower than using a ball mill. Samples of waste rock material after crushing and fly ash are taken into the drying oven to dry, respectively (Figure 3). The crushed waste rock is separated from the fly ash for ease of mixing in experiments.

Samples of rock and fly ash were mixed in ratios from 1/99 to 99/1 for the purpose of testing: (1) the ability of transportation in the pipeline, (2) the ability of separating water from the backfill, and (3) shrinkage of the backfill. In which the rock plays the role of the main fill material, bearing the main pressure, the fly ash plays the role of a conductor (with water) in the pipeline, and the fly ash is used for filling into the space between the stones in order to improve compaction of the backfill before it is given to the fill area.

Thus, it is necessary to do three experiments with mixing ratios of rock (a) and fly ash (b) to find the appropriate a/b ratio that satisfies all 3 conditions (1), (2), and (3). Do 3 experiments simultaneously.

3. EXPERIMENT 1. DETERMINING THE TRANSPORTATION ABILITY OF THE FILL MATERIALS IN THE PIPELINE

Target: Determine the transportation ability of the mixture of rock, fly ash, and water in the pipeline. Prepare test samples with different mixing ratios and allow them to hydrate to saturation. Set up the pipeline with three sections of changing direction from a height of 16.5m to a height of 0m (see Figures 7 and 9). Install 3-pronged elbows and one-way valves at the places of direction change. The one-way valve will add pressure if the flow gets stuck at the place of direction change (see Figures 8 and 9).

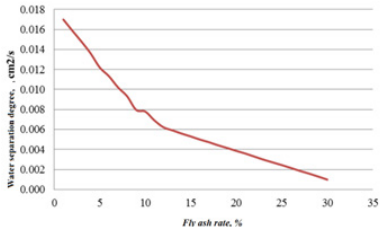

Fig. 9. Relationship between water separation and ratio of fly ash in the mixture

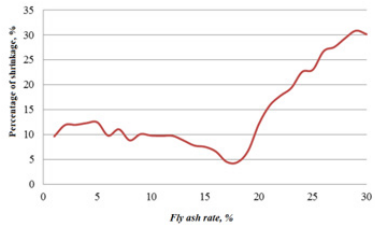

Fig. 10. Relationship between shrinkage and ratio of fly ash

In the implementation process, it shows that when the amount of fly ash is less than 18%, most of the samples cause pipe blockage. When water is added into the top of the pipe, the blockage happens at point B (elevation of 13.1m). Pressure is continually added by opening valve No. 1, the output is a suspension mixture (mainly water and fly ash, Fig. 4). Further experimenting with the ratios of fly ash from 18 to 30%, it shows that the mixture does not get stuck and the results are obtained as shown in Fig. 7a. When the amount of fly ash increases and the percentage of rock reduces, the mixture mainly consists of suspended ash and water with only a small amount of rock.

From the experiment, it is realized that when the ratio of a/b equals 82/18 and the minimum amount of water is used, the density of the mixture of water and fly ash reaches saturation of 1.29 tons/m³. However, when the natural height difference is 16.5 m, the tube gets stuck at turning point (B). This is due to insufficient pressure and the high density of a/b, which causes the heavy rock to sink quickly into the pipeline. Testing by adding water pressure at bends (D), (E), and (F) prevents pipe blockage, but the resulting product is a mixture of mud and water (Fig. 7b).

Case 1: The volume of fly ash is larger than the porosity of the rock (b ≥18%):

$$m.\gamma_n = V_{void} = V_t^{vl} - V_s^{vl} = V_t^{ash} + V_s^{rock}$$

$$- (V_s^{rock} + V_s^{ash}) = V_t^{ash} - V_s^{ash} = b\left(\frac{1}{\gamma_v^{ash}} - \frac{1}{\gamma_r^{ash}}\right) \quad (1)$$

$$\Leftrightarrow \frac{m}{\gamma_n} \geq b\left(\frac{1}{\gamma_v^{ash}} - \frac{1}{\gamma_r^{ash}}\right), \quad (2)$$

With "m" is ratio of water (according to weight) for transporting one material unit

Case 2: The volume of fly ash is smaller than the porosity of the rock (b ≤ 18%):

$$V_{void} = V_t^{rock} - V_s^{rock} - V_s^{ash} = a\left(\frac{1}{\gamma_v^{rock}} - \frac{1}{\gamma_r^{rock}}\right) - \frac{b}{\gamma_r^{ash}}$$

$$\Leftrightarrow \frac{m}{\gamma_n} \geq a\left(\frac{1}{\gamma_v^{rock}} - \frac{1}{\gamma_r^{rock}}\right) - \frac{b}{\gamma_r^{ash}} \quad (3)$$

Note: Choose $\gamma_n = 1$; $\gamma_v^{rock} = 1.24$; $\gamma_r^{rock} = 2.55$; $\gamma_v^{ash} = 0.522$; $\gamma_r^{tro} = 2.266$, *tons/m³* (4)

When the mixture is saturated, the factors affecting the transportation process are the solvent density and the volume ratio of the rock.

- Solvent density: the higher the density of the fly ash water suspension is, the more it prevents the deposition of rock;

$$\gamma_{solvents} = (b+m)(b/(\gamma_r^{ash}) + m)$$

- The volume ratio of rock in the mixture: The smaller the volume ratio of rock is, the more beneficial transportation is:

+ Case of b≤18%: $V_{rock}^{\%} = \frac{\gamma_v^{rock}}{\gamma_r^{rock}}$

+ Case of b≥18%: $V_{rock}^{\%} = \frac{a}{\gamma_r^{rock}} : \left(\frac{a}{\gamma_r^{rock}} + \frac{b}{\gamma_v^{ash}}\right)$

Results of Experiment 1 determined that the ratio of 82/18 < a/b < 70/30 is the effective transportation ratio both in terms of moving in the pipeline and the obtained mixture at the end of the pipe. Experimenting again at different ratios a/b = 73/27–70/27, i.e., the percentage of fly ash increased to 27–30%, the time of material transportation is about 95 seconds, the weight of the material that can be loaded is 0.02 m³, equivalent to a speed of 0.75 m/s and requiring 34 liters of additional water. The following experiments will confirm this ratio, no exceed 36 samples.

4. DETERMINATION OF THE SHRINKAGE RATIO AND WATER SEPARATION RATIO

4.1 Experiment 2. Determining the water separation ability of the mixture of rock and fly ash according to the mixing ratios

Target: Determining the water separation ability of the mixture of rock and fly ash and water with different a/b mixing ratios.

Prepare 36 samples for the experiment with ratios shown in table 2. Weigh the dry samples. Let the samples hydrate until saturation. Place these samples into PVC pipes with the same type and volume. Continuously pour an equal amount of water into the pipes (figure...), measure the time of draining from point 1 to point 2 (figure 8).

The experiment reached sample 32th, where it was found that when the mixing ratio a/b equals 68/32, the water separation gradually decreased to zero. The experiment was stopped because a larger fly ash ratio will be inappropriate to use in production reality. The water-filled block has poor water separation ability and the materials are easily transported to another place. Experiment results are shown in Table 1, column (4), and Figure 9. When the ratio of rock (a) is high, the water separation ability is better, and vice versa. If the proportion of rock is too high, then heavy materials will sink to the bottom of the pipe, causing blockage and making transportation difficult.

4.2 Experiment 3. Determining the shrinkage of the mixture of rock and fly ash after separating water

Target: Determining the volumetric shrinkage of the mixture of rock, fly ash, and water after water separation.

Prepare 100 samples of mixture of rock, fly ash, and water. Use the same type of PVC pipe with a height of 1 meter and a water filter at the bottom. Pour each sample into the PVC pipe and measure the height of the material in the pipe using a ruler with an accuracy of 0.1 mm. Then, pour water into the pipe as shown in Figure 4. Use a ruler to measure the subsidence of the backfill in the PVC pipe. The experimental results are shown in Table 2, columns (4), (5), (6) and Figure 10.

The experiment reached sample 36, which showed that when the mixing ratio a/b equals 64/36, the water separation gradually decreased to zero. The experiment was stopped because this ratio is not suitable with production reality. The water-containing backfill has poor water separation, making it easy for the material to flow to other places. When the ratio of rock (a) is high, the water separation is better, and vice versa. If the proportion of rock is too high, heavy materials sink to the bottom of the pipe, it will cause blockages and make transportation difficult.

The relationship for shrinkage ratio can be expressed as:

shrinkage ratio (%) = weight of water / (weight of solid + weight of water) (1)

When the proportion of fly ash is lower than the void in rock, the unfilled rock tends to be crushed by pressure, resulting in smaller particles and a reduced volume of the backfill. The optimal ratio is that the small particles fill all voids between the large particles. Volume of voids in rock:

$$V_{void} = \frac{a}{\gamma_v^{rock}} - \frac{a}{\gamma_r^{rock}} \quad (5)$$

The volume of fly ash in void:

$$b = 100 - a = \gamma_v^{ash} \times V_{void} \Rightarrow b = 100\left(1 - \frac{1}{1+\gamma_v^{ash}\times\left(\frac{1}{\gamma_v^{rock}} - \frac{1}{\gamma_r^{rock}}\right)}\right) \quad (6)$$

The relationship of shrinkage ratio is determined as follows: ratio of shrinkage (%) = weight of water / (weight of solid + weight of water) (1). If the proportion of fly ash has less volume than the void in rock, the unfilled rock tends to be crushed by pressure to create smaller particles and reduce the volume of the backfill. The right ratio means that the small particles fill all voids in the large particles.

Where a and b are respectively the ratio of rock and the ratio of fly ash (a+b =100); γ_v^{rock}= 1.20÷1.34 tons/m³, γ_v^{rock} = 2.45 to 2.63 tons/m³, and γ_v^{ash}= 0.52 to 0.56 tons/m³ are the volumetric weight, private weight of rock, and volumetric weight of fly ash. Different proportions of rock (a%) and fly ash (b%) will have different shrinkage, as shown in Table 2. Formulas (2), (3), and Tables 2 and 6 show that when the ratio of fly ash is high, the deformation of the backfill does not change much. The fly ash particles are too fine, so there is no space to fill, and the volume of the backfill is stable. The disturbance of the backfill from sample 6 to sample 19 hardly has a clear rule between the mixing ratio a/b and the volumetric change in the presence of water. The reason is due to water that washes away the fly ash particles. In reality, with higher water pressure, if the fly ash ratio is too high, it will be difficult to form backfills due to being swept away by water in the process of water separation from the backfill.

5. RESULTS AND DISCUSS

The results of the water separation test show that the higher the ratio of rock to fly ash (a/b) is, the greater the water separation of the backfill is. When this ratio (a/b) equals 7/3, the mixture of fly ash and rock becomes viscous. The results of the shrinkage test show that the peak shrinkage occurs in case of that the ratio of fly ash accounts for 27% and the ratio of rock accounts for 73%. Therefore, in order to achieve optimal shrinkage, the suitable mixing ratio is between 27–30% of fly ash and 73–70% of waste rock.

The testing of transportation in the pipeline showed that when the height difference is 16.5 m without the addition of pressure, and the ratio of rock to fly ash (a/b) is 82/18, the tube is blocked in the first bend at a height difference of 13.1 m. After adding a pressure difference to the water, the obtained backfill material at the output is mainly a mixture of mud and water. When the percentage of fly ash increases 27–30%, the material transportation time is about 95 seconds, the volume of the loaded material is 0.02 m³, equivalent to a speed of 0.75 m/s, and requires over 34 liters of water (0.034 m³ of water). Thus, in the production reality, it is necessary to pay attention to adding pressure or pressurized water in the bends or calculate the capacity of the pump appropriately to avoid the blockage of pipes.

6. CONCLUSIONS

The chemical compositions of the waste rock and fly ash used as fill materials in Mong Duong, Cam Pha, Quang Ninh, Vietnam are safe and do not contaminate groundwater in the longwall. The optimal mixing ratio of materials that is suitable with transportation conditions in the pipeline is from 70/30 to 80/20. This mixing ratio helps to create a safe conductor in order to transport into the longwall without the risk of tube blockage. However, it is still necessary to add pressure at the turning bends during the transportation process.

When the optimal mixing ratio (70/30 to 80/20) is used for waste rock and fly ash in Mong Duong, Cam Pha, Quang Ninh, Vietnam, the shrinkage ranges is from 8.8% to 12.3%. After 48 hours, additional fill materials should be pumped into the longwall to achieve a higher anti-subsidence effect. It is also important to consider the mechanical and physical characteristics of the wall rock when calculating the backfill materials and determining the appropriate pump capacity and timing to maximize the effectiveness of the fill materials in preventing collapse of the wall rock.

Literatura – References

1. A Bascetin et al. 2016 – A Bascetin, Tuylu, Adiguzel, U. Cinar. 2016. Determination of optimum mixture ratios of paste backfill materials for disposal of mineral processing tailings. SME Annual Meeting, Phoenix, AZ, P 1-4.
2. B.D. Thompson et al. 2012 - B.D. Thompson, W.F. Bawden, and M.W. Grabinsky. 2012. In situ measurements of cemented paste backfill at the Cayeli Mine, Can. Geotech. J. 49: 755–772 (2012) doi:10.1139/T2012-040.
3. Bai E et al. 2018 – Bai E., Guo W., Tan Y., Yang D. 2018 .The analysis and application of granular backfill material to reduce surface subsidence in China's northwest coal mining area. PLoS ONE 13(7): e0201112. https://doi.org/10.1371/journal. pone.0201112.
4. Changxiang Wang et al. 2019 - Changxiang Wang, Yin Liu, Hao Hu, Yangyang and Yao Lu. 2019. Study on Filling Material Ratio and Filling Effect: Taking Coarse Fly Ash and Coal Gangue as the Main Filling Component. Hindawi Advances in Civil Engineering Volume 2019, Article ID 2898019, 11 pages https://doi.org/10.1155/2019/2898019.
5. Chaoqun Dai et al. 2019 - Chaoqun Dai, Aixiang Wu, Yan Qi, Zhiqiang Chen. 2019. The Optimization of Mix Proportions for Cement Paste Backfill Materials via Box–Behnken Experimental Method. Journal of The Institution of Engineers (India): Series D volume 100, pages307–316 (2019) https://doi.org/10.1007/s40033-019-00108-7.
6. Dónal O'Sullivan and Alexandra Newman. 2014. Extraction and Backfill Scheduling in a Complex Underground Mine. Mine Interfaces 44(2), pp. 204–221, 2014, http://dx.doi.org/10.1287/inte.2013.0730.
7. Erhu Bai et al. 2019 - Erhu Bai, Wenbing Guo, Miningjie Muo, Gaozhong Lou& Yi Tan. 2019. Analysis and Application of Backfill Mining in Thin Coal Seams for Preventing Building Damage. Sains Malaysiana 48(9)(2019): 1823–1832 http://dx.doi.org/10.17576/jsm-2019-4809-03.
8. F.P. Hassani et al - F.P. Hassani, A. Mortazavi, and M. Shabani. An investigation of mechanisms involved in backfill-rock mass behaviour in narrow vein mining. The Journal of The Southern African Institute of Mining and Metallurgy, Volume 108, P463-472.
9. Fabrice Kazambua Beya et al. 2019 - Fabrice Kazambua Beya, Mamert Mbonimpa, Tikou Belem, Li Li, Ugo Marceau, Patrick Kayumba Kalonji, Mostafa Benzaazoua and Serge Ouellet. 2019. Mine Backfilling in the Permafrost, Part I: Numerical Prediction of Thermal Curing Conditions within the Cemented Paste Backfill Matrix. Minerals 2019, 9, 165; doi:10.3390/min9030165;
10. Guo et al. 2014 - Guo, G.L., Zhu, X.J. & Zha, J.F. 2014. Subsidence prediction method based on equivalent mining height theory for solid backfilling mining. Transactions of Nonferrous Metals Society of China 24(10): 3302-3308.
11. Huang et al. 2011 - Huang, Y.L., Zhang, J.X., Zhang, Q. & Nie, S.J. 2011. Backfilling technology of substituting waste and fly ash for coal underground. Environmental Engineering and Management Journal 10(6): 769-775.
12. J Mgumbwa and T Nester. 2014. Paste improvement at La Mancha's Frog's Leg underground mine, Mine Fill 2014, Perth, Australia, DOI https://doi.org/10.36487/ACG_rep/1404_22_Mgumbwa.
13. Jean Béket Dalcé et al. 2019 – Jean Béket Dalcé, Li Li and Pengyu Yang. 2019. Experimental Study of Uniaxial Compressive Strength (UCS) Distribution of Hydraulic Backfill Associated with Segregation. Minerals 2019, 9, 147; doi:10.3390/min9030147.
14. Jixiong Zhang et al. 2019 - Jixiong Zhang, Meng Li, Abbas Taheri, Weiqing Zhang , Zhongya Wu and Weijian Song. 2019. Properties and Application of Backfill Materials in Coal Mines in China. Minerals 2019, 9, 53; doi:10.3390/min9010053.
15. Kambiz Tahzibi1 et al. 2016 - Kambiz Tahzibi1, Mehdi Nasiri, Bijan Mashoof, Shokrollah Lotfi. 2016. Experimental and Analytical Studies to Achieve an Optimised Cemented Backfill Mix to be Used in a Cut-Fill Mining Method. International Journal of Mining Engineering and Mineral Processing 2016, 5(1): 1-8 DOI: 10.5923/j.mining.20160501.01.
16. Khaldoun Abdelhadi1 et al. 2018 - Khaldoun Abdelhadi1, Ouadif Latifa1, Bahi Lahcen1 , Baba Khadija. 2018. Underground Cemented Backfill, a Design Procedure for an Integrated Mining Waste Management. MATEC Web of Conferences 149, 02086 (2018) https://doi.org/10.1051/matecconf/201814902086.
17. Krzysztof Skrzypkowski. 2018. Compressibility of materials and backfilling mixtures with addition of solid wastes from flue-gas treatment and fly ashes. E3S Web of Conferences 71, 00007 (2018) https://doi.org/10.1051/e3sconf/20187100007.
18. La Nghia Hieu. The waste dump only loads eleven days, the thermal plant is in danger of stopping production, https://thanhnien.vn/thoi-su/bai-thai-chi-con-tai-11-ngay-nha-may-nhiet-dien-co-nguy-co-dung-san-xuat-948315.html.
19. Liang Cui and Mamadou Fall. 1976. Multiphysics Modeling and Simulation of Strength Development and Distribution in Cemented Tailings Backfill Structures. International Journal of Concrete Structures and Materials DOI 10.1186/s40069-018-0250-y ISSN 1976-0485 / eISSN 2234-1315;

20. Milena Kostović. 2019. Paste backfill materials for underground mining - some experiences in serbia – part I. Underground mining engineering 35 (2019) 57-64 , university of Belgrade - faculty of mining and geology ISSN 03542904.

21. Minh Hang. Slag ash from Mong Duong thermal plants 1 and 2: How is it treated?, https://baoxaydung.com.vn/tro-xi-nha-may-nhiet-dien-mong-duong-1-va-2-duoc-xu-ly-nhu-the-nao-234821.html.

22. Morteza Sheshpari. 2015. A Review of Underground Mine Backfilling Methods with Emphasis On Cemented Paste Backfill. Electronic Journal of Geotechnical Engineering January 2015, Vol. 20 [2015], Bund. 13, p 5183- 5208.

23. Nagaratnam Sivakugan et al. 2015 - Nagaratnam Sivakugan, Ryan Veenstra, Niroshan Naguleswaran. 2015. Underground Mine Backfilling in Australia Using Paste Fills and Hydraulic Fills. Int. J. of Geosynth. and Ground Eng. (2015) 1:18, DOI 10.1007/s40891-015-0020-8.

24. Ning Jiang et al. 2017 - Ning Jiang, Jinhai Zhao, Xizhen Sun, Liyang Bai, Changxiang Wang. 2017. Use of fly-ash slurry in backfill grouting in coal mines. Heliyon 3 (2017) e00470. doi: 10.1016/j.heliyon.2017. e00470.

25. Peng Huang et al. 2018 – Peng Huang, AJS (Sam) Spearing, Ju Feng, Kashi Vishwanath Jessu and Shuai Guo. 2018. Effects of solid backfilling on overburden strata movement in shallow depth longwall coal mines in West China. Journal of Geophysics and Engineering, J. Geophys. Eng. 15 (2018) 2194–2208 (15pp) https://doi.org/10.1088/1742-2140/aac62c.

26. Pengfei Zhang et al. 2019 – Pengfei Zhang, Yubao Zhang , Tongbin Zhao, Yunliang Tan and Fenghai Yu. 2019. Experimental Research on Deformation Characteristics of Waste-Rock Material in Underground Backfill Mining. Minerals 2019, 9, 102; doi:10.3390/min9020102.

27. Pengyu, Y. and Li, L. 2015. Investigation of the short-term stressdistribution in stopes and drifts backfilled with cemented paste backfill. International Journal of Mining Science and Technology, Vol. 25 (Issue No. 5), pp. 721-728.

28. Qingliang et al. 2014 - Qingliang Chang, Jianhang Chen, Huaqiang Zhou, and Jianbiao Bai. 2014. Implementation of Paste Backfill Mining Technology in Chinese Coal Mines. Hindawi Publishing Corporation ę e Scientific World Journal Volume 2014, Article ID 821025, 8 pages http://dx.doi.org/10.1155/2014/821025.

29. R. Cooke. 2001. Design procedure for hydraulic backfill distribution systems. The Journal of The South African Institute of Mining and Metallurgy, MARCH/APRIL 2001, p 97-102.

30. R. Rankine et al. 2007 - R. Rankine, M. Pacheco, N. Sivakugan. 2007. Underground Mining with Backfills. Soils and Rocks, São Paulo, 30(2): 93-101, May-August, 2007.

31. SD Widisinghe et al. 2014 - SD Widisinghe, N Sivakugan, VZ Wang. 2014. Loads on barricades in hydraulically backfilled underground mine stopes. Mine Fill 2014, Perth, Australia, doi https://doi.org/10.36487/ACG_rep/1404_08_Widisinghe.

32. Von M.Eng. and Manoon Masniyom. 2009. Systematic Selection and Application of Backfill in Underground Mines. Doctor-Ingenieur, Der Fakultät für Geowissenschaften, Geotechnik und Bergbau der Technischen Universität Bergakademie Freiberg genehmigte, 2009.

33. Yanchun Yin et al. 2019 - Yanchun Yin, Tongbin Zhao, Yubao Zhang, Yunliang Tan, Yue Qiu, Abbas Taheri and Yuan Jing. 2019. An Innovative Method for Placement of Gangue Backfilling Material in Steep Underground Coal Mines. Minerals 2019, 9, 107; doi:10.3390/min9020107.

34. Yanlong Zhou et al. 2020 – Yanlong Zhou , Keping Zhou , and Yun Li. 2020. A New Decision Method of Filling Ratio Based on Energy Matching of Surrounding Rock and Backfill. Hindawi Geofluids, Volume 2020, Article ID 8856537, 7 pages https://doi.org/10.1155/2020/8856537.

35. Yue Zhao et al. 2019 - Yue Zhao , Amin Soltani, Abbas Taheri, Murat Karakus and An Deng. 2019. Application of Slag–Cement and Fly Ash for Strength Development in Cemented Paste Backfills. Minerals 2019, 9, 22; doi:10.3390/min9010022.

36. Walawska B., Szymanek A, The effect of structure modification of sodium compounds on the efficiency in removing SO2 and HCl from fumes in the conditions of circulating fluid bed, Chemical and Biochemical Engineering Quarterly 31 (3) 261–273 (2017)

37. Walawska B, Szymanek A, Szymanek P. Impact of decomposition temperature on the surface area of sodium bicarbonate Przemysł Chemiczny 2012, pp.1049-1052

38. Sambor A, Szymanek A Analysis of the migration of chemical compounds from fly ash exposed the weather condition ,Chemical and Process Engineering. 2014, ISSN:0208-6425

Selecting Parameters to Design Auxiliary Ventilation in Underground Mine

Phuong Thao DANG[1)]

[1)] Mining Faculty, Hanoi University of Mining and Geology, Hanoi, Vietnam; 18 Vien Street, Duc Thang Ward, Bac Tu Liem District, Hanoi, Vietnam; email: dangphuongthao@humg.edu.vn

http://doi.org/10.29227/IM-2023-02-40

Submission date: 29-08-2023 | Review date: 23-09-2023

Abstract

In recent years, Quang Ninh coal mines are continually expanding on size and depth, the total length of the roadway each year amounts about ten thousands meters in order to reach new production zones. The length of new roadways is usually longer, leading to increase to the airflow demand. Ventilation is one of the main factors effecting driving progress of the roadway. The estimation of airflow requirements is usually based on the minimum amount of airflow required at the heading during driving roadways or at the working face, in other words, when the ventilation ductwork is at its maximum length.

Therefore, determination of maximum ventilation length of ductwork has been undertaken. This results allow the selection of a reasonable fan to meet the ventilation requirements when driving the roadway. Also, this value is an important parameter for designing auxiliary ventilation system that operates more efficiently on a lower cost.

Keywords: *air leakage, maximum ventilation length, auxiliary ventilation, duct, working face*

Introduction

Auxiliary ventilation is one of critical importance considerations in coal underground mine. The systems must be supplied a fresh air to ensure a safe and comfortable environment conditions in the working face. Therefore, ventilation system needs to be ensured technical standard and safety regulations, also get optimized both capitals and operating cost.

In fact, in coal mine in Vietnam, when driving roadways, the most common auxiliary ventilation system used is the force system, in which the fresh air is led to the face through the fabric duct. The auxiliary ventilation system is comprised the ductwork and the axial fans. Recently, mines have equipped with auxiliary fans to meet requirements of ventilation. Fan requirements for mechanized roadway depend on the length of the roadways and airflow requirements. The problem is that mines normally select fan based on experience. In practice, one mine use a fan while another mine use two fans with the same conditions (the airflow requirements, the length of the roadways). It can be noticed, if one fan satisfies the air flow, two fans will "redundant" that can increase system operating costs. The another problem is that both cases are aimed at ensuring ventilation by selecting number of fans and not paying much attention to air ducting system to the face. The fan consumes energy to overcome duct resistance to bring fresh air into the face, so duct needs to have special technical characteristics to improve the efficiency of the fan. The cost of fan is no less than the cost of the ducting system. There is a widely-held belief in the mining community that more fan power in a ventilation ducting system will produce more airflow. However, in most cases, this is either not true in any practical sense, or is a very expensive way to achieve an increase, in both capitals and operating costs [1]. Economic fact associated with mine ventilation is well known to the practising engineer as ventilation accounts for 40 to 50% of a mine's total energy consumption [2].

The estimation of air volume requirements is normally based on the minimum amount of airflow required at the heading during the final stages of development or at the stope face during the final stages of production; i.e. when the ventilation ducting is at its maximum length [3]. Therefore, determination of maximum ventilation length with a given ductwork as well as ventilation parameters in auxiliary ventilation system have been investigated in order to optimize parameters to design auxiliary ventilation in underground mine.

1. Optimal fan selection in auxiliary ventilation systems

For each auxiliary ventilation system with a given ductwork, airflow amount of the fan can bring to the working places needs to be determined. One of the important problem of ventilation design when driving roadway is to calculate the maximum length of ductwork that a fan has enough capacity to ensure to bring air to the face.

In case the roadways are not long, solving the above problem is choosing the one appropriate fan for auxiliary ventilation. And ducts must have low resistance, air leakage as well as ensure construction quality when installed in the roadway cross section.

In case the roadways are long. The solution to the problem is to calculate the maximum length of ductwork that a fan can ensure to reach fresh air to prepared face. From that, design a reasonable distance between the fans working in series (the outlet of one fan is the direct inlet to the next fan) in order to prevent pressure drop in the ductwork before the next fan's inlet, causing problems with the fan motor.

As can be seen in Figure 1, distance between the fans installed in series can be as [4]:

a. The distance between the fans is calculated in theory.

b. The distance between the fans is far causing a ducting pressure loss at the inlet of the next fan in series. This can cause problems with the fan motor.

c. The distance between the fans is recommended for installing fans based on the maximum ventilation length

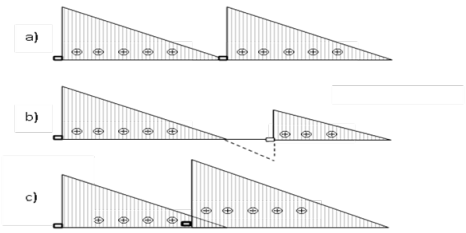

Fig. 1. Schematic of fans installation in series whilst in a series operation system

Fig. 10. Relationship between shrinkage and ratio of fly ash

Q (m³/s) / L(m)	2	2.3	2.5	2.8	3	3.2	3.4	3.5	3.8	4.0
100	1.024	1.026	1.027	1.028	1.030	1.030	1.032	1.033	1.035	1.035
200	1.091	1.097	1.102	1.111	1.118	1.120	1.124	1.125	1.131	1.135
300	1.203	1.214	1.221	1.230	1.238	1.242	1.249	1.252	1.261	1.272
400	1.323	1.345	1.368	1.378	1.394	1.415	1.435	1.450	1.476	1.488
500	1.542	1.568	1.590	1.618	1.642	1.666	1.688	1.678	1.798	1.716
600	1.749	1.776	1.798	1.838	1.889	1.908	1.930	1.946	1.977	1.995
700	1.976	2.032	2.078	2.133	2.169	2.193	2.218	2.233	2.268	2.296

Tab. 2. Values of aerodynamic characteristic of the fan YBT-22

Flow rate, m³/s	3.9	4	4.15	4.27	4.5	4.66	4.83	5
Pressure, mmH₂O	316	316	316	314	302	291	277	261
Flow rate, m³/s	5.16	5.33	5.5	5.67	5.83	6	6.18	
Pressure, mmH₂O	245	228	206	179	149	113	70	

estimated, it is estimated the reasonable distance between the fans working in a series operation system.

Netherless, it is necessary that the use of fans and their operation in optimal conditions lead to savings in energy consumption.

2. Model of conceptual analysis for calculating maximum ventilation length

For example, determining the relationship between the maximum length of duct which the fan can bring the required airflow to the face, is difficult to solve by graph method if not combined with analytical methods.

Underground mine ventilation network analysis has not been much changed since 1935 when McElroy conducted the study of the engineering factors in the underground mine ventilation [5–6]. In the general case, the concept mathematical model of the auxiliary ventilation system is described by the following expression [7]:

$$R_o.p.Q^2=n.f(Q) \quad (1)$$

Where: R_0: Theoretical friction resistance of ductwork (no air leakage in ductwork), kμ;
f (Q): Analytic expression of the fan aerodynamic characteristic curve;
p: Duct leakage coefficient;
Q: Quantity of airflow, m^3/s;
n: Numbers of fans in series;

Resistance Ro is determined by the formula [8]:

$$R_0 = 6.48 * 0.00048 * L/D^5 (k\mu) \quad (2)$$

Where: α: Friction factor for the duct, α= 0.00048 $KgF.s^2/m^4$;
L: Distance between two cross sections of duct, m;
D: Diameter of the duct, m.

Equation (1) can be represented as follows:

$$6,48.\alpha.L/D^5 .p.Q^2=n.f(Q) \quad (3)$$

Estimating duct leakage coefficient – p and fan characteristic curve – H=f(Q) in order to calculate the maximum ventilation length, which the fan can generate the required air flow.

2.1 Determining leakage coefficient

Level of air leakage is mainly influenced by the following factors: total length, diameter of the ducting and airflow in the ducting system. The experimental data are made on 0.7 m diameter ducts over sections of ducts installing towards the working face in actual field conditions in Vang Danh Coal mine in Quang Ninh province as shown in Tab.1. A conceptual prediction model has been proposed based on experimental data at Vang Danh Coal mine [9–10].

$$p=f(L,Q) \quad (4)$$

Let p, L and Q represent leakage coefficient, duct length and quantity of airflow in the ducting system respectively. It is assumed to express p in the form:

$$ln(p-1)=lnc+b_1\ lnL+b_2\ lnQ \quad (5)$$

Where: p: Leakage coefficient;
L: Duct length, m;
Q: Quantity of airflow in the ducting system, m^3/s;
lnc, b_1, b_2, constants.

Each set of data: ln (p_i), ln (L_i) and ln (Q_i) under given data – duct diameter, with i=1, 2…n.

With ducting length L_i, the quantity of airflow in the ducting system Q_i is measured; the air leakage coefficient p_i is calculated as $p_i=Q_0/Q_i$;
Where: Q_0 the quantity of airflow beyond the fan, m^3/s;

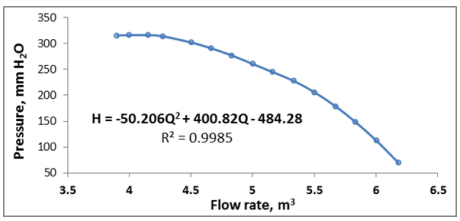

Fig. 2. Pressure-volume characteristic curve for fan YBT-22

Tab. 3. Values of aerodynamic characteristic of the fan SDF(A)-II-5.3/ 2x7.5

Flow rate, m³/s	3.3	3.5	3.7	3.8	4	4.3	4.5
Pressure, mmH₂O	405	407	407	406	403	393	375
Flow rate, m³/s	4.8	5	5.3	5.5	5.8	6	6.2
Pressure, mmH₂O	347	311	269	224	174	123	88

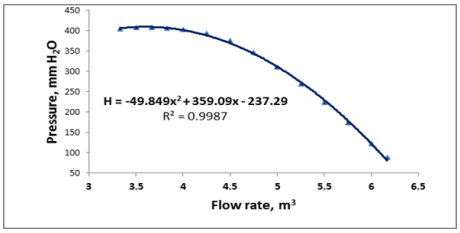

Fig. 3. Pressure-volume characteristic curve for fan SDF (A)-II-5.3/ 2x7.5

Q_i the quantity of airflow reaching the end of the ducting length – L_i.

Linear regression analysis by using Stata software to fit these experimental data can derive the relationship between the air leakage coefficient, the quantity of the air in the ductwork and the ducting length. Therefore, the air leakage coefficient for the ductwork of 0.7 m diameter can be estimated based on the experimental data at Vang Danh Coal mine by the regression method.

As a result obtained from Stata software, the air leakage coefficient for the duct of 0.7 m diameter can be found based on data at Vang Danh Coal mine:

$$p= 1 + 3.06397.10^{-6}.L^{1.88078}Q^{0.47215} \quad (6)$$

Use the F-test can evaluate Pro (F) = 0.0000 with significance level is 0.5. This low a value would imply that the regression parameters are nonzero and the regression equation does have some validity in fitting the data [11].

2.2 Analysis of the fan characteristic curve H=f(Q)

Drawing figure representing the relationship between fan flow rate and pressure of fan to find fan characteristic curve. The figures of the fan characteristic curves of the fan YBT-22 and the fan SDF (A)-II-5.3/ 2x7.5 are determined by data describing the fan characteristic as shown in table 2 and table 3.

The fan curve H=f(Q) for fan YBT-22 in the form of an inverse curve figure 2. Quadratic polynomial fit to these data is as follows:

$$H=-50.206.Q^2 + 400.82.Q - 484.28 \text{ for fan YBT-22} \quad (7)$$

The value of the correlation coefficient r^2= 0.9985, showing that the function H = f(Q) describes quite accurately the characteristic curve of the fan.

The fan curve H= f(Q) for fan $SDF_{(A)}$-II-5.3/ 2x7.5 can be obtained by using the same procedure, as shown in figure 3:

$$H = -49.849.Q^2 + 359.09.Q - 237.29 \text{ for fan } SDF_{(A)}\text{-II - 5.3/ 2x7.5} \quad (8)$$

Correlation coefficient r^2= 0.9987 is shown that a regression line to be considered reliable.

2.3 Calculating maximum ventilation length

Combining equation (3) and equation (7), gives:

$$6,48.\alpha.L/D^5 .p.Q^2=-50.206.Q^2+400.82-484.28 \quad (9)$$

For fan YBT-22

Currently, in Quang Ninth mines, airflow volume Q supplying to the face changes from 2 to 8 m³/s for the duct of D = 0.6 ÷ 0.8 m; sometimes 1.0 m for large cross-section roadway.

Under the conditions of this study: using the fan YBT-22, the ductwork of 0.7 m diameter and amount of airflow required at the face Q= 4m³/s,

$$\text{Substituting values } p= 1 + 3.06397.10^{-6}.L^{1.88078}Q^{0.47215} \quad (10)$$

into (Eq. 9) then obtains maximum ventilation length L_{max} = 566.25 m.

By using the same analytical procedure as above, under the conditions of this study: using the fan SDF(A)-II-5.3/2x7.5 , the ductwork of 0.7 m diameter and amount of airflow required at the face Q= 4m³/s, maximum ventilation length L_{max} for SDF(A)-II-5.3/2x7.5 is 860.22 m.

Conclusion

Analysis of fan characteristics and ductwork parameters in order to assess the reliability of the ventilation level when driving roadways. From the analytic equations it is possible to determine the maximum ventilation length that the auxiliary fan has enough capacity to ensure to bring the required airflow to the face. The equations to solve the problem of selecting the number of fans need to be used for the ducting

system.These data can help designers and operators to select the appropriate fan in auxiliary ventilation systems.

A conceptual prediction model has been proposed based on the experimental data at Vang Danh Coal mine.

In addition, this is the basis for making a plan to equip ducts and fans to meet production requirements for each stage in underground coal mines. The research results were used to optimize the auxiliary ventilation system that can save costs and energy.

Acknowledgements

Author would like to thank to Vang Danh coal company Team for the support with site access and field investigation. Author also wish to gratefully acknowledge Ass. Prof. Vu Chi Dang for his contributions to the paper. Paper was presented during the 7th International Conference of Scientific research cooperation between Vietnam and Poland, AGH UST, Krakow, Poland.

Literatura – References

1. D J Brake, Auxiliary ventilation design - why and how mines waste so much power on inferior systems, in Proceedings Australian Mine Vent Conference 2017, pp 27-34 (The Australasian Institute of Mining and Metallurgy: Melbourne).
2. De souza, E., Cost saving strategies in mine ventilation. CIM Journal, Vol. 9, №.2, 2018
3. De souza, E., 2004, Auxiliary ventilation operation practices, Proceedings of the 10th U.S., North American Mine Ventilation Symposium, Leiden, Netherlands: Balkema, pp. 341–348.
4. Dang Vu Chi, Phương pháp giải tích với bài toán thông gió khi đào đường lò, Hội nghị Khoa học lần thứ 17 Trường Đại học Mỏ- Địa chất, Hà nội, 31, 2006 (in Vietnamese)
5. McPherson MJ. Subsurface ventilation and environmental engineering. Springer Science & Business Media; 2012
6. Kingery, D.S., Introduction to Mine Ventilating Principles and Practices, US Bureau of Mines Bul (US Bureau of Mines, Washington DC), (1960)
7. D.A.Telyakovsky, V. Komarov, Mine Ventilation, Mir Publishers, Moscow (1969).
8. A.I. Ksenofontova, Hanbook for Mining ventilation, State scientific and technical publishing house for mining, Moscow 1962 (In Russian)
9. Phuong Thao Dang, Zinovii Malanchuk, Vitalii Zaiets (2021); Investigation of resistance and air leakage of auxiliary ventilation ducting in underground mine in Quang Ninh; ICFS.
10. Phuong Thao Dang, Vu Chi Dang (2019); Study on relationship of duct leakage and parameters of duct in Quang Ninh; Journal of the Polish Mineral Engineering Society
11. Douglas C. Montgomery, Elizabeth A. Peck, G. Geoffrey Vining, Introduction to linear regression, Wiley; Fifth edition (Mar. 2012)

Fracture Mechanism of Hard Main Roof and Determining the Width of Coal Pillars when Extracting Flat-lying Coal Seams

Quang Phuc LE[1)], Van Chi DAO[2)], Phi Hung NGUYEN[3)], Thai-Tien Dung VU[4)]

[1)] Faculty of Mining, Hanoi University of Mining and Geology, 18 Vien Street, Hanoi 100000, Vietnam; email: lequangphuc@humg.edu.vn
[2)] Faculty of Mining, Hanoi University of Mining and Geology, 18 Vien Street, Hanoi 100000, Vietnam; email: daovanchi@humg.edu.vn
[3)] Faculty of Mining, Hanoi University of Mining and Geology, 18 Vien Street, Hanoi 100000, Vietnam; email: nguyenphihung@humg.edu.vn
[4)] Faculty of Mining, Hanoi University of Mining and Geology, 18 Vien Street, Hanoi 100000, Vietnam; email: vuthaitiendung@humg.edu.vn

http://doi.org/10.29227/IM-2023-02-41

Submission date: 29-08-2023 | Review date: 25-09-2023

Abstract

In underground coal mining, the stability of roadways and gob-side entry depends on the coal pillar width. An unreasonable width of the coal pillar will cause the roadway to be in a dangerous zone of influence of the abutment pressure, leading to severe roadway deformation. This paper studies the fracture mechanism of the hard main roof and reasonable coal pillar width to protect the stability of gob-side entry driving. The research results show that when mining a coal seam under a hard main roof, the console of the main roof on the edge of the coal seam has the form of hinge structure. The great load of the roof layers and the rotation of the console are the main causes leading to the variation of the stress field in the coal seam. According to the development law of the stress field, after the main roof completes the collapse process, the peak of the maximum stress will move deep into the solid coal seam, and on the edge of the coal seam it will form a low-stress zone. Research results from the case of Seam #11 of Khe Cham coal mine, Vietnam show that the gob-side entry will be well stabilized when the narrow coal pillar between it and the boundary of the gob is 4–5 m.

Keywords: *failure mechanism, coal pillar, stress distribution, roadway deformation, retained roadway, hard main roof, gob-side entry*

Introduction

In Vietnam, coal is mainly mined in the Quang Ninh coal basin (Figure 1). According to statistics, the Quang Ninh coal basin ensures nearly 90% of Vietnam's state-owned coal production. The main technology of underground coal mining in Vietnam is the longwall mining system. The panels are prepared with two roadways and a 20–30 m wide coal pillar between them. In particular, the coal pillar has the role to protect and maintain of the retained of one of the two roadways for the next panels. As a result, coal losses in the coal pillars are large, accounting for about 20–30% of the coal reserves of the mined panel (Vietnam, 2016). In particular, the loss of coal in the pillars will increase when exploiting coal seams with hard main roof and at great depths. Currently, underground coal mining activities in Vietnam are carried out at depths of greater than 350–400 m. Statistical results show that underground coal mines in Vietnam contain about 30–85% of coal seams with hard roof (Zubov & Le, 2022). Therefore, this is a challenge for coal pillar design and loss of coal reduction in underground coal mines in Vietnam.

The cases that occur when mining coal seams with hard main roofs, it affects roadway stability issues, such as heaving floors, collapsing of ribs, etc., which occur frequently. It increases the risk of occupational accidents and is the cause of increased production costs and reduced labor productivity. This finally affects the competitiveness of mining companies. Most of these problems occur because the coal pillar is not wide enough, and the roadway is located in the high-stress region of the abutment pressure. At that time, they will be directly affected by the static and dynamic loads of the formation and collapse of the main roof console in the gob. When the main roof breaks, it will rotate and collapse on the gob. And on the edge of the coal pillar, the immediate roof was crushed, and the effect of high abutment pressure caused the pillar to compact and collapse. This is the cause of the severe deformation of the roadway, which is protected by the coal pillar. The long console formation of the hard main roof above the pillar, and the overloaded strata exert great abutment pressure, causing the coal seam to be compressed into the roadway. The deformation of the roadway sometimes leads to inaccessibility of the working face, making it difficult to repair, transport and ventilate. Especially the work of maintaining stability at the intersection between the roadway and the working face. In addition, shear forces along the fracture line of the main roof can extend to the site of the roadway, causing serious rock bust problems.

The balance between the requirement of roadway stability when mining the coal seam under the hard main roof and reducing the loss of coal in the pillar is a difficult problem. The articles (Wang et.al., 2019, He et.al., 2018, Qi et.al., 2019, Ma et.al., 2018) have presented the no-pillar exploitation method with the technique of directional roof cutting. They proved that the no-pillar mining technique with automatically formed gob-side entry retaining is feasible for longwall mining and achieves the goal of safe and efficient mining. However, the high cost to implement and a large amount of work necessary to be done at the intersection between the roadway and the working face. The presence of a hard-to-collapse main roof poses a high risk of rock bust incidents. Dynamic and static loads of the curving process, rotatory, and sagging of the main roof console along the line behind the first working face are known to cause accident risks in this solution. In addition, the gas pressure caused by the massive collapse of the main roof in the gob has a serious effect on the labor safety and stability

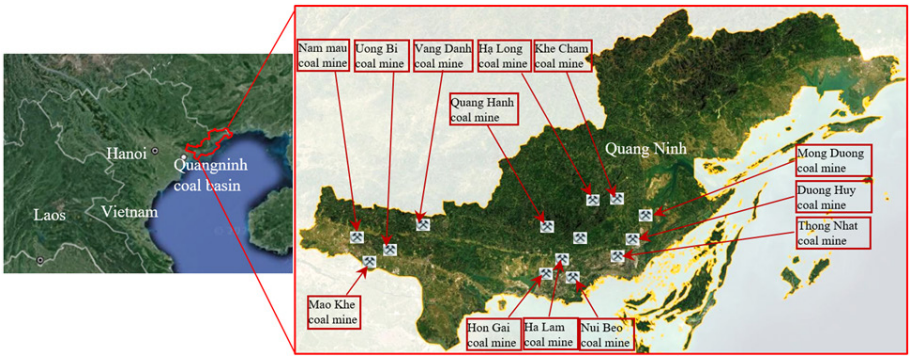

Fig. 1. Location of Quang Ninh coal basin in North Vietnam

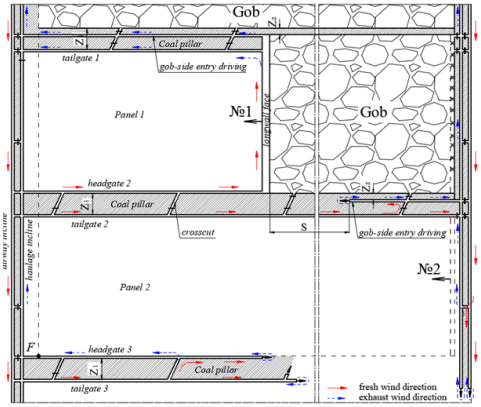

Fig. 2. Longwall mining system, in which coal pillar will be extracted together with the adjacent longwall face

of the roadway. In the second option, methods of constructing artificial pillars to replace coal pillars have also been studied (Zhao et.al., 2019, Wu et.al., 2019). In particular, artificial pillars are built of wood, stone, concrete, or other materials. This method has proven to be advantageous in reducing coal loss in the pillars. However, the excessive consumption of insert material and high technical requirements put limits on the popularity of this method. Therefore, it is necessary to search for a more efficient and economical method to improve the sustainability and safety of mining (Zhen et.al., 2019).

In study (Zubov & Le, 2022) has shown that the road is guaranteed to be stable when in a solid coal seam, or the low-stress zone at the edge of the coal seam. That is, a wide coal pillar must be designed to ensure the stability of the retained roadway. Then a new gob-side entry done along the gob (after the fracture of the main roofs) would be optimal. It will ensure that the coal pillar will be extracted together with the adjacent longwall face (Figure 2). The tailgate is also guaranteed to be stable because of the wide coal pillar that protects it. After the complete fracture of the main roof, the gob-side entry is safer when done in the low-stress zone under the console.

When applying the solution in Figure 2, the problem of reducing coal loss in the coal pillar has been improved. However, the task posed in the coal seam mining process has a hard main roof to predict the stress-deformation state of the surrounding rock and determine the width of the coal pillar. In Figure 2, the width of the coal pillars (Z1, Z2) will determine the stress-deformation state of the surrounding rock as well as the stability of the roadway (Zhang et.al., 2018, Liang et.al, 2018) . The decrease in strength of the coal pillar is considered as the reduction ratio between the width and the height of the pillar (Mark et.al, 2010), and the small coal pillar will put the roadway in a stress-releasing state, while the wide pillar will put it at high-stress state (Li et.al., 2015). Shabanimashcool and Li (Shabanimashcool & Li, 2013) found that the stress in the wide coal pillar would fluctuate up and down in process mining at the adjacent longwall face. And it also depends on the periodic collapse of the roof rock in the gob. The conclusions in the study of Wang et al. (Wang et.al, 2013) suggest that the risk of rock burst for the retained roadbed will increase significantly when there is no elastic zone in the coal pillar. Bai et al. (Bai et.al., 2015) used the law of stress development to analyze the roof-sagging mechanism of the retained roadway. They have determined that the width of a coal pillar less than 5 m or more than 22 m will ensure better roadway stability than a coal pillar of medium width. Mohammadi et al. (Mohammadi et.al., 2016) demonstrated that the expansion of the plastic failure zone in the rock surrounding the retained roadway occurred when the width of the coal pillar was reduced from 30 m to 10 m based on computational geometry. Shen et al. (Shen et.al., 2018) concluded that the ratio of the width to the height of the coal pillar also plays a significant role in the stability of the pillar. When there is a delamination plane in the roof rock layer, the roof of the retained roadway will easily slip when the ratio between the width and height of the coal pillar is less than 8. Many other important studies have been done to study the stress distribution in the surrounding rock and the solution to stabilize the roadway next to the narrow coal pillar (Shen et.al., 2018, Jiang et.al., 2017, Zhang et.al., 2018, Yu et.al., 2020, Zubov et.al., 2023, Le et.al., 2022, Le et.al., 2020).

When mining coal pillars on the same line as the adjacent longwall face, the ventilation task has posed a requirement to excavate a gob-side entry after completing the collapse of the main roof in the gob. Hao et al. (Hao et.al., 2020) used an equiv-

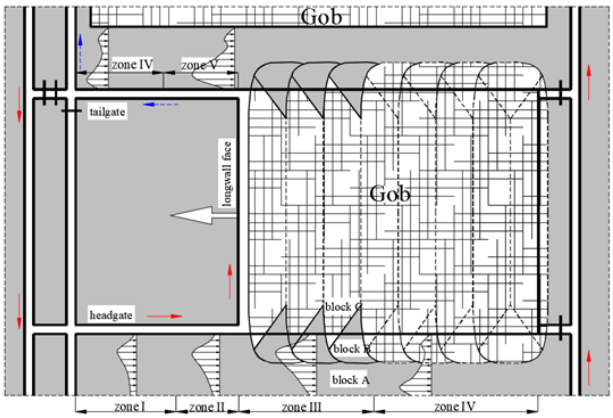

Fig. 3. Law of main roof collapse and characteristics of stress-deformation changes of the surrounding rock

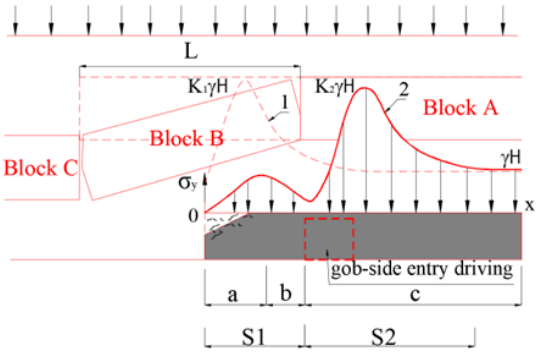

Fig. 4. Mechanical model of the "hanging-collapse" structure of the main roof and the stress distribution on the edge of coal seam

alent material model to determine the location of the gob-side entry. They assume that the gob-side entry will be stable when it is excavated in the low stress zone on the gob side. That is, the distance between gob-side entry and gob is not more than 5 m, and this result is successfully applied at Shengyuan coal mine 4#, China. Yang Yu et al. (Yu et.al., 2020) also evaluated that the fracture, rotation, and sagging processes of the main roof negatively affected the stability of the gob-side entry. With numerical simulation, they determined the reasonable distance between the gob-side entry and the gob to be 6 m. Li et al. (Li et.al., 2022) performed field investigation, theoretical calculations, and numerical simulation for a specific case in the Xinji coal mine, China. They have determined that a reasonable distance between the gob-side entry and the gob is 5 m. When the width of the pillar is reduced to 3–4 m, the coal pillar is destroyed, and when it is increased to 8 m, the gob-side entry is in the region of concentrated stress, leading to it being unstable. These studies are useful in common applications of retained roadway protection and gob-side entry. However, there is a lack of studies on the fracture mechanism of the hard main roof and the rationality of the coal pillar width. Therefore, there is a need for additional analysis and experimental studies on this issue.

In this paper, the theoretical analysis method for the formation of the stress-strain state of the rock mass has been performed. After that, an experimental study on the equivalent material model and numerical model was applied to evaluate the fracture mechanism of the hard main roof and determine the coal pillar width.

Research Methods

In this paper, the method of theoretical analysis of the fracture mechanism of the hard main roof is used. This is the basis for evaluating the collapse rule of the main roof in the gob, thereby leading to the principle of determining the position of gob-side entry driving. Then, a physical model and a computer program are used to simulate the mining of the panels, the stress distribution in the surrounding rock, and the deformation of the gob-side entry. In the case study, we use typical geological conditions of coal seam #11 of Khe Cham coal mine in Quang Ninh coal basin, where the thickness of the hard main roof is 10–20m.

Results and discussion

Theoretical analysis of the fracture mechanism of the main roof and the formation of the stress-strain state of the rock mass on the edge of the coal seam:

The studies (Shen et.al., 2018, Wang et.al., 2020) all show that the rule of roof collapse is cyclical, as shown in Figure 3. On the coal seam around the gob, the formation of the console beam of the roof rock depends on many factors, such as the collapse step of the main roof, the slope angle of the coal seam, the thickness of the coal seam, and the immediate roof rock layer. Figure 3 shows 5 main stages of the stress-strain state, including: Zone I – initial stress zone; Zones II and V – zones of influence of static pressure, forming in front of the working face; Zone III – zone of influence of both static and dynamic pressure, forming behind the working face; and Zone IV – stable lateral stress zone, formed after the collapse of the main roof in the gob.

Among these, zones II and V are dangerous mine pressure zones with a high probability of rock bursts. Zone 3 – right behind the working face, is the place where the high stress concentration is due to the formation of the console of the main roof and the intense displacement of the surrounding

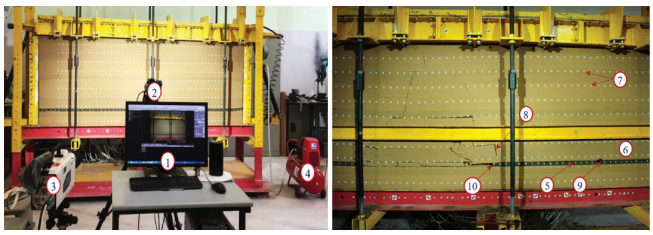

Fig. 5. Law of main roof collapse and characteristics of stress-deformation changes of the surrounding rock

Tab. 1. Physical and mechanical characteristics of rocks in the field and on models (Le & Dao, 2023, Le, 2021)

Type rock	Tensile strength (MPa)	Cohesion (MPa)	Friction angle (degree)	Uniaxial compressive strength (MPa)		Density (kg/m³)	
				Prototype	On the model	Prototype	On the model
Sandstone	1,6	3.22	34.2	83,2	0,64	2785	1853
Mudstone	0,9	2.14	30.1	50,6	0,39	2552	1700
Siltstone	1,2	1.83	26.4	16,5	0,21	2253	1500
Coal	0,4	1.54	19.3	14,5	0,21	1454	967

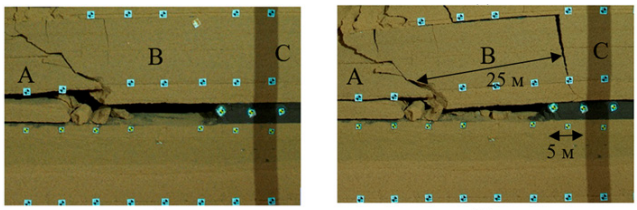

a) b)

Fig. 6. Fracture mechanism of hard main roof: a – the formation and sagging displacement of the main roof; b – collapse of the main roof

rock. The loading of the rock layers to the console of the roof during this period is enhanced over time, and at the same time, the collapse of the edge of the coal pillar occurs on the boundary of the gob. The result of this process is the sagging, rotation, and eventually fracture of the console of the main roof at the boundary of the gob. Before the fracture of the console occurs, the peak of the maximum stress is 2–5 m from the gob. This is an area of increased stress and possible rock bursts. After the console breaks, the load of the roof rock layers is transferred to the collapsed rock in the gob, and the stress on the edge of the coal seam is reduced. The peak of the maximum stress moves deep into the coal seam. At the end of the collapse of the roof rock, the displacement of the surrounding rock stops, and the stress distribution on the edge of the coal seam reaches a new steady state (as in zone IV in Figure 3).

Thus, to ensure the stability of the retained roadway, it should be outside the danger zone of abutment pressure. Surveying the displacement of the main roof shows that, when the roadway is outside the affected area of increased abutment pressure, its stability does not depend on the reception of protection solutions. Therefore, this can be the main factor in choosing the location of the roadway and the solutions to protect it in the mine design.

In the case of coal seam mining with a hard main roof, the sagging, rotation, and fracture of the roof rock layers will have a great influence on the retained roadway. Therefore, the location of the retained roadway should be chosen outside the abutment pressure zone. If the coal pillar is not width enough, the static and dynamic loads of the fracture of the roof rock will break the supporting structure and lead to deformation of the roadway.

As analyzed, in the process of coal pillar mining, gob-side entry is necessary and excavated according to ventilation requirements. However, if the movement of the roof rock has not ended, then excavating the gob-side entry will be detrimental, and there is a potential risk of a rock burst. Because the edge of the coal pillar has not been completely unloaded from the main roof, it will be difficult for the gob-side entry to be stable. Therefore, it is necessary to ensure that the gob-side entry is performed at a safe time behind the previous longwall face during coal seam mining. According to statistics, in the current underground coal mines in Vietnam, the working surface has an average moving speed of 25–30 m/month. Corresponding to this, the distance from the previous working face to the gob-side entry (parameter S in Figure 2) is about 200 m to 240 m.

Although it is known that the collapse process of the main roof is characterized by the geotechnical condition and the length of the console. However, with the cyclical collapse of the main roof (Figure 3), the suitable location for excavating the gob-side entry is in the reduced stress zone under the hard main roof at the gob side (under block A, Figure 4). Because, in this location, the hard main roof acts as a stable beam to pick up the load of the rock layers above and transfer the pressure deep into the coal seam. At the same time, it prevents the transfer of loads from the roof rocks to the edge of the coal seam. And the load acting on the support frame of the roadway will be determined only by the immediate roof. Therefore, the gob-side entry excavated at this location is advantageous in that it remains stable despite the small amount of displacement of the surrounding rock. The distance from the gob-side entry to the gob is not less than the distance from the crack of the main roof to the gob. According to experience, the fracture of the main roof is located on the coal seam at a distance of 4.0–5.0 m from the gob.

It should be noted that, under the collapse rule of the main roof (Figure 3), the console can hang in the gob for a relatively long time. The mechanical model of its formation and collapse is shown in Figure 4.

In Figure 4, before and after the main roof is broken, the stress distribution is shown by curves 1 and 2. The internal

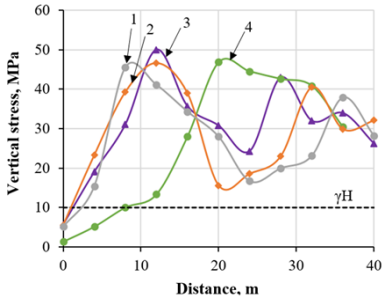

Fig. 7. Stress distribution on the edge of coal seam: 1 – before the collapse of the main roof with a console of 10 m; 2 – before collapsing main roof with a console of 15 m; 3 – before collapsing main roof with a console of 20 m; 4 – after the main roof collapse

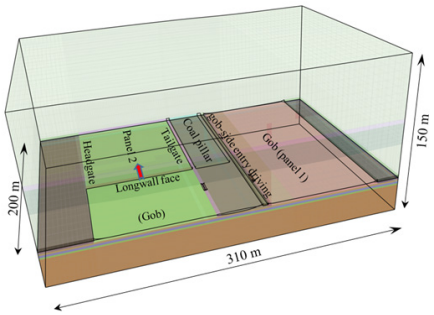

Fig. 8. Configuration of longwall model using FLAC3D

force of the coal seam on the edge is formed by three corresponding zones to support the load of the roof rock layers: a plastic deformation zone (a), an elastic region (b), and an initial stress region (c). Over time, and with the increased load from the roof rock layers, in the "a" area of the coal seam, a landslide triangle is formed. This triangular block has the greatest effect on the stability of the surrounding rock of the gob-side entry. Under the influence of stress, the coal seam and immediate roof connect with adjacent blocks to form a hinged structure. This structure is relatively stable because it is horizontal and subject to the pushing action of the adjacent rock mass. The junction between the elastic zone “b” and the initial stress zone “c” exhibits sufficient strength for the coal seam not to deform, and thus the main roof will rotate and crack at this section.

When the main roof is cracked, the pressure is transmitted to the edge of the coal seam and is divided into two zones: Zone S1 has a console head resting on the edge of the coal seam, an external stress field (reduced stress zone); Zone S2 is located under the hard main roof, an internal stress field (stress increase zone). The abutment pressure in the "external stress field" arises from the movement of the console at fracture.

The basic rule for determining the width of coal pillars located between the gob-side entry and the gob is to ensure the gob-side entry is in the reduced stress zone of the coal seam. That is, it should be excavated in the "external stress field" and the reduced stress zone of the "internal stress field", which provide a favorable stress environment for the stability of the surrounding rock. This is the basic element for gob-side entry stability, reducing repair costs. Then, the width of the coal pillar will correspond to the width of the "external stress field", where the maximum reaction of the coal seam will appear to support the roof rock. At the same time, the outer console head resting on the collapsed rock in the gob will unload most of the load of the roof rock layers.

Case studies

Research using equivalent materials model

With the task of studying the fracture mechanism of the main roof and the stress distribution on the coal seam, an equivalent material model was built. The model has dimensions of 2800 mm in length, 200 mm in width, and 1000 mm in height. The input data to make the model corresponds to the coal seam #11 mining conditions of the Khe Cham coal mine. The coal seam has a thickness of 3 m, a slope angle of 9 degrees, and is mined at a depth of 400 m. The coal seam has a small slope angle, so in this research model, the rock layers and the coal seam are built in the horizontal direction (Figure 5) (Zubov & Le, 2022). The characteristics of the similarity ratio between the model and the field are determined according to Equation 1.

$$\begin{cases} C_L = {}^{L_m}/_{L_p} = {}^{1}/_{100} \\ C_\mu = {}^{\mu_m}/_{\mu_p} = 1 \\ C_\rho = {}^{\rho_m}/_{\rho_p} = {}^{1}/_{1.5} \\ C_\sigma = {}^{\sigma_m}/_{\sigma_p} = {}^{1}/_{130} \end{cases} \quad (1)$$

here L_p, μ_p, ρ_p, and σ_p, respectively, geometric dimensions, Poisson's ratio, density, and uniaxial compressive strength of rock layers in the field; L_m, μ_m, ρ_m, и σ_m, respectively, geometric dimensions, Poisson's ratio, density, and uniaxial compressive strength of rock layers in the model.

Figure 5 depicts the research model and related tools. The physical and mechanical parameters of rock in the field and in the model are shown in Table 1. The results of the model study are shown in Figure 6.

Figure 6 shows the visual observation of the main roof's fracture mechanism on the model. The results show that when exploiting a coal seam with a hard main roof, a cantilever beam with a large length (about 25 m) is created on the edge of the coal seam. The crack location of the main roof is above the coal seam at a distance of 5 m to the gob.

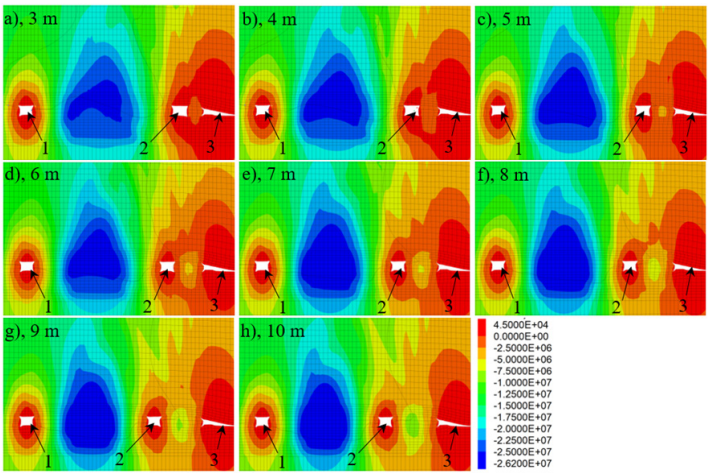

Fig. 9. Vertical stress distribution in the surrounding rock of gob-side entry driving with different narrow pillar widths: 1 – Tailgate; 2 – gob-side entry driving; 3 - gob.

The stress data distributed on the edge of the coal seam is obtained from stress sensors installed on the model. The stress sensors are connected to the computer and stored and processed in real-time. The results of stress distribution on the edge of the coal seam are shown in Figure 7.

Figure 7 shows that, when the console of the main roof has not collapsed, even in cases of different console lengths, the peak of the maximum stress is distributed over a distance of 8–11 m from the boundary of the gob. For example, when the console is 10 m long, the maximum stress is 45.5 MPA at a location 8 m from the boundary of the gob. When the console of the main roof is 15 m or 20 m, the peak of the maximum stress increases to 48.8 MPA, and the distance to the gob is 11 m. It can be observed that, in most cases when the console has not collapsed, the high-stress area is distributed on the edge of the coal pillar at a distance of 8–11 m. However, after the collapse of the console, the peak of the maximum stress moved deep into the coal seam and stopped at a distance of 20 m from the boundary of the gob. At this time, within 10 m on the edge of the coal seam, the stress decreases and is lower than the initial stress.

Thus, from the simulation results, it can be concluded that the sagging and rotation of the console of the main roof have created a strong compressive pressure at the edge of the coal seam and gradually formed many cracks. When the console beam's rotation is maximized, and then it collapses, one head of it rests on the collapsed rock in the gob and unloads almost the entire load of the roof rock layers. As a result, there will be very little stress on the edge of the coal seam, where the main console breaks, and this location is good for the excavation of a gob-side entry. As shown in Figure 7, a reasonable location to excavate a gob-side entry is within a distance of 4–8 m from the boundary of the gob.

Research with numerical model

A numerical simulation is constructed based on the computer program FLAC3D to study the stability of retained roadway and stress distribution when coal pillar width varies (Itasca, 2019). FLAC3D is a computer program for numerical modelling of continuum media to investigate the stress-strain state of rock mass. FLAC3D uses an explicit finite volume method to represent complex behaviors of rock mass, experiencing large displacements and deformations and considering non-linear material behavior. The program is capable of modelling material failure over large areas.

The model has a length of 310 m, a width of 200 m, and a height of 150 m, as shown in Figure 8. This model size was determined through a trial-and-error process considering the size and density of finite volume. Panels 1 and Panel 2 and associated roadways are included in the model. The roadway's and gob-side entry driving width and height are 4.0 and 3.0 m, respectively. With the research results of [2], under similar conditions at Khe Cham coal mine, the tailgate is guaranteed to be stable when the distance between it and the gob is over 40 m. In this study, numerical modeling is used to determine the location of the gob-side entry. Thus, the distance between the retained roadway and the gob is fixed at 40 m. The distance between the gob-side entry and the gob built in the cases is 3, 4, 5, 6, 7, 8, 9, and 10 m (narrow pillar), respectively. The overburden stress is 7.0 MPa applied to the top boundary. The specific gravity of rocks is 2500 kg/m^3 with a gravity of 10 m/s^2 (Le et.al., 2020). The horizontal boundaries of model are fixed in X direction while the bottom boundary is fixed in Y direction. The Mohr-Coulomb constitutive law is used for materials. The physical-mechanical properties of coal and rocks used in the model are based in Table 1. The results are shown in Figure 9, and 10.

Stress distribution characteristic analysis:

The vertical stress distribution in narrow coal pillars between the gob and gob-side entries (Figures 9, 10) shows that, when the narrow pillar width is from 3 to 9 m, the vertical stress in the narrow coal pillar is less than the initial stress (γH). Especially when the pillar width is 3 m, the maximum stress value is only about 3.1 MPA. Figure 9a shows that the coal pillar seems to have a plastic failure because the stress concentration value in the coal pillar is larger than the value of the critical compressive strength of the coal. As a result, the coal pillar loses its bearing capacity and does not guarantee the separation between the gob-side entry and gob. When the narrow pillar width is 10 m, the maximum stress value is about 10.6 MPA (the stress concentration factor is 1.06). Thus, the maximum stress value in the narrow pillar increases in proportion to the increase in the width of the pillar. This is

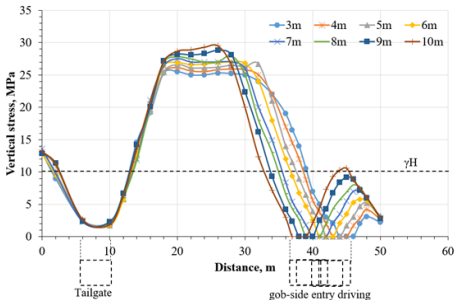

Fig. 10. Distribution of vertical stress with different narrow pillar widths

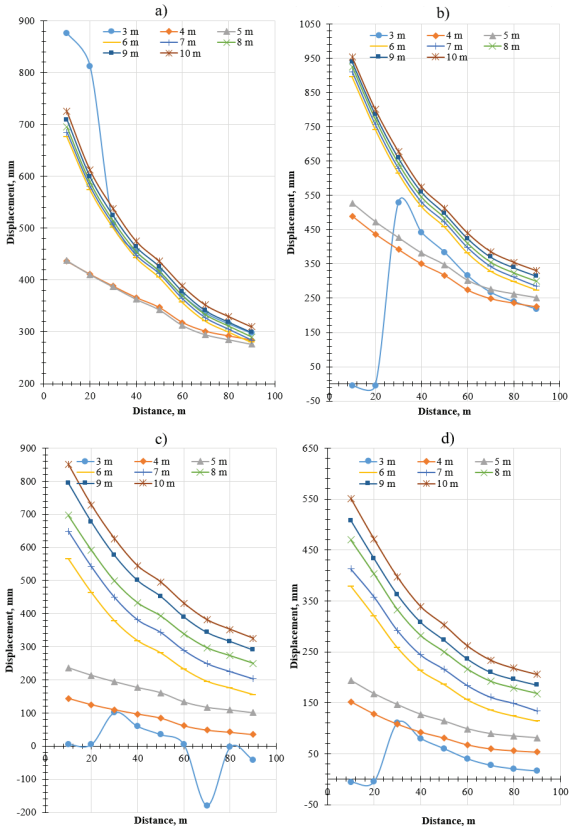

Fig. 11. Convergence of the roadway different narrow pillar width: a – roof sagging; b – displacement of solid coal side; c – floor heave; d – displacement of narrow coal pillar side.

similar to the theoretical analysis in Figure 4, where the edge of the coal seam adjacent to the gob is broken by the main roof's fracture and collapse mechanism.

When the width of the coal pillar is 4 m or 5 m, the maximum vertical stress in the coal pillar is 4.2 MPA and 5.2 MPA, respectively. The stress concentration zone in the coal pillar is gradually being formed. However, both of these cases give a stress value less than the initial stress, i.e., 10.0 MPA. As the width of the coal pillar increases to 6 m, 7 m, 8 m, and 9 m, the vertical stress in the coal pillar is essentially increasing to equal the initial stress. Its maximum vertical stress values are 5.6 MPA, 7.0 and 8.1 MPA, and 9.2 MPA, respectively. Observations in Figures 9d, 9e, 9f, and 9g show that the area of stress concentration is gradually increasing in the core of the coal pillar. This can be explained by the stress superposition when excavating the gob-side entry and the residual stress caused by the mining operation on the previous longwall face. With increasing the pillar width, the stress superposition effects will be more obvious, causing the stress concentration value to increase gradually. An increased stress concentration would be a bad sign for the stability of the gob-side entry. Because then the coal pillar will receive more load from the roof rock layers, the possibility of a rock burst increases. When the width of the coal pillar is 10 m, the vertical stress in the coal pillar is 10.6 MPA and exceeds the initial stress. The area of concentration of stress in the coal pillar has been clearly seen (Figure 9h). The coal pillar seems to be intact. But it should be noted that a high-stress concentration in a coal pillar is not good. It can cause rock explosion risks and harder support for gob-side entry.

Deformation characteristic analysis of gob-side entry:

Different stress environments in a narrow coal pillar can lead to different displacements. In this case study, the section performing deformation control of the gob-side entry was performed in front of working face #2 (at a distance of 20 m). Analyzing the convergence of the gob-side entry, the displacement values gradually increased, corresponding to the

increase in the width of the narrow coal pillar (Figure 11). However, the displacement analysis results show that, with a width of 3 m of the narrow pillar, the gob-side entry is completely deformed at a distance of 20 m in front of working face #2. Therefore, a coal pillar with a width of 3 m is not guaranteed to stabilize the roadway and separate the gob-side entry and gob. When the width of the coal pillar is 4 to 5 m, the convergence of the gob-side entry is much smaller than in the other cases. Specifically, with the widths of the pillars of 4 m and 5 m, the roof convergence is 430 m, respectively. But, with a pillar width of 6 m to 10 m, the corresponding roof convergence increases from 676 mm to 725 mm, respectively. The convergence of the left rib of the gob-side entry is 489 mm and 528 mm, respectively, for the widths of the coal pillars of 4 m and 5 m. Conversely, if the width of the coal pillar is 6 m, this value is 895 mm, and 953 mm corresponds to the coal pillar with a 10 m width.

The convergence of the right rib is 144 mm and 236 mm, respectively, of the coal pillar with a width of 4 m and 5 m. Meanwhile, this value is 566 mm and 851 mm when the width of the coal pillars is 6 m and 10 m, respectively. The floor convergence is 152 mm and 193 mm, with the cases of coal pillars having widths of 4 m and 5 m, respectively. As the coal pillar width increased from 6 m to 10 m, the floor convergence increased from 379 mm to 551 mm, respectively. Thus, it can be seen that a coal pillar with a width of 4–5 m is suitable for the case of excavating gob-side entry. In this case, the converging values of the gob-side entry are always two times smaller than in the other cases.

As such, when excavating a gob-side entry, the coal pillar between it and the gob with a width of 3 m will be destroyed. However, then the deformation of the gob-side entry will increase proportionally with the distance between it and the gob. This is quite similar to the results of the analysis of the main roof's fracture mechanism mentioned in Figure 4. That is, after the main roof's fracture process, the larger-width coal pier will place the gob-side entry in the area of maximum abutment pressure. Therefore, with the requirement for the reduction of coal loss and improving the level of work safety, on the basis of the theoretical analysis of the main roof's fracture mechanism and the case study results, the optimal distance between the gob-side entry and the boundary of the gob should be chosen at a distance of 4–5 m.

Conclusion

The fracture mechanism of the main roof on the edge of the coal seam has been theoretically analyzed. The results show that, after the main roof collapses, two stress fields will be formed on the edge of the coal seam, including an external stress field (S1) and an internal stress field (S2). The boundary of these two stress fields is determined at the crack location of the main roof. A favorable location to excavate a gob-side entry should be located in the S1 zone.

A study by an equivalent material model shows that the fracture location of the main roof is 4–5 m from the boundary of the gob. After the collapse of the main roof, the peak of the maximum stress moved deep into the coal seam. Then, on the edge of the coal seam, there is a reduced stress zone due to the console of the main roof breaking and unloading into the gob. With this method, a favorable location to excavate a gob-side entry should be located between 4 m and 8 m from the boundary of the gob.

Numerical simulation has demonstrated that a coal pillar which is too narrow (3 m) will be easily destroyed, and it does not guarantee stability and separation between the gob-side entry and the gob. As the pillar width increases, the stress concentration in the pillar also increases. However, the great stress concentration will not be favorable for maintaining the stability of the gob-side entry and coal pillar because the coal pillar has to play the main role in supporting the load of the roof rock layers. The deformation monitoring results show that the gob-side entry is stable when the width of the coal pillar is 4–5 m. As the pillar width increases, the stress concentration increases that leads to greater deformation of the gob-side entry.

Acknowledgment

The authors are grateful to the Hanoi University of Mining and Geology, Vietnam (Grant No. T23-32) for financial support of the work.

Literatura – References

1. Decision on approval for adjusted master plan for Vietnam's coal industry development to 2020 andvision towrads 2030. 2016, Hanoi, Vietnam, March 14, – 142pp. (in Viet Nam);
2. ZUBOV VP, LE QUANG PHUC. Development of resource-saving technology for excavation of flat-lying coal seams with tight roof rocks (on the example of the Quang Ninh coal basin mines). Journal of Mining Institute. 2022, Vol. 257, p. 795–806;
3. WANG, K., ZHAO, T., YETILMEZSOY, K., & ZHANG, X. Cutting-caving ratio optimization of fully mechanized caving mining with large mining height of extremely thick coal seam. Advances in Civil Engineering. 2019, Vol. 2019, p. 1-11.;
4. WANG, Q., HE, M., YANG, J., GAO, H., JIANG, B., & YU, H. Study of a no-pillar mining technique with automatically formed gob-side entry retaining for longwall mining in coal mines. International Journal of Rock Mechanics and Mining Sciences. 2018, Vol. 110, p. 1-8.;
5. QI, F., & MA, Z. Investigation of the roof presplitting and rock mass filling approach on controlling large deformations and coal bumps in deep high-stress roadways. Latin American Journal of Solids and Structures. 2019, 16 pp;
6. MA, Z., WANG, J., HE, M., GAO, Y., HU, J., & WANG, Q. Key technologies and application test of an innovative noncoal pillar mining approach: a case study. Energies. 2018, Vol. 11(10), p. 2853;
7. ZHAO, H. State-of-the-art of standing supports for gob-side entry retaining technology in China. Journal of the Southern African Institute of Mining and Metallurgy. 2019, Vol. 119(11), p. 891-906.;
8. WU, B., WANG, X., BAI, J., WU, W., ZHU, X., & LI, G. Study on crack evolution mechanism of roadside backfill body in gob-side entry retaining based on UDEC trigon model. Rock Mechanics and Rock Engineering. 2019, Vol. 52, p. 3385-3399;
9. ZHEN, E., GAO, Y., WANG, Y., & WANG, S. Comparative study on two types of nonpillar mining techniques by roof cutting and by filling artificial materials. Advances in Civil Engineering. 2019, Vol. 2019. https://doi.org/10.1155/2019/5267240;
10. Zhang, G. C., Tan, Y. L., Liang, S. J., & Jia, H. G. Numerical estimation of suitable gob-side filling wall width in a highly gassy longwall mining panel. International Journal of Geomechanics. 2018, Vol. 18(8), 04018091.
11. ZHANG, G., LIANG, S., TAN, Y., XIE, F., CHEN, S., & JIA, H. Numerical modeling for longwall pillar design: a case study from a typical longwall panel in China. Journal of Geophysics and Engineering. 2018, Vol. 15(1), p. 121-134.
12. ESTERHUIZEN, E., MARK, C., & MURPHY, M. M. Numerical model calibration for simulating coal pillars, gob and overburden response. In Proceedings of the 29th international conference on ground control in mining. Morgantown: West Virginia University. 2010, p. 46-57.
13. LI, W., BAI, J., PENG, S., WANG, X., & XU, Y. Numerical modeling for yield pillar design: a case study. Rock Mechanics and Rock Engineering. 2015, Vol. 48, p. 305-318.
14. SHABANIMASHCOOL, M., & LI, C. C. A numerical study of stress changes in barrier pillars and a border area in a longwall coal mine. International Journal of Coal Geology. 2013, Vol. 106, p. 39-47.
15. WANG, H., JIANG, Y., ZHAO, Y., ZHU, J., & LIU, S. Numerical investigation of the dynamic mechanical state of a coal pillar during longwall mining panel extraction. Rock mechanics and rock engineering. 2013, Vol. 46, p. 1211-1221.
16. BAI, J. B., SHEN, W. L., GUO, G. L., WANG, X. Y., & YU, Y. Roof deformation, failure characteristics, and preventive techniques of gob-side entry driving heading adjacent to the advancing working face. Rock Mechanics and Rock Engineering. 2015, Vol. 48, p. 2447-2458.
17. MOHAMMADI, H., EBRAHIMI FARSANGI, M. A., JALALIFAR, H., & AHMADI, A. R. A geometric computational model for calculation of longwall face effect on gate roadways. Rock Mechanics and Rock Engineering. 2016, Vol. 49, p. 303-314.
18. SHEN, W. L., BAI, J. B., LI, W. F., & WANG, X. Y. Prediction of relative displacement for entry roof with weak plane under the effect of mining abutment stress. Tunnelling and Underground Space Technology. 2018, Vol. 71, p. 309-317.
19. SHEN, W., XIAO, T., WANG, M., BAI, J., & WANG, X. Numerical modeling of entry position design: a field case. International Journal of Mining Science and Technology. 2018, Vol. 28(6), p. 985-990.
20. JIANG, L., ZHANG, P., CHEN, L., HAO, Z., SAINOKI, A., MITRI, H. S., & WANG, Q. Numerical approach for goaf-side entry layout and yield pillar design in fractured ground conditions. Rock Mechanics and Rock Engineering. 2017, Vol. 50, p. 3049-3071.
21. ZHANG, G. C., HE, F. L., LAI, Y. H., & JIA, H. G. Ground stability of underground gateroad with 1 km burial depth: a case study from Xingdong coal mine, China. Journal of Central South University. 2018, Vol. 25(6), p. 1386-1398.

22. Yu, Y., Bai, J., Wang, X., & Zhang, L. Control of the surrounding rock of a goaf-side entry driving heading mining face. Sustainability. 2020, Vol. 12(7), p. 2623. https://doi.org/10.3390/su12072623

23. ZUBOV V.P., THAN VAN DUY & FEDOROV A.S. Technology of underground mining of thick coal seams with low strength properties. Ugol'. 2023, (5), p. 41-49. DOI: 10.18796/0041-5790-2023-5-41-49.

24. LE TIEN DUNG, OH JOUNG. Longwall face stability analysis from a discontinuum-Discrete Fracture Network modelling. Tunnelling and Underground Space Technology. 2022, Vol. 124, p. 104480.

25. LE TIEN DUNG, NGUYEN CHI THANH, DAO VAN CHI. Estimation of coal and rock mechanical properties for numerical modelling of longwall extraction. Inżynieria Mineralna – Journal of the Polish Mineral Engineering Society. 2020, Vol. 46(2), p. 41-47.

26. HAO, L. I. U., ET AL. Reasonable Width of Narrow Coal Pillars Along Gob-side Driving Entries in Gas Outburst Coal Seams: Simulation and Experiment. In: IOP Conference Series: Earth and Environmental Science. IOP Publishing. 2020, p. 052042.

27. YU, YANG, ET AL. Control of the surrounding rock of a goaf-side entry driving heading mining face. Sustainability. 2020, Vol 12(7): 2623; https://doi.org/10.3390/su12072623

28. LI, LIANGSHAN, ET AL. Pressure Relief and Bolt Grouting Reinforcement and Width Optimization of Narrow Coal Pillar for Goaf-Side Entry Driving in Deep Thick Coal Seam: A Case Study. Minerals. 2022, Vol. 12(10): 1292. https://doi.org/10.3390/min12101292

29. SHEN, W. L., GUO, W. B., NAN, H., WANG, C., TAN, Y., & SU, F. Q. Experiment on mine ground pressure of stiff coal-pillar entry retaining under the activation condition of hard roof. Advances in Civil Engineering. 2018. Article ID 2629871, 11 pages https://doi.org/10.1155/2018/2629871;

30. WANG, Y., WANG, H., HE, M., WANG, Q., QIAO, Y., & YANG, J. Mine pressure behavior characteristics and control methods of a reused entry that was formed by roof cutting: a case study. Shock and Vibration. 2020, p. 1-15.

31. ITASCA. Fast Lagrangian Analysis of Continua User's Guide; Itasca Consulting Group Inc.: Minneapolis, MN 55401, USA, 2019. https://www.itascacg.com/search;

32. LE, Q.P., DAO, V.C. Roof Condition Characteristics Affecting the Stability of Coal Pillars and Retained Roadway. Environmental Science and Engineering. Springer, Cham. 2023, p. 463-477. https://doi.org/10.1007/978-3-031-20463-0_29;

33. LE QUANG PHUC. Cause and Solution to Roadway Deformation in Vietnam Underground Coal Mines. Inżynieria Mineralna. 2021, No.2, Vol.1, p. 381-390. http://doi.org/10.29227/IM-2021-02-35;

34. LE QUANG PHUC, ZUBOV V.P., PHUNG MANH DAC. Improvement of the Loading Capacity of Narrow Coal Pillars and Control Roadway Deformation in the Longwall Mining System. A Case Study at Khe Cham Coal Mine (Vietnam). Inżynieria Mineralna. 2020, Vol. 1(2), p. 115-122. DOI: 10.29227/IM-2020-02-15;

35. Szymanek A., Nowak W. Mechanically activated limestone, Chemical and process engineering, 28,127-137, 2007. ISSN0208-6425 IF 0,394

Understanding Saltwater Origins and Mechanisms in the Coastal Aquifers of Da Nang Area (Central Vietnam)

Thao Bach NGUYEN[1,2)], Nhan Dang DUC[3)], Bang Duc DAO[1)]*

[1)] Hanoi University of Mining and Geology (HUMG), 18 Vien str,. Bac Tu Liem, Hanoi, Vietnam
[2)] Research and Advanced Technology Applications in Environmental, Material and Earth Sciences Research Team, Hanoi University of Mining and Geology, Vietnam
[3)] Institute for Nuclear Sciences and Technology, 179 Hoang Quoc Viet St., Ha Noi, Vietnam
* Correspondence: nguyenbachthao@humg.edu.vn (T.B.N); 84 4 9133 133 09

http://doi.org/10.29227/IM-2023-02-42

Submission date: 27-08-2023 | Review date: 26-09-2023

Abstract

Saltwater intrusion in the rapidly developing city of Da Nang in central Vietnam is currently causing various water-related challenges, including inadequate water supply and water pollution. An integrated SWAT-MODFLOW numerical model was used to investigate the origin and mechanism of saltwater in Holocene and Pleistocene aquifers. Geophysical and isotopic approaches were used to validate the SEAWAT model applied for simulating saltwater intrusion. The results suggest that the ebb and flow of tides, as well as water levels in rivers primarily impact coastal aquifers. However, effective water resource planning and management, along with maintaining the natural recharge of fresh water from local rain during the rainy season, could enable the rational and efficient utilization of groundwater, reducing saltwater intrusion in many areas. During the dry season, groundwater is recharged from higher altitude areas. The current saltwater intrusion mainly occurs along the rivers up to the hydraulic dam. Simulated models, using scenarios of stop abstracting groundwater, but changing to the use of surface water for drinking water, show that the area of saline water shrinks quickly after 30 years, reducing from 59.6 km² to 39.5 km² and from 40.2 km² to 28.6 km² in the Holocene and Pleistocene, respectively.

Keywords: *saltwater intrusion, groundwater modeling, sustainable groundwater development, coastal aquifers, surface water interaction, water resource management*

1. Introduction

Currently, the world's population is grappling with the pressing issue of water scarcity and saltwater intrusion. The availability of water has become a major concern for many regions, especially those that are arid or semiarid. In the past, the management of water resources has typically treated surface water and groundwater as distinct and separate from each other [1], even though they are closely interconnected components of the hydrological cycle [2]. In Vietnam, most of the water resources management is focused on surface water [3,4], while issues concerning groundwater are neglected and not managed properly. In many studies, modelling has been identified to be the most effective approach for estimating both surface and groundwater availability [5,6,7,8].

Saltwater origin and mechanisms in coastal aquifers in Vietnam have been studied extensively and the main causes identified are groundwater exploitation [9]; inter-aquifer leakage due to diffusion and density flow or high hydraulic gradient [10].

A major urban center located in the central region of Vietnam is Da Nang with over 70 km of coastline and is renowned for its pivotal role in tourism, industry, and agriculture. Despite this, the city is facing multiple challenges such as high population density, water scarcity, environmental pollution, and saltwater intrusion. Due to its vast coastline, the aquifers in this region are greatly impacted by the saline intrusion, but no study has yet analyzed this phenomenon using numerical models. A survey was conducted to create a hydrogeological map of the city, and it was revealed that about 30% of the aquifer area in this region is affected by salinity [11]. Thus, it is essential to evaluate the current condition of saltwater intrusion and identify an effective solution to this problem.

In this study, geophysical, hydrogeochemical and isotopic methods were applied to investigate the distribution of saltwater and its origin and mechanism in the coastal aquifers. The status of saltwater intrusion in the Da Nang area was assessed using a coupled SWAT-MODFLOW numerical model. The model was calibrated and employed to forecast potential scenarios of saltwater intrusion, considering the influence of economic and urban development through changes in groundwater pumping and recharge rates.

2. Study area

The focus of this study is the coastal region of Da Nang, as highlighted in Figure 1a. The area spans a total of 360 km². The Han River (Figure 1a) acts as the boundary between the coastal plain and the southern parts of the city, while sand dunes can be found in the Ngu Hanh Son and Nam O areas, largely due to wind activity. The geology and hydrogeology of the study region drawn for a cross-section A–B and C–D is shown in Figure 1b. and comprises three primary hydrogeological formations: aquitards, porous aquifers, and fracture aquifers.

The study area is predominantly covered by porous sediments from the Holocene and Pleistocene ages (a blue color, Figure 1). Holocene deposits in the study region are found with thickness varying from 5 m to 29 m and containing sand, silty sand and gravel (light blue, Figure 1). The area of the Holocene aquifer (qh) is around 160 km², with an outcrop area of approximately 90 km². The groundwater levels in this aquifer

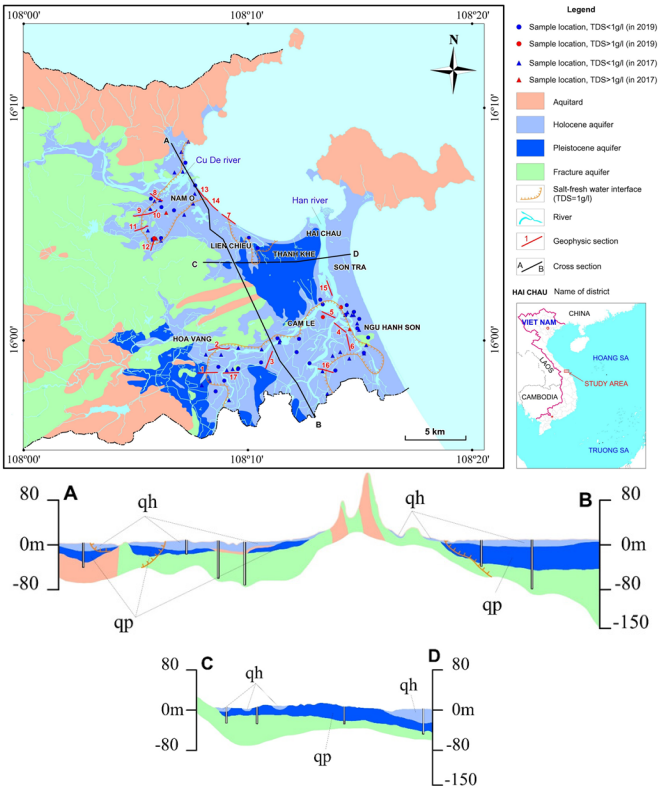

Fig. 1. (a) Hydrogeological map and location of sampling wells and (b) cross-section along A–B and C–D line shown in the map

vary seasonally, and it is in the range of 0.45 to 3.0 m from the surface in the Lien Chieu Hai Chau area, 1.8 to 11.2 m in the Son Tra – Ngu Hanh Son area.

Following the Holocene, there are fine to coarse sand, as well as sand with gravel and pebbles of the Pleistocene age with a thickness up to 34 m, average is about 25 m. The sediment in the Pleistocene deposit contains gravel sand to silty sand (dark blue, Figure 1). The area of the qp aquifer is around 160 km².

An observation for the water level in different boreholes and geological structures revealed that qh and qp aquifers are the same hydraulic system in the study area.

The fissure aquifer in the study zone possesses an area of less than 40 km² (green color in Figure 1), majority of those areas encompassed by younger sediments, predominantly composed of sericite schist, calcareous limestone, quartz schist, and shale, the aquifer is considered to have a moderate to poor capacity for water storage.

In light of the hydrogeological characteristics, the Holocene and Pleistocene porous aquifers need particular attention because water from these aquifers is currently exploited as the clean water source of the local population. Both, however, are under the vulnerability of saline intrusion.

3. Methods

3.1. Sampling procedure and field measurement

Water from 35 boreholes was sampled during two sampling campaigns in Dec/2019 (dry season) and May/2020 (wet season) for major cations and anions, TDS and isotopic compositions of deuterium (^2H) and oxygen 18 (^{18}O) in water determination. The positions of boreholes from those samples were taken were selected around the saltwater boundaries from hydrogeological mapping in 2012 (Figure 1). The isotopic compositions of ^{18}O and ^2H ($\delta^{18}O$, δ^2H) in water samples are expressed in delta (δ) notation by Equation (1) and (2):

$$\delta^{2}H = \left(\frac{^{2}R_{sample}}{^{2}R_{std}} - 1\right) x1000 \quad (1)$$

$$\delta^{18}O = \left(\frac{^{18}R_{sample}}{^{18}R_{satd}} - 1\right) x1000 \quad (2)$$

Where $^2R_{sample}$, $^2R_{std}$, $^{18}R_{sample}$ and $^{18}R_{std}$ are, respectively, the ratios of abundances (in mole) of the heavier (^2H or ^{18}O) to those of the lighter isotopes (^1H or ^{16}O) in water samples subjected to analysis and in standard. The standard for water isotopic composition determination is VSMOW2 (Vienna Standard of Mean Ocean Water batch 2), supplied by the International Atomic Energy Agency (IAEA) located in Vienna, Austria.

Before taking groundwater samples, the groundwater levels in boreholes were recorded, then the stagnant water in each sampling borehole was pumped out till the pH, temperature, EC in water became unchanged. The pH, temperature and EC of water were measured using a WTW Multi 197i device equipped with appropriate probes.

Groundwater samples were taken from the boreholes and passed through polycarbonate membranes with a pore size of 0.45 µm to eliminate suspended solids. For major cations analysis, 50 mL of the filtered samples were acidified by HNO_3 acid (65%, PA grade, Merck, Germany) to pH 1–2. The samples were kept in HDPE (high-density polyethylene) bottles for transport to the laboratory. For major anions determination, 50 mL of the filtered samples were stored without acidification in HDPE bottles for transport to the laboratory. For water isotopic composition analysis 50 mL of the filtered water was taken and stored in HDPE bottles with double caps to avoid evaporation. The samples were subjected to analyses within 2 weeks of the sampling day.

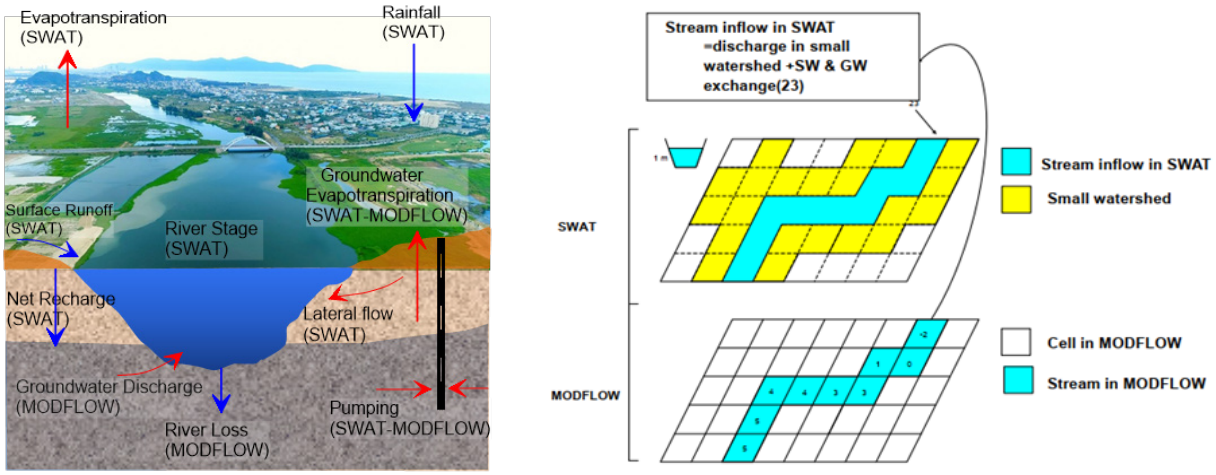

Fig. 2. A combination of surface water and groundwater models for hydrological analysis in Da Nang coastal area (a) [6] and the linkage of a river in MODFLOW with SWAT (b) [19]

Rainwater was collected using a device made according to the IAEA's recommendation [12]. The device was installed on the roof of an office building located within the study area. Sea water was sampled at a distance of 20 meters from the shore, at a depth of 0.5 m from the surface for $\delta^{18}O$ and $\delta^{2}H$ analyses.

3.2. Analytical procedure

The major ionic contents of water samples were analyzed at the Centre for Excellence in Analysis and Experiment (CEAE) of the Hanoi University of Mining and Geology (HUMG) by using ion chromatography (IC) method on a DIONEX 600.

The water isotopes compositions were analyzed by laser spectrometry method on a Picaro's cavity ring down spectrometer CRDS L2130-I at the Laboratory of Water Resources of the Ha Noi University of Natural Resources and Environment (HUNRE). The results of $\delta^{18}O$, $\delta^{2}H$ were expressed in ‰ relative to the VSMOW2.

3.3. Geophysical method

Electrical resistivity tomography (ERT) was used in this study to validate the developed saltwater numerical model. The ERT technique provides a continuous characterization of subsurface electrical conductivity (by the means of electrical resistivity distribution) [13,14]. Besides, the ERT method provided high-quality electrical resistivity data obtained [15] with substantial spatial precision and the capability to survey underground areas continuously in both 2D and 3D dimensions [16] that were used to calibrate the numerical model in this study.

In the research area, 17 ERT profiles across the salt-fresh water interface were measured (Figure 1a) by using a multi-electrode SuperSting R1/IP equipment, with inter-electrode spacing of 10m.

3.4. Numerical model

MODFLOW is a comprehensive groundwater modeling system that employs finite-difference technology to simulate three-dimensional flow. The governing equation for MODFLOW is based on Darcy's Law [17,18], which is represented by a partial differential equation, and it is described in Equation (3).

$$\frac{\partial}{\partial x}\left(K_{xx}\frac{\partial h}{\partial x}\right)+\frac{\partial}{\partial y}\left(K_{yy}\frac{\partial h}{\partial y}\right)+\frac{\partial}{\partial z}\left(K_{zz}\frac{\partial h}{\partial z}\right)-W=S_s\frac{\partial h}{\partial t} \quad (3)$$

The Equation (3) takes into account several variables such as hydraulic conductivities in the x, y, and z axis (K_{xx}, K_{yy}, and K_{zz}), piezometric head (h), volumetric flux per unit volume (W), specific storage of the porous medium (S_s), and time (t). The hydraulic conductivities in the major axes, which are parallel to the x, y, and z axis, are used to calculate the rate of flow in each direction. The height of the water column above a reference point, known as the piezometric head, is a crucial factor for understanding the pressure distribution in the aquifer. Sources or sinks of water that may affect the flow direction and rate are represented by the volumetric flux per unit volume. The specific storage of the porous medium indicates the quantity of water stored in a unit volume of the medium under unit hydraulic gradient change. Time plays a crucial role in modelling the behavior of groundwater over time. Thus, Equation (3) provides a comprehensive framework for understanding the complex behavior of groundwater in various geological settings.

3.4. SWAT-MODFLOW integration

The combination of surface water and groundwater models can provide valuable insights into the spatial-temporal replenishment of groundwater and the interaction between river water and groundwater. SWAT-MODFLOW is a powerful tool that can simulate these complex interactions [6,19]. Figure 2a illustrates that SWAT is used to model the top layers such as the root zone, vadose zone, and shallow aquifer, while MODFLOW is used to model the lower layer, which is the deep aquifer.

In this study, both the SWAT and MODFLOW models were employed to evaluate recharge rates, first separately and then in combination. The SWAT model was initially used to evaluate recharge rates and calculate groundwater recharge values at the hydrological response units (HRUs) level. In order to combine the SWAT and MODFLOW models, the HRU recharge rates had to be transferred and utilized as input data for MODFLOW, as illustrated in Figure 2b. Since SWAT is semi-distributed, it was uncertain where each HRU was located within the sub-basins. To overcome this issue, a single HRU was created for each sub-basin based on the dom-

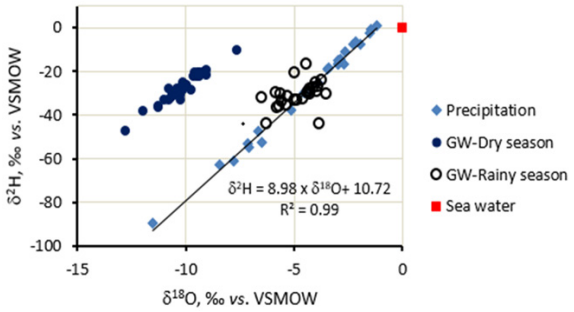

Fig. 3. Isotopic compositions in groundwater samples analyzed along with the local meteoric water line in a coastal area of Da Nang city in 2020

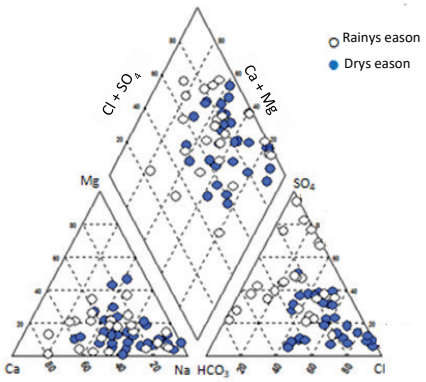

Fig. 4. Piper diagram showing the chemistry of groundwater in the study area

inant soil, land use, and slope option [2]. By combining the two models and accounting for the limitations of each, it was possible to obtain a more accurate and comprehensive understanding of the groundwater replenishment process.

4. Results and discussion

4.1. Isotopic compositions in water as indicators for the genesis and recharge area of groundwater in the study region

The isotopic compositions of groundwater from the study area is displayed alongside the local meteoric water line (LMWL) for the Da Nang city area in Figure 3. The LMWL in this region follows a model with a slope of 8.98 and an intercept of 10.71, as depicted in Figure 3. These values are slightly different from the Global Meteoric Water Line (GMWL) of 8 and 10, respectively, as established by Craig [22]. The variation in the values of slope and intercept of the LMWL could be attributed to the unique weather conditions in Da Nang city, which is characterized by high atmospheric temperatures and humidity throughout the year.

In the rainy season isotopic compositions in groundwater (open dots in Figure 3) from the study area positioned close to the LMWL indicate that groundwater in this area is recharged from the local precipitation. The only point positioned below the LMWL, possibly is being affected by seawater making the isotopic signatures in water from that borehole to be enriched.

For the dry season, a quite different trend of the δ^2H vs. $\delta^{18}O$ relationship for groundwater was observed (solid dots in Fig.3). Oxygen 18 in the water was depleted but deuterium was enriched. The reason for this could be the recharge area was at a higher altitude for which isotopic compositions in precipitation were depleted, and the flow direction of the recharge would be through and beneath a landfill. In fact, a large landfill is currently located around 12-15 km towards Northwest of Da Nang for storing and processing waste from the city. The leachate from the landfill containing sulphide (H_2S) and methane (CH_4) as the products of domestic waste bio-decomposition leak into aquifers. This leakage would be so intensive during the dry season because of not enough pressure from recharge to protect from the infiltration of the leachate to aquifers. It was reported that hydrogen in H_2S and CH_4 generated from domestic waste is enriched in deuterium [23,24] and the enriched deuterium in sulphide and methane participated in the isotopes exchange with hydrogen in water in aquifers making deuterium in water to be enriched. However, oxygen 18 has no chance to take part in isotopes exchange, therefore its signature was unchanged as it was from the recharge area.

4.2. The chemical composition of the groundwater in the area under investigation

Table 1 showed the hydrogeochemical properties and stable isotopic compositions of groundwater in the rainy season. Similarly, Table 2 displays the corresponding results for the dry season. The data in Table 1 and Table 2 provide valuable insights into the dynamics of groundwater quality and its potential impact on the environment and human health.

The chemical characteristics of groundwater in the study area were presented in a Piper diagram shown in Figure 4.

As seen from Figure 4 groundwater in the area is dominated by Na-Ca-Cl-SO_4 type. However, some boreholes, e.g. BS1, BS12, BS27 HV40, in the rainy were found to have chloride concentrations that exceeded the national standard for groundwater quality set by the Ministry of Natural Resources and Environment [21] by up to 4 times (BS27, Table 1). The high levels of chloride in groundwater may be attributed to the ongoing salt intrusion occurring in the study area

Tab. 1. Analysis of the chemical composition and stable isotopes of groundwater during the rainy season (4/2019)

No	Field code	Ca^{2+} (mg/l)	Mg^{2+} (mg/l)	Na^{+} (mg/l)	SO_4^{2-} (mg/l)	Cl^{-} (mg/l)	HCO^{3-} (mg/l)	$d^{18}O$ (‰)	$d^{2}H$ (‰)
1	BS1	32.06	48.76	590.41	87.51	1032.34	34.97	-10.22	-30.75
2	BS2	33.67	9.73	58.67	91.51	71.05	69.46	-11.94	-38.23
3	NHS12	33.67	6.93	52.75	80.33	71.02	53.74	-10.67	-32.21
4	BS3	34.27	3.53	20.27	43.09	35.50	60.47		
5	BS5	13.03	3.28	57.97	15.84	63.19	81.45	-12.8	-47.61
6	BS6	96.99	40.25	94.83	297.57	120.70	166.37	-9.1	-20.01
7	BS7	38.08	4.86	26.36	31.04	71.01	49.31	-9.18	-20.61
8	BS8	36.07	0.49	71.66	12.64	78.10	152.30	-10.53	-31.15
9	BS10	34.67	3.04	76.88	98.64	85.20	53.34	-10.19	-27.95
10	BS11	15.63	12.16	82.74	18.21	129.22	83.76	-11.26	-36.48
11	BS12	123.45	58.85	1278.34	310.64	2130.0	27.15	-10.22	-33.19
12	BS13	21.04	10.71	39.62	52.15	62.48	50.01	-11.24	-35.85
13	BS14	19.24	12.65	34.41	53.29	67.45	30.60	-10.75	-32.98
14	BS15	39.26	8.51	50.06	90.94	90.17	24.47	-10.63	-30.25
15	BS16	12.42	3.77	36.71	13.07	65.32	25.56	-9.95	-26.34
16	BS17	20.04	7.32	26.72	8.31	43.31	84.09	-10.13	-25.33
17	BS18	29.26	25.78	150.02	48.81	173.24	258.46	-10.13	-28.88
18	BS20	13.43	3.16	70.41	21.06	68.16	99.88	-9.05	-21.79
19	BS21	16.03	2.43	53.88	29.61	84.49	21.33	-9.65	-22.51
20	BS22	25.45	8.15	62.13	62.13	58.93	103.61	-9.74	-28.92
21	BS23	4.01	2.07	7.91	3.75	28.40	9.86	-10.78	-28.25
22	BS24	2.20	5.59	9.55	4.32	30.53	2.50	-10.37	-27.88
23	BS25	25.45	13.51	197.89	118.55	223.65	136.13	-9.03	-19.66
24	BS26	4.61	5.59	8.67	8.65	32.66	59.33	-11.01	-33.32
25	HV40	30.20	18.02	374.67	113.42	600.66	19.34	-7.61	-10.38
26	BS27	47.01	17.88	786.83	264.59	1084.88	153.15	-9.98	-26.78
27	HV41	10.02	1.22	15.58	9.79	38.34	48.56	-9.37	-22.36
28	BS28	10.60	5.96	130.02	100.31	137.03	50.48	-9.34	-20.43
29	BS29	19.60	1.58	30.02	28.19	55.38	22.64	-9.4	-20.88
30	BS30	22.04	5.11	40.27	57.85	41.18	55.72	-9.56	-20.73
31	BS31	29.06	4.86	68.87	32.18	116.40	55.09	-9.46	-22.33
32	BS32	33.62	3.44	37.95	57.00	66.74	38.61	-10.24	-27.79

Tab. 2. Hydrochemical and stable isotopic composition of groundwater in the dry season (12/2020)

No	Field code	Ca^{2+} (mg/l)	Mg^{2+} (mg/l)	Na^{+} (mg/l)	SO_4^{2-} (mg/l)	Cl^{-} (mg/l)	HCO^{3-} (mg/l)	$d^{18}O$ (‰)	$d^{2}H$ (‰)
1	BS1	118.27	46.01	347.22	818.63	263.88	24.23	-5.66	-29.89
2	BS1A	116.47	44.43	348.31	781.00	273.17	22.83	-6.30	-43.94
3	NHS12	18.81	4.13	8.49	16.33	1.41	71.03	-6.55	-31.88
4	BS3	38.28	4.26	8.63	31.95	45.64	48.40	-4.45	-16.59
5	BS7	41.48	10.09	22.81	68.16	25.01	89.38	-5.03	-20.53
6	BS10A	17.01	6.66	26.32	17.75	68.00	38.57	-5.90	-29.28
7	BS11	13.02	18.02	43.15	117.15	7.25	35.14	-5.82	-36.34
8	BS12	160.28	60.15	1118.1	2105.15	86.02	33.42	-5.69	-35.78
9	BS13	29.02	16.42	25.72	65.32	63.68	46.97	-5.62	-33.54
10	BS15	43.23	16.49	38.85	93.72	90.26	42.97	-3.89	-43.98
11	BS17	12.02	4.86	19.11	35.51	12.78	34.78	-4.33	-29.94
12	BS18	35.67	25.17	103.11	174.66	85.41	101.52	-4.00	-28.73
13	BS20	12.82	6.32	37.95	55.38	19.97	51.34	-3.55	-29.92
14	BS21	21.41	6.93	32.25	63.91	27.49	41.33	-4.61	-32.21
15	BS24	16.01	0.49	15.62	18.46	1.98	58.46	-5.01	-32.95
16	BS25A	1.22	2.07	21.75	19.17	2.71	35.48	-5.35	-31.33
17	BS25	50.11	6.08	198.72	159.75	160.55	232.17	-4.01	-24.84
18	HV40	73.51	25.91	859.82	1309.95	274.64	36.25	-4.34	-28.74
19	BS27	86.69	32.12	909.32	1469.7	196.72	63.80	-4.31	-27.79
20	HV41	10.81	3.77	20.52	26.98	10.33	47.02	-4.12	-27.15
21	BS28	40.08	11.67	35.15	78.11	91.41	24.42	-3.76	-23.96
22	BS29	14.03	0.61	9.82	21.32	3.03	31.47	-4.90	-32.74
23	BS30	18.44	0.61	26.25	24.14	39.95	36.71	-5.40	-35.31
24	BS31	59.12	0.61	17.15	39.76	65.38	77.49	-4.41	-29.62
25	BS32	32.02	4.86	38.81	78.12	31.50	51.04	-3.94	-26.51

4.3. Distribution of salinity

The classification of water types according to TDS (total dissolved solids) is an important step in water resource management. Zhou [20] proposed a classification system based on TDS levels, which includes four categories: brine (TDS > 50 g/l), saline water (TDS = 3–50 g/l), brackish water (TDS = 1–3 g/l), and freshwater (TDS < 1 g/l). This system allows for a clear understanding of the quality of water resources and helps to guide decision-making related to their use and management. An understanding of the TDS levels present in various water sources can help in assessing the suitability of water for different applications, such as drinking, irrigation, or industrial use. Data from 35 sampling locations were used to generate a limit between fresh and salt water. Among points that were collected during 2020 (in dry and rainy seasons), TDS varies from 0.1 to 3.6 g/l. Five samples with TDS higher than 1 g/l are located along the Han and Cu De rivers (Figure 1.a). It was revealed that a sharp contrast of electrical resistivity along Profile 2, 13 (Figure 3). Below surface up to 15 m depth, resistivity varies from about 15 Ohm.m close to the river and up to more than 50 Ohm.m is observed corresponding to superficial Holocene sediments made of sandy clay or unsaturated zone. Resistivity readings ranging from 1 to 10 Ohm.m at a depth of 15–30 m suggest the presence of salt and brackish water from the nearby river. Aquifer with freshwater is reflected by a high resistivity (> 40 Ohm.m) below 30 m depth due to the presence of gravel. The low resistivity zone in the deep part close to the river is demonstrated as salty water affected by surface water from the river.

4.4. Saltwater intrusion modelling in the study area

Saltwater intrusion modelling was validated and calibrated by using EC measurement data from boreholes and elec-

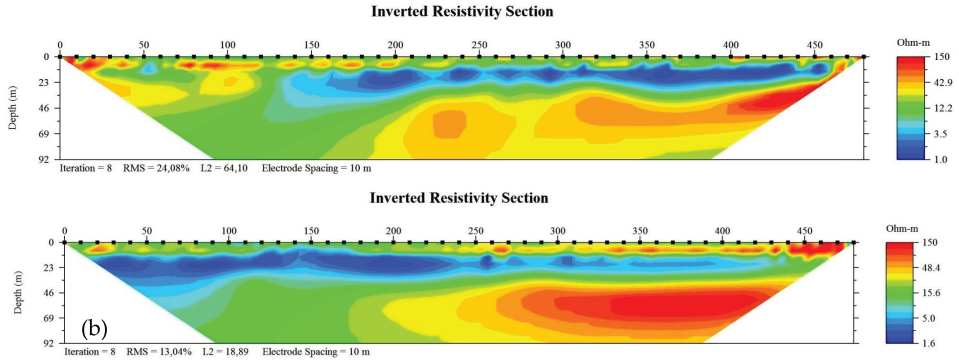

Fig. 5. 2-D electrical resistivity tomography (ERT) of section 2 (a) and section 13 (b)

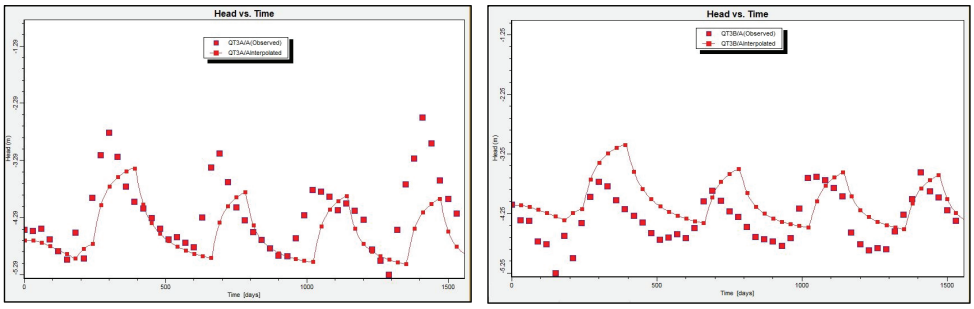

Fig. 6. Simulated and observed groundwater head values at observation borehole QT3A (a) and QT3B (b)

trical resistivity tomography (ERT) measurement in two campaigns 2019–2020. The results from the calibrated numerical model in the Holocene and Pleistocene aquifers in the rainy season (May/2020) show that the salinity area with TDS higher than 1 g/l in the water of the Holocene aquifer decreases faster than in Pleistocene aquifer compared to which in the rainy season of the year 2012. The salinity decreases because of the precipitation recharge to these aquifers. The replenishment of the aquifer due to rain and the pumping process both impact the aquifer, causing it to pale. In areas located nearby the Han and Cu De River, and the coastline, the salinity level rises with the passing of time.

Figure 6 displays a comparison between the simulated water heads at observation borehole QT3A (Holocene aquifer) and QT3B (Pleistocene aquifer) and the water heads that were acquired from the existing pumping rates. The changes in the water heads ranged from 0.2 to 1 meter, and they depended on the position of the observation borehole. Those boreholes located in proximity to pumping wells showed a higher degree of change. Based on the results of the numerical modeling for saltwater intrusion in the Holocene and Pleistocene aquifers in April 2020, it was observed that the area of Holocene aquifer with initial high salinity decreased at a faster rate than that of Pleistocene aquifer. This difference may be due to the higher levels of precipitation recharge in Pleistocene aquifer, as shown in Figure 7.

This is a result of the high influence of rivers and the sea on the surface aquifer. Figure 7 indicates areas with TDS greater than 1g/l of Holocene and Pleistocene aquifers during wet season (April/2020). Accordingly, the total area with salinities higher than 1 g/l is 41.8km^2 and 53.4km^2 for Holocene and Pleistocene aquifers, respectively (Figure 7).

4.5. Saltwater intrusion due to recharge and pumping in coastal aquifers

The potential control of saltwater intrusion by reducing groundwater pumping or by increasing surface water infiltration was assessed using the calibrated model. To predict the saltwater intrusion in 2020, four distinct scenarios were simulated:

- status quo: with the current groundwater pumping rate and recharge from rain/surface water
- stop pumping: use 100% surface water resource for water supply
- double pumping rates: increase GW pumping rate to fit the demand of drinking water of the city
- no recharge occurs: no recharge area due to urban development

Predicted saltwater areas with different scenarios for both aquifers Holocene and Pleistocene in the years 2035 and 2050 are shown in Table 3.

Most of the pumping wells in this area penetrated to Pleistocene aquifer, the simulated model shows the saltwater area in both aquifers decrease quickly when all pumping wells stop, the saltwater area decreases 23.4% and 28.9% in Pleistocene and Holocene aquifer respectively in 2050. The simulated salt intrusion model from the scenario of groundwater of pumping rate doubled to fit the water demand in future times is relatively similar to the scenario of no recharge to groundwater due to urban development.

5. Conclusions

In Da Nang area, data from groundwater analysis and ERT measurements shows the distribution of saltwater (TDS>1g/l) in Holocene with about 60.3km^2 and in the Pleistocene aquifer with 41.3km^2. In some boreholes, water contains chloride at a concentration exceeding 4 times compared to the National Standard for groundwater quality. Hydrochemical and

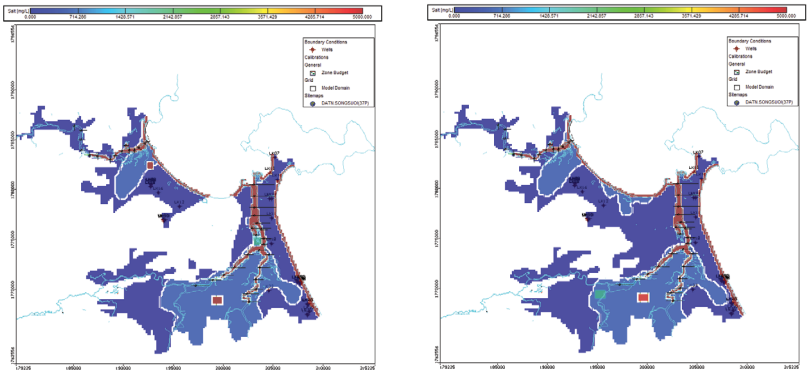

Fig. 7. Saltwater intrusion distribution in groundwater of the study site in April 2020 (modeled using Visual MODFLOW) (a) Depicting the distribution in the Holocene aquifer; (b) Depicting the distribution in the Pleistocene aquifer

Tab. 3. Predicted saltwater areas with different scenarios for Holocene and Pleistocene aquifer

Scenarios	**Area of saltwater with TDS > 1g/l (km²)**					
	Holocene aquifer			Pleistocene aquifer		
	In 2020	In 2035	In 2050	In 2020	In 2035	In 2050
status quo	60.3	53.0	41.3	41.3	37.6	31.2
stop pumping	59.6	51.2	39.5	40.2	35.3	28.6
2x pumping rates	60.2	56.4	44.3	41.8	38.8	35.4
no recharge	60.8	57.9	45.4	41.4	38.0	37.2

stable isotopic data of 35 points from both aquifers demonstrated that in the rain season, groundwater is recharged from the local precipitation, in the dry season groundwater is recharged from a higher altitude area and the flow direction of the recharge would be through and beneath a landfill. The replenishment of groundwater from surface sources is a valuable resource that can reduce the extent of saltwater intrusion in many areas. Along the river downstream up to the hydraulic dams, saltwater in groundwater mainly recharges by surface water from rivers.

The study area was simulated for surface and groundwater, including saltwater intrusion, through the development of an integrated SWAT and MODFLOW model. Thanks to groundwater pumping management, with freshwater recharge from the surface, the area of saline groundwater in both aquifers is decreasing. Double pumping rate scenario and no recharge scenario give the same salt intrusion effect to qh and qp aquifers. In this area, groundwater is an effective resource for water supply to the city, but detailed studies are needed to control saltwater intrusion into aquifers.

Acknowledgments

This research was funded by the Ministry of Education and Training of Vietnam (Program 562) under the grant encoded B2019-MDA-562-16.

Literatura – References

1. Winter, T. C., Harvey, J. W., Franke, O. L. & Alley, W. M. Ground water and surface water: A single resource. 1998. Circular.
2. Dowlatabadi, S. & Zomorodian, S. Conjunctive simulation of surface water and groundwater using SWAT and MODFLOW in Firoozabad watershed. KSCE Journal of Civil Engineering, 2015, 20.
3. Chau, T. K. A. K., D. X. Study on water balance in Sesan river basin in drought year 2015/2016. Journal of Meteorological, 678, 2017, 44-53.
4. Au, N. T. T., Liem, N. D., Loi, N. K. Applying GIS technique and SWAT model to assessing water discharge in Dakbla watershed. Journal of National University, 29, 2013,1-13
5. Nguyen, B. T., Anh., C. V., Trinh., N. D., Son., H. T. & Nguyen, V. D. Saltwater intrusion in aquifers of Danang area and solution for sustainable groundwater development. Journal of Mining and Geology Science and Technology, 2018, 10-20.
6. Nguyen, B. T. & Khoa, T. V. L. Integrated SWAT-MODFLOW model to study saltwater intrusion in Da Nang coastal city. IOP Conference Series: Earth and Environmental Science, 2022, 1071, 012037.
7. Voss, C. I. & Souza, W. R. Variable density flow and solute transport simulation of regional aquifers containing a narrow fresh-water-saltwater transition zone. Water Resources Research, 1987, 23, 1851-1866.
8. ABD-ELHAMID, H. F. & JAVADI, A. A. A density-dependant finite element model for analysis of saltwater intrusion in coastal aquifers. Journal of Hydrology, 2011, 401, 259-271.
9. Long, P. N. & Dat, H. T. Application of GIS-Base GALDIT for vulnerability assessment to saltwater intrusion of Holocene coastal aquifer: a case of Quang Nam - Da Nang city, Vietnam. Science of the Earth, 2020, 42, 298-310.
10. Hoan, H. V., Larsen, F., Lam, N. V., Nhan, D. D., Luu, T. T. & Nhan, P. Q. Salt Groundwater Intrusion in the Pleistocene Aquifer in the Southern Part of the Red River Delta, Vietnam. VNU Journal of Science: Earth and Environmental Sciences, 2018, 34.
11. Nguyen, B. T., Anh., C. V., Trinh., N. D., Son., H. T. & Nguyen, V. D. Saltwater intrusion in aquifers of Danang area and solution for sustainable groundwater development. Journal of Mining and Geology Science and Technology, 2018, 10-20.
12. IAEA. Water and environment newsletter of the Isotope Hydrology Section. International Atomic Energy Agency. 2002.
13. Loke, M. H. & Barker, R. D. Rapid least-squares inversion of apparent resistivity pseudosections by a quasi-Newton method1. Geophysical Prospecting, 1996, 44, 131-152.
14. Zarroca, M., Bach, J., Linares, R. & Pellicer, X. M. Electrical methods (VES and ERT) for identifying, mapping and monitoring different saline domains in a coastal plain region (Alt Emporda, Northern Spain). Journal of Hydrology, 2011. 409, 407-422.
15. Bauer, P., Supper, R., Zimmermann, S. & Kinzelbach, W. Geoelectrical imaging of groundwater salinization in the Okavango Delta, Botswana. Journal of Applied Geophysics, 2006, 60, 126-141.
16. Batayneh, A. T., Elawadi, E. A. & Al-Arifi, N. S. Use of Geoelectrical Technique for Detecting Subsurface Fresh and Saline Water: A Case Study of the Eastern Gulf of Aqaba Coastal Aquifer, Jordan. Journal of Coastal Research, 2010, 26, 1079-1084.
17. Mehl, S. & Hill, M. C. Development and evaluation of a local grid refinement method for block-centered finite-difference groundwater models using shared nodes. Advances in Water Resources, 2002, 25, 497-511.
18. Chiang, W.-H. & Kinzelbach, W. Processing Modflow A Simulation System for Modeling Groundwater Flow and Pollution. 1998.
19. Kim, N. W., Chung, I. M., Won, Y. S. & Arnold, J. G. Development and application of the integrated SWAT–MODFLOW model. Journal of Hydrology, 2008, 356, 1-16.
20. Zhou, Y., Wang, Y., Li, Y. et al. Hydrogeochemical characteristics of central Jianghan Plain, China. Environ Earth Sci 68, 2013, 765–778. https://doi.org/10.1007/s12665-012-1778-9
21. MONRE. National technical regulation on groundwater quality. Ministry of Natural Resources and Environment, QCVN 09: 2015/BTNMT.
22. Craig, H. Isotopic Variations in Meteoric Waters. Science, 1961, 133, 1702-1703.
23. Hackley, K. C., Liu, C. L. & Coleman, D. D. Environmental Isotope Characteristics of Landfill Leachates and Gases. Groundwater, 1996. 34, 827-836.
24. Clark, I. & Fitz, P. Environmental Isotopes in Hydrology. Lewis Publishers. 1998.

Emission Reduction in Oil & Gas Subsurface Characterization Workflow with AI/ML Enabler

Thuy Nguyen Thi THANH[1)], Samie LEE[1)], The NGUYEN[1)], Le Quang DUYEN[2)]

[1)] SLB: Schlumberger Vietnam Services - 7th Floor, Havana Tower, 132 Ham Nghi Street, Ben Thanh Ward, Ho Chi Minh City, Vietnam; Schlumberger Oilfield Support Sdn. Bhd - Wisma Rohas Purecircle, No.9 Jalan P.Ramlee, 50250 Kuala Lumpur, Malaysia
[2)] HUMG: Faculty of Petroleum and Energy, Hanoi University of Mining and Geology, No.18 Vien Street - Duc Thang Ward- Bac Tu Liem District - Ha Noi
Corresponding author email: tthanh3@slb.com, slee21@slb.com, tdac@slb.com, lequangduyen@humg.edu.vn

http://doi.org/10.29227/IM-2023-02-43

Submission date: 24-08-2023 | Review date: 27-09-2023

Abstract

According to (McKinsey & Company, 2020), drilling and extraction operations are responsible for 10% of approximately 4 billion tons of CO_2 emitted yearly by Oil and Gas sector. To lower carbon emissions, companies used different strategies including electrifying equipment, changing power sources, rebalancing portfolios, and expanding carbon-capture-utilization-storage (CCUS). Technology evolution with digital transformation strategy is essential for reinventing and optimizing existing workflow, reducing lengthy processes and driving efficiency for sustainable operations.

Details subsurface studies take up-to 6–12 months, including seismic & static analysis, reserve estimation and simulation to support drilling and extraction operations. Manual and repetitive processes, aging infrastructure with limited computing-engine are factors for long computation hours. To address subsurface complexity, hundred-thousand scenarios are simulated that lead to tremendous power consumption. Excluding additional simulation hours, each workstation uses 24k kWh/month for regular 40 hours/month and produces 6.1kg CO_2.

Machine Learning (ML) become crucial in digital transformation, not only saving time but supporting wiser decision-making. An 80%-time-reduction with ML Seismic and Static modeling deployed in a reservoir study. Significant time reduction from days-to-hours-to-minutes with cloud-computing deployed to simulate hundreds-thousands of scenarios. These time savings help to reduce CO_2-emissions resulting in a more sustainable subsurface workflow to support the 2050 goal.

Keywords: *CO_2 emission, net zero carbon, machine learning, CCUS, digital transformation, emission reduction, digital subsurface workflow*

Introduction

Sustainability and emissions reduction have attracted attention in the oil and gas industry to optimize recovery and increase efficiency. According to (McKinsey & Company, 2020), oil and gas drilling and extraction operations are responsible for 10% of approximately 4 billion tons of CO_2 emitted yearly to the atmosphere. This has made an enormous impact in the oil and gas industry and on analyzing carbon footprint reduction opportunities.

A report by the International Energy Agency estimates that the use of Artificial Intelligence and Machine-Learning (AI/ML) could reduce global greenhouse gas emissions by up to 4% by 2030, which is equivalent to nearly 2.4 gigatons of carbon dioxide. The use of AI/ML enables workflows, i.e., Subsurface Reservoir Characterization and Field Development Planning enabler workflows, and has the potential to play a significant role in reducing carbon emissions and mitigating the impacts of climate change.

In this paper, we will present an overview of AI/ML Subsurface Characterization Workflows for optimizing performance in reservoir management and operations while reducing their emissions footprint. We will outline via AI/ML subsurface workflows to showcase the areas of improvement over data insights and domain sciences to manage and reduce reservoir uncertainty.

Conventional Subsurface Reservoir Characterization and Key Challenges

The Subsurface Reservoir Characterization is an integral part of sequences geoscience processing and interpretation workflows. A prolonged data-gathering process may require due to inadequate data management and governance in obtaining necessary workable datasets to proceed with the study. The interpretation scopes also required significant turnaround time due to the multiple iterations of Quality Check (QC) and review processes, silos domain data processing and interpretation, and complex domain workflow for complex reservoir environment. Moreover, most conventional reservoir characterization employs core data measurements and local correlations as input for reservoir properties modeling, whereby a strong correlation between core-log is not always available. Therefore, higher reservoir uncertainties may also require multiple screening and simulation runs to better quantify and address the reservoir uncertainties. Infrastructure limitation has always been a major challenge to most of the Oil and Gas Operators where the complicated procedure is involved whenever storage or RAM needs to be upgraded. Infrastructure ownership and maintenance further contribute to a higher cost where upfront CAPEX allocation is required. The subsurface domain workflow gaps and work inefficiency with the on-premises solution also serve as another concern, in addition to poor data management which ultimately leads to poor business investment decisions due to data unreliability.

Digital Transformation

To resolve those complex challenges of the subsurface environment and optimize its processing and interpretation

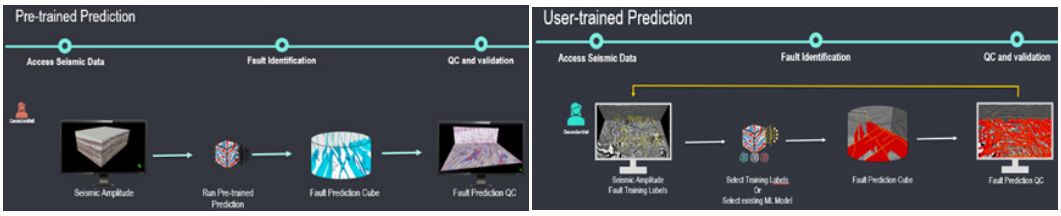

Fig. 1. Two model types of ML Fault Prediction

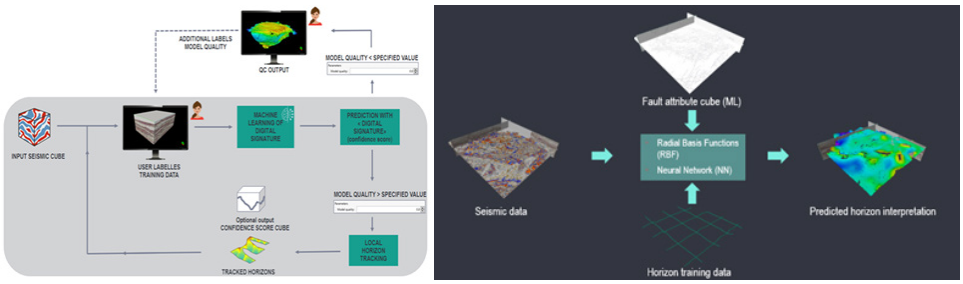

Fig. 2. ML Horizon Prediction Workflow

workflows, the majority of Oil & Gas Operators have to keep upgrading their IT infrastructure every few years to accommodate the evolution of technology and fast-changing applications. Each new user laptop or workstation has a carbon footprint of 331 kg CO_2 which 75–80% is from manufacturing processes (Circular Computing, n.d.). If multiplying these numbers by hundreds or thousands, it will contribute to the increase in CO_2 emission. Hence, migrating operators' IT architecture and workflows to digital cloud solutions will enable them to build up a more sustainable workflow that supports the achievement of CO_2 emission reduction.

Firstly, ability accessing to High Cloud Computing (HPC) simulation power will ease the need of purchasing a new laptop or workstation as well as speed up the simulation running time.

Secondly, Oil and Gas Operators will be able to build an efficient collaborative working environment, enabling access to intelligent insights from the data with cloud technology. In addition, it allows the embedded of Artificial Intelligence/ Machine Learning (AI/ML) application into the traditional reservoir characterization study to have a more data-driven insights for accurate outputs. More importantly, a much shorten turn-around time from days-to weeks which traditionally could takes months-to-years to complete. (Woodside Energy, n.d.) (OMV, n.d.) (ADNOC, n.d.)

Last but not least, digitalizing the current subsurface characterisation workflow will allow the testing of different scenarios for uncertainty analysis and provide an in-depth understanding of the geological settings of Areas of Interest (AOI) before any decision-making required.

AI/ML Enablers Subsurface Reservoir Characterization Workflows

Many of the worldwide Oil and Gas Giant Operators invested tremendously in the development of AI/ML cloud-based subsurface workflows or applications. An example, BP Ventures invested five million pounds in the "Sandy" platform that is capable of linking information to identify new connections and workflows and creating a robust knowledge graph of BP's subsurface assets. This project is expected to reduce project life cycles by reducing the time necessary for data collection, interpretation, and simulation.

In a similar feat, Shell International Petroleum Company has partnered with Microsoft Corporation in different projects to improve its processes. From the use of the Microsoft DevOps platform to improve teamwork and standardize operations to partnering to reduce carbon emissions.

In the following sessions, we would like to share several AI/ML workflows that have the potential to improve exploration accuracy and reduce repetitive routine processing workflows and interpretation uncertainty. This body of information can serve as a guideline for adopting AI/ML in subsurface reservoir characterization – a trend of more effective and efficient industry-tailored intelligence solutions.

(A) Automated Wellbore and Log Interpretation

Oftentimes, the Petrophysicist are expected to evaluate the potential of reservoir properties and volumetric in-places in time-constraint situations while maintaining the consistency and accuracy of parameters and interpretations. Nevertheless, more challenges may arise when working with older wells and vintage data where data maybe appears to be incomplete and inadequate. Traditionally, weeks-to-months needed for a Petrophysicist to complete the scopes for data screening and review, key well formation evaluation, establish of core-log correlations, multiwell evaluations, poro-perm, rock-typing and saturation modeling.

The Automated Machine Learning Wellbore and Log Interpretation include automated Log Data Quality Checks (LogQC) and Composite Log Preparations, followed by Formation Evaluation for volumetric calculations to reduce the repetitive scopes for a Petrophysicist to hours-to-days.

Automating the log data QC and conditioning processes could significantly reduce repetitive human manual efforts thus increasing the process cycle efficiency in the reservoir characterization process. Taking advantage of a high-computing engine of machine learning, automation, and new technologies to speed up this manually intensive task will ultimately make more quality ranked data available for the interpretation workflows in a smaller fraction of the time.

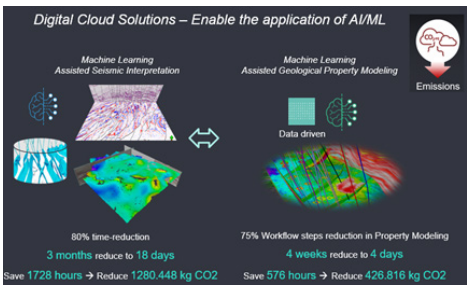

Fig. 3. CO_2 emission reduction using AI/ML workflow

The scope of work for the automated wellbore and log interpretation could include a series of data quality checks from 'Family and Unit check & correct', 'First & Last Reading detection', 'Depth-shift check', 'Resampling & Splicing', 'Bad-hole Flagging', 'Outlier Detection', 'Log Normalization', 'Log Prediction', etc. The automated log interpretation could automatically compute lithology and QC the conditioned log data using hierarchical Element Analysis (ELAN). The outputs of auto-petrophysical interpretation could be used as inputs to subsequent Rock-Typing and Saturation Height Modeling workflow. Lastly, a statistical method that looks at the variability of the input data and the changes made by the algorithms to establish a traffic light validation for accessing the uncertainties and assurance.

(B) Machine-Learning-Assisted-Seismic-Interpretation (ML-ASI)

Although the Seismic Interpretation has long been a crucial part of subsurface characterization workscope, there is still an enormous operational obstacle when it comes to interpretation and extracting the most value out of such information. A time-consuming process that frequently yields inconsistent results is caused by the combination of large amounts of data and a series of repetitive, time-consuming, and subjective workflow and interpretation approaches.

The Machine-Learning Assisted Seismic Interpretation (ML-ASI) has defined a new style of working that has resulted in enabling higher productivity and efficiency in delivering the seismic interpretation. The Seismic Interpreter now has the opportunity to test and run multiple scenarios with much lesser turnaround time to enable faster decision-making. The Elastic Cloud-Computing and Domain-Driven ML-ASI have the ability to significantly improve seismic interpretation efficiency and reveal an immense amount of information from expensive and unwieldy seismic datasets.

In this paper, using the Petrel platform in a cloud environment as an example, we will explain how ML-ASI can accelerate the existing seismic interpretation process in the modern subsurface workflow.

Two innovative Machine-Learning (ML) methods were developed, starting with Fault Interpretation, based on the fundamental design of Deep Convolution Neural Networks (CNN) U-Net Architecture. These methods were then modified for use in the seismic interpretation.

Utilizing a range of seismic data sets, the first method required to have a pre-trained model to be developed. Observed fault locations were designated as positive training examples. To further enhance our understanding of the possible structure in the data, the pre-trained fault prediction offers an accurate estimation of where the faults will be located. The main benefit of this method is that the acquisition of this information without the need for tedious data preparation, parameterization, manual picking, or training labels tailored to particular sets of data.

As for the second method, the user must input their fault labels from the particular dataset of interest, which employs a user-supervised model. Since it was only trained on the relevant dataset, this could increase the prediction's quality. In comparison to the first pre-trained approach, this supervised method relies on minimum interpreter labeling however could produces a more accurate fault prediction. To perform better than humans, the traditional Deep-Neural-Network-Based categorization schema typically needs a lot of training data. One of the key difficulties was that the workflow's principal goal was to execute tasks with the least amount of human intervention possible. The machine can usually be trained with just a handful of lines.

During the exploration stage whereby time is essential and information is limited, the pre-train model can provide preliminary ideas about the area's fault structure system. Then, combined with geological understanding and minimum interpretation guidelines, the user-trained model will deliver the completed fault model within days or weeks, instead of weeks or months previously.

In the development stage, especially when planning for infilled wells, re-interpreting the existing data is always considered. However, human bias will eventually lead to the same output, or low data quality of interpretation. Leveraging ML to get the data-driven output will provide better outcomes and a different perspective for interpreters. In addition, if there are limited resources available for this re-interpreting study, ML will help to reduce time significantly.

Currently, the majority of workflows for autonomous fault identification and extraction include these four steps:

- Seismic conditioning or filtering to improve signal-to-noise (SNR) ratio.
- Edge detection based on one or combined (multi-scale) seismic attributes.
- Edge enhancement.
- Fault patches/surfaces extraction.

The quality of the seismic data typically affects the first two phases. The faults may be selected directly from the edge attribute set if they are well-imaged on the seismic volume. However, preconditioning the seismic and adjusting the resulting edge attributes to the needs of the interpretation will be more difficult with a low-quality seismic image. A common trade-off is between gaining detail and decreasing SNR. To help shorten the time needed for this stage, the Petrel ML method often does not require any preconditioning.

Moving to Machine-Learning Assisted Horizon Interpretation, the idea behind this approach is a semi-automated method. Users can submit single points, or a continuous horizon reflection pick of the training data as labelled seismic reflection events. The prediction from the ML model is used to detect high confidence, and the ML model is generated using labels. Users can produce a confidence cube based on how closely it resembles QC.

An overview of the Horizon prediction workflow is provided below to illustrate the concept. However, depending on the model quality value, the procedure may go through numerous rounds to meet the value. When it's done, the algorithm can continue with ML-Based Horizon Prediction by lowering the model quality value or by adding more labels to the same horizon interpretation.

In further detail, the algorithm learns the pattern while tracking and makes use of Radial Basis Functions (RBF). It utilizes pattern recognition in the same trace that labels are used. By analyzing neighboring values in a vertical direction and determining the confidence score values for additional expansion, it broadens a horizon.

The Neural Network is executed once the label has accumulated sufficient training data to create a more reliable model. In contrast to Radial Basis Functions, which learn patterns, Neural Net weights store class information. For training and later for prediction, the algorithm feeds the selected training data into one of the models. The iterative procedure comes to an end when it reaches the model quality value that reduces the chance of tracing the incorrect event. When tracking needs to be stopped or continued, it might be utilized as a signal.

The production of anticipated horizon interpretation can be supported by the fault attribute cube produced by the preceding ML stage. A horizon interpretation and confidence score cubes are this method's outputs.

Only one waveform may be tracked at a time by conventional waveform trackers, which rely on cross-correlation. Additionally, the settings may be overly convoluted when a horizon prediction method based on ML can track numerous waveforms simultaneously. It is more effective at extracting the particular waveform that is present around a reflector. In contrast to conventional trackers, it prevents cycle skipping. Even with the bare minimum parameters, it can produce reliable results.

Lastly, the output from both automated fault extraction and horizon using ML will be directly consumed in the structural model process without any further modification. Whether the stage of subsurface study is exploration or development, leveraging the application of ML seismic interpretation definitely helps to shorten the turnaround time, remove unnecessary manual steps and focus on the analysis of complex geological structures and validate its uncertainty.

The structure of AOI or the types of studies that the Oil and Gas industry is conducting nowadays are becoming increasingly complex and demanding a significant amount of time and resources to finish. Hundreds-to-thousands of simulation hours run continuously every day, six-to-nine months or a year of study have contributed to the release of CO_2 emission. Therefore, the assistance of Machine-Learning with significant time saving not only supports the reduction of CO_2 but also provides a more accurate structural model and allows various scenarios analysis to be performed. Several studies such as (INPEX, n.d.) have shown 80% time-reduction after applying ML for Seismic Interpretation.

(C) Machine-Learning Assisted Geological Property Modeling (EMBER)

Perhaps the most often utilized method in reservoir description to date is the classification of geological features like faults using seismic data. Another interesting field is the use of Generative Adversarial Networks (GANs) for property modeling, which are based on large analogue training data sets. However, there hasn't been as much work made towards integrating geostatistical techniques with ML algorithms for property modeling. These techniques can be used to estimate and virtually realize reservoir properties like porosity and permeability. Despite being highly useful and becoming the standard for modeling reservoir features, they do require a few workarounds in real-world circumstances.

The Embedded Model Estimator (EMBER) approach uses a combination of ML and conventional geostatistical estimation and simulation methods to quickly and accurately estimate reservoir parameters. This machine learning-based method aims to generate reservoir characteristics from input well data as well as additional information such as seismic attributes/features.

EMBER produces modeling results with a significant reduction in effort compared to traditional petrophysical modelling algorithms, which rely on labor-intensive manual data analysis, including stationarity determination and factoring, trend removal, and variogram analysis per zone, region, and direction. Such cutting-edge hybrid modeling techniques can perform noticeably better than any traditional technique. Little setup time and exposure to complicated geostatistical contexts are required for the approach. It enables reservoir model construction to move along much more quickly and consistently, which has an adverse impact on field development planning.

Without running dozens of repetitive processes for each zone and/or facies as well as performing different scenarios set up to populate reservoir properties distribution, which can take many hours or days; EMBER enables 70–75% workflow steps reduction in those property modeling process, stated by many operators such as (Pertamina Hulu Mahakam, n.d.). Additionally, a 15–20% improved accuracy of reservoir properties prediction was reported. Generally, EMBER supported the acceleration of the geological property modeling process and improvement of output.

Emissions Reduction

The U.S. Department of Energy claims that buildings account for over 76% of electricity use and only about 20% of electricity comes from renewable sources. It tends to be an obvious starting point when calculating greenhouse gas emissions and carbon footprint because electricity is relatively easy to measure – and just about everyone uses it.

As the emission factor for electricity is 0.256kg of CO_{2e} per kWh, each laptop uses an average of 24k kWh per month for the standard 40 hours per month, excluding additional simulation hours, producing 6.1kg of CO_{2e}. (PlanetMark, n.d.)

In Oil & Gas subsurface reservoir characterization workflow, the simulation of hundreds and thousands of scenarios

to increase the accuracy of outputs will require machines running continuously for days, weeks, and months. Hence, contributing to the release of CO_2 emissions significantly.

Moving to a digital platform, not only helps Oil & Gas operators minimise the purchase of new laptops as longer lifecycle usage but also enables the application of AI/ML to shorten the subsurface study duration and simulation time.

According to (Sustainable Energy Development Authority Malaysia, n.d.), each hour saving equals to 0.741kg CO_2 reduction. As stated earlier, many studies have shown Machine Learning Assisted Seismic Interpretation workflow has reduced 80% processing time from 3 months to 18 days, saving up to 1728 hours and reducing 1280.448kg CO_2. (INPEX, n.d.).

Studies also reported Machine-Learning Assisted Geological Property Modeling helped to reduce 75% of workflow steps and make the process simpler and faster from 4 weeks to 4 days, saving 576 hours and reducing 426.816 kg CO_2. (Pertamina Hulu Mahakam, n.d.)

Conclusions

The Machine-Learning workflows presented in this paper have allowed us to resolve most of the common or known processing and interpretation challenges that a conventional subsurface characterization study would require tremendous effort to handle. An advantage of machine-learning methods is that they can be implemented to produce results without the need to have a complete and established reservoir model. The principal challenge of machine learning lies in attaining enough training information, which is essential in obtaining an adequate model that allows for a prediction with a high level of accuracy.

A significant time reduction from months-weeks to days-hours potentially shortens the overall subsurface evaluation timeframe with Machine-Learning applications and reduces the carbon emissions and footprint.

Acknowledgements

The authors would like to thank Dr. Le Quang Duyen from Hanoi University of Mining and Geology for his support in this publication.

We also would like to express our sincere appreciation to the SLB team for the permission to submit the content and data that used in this publication.

Literatura – References

1. ADNOC, n.d. [Online] Available at: https://www.youtube.com/watch?v=ruElQ1oInt0
2. Circular Computing, n.d. [Online] Available at: https://circularcomputing.com/news/carbon-footprint-laptop/#-Carbon%20Footprint%20During%20Production%20of%20A%20Laptop
3. INPEX, n.d. SLB Software. [Online] Available at: https://www.software.slb.com/videos/inpex-leaders-discuss-the-digital-transformation-of-ep
4. McKinsey & Company, 2020. The future is now: How oil and gas companies can decarbonize.
5. OMV, n.d. [Online] Available at: https://www.omv.com/en/news/201217-schlumberger-and-omv-announce-enterprise-deployment-of-ai-and-digital-solutions-enabled-by-the-delfi-cognitive-ep-environment
6. Pertamina Hulu Mahakam, n.d. SLB Software. [Online] Available at: https://www.slb.com/resource-library/case-study/so/Pertamina%20Hulu%20Mahakam%20utilizes%20machine%20learning%20to%20reduce%20property%20modeling
7. PlanetMark, n.d. [Online] Available at: https://www.planetmark.com/how-to-measure-the-carbon-impact-of-working-from-home/
8. Sustainable Energy Development Authority Malaysia, n.d. [Online] Available at: https://www.seda.gov.my/statistics-monitoring/co2-avoidance/
9. Woodside Energy, n.d. SLB Software. [Online] Available at: https://www.software.slb.com/videos/schlumberger-announces-enterprise-wide-deployment-of-delfi-environment-for-woodside-energy
10. Thuy Nguyen Thi Thanh et al., EAGE Conference on Digital Innovation for a Sustainable Future, 13-15 September 2022, Bangkok. Available at: Reinventing Digital Subsurface of Operator through DELFI PTS cloud digital solution at Enterprise Scale | Earthdoc
11. Joy Ugoyah and Anita Mary Igbine (2021), University of Port Harcourt, SPE-207152. Available at: Applications of AI and Data-Driven Modeling in Energy Production and Marketing Processes | Request PDF (researchgate.net)

Other Case Studies Avaialble at:

1. Redefining seismic interpretation - Machine learning for fault interpretation, enhancing efficiency, accuracy and auditability through a cloud-based approach
2. Accelerating seismic fault and stratigraphy interpretation with deep CNNs: A case study of the Taranaki Basin, New Zealand
3. Application of Machine Learning-Assisted Fault Interpretation on Large Carbonate Field with Subtle Throws
4. Large Fault Extraction Using Point Cloud Approach to a Seismic Enhanced Discontinuity Cube
5. Redefining seismic interpretation: Enhancing fault interpretation efficiency and accuracy with Deep Convolutional Neural Network and elastic cloud compute
6. [2011.05561] An application of an Embedded Model Estimator to a synthetic non-stationary reservoir model with multiple secondary variables (arxiv.org)
7. Tight Integration of Decision Forests into Geostatistical Modelling | Earthdoc
8. Walawska B., Szymanek A, The effect of structure modification of sodium compounds on the efficiency in removing SO2 and HCl from fumes in the conditions of circulating fluid bed, Chemical and Biochemical Engineering Quarterly 31 (3) 261–273 (2017)
9. Szymanek A., Nowak W. Mechanically activated limestone, Chemical and process engineering, 28,127-137, 2007. ISSN0208-6425 IF 0,394
10. Szymanek A., de las Obras-Loscertales M., Pajdak A.Effect of sorbent reactivity on flue gas desulphurization in fluidized-bed boilers under air firing mode. The Canadian Journal of Chemical Engineering, Volume 96, April 2018, 895-902

Effectiveness of a Mobile Application-Based Intervention to Improve Knowledge and Practice Regarding Silicosis Among High-Risk Workers of Dust Exposure in a Northern Province of Vietnam

Nguyen Thi THU HUYEN[1,2], Ta Thi KIM NHUNG[1], Pham Thi QUAN[2], Nguyen THANH THAO[1], Nguyen NGOC ANH[1], Nguyen Thi LIEN HUONG[2], Le Thi HUONG[1], Luong MAI ANH[3], Le Thi THANH XUAN[1]

[1] School of Preventive Medicine and Public Health, Hanoi Medical University, Hanoi, Vietnam
[2] Ministry of Health, Hanoi, Vietnam
[3] Vietnam Health Environment Management Agency, Ministry of Health, Hanoi, Vietnam
* Corresponding author: Le Thi Thanh Xuan - lethithanhxuan@hmu.edu.vn

http://doi.org/10.29227/IM-2023-02-44

Submission date: 20-08-2023 | Review date: 26-09-2023

Abstract

Objectives: to analyze changes in knowledge and practices regarding silicosis in groups of workers at high risk of silicosis before - after an intervention. Methods: The study was conducted from 2018 to 2019 based on structured questions related to knowledge and practices of silicosis of workers directly exposed to silica dust in a Northern province of Vietnam. The mobile app-based intervention was applied to steel workers, then compared with ironworkers in improvements in silicosis knowledge and practices. Results: Significant changes in the intervention group related to workers' knowledge about the signs suggestive of silicosis, disease consequences, measures to reduce the risk of silicosis, and participation in annual occupational disease examinations were reported. Conclusion: Mobile application-based interventions could improve silicosis knowledge and practice among workers at high risk of exposure to silica dust.

Keywords: *knowledge, practice, workers, silicosis, mobile application, effectiveness*

1. Introduction

According to the World Health Organization, silicosis is one of the oldest occupational diseases. The prevalence of silicosis among workers exposed to dust in developing countries was about 20–50% [1]. In Vietnam, silicosis has been diagnosed in Vietnam since 1976, accounting for 88% of all cases of an occupational disease diagnosed in Vietnam during the period 1976–1997 [2, 3]. According to a recent report by the Vietnam Health Environment Management Agency, silicosis is still one of the most common occupational diseases in Vietnam and has not tended to decrease [4]. During the period 2018–2019, a study was conducted in five provinces of Vietnam on workers at high risk of exposure to silica dust, and study results showed that the rate of workers participating in the study with silicosis was 12.27% [5]. Workers in the construction materials, mining, and metallurgy industries are often exposed to adverse factors such as silica dust, which has adverse effects on health [6, 7, 8, 9]. Currently, there is no specific treatment for silicosis, and thousands of people has died every year because of this disease. However, silicosis is a preventable disease by improving workers' knowledge about the disease. In the world, at present, there are only a few studies on the knowledge and practice of workers about silicosis, typically a study conducted in South Africa showed that the percentage of workers with correct knowledge about silicosis was 20.7% [10]. In Vietnam, a research by Le Thi Thanh Xuan and Le Thi Huong (2018) showed that 44.3% of workers did not know the signs of silicosis, and 31.5% of tuberculosis did not know the consequences of this disease. The percentage of employees complying with occupational disease prevention measures was still limited. The rate of workers having annual medical examinations was 66.6%, compliance with occupational hygiene was 64.7%, and annual occupational disease examinations were 39.1% [11, 12] Interventional studies on the change in knowledge and practice of workers were largely lacking. In recent decades, the use of mobile technology including mobile applications, text messaging, etc. to improve human health has attracted more attention. Medical applications on smartphones have developed more and more widely. These applications have various content such as drug references, medical training, and document search, supplementing knowledge for users [13, 14, 15, 16]. The development of applications for the health field has made an important contribution to maintaining or improving people's healthy behaviors, quality of life, and well-being [17]. These mobile-based intervention studies have assisted people in the management of many chronic diseases through improved knowledge and associated risk behaviors [18, 19, 20, 21, 22, 23, 24, 25].

Thai Nguyen province which is a province in the North of Vietnam has abundant mineral resources. Therefore, Thai Nguyen province has a great advantage in developing metallurgical and mining industries. These industries have attracted thousands of workers. However, these manufacturing industries also generate a large amount of silica dust in the working environment. The top concern of managers is the health of workers, including silicosis. Currently, there is no intervention study to change the knowledge and practice of workers about silicosis in Thai Nguyen province. Therefore, the study was conducted to evaluate the effectiveness of mobile application-based intervention in improving knowledge

Tab. 1. Demographic characteristics of study subjects

Characteristics		Steel factory (n=309)		Iron factory (n=356)		Total (n=665)	
		n	%	n	%	n	%
Gender	Male	286	92.6	276	77.5	562	84.5
	Female	23	7.4	80	22.5	103	15.5
Age group (years)	20 – 29 years	64	20.7	49	13.8	113	17.0
	30 – 39 years	157	50.8	165	46.3	322	48.4
	40 – 49 years	64	20.7	110	30.9	174	26.2
	≥ 50 years	24	7.8	32	9.0	56	8.4
	$\bar{X}$ ± SD (min; max)	36.0 ± 7.7 (22; 59)		38.1 ± 7.8 (22; 55)		37.2 ± 7.8 (22; 59)	
Education level	Under high school	3	1.0	9	2.6	12	1.7
	High school	58	18.8	53	14.9	111	16.7
	Technical/vocational school	120	38.8	160	44.9	280	42.2
	College/university	128	41.4	134	37.6	262	39.4
Silica exposure time	< 10 năm	155	50.2	129	36.2	284	42.7
	10 – 19 năm	114	36.9	117	32.9	231	34.7
	≥ 20 năm	40	12.9	110	30.9	150	22.6
	$\bar{X}$ ± SD (min; max)	11.0 ± 8.2 (1; 39)		14.0 ± 8.7 (1; 36)		12.6 ± 8.6 (1; 39)	

and practice on silicosis of workers at high risk of exposure to silica dust in the North of Vietnam. The research results provided evidence for the authorities and businesses to make appropriate policies and programs to prevent silicosis for workers at high risk of exposure to silica dust.

2. Materials and Methods

2.1. Study Setting and Participants

A study was conducted from 2018 to 2019 at two factories that generated silica dust in the working environment in Thai Nguyen province. The study was conducted in 3 stages:

(1) Stage 1: an assessment of the knowledge and practice regarding the silicosis of workers in the two factories before the intervention was carried out in December 2018.

(2) Stage 2: the development and application of interventions at the factory were carried out from January 2019 to December 2019.

(3) Stage 3: assessing workers' change in knowledge and practice about silicosis post-intervention in December 2019. The effectiveness of the mobile application-based intervention was evaluated.

Eligible criteria for selecting participants were as follows: (1) workers who were directly exposed to silica dust while working, (2) working time at the factory at least 1 year or above, (3) consenting and participating fully in the study, (4) have a smartphone to access the intervention application on the phone. Exclusion criteria included the participants refusing to participate by signing an informed consent form.

2.2. Sample and Sampling

The following formula was used for calculating the sample size in the study:

$$n = \frac{Z^2_{(1-\alpha/2)}.p.(1-p)}{d^2}$$

Where n is the minimum sample size, Z(1-α/2) = 1,96 (α=0,05) is the statistic corresponding to a level of confidence (95%), p = 0,13 (the proportion of workers in the mining sector exposed to silica dust and suffering from silicosis – according to study result by Le Thi Hang 2007) [26]; and d = 0.03 is precision (corresponding to effect size). A minimum sample size of 600 can be calculated.

In fact, before the intervention, research recruited 667 participants, including 309 employees of the Steel factory (out of a total of 352 employees of the steel factory) and 358 employees of the Iron Factory (out of the total of 403 workers of the iron factory). In post-intervention, 665 workers were participating in the study (309 employees of the Steel Factory and 356 employees of the Iron Factory), because there were 2 workers of the Iron factory who did not participate in the post-intervention survey. Thus, the sample size of the study for analysis in this study was 665 workers.

2.3. Intervention package

a) Intervention group

Based on the baseline survey results, the Steel Factory had a higher rate of workers suffering from silicosis than the Iron Factory (11.7% compared with 10.1%). Besides, the percentage of workers in the Steel Factory who had correct knowledge of the signs and symptoms of silicosis and its consequences was lower than this rate in the Iron Factory. In addition, we also received the support and commitment to willingly participate in the research of the Steel Factory's Board of Directors. Therefore, we conducted an intervention at the Steel Factory (Intervention group).

The "VIHEMA Survey" application on smartphones had been developed by researchers, experts, and engineers from the Vietnam Health Environment Management Agency to provide information on silicosis. The application was available on both Android and iOS platforms.

The application consists of two main parts: Part 1: providing knowledge related to silicosis, including 4 main contents: (1) legal documents related to silicosis, (2) information about causes of silicosis, (3) signs and symptoms suggestive diagnosis of silicosis, (4) measures prevented silicosis. Part 2: providing questions to assess the level of knowledge and practice of workers related to silicosis.

Tab. 2. Intervention effectiveness on knowledge regarding silicosis (i-group: intervention group; c-group: control group); * The effectiveness of the intervention decreased (between the intervention group and the control group)

Variables	Intervention group (n=309)		Control group (n=356)		Efficiency indicators		Effectiveness (%)	p-value (i-group/ c-group)
	Baseline (%)	4 months (%)	Baseline (%)	4 months (%)	i-group (%)	c-group (%)		
Signs and symptoms of silicosis								
Cough	55.7	70.9	61.2	64.2	27.3	4.9	22.4	< 0.001
p-value	< 0.001		0.15					
Sputum	45.0	56.6	47.8	55.6	25.8	16.3	9.5	< 0.001
p-value	< 0.01		< 0.001					
Chest pain	57.6	61.8	64.8	68.7	7.3	6.0	1.3	< 0.05
p-value	0.26		0.57					
Shortness of breath	59.9	61.5	65.6	63.4	2.7	3.4	0.7*	0.82
p-value	0.68		0.12					
Fever	22.7	28.2	27.1	29.3	24.2	8.1	16.1	< 0.01
p-value	< 0.01		0.16					
Consequences of silicosis								
Declining in health	81.2	84.8	82.1	80.2	4.4	2.3	2.1	0.76
p-value	0.23		0.45					
Increasing risk of getting other serious	33.7	45.6	36.6	43.9	35.3	19.9	15.4	< 0.001
p-value	< 0.01		< 0.01					
Declining worker power	69.9	73.5	74.0	75.1	5.2	1.5	3.7	0.28
p-value	0.27		0.68					
Reducing labor income	39.5	57.9	44.4	46.6	46.6	5.0	41.6	< 0.001
p-value	< 0.001		0.36					
Preventing silicosis								
Wearing mask	78.0	89.0	76.3	70.7	14.1	7.3	6.8	0.22
p-value	< 0.01		< 0.01					
Wearing protective clothes at the worksite	41.4	42.7	36.9	42.2	3.1	14.4	11.2*	0.02
p-value	0.64		< 0.001					
Providing periodic medical examinations	57.9	64.4	52.2	55.6	11.2	6.5	4.7	0.01
p-value	0.09		0.01					
Providing periodic occupational medical examinations	54.0	62.1	49.4	51.4	15.0	4.0	11.0	< 0.01
p-value	0.02		0.09					
Occupational health and safety compliance	63.4	68.6	60.1	62.8	8.2	4.5	3.7	0.02
p-value	0.13		0.01					

The intervention program was implemented in 4 months, from August 2019 to November 2019. Each participant was provided an account and password to access the application. To manage participants' compliance with a mobile app-based intervention, we monitored the frequency of application visited every 2 weeks for the first month and fed back to the users with an audio notification on the application reminding the users to access the application.

b) Control group

The subjects in the control group which was at the Iron factory received only conventional education through periodic factory training sessions (Control group).

2.4. Instruments and Measures

Research subjects were interviewed directly through a pre-designed closed-ended structured questionnaire based on Circular 15/2016/BYT of the Ministry of Health on covered occupational diseases [2]. The questionnaire also referenced the questionnaire of the study on knowledge and attitudes about silicosis in South Africa [10]. The questionnaire focused on the demographic characteristics of the study subjects; the knowledge and practice of workers about silicosis. Most of the questions were used as closed-ended questions with two options namely "Yes" and "No" for each question. By evaluating the improvement of workers' knowledge and practice about silicosis, the research team determined the effectiveness of a mobile app-based intervention for workers exposed to silica dust at work.

2.5. Statistical analysis

Data were analyzed on Stata software version 14.0. Descriptive statistics were applied to present the frequency, percentage of complete knowledge, and appropriate practice of the study subjects related to silicosis. The effectiveness of the intervention was assessed through efficiency indicators (comparison pre and post-intervention to see changes in knowledge and practice regardings silicosis).

2.6. Ethical Consideration

The study was approved by The Hanoi Medical University Review Board (No.42/BB HDDD DHYHN on October 31st, 2018), and the study adhered to the principles of the Declaration of Helsinki. All participants signed a written informed

Tab. 3. Intervention effectiveness on practices related to silicosis (i-group: intervention group; c-group: control group); * The effectiveness of the intervention decreased (between the intervention group and the control group)

Silicosis prevention practices	Intervention group (n=309)		Control group (n=356)		Efficiency indicators		Effectiveness (%)	p-value (i-group/c-group)
	Baseline (%)	4 months (%)	Baseline (%)	4 months (%)	i-group (%)	c-group (%)		
Using Personal Protective Equipment (PPE)								
Hard hat	98.7	98.1	96.6	94.4	0.6	2.3	1.7*	< 0.05
p-value	0.53		< 0.05					
Safety shoes	96.4	96.4	95.5	95.3	0.0	0.2	0.2*	0.83
p-value	-		0.81					
Mask	100.0	100.0	100.0	100.0	0.0	0.0	-	-
p-value	-		-					
Gloves	98.4	97.7	96.1	97.2	0.7	1.1	0.4*	0.62
p-value	0.48		0.16					
Protective clothes	99.4	98.7	97.8	97.2	0.7	0.6	0.1	0.21
p-value	0.32		0.41					
Safety glasses	75.4	70.2	51.7	46.9	6.9	9.3	2.4*	< 0.001
p-value	0.03		< 0.01					
Personal measures preventing silicosis								
Periodic medical examinations	80.3	83.5	81.3	82.7	4.0	1.7	2.3	0.18
p-value	0.23		0.49					
Periodic occupational medical examinations	68.9	83.8	58.7	60.9	21.6	3.7	17.9	< 0.001
p-value	< 0.001		0.37					
Compliance with occupational safety	83.2	90.9	81.2	81.7	9.3	0.6	8.7	0.01
p-value	<0.01		0.80					
Compliance with occupational hygiene	77.3	84.1	79.2	77.2	8.8	2.5	6.3	0.21
p-value	<0.01		0.39					
Compliance Factory Rules	71.2	76.4	72.1	73.7	7.3	2.2	5.1	0.05
p-value	0.03		0.48					

consent form for their willingness to participate. The research problem did not affect the health or other problems of the subject. The information collected from the subjects is for research purposes only.

3. Results

The majority of participants were male (accounting for 84.5%). The proportion of male workers in steel mills was 92.6%, and this rate in iron factories was 77.5%. The respondents were mainly the 30–39 years old group (48.4%) and had a technical/vocational school education level of 42.2%. The average age of participants in the steel factory and iron factory was 11.0 years and 14.0 years, respectively. However, participants in the age group of fewer than 10 years accounted for the majority in both factories (50.2% and 36.2% respectively, table 1).

Table 2 presents intervention effectiveness on knowledge regarding silicosis. In the group of workers receiving the intervention, the percentage of workers whom correctly knowledge the signs and symptoms of silicosis (cough, sputum, fever) and the consequences of silicosis (increased risk of other diseases and reduced labor income) increased compared with pre-intervention ($p<0.05$).

Compared with the control group, the percentage of workers in the intervention group correctly knowledge the signs and symptoms of silicosis (such as cough, sputum, chest pain, and fever) and the consequences of silicosis (such as the increased risk of other diseases, reduced labor income) increased significantly after the intervention ($p < 0.01$). Intervention effectiveness on the knowledge about signs/symptoms and consequences of silicosis increased (ranging from 1.3–41.6%). The percentage of workers in the intervention group who had proper knowledge regarding preventing silicosis (such as wearing protective clothing at the worksite, providing periodic medical examinations, and annual occupational medical examinations, and compliance with occupational health and safety) increased significantly in post-intervention ($p<0.01$). Intervention effectiveness in preventing silicosis knowledge increased (ranging from 3.7–11.0%).

Table 3 illustrates the changes in practices related to silicosis among our study participants. The percentage of respondents wearing masks at the workplace reached 100% in both groups.

Compared with the control group, in the intervention group, the percentage of participants using glasses at the worksite decreased significantly ($p<0.05$) and the intervention effectiveness on wearing glasses decreased (2.4%).

Table 3 showed that the percentage of participants in the intervention group who performed annual occupational medical examinations, compliance with occupational safety, occupational hygiene, and factory rules to prevent silicosis increased significantly ($p<0.05$). Compared with the control group, the percentage of participants in the intervention group who performed annual occupational medical examinations increased significantly after the intervention ($p<0.001$), and the intervention effectiveness increased (17.9%). The per-

centage of respondents in the intervention group who complied with occupational safety increased significantly and the intervention effectiveness increased by 8.7%.

4. Discussion

The study was an initial survey in Vietnam to assess the effectiveness of mobile application-based interventions in improving workers' knowledge and practice of silicosis. The study results showed that the mobile application could contribute to improving the knowledge and practice of participants regarding silicosis, which in turn could contribute to preventing this disease. The study was implemented at 02 factories with a total of 665 participants, including 309 workers at the Steel Mills and 356 workers at the Iron Factory. These were two factories with full characteristics of the metallurgical industry in Thai Nguyen. The production process at the two factories generated many harmful occupational factors such as dust, noise, adverse microclimate, restrictive working posture, and especially silica dust in the labor environment.

Most of the study participants were male. This might be due to the specific working conditions of the metallurgical industry, which was hard labor, so it needed mainly male workers. The study results were similar to the other authors' research results [27, 28, 29, 30]

The workers in our study mainly had higher education levels than those in some factories with typical hard labor characteristics. In the study of the authors Souza T.P., Gizaw Z., and Ferrante G. the majority of workers had a high school education or less [31, 32, 33]. With such a level of education, workers living in two factories have a background in absorbing new knowledge faster.

Workers at the two factories had almost no change in the workplace since starting work. Therefore, the working age was generally calculated as the time from the beginning of working at the factory to the time of doing the study. In addition, we aimed to exploit both workers' other work and the time working exposed to silica dust before working at the two present factories. The purpose of this action was to accurately calculate a worker's exposure to silica dust. However, the workers involved in this study had never worked in jobs that were exposed to silica dust. The average age of workers in the two factories was lower than that of workers in the Souza T.P. study (20.4 ± 12.8 years) [31].

The baseline assessment showed that the percentage of workers in the Steel factory correctly knowledge the signs and symptoms of silicosis (cough, sputum, chest pain, shortness of breath, fever) and the consequences of silicosis (declined in health, declined worker power, decreased in labor income) were lower than in the Iron Factory. Therefore, the study conducted intervention on workers of Steel factory.

Currently, the number of smartphone users was becoming larger and large. The age of users has also expanded, including young people as well as the elderly. According to data provided by Statista, by the end of 2020, 78.05% of the world's population used smartphones [34]. Many studies around the world have recorded the positive effect of the intervention methods based on mobile technology in improving the knowledge, attitude, and practice of the research subjects. These mobile-based intervention studies have helped study subjects to improve their risk behaviors, manage, and prevent a variety of chronic diseases [18, 19, 20, 21, 22, 23, 24, 25]. When comparing interventions by mobile technology, the use of intervention as a communication application brought more advantages such as intervention information being stored and continuously updated on the communication application. This helped the intervention subjects to review regularly the content related to the research topic. In addition, we also integrated images and videos related to research topics into the application that text messages cannot deliver. This supported well the subjects participating in the research.

In the pre-intervention, the percentage of study participants who knew about the signs suggestive of silicosis such as cough, sputum, chest pain, shortness of breath, and fever ranged from 22.7% to 65.6%. These results were different from the results in the Indian study of Nandi S [35]. This difference can be explained by the different study populations. This result also suggested that we needed to improve the knowledge of workers regarding the signs and symptoms of silicosis. After the intervention, the percentage of participants who had correct knowledge about the signs and symptoms of silicosis increased. The rate of respondents knowing that cough was a symptom suggestive of silicosis increased from 55.7% to 70.9% after the intervention ($p<0.05$). The percentage of participants who knew that sputum was a symptom suggestive of silicosis increased from 45.0% to 56.6% after the intervention ($p<0.05$). Compared with the control group, the percentage of workers who knew about the signs and symptoms suggesting silicosis increased, and the intervention effectiveness increased significantly from 1.3% to 22.4% ($p<0.05$). In our opinion, this improvement had helped workers to proactively detect the disease early. When workers have had such signs and symptoms, they could go to the hospital earlier to screen for disease and prompt treatment.

Regarding the knowledge of the consequences of silicosis, declining health accounted for the highest rate, followed by declining worker power and income reduction. This result was higher than the research results of the author Phan Thi Mai Huong and the author Le Thi Thanh Xuan [11, 36]. These consequences caused disease burden as well as economic effects for individuals, families, and society. In this study, the percentage of workers in the intervention group whom correctly knowledge the consequences of silicosis increased. Compared with the control group, the effectiveness of the intervention increased, ranging from 2.1% to 41.6%. In which, the percentage of workers who correctly knew silicosis increased the risk of other diseases (from 33.7% to 45.6%) and reduced the workers' income (from 39.5% to 57.9%) increased significantly after the intervention ($p<0.001$). Our findings on positive changes in knowledge among study participants may help high-risk workers would have positive changes in attitudes and practices to prevent diseases.

If the workers did not know about the signs and symptoms of silicosis and the consequences of the disease, the workers would have a subjective attitude when preventing the disease. Therefore, the study should enhance knowledge about signs, symptoms, and consequences for these workers. This result suggested that we come up with specific and appropriate interventions for the study.

Regarding measures to prevent silicosis, the majority of participants knew that wearing a mask, compliance with oc-

cupational safety and health, annual health examination, and annual occupational medical examination could prevent silicosis. Our study gave better results than the results of other authors [10, 35]. The two factories in this study might have included these contents in the periodic occupational safety and health training, so the subjects in the study might have better knowledge than other researchAlthough occupational medical examination was the earliest method to detect silicosis, only about half of the workers participating in the study knew about this method. This rate suggested that we needed to coordinate with the two factories to improve the knowledge of employees about methods to detect silicosis early, especially annual occupational medical examinations. After the intervention, our study had positive results on this issue. The percentage of employees who were correctly knowledge about measures to reduce the risk of silicosis increased post-intervention. In which, the percentage of workers who knew that wearing a mask is an effective measure to prevent silicosis increased significantly after the intervention (from 78.0% to 89.0%) ($p<0.01$). The efficiency indicators in the intervention group increased from 3.1% to 15.0% and the intervention effectiveness increased (ranging from 4.7% to 11.0%) ($p<0.05$).

In the intervention group, the percentage of employees participating in annual health check-ups increased from 80.3% to 83.5%. In particular, the percentage of employees participating in annual occupational medical examinations increased significantly from 68.9% to 83.8%, the intervention efficiency increased by 17.9% ($p<0.001$). The rate of employees complying with occupational safety increased statistically significantly from 83.2% to 90.9% after the intervention and the effectiveness increased by 8.7% ($p<0.05$). The rate of employees complying with occupational hygiene increased significantly from 77.3% to 84.1% after the intervention ($p<0.01$) and the intervention effectiveness increased by 6.3%. The rate of employees complying with factory rules increased from 71.2% to 76.4% ($p<0.05$) and the intervention effectiveness increased by 5.1%.

The study had some limitations that needed to solve in other studies. Firstly, research on the knowledge and practice of workers about silicosis in Vietnam was rare. Therefore, the questionnaire might not fully reflect the purpose and objectives of the study. Secondly, the study used mobile application-based intervention, which would make it difficult for some elderly workers to use the application.

Despite the above limitations, the research results showed that the mobile application-based intervention had changed the knowledge and practice of the study subjects in preventing silicosis. This brought certain effects on employees. The research results also showed that the responsibility to prevent silicosis was not only the employers but also the employees.

5. Conclusions

Mobile application-based interventions could contribute to improving participants' knowledge and practices regarding silicosis. Therefore, factories should apply and extend mobile health applications as a measure of workplace health promotion and drive workers to adopt the use of mobile health applications.

Knowledge of workers about signs and symptoms of silicosis (cough, sputum, chest pain, fever), consequences of silicosis (increased risk of getting other serious, reduced labor income), and measures to prevent silicosis (periodic health examination, annual occupational medical examination, compliance with occupational safety and health) had improved markedly after the intervention. The percentage of workers wearing masks at the workplace reached 100% in both groups. The percentage of workers participating in annual occupational medical examinations increased significantly (intervention effectiveness increased by 17.9%).

Declarations

Acknowledgments: We would like to thank Professor. Le Thi Huong, Head of the School of Preventive Medicine and Public Health, at Hanoi Medical University, allowed us to participate in this research.

Consent to participate: A consent form was sent to participants before the study was conducted.

Ethics approval: Subjects were adequately informed about the purpose of the study and participated voluntarily. The research problem did not affect the health or other problems of the subject. The information collected from the subjects is for research purposes only.

Availability of data and materials: Data are available from the corresponding author upon reasonable request.

Competing Interest: All authors declare no conflict of interest.

Funding: This research received no external funding.

Authors' Contributions: Conceptualization, H.T.T.N, N.T.K.T, X.T.T.L; data curation, H.T.T.N, N.T.K.T, Q.T.P, T.T.N, A.N.N, H.T.L.N, H.T.L, A.M.L and X.T.T.L; formal analysis, H.T.T.N, N.T.K.T, X.T.T.L; investigation, H.T.T.N, X.T.T.L, N.T.K.T, Q.T.P, T.T.N, A.N.N, H.T.L.N, H.T.L, A.M.L; methodology, X.T.T.L., H.T.T.N, N.T.T.K, Q.T.P, H.T.L; project administration and supervision, X.T.T.L., H.T.T.N, Q.T.P, N.T.K.T, T.T.N, A.N.N, H.T.L,; visualization, H.T.T.N, X.T.T.L., H.T.L; writing original draft, H.T.T.N, X.T.T.L., N.T.K.T; writing, reviewing & editing, H.T.T.N, N.T.K.T, Q.T.P, T.T.N, A.N.N, H.T.L.N, H.T.L, A.M.L and X.T.T.L. All authors commented on previous versions of the manuscript. All authors read and approved the final manuscript.

Consent for publication: Not applicable

Literatura – References

1. Churchyard G.J., Ehrlich R., WaterNaude J.M., et al. 2004. Silicosis prevalence and exposure-response relations in South African goldminers. Occupational and environmental medicine. 2004;61(10):811-816. doi:10.1136/oem.2003.010967
2. Vietnam Ministry of Health. Circular 15/2016/TT-BYT: Regulations on occupational diseases covered by social insurance. 2016
3. Tran Thi Ngoc Lan, Phan Hong Son, Le Van Trung, et al. 2003. Distribution of Silica- exposed Workers by Province and Industry in Viet Nam. Int Arch Occup Environ Health. 2003;9:128–133.
4. Nguyen Khac Hai. 2006. Orientation of occupational medicine activities in Vietnam in 2006 - 2010. The 3rd Scientific Conference on Occupational Medicine.
5. Huyen Thi Thu Nguyen HTL, Huong Thi Lien Nguyen, Quan Thi Pham, Duy Van Khuong, Anh Ngoc Nguyen, Nguyen Tran Nhu, Thao Thanh Nguyen, Doanh Quoc Nguyen, Huong Thi Mai Phan, Nhung Thi Kim Ta, Anh Mai Luong, Xuan Thi Thanh Le. 2020. Silicosis prevalence and associated factors among high-risk population group in Vietnam in 2018-2019. Lecture Notes in Civil Engineering. 2020;1(LNCE 109):453-468.
6. Trinh Cong Tuan. 2016. Situation of Silicosis at some mining, stone processing and construction material production in Binh Dinh province in 2016.(In Vietnamese)
7. Le Thi Hang. 2007. Study on epidemiological characteristics of silicosis in construction material production workers and effectiveness of interventions. Vietnam Military Medical Academy. Doctoral thesis.
8. Dao Xuan Vinh, Truong Viet Dung and Le Thi Hang. 2006. Incidence, incidence index and some related factors of silicosis in construction material production workers. Journal of Practical Medicine. 2006;555(10):72 - 74. (In Vietnamese)
9. Ta Thi Kim Nhung, Nguyen Ngoc Anh, Le Thi Thanh Xuan, et al. 2019. Situation of silicosis among workers in an Iron factory and some related factors in 2018. Vietnam Medical Journal. 2019;478:96-100. (In Vietnamese)
10. Select Research (Pvt) LTD. 2017. Knowledge, Attitudes and Practises (KAP) on TB, HIV and Silicosis Among Key Populations Aged 15 and 59 years in Southern Africa.
11. Le Thi Thanh Xuan, Le Thi Huong, Khuong Van Duy, et al. 2019. Knowledge and attitude of workers about silicosis at a company in Hai Duong province in 2018. Vietnam Medical Journal. 2019;484(1 - tháng 11):92-96. (In Vietnamese)
12. Le Thi Huong, Le Thi Thanh Xuan, Khuong Van Duy, et al. 2019. Practice of workers at a company in Hai Duong province on prevention of silicosis in 2018. Vietnam Medical Journal. 2019;483(2 - tháng 10) (In Vietnamese)
13. I Illiger K., Hupka M., von Jan U., et al. 2014. Mobile technologies: expectancy, usage, and acceptance of clinical staff and patients at a university medical center. JMIR Mhealth Uhealth. Oct 21 2014;2(4):e42. doi:10.2196/mhealth.3799
14. Payne K.B., Wharrad H. and Watts K. 2012. Smartphone and medical related App use among medical students and junior doctors in the United Kingdom (UK): a regional survey. BMC Med Inform Decis Mak. Oct 30 2012;12:121. doi:10.1186/1472-6947-12-121
15. Johnson A.C., El Hajj S.C., Perret J.N., et al. 2015. Smartphones in medicine: emerging practices in an academic medical center. J Med Syst. Jan 2015;39(1):164. doi:10.1007/s10916-014-0164-4
16. Ventola CL. 2014. Mobile devices and apps for health care professionals: uses and benefits. P T. May 2014;39(5):356-64.
17. Gazdecki A. 9 Mobile Technology Trends For 2017 (Infographic). Accessed 12August2022, https://www.bizness-apps.com/blog/mobile-technology-trends/
18. Duong Van Tu, Dao Thi Dung, Tong Thi Hong Nhung, et al. 2022. Intervention effectiveness using mobile text messages to improve knowledge, attitudes and practices of parents in dental health care for 3-year-old children in some public preschools in Ha Nam province. Journal of Community Medicine. 2022;63(1):106-111.
19. Haghighinejad H., Liaghat L., Malekpour F., et al. 2022. Comparing the effects of SMS-based education with group-based education and control group on diabetes management: a randomized educational program. BMC Prim Care. Aug 19 2022;23(1):209. doi:10.1186/s12875-022-01820-w
20. Yao P., Fu R., Craig Rushing S., et al. 2018. Texting 4 Sexual Health: Improving Attitudes, Intention, and Behavior Among American Indian and Alaska Native Youth. Health Promot Pract. Nov 2018;19(6):833-843. doi:10.1177/1524839918761872
21. Liao Y., Wang Y., Tang J., et al. 2022. Predictors of long-term abstinence in a randomized controlled trial of smoking cessation by mobile phone text messaging ('Happy Quit') in China. Tob Prev Cessat. 2022;8:31. doi:10.18332/tpc/152255

22. Cucciniello M., Petracca F., Ciani O., et al. 2021. Development features and study characteristics of mobile health apps in the management of chronic conditions: a systematic review of randomised trials. NPJ Digit Med. Oct 5 2021;4(1):144. doi:10.1038/s41746-021-00517-1

23. Chandran V.P., Balakrishnan A., Rashid M., et al. 2022. Mobile applications in medical education: A systematic review and meta-analysis. PLoS One. 2022;17(3):e0265927. doi:10.1371/journal.pone.0265927

24. Ahmad K., Alam F., Qadir J., et al. 2022. Global User-Level Perception of COVID-19 Contact Tracing Applications: Data-Driven Approach Using Natural Language Processing. JMIR Form Res. May 11 2022;6(5):e36238. doi:10.2196/36238

25. Al Raimi A.M., Chong M.C., Tang L.Y., et al. 2022. The effect of mobile applications in enhancing asthma knowledge among school children with asthma in Malaysia. J Pediatr Nurs. Jul-Aug 2022;65:e63-e71. doi:10.1016/j.pedn.2022.02.012

26. The National Assembly of Vietnam. Law no: 84/2015/QH13: Law on Occupational Safety And Hygiene (2015).

27. Huynh Thanh Ha and Trinh Hong Lan. 2008. Survey on occupational silicosis at some construction material production facilities of Di An construction company - Binh Duong. Journal of University of Medicine and Pharmacy at Ho Chi Minh City. 2008;4(12):240 - 246. (In Vietnamese)

28. Nguyen Duc Viet. 2011. Working environment and health of workers at cement company X78 in 2010 - 2011. Hanoi Medical University; Medical Doctor Graduation Thesis.2011.

29. Vu Van Trien, Ngo Quy Chau, Bui Van Nhon, et al. 2013. Respiratory dysfunction of workers on Nhat Tan bridge construction project. Journal of Practical Medicine. 2013;886(11):28 - 30. (In Vietnamese)

30. Ta Thi Kim Nhung. 2017. Situation of health, illness and some elated factors of workers producing Supephosphate Lam Thao Company in 2017. Hanoi Medical University; Medical Doctor Graduation Thesis.

31. Souza T.P., Watte G., Gusso A.M., et al. 2017. Silicosis prevalence and risk factors in semi-precious stone mining in Brazil. Am J Ind Med. Jun 2017;60(6):529-536. doi:10.1002/ajim.22719

32. Gizaw Z., Yifred B., and Tadesse T. 2016. Chronic respiratory symptoms and associated factors among cement factory workers in Dejen town, Amhara regional state, Ethiopia, 2015. Multidiscip Respir Med. 2016;11:13. doi:10.1186/s40248-016-0043-6

33. Ferrante G., Baldissera S., and Campostrini S. 2017. Epidemiology of chronic respiratory diseases and associated factors in the adult Italian population. Eur J Public Health. Dec 1 2017;27(6):1110-1116. doi:10.1093/eurpub/ckx109

34. Statista. Number of smartphone subscriptions worldwide from 2016 to 2027. Accessed 20July-2022, https://www.statista.com/statistics/330695/number-of-smartphone-users-worldwide/

35. Nandi S., Burnase N., Barapatre A., et al. 2018. Assessment of Silicosis Awareness among Stone Mine Workers of Rajasthan State. Indian J Occup Environ Med. May-Aug 2018;22(2):97-100. doi:10.4103/ijoem.IJOEM_63_18

36. Phan Thi Mai Huong, Nguyen Ngoc Anh, Ta Thi Kim Nhung, et al. 2020. Knowledge about silicosis of workers at two companies and some related factors in Dong Nai in 2020. Journal of Medical Research. 2021;144(8):329-340. (In Vietnamese)

3D LoD3 Modeling of High Building Using Terrestrial Laser Scanning and Unmanned Aerial Vehicle: A Case Study in Halong City, Vietnam

Le Thi THU HA[1,2], Nguyen QUOC LONG[1,3]

[1] Hanoi university of Mining and Geology, 18 Vien Str., Duc Thang Ward, Hanoi 100000, Vietnam; email: lethithuha@humg.edu.vn
[2] Geomatics in Earth Sciences Research Group, Hanoi University of Mining and Geology, 18 Vien Str., Duc Thang Ward, Hanoi 100000, Vietnam
[3] Innovations for Sustainable and Responsible Mining (ISRM) Research Group, Hanoi University of Mining and Geology, 18 Vien Str., Duc Thang Ward, Hanoi 100000, Vietnam; email: nguyenquoclong@humg.edu.vn

http://doi.org/10.29227/IM-2023-02-45

Submission date: 20-08-2023 | Review date: 28-09-2023

Abstract

3D urban building models play an important role in the association, convergence and integration of economic and social urban data. 3D building reconstruction can be done from both the lidar and image-based point clouds, however, the lidar point clouds has dominated the research giving the 3D buildings reconstruction from aerial images point clouds less attention. The UAV images can be acquired at low cost, the workflow can be automated with minimal technical knowhow limitation. This promotes the necessity to understand and question to what extent the 3D buildings from UAV point clouds are complete and correct from data processing to parameter settings. This study focuses on proposing a process for building 3D geospatial data for a smart city using geospatial data collected by UAV and Terrestrial Laser Scanner. The experimental results have produced 3D geospatial data of high building in LoD3, with the root mean square error of the received test points mΔx=3.8 cm, mΔy=3.1 cm, and mΔH=7.5 cm.

Keywords: *3D LoD3 model of high building, Unmanned Aerial Vehicle (UAV), Terrestrial Laser Scanners (TLS)*

1. Introduction

Tree-dimensional geoinformation is data that describes geographic features in 3D space with a set of (x; y; z) coordinates [1]. 3D urban building models play an important role in the association, convergence and integration of economic and social urban data and have been widely used in various fields, e.g., smart cities construction, social comprehensive management, and emergency decision-making [2]. The amount of detail that is captured in a 3D model, both in terms of geometry and attributes, is collectively referred to as the level of detail (LOD), indicating how thoroughly a spatial extent has been modelled. As a result, the LOD is an essential concept in geographical information science (GIS) and 3D city modelling [3]. The CityGML 2.0 standard from the Open Geospatial Consortium (2012) defines five LODs from LOD0 to LOD4. The five LODs have become widely adopted by the stakeholders in the 3D GIS industry and they now also describe the grade and the design quality of a 3D city model, especially its geometric aspect [1].

In recent years, advanced technologies have made it possible to create precise and detailed 3D models to represent buildings as built [4]. Different data acquisition techniques are used to create the 3D object modeling, including satellite [5], airborne, unmanned aircraft systems (UAS; i.e. drones) [6,7], mobile mapping [8,9,10], ground (static), handheld devices [11,12], and crowd sensed [13]. Another viewpoint to distinguish acquisition approaches is by the type of the technology (sensors). These are most prominently: lidar, radar, camera (photogrammetry), and total stations [14,15,16].

Terrestrial laser scanner (TLS) produces high resolution point cloud of the measured object. TLS has been extensively used in precise geodetic application (e.g., 17,18,19,20). However, TLS has limitations in some applications. For example, in 3D building model applications, the area covered by the TLS is limited by the sensor line of sight. Unmanned aerial system is a cost-effective and efficient surveying tool which can capture precise images of inaccessible areas.

Meanwhile, UAV has been widely used in mapping, geoscience and scientific research applications (e.g., 21,22,23,24,25). Aerial imageries produce an overall decent 3D city models and generally suit to generate 3D model of building roof and some non-complex terrain. However, the automatically generated 3D model, from aerial imageries, generally suffers from the lack of accuracy in deriving the 3D model of road under the bridges, details under tree canopy, isolated trees, etc…[26].

Moreover, the automatically generated 3D model from aerial imageries also suffers from undulated road surfaces, non-conforming building shapes, loss of minute details like street furniture, etc. in many cases. On the other hand, laser scanned data and images taken from mobile vehicle platform can produce more detailed 3D road model, street furniture model, 3D model of details under bridge, etc. However, laser scanned data and images from mobile vehicle are not suitable to acquire detailed 3D model of tall buildings, roof tops, and so forth [27]. Our proposed approach to integrate multi sensor data compensated each other's weakness and helped to create a very detailed 3D model with better accuracy.

In this paper, we have introduced a technique to integrate two different data acquisition techniques, including terrestrial laser scanner, and unmanned aerial system. This study combines UAV and TLS technologies to collect and process data to build a highly detailed 3D model (LoD3) for the high building in Ha Long city, Quang Ninh province. The combined use of UAV and TLS technologies has proven to be possible to create

Fig. 1. Data acquisition techniques FARO FOCUS3D X130 TLS (a), and location of TLS station (b)

Tab. 1. Terrestrial laser scanner specification

Sensor	Wavelength (nm)	Maximum distance (m)	Vertical range (Deg.)	Field of View (Deg.)	Speed points/second
FARO Focus 3D X130	1550	330	270	360	976,000

Fig. 2. Data acquisition techniques DJI Phantom 4 Pro V2.0 (a), and describe the case of taking photos of high buildings (b)

a highly accurate 3D model, the 1:500 scale of urban areas according to current standards.

2. Methodology

The methodology of this study can be categorized into three phases: data acquisition, data processing, result and accuracy assessment.

2.1 Phase 1: Data acquisition

In this phase, data collection was carried out by using the UAV and the FARO FOCUS3D X130. First thing that were done are recognizing the study area and determining the flight line according to the suitable situation. Phantom 4 pro V2.0 was used to obtain the aerial images. Meanwhile, FARO FOCUS3D X130 was used to collect the ground data.

2.1.1 TLS data collection

FARO FOCUS3D X130 TLS (Fig. 1a) has been used as the main scanning system to capture point cloud data from different locations in the area of interest. During the field operation, 11 scans have been completed around the building in order to capture the details of the building and create a good overlap between the scans. (Fig. 1b), FARO FOCUS3D X130 has an integrated camera that allows the acquisition of the images needed to assign RGB values to every single point cloud. Table 1 summarizes the used TLS sensor specifications in our study.

2.1.2 UAV image acquisition

The UAS data acquisition has been performed using a low-cost DJI Phantom 4 Pro (Fig. 2a) and table 2. In order to acquire a complete coverage of the building of interest, three flights have been planned and then executed. The first flight has been performed using camera oriented in the nadir direction with flight height from 50m to 175 m above the ground and with overlap greater than 80% and side lap greater than 20% (Fig. 2b). In addition, according to the shape of the building, two circular flights with an oblique camera configuration with a lens axis inclination about – 40 degree have been planned and then executed (Fig. 3). The total acquired number of images were 875 images.

2.2 Phase 2: Data Processing

In this processing phase, it is divided into 5 parts which are stated in Figure 4.

3. Results and accuracy assessment

3.1 The study site

Phat Linh Hotel Ha Long is a 5-star luxury hotel, located at A9, Lot 1, Ha Long Marine Boulevard, Ha Long city, Quang Ninh Province (Fig.5a). Phat Linh Hotel is a tall as being at least 120 meters, continuously habitable building having 25 floors (Fig.5b).

3.2 Point clouds from TLS

The data collected from FARO FOCUS3D X130 TLS is processed using SCENE software. The data went through few steps consist of data importing, data registration and data cleaning. Coordinates of known points has already inserted in the field and eventually georeferencing part can also be skipped. Georeferencing is a process that enables to reorient the entire dataset to the corresponding coordinates of the tie

Tab. 2 Specification of DJI Phantom 4 Pro V2.0

No	Parameters	Specifications details
1	Weight (Battery & Propellers Included)	1375 g
2	Max Speed	S-mode: 45 mph (72 kph) A-mode: 36 mph (58 kph) P-mode: 31 mph (50 kph)
3	Max Flight Time	Approx. 30 minutes
4	Satellite Positioning Systems	GPS/GLONASS
5	Hover Accuracy Range	* Vertical: ±0.1 m (with Vision Positioning) ±0.5 m (with GPS Positioning) * Horizontal: ±0.3 m (with Vision Positioning) ±1.5 m (with GPS Positioning)

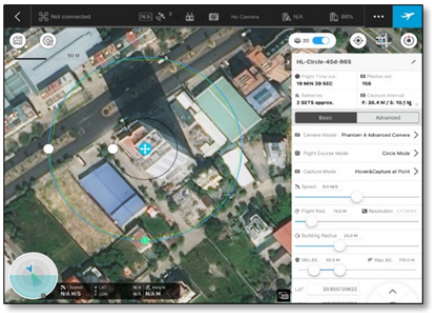

Fig. 3. Settings for UAV flying

point constraints measured using a GPS or total station with the coordinate from laser scanner. Cleaning process means user need to clean the unwanted point clouds collected during the scans. For example, trees that being scanned needs to be cleaned out from the point cloud. In this study, Autodesk Recap is used in this study to carry out the cleaning.

The processing TLS data includes steps:

1. Create project,
2. Import data of scanning stations (Import),
3. Process scan stations (Processing),
4. Merge scan stations and evaluate accuracy (Registration),
5. Create a cloud point cloud (Create point cloud), and export point cloud (Export).

With TLS data, scans are dumped in SCENE software, handling PC creation and station pairing.

The result of the processing is a point cloud as shown in Figure 7.

3.3 Point clouds from UAV

UAV image data processed on the software is Agisoft Metashape. Software Agisoft uses SfM algorithms include steps:

(1) Identify the above features image through the use of a special transformation algorithm multi-scale feature (SIFT);
(2) Matching points featured;
(3) Orientation in and out of the image;
(4) Creating dense PCs.

3.4 Integration of point clouds from UAV and TLS

The Iterative Closest Point (ICP) algorithm always converges monotonically to the nearest local minimum of a mean-square distance metric, and experience shows that the rate of convergence is rapid during the first few iterations. Therefore, given an adequate set of initial rotations and translations for a particular class of objects with a certain level of "shape complexity," one can globally minimize the mean-square distance metric over all six degrees of freedom by testing each initial registration. For example, a given "model" shape and a sensed "data" shape that represents a major portion of the model shape can be registered in minutes by testing one initial translation and a relatively small set of rotations to allow for the given level of model complexity.

One important application of this method is to register sensed data from unfixtured rigid objects with an ideal geometric model prior to shape inspection. The described method is also useful for deciding fundamental issues such as the congruence (shape equivalence) of different geometric representations as well as for estimating the motion between point sets where the correspondences are not known.

To improve the accuracy of the point cloud after merging, the ICP method is used. Before concatenation, the UAV and TLS point clouds are filtered for noise. Filter noise from point clouds to remove points of unimportant objects such as wires, trees, etc. or points that were wrong in previous processing. In addition, noise filtering also reduces the capacity of the point cloud. Because the TLS point cloud has a higher density of points and higher accuracy, it is used as the base point cloud and the UAV point cloud is the composite point cloud.

The data concatenation process consists of two steps: Coarse Alignment and Fine Alignment. In which, in the raw coupling step, it is necessary to select at least 4 duplicate points on two points cloud. This can be a focal point, a control point, or a sharp feature on two points cloud. At the exact match step, the number of points participating in the matching process increases significantly, so the data matching accu-

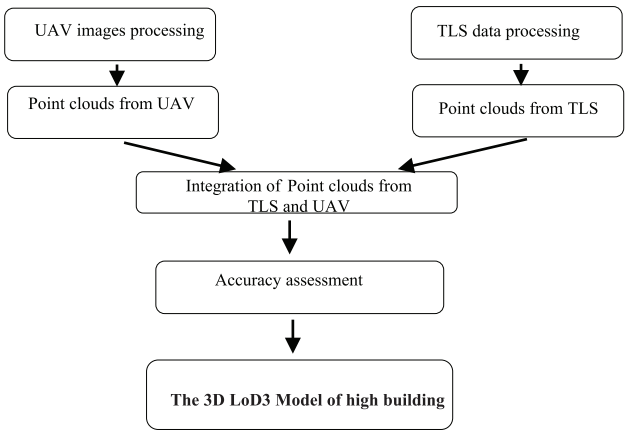

Fig. 4. Flowchart in data processing phase

Fig. 5. The study site

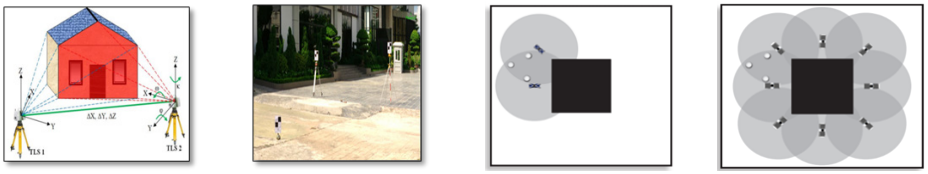

Fig. 6. How TLS work|

racy also increased and the processing time will be longer. The two steps of point cloud data concatenation are performed on Cloudcompare software (Fig. 9).

3.5 Accuracy assessment

The 8 points were used as checkpoints to check the accuracy of the integration of point clouds from UAV and TLS. The reliability of these dataset was evaluated through the value of root mean square error between the coordinates of the points on orthophoto generated and the coordinates from GPS. The lower the value of RMSE indicates a higher accuracy. The value of RMSE is shown in Table 3.

The results of the comparison between the point cloud integrating UAV and TLS technology with the point cloud built from TLS of high building (Fig. 12).

3.5 Building the 3D LoD-3 model for a high building from point clouds UAV and TLS on Sketchup Pro 2021 software.

After being satisfied with the integration result obtained, the integrated data is utilized to generate a 3D model as a final product of this study. Sketch Up software is used to build the 3D model of high building. Figure 13b shows the 3D model of high building as a final product of integration points cloud process.

Line drawings are generated from the mesh of points by using the point cloud as the basis from which geometric features are traced, and elevations at 1:500 scale (Fig. 13c)

4. Conclusion

The main purpose of integration was to produce a complete 3D LoD3 model of high building through the generation of point clouds. The integration was facilitated by the fact that the two points cloud are in the same coordinate system. In this study, the use of FARO FOCUS3D X130 TLS also facilitate in data acquisition and processing since it has the geodetic positioning advantages. Due to that, the point cloud generated from the laser scanner can be directly imported into the software for integration purposes.

Our work consisted in the evaluation of the 3D LoD3 Model of high building and the extraction of structural elements from point clouds from two technologies, namely: drone photogrammetry and terrestrial laser scanning, as well as the evaluation of the contribution of their integration.

The integration of the two sets of point clouds improves the completeness of the coverage, which allows the modeling of the complex objects of this high building. If drone oblique images are not available, we can use the TLS to capture the

Fig. 7. Point clouds from TLS data

Fig. 8. Point clouds from UAV images

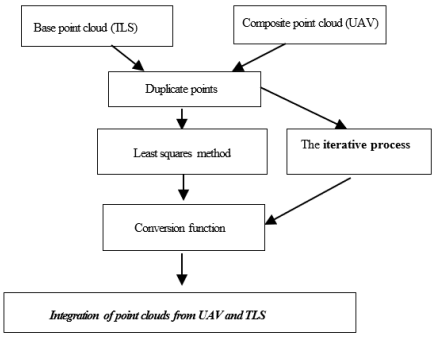

Fig. 9. Flow chart of the ICP methodology

Fig. 10. High building's TLS point cloud after noise filtering (a), High building's UAV point cloud after noise filtering (b), High building's UAV and TLS point cloud after precision matching (c)

Fig. 11. Distribution of image control points and checkpoints for high building

Tab. 3. Results of assessing the accuracy of point clouds from UAVs and TLS high buildings

No	M_x (cm)	M_y (cm)	Mp (cm)	M_h (cm)
3	-0,8	-0,8	1,1	0,9
6	0,4	-3,2	3,3	-1,7
18	4,4	-0,6	4,4	6,1
23	3,8	2,0	4,3	4.3
197	-2,3	-2,9	3,7	-0,9
203	-6,3	-1,9	6,5	-0,7
205	-5,9	-5,7	8,2	-2,4
212	-2,0	4,4	4,8	-19,5
RMSE	**3,8**	**3,1**	**5,0**	**7,5**

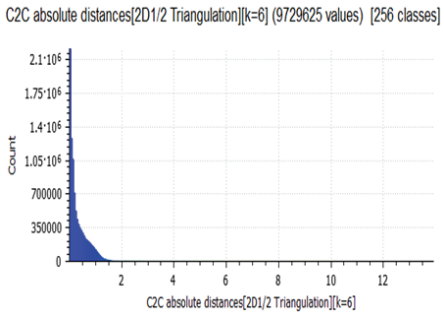

Fig. 12. Histogram of the distance between two point clouds from UAV and TLS and point cloud TLS

Fig. 13. The 3D LoD-3 model for a high building from point clouds UAV and TLS on Sketchup Pro 2021 software

facades and the drone nadir images for the roof and integrate them to have full coverage on the building.

Declarations

Acknowleagements: The article is supported data and funding from the project of the University of Mining and Geology, code T22-48 with the name "Research to establish high-detailed 3D model of construction works (LoD-3) by a combination of unmanned aerial vehicle (UAV) and ground laser scanning" and from the project of the Ministry of Natural Resources and Environment: "Research and application of geospatial technology to build 3D geospatial data for management coastal smart city in Vietnam conditions, pilot in Ha Long city, Quang Ninh province", code: TNMT.2021.04.04.

Consent to participate: A consent form was sent to participants before the study was conducted.

Ethics approval: Subjects were adequately informed about the purpose of the study and participated voluntarily. The research problem did not affect the health or other problems of the subject. The information collected from the subjects is for research purposes only.

Availability of data and materials: Data are available from the corresponding author upon reasonable request.

Competing Interest: All authors declare no conflict of interest.

Funding: This research received no external funding.

Authors' Contributions: Conceptualization, L.T.T.H, N.Q.L; data curation, L.T.T.H, N.Q.L; formal analysis, L.T.T.H; investigation, L.T.T.H, N.Q.L; methodology, L.T.T.H, N.Q.L; project administration and supervision, L.T.T.H, N.Q.L; visualization, L.T.T.H, N.Q.L; writing original draft, L.T.T.H; writing, reviewing & editing, N.Q.L. All authors commented on previous versions of the manuscript. All authors read and approved the final manuscript.

Consent for publication: Not applicable

Literatura – References

1. Biljecki F, Ledoux H, Stoter J. 2014. Redefning the Level of Detail for 3D models. GIM International, 28(11): 21–23.
2. MLTM. 2009. 3D Spatial Information Construction for Ubiquitous National Administration, 2009.
3. Biljecki, F.; Ledoux, H.; Stoter, J. 2016. An improved LOD specification for 3D building models. Comput. Environ. Urban Syst. 59, 25–37.
4. M. Bouziani, H. Chaaba, M. Ettarid, 2021. Evaluation of 3D building model using terrestrial laser scanning and drone photogrammetry. The International Archives of the Photogrammetry, Remote Sensing and Spatial Information Sciences, Volume XLVI-4/W4-2021 16th 3D GeoInfo Conference 2021, 11–14 October 2021, New York City, USA.
5. Tack F, Buyuksalih G, Goossens R 2012. 3D building reconstruction based on given ground plan information and surface models extracted from spaceborne imagery. ISPRS Journal of Photogrammetry and Remote Sensing, 67: 52–64.
6. Colomina I, Molina P. 2014. Unmanned aerial systems for photogrammetry and remote sensing: A review. ISPRS Journal of Photogrammetry and Remote Sensing, 92: 79–97.
7. Nex F, Remondino F. 2013. UAV for 3D mapping applications: a review. Applied Geomatics, 6(1): 1–15.
8. Böhm J, Brédif M, Gierlinger T, Krämer M, Lindenberg R, Liu K, Michel F, Sirmacek B. 2016. Te IQmulus urban showcase: automatic tree classifcation and identifcation in huge mobile mapping point clouds. Int. Arch. Photogramm.Remote Sens. Spatial Inf. Sci., XLI-B3: 301–307.
9. Kaartinen H, Hyyppä J, Kukko A, Jaakkola A, Hyyppä H. 2012. Benchmarking the Performance of Mobile Laser Scanning Systems Using a Permanent Test Field. Sensors, 12(12): 12814–12835.
10. Früh C, Zakhor A. 2004. An Automated Method for Large-Scale, Ground-Based City Model Acquisition. International Journal of Computer Vision, 60(1): 5–24.
11. Rosser J, Morley J, Smith G. 2015. Modelling of Building Interiors with Mobile Phone Sensor Data. ISPRS International Journal of GeoInformation, 4(2): 989–1012.
12. Sirmacek B, Lindenbergh R. 2014. Accuracy assessment of building point clouds automatically generated from iphone images. Int. Arch. Photogramm. Remote Sens. Spatial Inf. Sci., XL- 5: 547–552
13. Hartmann W, Havlena M, Schindler K. 2016. Towards complete, geo-referenced 3D models from crowd-sourced amateur images. ISPRS Ann. Photogramm. Remote Sens. Spatial Inf. Sci., III-3: 51–58.
14. Stilla U, Soergel U, Toennessen U. 2003. Potential and limits of InSAR data for building reconstruction in built-up areas. ISPRS Journal of Photogrammetry and Remote Sensing, 58(1-2): 113–123.
15. Shahzad M, Zhu XX. 2015. Robust Reconstruction of Building Facades for Large Areas Using Spaceborne TomoSAR Point Clouds. IEEE Transactions on Geoscience and Remote Sensing, 53(2): 752–769.
16. Fischer A, Kolbe TH, Lang F, Cremers AB, Förstner W, Plümer L, Steinhage V. 1998. Extracting Buildings from Aerial Images Using Hierarchical Aggregation in 2D and 3D. Computer Vision and Image Understanding, 72(2): 185– 203
17. Barnhart, T.B., Crosby, B.T. 2013. Comparing two methods of surface change detection on an evolving thermokarst using high-temporal-frequency terrestrial laser scanning, Selawik River. Alaska Rem. Sens. 5, 2813–2837.https://doi.org/10.3390/rs5062813
18. Erdélyi, J., Kopáčik, A., Lipták, I., Kyrinovič, P., 2017. Automation of point cloud processing to increase the deformation monitoring accuracy. Appl. Geomat. 9 (2), 105–113. https://doi.org/10.1007/s12518-017-0186-y.
19. Fan, J., Wang, Q., Liu, G., Zhang, L.u., Guo, Z., Tong, L., Peng, J., Yuan, W., Zhou,W., Yan, J., Perski, Z., Sousa, J., 2019. Monitoring and analyzing mountain glacier surface movement using SAR data and a terrestrial laser scanner: a case study of the Himalayas North Slope Glacier Area. Rem. Sens. 11 (6), 625. https://doi.org/10.3390/rs11060625.
20. Xu, Z., Xu, E., Wu, L., Liu, S., Mao, Y., 2019. Registration of terrestrial laser scanning surveys using terrain-invariant regions for measuring exploitative volumes over open-pit mines. Rem. Sens. 11 (6), 606. https://doi.org/10.3390/rs11060606
21. Harmening, C., Neuner, H., 2020. A spatio-temporal deformation model for laser scanning point clouds. J. Geod. 94, 1–25. https://doi.org/10.1007/s00190-020-01352-0.
22. Whitehead, K., Hugenholtz, C.H., 2014. Remote sensing of the environment with small unmanned aircraft systems (UASs), part 1: a review of progress and challenges. J. Unmanned Vehicle Syst. 02, 69–85. doi:10.1139/juvs-2014-0006
23. Sayab, M., Aerden, D., Paananen, M., Saarela, P., 2018. Virtual structural analysis of Jokisivu open pit using 'structure-from-motion' Unmanned Aerial Vehicles (UAV) photogrammetry: Implications for structurally-controlled gold deposits in Southwest Finland. Rem. Sens. 10, 1–17. https://doi.org/10.3390/rs10081296.

24. Chakra, C., Gascoin, S., Somma, J., Fanise, P., Drapeau, L., 2019. Monitoring the snowpack volume in a sinkhole on mount Lebanon using time lapse photogrammetry. Sensors (Switzerland) 19 (18), 3890. https://doi.org/10.3390/s19183890.

25. Díaz, G.M., Mohr-Bell, D., Garrett, M., Muñoz, L., Lencinas, J.D., 2020. Customizing unmanned aircraft systems to reduce forest inventory costs: can oblique images substantially improve the 3D reconstruction of the canopy? Int. J. Rem. Sens. 41 (9), 3480–3510. https://doi.org/10.1080/01431161.2019.1706200.

26. S. Chhatkuli, T. Satoh, K. Tachibana, 2015. Multi sensor data integration for an accurate 3D model generation. The International Archives of the Photogrammetry, Remote Sensing and Spatial Information Sciences, Volume XL-4/W5, 2015 Indoor-Outdoor Seamless Modelling, Mapping and Navigation, 21–22 May 2015, Tokyo, Japan.

27. Allysa Mat Adnan, Norhadija Darwin, Mohd Farid Mohd Ariff, Zulkepli Majid, Khairulnizam M Idris, 2019. Integration between unmanned aerial vehicle and terrestrial laser scanner in producing 3d model. The International Archives of the Photogrammetry, Remote Sensing and Spatial Information Sciences, Volume XLII-4/W16, 2019 6th International Conference on Geomatics and Geospatial Technology (GGT 2019), 1–3 October 2019, Kuala Lumpur, Malaysia.

Geological and Geochemical Characteristics of the Pac Lang Gold Deposits, Northeastern Vietnam and Their Potential Prospects

KHUONG The Hung[1)], NGUYEN Van Dat[2)], NGUYEN Thi Cuc[1)], PHAM Nhu Sang[1)]*

[1)] Faculty of Geosciences and Geoengineering, Hanoi University of Mining and Geology 18 Vien Street, Duc Thang, Bac Tu Liem, Hanoi, Vietnam
[2)] Vietnam Institute of Geosciences and Mineral Resources – VIGMR, 67 Chien Thang Street, Thanh Xuan, Hanoi, Vietnam
* Corresponding author: khuongthehung@humg.edu.vn

http://doi.org/10.29227/IM-2023-02-46

Submission date: 18-08-2023 | Review date: 20-09-2023

Abstract

The Song Hien Rift basin, located in northeast Vietnam, has been identified as an important region for gold deposits, including the Pac Lang deposit. Several methods like petrographic observations, elemental analyses, and geochemical elements and vertical zoning models of primary halo have been used to describe geological characteristic of this deposit. The investigation focused on examining the geological events that occurred both before and after the formation of the ore. The use of ICP-MS analysis and element concentration contrast enabled an effective assessment of the relative degrees of denudation that occurred at the Pac Lang deposit. The findings of this study were consistent with prior research on ore deposit geology, geochemical primary-halo, and examination of geochemical indicator zoning patterns for gold ore bodies. The study's application of singularity analysis for evaluating the degree of denudation provides important geological information that can aid in data interpretation. The results of the study can also have significant reference value in furthering our understanding of the post-ore deformation of deposits and in the investigation of unknown orebodies in northeast Vietnam. There indicate that, the research's findings suggest that the use of singularity analysis to evaluate the degree of denudation is a valuable tool for exploring potential gold deposits and enhancing our knowledge of gold deposit geology in northeast Vietnam. Overall, this study contributes to the existing body of knowledge on gold deposits in the Song Hien Rift basin and can serve as a useful reference for future research in the area.

Keywords: *geology, geochemistry, Pac Lang gold deposit, Vietnam*

1. Introduction

Gold, with its captivating allure and enduring value, has fascinated humanity for centuries. From ancient civilizations to modern-day societies, this precious metal has played a significant role in shaping economies, cultures, and even has a big influence for mankind development. Understanding the origin and formation of gold deposits has been a subject of intense scientific investigation, with researchers striving to unravel the intricate processes that lead to their creation. One aspect that has recently garnered attention is the denudation of gold deposits, which refers to the erosion and stripping away of overlying rocks and sediments, ultimately exposing the concealed gold beneath.

The denudation of gold deposits is a complex phenomenon that involves the interplay of various geological, geochemical, and environmental factors. Over geological timescales, tectonic forces, such as uplift and subsidence, along with climatic changes and erosion, act as powerful agents in unearthing these hidden treasures. These processes not only reveal the underlying gold deposits but also influence their distribution, concentration, and potential economic feasibility. In recent times, the identification of industrial metal ore deposits on a global scale has brought to light an interesting trend wherein new deposits tend to be concentrated in well-established ore regions, while concealed ore deposits are often discovered within extensively researched mineralization areas. This observation underscores the importance of conducting comprehensive investigations, surveys, and explorations into geological features that lie deeply buried. Following the formation of ore deposits, they frequently undergo alteration processes induced by geological activities occurring within or above the Earth's crust, as well as through interactions among different components of the lithosphere. These processes play a critical role in determining the positioning and subsequent preservation of the ores. Among these processes, denudation emerges as a significant factor influencing alteration (Zhai et al., 2000). For example, in the case of a vertical metal hydrothermal mineralization system, the altered mineralization zones situated in the upper portion of the sediment are prone to weathering and denudation, while the ore sources located in the lower sections of the sediments are more likely to be safeguarded (Zhai, 1999). In order to evaluate the rate of sediment denudation, identify undiscovered ore deposits, investigate geochemical peculiarities, and facilitate mineral exploration, quantitative assessments of ore denudation depth are commonly employed (Li et al., 2006; Liu and Ma, 2007).

2. Geological background

2.1. Regional geology

Northeastern Vietnam is home to a significant large-scale gold-polymetallic concentration area in the country. Up to this point, approximately 50 gold deposits and occurrences have been discovered in this region (Tri and Khuc, 2011). However,

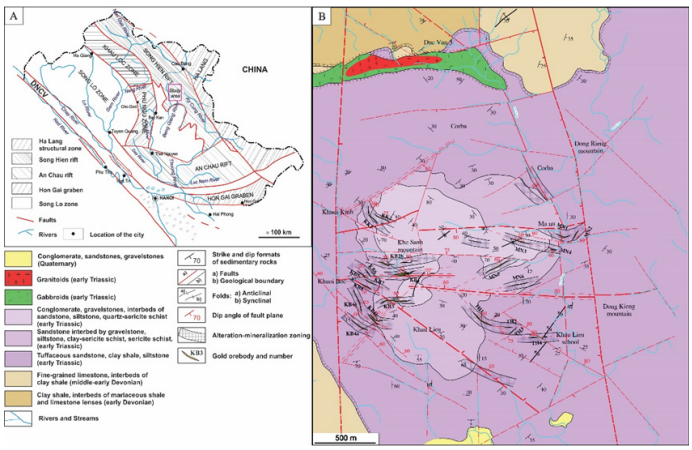

Fig. 1. A – Tectonic map of Northeast Vietnam and location of the study area (Dovjikov et al., 1965); B – Geology and mineral map of the Pac Lang gold deposit (Hoang Van Quang et al., 1997)

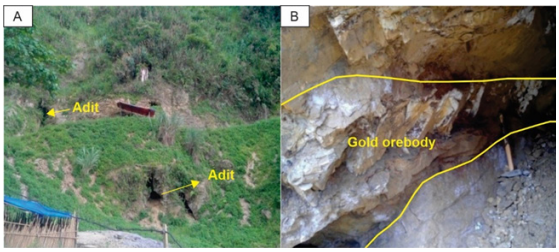

Fig. 2. Gold ore bodies in the Khuoi Boc (PL.3009) (A) and Khuoi Kinh (PL.3003) (B) areas exist in the form of veins (photo from Nguyen Van Dat et.al., 2017)

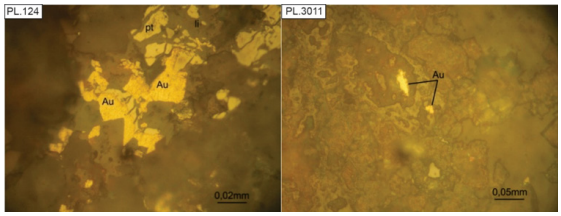

Fig. 3. Native gold concentrates in small nests, pseudomorph irregular shapes while being intercalated with pyrite. Moreover, it undergoes limonite alteration, as observed in samples PL.124 and PL.3011 (after Le Thanh Huong, 2017 in Nguyen Van Dat (2017))

certain deposits that share a similar metallogenic background and are influenced by comparable ore-controlling conditions (e.g., anticline and fault compound) exhibit distinctive characteristics in terms of exposed orebodies, deposit scale, and the intensity of geochemical anomalies associated with mineralization. While the diverse range of ore-forming processes may give rise to various mineralization products, denudation likely plays a pivotal role in responding to post-ore alteration is running simultaneously with gold precipitation during the hydrothermal circulation of the ore forming fluids.

The Pac Lang gold deposit is located at the western edge of the Song Hien zone, adjacent to the Bac Thai convexity complex (Fig. 1A). It is characterized by a deep depression that originated during the Middle Paleozoic and experienced significant tectonic activity in the Permian-Triassic period. As a result, the Mesozoic overlap may be associated with the intracontinental rift, which is connected to the late Permian-early Triassic mantle upwelling. The area primarily consists of terrigenous or terrigenous intercalated tufogen sedimentary rocks belonging to the Song Hien formation. In the northern region, there are additional carbonate and terrigenous sedimentary formations known as the Na Quan and Mia Le formations (Fig. 1B; Hoang Van Quang et al., 1997).

In the study area, there is a intrusive magmatic body in the form of vein belts, measuring 1200m in length and 100–200m in width (Fig. 1B). This body exhibits contrasting compositions, consisting of gabbrodiabase and granite porphyry, and is located along the sub-latitude fault in close proximity to the provincial road DT209.

The Song Hien formation, consisting of tufogen terrigenous sedimentary rocks, contains ores of interest. The potential source of these ores could be associated with the magmatic rocks found in the Cao Bang complex. These magmatic rocks exhibit a mafic to sub-alkaline acid composition and are characterized by copper magma eruptions, which differ from the formations found in the Song Hien formation.

The northwest-southeast and sub-latitude fault systems play a crucial role in creating fractured and compressed zones that host gold mineralization. Additionally, the sub-meridian faults are post-generation systems that cause shear and displacement of the ore mineralization controlling structures.

2.2. Characteristics of the Pac Lang gold deposits

2.2.1. Features of ore veins and gold orebodies

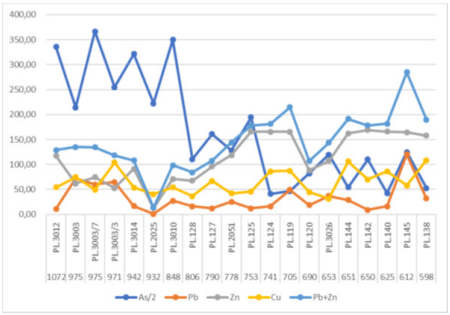

Fig. 4. Correlation relationship between the elemental content of As, Cu, Pb, and Zn and the ore-forming depth (due to the relatively large elemental content of As, As/2 is used here)

Tab. 1. Distribution order by the lithological structure of the Pac Lang gold deposit

Distribution location	Distribution order by the lithological structure	Mineral symbiotic complex	Distribution location
The upper part	Felzit, siltstone, sandstone, gravel of the Song Hien Formation. Mahogany brown siltstone, thick layer, quartz-sericite slab, black clay.	Quartz-gold-poor sulfide (pyrite, galenite, sphalerite, chalcopyrite). Large grain pyrite sulfide.	In the ranges of IV, III, II, I, Khuoi Boc, Khuoi Kinh, Mo Coi hill, and the Manu longwall route. These areas create a rather highly-distributed area by the stratigraphic structure
The lower part	Graphitized black shale, blue-gray quartzite, with dark siltstone.	Quartz-pyrite (with chalcopyrite, galenite-sphalerite-gold. Medium-grained pyrite, small-grained sulfide minerals.	The lower part of the Manu mining area

In the research area, gold ore bodies have various forms, including simple veins, complex veins, vein systems, lens-shaped bodies, stockwork bodies, and ore shoots.

In the sublatitude direction, ore bodies exhibit complex structures. When observing the ore body along its strike, simple vein segments with consistent thickness, dip angles, and relatively stable altered wall rocks become apparent. Additionally, several sections of the ore body branch out along the same orientation but at varying dip angles or perpendicular orientations, creating branching patterns that can resemble tree branches or cluster-like formations, sometimes similar to horse-tail shapes.

The ore body displays zonation, often with gold-containing quartz veins. The zonation within the ore body progresses as follows: In the center lies a core of quartz, usually containing gold sulfides, surrounded by phyllites and sericite, infiltrated by sulfides. Beyond the core is the primary rock, heavily fractured and fissured, with some sections cross-cut by quartz veins, and with boundaries not always distinctly defined, occasionally existing only within the walls or pillars of the ore body, with some sulfide infiltration. The outermost part of the ore body consists of less altered primary rock.

In the northwest-southeast direction, gold ore bodies are oriented with strike and dip values of approximately 40–60/220–240. These ore bodies commonly take the form of quartz-veins containing gold, exhibiting either simple structures or elongated lenses. The vein structures are relatively straightforward, with thickness ranging from 0.1 to 0.5m, and the elongated lenses extend for 5–40m with a thickness of 0.1–0.5m. The surrounding rocks show less alteration, and the gold content in these veins is generally quite low.

In the northeast-southwest direction, gold ore bodies are oriented with strike and dip values of approximately 300–310/40–80. These ore bodies frequently occur as vein systems or lens systems. The veins or lenses have a small thickness, ranging from 0.1 to 0.2m, spaced at intervals of 1–2m, and running parallel to each other, with observable lengths varying from 5 to 20m.

Furthermore, at the intersections of various fracture systems, rocks experience thrust folding and intense fracturing, leading to the formation of ore nests. These ore shoots typically bulge in the middle and taper towards both ends, with an average length of about 25m and some bulging areas extending up to 20m. These ore nests have a strike direction of 130° and a dip angle of 65°; a typical example of such ore nests is found in the I, II, III, IV areas.

2.2.2. Structural and textural gold ores

At the Pac Lang gold mine, a variety of ore structures are encountered, encompassing disseminated, veinlet, infiltration, pseudobedding, breccia, and banded structures.

Disseminated structures are observed within quartz veins with minimal fracturing, displaying a firm, milky-white color, and containing minute proportions of pyrite and limonite minerals. This type of structure is characteristic of ore shoots and quartz lens formations, which exhibit low and highly variable gold content.

The veinlet infiltration structure is a distinctive feature of gold–quartz–polymetallic sulfide ore. Sulfide veins are unevenly distributed within the quartz background, with veinlet sizes ranging from a few mm to 20mm.

Breccia and banded structures are commonly found in numerous ore bodies. In these structures, quartz, pyrite, and other fractured minerals form brecciated slates that are cemented by subsequent generations of quartz and pyrite.

Additionally, pseudobedding, foliation, and mesh-like structures are present in certain areas of high-grade gold ore bodies and in generations containing low-grade mineralization.

The typical ore textures in the mining area encompass euhedral, semi- euhedral, and anhedral textures, which are characteristic of minerals such as pyrite and sphalerite. Anhe-

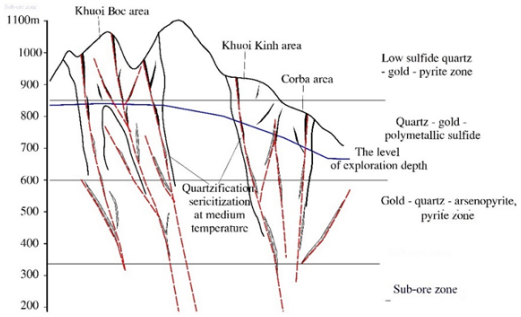

Fig. 5. Model of gold – quartz – sulfide ore zoning according to the depth of the Pac Lang gold deposit (Nguyen Van Dat et al., 2017)

dral textures are distinctive of galena; erosion features typify pyrite in the initial stage; and bone-shaped textures form due to the replacement of pyrite by limonite and goethite during oxidation processes.

3. Materials and methods

3.1. Analytical methods

Geochemical samples are collected from cross-sections of the ore body, typically selected to adequately represent the targeted region or ore body classification under investigation. The selection of sampling locations may be informed by existing geochemical data or a meticulously devised research plan. Subsequently, 70 geochemical samples undergo comprehensive analysis utilizing ICP-MS for the quantification of 17 elemental components, mineralogical examination, and handheld Xmet device measurements. The resulting analytical data is then synthesized and meticulously processed to facilitate the evaluation denudation of ore mineralization. This assessment is based on the vertical geochemical zoning characteristics of ore-forming elements, particularly pertaining to denudation depth.

3.2. Assessment of ore body's size, morphology, and localization

Based on research documents on thickness, the length in the strike direction, and the height in the dip direction of ore bodies in hundreds of hydrothermal deposits of tungsten, fluorite, molybdenum, gold, copper, tin, and uranium in the world. Lir (1984) established the correlation between the length in the strike direction (l) with the height in the dip direction (h) of the hydrothermal ore bodies and calculated the coefficient (k) of these parameters by the following formula:

$$k = h/l \tag{1}$$

According to the formula (1), the coefficient k = 0.6 for the vein-type gold ore. From the strike direction dimensions of the gold ore bodies in the 03 study areas, it is possible to calculate the relative existence depth of the gold ore bodies. However, due to the discontinuous characteristics and low stability of gold ores, it is necessary to evaluate the overall ore zone to have an accurate assessment of the ore existence depth.

3.3. Assessment of the denudation rate

The vertical alteration in ore deposition conditions is one of the most important causes leading to the formation of mineral formations with different compositions.

One of the methods to assess the distribution depth of gold ore bodies is to calculate the vertical distribution of ore-forming elements, thereby calculating the ore body's denudation coefficient by the formula proposed by Beus and Grigoryan (1977) as follows:

$$K_z = \frac{Ag \times Pb \times Zn}{Cu \times Co \times Bi} \tag{2}$$

In which: K_z is the denudation coefficient; Ag, Pb, Zn, Cu, Co, Bi are elemental contents of Ag, Pb, Zn, Cu, Co, and Bi (ppm); Kz < 0.1 under the ore-forming zone; $0.1 \leq K_z \leq 10{,}000$ in the ore-forming zone; $K_z > 10{,}000$ on the ore-forming zone.

4. Results and Discussion

3.1. Geochemical singularities

3.1.1. Correlation between elemental contents and ore formation depth

The results of the ICP-MS analysis of 70 ore samples in cross-section from the top of the Khuoi Boc peak in the Khuoi Kinh area to the lower longwall floors in the Manu area, as well as comparisons of the contents of some key elements and the sampling height, allow for the construction of a graph showing the relationship between the elemental content and ore formation depth (Figure 4).

On the Figure 4, the contrast in elemental content values can be seen at the position of the sample PL.128, which was collected from a longwall at an elevation of about 800–850m.

As can be seen that from the position of the sample PL.128 to the positions of the higher sampling locations, the As content increases significantly, whereas, the content of Cu, Zn, and Pb elements is much lower. From the position of the sample PL.128 to the lower sampling locations, the As content decreases remarkably along with the steady increase of Cu, Zn, and Pb.

This is the elemental geochemical characteristic of two different mineralization zones when the upper zone is characterized by arsenopyrite and pyrite minerals, the lower zone is characterized by an increase in polymetallic minerals such as galenite, sphalerite, and chalcopyrite, etc.

In the Pac Lang gold deposit, the elevation range of +800m to +850m marks the dividing line between the two main mineralization zones.

3.1.2. Ore zoning features

Vertical zoning: Based on actual observation and synthesis of gold ore documents of the Pac Lang deposit, the main ore zoning features are shown as follows. The upper part is the large size quartz veins that are poor in sulfide ore and contains gold in their mineral pillars; the middle part is hydrothermal quartz veins without ore and their local mineral pillars con-

Tab. 2. Range of ore-forming depth of gold ore bodies in the Pac Lang gold deposit

No.	Area	Ore body	Depth of the ore body's denudation surface (m)	Controlled ore-forming depth (m)	Forecasted ore-forming depth (m) (-50m)	Range of ore formation depth
1	Khuoi Kinh	KK1	1030	816	766	264
2		KK2	1068	902	852	216
3	Khuoi Boc	KB1	1083	878	828	255
4		KB2	1089	934	884	205
5		KB3	1060	807	757	303
6		KB4a	1015	758	708	307
7		KB4b	1008	777	727	281
8		KB4c	960	831	781	179
9		KB5	842	808	758	84
10		KB6	882	769	719	163
11		KB7	920	807	757	163
12		KB8	920	796	746	174
13	Manu	MN1	662	581	531	131
14		MN2	705	586	536	169
15		MN3	764	594	544	220
16		MN4	664	537	487	177
17		MN5	774	529	479	295
18		MN6	742	612	562	180
19	School	TH1	852	706	656	196
20		TH2	743	662	612	131
21		TH3	751	637	587	164
22		TH4	651	516	466	185
Average			**872.05**	**720.14**	**670.14**	**201.91**
Range of ore-forming depth of the ore field						**623**

Tab. 3. The height in the dip direction of the gold ore bodies of the Pac Lang gold deposit (Lir, 1984)

No.	Area	Ore bodies	Length in the strike direction (m)	Height in the dip direction (m)
1	Khuoi Kinh	KK1	182.8	109.68
2		KK2	143.6	86.16
3	Khuoi Boc	KB1	194.5	116.70
4		KB2	143.2	85.92
5		KB3	255.1	153.06
6		KB4a	142.7	85.62
7		KB4b	143.3	85.98
8		KB4c	206.3	123.78
9		KB5	81.0	48.60
10		KB6	82.9	49.74
11		KB7	110.3	66.18
12		KB8	106.5	63.90
13	Manu	MN1	132.0	79.20
14		MN2	112.5	67.50
15		MN3	168.9	101.34
16		MN4	81.5	48.90
17		MN5	230.0	138.00
18		MN6	163.3	97.98
19	School	TH1	207.2	124.32
20		TH2	89.0	53.40
21		TH3	87.0	52.20
22		TH4	161.7	97.02
Average			**146.60**	**87.96**

Tab. 4. Existence depth of the gold ores in the Pac Lang gold deposit by the ore body shape (Bogaski, 1982)

No.	Area	Ore bodies	Length in the strike direction (m)	Height in the dip direction (m)	Order No.	Existence depth
1	Khuoi Kinh	KK1	182.80	109.68	2	219.36
2		KK2	143.60	86.16	2	172.32
3	Khuoi Boc	KB1	194.50	116.70	2	233.40
4		KB2	143.20	85.92	2	171.84
5		KB3	255.10	153.06	2	306.12
6		KB4a	142.70	85.62	2	171.24
7		KB4b	143.30	85.98	2	171.96
8		KB4c	206.30	123.78	2	247.56
9		KB5	81.00	48.60	2	97.20
10		KB6	82.90	49.74	2	99.48
11		KB7	110.30	66.18	2	132.36
12		KB8	106.50	63.90	2	127.80
13	Manu	MN1	132.00	79.20	2	158.40
14		MN2	112.50	67.50	2	135.00
15		MN3	168.90	101.34	2	202.68
16		MN4	81.50	48.90	2	97.80
17		MN5	230.00	138.00	2	276.00
18		MN6	163.30	97.98	2	195.96
19	School	TH1	207.20	124.32	2	248.64
20		TH2	89.00	53.40	2	106.80
21		TH3	87.00	52.20	2	104.40
22		TH4	161.70	97.02	2	194.04
Average			**146.60**	**87.96**	2	**175.93**

Tab. 5. Calculation of denudation coefficient by the formula proposed by Beus and Grigoryan (1977) based on the sample ICP-MS analysis results in the whole Pac Lang gold deposit

No.	Sample No.	Analysis results (ppm)						Denudation coefficient K_z
		Ag	Pb	Zn	Cu	Co	Bi	
1	PL.119	0.38	49.04	165.70	87.16	48.49	0.92	0.79
2	PL.120	0.37	18.93	88.14	44.60	10.64	1.74	0.74
3	PL.123	0.45	29.39	50.85	42.85	19.94	0.95	0.83
4	PL.124	0.53	16.04	165.38	86.04	14.54	1.81	0.62
5	PL.125	0.48	12.26	166.17	45.79	21.96	0.84	1.17
6	PL.127	0.42	11.94	95.70	66.96	10.76	0.61	1.08
7	PL.128	0.71	16.39	67.63	36.73	10.46	0.64	3.22
8	PL.129	0.48	21.33	342.51	50.33	23.98	0.92	3.18
9	PL.138	1.46	31.74	158.06	108.66	23.15	2.41	1.21
10	PL.140	0.70	16.08	165.79	86.14	14.22	1.24	1.24
11	PL.142	3.04	8.87	169.14	70.07	20.84	0.69	4.53
12	PL.144	1.27	28.92	162.34	106.22	23.51	3.02	0.79
13	PL.145	0.46	120.43	164.48	57.84	24.74	3.66	1.74
14	PL.2025	0.84	1.09	12.74	40.61	5.49	0.55	0.10
15	PL.2051	0.60	25.34	118.96	41.92	16.55	0.78	3.35
16	PL.3003	0.74	132.68	122.14	74.54	9.92	2.80	5.80
17	PL.3003/1	0.65	47.54	192.28	73.81	17.94	2.69	1.66
18	PL.3003/3	0.84	115.20	102.97	103.88	29.20	1.59	2.07
19	PL.3003/5	0.88	207.25	117.09	39.55	19.40	0.66	42.30
20	PL.3003/7	2.34	59.66	114.67	49.66	23.40	1.16	11.85
21	PL.3003/9	0.97	149.81	190.67	77.42	29.34	0.80	15.15
22	PL.3003/11	0.67	100.76	218.02	56.71	20.24	0.96	13.37
23	PL.3009	2.33	42.36	178.33	65.53	10.96	0.71	34.33
24	PL.3010	4.58	27.32	71.02	54.38	10.65	0.99	15.56
25	PL.3012	1.05	11.32	117.48	54.43	12.91	0.50	3.95
26	PL.3014	1.03	16.92	91.17	53.94	11.23	0.85	3.07
27	PL.3026	0.83	36.79	106.98	31.59	7.02	1.11	13.30
Average		**1.08**	**50.20**	**137.64**	**63.24**	**18.20**	**1.32**	
K_z of the whole gold deposit		**4.91**						
The average value of ore gold samples		**1.41**	**78.97**	**135.24**	**61.29**	**16.85**	**1.24**	
Average K_z of ore gold samples		**11.78**						

tain sulfide-poor gold, and the lower part is quartz-pyrite veins containing gold in the graphite black shale. The distribution order of the lithographic structure can be divided into different zones as shown in Table 1.

Based on the ore zoning features and actual survey results, the author has built a cross-sectional model of the gold–quartz–sulfide ore zoning at the Pac Lang gold deposit (Figure 5).

Horizontal zoning: On the map, the Pac Lang gold deposit's region shows the horizontal zoning of the ore very well. This region can be separated into two primary ore zones, the polymetallic gold–quartz–sulfide ore zone, and the gold–quartz–pyrite ore zone, running from the northeast to the southwest.

The polymetallic gold–quartz–sulfide ore zone, which is found mainly in the Manu and Corba areas, forms a strip about 500–600m wide and extends from the northwest to the southeast;.

The gold–quartz–pyrite ore zone, which is distributed along the high mountain peaks from Khuoi Kinh and Khuoi Boc areas down to the School area, forms a strip many kilometers wide and stretches from the northwest to the southeast.

3.2. Prospective deep-buried mineral predictions

3.2.1. The ore-forming depth

It is feasible to determine the range of ore-forming depth for each ore body and the entire gold deposit by examining the depth of the ore body's denudation surface (the elevation of the outcrop) and the controlled ore-forming depth. Table 2 lists the results of the calculations for the range of formation depths of ore bodies.

The above-mentioned calculation results show that the development depth of the ore bodies at the Pac Lang gold deposit is relatively deep, the ore bodies are controlled and exploited to a relatively large depth from 84m to 307m, with an average of 201. 91m. The range of ore-forming depths of the whole gold deposit is 623m, indicating that the ore formation in the area has a high capacity to existing at depth. Furthermore, it is predicted that ore can develop to a depth of >450m.

3.2.2. The ore body's morphology and size

According to Lir (1984), the ratio between the height of the ore bodies in the dip direction and the length in the strike direction of the hydrothermal gold ore bodies has the coefficient k = 0.6. Based on the collected results on the length along the strike direction and the size of the ore bodies, and the formula (1), it is possible to calculate the distribution height of the ore bodies in the dip direction as shown in Table 3.

Tab. 3. The height in the dip direction of the gold ore bodies of the Pac Lang gold deposit (Lir, 1984)

On the other hand, according to Bogaski (1982), all 243 hydrothermal ore deposits in southern Siberia have a height in the dip direction equal to the length in the strike direction of the ore bodies. This finding is true for all three vertical forms of ore body existence, namely, single, intermittent, and stepwise.

Field survey results show that most of the gold ore bodies in the Pac Lang gold deposit are in the form of veins, sockets, cylinders, and intermittent lenses. Therefore, it is assumed here that the gold ore bodies have the existence number of 2 orders.

Then, regarding the existence form of hydrothermal ore bodies, the calculation results of the relative depths of gold ore bodies in the Pac Lang gold deposit are shown in Table 4.

The calculation results indicate that the ore bodies in the gold deposit have relatively high development prospects,

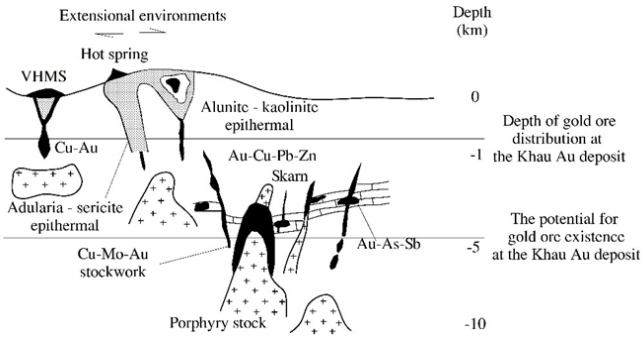

Fig. 6. The distribution model of original gold deposits by depth (Groves et al., 1998)

reaching 175.93m on average. Some ore bodies have a depth of 200–300m such as KK1, KB1, KB3, KB4c, MN3, and TH1.

3.2.3. The characteristics of the denudation rate

The change in vertical ore deposition conditions is one of the most important causes leading to the mineral formations with different compositions. The calculation of the denudation coefficient K_z by the formula (1) can assess the possibility of the existence of ore bodies deep-seated in the study area. Based on the ICP-MS analysis results of 27 samples at the Pac Lang gold deposit, the calculation results of the denudation coefficient K_z are shown in Table 5.

Calculation results of K_z by the formula (2) for the Pac Lang gold deposit show that the average K_z value of the whole gold deposit is 4.91 and of the ore samples are 11.78, all in the range from 0.1 to 10,000. No K_z value is less than 0.1 (below the value showing the ores or the ore bodies here have been completely denudated/eroded).

In general, the K_z value of the Pac Lang gold deposit is relatively low. Some areas with a low denudation rate include Khuoi Boc, Khuoi Kinh, and Mo Coi hill (Table 5), where the typical ore type is low-sulfide gold–quartz–pyrite, so the existence possibility of deep ore mineralization in these areas is still very promising.

The areas of Manu and School have a lower value of denudation coefficient, so the denudation rate is higher. These are also areas with low terrains and their typical ore type is gold–quartz–polymetallic sulfide. In these areas, the ore bodies of the sulfide-poor gold–quartz–pyrite ore zone have basically been completely denudated, and therefore, these areas have little potential for deep ore mineralization.

Evaluation of the ore body denudation depth: The ore formation distribution characteristics in ore-forming models indicate that the medium to low-temperature hydrothermal gold ore is formed at medium depth, with the depth fluctuating from about 800–1000m (Groves et al., 1998).

The study results on the ore mineralization characteristics, hydrothermal changes, and zoning features show that the gold–quartz–sulfide ore mineralization of the Pac Lang gold deposit is consistent with the distribution model of gold mines by depth mentioned by Groves et al. 1998) (Figure 6).

According to this model, the gold ore in the Pac Lang gold deposit is distributed at a depth of 0.5–1.2km and has a denudation rate of about 200–350m. Thus, based on the above-mentioned distribution model, it can be seen that the Pac Lang gold deposit has the ability to exist very deep and can go down to a depth of -5km.

5. Conclusion

Based on trace element geochemistry and assessment of the denudation rate of the Pac Lang gold deposit, the following conclusions can be made:

The ore mineralization at the Pac Lang gold deposit can be classified into three main zones: The gold–quartz–pyrite–poor sulfide zone; the gold–quartz–polymetallic sulfide zone, and the gold–quartz–arsenopyrite and pyrite zone.

The calculation results indicate that the depth range of gold ore formation in the deposit is approximately 623m. Based on the morphology of gold ore bodies and the average size of ore bodies in the Pac Lang gold deposit, the forecasted existence depth is estimated to be around 175.93m.

The denudation coefficient K_z for the gold ore in the deposit is calculated to be 11.78. This denudation coefficient suggests a moderate to strong denudation rate and places the deposit in the ore-forming zone, with the denudation depth estimated to be around 200–350m.

The study suggests the possibility of hidden gold ore deposits at even greater depths, potentially reaching depths of up to -5km.

Acknowledgements

This research is supported by the Ministry of Education and Training of Vietnam, under grant number B2023-MDA-08.

Literatura – References

1. Beus, A.A., Grigoryan, S.V., 1977. Geochemical exploration methods for mineral deposits. Applied Publishing Ltd. USA, 31-270pp.
2. Bogaski, K.L., 1982. Basis for the assessment of mineral deposits and mining enterprises. Mining Journal, 9: 3-9 (in Russian).
3. Dovjikov, A.E. (ed.), My, B.P., Vasilevskaia, E.D., Jamoida, A.I., Ivanov, G.V., Izokh, E.P., Huu, L.D., Mareitchev, A.I., Chien, N.V., Tri, N.T., Luong, T.D., Quang, P.V. & Long, P.D., 1965. Geology of North Vietnam. Explanatory note of the Geological Map of North Vietnam at 1:500,000 scale. Geological Department of Vietnam, Ha Noi, 584 pp.
4. Groves, D.I., Goldfarb, R.J., Gebre-Mariam, M., Hagemann, S.G. & Robert, F., 1998. Orogenic gold deposits: A proposed classification in the context of their crustal distribution and relationship to other gold deposit types. Ore Geology Reviews, 13: 7-27.
5. Hoang Van Quang (ed. 1997). Report on the results of geological mapping at a scale of 1:50,000 for the Bang Khau-Yen Lac sheet group. Center for Information, Archives and Geological Journal, Hanoi.
6. Li, H., Zhang, G., Yu, B., 2006. The model of structural superimposed halo in prognostic and efficiency for blind orebodies in gold ore-district. Geological Publishing House, Beijing, pp. 146 (in Chinese).
7. Lir, Iu.V. (ed. 1984). Average size of hydrothermal ore bodies along strike and dip direction. Nhedra Publisher, 106pp (in Russian).
8. Liu, C., Ma, S., 2007. The main achievements of the study on primary halo in the past 50 years in China. Computing Techniques for Geophysical and Geochemical Exploration, 29 (Supplement): 215-222 (English abstract).
9. Nguyen Van Dat (ed. 2017). Establishing prospective zoning types of gold-quartz-sulfide ore in the deep concealed region of Northwest Vietnam. Ministry of Natural Resources and Environment, code TNMT.2017.03.04 (in Vietnamese).
10. Tri, T.V. & Khuc, V. (ed.), 2011. Geology and Earth Resources of Vietnam. General Department of Geology and Minerals of Vietnam, Publishing House for Science and Technology, Hanoi.
11. Zhai, Y., Deng, J., Peng, R., 2000. Research contents and methods for post-ore changes, modifications and preservation. Earth Science-Journal of the China University of Geosciences, 25(4): 340-345 (English abstract).
12. Zhai, Y.S., 1999. On the Metallogenic System. Frontiers in Earth Science, 6(1): 13-27 (English abstract).
13. Szymanek A., de las Obras-Loscertales M., Pajdak A.Effect of sorbent reactivity on flue gas desulphurization in fluidized-bed boilers under air firing mode. The Canadian Journal of Chemical Engineering, Volume 96, April 2018, 895-902.

Geological Hazard Investigation Combined with Mathematical Modeling in Flood Risk Assessment: A Case Study of Hoang Long River, Ninh Binh Province, Vietnam

Nhu Y NGUYEN[1)], To Xuan BAN[2)], Dang Dinh KHA[1)]*

[1)] Faculty of Hydrology, Meteorology and Oceanography, University of Science, Vietnam National University, Hanoi
[2)] Faculty of Geosciences and Geoengineering, Hanoi University of Mining and Geology
* Corresponding email: toxuanban@humg.edu.vn

http://doi.org/10.29227/IM-2023-02-47

Submission date: 29-08-2023 | Review date: 27-09-2023

Abstract

The primary function of the river dike system is to safeguard lives and property from flood hazards. However, due to aging infrastructure and various geological or anthropogenic factors, certain vulnerable sections of the dike system can emerge as the water level in the river increases. Flood maps are one tool that presents vital information for authorities and residents in the flood risk mitigation. This study's primary goal is to provide a flood map under the dike break condition using the estimated fracture size parameters from a geo-radar survey and the MIKE FLOOD model. This approach addresses the observed research gap by utilizing a survey database instead of relying on empirical models which are capable to produce the conservative estimates of the dike breach outflow. A case study is conducted on the Hoang Long River dike system in Ninh Binh Province, Vietnam.

Keywords: *flood risk assessment, dike break, dike failure, geo-radar, breach outflow, MIKE FLOOD*

1. Introduction

The dike system plays a vital role in protecting individuals, assets, and the environment from the risk of rising river water levels. Under the impact of climate change, the flow conditions have become more severe (Zagonjolli M., 2007). Meanwhile, river dikes, constructed long ago, often suffered from damages caused by geological hazards (such as earthquakes and subsidence) (Dat T.T. và nnk, 2019) as well as pressure from human activities (such as using dikes systems as traffic routes) (Hue N.H. và nnk, 2019). The condition of these dike system raises concerns for the residents living in the vicinity. The damage caused by the dike breaks depends on many factors, including the inundation water depth, flow velocity, breach outflow, population density, property distribution, and the adaptive capacity of residents in the affected area (Nguyen M.T. và nnk, 2021). Among these factors, determining the fracture size of the dike breach is the first essential technical steps in dike break simulation (Froehlich D.C., 2008) which the output of this modeling holds significant value for society. The dam breach parameters are usually estimated using the empirical formula related to geometrical properties: the dam's height, the slope, and the reservoir capacity (Dat T.T. và nnk, 2019; Froehlich D.C., 2008). Although it might not be effective, the simplicity of this empirical approach can be explained for the widespread use of empirical models in practical application.

Various studies have used numerical models to investigate dike failure's impact, for example, HEC-RAS (Brunner G.W., và nnkand CEIWR-HEC., 2016), MIKE FLOOD (DHI Water and Environment., 2014), NWS-DAMBRK (Fread D.L., 1991), or NARX (Bomers A., 2021) neural network. Ansori et al (2021) used HEC-RAS to simulate the dam failure of Way Apu reservoir in Malaysia with different design frequency discharge. In the work of Dat et al. (2019), MIKE FLOOD was used to simulate various dam break scenarios for the DakDrinh reservoir in Viet Nam and define the affected area. Anouk Bomers (2021) (2021) combined the HEC-RAS hydraulic model and the NARX artificial neural networks model to reduce the computer's weight processor when evaluating the fracture flow.

It is generally acknowledged that breach parameters are the most significant uncertainty in dam break studies spite the model used (ASCE/EWRI, 2011) (Wu W., 2011). This work tries to fill the lack of studies observed, using an extensive database instead of empirical approaches, or hypothetical values. Therefore, the main objective of this study is to exploring the dam breach parameters at critical locations using the geo-radar observation and to simulate flooding due to dike break using MIKE FLOOD model.

2. Material and methods

2.1 Description of study site

Hoang Long River is a tributary of the Day River, the largest river in Ninh Binh province. The upstream of the Hoang Long River is called the Boi River. The Hoang Long River has a length of about 125km, and the basin area is 1550 km². Hoang Long River flows through a lowlands area with only a 2–4m elevation. These terrain conditions cause severe flooding quickly after heavy rain. Hoang Long River has a complex hydrological regime; in the flood season, the river is affected by the Boi River upstream, and the downstream is greatly affected by floods from the Red River.

The Hoang Long River has a primary dike system for flood protection, consisting of the Ta Hoang Long Dike and the Huu Hoang Long Dike. This dike wall height adheres to the flood control level of the approved plan of +5.53 meters

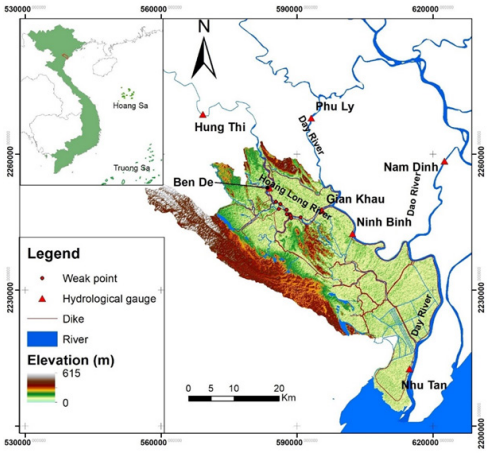

Fig. 1. Area of study

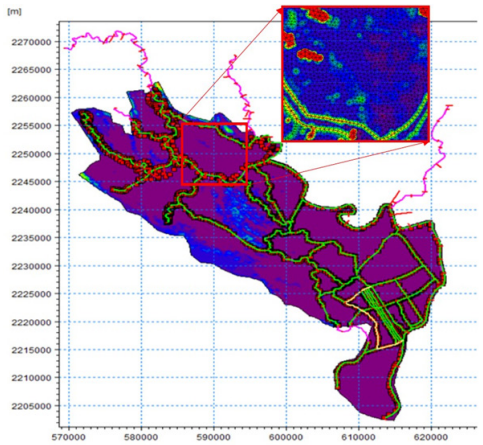

Fig. 2. Hydrologic and hydraulic coupling in MIKE FLOOD

(The Ministry of Agriculture and Rural Development., 2012). However, this dikes network was built over different dike periods. The earth-fill layer is not uniform and is constructed in multiple stages to meet the flood prevention requirements of the potentially endangered areas. These dikes have been renovated recently to serve road traffic for the locality's socio-economic development. This use has increased pressure on the dike system and dike safety (Hue N.H. và nnk, 2019).

2.2 Method and materials

MIKE FLOOD model

The MIKE FLOOD model developed by the Danish Hydraulic Institute was used to simulate inundation caused by dike failure (The Ministry of Agriculture and Rural Development., 2012). The model is integrated with (i) MIKE 11 model with the dike break module (DamBREK) to simulate unidirectional flow in the river and (ii) MIKE 21 model to simulate 2-D flow in flooded areas. Although the MIKE 11 model has outstanding advantages in simulating 1D flow in complex river networks, and MIKE 21 model can simulate the surface flow. However, MIKE 11 alone will be challenging to simulate overflow if flow directions are unknown in advance and can not define the velocity field. Using MIKE 21 to simulate the surface and mainstream flow requires reducing the mesh size to the extent which can show the channel's topography change. As a consequence, the computational time is a dramatic increase. To utilize the advantages of 1-D and 2-D models and overcome their disadvantages, MIKE FLOOD allows the coupling of MIKE 11 and MIKE 21 models in the simulation. This coupling model allows increasing the mesh size of the model. (i.e., reducing computation time), simulating the surface and stream flow. Therefore, the MIKE FLOOD model was employed in this study.

Materials

The hydrometeorological data, riverbed, and floodplains topography are collected for the inundation model. The hourly rainfall data at Ninh Binh meteorological station and seven hydrological stations (Nhu Tan, Ninh Binh, Gian Khau, Ben De, Nam Dinh, Phu Ly, and Hung Thi) were obtained from 2008 to 2020. The flood water level collected at seven hydrological stations is used for the model's boundary conditions and model verification. These data were provided by the National Center for Hydrometeorological Forecasting (NCHMF)(https://nchmf.gov.vn/). Riverbed topographic data collected from multiple sources throughout 2005 and 2019 includes 113 river cross-sections defining the 333km river lengths. Topographic data of floodplain areas are extracted from topographic maps at a scale of 1:10,000 m provided by the Vietnam Ministry of Natural Resource and Environment.

Establishing of coupled link 1D-2D in MIKE FLOOD model

a) Establishing network in 1D model

Fig. 3. The location of the levee subsidence on the left bank of the Hoang Long River

Tab. 1. The abnormal points along the Ta Hoang Long and Huu Hoang Long levees

Levee	#	Anomalies	Coordinates		Depth from the surface (m)	Predicted abnormal points
			Longitude	Latitude		
Huu Hoang Long	1	H1	105° 49' 43.23"	20° 19' 20.20"	2.4	Termite voids
	2	H2	105° 49' 55.49"	20° 19' 13.46"	1.8	Termite voids
	3	H3	105° 50' 25.66"	20° 18' 38.82"	3.8	Termite voids
	4	H4	105° 51' 42.48"	20° 18' 03.28"	2.5	Termite voids
Ta Hoang Long	6	T1	105° 49' 13.26"	20° 20' 03.98"	2.0	Termite voids
	7	**T2**	**105° 49' 42.60"**	**20° 19' 48.29"**	**1.0**	**Termite voids**
	8	T3	105° 49' 54.38"	20° 19' 41.35"	5.7	Termite voids
	9	T4	105° 49' 58.99"	20° 19' 38.39"	1.0	Termite voids
	10	T5	105° 50' 05.64"	20° 19' 33.34"	0.9	Termite voids

Tab. 2. The parameters of dike failures

Elevation of dike failure water level (m)	Initial failures		Limitation failures	
	$Z_{Initial}$ (m)	$B_{Initial}$ (m)	Z_{End} (m)	B_{End} (m)
4.3	4.33	10	2.5	110

The hydraulic system includes the Day River, Dao River, Hoang Long River, and inland waterways. The Day River is the longest in this network, stretching 105.5 km (from Phu Ly station to Cua Day), followed by the Hoang Long River at 60.7 km (from Hung Thi station to the Day River confluence) and the Dao River at about 24.5 km (from Nam Dinh station to the Day River confluence). Other rivers have a length in the range from 7 to 24 km. The total simulated length of the rivers is 407.5km with 259 river cross-sections. Figure 2 depicts the location and length of the rivers.

The water level at the Hung Thi, Phu Ly, and Nam Dinh stations define the upper boundaries of the river system. The tidal water level at the Day mouth calculated from the harmonic constant is defined as the lower boundary (Huan N.M., 2015).

b) Establishing computation mesh in 2D, MIKE FLOOD

The study defined the computational domain from the topographic map of the 1:10,000 scale. It includes the entire Ninh Binh province, with an area of 1387 km^2. The study area is discretized into 30686 elements, with the size varying in a range of 20–250m. The fine mesh is defined for important and complex areas (such as urban and residential areas). The flat area, like a paddy field, is defined with the larger grid cell size. In the MIKE FLOOD model, the 2-D model is connected to the 1-D model through side connections (Figure 2).

c) The location of vulnerable levees using Georadar physical survey (GPR)

The study surveyed various dike sections to determine the locations of vulnerable points along the levee system. The preliminary survey results identified four weak points on the right bank of the Hoang Long River levee and six weak points on the left bank, showing signs of subsidence and surface cracks (Figure 3, Table 1). The research team continued to utilize geo-radar physical survey, also known as Ground Penetrating Radar (GPR), a geophysical exploration method that uses electromagnetic wave propagation through the ground. By emitting radiofrequency electromagnetic waves into the subsurface as pulses, the radar system records the reflections when encountering boundaries or inhomogeneities in the electrical properties of the subsurface, capturing the data with receiving antennas. Using various processing, analysis, and interpretation techniques on the recorded electromagnetic wave field, anomalies-causing objects can be inferred. Ground-penetrating radar method offers several advantages in shallow geological surveys, such as non-destructiveness, ease of mobility, fast data acquisition, high resolution, and accuracy. The results obtained from geo-radar measurements can correlate with other geological and geophysical survey findings to elucidate geological factors, such as boundaries between soil and rock layers, and determine the position, depth, and size of anomalous objects within levee bodies or embankments. This study utilized the GSSI SIR-30 geo-radar system with a 100MHz frequency, antenna model 3207/3207A, and a noise-resistant display to measure continuously over vulnerable sections. Using a frequency filter ranging from 25 to 300MHz allows for a maximum depth penetration of 13 meters from the ground surface.

The geo-radar measurement of the dike anomalies objects allows for the finding of the geological characteristics of the dike. The main components of the dike consist of loose materials, including clay and clay-sand mixtures. The structure of these geo-radar anomalies suggests that they may indicate the development of termite voids within the dike. If left undetected and untreated, these termite voids within the levee can grow, expand, cause seepage, and potentially lead to subsidence, slope failure, and destruction and pose hidden risks of levee failure (Figure 4). Among the weak points, the survey team observed significant anomalies at location T2 on the left bank of the Hoang Long River levee, making it the most vulnerable point in this area. Based on the measured signals, the survey team estimated the size of the weak section, as shown in Table 2.

3. Results and discussion

3.1 Calibration and validation

The calibration and verification are to determine the appropriate parameters for the study area and to simulate the

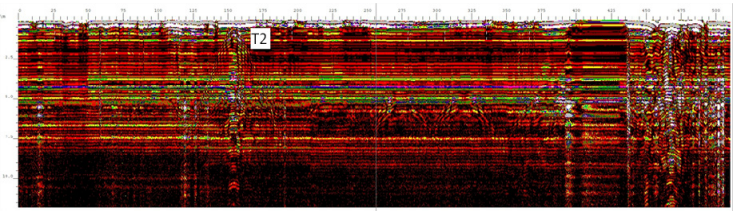

Fig. 4. Abnormal points detected by georadar (T2) on Ta Hoang Long levee

Tab. 3. Model's performance evaluation indicators

	Station	Nash	R^2	Peak flood errors (cm)
Calibration	Ben De	0.91	0.95	26
	Gian Khau	0.81	0.94	21
	Ninh Binh	0.88	0.93	17
Validation	Ben De	0.93	0.95	15
	Gian Khau	0.96	0.96	22
	Ninh Binh	0.96	0.95	21

Tab. 4. Comparison between simulated and measured flood marks

#	Coordinate		Year of 2008 Flood event			Year of 2017 Flood event		
	Longitude X	Latitude Y	Observed (m)	Simulated (m)	Error (m)	Observed (m)	Simulated (m)	Error (m)
1	106.076	20.103	1.1	1.09	0.01	1.05	1.09	-0.04
2	106.071	20.104	1.09	0.93	0.16	1.05	1.08	-0.03
3	106.085	20.084	1.1	1.06	0.04	1.04	1.08	-0.04
4	106.081	20.093	1.11	1.05	0.06	1.05	1.11	-0.06
5	106.089	20.083	1.09	1.05	0.04	1.04	1.04	0
6	106.086	20.091	1.09	1.05	0.04	1.05	1.1	-0.05
7	106.078	20.105	1.12	1.02	0.1	1.07	1.1	-0.03
8	106.079	20.084	1.1	1.06	0.04	1.05	1.04	0.01
9	106.090	20.063	1.1	1.08	0.02	1.05	1.1	-0.05
10	106.079	20.095	1.09	1.03	0.06	1.06	1.09	-0.03
11	106.081	20.101	1.11	1.1	0.01	1.05	1.09	-0.04

dike break scenario later. The large floods in the study area were used for this purpose. The first flooding occurred from October 29, 2008, to November 4, 2008, with the observed rainfall reach 327mm at Ninh Binh station. The water level on the Day river reached 332 cm at Ninh Binh station, causing severe inundation for the river basin. The second flooding occurred from October 3, 2017, to October 13, 2017 making the water level on the Day river reaching 394 cm (at Ninh Binh station). These events are considered as the historical flood events, resulting the severe inundation for the area. Nash-Sutcliffe (Nash J.E., 1970), flood peak error, and coefficient of determination (R2) are used to evaluation the model performance at three hydrological stations.

The comparison between simulated and measured water levels show a good agreement regarding phase and values (Figure 5–10). The Nash-Sutcliffe values range from 0.81 to 0.96 at all three stations during calibration and validation periods. The R2 values range from 0.93 to 0.95 for calibration and validation. The peak flood errors for all stations range from 25 to 26 cm (Table 3).

The study used flood mark data from the flooding events in November 2008 and October 2017 to evaluate the model's performance in flood-prone areas. The comparison of water levels at the flood marks indicates the discrepancy between the simulated and measured values ranging from 0.1 to 0.3 meters (Table 4). These findings suggest that the model well captures the flood extent in the inundated areas. Flood maps for the 2008 and 2017 flood events are presented in Figures 11 and 12, respectively.

The calibration and validation process of the 1-2D hydrodynamic model in MIKE FLOOD demonstrates a good flow simulation in rivers and over flood-prone areas. The Manning's roughness coefficients in the river range from 0.025 to 0.038 ($m^2/^3/s$), while the coefficients over the flooded areas range from 0.03 to 0.056 (m1/3/s). The calibrated and validated model will simulate scenarios involving levee breaches.

Inundation area for dike breach scenarios

The verified model will be used to simulate the dike break scenario. The parameters for the dike breach are determined in Table 2. The study does not consider the influence of rainfall within the study area in evaluating the impact of flooding caused by the dike break. Only the assumption of high water levels in the Hoang Long River leading to the dike break is considered. The simulated results of the dike break scenario using the MIKE FLOOD model are extracted and used to create flood maps using ArcGIS 10.3 software, as shown in Figure 13.

According to the simulation results of the dike break scenario, the flooded area is mainly concentrated in the Gia Vien district, with a commonly observed depth of 2–3 meters covering 3,413 hectares (19.5% of Gia Vien district's total area). The area with an inundation depth of 0.3 to 1.0 meters covers 1,719 hectares (9.8%), while the area with an inundation depth between 1 and 2 meters covers 2,234 hectares (approximately 12.75%) (Figure 13). This information will be crucial for the residents and the authorities to respond to dike break incidents.

4. Conclusions

The safety of dike systems plays a crucial role in protecting human lives and property against the threats posed by river floods. However, levee systems are prone to geological hazards and human-induced damage. Therefore, it is necessary to conduct investigations and surveys to identify vulnerable points in dike systems to implement appropriate response, repair, or improvement measures. In this regard, developing dike breach scenarios is one approach to enhance the capacity to cope with the consequences of dike break. This study conducted a survey to identify weak points in the Hoang Long River dike system in Ninh Binh province. Based on this information, the size, and potential breach locations were determined to simulate the dike breach scenario using the MIKE FLOOD model. The verified model represents well

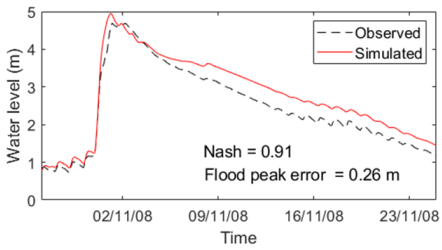

Fig. 5. Simulated and measured water levels at the Ben De station (October 2008 flood event)

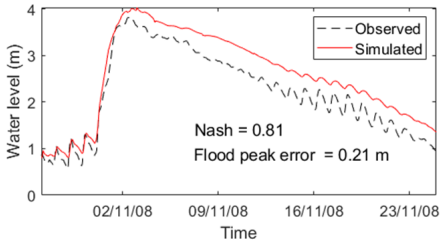

Fig. 6. Simulated and measured water levels at the Gian Khau station (October 2008 flood event)

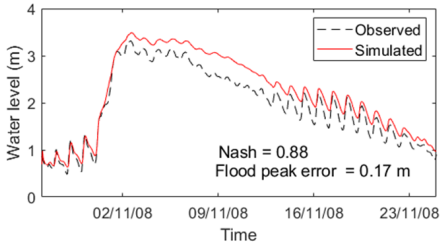

Fig. 7. Simulated and measured water levels at the Ninh Binh station (October 2008 flood event)

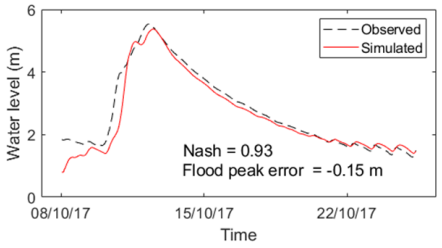

Fig. 8. Simulated and measured water levels at the Ben De station (October 2017 flood event)

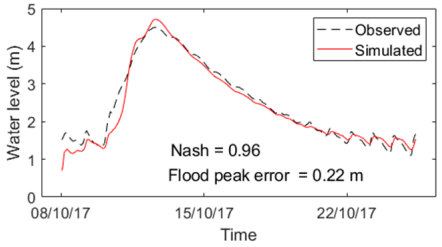

Fig. 9. Simulated and measured water levels at the Gian Khau station (October 2017 flood event)

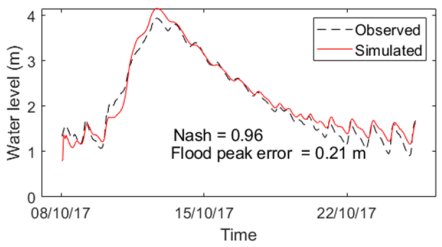

Fig. 10. Simulated and measured water levels at the Ninh Binh station (October 2017 flood event)

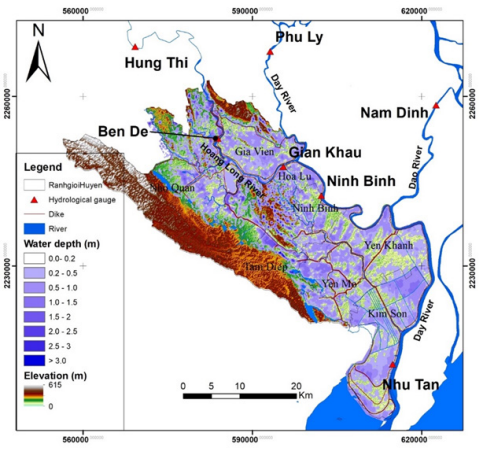

Fig. 11. Flood map of the year of 2008 flood event

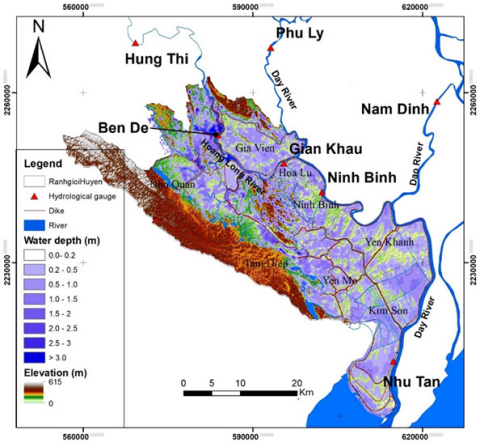

Fig. 12. Flood map of the year of 2017 flood event

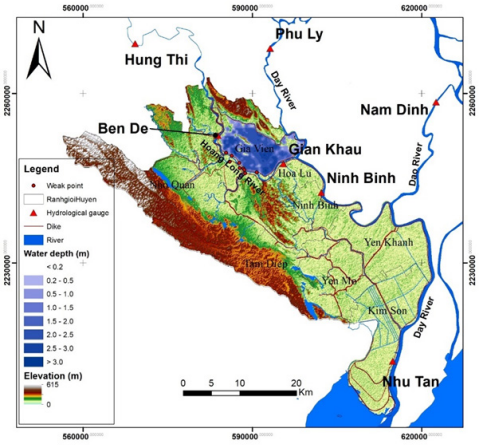

Fig. 13. Flood map according to the dike break scenario.

the historical flood events. The simulation results revealed a Hoang Long dike break's affected area and flood depth. This information will assist managers and residents in developing appropriate strategies to minimize human and property losses during a dike break incident. The results of this approach, overall, tend to be conservative in terms of estimating the fracture size of the dike breach and subsequently, the flood map. The study also demonstrated the potential use of the model for different scenarios or similar regions. Nevertheless, it should be noted that the geo-radar survey method has a depth limitation of 20–30 meters, indicating the need for additional approaches to estimate fracture parameters.

Acknowledgments

Nhu Y Nguyen was funded by Vingroup JSC and supported by the Postdoctoral Scholarship Programme of Vingroup Innovation Foundation (VINIF), Vingroup Big Data Institute (VinBigdata), code VINIF.2021.STS.25.

Literatura – References

1. Ansori M.B., 2021. Flood Inundation and Dam Break Analysis for Disaster Risk Mitigation (a Case Study of Way Apu Dam). . International Journal of GEOMATE, 21, 84–92.
2. Bomers A., 2021. Predicting outflow hydrographs of potential dike breaches in a bifurcating river system using narx neural networks. Hydrology, 8.
3. Brunner G.W.and CEIWR-HEC., 2016. HEC-RAS River Analysis System: User Manual 1D and 2D Version 5.0. US Army Corps of Engineers, 1–790.
4. Dat T.T., Tri D.Q., & and Troung D.D., 2019. he Application of Mike Flood Model in Inundation Simulation with the Dam- break Scenarios : A Case Study of DakDrinh Reservoir in Vietnam The Application of Mike Flood Model in Inundation Simulation with the Dam-break Scenarios : A Case Study of DakDrinh. International Journal of Earth Sciences and Engineering, 12, 60-70.
5. DHI Water and Environment., 2014. MIKE Flood - User Manual. Hydrodynamic Module User Guide, pp. 1–162.
6. Fread D.L., 1991. BREACH: an erosion model for earthen dam failures. Silver Spring. National Weather Service, Office of Hydrology.
7. Froehlich D.C., 2008. Embankment Dam Breach Parameters and Their Uncertainties. Environmental Protection, 134.
8. Huan N.M., 2015. Building Spatial Distribution of Tidal Harmonizing Constituents for Central Vietnam Sea Journal of Science: Natural Sciences and Technology, 31, 157–166.
9. Hue N.H., Huong D.C., & and Thanh N.H., 2019. Technical Solution to Improve the Existing River Dikes for both Flood Prevention and Transportation Purposes. IOP Conference Series: Materials Science and Engineering, 507.
10. Nash J.E., S. J. V., 1970. River flow forecasting through conceptual models part I - A discussion of principles. Journal of Hydrology, 10, 282–290.
11. Nguyen M.T., Sebesvari Z., Souvignet M., Bachofer F., Braun A., & Garschagen M., 2021. Understanding and assessing flood risk in Vietnam: Current status, persisting gaps, and future directions. Journal of Flood Risk Management, 14, 1–24.
12. The Ministry of Agriculture and Rural Development., 2012. Decision 1629/QĐ-BNN-TCTL dated July 10, 2012. Decision on the dike classification and grading in Ninh Binh province.
13. Wu W., 2011. Earthen Embankment Breaching. Journal of Hydraulic Engineering, 137, 1549–1564.
14. Zagonjolli M., 2007. "Dam break modelling, risk assessment and uncertainty analysis for flood mitigation", Taylor & Francis Group Plc, pp. 1–162
15. Sambor A, Szymanek A Analysis of the migration of chemical compounds from fly ash exposed the weather condition ,Chemical and Process Engineering. 2014, ISSN:0208-6425
16. Szymanek A., de las Obras-Loscertales M., Pajdak A.Effect of sorbent reactivity on flue gas desulphurization in fluidized-bed boilers under air firing mode. The Canadian Journal of Chemical Engineering , Volume 96, april 2018, 895-902

Radon-Radium Thermal Mineral Water in Vo Am Ecotourism Project Area, Ngoc Luong Commune, Yen Thuy District, Hoa Binh Province, Vietnam

BAN To Xuan[4)], DUNG Le Tien[1)], DUC Tran Van[2)], TRONG Nguyen Huu[1)], TUAN Truong Duc[3)]*

[1)] University of Mining and Geology
[2)] Ministry of Sciences and Technology
[3)] Northern Vietnam Geological Mapping Division
[4)] University of Mining and Geology; email: toxuanban@humg.edu.vn

http://doi.org/10.29227/IM-2023-02-48

Submission date: 29-08-2023 | Review date: 27-09-2023

Abstract

Ngoc Luong thermal mineral water at Vo Am ecotoursim, Ngoc Luong commnune, Yen Thuy district, Hoa Binh province, northern Vietnam. The thermal mineral water source is at karstic-fractured limstones of Dong Giao Formation aged Anisi. Methods used in this study conists of basic field survey of hydrogeology, resistivity, borehole drilling, pumping tests, and thermal mineral water sample analysis. The thermal mineral water is classified as radon-radium, low mineralised thermal mineral water. The water source is originally related to the deep Moc Chau-Tam Diep Fault directing northwest-southeastward. Its exploration reserve is estimated at 1,497 m³/d with good quality, sastifying all national criterals for the use of domestic supply, bathing, and medical treatment. This is one of ten rare thermal-mineral water sources in Vietnam, containing radon and radium. It is thefore necessary to have good management to ensure the thermal-mineral water to be effectively exploited, used, and protected.

Keywords: *thermal mineral water, Ngoc Luong, Hoa Binh, Vietnam*

1. Introduction

Ngoc Luong thermal mineral water source is located in Vo Am eco-tourism area in Ngoc Luong commune, south of Yen Thuy district (Hoa Binh province), having a boundary with Nho Quan district, Ninh Binh province, about 15km away from Hang Tram town (Figure 1). For a long time, local people have used Ngoc Luong thermal mineral water to bathe effectively for bone and joint diseases (To Xuan Ban, 2021). The Ngoc Luong thermal mineral water has yet listed in the 1996 Vietnam atlas of mineral water and not in a list of the list of 400 national thermal mineral water sources reported by Ho Minh Tho (2019).

Located 10–15km away to the east and southeast of Ngoc Luong source are some thermal mineral water spots such as Kenh Ga, Cuc Phuong, and Thuong Sung in Ninh Binh province (Ho Minh Tho, 2019; Vo Cong Nghiep, 2000). Further to the northwest about 30 to 45 km, in Kim Boi district (Hoa Binh province), there are natural resources of Kim Boi, Sao Bay, Xom Denh (Vo Cong Nghiep, 2000). These thermal mineral water sources have been exploited for bathing and health care. Raw materials from Thuong Sung and Kim Boi are exploited and bottled. The distinctive feature of Ngoc Luong in comparation with other surrounding thermal mineral water is rich in Radon (Rn) and Radium (Ra) contents (To Xuan Ban, 2021), which is effective in treatment of born-relating disses and improving joint function when bathing.

2. Methods

Methods used in this work include basic field investitagtion of hydrogeology, geophysics (resistivity), pumping tests and sample analysis for thermal mineral water. The field investigation is to study the geology and hydrogeology of the site for the potential of thermal mineral water. Resistivity works involves to alocate anorm relating to thermal mineral water in the area. The pumping test was carried out at three discharge rates of 43.0 m³/h, 30.5 m³/h, and 25.0 m³/h at two boreholes at which then were pumped for experimental exploitation at discharge of 25 m³/h for period of 6 months. The two boreholes were then monitored for water levels and temperatural for 12 months. There were 9 groups of water samples at the area to analyze with about 130 thermal water parameters.

3. Results and discussion

3.1. Hydrogeological setting

As with other thermal mineral water sources of Thuong Sung, Kenh Ga, Kim Boi, Sao Bay Xom Denh, etc., Ngoc Luong thermal mineral water resource distributes in the Anisi limestones of the Dong Giao Formation (T2adg). There is an exploration well named as NL2/1 for assessing water reserve and a monitoring borhole QT1 (NL1) penetrating the limestone of Dong Giao limestone Formation (T2adg) overlain by Quaternary sediments of Thai Binh Formation which has a thickness of 2 to 3m (Figure 1 and Figure 2).

Hydrogeological stratigraphic column of NL2/1 well shows 2 layers: the above thin layer of Quaternary sediments directly overlying the below the fracture-karstic aquifer of up to 60m below ground surface. The fracture-karstic aquifer constists of cracked and irregularly karstified massive blueish grey limestones. The karstification of limestones is irregular with short unconected kartsic caves with cave heigh of 0.5 to 1.2m. Backfilling caves are also different with two emplty caves above and one below filling with clay materials. Aquifer thickness at NL2/1 well is 25m. The aquiclude consists of blueish grey limestones and dolomitestones which are mas-

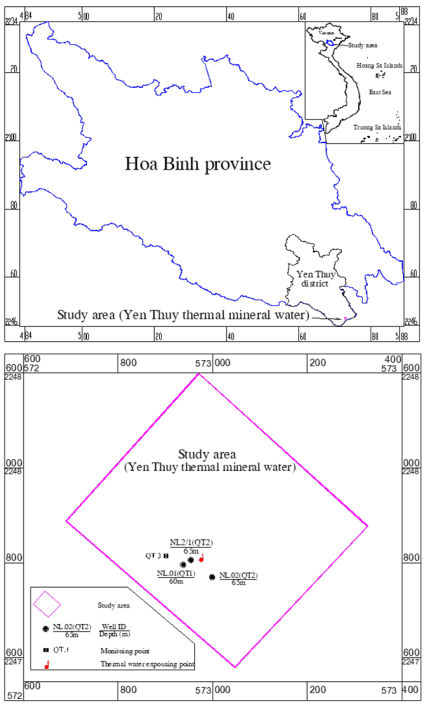

Fig. 1. A sketch map showing location of Ngoc Luong thermal mineral water

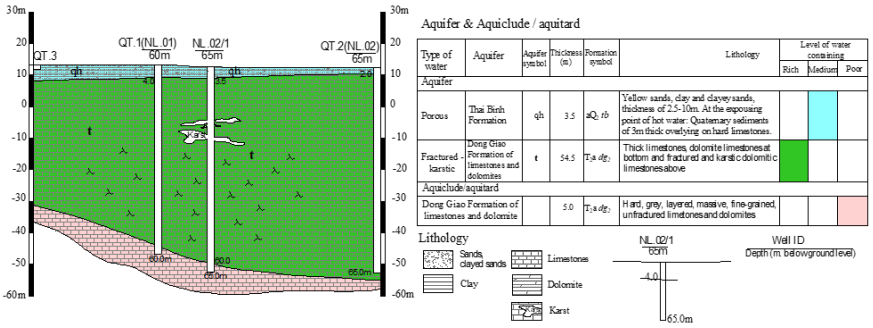

Fig. 2. Hydrogeological cross-section at Ngoc Luong thermal mineral source

sive, unfractured or weekly fractured locating at depth greater than 60 bewlow surface (Figure 3).

Field investigation and pumpinng tests at Well NL2/1 and 2 monioting wells QT1 abd QT2 indicates that thermal water at Well NL2/1 is confined (To Xuan Ban, 2021). Thermal mineral water source from deep below, extruding to the surface via cracks and fractures and exposing on the surface in the form of extrusion and effervescent circuits. The water pumping test of 15 days long (45 shifts) and trial exploitation of 6 months long with an abtraction rate of 600 m^3/day at Well NL2/1 along with monitoring time of 12 months at the monitoring Well QT1 and QT2) were carried. The results are shown in Table 1, Table 2 and Table 3.

3.2. Quality of thermal mineral water

To evaluate the quality of the Ngoc Luong thermal mineral water source, 9 sets of samples were analyzed, each set was analyzed with 130 parameters. Of 9 sample sets, 3 sets were taken at pumping tests (3 times water abstraction), another 3 sets of samples were taken in 6 months of trial exploting pumping and the last 3 sets of samples taken in 12 months of monitoring. The results were summazed, compared with the standards of water quality.

The basic chemical composition of water

The basic chemical composition of the thermal mineral water includes 17 parameters: color, turbidity, taste, pH, total dissolved solids (TDS); cations (Na^+, K^+, Ca^{+2}, Mg^{+2}, Fe^{+3}); anions (Cl^-, HCO_3^-, SO_4^{-2}), free CO_2, total hardness. Figure 3 indicates that the chemical composition of the samples was taken under different conditions and time, but the distribution was concentrated and stable in the calcium magnesium bicarbonate field. That shows that the water source is not mixed and does not fluctuate over time.

Classification of the Ngoc Luong thermal mineral water

According to Circular No.52/2014/TT-BTNMT of Vietnam Ministry of Natural Resources and Environment (2014), Ngoc Luong thermal mineral water is classified as a natural thermal mineral water with low mineralization, radon, radium (Table 4). The nominal values have very stable values, being unchanged with season and to the experimental pumping tests.

The thermal mineral water for drinking botter

Assessment according to QCVN 6-1: 2010/BYT of Ministry of Health Portal of Vietnam (2010), including 25 criteria Sb, As, Ba, B, Cu, CN, F, Pb, Mn, Hg, Ni, NO_3, NO_2, Se, sur-

Tab. 1. Summary of 15-day-pumping tests at NL2/1 well and monitoring at QT1 and QT3

Times	Pumping well				Monitoring wells			
	NL2/1				NL1 (QT1)		Surface water (QT3)	
	Discharge rate Q (m^3/h)	Drawdown S (m)	Specific discharge q (l/s.m)	Temperature (°C)	Drawdown S (m)	Temperature (°C)	Variation in temperature (degree Celcis)	Variation in water level* (m)
1st	43.0	5.17	2.30	41.0	2.60	40.5	14-23	0.5-0.8
2nd	30.5	4.38	2.12	41.0	1.75	41.0	15-24	0.9-1.1
3rd	25.0	2.88	2.41	41.0	1.66	41.0	15-23	0.8-1.3

Tab. 2. Summary of a 6-month-long pumping test

	Pumping Well NL2/1				Monitoring Well QT1 (NL1)			Monitoring QT3 (Surface water at the trend)*		
	Elevation of water level (m)	Water level (m)	Discharge rate (m^3/h)	Temperature (^{0}C)	Elevation of water level (m)	Water level (m)	Temperature (^{0}C)	Elevation of water level (m)	Water level (m)	Temperature (^{0}C)
Average	8.63	3.98	25	40.05	8.60	4.63	40.19	13.09	0.25	28.34
Maximum	8.70	4.05	25	40.64	8.65	4.7	40.64	13.34	0.57	35.83
Minimum	8.58	3.91	25	39.06	8.54	4.58	39.54	12.77	0.00	20.74

Tab. 3. Summary of 12-month-long monitoring record at QT1, QT2, and QT3

	Well NL2/1		Well QT1		NL2 QT2		Surface water QT3	
	Elevation of water level (m)	Temperature (^{0}C)	Elevation of water level (m)	Temperature (^{0}C)	Elevation of water level (m)	Temperature (^{0}C)	Elevation of water level (m)	Air temperature (^{0}C)
Min	11.25	39.0	10.05	39.00	12.61	28.00	12.54	17.00
Max	11.67	41.0	10.50	40.00	13.02	29.00	13.31	38.00
TB	11.52	40.3	10.37	39.92	12.91	28.85	13.08	26.45

factants, pesticide residues and PCBs, mineral oils, polycyclic aromatic hydrocarbons, E. Coli or heat-resistant coliform, Total Coliform, Streptococi feacal, Pseudomonas aeruginosa, Spores of sulfite-reducing anaerobic bacteria.

The thermal mineral water for drinking water

Assessment according to QCVN 01-1:2018/BYT of Ministry of Health Portal of Vietnam (2018), including 99 indicators belonging to the groups of microbiological parameters, inorganic organoleptic parameters, parameters of disinfectant chemicals and by-products, and level of radiation contamination.

Combining QCVN 6-1:2010/BYT (2010) and QCVN 01-1:2018/BYT (2018) of Ministry of Health Portal of Vietnam indicates that Ngoc Luong hot mineral water source in borehole NL2/1 is qualified for drinking and bottling.

Ngoc Luong thermal mineral water for bathing

In comparation with the table of criteria and standards of therapeutic mineral water (total mineralization, free CO2, total (H_2S+HS^-), H_2SiO_3, (Fe^{+2}+Fe^{+3}), F^-, As, Br, I, Rn, Ra and temperature), Ngoc Luong mineral water source meets three criteria. That is the temperature and radon and radium content. Specifically: the temperature is higher than the specified value to 100 C; average radon (Rn) content of 2.52 nCi/l, more than 2 times higher than the regulation; radium (Ra) content averaged 5.45.10–11 g/l, 5 times higher than prescribed. With the above characteristics, Rn and Ra Ngoc Luong hot mineral water sources are very rare in the Northern region and in the territory of Vietnam.

3.3. Reserves of Ngoc Luong thermal mineral water

Ngoc Luong thermal mineral water source is distributed in the fractured zone, karstic systems of limestones, dolomitic limstones (To Xuan Ban, 2021). To Xuan Ban (2021) reported total reserves and resources in Well NL2/1 is 1497 m^3/day (combination grade B and C1; with grade B of 600 m^3/day and grade C1 of 897 m^3/day). Compared with neighboring non-renewable sources, Ngoc Luong thermal mineral water resource is in the group of large reserves.

3.4. Origin of Ngoc Luong thermal mineral water

Origin models of thermal mineral water

Natural thermal mineral water is a special type of water of geological origin, overflowing on the ground or located at a small depth, which can be exploited and used for very different purposes depending on the characteristics of the source. Thermal mineral sources are natural underground water formed by a geological process, with temperature, mineral composition and chemical, physical, microbiological properties, purity, meeting standards and regulations. Technical standards can be exploited for use in drinking, bottling, bathing, and medical treatment. Thermal mineral water often contains a small amount of dissolved chemical compounds in the form of cations and anions. The pH of thermal mineral water ranges from very acidic to alkaline, silicon-saturated alkaline chloride, calcium bicarbonate. Some sources contain iron cations and other metals. The temperature, chemical composition change from one source to another and over time, seasonally, affected by neighboring groundwater sources.

Thermal mineral water is derived from groundwater and rain water (meteorological water). These water move deep down. At the great depths of the Earth's crust, water is heated by heat sources and moves back to the upper part and extrudes to the surface. The most favorable path of moving downwards and extruding back to the surface is tectonic faults, especially deep faults, strongly deformed and fractured soil and rock (Figure 4).

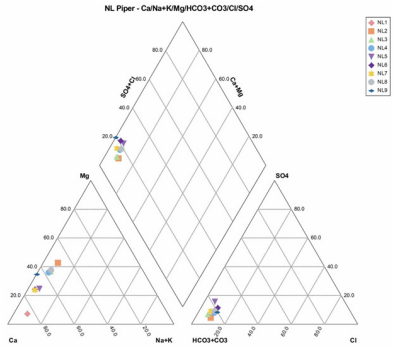

Fig. 3. A piper diagram showing sample analysis of Ngoc Luong thermal mineral water

Tab. 4. Classification of Ngoc Luong thermal mineral water according to the Circular No.52/2014/TT-BTNMT [* Standard according to TT 52/2014 of Vietnam Ministry of Natural Resources and Environments. ND: Not ditected]

#	Parameters	Unit	TT52/2014 /BTNMT*	Name of mineral water	Results of Well NL2/1	Assessment
1	TDS	mg/l	≥ 50 – 500	Low mineral water	297	Acceptable
2	CO_2 (free gas)	mg/l	≥ 500	Carbonic mineral water	30.57	
3	Total ($H_2S + HS^-$)	mg/l	≥ 1	Sulphuric mineral water	ND	
4	$H_2SiO_3^+$	mg/l	≥ 50	Silic minerl water	ND	
5	Iron ($Fe^{2+} + Fe^{3+}$)	mg/l	≥ 10	Ironic mineral water	ND	
6	Flourite (F^-)	mg/l	≥ 1.5	Flourite mineral water	ND	
7	Asenic (As^-)	mg/l	≥ 0.7	Asenic mineral water	ND	
8	Brom (Br^-)	mg/l	≥ 5	Bromic mineral water	ND	
9	Iod (I)	mg/l	≥ 1	Iodic mineral water	ND	
10	Radon (Rn)	nCi/l	> 1 nCi/l	Radonic mineral water	2.52 nCi/l	Acceptable
11	Radi (Ra)	g/l	> 10^{-11} g/l	Radii mineral water	5.45*10^{-11}g/l	Acceptable
12	Temperature	° C	≥ 30	Thermal mineral water	40° C	Acceptable

The analysis results of oxygen isotope δ18O and hydrogen δ2 H from hot mineral water sources around the world show that most of the thermal mineral water is formed by the mixing of meteorological water and thermal water from magma sources at different ratios. The heat sources that create hot water mineral include residual heat source of magma blocks, geothermal gradient source, heat source due to radioactive decay reactions.

Chemical compounds are present in thermal mineral water sources due to many reasons: provided by gases or hydrothermal solutions of magma during crystallization, during metamorphism. On the way to move upwards, hot water sources with high temperatures, containing gases cause chemical reactions with surrounding minerals and rocks, and are supplied with additional chemical components. The dissolution process is very favorable when the hot water source moves through the limestone strata, ore bodies containing sulfur minerals. Many hot water springs are surface manifestations of underground "thermothermal" mineral deposits. For example, when the source of hot water moves in limestone layers will have a following reaction:

$$CaCO_3 + H_2O + CO_2 \leftrightarrow Ca^{+2} + 2HCO_3^-$$

The source will receive more calcium bicarbonate. When the hot water source moves through the sulphur ore bodies, it is possible to receive more sulphate according to following reaction:

$$2FeS_2 + 7O_2 + 2H_2O \leftrightarrow 2Fe^{2+} + 4SO_4^{-2} + 4H^+$$

As a result of the processes of dissolving, mixing, acquiring more components due to chemical reactions, from an initial meteorite water source, it has developed into many sources of thermal mineral water with different chemical compositions. In fact, in Hoa Binh province, the source of Sao Bay (Kim Boi district, Hoa Binh province) Aqueous Minerals is located near pyrite ore bodies, so the sulphate content is higher, higher than that of Ngoc Luong, Bo, Kim Boi, Dinh hamlets (Cao The Dung, 2013, 2015; Tran Ngoc Minh, 1997).

In areas where thermal mineral water is developed, large-scale heat sources in the depths may appear. The temperature in the depths can be up to several hundred degrees, exploited for different needs such as electricity generation, heating and many other applications. For example, the geothermal energy of the Malawi rift, Mozambique in South Africa (Estefanny Davalos-Elizondo, Eliot A. Atekwana, et al.D. A. L. Davila, 2021) is very large (Figure 5). Thermal mineral water points with temperature from 35 to 80°C, the type of hot mineral water is sodium sulfate (bicarbonate), sodium bicarbonate (sulphate) and sodium chloride (sulphate). Depending on the location, at a depth of up to 1000m, the temperature rises to 100°C, the depth of 2500m, the temperature rises to 150°C. Figure 5 indicates cold meteoric rainwater moves down deep along faults heated by heat sources; parent water continues to be heated further as it approaches the heat source, and mixing water after being heated, goes up and mixes with the aquifer farming and adding CO_2 (Emmanuel A. Njinju et al., 2019; Estefanny Davalos-Elizondo, Eliot A. Atekwana, Estella A. Atekwana, et al., 2021).

Radon-radium thermal mineral water in the Moc Chau-Tam Diep deep fault zone

The Moc Chau-Tam Diep deep fault has been known in many geological documents in Vietnam, extending for more than 100 km from Mai Chau (Son La province) through Ngoc Luong (Yen Thuy, Hoa Binh province) to Tam Diep area (Ninh Binh province) in northwest southeast direction (Cao Dinh Trieu & Pham Huy Long, 2002). The fault of large scale coincides with the topographic elevation levels and indicates with

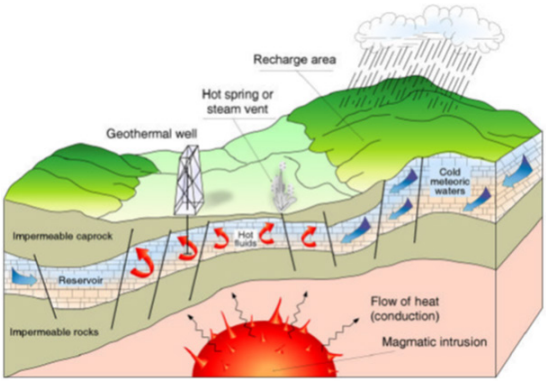

Fig. 4. A simple model explaining the form of a source of thermal mineral water and geothermal system (Mary H.Dicson & Mario Fanelli, 2004)

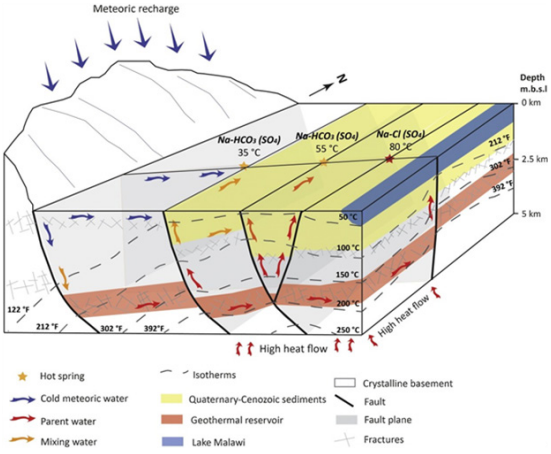

Fig. 5. A schematic geothermal conceptual model of the Malawi Rift Zone, explaining the form of thermal mineral water and heat sources (Dávalos-Elizondo et al., 2021)

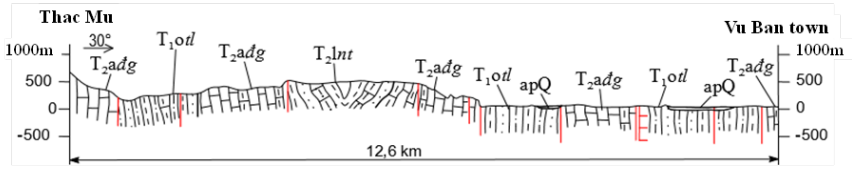

Fig. 6. Geological cross-section showing the allocation of Thac Mu-Vu Ban within the Moc Chau – Tam Diep tectonic zone. Note: T1tl: Tan Lac Formation (Brownish red sandstones, siltstones, claystones); T2ađg: Dong Giao Formation (limstones, dolomitic limestones, dolomite); T2lnt: Nam Tham Formation (clayed limestones, siltstones, schist), aqQ: alluvium-prolovium sediments (gravels, sands, silts, clays)

Vu Ban - Hang Tram (Hoa Binh province) - Tam Diep (Ninh Binh province) negative topographic valley line, filled with Quaternary sediments. According to the section from Vu Ban town (Hoa Binh province) through Con River, to Thac Mu (Lac Son, Hoa Binh province), the deformation zone is over 12 km wide (Le Tien Dung & To Xuan Ban, 2021), conisisting of limestones and shale bands of milonitization, slab slope angle 85–900 interspersed with dolomitic cataclasite limestone beds and tectonic gritstones (Figure 6 and Figure 7).

According to Cao Dinh Trieu and Pham Huy Long (2002), the Moc Chau-Tam Diep fault, plugged to the northeast, 100km long and 20km wide, includes a series of faults of the same nature. The slope is right, plugging to the northeast, forming a zone of step structure, the foundation surface crystallizes within 2–3km. Conrad face (12–14 km) and Moho face (26–30 km) (Nguyen Van Hoanh, 2005). The influent depth of the fault is 35–40km. The zone coincides with the band-positive structure, the Bouguer gravity anomaly varies in the range of -50 to +10 mGal, the relative positive structure of the magnetic field has a variable value in the range of from -200 to +40. The fault bodies of the zone coincide with the gravity anomalous horizontal gradient with an average value of 1.0–2.5 mGal/km and the horizontal anomalous gradient from the air with an average intensity of 8.0–12 nT/kilometer. Along the fault, earthquakes of magnitude Ms approximately 4.0–4.9 magnitude are observed and hot mineral water sources.

3.5. Therapeutic effects of radon-radium thermal mineral water at Ngoc Luong

Ho Minh Tho (2019) reported that among 400 sources of thermal mineral water in Vietnam, there are only 8 sources having radii and 8 sources featured with radon in water. The Ngoc Luong thermal mineral water sources is istingushed to have both radon and radii. The nearsest sources to Ngoc Luong are La Phu flouride-radon thermal mineral water located in Thanh Thuy district, Phu Tho province, and Tan Vien radii thermal mineral water located at Tan Linh moutain, Ba Vi district, Hanoi.

Accoring to the medical studies of La Phu source, the fouride-radon thermal mineral water featured with present of

Fig. 7. Deformed limestone (right) and claystone steep dipping in Moc Chau-Tam Diep milonite fractured zone

Fig. 8. Local people taking bath with thermal water abstracted from the Welll NL02 at Ngoc Luong thermal mineral water sources

radi element have more use and effect (www.tnmtphutho.gov.vn). Bathing: when soaking or submerging whole or part of man body in the mineral water, radon can penetrate through skin to the bloodstream and reach the cells. This therapy is effective for treating diseases of cardiovascular, musculoskeletal, and peripheral nervous system. Drinking: drinking radon-mineral water at appropriate level of doses has strong effect on body because it adsorps radon into blood, absorbing more radiation than bathing therapy. Radon in water also helps to improve function, enhance the secretion of gastric juice and the activity of the stomach, and improve the lipid exchange. Inhalating: this therapy is effective for respiratory and circulatory diseases. Enema pumping: enema, pushing radon-mineral water into rectum to treat some intestinal diseases. Mud bathing: covering body with mud containing radon-mineral water to treat diseases relating to joints, nervous system, circulatory system and de featuring with flouride – radon found in the thermal water to treat diseases relating to joints, nervous system, circulatory system, and dermatology.

There has yet been any medical research to evaluate curative effects of the Ngoc Luong thermal mineral water. However, over the years, local people daily come to bathe with Ngoc Luong thermal mineral water because of its effectiveness in treatment of osteoarthritis and cardiovascular diseases (Figure 8).

4. Conclusions

Ngoc Luong thermal mineral water source is in the Vo Am eco-tourism project area, Yen Thuy district, Hoa Binh province, Vietnam. The thermal mineral water belongs to the group of calcium bicarbonate, distributed in the system of fractures, karstic caves of the Dong Giao Formation aged Anizi.

Thermal mineral water has a high temperature (40°C), the content of physico-chemical indicators is stable, meeting the requirements for bottling, bathing, caring and health recovering. Identification of Ngoc Luong water source is of natural thermal mineral water, low mineralization, radon, radium.

The radon and rdium contents of Ngoc Luong thermal mineral water are higher than that of other thermal mineral water sources located around Hoa Binh and Ninh Binh provinces, which is believed to be in relation to the Moc Chau – Tam Diep deep fault. The presence of radon and radium in Ngoc Luong thermal mineral water increase its effect for healing, bathing, and restoring health.

From the fact that the source of Ngoc Luong NKN is very effective for bathing, treating bone, joint and cardiovascular diseases. To improve the efficiency of using Ngoc Luong renewable resources, it is necessary to conduct systematic scientific studies, evaluate the properties of hydrotherapy, thermotherapy, mineralotherapy, and propose procedures for the use of mineral resources. scientific, reasonable, economical, and effective.

Literatura – References

1. Cao Dinh Trieu & Pham Huy Long, 2002. Fault tectonics in Vietnamese territory. Hanoi: Science and Technics Publishing House.
2. Cao The Dung, 2013. Report on mineral water exploration at KB1 borehole, Bo town, Kim Boi district, Hoa Binh province. . Retrieved from
3. Cao The Dung, 2015. Report on exploration of mineral water at SB1 and SB2 Boreholes, Sao Bay village, Kim Boi district, Hoa Binh province. . Retrieved from
4. Dávalos-Elizondo, E. , A., E. A., , Atekwana, E. A., Tsokonombwe, G., & and Laó-Dávila, D. A., 2021. Medium to low enthalpy geothermal reservoirs estimated from geothermometry and mixing models of hot springs along the Malawi Rift Zone: Geothermics, v. 89.
5. Emmanuel A. Njinju, Estella A. Atekwana, D. Sarah Stamps, Mohamed G. Abdelsalam, Eliot A. Atekwana, Kevin L. Mickus, S. F., và nnk,Nyalugwe, V. N., 2019. Lithospheric Structure of the Malawi Rift: Implications for Magma-Poor Rifting Processes. Tectonics Volume 38, Issue 11 p. 3835-3853.
6. Environment, M. o. M. R. a., 2014. Circular No. 52/2014/TT-BTNMT dated 9th September 2014 of Vietnam Ministry of Natural Resources and Environment on Regulations on decentralization of reserves and resource of mineral water and natural thermal water
7. Estefanny Davalos-Elizondo, Eliot A. Atekwana, Estella A. Atekwana, Gift Tsokonombwe, & Davila, D. A. L., 2021. Medium to low enthalpy geothermal reservoirs estimated from geothermometry and mixing models of hot springs along the Malawi Rift Zone. Geothermics. Volume 89, January 2021, 101963.
8. Estefanny Davalos-Elizondo, Eliot A. Atekwana, E. A. A., Gift Tsokonombwe, , & D. A. L. Davila, 2021. Medium to low enthalpy geothermal reservoirs estimated from geothermometry and mixing models of hot springs along the Malawi Rift Zone. Geothermics. Volume 89, January 2021, 101963.
9. Ho Minh Tho, 2019. Solutions for rational exploitation, use and protection of thermal mineral water resources in Vietnam. Report of science and technology project, Hanoi.
10. Le Tien Dung & To Xuan Ban, 2021. Report on implementation of science and technology project entitled Research and build a database on natural tourism resources for sustainable tourism development in Hoa Binh province. Hoa Binh province.
11. Mary H.Dicson & Mario Fanelli, 2004. What is Geothermal Energy, Istituto di Geoscienze e Georisorse, CNR , Pisa, Italy, 2004.
12. Ministry of Health Portal, 2010. QCVN 6-1: 2010/BYT. National technical regulation for bottled/packaged natural mineral waters and drinking waters.
13. Ministry of Health Portal, 2018. QCVN 01-1:2018/BYT. National technical regulation on Domestic Water Quality.
14. Nguyen Van Hoanh, 2005. Ninh Binh Geological map (F-48-XXXIV), scale 1:200,000. General Department of Geology and Mineral Resources of Vietnam.
15. To Xuan Ban, 2021. Report on exploration results of hot mineral water in Ngoc Luong commune, Yen Thuy district, Hoa Binh province. Hanoi.
16. Tran Ngoc Minh, 1997. Searching for mineral water in Thuong Sung area, Ninh Binh. Cuc Phuong Mineral Water Company, Ninh Binh. Geological Archives, Hanoi.
17. Vo Cong Nghiep, 2000. Atlas of thermal and mineral water of Vietnam. Department of Geology of Vietnam.

Prediction of Road Subsidence Caused by Underground Mining Activities by Artificial Neural Networks

Hung Viet NGUYEN[1)], Duyen Quang LE[2)], Long Quoc NGUYEN[3,4)], Tomasz LIPECKI[5)]*

[1)] Faculty of Information Technology, University of Transport and Communications, Hanoi, Vietnam; ORCID https://orcid.org/0009-0005-1104-5161
[2)] Faculty of Petroleum and Energy, Hanoi University of Mining and Geology, Hanoi, Vietnam; ORCID https://orcid.org/0000-0001-6953-4762
[3)] Faculty of Geomatics and Land Administration, Hanoi University of Mining and Geology, Hanoi, Vietnam; ORCID https://orcid.org/0000-0002-4792-3684
[4)] Innovations for Sustainable and Responsible Mining (ISRM) Research Group, Hanoi University of Mining and Geology, Hanoi, Vietnam;
[5)] Faculty of Geo-data Science, Geodesy and Environmental Engineering, AGH University of Krakow, Kraków, Poland; ORCD https://orcid.org/0000-0002-3204-7343
* Corresponding author: lequangduyen@humg.edu.vn

http://doi.org/10.29227/IM-2023-02-49

Submission date: 30-08-2023 | Review date: 29-09-2023

Abstract

Mining-induced road subsidence is a significant concern in areas with extensive underground mining activities. Therefore, the prediction of road subsidence is crucial for effective land management and infrastructure planning. This paper applies an artificial neural network (ANN) to predict road subsidence caused by underground mining activities in Vietnam. The ANN model proposed in this study is adopted relying on the recursive multistep prediction process, in which the predicted value in the previous step is appended to the time series to predict the next value. The entire dataset of 12 measured epochs covering 12 months with a 1-month repeat time is divided into the training set by the first 9 measured epochs and the test set by the last 3 measured epochs. K-fold cross validation is first applied to the training set to determine the best model's hyperparameters, which are then adopted to predict land subsidence of the test set. Absolute errors of the predicted road subsidence depend on the separated time between the last measured epoch and the predicted epoch. Those errors at the 10th month of the three tested points are 3.0%, 0.1 %, and 0.1%, which increase to 4.8%, 3.3%, and 1.5% at the 11th month, and 7.2%, 2.5% and 1.3% at the 12th month. The absolute errors are found to be small, which were all ranged with 0.5 mm and demonstrates that the proposed method utilizing ANN in this study can produce good prediction for road subsidence time series at mining areas.

Keywords: *subsidence prediction, underground mine, machine learning, ANN*

1. Introduction

In many nations, including developing countries, mining activities have played an important role in economic development (Hilson, 2002), which includes resource provision with valuable minerals, metals, and other resources to various industrial sectors, e.g., manufacturing, construction, energy (Fan, Yan, & Sha, 2017). However, the relationship between mining activities and economic development has been proved to be complex (Knierzinger, 2014). Additionally, the mine industry provides jobs (Fleming & Measham, 2014) in various sectors, e.g., geology, surveying, electrics. The Vietnamese mining industry has a long history, which made contributions to the Vietnam's economy (B. N. Nguyen, Boruff, & Tonts, 2021). Vietnam has diversity in ore occurrence with around 70 types of minerals (B. N. Nguyen, Boruff, & Tonts, 2017), among which coal is the main mineral source – most of the Vietnam coal mines located in Quang Ninh province. Of those, the percentages of underground and open pit coal mines are about 60% and 40% respectively, with the exploration volume projected to increase yearly (B. N. Nguyen et al., 2021). With some open-pit coal mines being transmitted to underground mines due to their increasing depths, the proportion of underground mines is increasing (Q. N. Nguyen, Nguyen, Pham, & Chu, 2021). The roles of Vietnam coal are not only economic growth in terms of mineral export but also political energy security in terms of coal-fired electricity generation (Dorband, Jakob, & Steckel, 2020).

In spite of the economic contributions, mining activities also result in environmental challenges (Mohsin, Zhu, Naseem, Sarfraz, & Ivascu, 2021), of which surface subsidence is a popular outcome. This environmental problem in turn poses significant risks to infrastructure, environmental stability, and human safety in mining areas (Marschalko et al., 2012). Mining-induced land subsidence can be measured by different methods, such as leveling (e.g., Todorović, 1993), Global Navigation Satellite System (GNSS) (e.g., Bian, Zhang, Zhang, & Zheng, 2014; Jing-xiang & Hong, 2009), and Interferometric Synthetic Aperture Radar (InSAR) (e.g., Bui et al., 2021; Kim, Tran, Bui, & Lipecki, 2021; Q. L. Nguyen, Tran, & Bui, 2021). Land subsidence caused by mining activities can be measured after the Earth's surface has subsided, efficient management and prediction of mining-induced land subsidence in the future are also crucial for sustainable mining practices and land use planning (Ma, Li, & Zhang, 2017). The traditional empirical approach based on a combination of experience and analysis of a large set of observations (Aston, Tammemagi, & Poon, 1987), and the analytical approach relying on computerized mathematical models (Bahuguna,

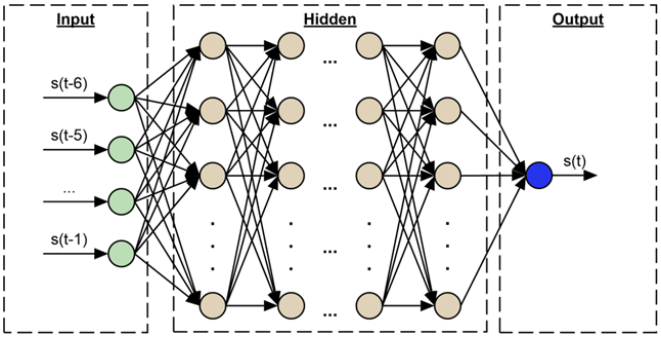

Fig. 1. Structure of artificial neural network with input, hidden, and output layers used in this study

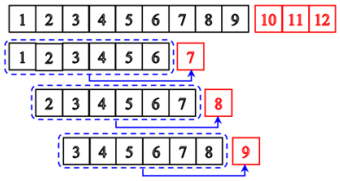

Fig. 2. Recursive multistep prediction process in this study. Black squares indicate inputs of the model and red squares correspond to outputs

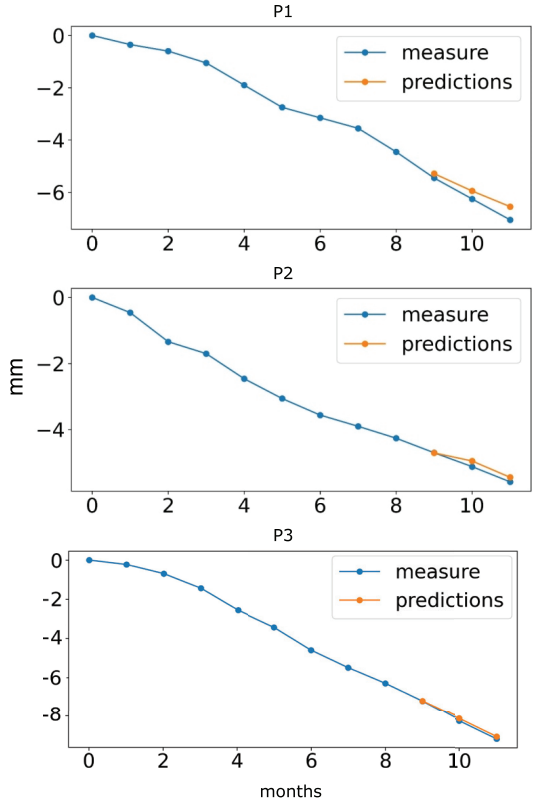

Fig. 3. Comparison between measured and predicted subsidence [mm] of point P1, P2 and P3

Srivastava, & Saxena, 1991) have been widely adopted. However, these methods often lack accuracy and predictive capability. In recent years, Artificial Neural Networks (ANNs) have emerged as a promising tool for subsidence prediction due to their ability to capture complex nonlinear relationships within datasets (e.g., Ambrožič & Turk, 2003; Lee, Park, & Choi, 2012; Rafie & Samimi Namin, 2015). This is because of the advantages of ANN that is an advanced computing system stimulating human neural networks. It is therefore a kind of data-driven self-learning, self-organizing system capable of solving a nonlinear dynamic system (Ambrožič & Turk, 2003).

In this article, ANN is adopted to predict underground mining-induced road subsidence, leveraging their strengths in pattern recognition, adaptive learning, and generalization, so as to introduce an alternative method of land subsidence in mining areas. By exploring the capabilities of the ANN models applied to underground mining-induced road subsidence, this study aims to contribute to the advancement of subsidence prediction techniques and support sustainable mining practices.

2. Neural Networks and Model Evaluation

2.1 Artificial Neural Networks

Tab. 1. Subsidence corresponding to the training set incorporating values from the first nine months. (Units: mm)

Month	Point P1	Point P2	Point P3
1	0	0	0
2	-0.4	-0.5	-0.2
3	-0.6	-1.3	-0.7
4	-1.1	-1.7	-1.4
5	-1.9	-2.5	-2.6
6	-2.8	-3.1	-3.4
7	-3.2	-3.6	-4.6
8	-3.6	-3.9	-5.5
9	-4.5	-4.2	-6.3

Tab. 2. Comparison of measured and predicted subsidence at Point 1

Month	Measured (mm)	Predicted (mm)	Abs. Error (mm)	Rel. Error (%)
10	-5.5	-5.3	-0.2	3.0
11	-6.3	-5.9	-0.4	4.8
12	-7.1	-6.5	-0.6	7.2

Tab. 3. Comparison of measured and predicted subsidence at Point 2

Month	Measured (mm)	Predicted (mm)	Abs. Error (mm)	Rel. Error (%)
10	-4.7	-4.7	0	0.1
11	-5.1	-4.9	-0.2	3.3
12	-5.6	-5.4	-0.2	2.5

Tab. 4. Comparison of measured and predicted subsidence at Point 3

Month	Measured (mm)	Predicted (mm)	Abs. Error (mm)	Rel. Error (%)
10	-7.2	-7.2	0.0	0.1
11	-8.2	-8.1	-0.1	1.5
12	-9.1	-9.0	-0.1	1.3

ANNs are among the artificial intelligence powerful tools used in land subsidence prediction owing to their ability to learn complex patterns with a large dataset by which accurate predictions can be conducted (e.g., Ambrožič & Turk, 2003; Yang & Xia, 2013). ANNs are computational models inspired by the structure of the human brain, and thus neural networks (Zou, Han, & So, 2009). They compose of a number of interconnected artificial neuron layers, which is divided into input, hidden, and output layers (see Figure 1). The input layer imports the input features then passes them through the hidden layers, in which computations are conducted with a series of weighted connections by which the predicted variables are estimated in the output layer. The weights are initially assigned with random values in the input layer, which are then propagated through the hidden and output layers. The weights are subsequently adjusted by optimization algorithms, e.g., gradient descent and backpropagation (Amari, 1993). In this way, ANN can accurately predict the output variables via adjusting the weights.

In an ANN, each layer involves one or more neurons depending on the specific problem under investigation. In this study, the input layer includes six neurons corresponding to six previous subsidence measurements from s(t-6) to s(t-1) used to predict the subsidence at the time t (i.e., s(t)). The hidden layer section includes one or more layers with each incorporating a number of nodes. In this study, the 'optimal' number of hidden layers, hidden nodes, and iterated backpropagation epochs are experimentally determined by the so-called k-fold cross validation (Fushiki, 2011).

There are a total of 12 subsidence observations measured once a month, corresponding to a year of measurement. With this number of observations, we divide the dataset into the training set incorporating the first nine measurements and the remaining three months are selected as the test set. To train the model based on the training set, we use the previous six measurements as the inputs and the next measurement as the output as shown in. This process is called recursive multistep prediction. Specifically, the first six months are first used as the inputs and the seventh month as the output. Then, the time series is one-step moved forward with the second month to the seventh month as inputs and the eighth month as output. Likewise, the third month to the eighth month are used as the inputs to predict the ninth month. In this way, the back propagation process is utilized based on the differences between predicted and measured values at the months 7, 8, and 9 (see Figure 2). The model's parameters after training are then used to predict subsidence at the months 10, 11, and 12. To this end, the values from the fourth month to the ninth month are used to predict the subsidence of the tenth month. Then, the predicted at then tenth month is appended to the time series to predict the eleventh month. Finally, a similar process is adopted to predict subsidence of the twelfth month.

2.2 Model Performance Evaluation

To evaluate the performance of mining-induced road subsidence prediction by ANN in this study, two validation metrics are employed in this study, including absolute and relative errors, which are:

$$Abs.Err_i = \eta_i - \hat{\eta}_i \tag{1}$$

$$Rel.Err_i = \frac{\eta_i - \hat{\eta}_i}{\eta_i} \times 100\% \tag{2}$$

where η_i and $\hat{\eta_i}$ are the measured and predicted subsidence.

3. Numerical Examples

In this study, three points measured by the leveling method over an underground mine in Vietnam are tested as numerical examples. The three points are named P1, P2, and P3 located in a road where transportation for mining is active. As mentioned above, each point was measured with 12 epochs at a monthly interval. The first nine months are selected as the training set, i.e., to train the model, and the last three months as the test set, i.e., to forecast subsidence. Programming code

is written in Python with the scikit-learn package (Pedregosa et al., 2011). Table 1 shows the measurements of the three tested points corresponding to the training set of the first nine months.

Road subsidence of the last three months are predicted relying on the parameters found from the training set with the results shown in Table 2 (Point 1), Table 3 (Point 2), and Table 4 (Point 3). In those tables, the predicted values are compared with the measured values by which the absolute (Abs.) errors in mm are computed. Additionally, the relative (Rel.) errors are computed by dividing the absolute errors by the measured subsidence in percent (%). The results indicate that longer separations between the predicted time and the last value of the training time results in higher relative errors. Relative errors at the 10th month of the three points are 3.0%, 0.1 %, and 0.1%, which increase to 4.8%, 3.3%, and 1.5% at the 11th month, and 7.2%, 2.5% and 1.3% at the 12th month. In all cases, the absolute errors are small, which are all less than 0.5 mm, which indicates that the proposed method utilizing ANN in this study can produce good prediction for road subsidence time series at mining areas. This is confirmed by the results shown in Figure 3, in which the measured and predicted subsidence are very close.

4. Conclusions

This study has applied ANN to predict road subsidence measured by leveling caused by underground mining in Vietnam. The recursive multistep prediction process is designed and adopted, in which the first nine months are used as inputs to train the model of which the parameters are then used to predict subsidence for the last three months. Three points located at the road of the mine were measured with 12 epochs. subsidence was measured by the leveling method for each epoch.

The hyperparameters of the ANN model, including the number of hidden layers, hidden nodes, and iterated epochs, were determined by k-fold cross validation before they were utilized to estimate the model's parameters by the training set and predict land subsidence for the test set. The proposed ANN model with 'optimal' hyperparameters found in this study was demonstrated to be a good tool for underground mining induced road subsidence. The absolute errors were found to be small, which were all ranged with 0.5 mm. The absolute errors depend on the separations between the month in which the prediction was made and the last value in the training set. Relative errors at the 10th month of the three tested points are 3.0%, 0.1%, and 0.1%, which increase to 4.8%, 3.3%, and 1.5% at the 11th month, and 7.2%, 2.5% and 1.3% at the 12th month.

Acknowledgements

This research is funded by the University of Transport and Communications (UTC) under grant number T2023-CN-003.

Conflicts of Interest

The authors declare no conflict of interest.

Literatura – References

1. Amari, S.-i. (1993). Backpropagation and stochastic gradient descent method. Neurocomputing, 5(4), 185-196. doi:10.1016/0925-2312(93)90006-O
2. Ambrožič, T., & Turk, G. (2003). Prediction of subsidence due to underground mining by artificial neural networks. Computers & Geosciences, 29(5), 627-637. doi:10.1016/S0098-3004(03)00044-X
3. Aston, T. R. C., Tammemagi, H. Y., & Poon, A. W. (1987). A review and evaluation of empirical and analytical subsidence prediction techniques. Mining Science and Technology, 5(1), 59-69. doi:10.1016/S0167-9031(87)90924-8
4. Bahuguna, P. P., Srivastava, A. M. C., & Saxena, N. C. (1991). A critical review of mine subsidence prediction methods. Mining Science and Technology, 13(3), 369-382. doi:10.1016/0167-9031(91)90716-P
5. Bian, H.-f., Zhang, S.-b., Zhang, Q.-z., & Zheng, N.-s. (2014). Monitoring large-area mining subsidence by GNSS based on IGS stations. Transactions of Nonferrous Metals Society of China, 24(2), 514-519. doi:10.1016/S1003-6326(14)63090-9
6. Bui, X.-N., Tran, V. A., Bui, L. K., Nguyen, Q. L., Le, T. T. H., & Ropesh, G. (2021). Mining-Induced Land Subsidence Detection by Persistent Scatterer InSAR and Sentinel-1: Application to Phugiao Quarries, Vietnam, Cham.
7. Dorband, I. I., Jakob, M., & Steckel, J. C. (2020). Unraveling the political economy of coal: Insights from Vietnam. Energy Policy, 147, 111860. doi:10.1016/j.enpol.2020.111860
8. Fan, S., Yan, J., & Sha, J. (2017). Innovation and economic growth in the mining industry: Evidence from China's listed companies. Resources Policy, 54, 25-42. doi:10.1016/j.resourpol.2017.08.007
9. Fleming, D. A., & Measham, T. G. (2014). Local job multipliers of mining. Resources Policy, 41, 9-15. doi:10.1016/j.resourpol.2014.02.005
10. Fushiki, T. (2011). Estimation of prediction error by using K-fold cross-validation. Statistics and Computing, 21(2), 137-146. doi:10.1007/s11222-009-9153-8
11. Hilson, G. (2002). Small-scale mining and its socio-economic impact in developing countries. Paper presented at the Natural resources forum.
12. Jing-xiang, G., & Hong, H. (2009). Advanced GNSS technology of mining deformation monitoring. Procedia Earth and Planetary Science, 1(1), 1081-1088. doi:10.1016/j.proeps.2009.09.166
13. Kim, T. T. H., Tran, H. H., Bui, L. K., & Lipecki, T. (2021). Mining-induced Land Subsidence Detected by Sentinel-1 SAR Images: An Example from the Historical Tadeusz Kościuszko Salt Mine at Wapno, Greater Poland Voivodeship, Poland. Inżynieria Mineralna, 48(2), 41-52. doi:10.29227/IM-2021-02-04
14. Knierzinger, J. (2014). The socio-political implications of bauxite mining in Guinea: A commodity chain perspective. The extractive industries and society, 1(1), 20-27. doi:10.1016/j.exis.2014.01.005
15. Lee, S., Park, I., & Choi, J.-K. (2012). Spatial Prediction of Ground Subsidence Susceptibility Using an Artificial Neural Network. Environmental Management, 49(2), 347-358. doi:10.1007/s00267-011-9766-5
16. Ma, C., Li, H., & Zhang, P. (2017). Subsidence prediction method of solid backfilling mining with different filling ratios under thick unconsolidated layers. Arabian Journal of Geosciences, 10(23), 511. doi:10.1007/s12517-017-3303-7
17. Marschalko, M., Yilmaz, I., Křístková, V., Fuka, M., Kubečka, K., Bouchal, T., & Bednarik, M. (2012). Optimization of building site category determination in an undermined area prior to and after exhausting coal seams. International Journal of Rock Mechanics and Mining Sciences, 54, 9-18. doi:10.1016/j.ijrmms.2012.05.021
18. Mohsin, M., Zhu, Q., Naseem, S., Sarfraz, M., & Ivascu, L. (2021). Mining Industry Impact on Environmental Sustainability, Economic Growth, Social Interaction, and Public Health: An Application of Semi-Quantitative Mathematical Approach. Processes, 9(6), 972. doi:10.3390/pr9060972
19. Nguyen, B. N., Boruff, B., & Tonts, M. (2017). Mining, development and well-being in Vietnam: A comparative analysis. The extractive industries and society, 4(3), 564-575. doi:10.1016/j.exis.2017.05.009
20. Nguyen, B. N., Boruff, B., & Tonts, M. (2021). Looking through a crystal ball: Understanding the future of Vietnam's minerals and mining industry. The extractive industries and society, 8(3), 100907. doi:10.1016/j.exis.2021.100907
21. Nguyen, Q. L., Tran, V. A., & Bui, L. K. (2021). Determination of Ground Subsidence by Sentinel-1 SAR Data (2018-2020) over Binh Duong Quarries, Vietnam. VNU Journal of Science: Earth and Environmental Sciences, 37(2), 69-83. doi:10.25073/2588-1094/vnuees.4605
22. Nguyen, Q. N., Nguyen, V. H., Pham, T. P., & Chu, T. K. L. (2021). Current Status of Coal Mining and Some Highlights in the 2030 Development Plan of Coal Industry in Vietnam. Inżynieria Mineralna. doi:10.29227/IM-2021-02-34

23. Pedregosa, F., Varoquaux, G., Gramfort, A., Michel, V., Thirion, B., Grisel, O., . . . Dubourg, V. (2011). Scikit-learn: Machine learning in Python. the Journal of machine Learning research, 12, 2825-2830.

24. Rafie, M., & Samimi Namin, F. (2015). Prediction of subsidence risk by FMEA using artificial neural network and fuzzy inference system. International Journal of Mining Science and Technology, 25(4), 655-663. doi:10.1016/j.ijmst.2015.05.021

25. Todorović, R. T. (1993). Precise Levelling Network Adjustment in Mining Subsidence Regions, Berlin, Heidelberg.

26. Yang, W., & Xia, X. (2013). Prediction of mining subsidence under thin bedrocks and thick unconsolidated layers based on field measurement and artificial neural networks. Computers & Geosciences, 52, 199-203. doi:10.1016/j.cageo.2012.10.017

27. Zou, J., Han, Y., & So, S.-S. (2009). Overview of Artificial Neural Networks. In D. J. Livingstone (Ed.), Artificial Neural Networks: Methods and Applications (pp. 14-22). Totowa, NJ: Humana Press.

Assessment of Air Quality Index in Annaba

Salem BADJOUDJ[1)], Aissa BENSELHOUB[2)], Souad NARSIS[2)], Nadiia DOVBASH[3)], Abdelaziz IDRES[1)], Khadouja Marame BENGHADAB[4)], Fares BOUTARFA[1)], Mohamed BOUNOUALA[1)], Stefano BELLUCCI[5)]

[1)] Laboratory of Valorization of Mining Resources and Environment, Mining Department, Badji Mokhtar University, Annaba, Algeria;
[2)] Environmental Research Center (C.R.E), Annaba, Algeria;
[3)] National Scientific Centre "Institute of Agriculture of the National Academy of Agricultural Sciences", Chabany, Ukraine
[4)] Laboratory of Metallurgy and Material Sciences, Badji Mokhtar University, Annaba, Algeria
[5)] INFN Frascati National Laboratories, Via E. Fermi 54, 00044 Frascati, Italy
* Correspondence: Dr.Aissa BENSEHOUB, Environment, Modeling and Climate Change Division, Environmental Research Center (C.R.E), sis at Campus Sidi Amar, 23001, Annaba, Algeria; email: aissabenselhoub@cre.dz

http://doi.org/10.29227/IM-2023-02-02

Submission date: 01-05-2023 | Review date: 03-06-2023

Abstract

In recent years, the world has been witnessing serious ecological imbalances due to the catastrophic situation and the damage caused to the environment. Human activities as waste disposal, cement units, smelting, chemical industries etc., are the main causes of pollution. Air pollution directly affects the human living standards, pollutants requires regular control in view of their direct impact on health, such as nitrogen oxide, sulfur dioxide, ozone, and particulate matter. Algeria adopts international standards to monitor the levels of pollution recorded in Algerian cities and compare them with global levels. In this context, quantitative estimates of polluted waste resulting from some industrial activities have been conducted in order to determine the degree of its danger and the extent of its contribution to the deterioration of the air quality. The monitoring of pollutants allowed us to identify the benefits of comprehensive environmental assessment. We determined the air quality index in Annaba using various pollutants parameters (dust, ozone, nitrogen dioxide and sulfur dioxide). A ten-point scale ranking of the overall air quality index of pollution accepted in Algeria allows making the differentiated assessment of negative impacts of existing industrial agglomerations on the environment. However, the analysis performed on samples DC1 and DC2 with SEM (TESCAN model VEGA II) and BSE detector (Backscattered Electrons) shows that the particles sizes are estimated to range from hundreds of microns to a few microns, a different morphology and irregular shape. Our results will enable policy makers to appropriate measures to be taken, and which are based mainly on sensitizing economic operators to environmental issues in order to adopt an environmentally friendly industrial system.

Keywords: *PM, atmospheric pollution, AQI, thresholds, northeastern of Algeria*

Introduction

In recent years, the world has been witnessing serious ecological imbalances due to the catastrophic situation and the damage caused to the environment (Benselhoub et al., 2015b; Kumar et al., 2021). Human activities as waste disposal, cement units, smelting, chemical industries etc., are the main causes of air pollution (Kharytonov et al., 2016; Hassan et al., 2022). Air pollution directly affects human health and standard of living in light of the increase in industries that produce polluting materials and the aggravation of the resulting dangers, which has become an impediment to the normal life of many people (Benselhoub and Kanli, 2020; Kanchan, 2015). Algeria has recorded many cases of concern, especially children, who suffer from health as a result of the waste that spreads in the atmosphere due to gaseous emissions from multiple sources. A pollutant is a body of anthropogenic origin or not, in solid, liquid or gaseous state, contained in the atmosphere and which is not part of the normal composition of the air or which is present there in abnormal quantity (Kharytonov et al., 2017; Bishoi et al., 2009). According to a criterion of toxicity, specificity of sources and the pollution generated, the main pollutants measured by air quality monitoring bodies are nitrogen oxides (NOX), sulfur dioxide (SO_2), carbon monoxide (CO), suspended particles (SP), lead (Pb), volatile organic compounds (VOC) and ozone (O_3) (Benselhoub et al.,2015a; Tang et al., 2018).

Among the pollutants in question, particles are among the most studied. Their effects depend on their size, nature and composition, which varies according to their origin. Their size is expressed in relation to their mean aerodynamic diameter (Ø) (Mekti et al., 2021; Sulejmanović et al., 2014).

Particles in suspension in the urban atmosphere constitute a vast and chemically and physically heterogeneous group. The toxicity of dust is essentially linked to the fraction of aerodynamic size less than 10 µm (“particulate matter 10” ‘’PM10”) (Benselhoub et al., 2015b; Akinfolarin, 2017). They can penetrate to the lower respiratory tract, carrying on their surface other pollutants that can be toxic, which leads to biological and health significance. Suspended particles, in particular PM10, represent a major indicator of air quality from a health point of view, as they are numerous and consistent, beyond geoclimatic contexts, populations and sources of emissions , studies attributing to them a responsibility in the occurrence of a wide range of biological and health effects (Chaudhuri et al., 2018). As a result of air pollution in industrialized countries, sectors of the economy such as agriculture and forestry suffer largely. The intensity and volume of damage to vegetation near large settlements and industrial facilities is constantly increasing (Stankevich et al., 2015).

Based on the presented material, a ten-point scale ranking of the overall index of air pollution accepted in Algeria allows

Fig. 1. Geographical location of the study area (Benselhoub et al., 2015b)
Rys. 1. Położenie geograficzne badanego obszaru (Benselhoub i in., 2015b)

making the differentiated assessment of negative impacts of existing industrial agglomerations on the environment. Therefore, the aim of our study was to determine the air quality index (AQI) in Annaba, NE Algeria.

Material and Methods

Description of the study area

The province of Annaba is situated between latitudes 36° 30N and 37° 30N and longitude 7° 20E and 8° 40E. Its area is 1411.98 km²; its population has increased recently to 650.000 inhabitants, which is in general concentrated at the level of municipalities and hamlets. It is bounded to the south by the province of Guelma, to the west by the province of Skikda, in the east by the province of El Tarf and to the north by the Mediterranean Sea (Fig.1) (Benselhoub et al., 2015b). The climate is typically Mediterranean with an average annual temperature of 18°C, and an annual rainfall ranging from 650 to 1000 mm, with a winter peak and a deficit during summer. The city of Annaba is bounded to the north and the west by the Edough massif (highest altitude: 850 m), the Mediterranean Sea to the east and the Seybouse alluvial plain to the south. The Edough massif is characterized by a basement of gneiss, schist, and micaschist. Alluvial plain featured by Tertiary gravelly and sandy clayed layers at depth and arable Quaternary clay cover (Benselhoub et al., 2015c).

Socio-economic and industrial context of the Annaba region

Annaba region is known for its great agricultural and industrial activity. Agriculture in this region is observed throughout the plain, with a very wide variety of crops, cereals, market gardening and arboriculture. The industrial sector in the region is intense and remarkable; it is positioned especially along the Meboudja River. Three categories of industries are observed:

- Heavy industries with El Hadjar Metallurgical Complex, SIDER, SNVI and Ferrovial, etc.
- Chemical industries with the phosphate and nitrogen fertilizer complex (FERTIAL);
- Agro-food industries presented by ORELAIT and several food industries or processing represented by small businesses. All urban and industrial discharges flow directly into the rivers, except that of the FERTIAL plant, which release these wastes to the sea (Benselhoub et al., 2015c).

Air pollution and its impact on human health and the environment

Atmospheric pollution or "air pollution" is a type of pollution characterized by altered levels of air quality and purity. This degradation is generally caused by one or more elements (particles, substances, materials, etc.) whose degrees of concentration and duration of presence are sufficient to produce a toxic and/or ecotoxic effect (Monforte and Ragusa, 2018), which explains why this kind of pollution is a public health issue, both globally and individually.

The quality of the air we breathe has undergone a significant change over the past decade, mainly due to the "introduction by man" directly or indirectly, into the atmosphere, of substances with harmful consequences danger on:

- Human health;
- Biological resources and ecosystems;
- Material goods;
- Climate (Kampa and Castanas, 2008).

All human activities (industry, transport, heating, agriculture, incineration of waste in the open air, etc.) affect the quality of the air we breathe and generate atmospheric pollution. Nature itself, through pollens, volcanoes, the biological activity of soils, oceans and plants also contributes to this pollution.

In Annaba region, the main air pollutants mainly came from (Boutarfa et al.,2022):

- Human activities, in particular road traffic;
- Emissions from aging industrial installations (stationary sources) and all activities using combustion;
- Thermal installations;
- Domestic heating;
- Incineration of waste in the open air.

According to statistics from the World Health Organization (WHO), three million people die every year as a result of air pollution around the world, in particular: Children (immature respiratory system), old people, and people suffering from respiratory and cardiovascular diseases (WHO, 2016).

In Algeria, a study was performed by the program of technical assistance of the Mediterranean environment (METAP), the deterioration of environment in Algeria costing $ 1.7 billion per year, or 3.6 percent of GDP. Additionally, the national report on the state of environment demonstrated that 30% of

Tab. 1. Effects of Pollutants on Human Health and Environment

Tab. 1. Wpływ zanieczyszczeń na zdrowie człowieka i środowisko

Pollutants	Environmental impacts	Health effects
Nitrogen dioxide (NO_2)	- Damages diverse plants and ozone formation. - Acid Rain. - Greenhouse effect (indirectly).	- Penetrates the deep respiratory tract where it weakens the pulmonary mucosa against infectious attacks, especially in children. - An irritating gas that penetrates the finest ramifications of the respiratory tract, causing bronchial hyper-reactivity in asthmatic patients and increases susceptibility of the bronchi to infections in children.
Sulfur dioxide (SO_2)	- Deterioration of plants and ecosystems as well as buildings. - Precursors of acid rain.	- Causes attacks in asthmatics. - Increases breathing difficulties and affect respiratory function in children.
Suspended particles < 10µm (PM10)	- Effects on crops. - Soiling of buildings.	- Mutagenic and carcinogenic properties. - Impaired respiratory function.
Ozone (O_3)	- Harmful effect on vegetation. - Contributes to the greenhouse effect and acid rain.	- An aggressive gas that easily penetrates to the finest respiratory tracts. - Causes coughing, lung damage and eye irritation.
Heavy metals	- Toxic Fallout.	- Neurotoxic. - Kidney, lung and bone toxicity. - Respiratory carcinogen.
Volatile organic compounds (VCO)	- Involved in the process of the greenhouse effect and the stratospheric ozone hole.	- The effects vary according to the nature of the chemical compound. - They range from simple olfactory discomfort to irritation, to a reduction in respiratory capacity, to mutagenic and carcinogenic effects.

consultations are for respiratory diseases, 40% of infant mortality (children under 1 year) is caused by respiratory diseases and 600.000 asthmatics suffer permanently (Benselhoub et al., 2022).

Air pollution does not only attack human health, but also affects our environment and our ecosystem represented by global phenomena at the local, regional and even continental scale, observed, through:

- Climate change;
- Problem of substances depleting the ozone layer;
- Deterioration of the disappearance of certain flora and fauna species.

Similarly, meteorological conditions can also favor pollution, on a local or continental scale, or contribute to their dispersion (Stankevich et al., 2015). Table 1 summarizes the impacts of pollution on human health and environment.

Parameters influencing air quality

Air quality is not only dependent on the amount of pollutants emitted by sources. It is also linked to the climatic, meteorological, topological and morphological conditions of the environment. Once emitted by a source of pollutant, its evolution in the atmosphere is dependent on the wind, the stability of the atmosphere, solar radiation, the topography and morphology of the environment.

Meteorological situations

Low-pressure situations (low pressures) generally correspond to fairly strong air turbulence and therefore good dispersion conditions. On the other hand, anticyclonic situations (high pressures) where the stability of the air does not allow the dispersion of pollutants leads to episodes of pollution. There is a clear relationship between wind speed and pollutant concentration levels. A weak wind therefore favors the accumulation of pollutants. Wind speed increases with altitude.

Wind effect

There is a clear relationship between wind speed and pollutant concentration levels. The dispersion of pollutants increases with wind speed and turbulence. A weak wind therefore favors the accumulation of pollutants. Wind speed increases with altitude. As pollutants rise, horizontal dispersion is facilitated by the wind. The stronger the wind, the lower the pollution levels in the city.

The evolution of the mean time profile of wind speeds recorded very moderate values. It characterizes a maximum period (depending on the reference site) that occurs between 12:00H, 19:00H, and a longer minimum period over the rest of the period (Fig 2).

The wind rose of the reference station clearly shows that the prevailing winds are from North East to South West. On the other hand, at the station of Annaba city and El Bouni is variable according to their position (within the urban fabric).

Influence of local topography

The topography of Annaba is favorable to the formation of temperature inversions which are situations allowing the accumulation of pollutants and consequently the rise in concentration rates. The effects of sea breezes, particular relief (land and slope), play an important role in the transport of clouds of pollutants. Indeed, the clouds of pollutants are carried by the land breeze at night towards the sea, and during the day, these clouds of pollutants return to the city by the sea breeze effect.

Algerian standards relating to air pollution

In 2006, and after developing a database relating to air quality due to road traffic, the Ministry of Territorial Planning and the Environment deemed it necessary to create Algerian standards relating to thresholds limited in case of air pollution to be respected. Thus, Decree No. 06-02 of January 7, 2006 comes into force after its adoption by the government. The executive Decree No. 06-02 of 7 Dhou El Hidja 1426 corresponding to January 7, 2006 definined the limit values, alert thresholds, and

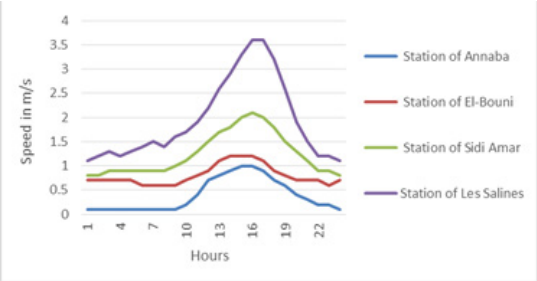

Fig. 2. Wind speed average hourly profile in Annaba province
Rys. 2. Średni godzinowy profil prędkości wiatru w prowincji Annaba

Tab. 2. Algerian norms relating to air pollutants
Tab. 2. Algierskie normy dotyczące zanieczyszczeń powietrza

	NO_2	SO_2	O_3
Information thresholds	400 µg/m³	350 µg/m³	180 µg/m³
Warning thresholds	600 µg/m³	600 µg/m³ (hourly average exceeded for three consecutive hours)	360 µg/m³

Tab. 3. Pollutants quantification
Tab. 3. Kwantyfikacja zanieczyszczeń

Pollutants / Stations	NO_2 µg/m³	O_3 µg/m³	PM µg/m³
Annaba	32	35	39
El Bouni	7	29	73
Sidi Amar	8	33	57
Les Salines	5	32	36

air quality objectives in the event of atmospheric pollution, and imposes the implementation of procedures for informing and alerting populations during a pollution episode. They exist for ozone, nitrogen dioxide and sulfur dioxide.

The information threshold is the concentration level beyond which short-term exposure could present a health risk. The alert threshold corresponds to a concentration level of polluting substances in the atmosphere beyond which short-term exposure presents a high risk for human health and the environment and above which emergency measures must to be taken (Benselhoub and Kanli, 2020). Table 2 shows the Algerian standards relating to the main air pollutants.

Pollutants momitoring

The calculation of the total index of atmospheric pollution in the city of Annaba is carried out according to the approved methodology, taking into account the data from the automatic weather stations. These indicators include particulate matter (PM), sulfur dioxide, nitrogen dioxide, and man-made ozone (Table 3).

Historically, the metallurgical complex of El Hadjar was considered as one of the main polluting sources in Annaba region (Benselhoub et al., 2015a). The table 4 shows the atmospheric emissions data of El Hadjar metallurgical complex in Annaba, according to a calculation model based on energy balances and emission factors.

From the data in table 5, we note the presence of a high content of iron (Fe) and silica (SiO2), and low content (traces) of sulfur (S) in ores from Ouenza and Boukhadra, such presence could possibly influence the environment and health (Boutemedjet et al., 2018).

Presentation and determination of the air quality index (AQI)

The definition of an AQI results from the desire to make information accessible to as many people as possible without entering into sometimes complex scientific considerations. This index is a qualitative assessment of air quality that has little scientific value. Indeed, it summarizes in a single parameter the results for pollutants whose effects on health can be very different and defines the air quality in relation to the pollutant for which the situation is the worst. We are therefore comparing very different data and we should in no case begin to establish statistics on these indexes (Kumar et al., 2022).

These indexes are based on the levels of ozone, nitrogen dioxide, sulfur dioxide and PM particles. They therefore do not take into account heavy metal or organic compounds whose effects result rather (but not always) from long-term exposure. The indexes therefore relate to the main irritant pollutants. For each of the pollutants, a concentration scale is defined to calculate a sub-index. The concentration scales are based both on the limit values imposed by international guidelines and on historical data (Table 6). The AQI is then determined as being the highest sub-index, therefore the poorest quality. If one of the sub-indexes is missing, the overall index is not calculated and a minimum of 50% valid data is required to calculate a sub-index. In this paper, we will only

Tab. 4. Atmospheric emissions data from El Hadjar metallurgical complex

Tab. 4. Dane dotyczące emisji do atmosfery z kompleksu metalurgicznego El Hadjar

	CO_2 (t/year)	Particles (t/year)	SO_2 (t/year)	NO_x (t/year)
Coke plant	142494.85	781.26	501.113	1145.08
PMA	339726.39	2813.58	1719.410	1250.48
HFx	1695980.18	1738.96	12.149	297.77
ACO1	162665.48	16.15	0.468	78.05
ACO2	85985.42	7.49	0.242	40.27
ACE	11622.49	0.35	0.046	8.40
LAC	59998.46	2.46	0.295	270.42
LAF/ Annealed	9392.59	0.48	0.046	10.78
LAF/ Galvanized	20202.84	1.02	0.099	23.18
LFR	55678.44	2.82	0.274	63.88
LRB	22334.67	1.13	0.110	25.62
TSS	47604.28	2.41	0.234	54.61
Coprosid	41984.90	2.13	0.206	48.17
AMM	3488.53	0.18	0.017	4.00
Fluid / Boilers	76507.03	3.88	0.376	87.77
PDE/ Power station	27882.57	1.41	0.137	31.99
Source:	2803549.09	5374.31	2235.086	3408.49
Environmental	*Department*	*of El Hadjar*	*Metallurgical*	*Complex*

Tab. 5. Chemical Analysis of Ores from Ouenza and Boukhadra mines

Tab. 5. Analiza chemiczna rud z kopalń Ouenza i Boukhadra

Content in (%) / Ores	Fe	SiO_2	$BaSO_4$	CaO	Mn	MgO	S
Ouenza mine	46	8	0.03	9	2	13	0.05
Boukhadra mine	55	10	0.20	3	2.10	0.14	0.10

Tab. 6. Air quality index (AQI)

Tab. 6. Wskaźnik jakości powietrza (AQI)

Index	PM10	SO_2	NO_2	O_3
	Daily Average	Hourly Average	Hourly Average	Hourly Average
1	0 – 9 µg / m^3	0 – 39 µg / m^3	0 – 29 µg / m^3	0 – 29 µg / m^3
2	10 – 19	40 – 79	30 – 54	30 – 54
3	20 – 29	80 – 119	55 – 84	55-79
4	30 – 39	120 – 159	85 – 109	80-104
5	40 – 49	160 – 199	110 – 134	105 – 129
6	50 – 54	200 – 249	135 – 164	130 – 149
7	55 – 79	250 -299	195 – 199	150 – 179
8	80 – 99	300 – 399	200 – 274	180 – 249
9	100 – 124	400 –599	275 – 399	250 – 359
10	> 125	> 600	> 400	> 360

use the sub- indexes precisely to avoid mixing up different concepts (Kumar et al., 2015; Benselhoub and Kharytonov, 2017). In table 6, we will refer to establish a distribution of the days according to the categories defined for the sub-indexes, site by site, the definition of a single index for the entire region being an overly simplistic notion that does not reflect local differences.

Taking into account the concentration of each of the four parameters, the corresponding sub-indexes are determined. The measured pollutants are considered excellent indicators of air quality.

The final score follows the highest value of the sub-index. According to the ten-point scale ranking, the air quality assessment is made in the following terms: Excellent, very good, good, pretty good, average, poor, very poor, bad, very bad, execrable (see table 6).

Results and Discussion

Particulate matter pollution

Throughout the world, the form of pollution that currently poses the most problems is that linked to the presence of increasingly fine particles in the atmosphere and emitted progressively in large quantities. The potential harm of these particles results from their size (the finer they are, the deeper they penetrate into the alveoli of the respiratory system) and the toxic compounds they carry (lead, carcinogenic polycyclic aromatic hydrocarbons, etc.). Fine particles and in particular the finest from diesel engines are nowadays a public health problem in all cities over the world.

The monitoring networks are thus equipped with analyzers for PM10 particles, PM2.5 respirable particles and increasingly PM1 (diesel particles). Both classes of particles PM10 and PM2.5 are strictly regulated by the WHO and by industrialized countries.The content of PM in Annaba is presented in the figure 3.

Dust concentrations are relatively high compared to the current standard of around 30 µg/m^3. Particulate pollution originates on the one hand from road traffic and industrial

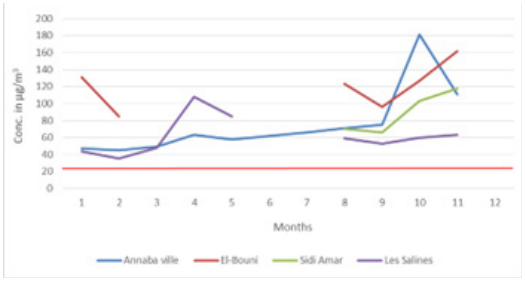

Fig. 3. Evolution of the PM content in Annaba province
Rys. 3. Ewolucja zawartości PM w prowincji Annaba

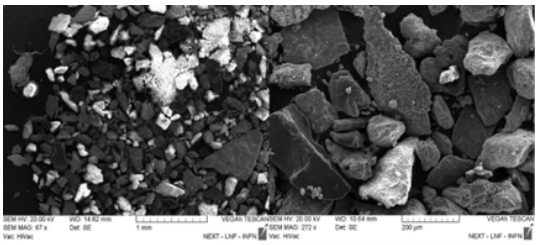

Fig. 4. Two different magnifications of the particles present in the dust DC1
Rys. 4. Dwa różne powiększenia cząstek obecnych w pyle DC1

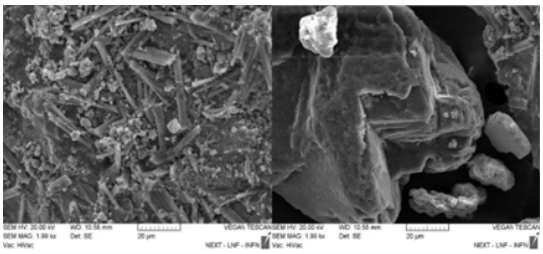

Fig. 5. Particle details of DC1
Rys. 5. Szczegóły cząstek DC1

activities at the edge of urban centers and on the other hand from low soil cover, resulting in the raising of dust at moderate wind and meteorological conditions, appearance of the sirocco during the dry period.

Dust morphology

The shape of PM generally can stimulate flight and reduce the sedimentation rate of a particle (Mekti et al., 2021). The speed is a function of the aerodynamic diameter. The PM collected from the dust collators (DC1 and DC2) at El Hadjar metallurgical complex of Annaba; have different morphology and irregular shape (figures 4, 5, 6, 7 and 8). The analysis was performed on samples called DC1 and DC2. They were visually shown in the form of granular powder.

For the study of these powders, it was carried out using a scanning electron microscope (SEM) of the TESCAN model VEGA II, which uses a tungsten filament thermionic source. The powders have been bonded on carbon-based adhesive tape placed on aluminum sample holder (stub). The images show a jagged surface with particles of different sizes and shapes.

The figure 4 shows the morphological variety of the particles present in the dust DC1.

The figure 5 illustrates the diversity in morphology of some DC1 particles. As we can see, some seem to show structures similar to "fibers" broken and supported or immersed in amorphous material; others instead resemble lamellar structures. It is estimated that particles range in size from hundreds of microns to tens of microns. The DC1 powders were metallized with a thin layer of platinum-gold because they were non-conductive and difficult to analyze.

The DC2 powders are formed by particles of different shapes and sizes.

Figure 6 shows the morphological variety of the particles present in the dust DC2.

The figure 7 shows the diversity in the morphology of some particles of DC2. As it is seen, some of them seem to show filiform structures immersed in amorphous material or different shapes. The particle size is estimated to range from hundreds of microns to a few microns. The DC2 powders were metallized with a thin layer of platinum-gold because they were non-conductive and difficult to analyze. On the DC2 sample, a measurement with BSE detector (Backscattered Electrons) was carried out, and which allows to have an image in the gray scale, that identifies the presence of species with different atomic numbers.

The figure 8 demonstrates the different atomic species presented in the sample DC2, the black color indicates the lowest atomic number, and the white color indicates the highest atomic number, relative to the area under consideration.

Air quality assessment in Annaba province. In view of the concentrations recorded, overall air quality can be considered as good in Annaba city (Fig. 9).

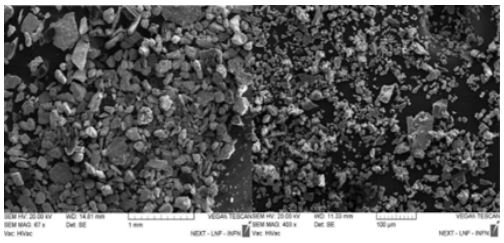

Fig. 6. Two different magnifications of the particles present in the dust of DC2
Rys. 6. Dwa różne powiększenia cząstek obecnych w pyle DC2

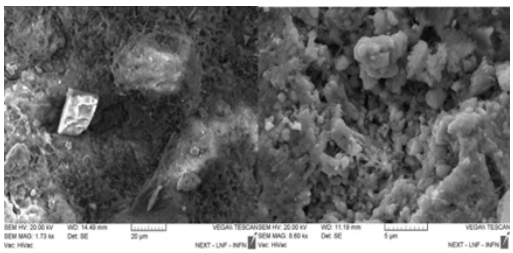

Fig. 7. Particle details of DC2
Rys. 7. Szczegóły cząstek DC2

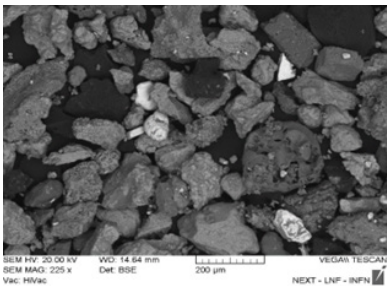

Fig. 8. BSE detector image of the sample DC2
Rys. 8. Obraz z detektora BSE próbki DC2

Sometimes, air quality has been affected by the presence of PM10 dust pollution.

From figure 10 the quality of the air is generally rated good to pretty good in Sidi Amar. However, air quality was affected, for a period equal to one quarter of the year, by heavy dust pollution and sometimes by nitrogen dioxide.

As shown in figure 11 the overall air quality in El Bouni can also be rated as good to medium. Nevertheless, the air quality is bad for an average period close to the month. Dust pollution is, as for other urban sites, the most significant. However, at Les Salines the air quality is generally considered very average to poor. The character of background pollution is not considered critical for all pollutants, with the exception of ozone for which critical thresholds and warnings have been exceeded during the summer period which is affected by strong sunshine and by the local breezes of land and sea.

Corresponding to figure 12, the poor air quality is due to the meteorological situation allowing poor dispersion of pollutants. Overall, air quality in the Annaba area varies from fairly good to bad. The poor quality is due in most cases to dust levels and to a lesser extent to photochemical pollution during the summer season.

Conclusion

Urban air pollution is a pervasive risk that cities must adapt to avoid significant and growing health and economic impacts. In fact, nearly 3 million people worldwide died due to excessive exposure to outdoor air pollution. In addition, the number of deaths due to ambient air pollution is expected to increase and become the main cause of premature mortality.

Historically, the metallurgical complex of El Hadjar was considered as one of the main polluting sources in the Annaba region. In ores from Ouenza and Boukhadra, we note the presence of a high content of iron (Fe) and silica (SiO_2), which presence could possibly influence the environment and health but the content of sulfur (S) is negligible (traces).

Dust concentrations are relatively high compared to the current standard of around 30 µg/m^3. Particulate pollution originates on the one hand from road traffic and industrial activities at the edge of urban centers and on the other hand from low soil cover, resulting in the raising of dust in the moderate wind and meteorological conditions, appearance of the sirocco during the dry period. The ozone pollution recorded during the summer period is due to the sunshine favored by the presence of the primary pollutants (NO_2, HC, CO).

The analysis performed on samples DC1 and DC2 with SEM (TESCAN model VEGA II) and BSE detector (Backscattered Electrons) shows that the particles sizes are estimated to range from hundreds of microns to a few microns, a different morphology and irregular shape.

Poor air quality is due to the meteorological situation allowing poor dispersion of pollutants. Overall, AQI in the

Fig. 9. Air quality in Annaba city
Rys. 9. Jakość powietrza w mieście Annaba

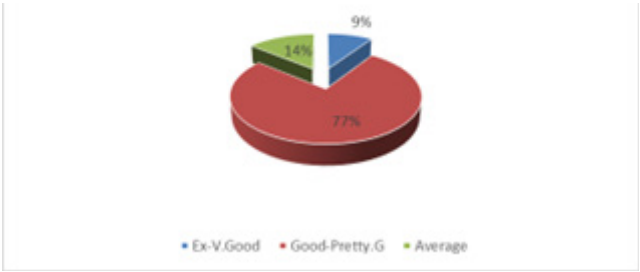

Fig. 10. Air quality in Sidi Amar
Rys. 10. Jakość powietrza w Sidi Amar

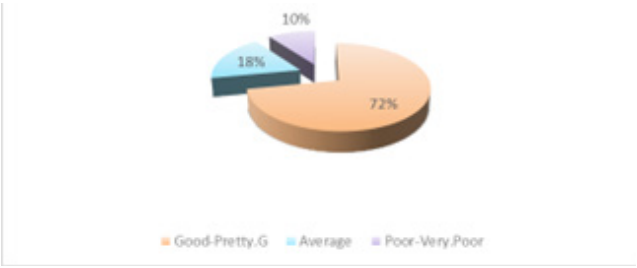

Fig. 11. Air quality in El Bouni
Rys. 11. Jakość powietrza w El Bouni

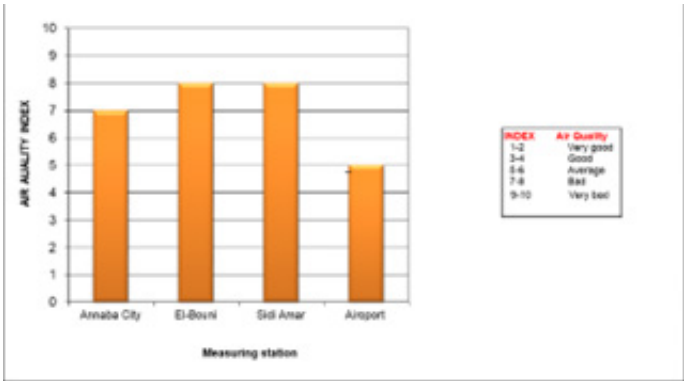

Fig. 12. Air quality index (AQI) in Annaba province
Rys. 12. Wskaźnik jakości powietrza (AQI) w prowincji Annaba

Annaba area varies from fairly good to bad. The poor AQI is due in most cases to dust levels and to a lesser extent to photochemical pollution during the summer season.

The ten-point scale ranking of the overall AQI of pollution accepted in Algeria allows making the differentiated assessment of negative impacts of existing industrial agglomerations on the environment. Such assessments will enable policy makers to appropriate measures to be taken, which are based mainly on sensitizing economic operators to environmental issues in order to adopt an environmentally friendly industrial system.

Acknowledgements

The authors express their gratefully acknowledgements to all colleagues from the Laboratori Nazionali di Frascati of the Istituto Nazionale di Fisica Nucleare (NEXT-LNF-INFN) for their assistance to carry out this research study.

Literatura – References

1. Akinfolarin, O. M., Boisa, N., & Obunwo, C. C. (2017). Assessment of particulate matter-based air quality index in Port Harcourt, Nigeria. Journal of environmental analytical chemistry, 4(4), 1-4.
2. Benselhoub A., Benghadab Kh.M, Dovbash N., Trirat T., Rouaiguia I. (2022). Consequences of air pollution on human health and environment in Algeria. All-Ukrainian scientific and practical conference "Environmentally safe technologies in crop growing under the conditions of marital state», Kyiv-Skyra, Ukraine, August 10, 2022, 8-9.
3. Benselhoub, A., & Kanlı, A. I. (2020). Environmental Impacts of Air Pollution on Human Health in Annaba Region (Northeast of Algeria). In Toxic Chemical and Biological Agents (pp. 209-216). Springer, Dordrecht.
4. Benselhoub, A and Kharytonov M. (2017). A comparison of approaches to the estimation of total airborne environment pollution in Algeria and Ukraine. Taurida Scientific Herald № 98 (in Ukrainian).
5. Benselhoub, A., Kharytonov, M., Bouabdallah, S., Bounouala, M., Idres, A., & Boukelloul, M. L. (2015b). Bioecological Assessment of Soil Pollution with Heavy Metals in Annaba (Algeria). Studia Universitatis "Vasile Goldiş", Seria Ştiinţele Vieţii, (25), 1.
6. Benselhoub, A., Kharytonov, M., Bounouala, M., Chaabia, R., & Badjoudj, S. (2015c). Estimation of soil's sorption capacity to heavy metals in Algerian megacities: case of Algiers and Annaba. INMATEH-Agricultural Engineering, 46(2).
7. Benselhoub, A., Kharytonov, M., Bounouala, M., Chaabia, R., & Idres, A. (2015b). Airborne soils pollution evaluation with heavy metals in Annaba region (Algeria). Metallurgical and Mining Industry, (7), 32-35.
8. Benselhoub, A. M., Kharytonov, M. M., Zaichenko, A. O., & Stankevich, S. A. (2015a). Environmental risks of man-made air pollution in Grand Algiers. Journal of the Georgian geophysical society, 18(19).
9. Bishoi, B., Prakash, A., & Jain, V. K. (2009). A comparative study of air quality index based on factor analysis and US-EPA methods for an urban environment. Aerosol and Air Quality Research, 9(1), 1-17.
10. Boutarfa F., Idres A., Benghadab Kh.M., Dovbash N., Benselhoub A.(2022).Environmental impacts of atmospheric emissions of El Hadjar metallurgical plant, International scientific and practical conference, Environmental safety and balanced natural use in agricultural production, Kyiv, Ukraine, July 7-8, 2022, 15-17.
11. Boutemedjet, A., Bounouala, M., Idres, A., & Benselhoub, A. (2019). Assessment of dust pollution related to granite quarry operations in kef Bouacida, Annaba (Algeria). Scientific Bulletin of National Mining University, (1).
12. Chaudhuri, S., & Chowdhury, A. R. (2018). Air quality index assessment prelude to mitigate environmental hazards. Natural Hazards, 91(1), 1-17.
13. D'Amato, G., Cecchi, L., D'amato, M., & Liccardi, G. (2010).Urban air pollution and climate change as environmental risk factors of respiratory allergy: An update. Journal of Investigational Allergology and Clinical Immunology, 20(2), 95–102.
14. Hassan, R., Rahman, M., & Hamdan, A. (2022, May). Assessment of air quality index (AQI) in Riyadh, Saudi Arabia. In IOP Conference Series: Earth and Environmental Science (Vol. 1026, No. 1, p. 012003). IOP Publishing.
15. Kampa, M., & Castanas, E. (2008). Human health effects of air pollution. Environmental Pollution, 151(2), 362–367.
16. Kanchan, K., Gorai, A. K., & Goyal, P. (2015). A review on air quality indexing system. Asian Journal of Atmospheric Environment, 9(2), 101-113.
17. Kharytonov, M., Benselhoub, A., Klimkina, I., Bouhedja, A., Idres, A., & Aissi, A. (2016). Air pollution mapping in the Wilaya of Annaba (NE of Algeria). Mining Science, 23.
18. Kharytonov, M., Benselhoub, A., Kryvakovska, R., Klimkina I, I., Bouhedja, A., Bouabdallah, S., ... & Vasylyeva, T. (2017). Risk assessment of aerotechnogenic pollution generated by industrial enterprises in Algeria and Ukraine.
19. Kumar, G., & Kumar, S. (2022). Air quality index–A comparative study for assessing the status of air quality before and after lockdown for Meerut. Materials Today: Proceedings, 49, 3497-3500.https://doi.org/10.1016/j.matpr.2021.05.575.
20. Kumar, B. A., Sagar, B. V., & Kunmar, B. P. (2015). Assessment of air quality index of Visakhapantam Urban area of Andhrapradesh. International Journal of Innovative Research and creative Technology, 1(4), 434-436.
21. Li, Y., Tang, Y., Fan, Z., Zhou, H., & Yang, Z. (2018). Assessment and comparison of three different air quality indices in China. Environmental Engineering Research, 23(1), 21-27.
22. Mekti, Z., Boutemedjet, A., Sekiou, O., Berdoudi, S., Chaib, A., Kouider, F., Rahmani, A., Benselhoub, A..(2021).airborne particulate matter pollution generated by phosphate export at the port of Annaba.Visnyk of Taras Shevchenko National University of Kyiv: Geology. v. 4(95). pp. 90-96.
23. Monforte, P., Ragusa, M.A. Evaluation of the air pollution in a Mediterranean region by the air quality index. Environ Monit Assess 190, 625 (2018). https://doi.org/10.1007/s10661-018-7006-7.

24. Murena, F. (2004). Measuring air quality over large urban areas: Development and application of an air pollution index at the Environ Monit Assess (2018) 190:625 Page 9 of 10 625 urban area of Naples. Atmospheric Environment, 38(36), 6195–6202.

25. Stankevich, S., Titarenko, O., Kharytonov, M., Benselhoub, A., Bounouala, M., Chaabia, R., & Boukeloul, M. L. (2015). Mapping of urban atmospheric pollution in the northern part of Algeria with nitrogen dioxide using satellite and ground-truth data. Studia Universitatis" Vasile Goldis" Arad. Seria Stiintele Vietii (Life Sciences Series), 25(2), 87.

26. Stankevich, S., Titarenko, O., Svideniuk, M., Kharytonov, M., Benselhoub, A., & Khlopova, V. (2016). Air pollution mapping with nitrogen and sulfur dioxides in the south-eastern part of Ukraine using satellite data. Mining Science, 23.

27. Sulejmanović, J., Muhić-Šarac, T., Memić, M., Gambaro, A., & Selović, A. (2014). Trace metal concentrations in size-fractionated urban atmospheric particles of Sarajevo, Bosnia and Herzegovina. International Journal of Environmental Research, 8(3), 711-718.

28. World Health Organization. (2016). Ambient air pollution: a global assessment of exposure and burden of disease. World Health Organization. https://apps.who.int/iris/handle/10665/250141.

Ocena wskaźnika jakości powietrza w Annabie

W ostatnich latach świat był świadkiem poważnych zaburzeń równowagi ekologicznej z powodu katastrofalnej sytuacji i szkód wyrządzonych środowisku. Działalność człowieka, taka jak usuwanie odpadów, cementownie, hutnictwo, przemysł chemiczny itp. są głównymi przyczynami zanieczyszczenia. Zanieczyszczenie powietrza bezpośrednio wpływa na standardy życia ludzi, zanieczyszczenia wymagają regularnej kontroli ze względu na ich bezpośredni wpływ na zdrowie, takie jak tlenek azotu, dwutlenek siarki, ozon i pył zawieszony. Algieria przyjmuje międzynarodowe standardy w celu monitorowania poziomów zanieczyszczeń rejestrowanych w algierskich miastach i porównywania ich z poziomami globalnymi. W tym kontekście przeprowadzono ilościowe szacunki zanieczyszczonych odpadów powstających w wyniku niektórych działań przemysłowych w celu określenia stopnia ich zagrożenia i zakresu ich wkładu w pogorszenie jakości powietrza. Monitorowanie zanieczyszczeń pozwoliło nam zidentyfikować korzyści płynące z kompleksowej oceny środowiska. Określiliśmy indeks jakości powietrza w Annabie, wykorzystując różne parametry zanieczyszczeń (pył, ozon, dwutlenek azotu i dwutlenek siarki). Dziesięciopunktowa skala rankingu ogólnego wskaźnika jakości powietrza zanieczyszczeń przyjętych w Algierii pozwala na zróżnicowaną ocenę negatywnego wpływu istniejących aglomeracji przemysłowych na środowisko. Jednak analiza przeprowadzona na próbkach DC1 i DC2 za pomocą SEM (TESCAN model VEGA II) i detektora BSE (Backscattered Electrons) pokazuje, że rozmiary cząstek szacuje się na od setek mikronów do kilku mikronów, o różnej morfologii i nieregularnym kształcie. Nasze wyniki umożliwią decydentom podjęcie odpowiednich środków, które opierają się głównie na uwrażliwieniu podmiotów gospodarczych na kwestie środowiskowe w celu przyjęcia przyjaznego dla środowiska systemu przemysłowego.

Słowa kluczowe: *PM, zanieczyszczenie atmosfery, AQI, wartości progowe, północno-wschodnia Algieria*

Mineralogical and Chemical Characteristics of Phosphates from the Djebel Onk Deposits (Tebessa, Algeria)

*Tourkia TAHRI[1)], Souad NARSIS[2)], Nacer BEZZI[1)], Abdellali BOUZENZANA[3)], Omar SEKIOU[2)], Tabet TRIRAT[4)], Theziri AMRANE[5)], Aissa BENSELHOUB[2)]**

[1)] Laboratory of Materials Technology and Process Engineering, University of Bejaia, Algeria
[2)] Environmental Research Center (C.R.E), Annaba, Algeria
[3)] Laboratory of Mining, Department of Mining and Geotechnical, Larbi Tebessi University, Tebessa Algeria
[4)] Badji Mokhtar University, Annaba, Algeria
[5)] Laboratory of Geodynamics of Natural Resources, University of Annaba, Algeria
*Correspondence: Dr.Aissa BENSEHOUB, Environment, Modeling and Climate Change Division, Environmental Research Center (C.R.E), sis at Campus Sidi Amar, 23001, Annaba, Algeria; email: aissabenselhoub@cre.dz

http://doi.org/10.29227/IM-2023-02-03

Submission date: 01-05-2023 | Review date: 03-06-2023

Abstract

Algeria has important phosphate reserves (2 billion tons) located in the east of the country at Djebel Onk. This mining district is located in the northwestern part of the Algerian Sahara near the Algerian-Tunisian border. The granulo-chemical and XRD analytical results confirm the phosphate depletion of Bled El Hadba layer and their enrichment in carbonate and dolomite, in comparison with the layer of Kef Essennoun. Phosphorite particles are heterogeneously grained. Although the two deposits are relatively close to each other, they show different mineralogical and chemical characteristics, which may cause the use of different mining exploitation methods.

Keywords: *phosphates, particle size, chemistry, petrography, Algeria*

1. Introduction

Algeria has rich mineral resources such as hydrocarbons, clays, and phosphate. Phosphate is mined in the region of Djebel Onk, which is located in the Tebessa region, and which contains more than two billion tons of phosphorite reserves distributed across different deposits [1]

Dejbel Onk mining district belongs to the Gafsa-Metlaoui-Onk basin, and phosphorite mineralization is found in five sectors: Kef Essennoun, Djemi Djema, Bled El Hadba, Djebel Onk North and Oued Betita [2-3].Phosphates are of great importance because of their applications in several sectors, particularly in the fertilizer and phosphoric acid industries. However, this sector imposes quality requirements on these phosphates concentrates [4-5] which consists in eliminating harmful impurities; such as, clays, silica, gypsum, etc. [6-7]. On the other hand, the deposits suffer from extensive resource exploitation by the SOMIPHOS group mining company, which causes environmental pollution. Another challenge is to recognize new economic sources in phosphorites, such as Rare Earth Elements (REE) [8-11].

Kef Essennoun deposit is characterized by a thick (~35 m) layer of Upper Thanetian phosphorites, divided into three sub-layers according to their P_2O_5 and MgO contents. The Bled El Hadba deposit is characterized by a ~30 m thick phosphorite layer [12] that occasionally contains marly phosphate intercalations with a marked drop in P_2O_5 contents [13].

This study aims to use several physicochemical methods to assess the mineralogical and chemical characteristics as well as the grain-size of the main minerals in each type of ores. Comparison of these characteristics will verify whether the enrichment procedures applied to beige minerals (Bled El Hadba) and (Kef Essennoun) are compatible with the common mineral processing method. Thus, the main objective of this research is to study the granulometry, mineralogy and chemical properties of the phosphate facies of the Kef Essennoun and Bled El Hadba deposits.

2. Geological Setting

The phosphate deposits near to Bir El Ater (Figure 1) are located in the transition between the eastern part of the Saharan Atlas to the north and the Sahara Platform to the south. The boundary between these two tectonic units is marked by the fault or flexure of the southernmost Atlas. The Atlas Mountains belong to the Alpine belt which was formed by the convergence of the Eurasian and African plates during the Miocene period [14].

The stratiform marine phosphate deposits are largely developed on the Algerian northeastern territory. These Tertiary phosphate fields (late Paleocene – early Eocene) belong to the large Mediterranean Phosphogenic Province which extends from Morocco to the Middle East (Iraq, Jordan, Syria etc.). The phosphate rocks of this province are predominantly of Cretaceous – Eocene ages [15-19].

The Algerian layers are from the lower Tertiary, mostly upper Thanetian, occasionally upper Thanetian - lower Ypresian Chouabine Formation, with a total thickness of 68 m. The main phosphate layer locally reaches a maximum thickness of 43 m. It is characterized by grains of phosphate pseudo--oolites and coprolites, and locally by a significant amount of fish teeth and fragments of phosphatic bones. The base of the Chouabine Formation is composed of lower Thanetian bituminous laminated marls, with irregular limestone intercalations containing a typical gastropod fauna.

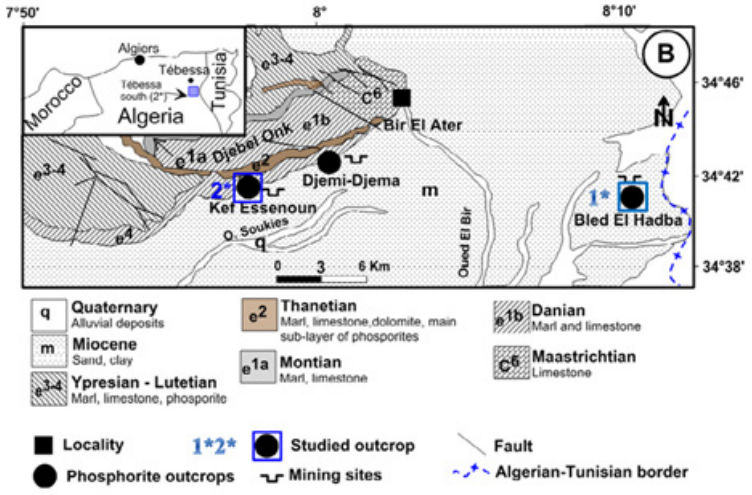

Fig. 1. Simplified geological sketch map of Djebel Onk region [22]
Rys. 1. Uproszczona mapa geologiczna regionu Djebel Onk [22]

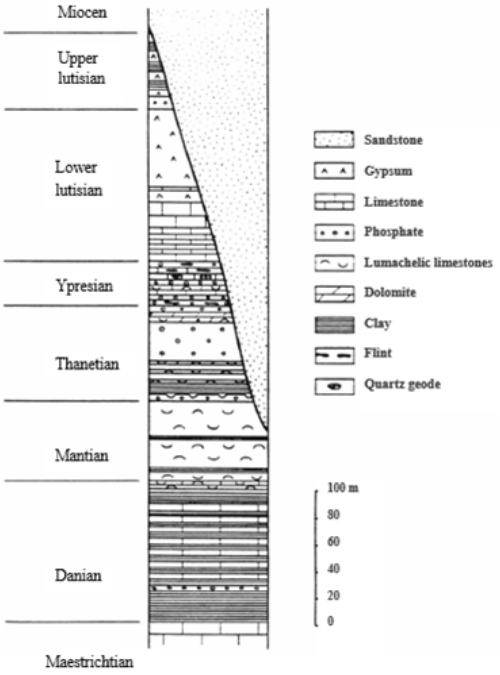

Fig. 2. Stratigraphic column of Jebel Onk [23]
Rys. 2. Kolumna stratygraficzna Jebel Onk [23]

The economically significant phosphorite layers at Djebel Onk (Tebessa) are in close spatial and chronological relation and share affinities with the layers known in Tunisia [20]. Many localities with phosphorite deposits, however, exhibit some differences in terms of petrography, geochemistry, and depositional environments [1]. Those located to the north of Tebessa (Djebel Dyr and El Kouif) are the equivalent of Ain Kerma, Kelaât Djerda and Sra Ouartane from Tunisia; they exhibit similar dimensions.

Those located south of Tebessa, such as Djebel Onk and the western side of Djebel Zrega, show considerable economic potential and are the equivalent of the Tunisian deposits in the Basin of Gafsa, such as the deposits of M'rata, Redeyef, Kef Eschfair and Metlaoui. The upper part of the phosphatic layer is represented by the YpresianMetlaoui Formation with a general thickness of 50 to 55 m. It is characterized by the presence of lumachelic limestones and marls with abundant flint concretion [21].

This large phosphate basin, located between Algeria and Tunisia (Figure 1), is also known as the Gafsa-Bir El Ater Basin. The Bled El Hadba (BEH) and Kef Essennoun (KES) deposits are located in this basin and represent the objective of this study (see Figure 2). The prospected area consists mainly of upper Cretaceous to lower Eocene marine sediments that are covered discordantly by thick continental sandy and argillaceous Miocene to Quaternary deposits.

3. Sampling and Methodology

Samples for petrographic and chemical analyses were taken from the outcrops of the three main phosphate sub-layers in both Kef Essenoun (KES) and Bled El Hadba (BEH), according to the structure of the deposits (top, main, and basal).

Six samples were taken (one for each sublayer), systematic from bottom to top in order to follow vertical evolution and determine the different types of facies for petrographic analy-

Fig. 3. Contact between the black and beige phosphates and the upper phosphatic dolomite of the Kef Essennoun (KES) deposit. A: Black phosphate; B: beige phosphate; C: Phosphatic dolomite

Rys. 3. Kontakt czarnych i beżowych fosforanów z górnym dolomitem fosforanowym złoża Kef Essennoun (KES). Odp.: czarny fosforan; B: beżowy fosforan; C: Dolomit fosforanowy

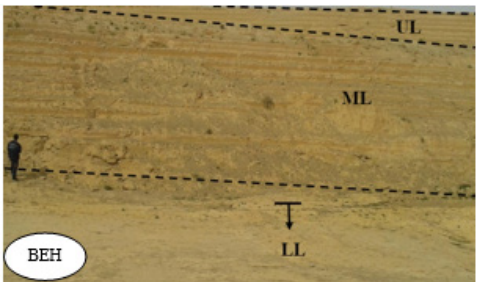

Fig. 4. Contact between the three sub-layers at the BEH deposit. UL: upper sub-layer; ML: main sub-layer; LL: lower sub-layer

Rys. 4. Kontakt trzech podwarstw na złożu BEH. UL: górna podwarstwa; ML: główna podwarstwa; LL: dolna warstwa podrzędna

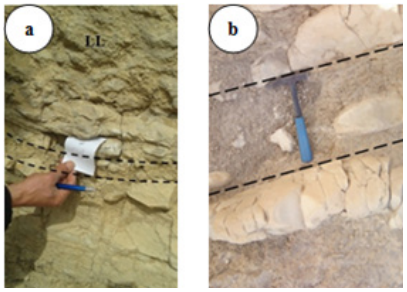

Fig. 5. Lower Thanetian phosphate layers (a): Bled-El Hadba and (b): Kef Essennoun

Rys. 5. Warstwy fosforanowe dolnego tanetu (a): Bled-El Hadba i (b): Kef Essennoun

ses. Thin sections were prepared from the six samples. The petrographic study was carried out using an optical microscope at the Department of Geology, University Annaba.

Two samples (one for each deposit) were taken in trenches (one trenches for each sublayer), mechanical preparation for these samples consisted of homogenization, crushing (≤ 4 mm), quartering, dry sieving (4 to 0.05 mm), grinding (<90 µm), and sieving through a series of dry sieve screens. Each grain size fraction was powdered (<90% passing through the 80 µm sieve) for chemical analyses provided to us by the Iron and Phosphate Exploitation Company (FERPHOS).

The dimensional classification (used to determine the weight distribution of particles of a material according to their dimensions) of the raw ore obtained after mechanical processing was carried out by the dry sieving method using a vibrating sieve on a series of sieves with openings ranging ≤ 2 mm. The different particle size fractions obtained after separation by sieving was grinded down to ≤ 100 µm, to facilitate chemical reaction during subsequent treatments. Based on previous studies [24-25] on this type of ore, we limited the duration of sieving to 10 to 15 minutes to avoid significant errors due to the crushing effect (attrition).

The X-ray diffraction was carried out with a powder X'Pert Pro Panalytical diffractometer using the copper line in the Laboratory of Material Technologies and Process Engineering (LTMGP) at the University of Bejaia. The determination of the major elements was carried out in the FERPHOS laboratory using the phosphomolybdate spectrophotometry, atomic absorption spectrometry (AAS) and calcimetry methods.

4. Results and Discussion

4.1 Petrographic data

The deposits of Djbel Onk (BEH and KES) are brittle phosphorites and are, therefore, classified as phospharenites [12-26]. The phosphatic facies is represented by homogenous fine grains (200 µm to 300 µm), rarely heterogeneous coarse-grained (up to 3 mm) phosphorites. Phosphatic particles are composed mainly of pellets, coprolites, bioclasts (mainly bone and fish teeth fragments), and glauconite. The rocks of the Kef Essennoun deposit are beige to brown in color at the top and dark grey to black at the bottom of the layer (Figure 3). Color variations are most likely related to organic matter contents [27].

Based on macroscopic, microscopic, and chemical studies we distinguish three phosphate sub-layers from the bot-

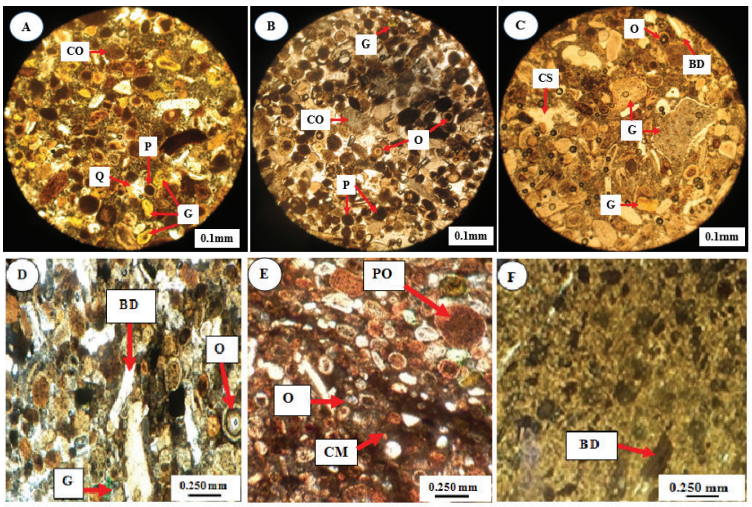

Fig. 6. Microscopic images of polished thin sections of Bled El Hadba (A, B and C) and Kef Essennoun (D, E and F) phosphates ores. BD: Bone Debris; PS: Pseudo-oolites; CM: Micritic Cement; G: Glauconite; O: Oolite; CO: Coprolites; P: Pellet; CS: Sparitic Cement; Q: Quartz

Rys. 6. Obrazy mikroskopowe wypolerowanych cienkich przekrojów rud fosforanowych Bled El Hadba (A, B i C) i Kef Essennoun (D, E i F). BD: szczątki kości; PS: Pseudo-oolici; CM: cement mikrytyczny; G: glaukonit; O: Oolit; CO: koprolity; P: Pellet; CS: cement sparytowy; P: Kwarc

tom to the top of the phosphorite layer in the BEH deposit (Figure 4):

Lower sub-layer (LL): The thickness is variable between 2.4 and 18 m, characterized by fine to medium-grained phosphorites with calcareous-dolomitic cement with rare limestone intercalations.

Middle sub-layer (ML): This section is thicker, reaching 29.75 m, which increases towards the western part of the basin. The beige, rarely dark-gray phosphates are fine-grained with clayey-marly matrix, occasionally sandy, soft and brittle. This section contains intercalations of phosphatic limestones with calcareous-dolomitic cement.

Upper sub-layer (UL): The thickness varies from 2.3 to 18 m. This layer disappears gradually towards the northwestern part of the section, near the studied area. The lithology is similar to that of the lower layer; it consists of beige, dark-gray, fine to medium-grained hard and compact phosphorites, with calcareous-dolomitic cement. Several quartz geode intercalations are occasionally observed.

The macroscopic observations of the outcrops allowed the determination of the following lithologies:

The Danian is composed of a thick layer of marls and whitish limestone that are overlain by intercalations of oyster limestones of Montian age surmounted by a medium phosphate bed rich in fish debris of Thanetian age (Figure 5). This is overlain by limestones with clays and marls, and black gypsum-rich marls.

The upper Thanetian is represented by a thick layer of phosphates (Figure 5 b).

The top of this phosphate layer consists of lower Ypresian phosphatic dolomites and phosphatic shark teeth-enriched (Elasmobranchii and cartilaginous fish) limestone, with intercalations of whitish limestones and flint. The teeth are represented by lateral-central and Hypotodusverticalis (superior side teeth). The change of lithology indicates a regressive tendency during the sedimentation of the deposits. This was followed by a reopening of the marine field during the late Ypresian represented by limestones and dolomites with flint.

Early Lutetian consists of dolomites and limestones with intercalations of quartz geodes. During the sedimentation of the upper Lutetian green clays, followed by limestones, marls and gypsum, the depth of the basin got significantly lower.

The uppermost beige phosphate of BEH (UL) is hard, coarse-grained and colored in its lower part by iron hydroxides. It contains shark teeth and bones, and bivalves can be observed in its lower part.

The middle phosphates of BEH, of brown color (ML), are fine-grained and friable.

The lowermost phosphates of BEH, of beige color (LL) are hard and contain white marl intercalations with a thickness up to 20 cm (Figure 5 a). The base of the bed is delimited by the presence of dark brown marls.

The phosphates of KES are represented by three types of facies: upper Thanetian black (A) and beige (B) phosphates, and lower Ypresian phosphatic dolomites (C).

The BHS deposit is poorer in P2O5 and richer in MgO contents than that of KES. Moreover, the natural size of apatite is finer than the material from KES. It is difficult to carry out a transfer of the data and parameters of the processes of treatment between these two deposits.

Petrographic examinations show that the phosphates of BHS (Figure 6) consist of pellets (50 µm to 100 µm), coprolites (0.5 to 1.6 mm), bone debris with varying shapes and sizes, oolites, quartz and glauconite (0.12 to 0.6 mm) that are cemented by carbonate, sparite (calcitic) or micrite (dolomitic). The cement of BHS deposits is generally dolomitic and calcitic but sometimes soft and not poorly-cemented [24].

The phosphates from the lower and upper part are characterized by an abundance of dolomitic and calcitic cement (75%) with the presence of a few heterogeneous grains: large-sized coprolites, bone debris, pseudo-oolites, glauconite, pellets and quartz of small grains (A, C). On the other hand, the phosphates of the intermediate sub-layer generally consist of fairly homogeneous grains: oolites, pseudo-oolites and pellets, with the presence of some small coprolites, bone debris, glauconite, and large quartz grains. These grains are bound by micritic cement (15%) of argillaceous nature however; the cement is also calcareous (B).

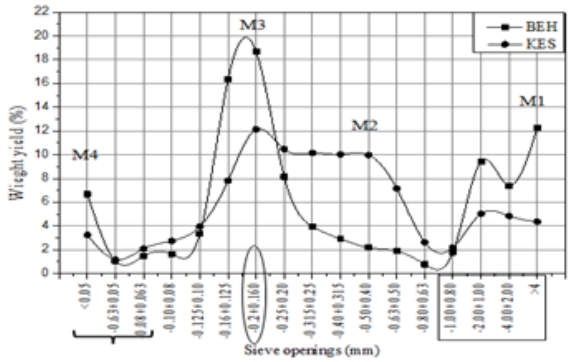

Fig. 7. Weight (%) versus size particle classes of KES and BEH samples
Rys. 7. Masa (%) a klasy wielkości cząstek próbek KES i BEH

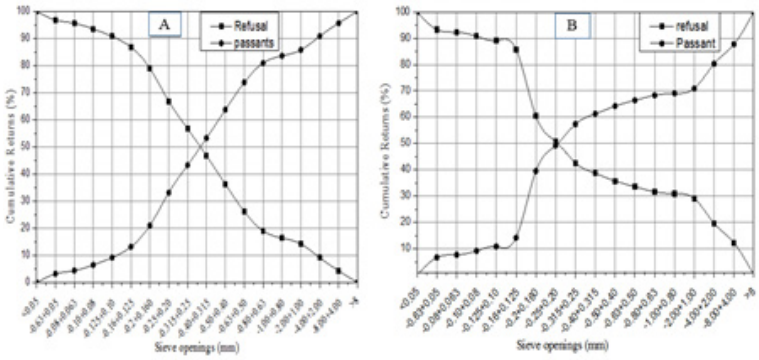

Fig. 8. Granulometry sieving of the KES and BEH phosphate samples
Rys. 8. Przesiewanie granulometryczne próbek fosforanów KES i BEH

The phosphates of KES consist predominantly of pellets, coprolites, bone debris, oolites and glauconite bound by a calcareous, sparitic or micritic cement.

Depending on the size and nature of the grains, the KES deposit includes three types of facies:

Black phosphate is generally composed of oolites and pseudo-oolites and black pellets with the presence of some coprolites and bone debris. It represents the lower part of the deposit of lower Thanetian age. The black color is due to the presence of organic matter (Figure 6D).

Beige phosphate is characterized by heterogeneity of the grains, and includes pseudo-oolites, glauconite, bone debris and coprolite. These grains are bound by calcareous cement. This type of phosphate is present in the productive sub-layer of the upper Thanetian (Figure 6E).

Dolomitic phosphate. It represents the upper part of the deposit (Figure 6F) and is characterized by the abundance of dolomitic cement with the presence of some coprolites, pseudo-oolites and bone debris.

4.2 Mineralogical and chemical analyses

The phosphatic elements of phosphorites exhibit a great diversity. These elements are peloids, nodules, oolites and oncoids, usually rounded to sub-rounded and lithoclasts, bioclasts and coproids, with less regular forms. The nonphosphatic fraction of the rock is divided into an endogangue included in the previously mentioned phosphatic elements and an exogangue that is external to them [13]. This distinction is important in mining geology because of the different treatment techniques. The endogangue is obviously more difficult to eliminate than the exogangue (example: pelophosphareenitis with endogangue pyrite and exogangue of clay rich in organic matter).

4.2.1. Mineralogical analyses

The volumetrically dominant phosphate mineral of Djebel Onk is carbonate fluorapatite [22]. The gangue minerals associated with phosphate particles in the phosphatic rocks are mainly quartz, calcite, dolomite, ankerite, siderite, feldspars, clay minerals, gypsum and organic matter [28].

4.2.2. Particle size analysis

The nature of the phosphate fractionallowsthe selection of the secondary components of the rock, which can be indicated in the name of the phosphorite by adding an adjective: argillaceous pelphospharenite, calcareous phospharenorudite, etc.

The exogangue is extremely variable in quantity, nature and aspect from one deposit to another. It consists mainly of carbonates, silica and silicates.

The endogangueis composed, as a whole, of non-apatitic fraction internal to the phosphatic elements [13].

The most common minerals are opal, quartz, illite and organic matter. The existence of organic matter (OM) in phosphate sediments has been reported by several authors [29-32].

Grain-size classification of the raw phosphates obtained after mechanical treatment and sieving for the two samples, BEH and KES, are reported in (Figure 7)

The distribution of grains in the raw ore is represented by four main modes (M1, M2, M3, and M4) of KES and BEH samples.

The mesh sizes of the phosphate elements are represented by the particle sizes 0.1 mm to 0.5 mm with 42.59 and 64.54%

Tab. 1. Major element contents versus sample size classes from BEH

Tab. 1. Zawartość głównych pierwiastków a klasy wielkości próby z BEH

Fraction	wt (%)									
	P_2O_5	MgO	CaO	SiO_2	Al_2O_3	Fe_2O_3	Na_2O	K_2O	LOI	Total
Total	**23.9**	**3.46**	**45.43**	**5.51**	**0.95**	**0.55**	**1.08**	**0.19**	**18.93**	**100**
> 4	19.92	2.22	48.69	4.61	0.8	0.3	0.64	0.21	22.61	100
- 4 + 2	20.4	4.09	46.56	3.61	2.25	0.29	0.89	0.24	21.67	100
- 2 + 1	22	4.19	47.6	3.91	2.41	0.31	0.68	0.24	18.66	100
- 1 + 0.80	22.4	3.51	47.08	4.32	2.74	0.34	1.21	0.31	18.09	100
- 0.80 + 0.63	22.6	3.42	47.13	4.03	3.29	0.36	1.25	0.35	17.57	100
- 0.63 + 0.50	24.8	3.23	46.01	6.06	4.05	0.34	1.08	0.31	14.12	100
- 0.50 + 0.40	**27.7**	3.12	46.01	5.41	3.19	0.3	1.38	0.33	12.56	100
- 0,40 + 0.315	**29.3**	2.86	47.2	4,16	3,12	0.25	1,36	0,44	11,31	100
- 0.315 + 0.250	**29.5**	2.45	47.89	3.63	2.25	0.2	1.24	0.29	12.55	100
- 0.250 + 0.200	**29,25**	2.15	48.15	3.69	2.07	0.22	1.44	0.32	12.71	100
- 0.20 + 0.160	**29.7**	1.89	49.64	3.41	2.23	0.21	1.35	0.31	11.26	100
- 0.160 + 0.125	**29,95**	1.32	47.26	4.29	3.2	0.34	1.21	0.34	12.09	100
- 0.125 + 0.10	**27.6**	1.2	44.1	4.6	3.5	0.27	1.16	0.56	17.01	100
- 0.10 + 0.08	18	3.25	43.08	5.51	3.28	0.23	0.92	0.57	25.16	100
- 0,08 + 0,063	11,9	4,36	42,2	5,63	3,3	0,22	0,81	0,55	31,03	100
- 0.63 + 0.05	9.1	4,25	41.3	5.77	3.4	0.36	0.75	0.5	34.57	100
<0,05	4,5	4	39,49	6,84	4,43	0,74	0,69	0,48	38,83	100

Tab. 2. Major element contents versus sample size classes from KES

Tab. 2. Zawartość pierwiastka głównego a klasy liczebności próby z KES

Fraction	wt (%)									
	P_2O_5	MgO	CaO	SiO_2	Al_2O_3	Fe_2O_3	Na_2O	K_2O	LOI	Total
Total	**28.23**	**2**	**47.8**	**3.04**	**0.68**	**0.25**	**1.16**	**0.35**	**16.49**	**100**
> 4	19.92	3.86	50.11	3.02	0.68	0.18	0.79	0.23	21.21	100
- 4 + 2	19.68	3.19	47.65	3.24	0.76	0.22	1.06	0.27	23.93	100
- 2 + 1	23.06	3.12	49.52	3.42	0.85	0.23	0.94	0.25	18.61	100
- 1 + 0.80	26.14	3.02	49.07	3.95	0.86	0.26	1.51	0.37	14.82	100
- 0.80 + 0.63	**28.79**	2.99	48.2	4.85	0.78	0.29	1.46	0.39	12.25	100
- 0.63 + 0.50	**29.99**	2.9	47.99	6.13	0.79	0.28	1.30	0.38	10.24	100
- 0.50 + 0.40	**30.19**	2.26	48.61	6.53	0.72	0.26	1.5	0.36	9.57	100
- 0.40 + 0.315	**30.34**	2.15	49.39	4.72	0.69	0.2	1.51	0.34	10.66	100
- 0.315 + 0.250	**30.18**	1.99	49.08	3.32	0.73	0.17	1.13	0.26	13.14	100
- 0.250 + 0.200	**30.01**	1.19	49.57	3.01	0.6	0.18	1.52	0.32	13.6	100
- 0.20 + 0.160	**29.74**	1.02	51.23	3.27	0.71	0.19	1.25	0.3	12.29	100
- 0.160 + 0.125	**28.71**	1	50.69	4.64	0.78	0.27	1.31	0.38	12.22	100
- 0.125 + 0.10	26.33	3.05	50.23	4.7	0.8	0.3	1.37	0.4	12.82	100
- 0.10 + 0.08	24.5	4.13	49.8	4.85	0.83	0.35	1.4	0.47	13.67	100
- 0.08 + 0.063	23.52	4.17	49.58	4.98	0.86	0.38	1.42	0.52	14.57	100
- 0.63 + 0.05	22.88	3.77	47.14	4.55	0.88	0.46	1.1	0.46	18.76	100
<0.05	20.21	2.16	41.66	4.68	0.95	0.61	0.56	0.33	28.84	100

respectively for the two types of the deposits of phosphates (BEH and KES).

The fine fractions smaller than 0,1 mm assigned to the elements of the gangue registered 10,84 and 9,09%, while the coarse fractions greater than 1mm with predominance in sterile elements of the gangue register considerable rates with 29.1 and 14.24% for (BEH and KES) respectively. On the other hand, figure 7 reports the evolution of the weight yield as a function of grain size classes by sieving. From the four granulometric modes, only M1 is the most pronounced. It is assigned partly to dolomite, very abundant in the coarse fraction greater than 1 mm [12].

The secondary modes M2 and M3 where the phosphatic elements are concentrated records proportions of grains with dimensions between 0.08 mm and 0.25 mm. The M4 mode with sizes smaller than 0.1mm is assigned to minerals of the gangue (silica and clay). The obtained output is higher in the intermediate fraction 0.1 to 0.5 mm for (KES) per report/ratio (BEH) which is assigned to the abundance of the phosphatic elements.

In Figure 8 FA, KES deposit illustrates the texture distribution of the rough ore. The percentage of the overall sample mass of KES phosphate ore is >50% and is represented by the range -0.40 +0.315 mm with a grain size class between -0.20 to +0.16 mm. Figure 8B illustrates the texture distribution of phosphates from the BEH deposit. The obtained results indicate that the granulometry is homogeneous. The percentage of the total sample mass of the BEH phosphate ore is >50% and is represented by the range -0.25 +0.20 mm with a grain size class between -0.20 to +0.16 mm.

4.2.3. Granulo-chemical analyses

The elements (oxides) P_2O_5, MgO, CaO, SiO_2, Al_2O_3, Fe_2O_3, Na_2O, K_2O contents of phosphates is directly correlated to the particle-size ranges of the BEH and KES samples, which are given in Tables 1 and 2 .The following observations emerge:

A small population appears in the field from 100 to 60 µm; this is attributed to the presence of dolomite, silica and clays;

A major population is centered around the 200 µm value; this is partly attributed to the phosphate elements of the arenite class.

A small population with coarse grains appears in the range 0.5 to 1 mm, and this corresponds to a mixture of grains consisting of phosphate and dolomite.

The P_2O_5 contents increase with a maximum in the particle size 0.08 to +0.125 mm and -0.500 to +0.100 mm and decrease considerably when the MgO contents increase. The evolution of MgO contents represents carbonates and dolomites located below the phosphatic layer. It seems that the pho-

sphate content increases with the decrease in dolomite and carbonate contents.

Major element contents of BEH and KES samples are given in Tables1 and 2.

From these analyses, the following remarks can be drawn:

The CaO/P_2O_5 ratio of BEH phosphates of 1.90 is higher than that of KES (1.69). Comparison with the CaO/P_2O_5 ratio of pure fluorapatite [33] indicates the presence of other Ca-minerals;

The KES phosphates are richer in CaO, Corg, and P_2O_5 than those of BEH;

The BEH phosphates show slightly higher MgO, loss on ignition (LOI), SiO_2 and Al_2O_3 contents compared to the KES phosphates;

The contents of remaining elements (Na_2O, K_2O, and Fe_2O_3) are similar in the two deposits.

5. Summary and Conclusions

Two types of phosphate ores were studied by granulo-chemical analyses and X-Ray diffraction (XRD) which allowed performing a comparative study of their granulometry, and chemical properties. The obtained results show that the phosphates grains are mainly coprolites, pseudo-oolites and pellets, bound by a dolomitic cement.

The phosphates of BEH are divided into three sub-layers from top to bottom: (1) the upper section with beige phosphates (UL) is very hard and relatively coarse-grained; (2) the middle section with brown phosphates (ML) is fine-grained and friable; and (3) the lower section with beige phosphates (LL) shows whitish marl intercalations (up to 20 cm). The phosphates of KES are represented by three types of facies: (1) the upper Thanetian black and (2) beige phosphates; and (3) the lower Ypresian phosphatic dolomites. In terms of particle size, the dimensional classification carried out by sieving revealed that the bulk of the overall mass of the raw ores is represented by the particle size range 0.08 to 0.125 mm and 0.50 to 0.10 mm: 70.36 (KES) and 61.56 % (BEH). This represents the optimal release mesh of separation of the phosphatic elements (class of the arenites).

The mineralogical study on BEH phosphates shows the presence of fluorapatite, hydroxylapatite and dolomite as the main minerals. Quartz, calcite and gypsum are minor minerals. KES phosphates are represented by carbonate-hydroxylapatiteand dolomite as the main minerals. Quartz and calcite are secondary minerals.

The results of the granulo-chemical and by XRD analyses point out the depletion in phosphate content of the layer of BEH and enrichment in carbonate and dolomite content of the BEH deposits compared to the KES deposits.

The CaO/P_2O_5 (1.90) ratio of BEH phosphates is higher than the ones from the KES phosphates (CaO/P_2O_5 = 1.69).

Despite the two deposits being located in the same region, each deposit has different mineralogical and chemical characteristics, which will need different method of exploitation in the mining operations.

Acknowledgments

We would like to thank FERPHOS mining company for the fieldwork access and assistance, the laboratory LTMGP of the University of Bejaia, the laboratory of mines of the University of Tebessa and the Mining Laboratory of Istanbul Technical University (Turkey) for various analyses.

Literatura – References

1. Kechiched, R., Laouar, R., Bruguier, O., Laouar-Salmi, S., Ameur-Zaimeche, O., Foufou, A., Preliminary data of REE in Algerian phosphorites: a comparative study and paleo-redox insights, Procedia Engineering, vol. 138, 2016, p. 19-29.
2. Visse, L., Monographies régionales 1er série Algérie n°27 - Genèse des gîtes phosphatés du Sud-Est Algéro-Tunisien - XIXe congrès géologique international, Protat frères, Alger, 1952.
3. Cielensky, S., Benchernine, N., Watkowski, T., Works of prospecting and assessment of phosphates in the region of Bir El Ater, Internal report EREM (Entreprise de Recherche et d'Exploration Minière), vol. 2, Algeria, 1988, p. 103. .
4. Bouzenzana, A., Harmful elements in concentrates them of phosphate and method of disposal case of "jebel-onk" Algeria, Journal of Ore Dressing, vol. 15, no. 30, 2013, p. 25-30.
5. Sinirkaya, M., Özer, K., Gülaboğlu, S. Investigation of the solubilities of sulfated and ground phosphate rock after sulfation in H2SO4 solution, Pamukkale University Journal of Engineering Sciences, vol. 20, no. 7, 2014, p. 253-257.
6. Bezzi, N., Aïfa, T., Hamoudi, S., Merabet, D., Trace elements of Kef Es Sennoun natural phosphate (Djebel Onk, Algeria) and how they affect the various mineralurgic modes of treatment, Procedia Engineering, vol. 42, 2012, p. 1915-1927.
7. Lassis, M., Mizane, A., Dadda, N., Rehamnia, R., Dissolution of Djebel Onk phosphate ore using sulfuric acid, Environmental Nanotechnology, Monitoring & Management, vol. 4, 2015, p. 12-16.
8. Long, X., Yuan, C., Sun, M., Zhao, G., Xiao, W., Wang, Y., Yang, Y., Hu, A., Archean crustal evolution of the northern Tarim craton, NW China: Zircon U–Pb and Hf isotopic constraints, Precambrian Research, vol. 180, no. 3-4, 2010, p. 272-284.
9. Kato, Y., Fujinaga, K., Nakamura, K., Takaya, Y., Kitamura, K., Ohta, J., Toda, R., Nakashima, T., Iwamori, H., Deep-sea mud in the Pacific Ocean as a potential resource for rare-earth elements, Nature geoscience, vol. 4, no 8, 2011, p. 535-539.
10. Emsbo, P., McLaughlin, P.I., Breit, G.N., Du Bray, E.A., Koenig, A.E., Rare earth elements in sedimentary phosphate deposits: Solution to the global REE crisis?, Gondwana Research, 2015, vol. 27, no 2, 2015, p. 776-785.
11. Kechiched, R., Laouar, R., Bruguier, O., Salmi-Laouar, S., Kocsis, L., Bosch, D., Foufou, A., Ameur-Zaimeche, O., Larit, H., Glauconite-bearing sedimentary phosphorites from the Tébessa region (eastern Algeria): Evidence of REE enrichment and geochemical constraints on their origin, Journal of African Earth Sciences, vol. 145, 2018, p. 190-200.
12. Bezzi, N., Gestion de la qualité et valorisation des Minerais de Phosphate De Bled El Hadba, Djebel Onk - Tebessa, PhD Thesis, Université Ferhat Abbas – Setif, Algeria, 2005.
13. Visse, L.D., Note préliminaire sur les coprolithes des phosphates de l'Afrique du nord, Compte rendu de Société Géologique de France, vol. 7-8, 1950, p. 119-121.
14. Gomez, F., Barazangi, M., Beauchamp, W., Role of the Atlas Mountains (northwest Africa) within the African-Eurasian plate boundary zone, Geology, vol. 28, no. 9, 2000, p. 775-778.
15. Notholt, A.J.G., Economic phosphatic sediments: mode of occurrence and stratigraphical distribution, Journal of the Geological Society, vol. 137, 1980, p. 793-805.
16. Sheldon, R.P., Association of phosphatic and siliceous marine sedimentary deposits, In: Hein, J.R. (Ed.), Siliceous sedimentary rock-hosted ores and petroleum, Van Norstrand Reinhold Co, New York, 1987, p. 58-80.
17. Notholt, A.J.G., Sheldon, R.P., Davidson, D.F., Phosphate deposits of the world, volume 2. Phosphate rock resources, Cambridge University Press, Cambridge, 1989.
18. Lucas, J., Prévôt-Lucas, L. (1995), Tethyan Phosphates and Bioproductites, In: Nairn, A.E.M., Ricou, LE., Vrielynck, B., Dercourt, J. (Eds.), The Ocean Basins and Margins, Volume 8. https://doi.org/10.1016/j.gexplo.2019.106396 Rare earth elements distribution of Tertiary phosphorites in Tunisia, In: Mineral Deposit Research: Meeting the Global Challenge. Springer, Berlin, Heidelberg, 2005, p. 1061-1064, https://doi.org/10.1007/3-540-27946-6_271
19. Kechiched, R., Laouar, R., Bruguier, O., Kocsis, L., Salmi-Laouar, S., Bosch, D., Ameur-Zaimeche, O., Foufou, A., Larit, H., Comprehensive REE + Y and sensitive redox trace elements of Algerian phosphorites (Tébessa, eastern Algeria): A geochemical study and depositional environments tracking, Journal of Geochemical Exploration, vol. 208, 2020, 106396, https://doi.org/10.1016/j.gexplo.2019.106396.
20. Chabou-Mostefai, S., Étude de la série phosphatée tertiaire du Djebel Onk, Algérie, Stratigraphie, Pétrographie, Minéralogie et Analyse Statistique, Thèse Doctorat, Université de Droit, d'Économie et des Sciences d'Aix-Marseille, France, 1987, 376.
21. Kassatkine, Y., Yahyaoui, A., Chatilov, S., The works of prospecting and assessment on phosphate executed in 1976-1978 in the mining district of Djebel Onk. Algeria, Internal report SONAREM (Société Nationale de Recherche et d'Exploration Minière), vol. 2, Algeria, 1980, p. 140.

22. Ranchin, G., Gisement de phosphate de chaux sédimentaire de Djebel Onk (Algérie), Rapport inédit, Société d'Etudes et de Réalisations Minières et Industrielles (SERMI), Paris,1963.

23. Larouci, M., Etude de la caractérisation et de la valorisation du minerai de phosphate de Djebel Onk – Algérie,Thèse de Doctorat, Université Orléans, 1988, 194 pages.

24. Hamdadou, M., Caractérisation petro-minéralogique et séquentielle du gisement de phosphate de Djebel Onk (Algérie), Thèse de Doctorat, ENSG Nancy, 1996.

25. Kechiched, R., Typologie géochimique et géostatistique des minerais de phosphates du gisement de Bled El Hadba – Djebel Onk (Algérie Orientale), Mémoire de Magistère, Université d'Annaba, Algérie, 2011, 175 pages.

26. Dass Amiour, M., Mezghache, H. & Elouadi, B., The use of three physico-chemical methods in the study of the organic matter associated with the sedimentary phosphorites in Djebel Onk Basin, Algeria, Arabian Journal of Geosciences, vol. 6, 2013, p. 309-319.

27. Bezzi, N., Merabet, D., Benabdeslem, N., Arkoub, H., Caractérisation physico-chimique du minerai de phosphate de Bled El Hadba – Tébessa, Annales de Chimie Science des Matériaux, vol. 26, no. 6, 2001, p. 5-23.

28. Benalioulhaj, S., Trichet, J., Comparative study by infrared spectroscopy of the organic matter of phosphate-rich (Oulad Abdoun basin) and black shale (Timahdit basin) series (Morocco), Organic Geochemistry, vol. 16, no. 4-6, 1990, p. 649-660.

29. Belayouni, H., Slansky, M., Trichet, J., A study of the organic matter in Tunisian phosphates series: Relevance to phosphorite genesis in the Gafsa Basin (Tunisia), Organic Geochemistry, vol. 15, no 1, 1990, p. 47-72.

30. Purnachandra Rao, V., Michard, A., Naqvi, S.W.A., Böttcher, M.E., Krishnaswamy, R., Thamban, M., Natarajan, R., Borole, D.V., Quaternary phosphorites off the southeast coast of India, Chemical Geology, vol. 182, no. 2–4, 2002, p. 483-502.

31. Piper, D.Z., Perkins, R.B., Rowe H.D., Rare-earth elements in the Permian Phosphoria Formation: Paleo proxies of ocean geochemistry, Deep Sea Research Part II: Topical Studies in Oceanography, vol. 54, no. 11-13, 2007, p. 1396-1413.

32. Slansky, M., Géologie des phosphates sédimentaires, Mémoire de Bureau de Recherche Géologiques et Minières (B.R.G.M. France), vol. 114, 1980, 92 pages.

Charakterystyka mineralogiczna i chemiczna fosforanów ze złóż Djebel Onk (Tebessa, Algieria)

Algieria posiada ważne rezerwy fosforanów (2 miliardy ton) zlokalizowane na wschodzie kraju w Djebel Onk. Ten obszar górniczy znajduje się w północno-zachodniej części algierskiej Sahary, w pobliżu granicy algiersko-tunezyjskiej. Wyniki analiz granulochemicznych i XRD potwierdzają zubożenie fosforanów w warstwie Bled El Hadba i ich wzbogacenie w węglan i dolomit, w porównaniu z warstwą Kef Essennoun. Cząstki fosforytu są niejednorodnie ziarniste. Chociaż oba złoża znajdują się stosunkowo blisko siebie, wykazują różne właściwości mineralogiczne i chemiczne, co może powodować stosowanie różnych metod eksploatacji górniczej.

Słowa kluczowe: *fosforany, wielkość cząstek, chemia, petrografia, Algieria*

Optimizing Dry Ultrafine Grinding of Talc in Attritor Mill

S.E. EL-MOFTY[1)], A.M. ELBENDARI[2)], A.A. EL-MIDANY[1)], M.K. ABDEL-RAHMAN[2)]

[1)] Mining, Petroleum, and Metallurgy Dept., Faculty of Engineering, Cairo University, Postal code 12613, Cairo, Egypt
[2)] Central Metallurgical R&D Institute, P.O. Box 87, Helwan, Cairo, Egypt
*Corresponding Author: S.E. EL-MOFTY, Mining, Petroleum, and Metallurgical Engineering Dept., Faculty of Engineering, Cairo University, Egypt; email: s_elmofty@eng.cu.edu.eg or mpm_cu@yahoo.com

http://doi.org/10.29227/IM-2023-02-04

Submission date: 01-05-2023 | Review date: 04-06-2023

Abstract

In this work, the parameters affecting the dry grinding of talc in the attritor mill were investigated. The attritor was tested with its initial design without balls then with balls as additional grinding media to prepare a feed passing 45 microns. The prepared feed (-45 mm) was used to produce a product with 10 μm or less using statistical design in presence of balls. The presence of balls enhances product fineness. The significance of the studied factors is: stirrer speed>mill filling >grinding time. In addition, the d_{50} was correlated with studied factors. The mean particle size (d_{50}) as low as 6 μm was obtained at 460 rpm, 20% mill filling, and after 60 min grinding time.

Keywords: *dry grinding, ultra-fine grinding, attritor mill, statistical design, talc*

1. Introduction

Grinding is an essential process for reducing particle size and preparing a material with specific size range or separating different minerals based on the difference in their mechanical properties [1-3]. Yet, fine grinding is a challenge where the conventional ball milling seems uneconomical especially when sizes below 10 μm are targeted [4-9]. Recently, the ultra-fine grinding of minerals attracts attention of numerous industrial applications such as advanced ceramics, porcelain, cement, paper coating, plastic and pigments. Ultra-fine talc (<10 μm), in particular, has wide applications. In plastics, ultra-fine size platy talc is used to improve its mechanical and surface properties such as stretch resistance [10]. In paper industry talc is used as a filler to control pitch and sticky materials and in coating formulation. In oil paints talc is used as an extender and suspending agent [11].

Attritor mill is one of modified designs of stirred media mill that produces fine particles for chemical, pharmaceutical and mineral processing industries [12-13]. The stirred mills are much more efficient for fine grinding than conventional ball mills. By introducing the stirred media mills, the fine grinding becomes more economically favorable in terms of high grinding rate and low energy consumption [5, 14-16]. In attritor mill, particles are subjected to various forces such as impact, rotational, tumbling, and shear; therefore, the fine powders in micron range can be easily achieved.

Therefore, this work aims at studying dry ultra-fine grinding of talc to produce fraction with a d_{50} less than 10 μm using attritor mill without or with alumina balls as additional grinding media. The main parameters affecting the grinding process such as grinding time, stirring speed, media size, and mill filling were investigated using either one-variable-at-a-time strategy or statistical design in terms of particle size (d_{50}) of the ground product. Moreover, the analysis of variance was used to determine the significance of the studied factors and derive a correlation of d_{50} of the ground product as a function of studied factors.

2. Experimental

2.1. Materials

Talc sample was supplied by El-Nasr Mining Co. It represents Bir Meseh, South of Shalatin locality, Eastern Desert, Egypt. Talc sample was crushed using a "Denver" jaw primary crusher in a closed circuit with a 6.63 mm screen. Representative batches were prepared by successive coning and quartering methods, one of which was finely ground to less than 200 mesh for XRD and chemical analysis.

2.2. Methods

2.2.1. Mineralogical and Chemical Analysis

Identification of the mineral composition of the considered sample was conducted by X-ray diffraction (XRD). Samples were analyzed by X-ray diffraction analysis pattern of the specimen, using the data of the powder pattern of ASTM. The samples for bulk mineral analysis as well as the pure mineral phases were finely ground, mounted randomly on an aluminum holder, and analyzed by X-ray diffraction. Different phases of the samples were identified by X-ray diffractometer (XRD, Brukeraxs D8 Advance, Germany) with Cu kα radiation (λ = 1.5406 Å) and secondary monochromator in the 2θrange from 2 to 75°

In addition, quantitative determination of the talc associated oxides was carried out using Panalytical XRF (Model advanced Axios, Netherlands). One gram of the sample was fired at 1000°C for 2 hours for calculating the loss on ignition (L.O.I). On the other hand, 10 g of the sample is pressed with 2 g wax as a binder in aluminum cup, and then exposed to X-rays as a disk.

2.2.2. Description of Attritor Mill

Vertical laboratory attritor mill (union process type 1S) consists of a stainless steel vessel of 9.5-liter capacity. It has a stainless steel shaft fitted with five arms made of stainless steel. The shaft is a belt-driven with a motor of 3Hp. The tank

Tab. 1. Factors and levels for Box Behnken experimental design

Tab. 1. Czynniki i poziomy dla eksperymentalnego projektu Boxa Behnkena

Variables	Symbol	-1	0	+1
Stirrer speed, rpm	A	270	365	460
Mill filling, %	B	20	30	40
Grinding time, min	C	30	45	60

Tab. 2. Chemical analysis of talc sample

Tab. 2. Analiza chemiczna próbki talku

Element	%	Element	%
SiO_2	46.33	SO_3	0.10
MgO	25.26	$Na_2O + K_2O$	0.12+0.015
CaO	9.48	P_2O_5	0.106
Al_2O_3	4.39	MnO	0.100
Fe_2O_3	2.21	F^-	0.193
TiO_2	0.27	L.O.I	11.40

Tab. 3. Box–Behnken design results in terms of d_{50}

Tab. 3. Wyniki obliczeń Boxa-Behnkena w zakresie d_{50}

Run	A: Stirrer speed, rpm	B: Mill filling, %	C: Grinding time, min.	d_{50}, µm
1	365	30	45	7.78
2	460	30	60	6.15
3	365	20	30	8.41
4	460	30	30	7.63
5	270	30	60	8.86
6	365	30	45	7.72
7	365	30	45	7.74
8	460	40	45	7.78
9	365	40	30	9.64
10	365	30	45	7.74
11	270	20	45	8.60
12	270	40	45	10
13	460	20	45	6.32
14	365	20	60	6.91
15	365	40	60	8.62
16	365	30	45	7.74
17	270	30	30	9.66

is jacketed for cooling and it includes a bottom discharge valve, and bar grid.

The grinding of talc is performed under dry conditions in the presence of 4 mm or 10 mm diameter alumina balls. The experiments were conducted in more details by varying different parameters; namely, grinding time (min), impeller speed (rpm), and mill filling by volume (%). The talc sample feed for attritor mill totally passed from 6.63 mm and its d_{50} equals 2.4 mm, Figure 1.

The attritor product at the end of each test was screened on 45 µm screen. The oversize fraction (+45 μm) was measured by screening, while the undersize fraction (-45 μm) was measured by COR-2000 Laser Particle Size Analyzer.

2.2.3. Statistical design

Box–Behnken experimental design [17-18] was used to investigate the significance of studied factors and for optimizing talc grinding process of -45 microns. The effects of stirring speed, mill filling and grinding time on the talc particle size (more specifically on d_{50} of the ground product) were studied. The design matrix consists of 15 randomized experimental runs. The levels of each factor are given in Table 1.

For this design, the optimal conditions were estimated using a second order polynomial function by which a correlation between studied factors and response (d_{50} of the ground product) was generated. Design-Expert 6.1 Software, Stat-Ease, Inc., Minneapolis, USA, was used for regression analysis of experimental data and to plot response surface. Analysis of variance (ANOVA) using F-test was used to estimate the significance of all terms in the polynomial equation as well as the statistical parameters within 95% confidence interval. The extent of fitting the experimental results to the polynomial model was expressed by the correlation coefficient, R2.

3. Results and Discussion

3.1. Mineral Characterization

The XRD analysis of talc sample, Figure 2, shows that it consists of talc $Mg_3(OH)_2Si_4O_{10}$ associated with chlorite ($(Mg,Fe)_5(Al,Si)_5O_{10}(OH)_8$), calcite ($CaCO_3$), quartz ($SiO_2$), and anatase ($TiO_2$). In addition, chemical analysis of sample, using XRF, is given in Table 2.

3.2. Grinding by Attritor Mill

3.2.1. Effect of ball size

The effect of ball size was studied at 35% mill filling, 270 rpm, and 30 min grinding time. Two ball sizes were tested as mono-size balls or as a mixture of the two balls sizes in different percentages. In the first set of experiments, all the balls are the same size (4 mm), the second set of experiments contains 50% of the ball charge from 4 mm balls and the other half consists of 10 mm, the third set of experiments uses 25% of the ball charge from 4 mm balls and 75% of the charge is 10 mm balls, while the fourth set consists of 100% of 10 mm balls.

Figure 3 represents the effect of ball size on weight % of fines. It is obvious that by increasing the percentage of 10 mm balls over 4 mm balls the product fineness increases. The weight % of -45 µm fraction increases by changing the ratio between the 4 mm balls to 10 mm balls. As the percentage of 10

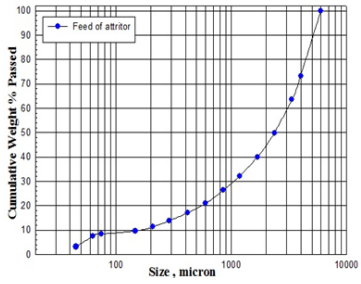

Fig. 1. Size analysis of Feed in Attritor mill
Rys. 1. Analiza wielkościowa paszy w młynie Attritor

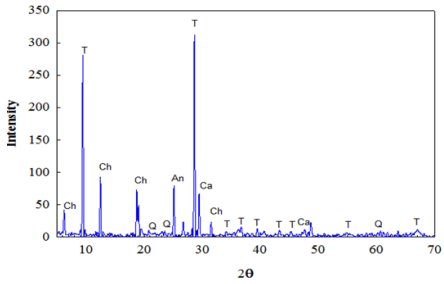

Fig. 2. XRD of talc sample
Rys. 2. XRD próbki talku

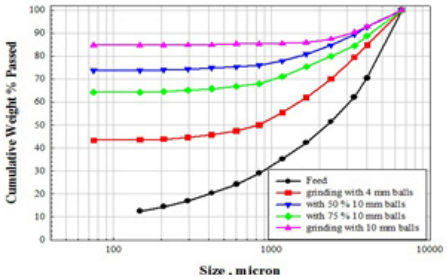

Fig. 3. Effect of different ball sizes on -45 µm wt% at 35% mill filling
Rys. 3. Wpływ różnych rozmiarów kulek na -45 µm % wag. przy 35% napełnieniu młyna

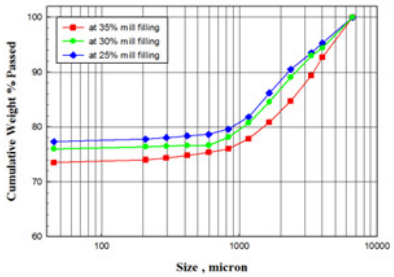

Fig. 4. Size distributions of product dry ground at different mill filling and balls size of (70% of 10 mm balls with 30% of 4 mm balls)
Rys. 4. Rozkład wielkości suchego produktu zmielonego przy różnym napełnieniu młyna i wielkości kulek (70% kulek 10 mm z 30% kulek 4 mm)

mm balls increases the weight percentage of fines increases. More clearly, the weight percentage of -45 µm changed from 50% at 100% 4 mm balls, passing through different 4 mm to 10 mm ratios, to about 85% at 100% 10 mm balls. This behavior can be attributed to the presence of large talc particles in the feed that requires large balls to be ground. The large balls is heavier and more efficient in breaking larger sizes. Whereas, the smaller balls is most probably needed in producing finer sizes [19-21].

3.2.2. Effect of Mill Filling

Different mill fillings (25%, 30%, and 35% by volume) at 270 rpm, and ball sizes (70% of 10 mm balls with 30% of 4 mm balls) at 30 min grinding time were tested. Figure 4 shows the effect of mill filling on the size distribution of the ground product as well as the percentage of -45 µm. It shows that the lower the mill filling is the higher the fines production. The weight % of -45 µm increases from 73% to 78% using 25% mill filling instead of 35% mill filling.

On the other hand, Figure 5 shows that the weight % of -45 µm increases using 100% of 10 mm ball at 25% mill filling to 85% compared to 78% in the case of using (70% of 10 mm with 30% of 4 mm balls). This means that the coarser ball size 10 mm is more effective than other ball sizes and mixtures. The load of 10 mm balls subjects the particles to higher stresses leading to their grinding.

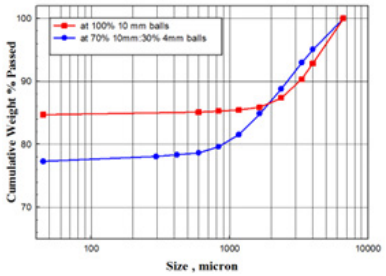

Fig. 5. Size distributions at different ball sizes at 25% mill filling
Rys. 5. Rozkłady wielkości przy różnych rozmiarach kulek przy 25% napełnieniu młyna

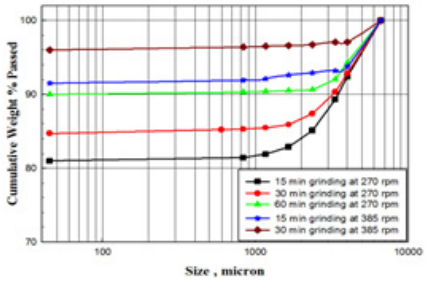

Fig. 6. Size distributions of ground products at 25% mill filling, different stirrer speeds and different times
Rys. 6. Rozkład wielkości zmielonych produktów przy 25% napełnieniu młyna, różnych prędkościach mieszania i różnych czasach

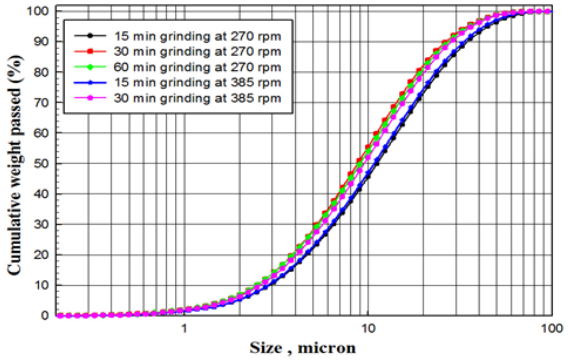

Fig. 7. Size distributions of -45 microns at different stirrer speeds and different times
Rys. 7. Rozkłady wielkości -45 mikronów przy różnych prędkościach mieszadła i różnych czasach

3.2.3. Effect of Stirrer Speed

Figure 6 shows the effect of stirrer speed at 25% mill filling, using 10 mm balls, at different grinding times. It is noticed that, for 15 min grinding time, the wt. % of -45 µm increases from 81% to 91.5% by increasing stirrer speed from 270 rpm to 385 rpm, respectively. While increasing the grinding time to 30 min, the weight % of -45 µm reaches 84.6% at 270 rpm and 95.6% at 385 rpm. It is clear from the size distribution of products that the grinding fineness increases by increasing stirrer speed. It has been shown that d_{50} in a fraction -45 µm at 385 rpm and 30 min grinding is 10.3 µm.

It can be concluded that the fineness of grinding products significantly increases with increasing both stirrer speed and time. The d_{50} of the ground products ranges from 9 to 12 µm, Fig.7. Therefore, to grind the all the sample to -45 um with d_{50} less than 10 µm, the optimization of the process using statistical design was studied.

3.3. Statistical design

The experimental design is used to optimize the dry grinding in attritor mill in terms of mill filling, stirrer speed, and grinding time. Table 3 shows Box-Behnken design results in terms of d_{50} of the products.

The standard deviation and R-Squared for d_{50} are 0.032, 0.9995, respectively. These values indicate the well-fitting of the experimental results to the polynomial model equation. The correlation between d_{50} and the studied facors is derived as follows:

$$d_{50},\ \mu m = +17.33 - (7.97X10^{-3} *A) - (0.2*B) - (0.14*C) + (4.0X10^{-3}*B2) + (1.13X10^{-3}*C2) - (8.8X10^{-5}*A*C) + (8.0X10-4*B*C)$$

where,
A : stirrer speed, rpm
B: Mill filling, %
C: grinding time, min

3.3.1. Effect of mill filling and stirring speed

Figure 8 shows the response surfaces for d_{50} at different values of mill filling and stirring speed at 30 min grinding time. It is noticed that by increasing stirring speed to 460 rpm

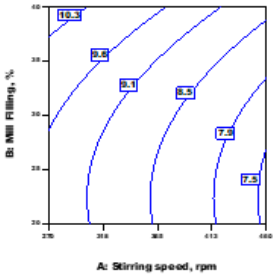

Fig. 8. Effect of stirrer speed and mill filling on d50 of the product at 30 min grinding time
Rys. 8. Wpływ prędkości obrotowej mieszadła i wypełnienia młyna na d50 produktu przy czasie mielenia 30 min

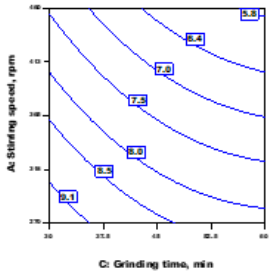

Fig. 9. Effect of stirring speed and grinding time on d50 at 20% mill filling
Rys. 9. Wpływ szybkości mieszania i czasu mielenia na d50 przy 20% wypełnieniu młyna

and decreasing mill filling to 20%, d_{50} decreases. The lowest d_{50} is 7.5 μm at 460 rpm stirring speed, 20% mill filling, and 30 minutes grinding time. Increasing the mill filling produces larger talc particles. This may be attributed to the lower collision probability between the media and talc particles because many hits will be among the media balls rather than with particles.

3.3.2. Effect of grinding time

Figure 9 shows the d50 as function of grinding time and stirring speed at 20% mill filling. The higher the grinding time is the lower the d_{50}. The combined effect of grinding time and stirring speed reduces the particle size from 9.4 μm to 5.8 μm. The smallest d_{50} is achieved at 460 rpm, 20% mill filling, and after 60 min grinding time.

4. Conclusions

Dry grinding of coarse talc feed in an attritor mill with/without balls, as grinding media, to produce fraction completely passes -45 μm was investigated. The results showed that a product with d_{50} ranges from 9-12 μm was obtained by grinding of 2.4 mm feed, with the larger ball size, the higher impeller speed, and lower mill filling. After preparing the fraction of -45 um fraction, its grinding is further studied by statistical design to investigate the significance of the studied factors.

In addition, a functional relationship between three grinding variables (i.e., mill filling, stirrer speed, and grinding time) and the product mean size d_{50} was obtained. It showed that the higher the speed and grinding time and the lower the filling is the higher the product fineness. A product as low as 6 μm can be achieved at optimum conditions (i.e., 460 rpm, 20% mill filling, and after 60 min grinding time).

Literatura – References

1. Chen J., Pan Z., Wang Y., 2018. Preparation of submicron-sized quasi-spherical silica particles via ultrafine grinding with chemical dissolution assistance, Powder Technology, 339: 585-594.
2. El-Midany A. A.; Selim A.Q.; Ibrahim S.S., 2011. Effect of Celestite-Calcite Mineralogy on Their Separation by Attrition Scrubbing, Particulate Science and Technology, 29: 272–284.
3. Sun C., Liu R., Ni K, Wu T, Luo X, Liang B, Zhang M., 2016. Reduction of particle size based on superfine grinding: Effects on structure, rheological and gelling properties of whey protein concentrate, Journal of Food Engineering, 186: 69-76
4. Chatterje, K.K., 2009, "Uses of industrial minerals, rock and fresh water", Chapter 43. Talc-Steatite-Soapstone, Nova Science Publishers, Inc., New York. pp. 425-437
5. Botin, J.A. (2009). Sustainable management of mining operations. SME: Society of Mining, Metallurgy and Exploration, Inc.
6. Roufail, R. (2011). The effect of stirred mill operation on particles breakage mechanism and their morphological features. Master's thesis, University of Waterloo.
7. Underle, U., Woodall, P., Duffy, M., Johnson, N.W., (1997). Stirred mill technology for regrinding McArthur river and Mount Isa zinc/lead ores. In: Proceedings of XX IMPC––Aachen, 21–26 September, 71–78.
8. Burgess, F., McGuire, I., Willoughby, R. (2001). Operation of sand mill detritors at Pasminco operations. In: Fine Particle Processing and Tailing Summit, July, Perth, Australia.
9. Mio, H., Kano, J., and Saito, F., 2004, "Scale-up method of planetary ball mill", Chemical engineering science, 59 (24) 5909-5916
10. El-Midany, A.A., Ibrahim, S.S. 2010, The effect of mineral surface nature on the mechanical properties of mineral-filled polypropylene composites", Polymer Bulletin, 64, 387-399.
11. Jayasundara, C.T., Yang, R.Y., Guo, B.Y., Yu, A.B., Govender, I., Mainza, A., and Rubenstein, J., 2011, "CFD–DEM modeling of particle flow in IsaMills–Comparison between simulations and PEPT measurements", Minerals Engineering, 24 (3) 181-187.
12. Jimbo, G., 1992, "Chemical Engineering Analysis of Fine Grinding Phenomena and Process", Chem. Eng. Japan, Vol. 25, p. 117.
13. Jankovic, A., 2003. Variables affecting the fine grinding of minerals using stirred mills, Minerals Engineering, 16, 337-345.
14. Choi, W.S., 1996, "Grinding Rate Improvement Using a Composite Grinding Ball Size for an Ultra-fine Grinding Mill", J. Soc. Powder Technol., Japan, 33:747.
15. Cayirli S., 2016. Dry grinding of talc in a stirred ball mill, E3S Web Conferences, Mineral Engineering Conference (MEC2016), Vol.8, article no. 01005.
16. Schilling, R.E., Yang, M., 2000, "Attritor grinding mills and new developments", Union process, Inc., Akron, Ohio.
17. Box G.E.P., Behnken D.W., 1960. Technometrics 2, 195 -202.
18. Box, G. E. P., W. G. Hunter, and J. S. Hunter, 1978. Statistics for Experimenters: An Introduction to Design, Data Analysis, and Model Building. Wiley, New York.
19. Schnatz, R., 2004. Optimization of continuous ball mills used for finish-grinding of cement by varying the L/D ratio, ball charge filling ratio, ball size and residence time, International Journal of Mineral Processing, 74S, S55-S63.
20. Austin, L.G., Shoji, K., Luckie, P.T., The effect of ball size on mill performance, Powder Technology, 14 (1976) 71 - 79
21. Bwalya, M.M., Moys, M.H., Finnie, G.J., Mulenga, F.K., 2014. Exploring ball size distribution in coal grinding mills, Powder Technology, 257, 68-73

Optymalizacja ultradrobnego mielenia talku na sucho w młynie Attritor

W niniejszej pracy zbadano parametry wpływające na mielenie talku na sucho w młynie Attritor. Attritor został przetestowany w początkowej wersji bez kulek, a następnie z kulkami jako dodatkowym medium mielącym w celu przygotowania nadawy przechodzącej przez 45 mikronów. Przygotowany wsad (-45 mm) został wykorzystany do wytworzenia produktu o uziarnieniu 10 µm lub mniejszym przy użyciu statystycznego projektu w obecności kulek. Obecność kulek zwiększa stopień rozdrobnienia produktu. Znaczenie badanych czynników to: prędkość mieszadła > wypełnienie młyna > czas mielenia. Ponadto d_{50} był skorelowany z badanymi czynnikami. Średni rozmiar cząstek (d_{50}) tak niski jak 6 µm uzyskano przy 460 obr/min, 20% wypełnieniu młyna i po 60 min mielenia.

Słowa kluczowe: *mielenie na sucho, mielenie ultradrobne, młyn attritor, projektowanie statystyczne, talk*

Embankments Stability of an Opencast Mine with the Proposal of a New Mining Method For its Reopening (Kef Essennoun, Algeria)

M.C. MEZAM[1)]*, M.A. BACHAR ASSED[2)], M. OULD HAMOU[3)], S. NARSIS[4)], A. BENSELHOUB[2)]*

[1)] Mining Department of National Polytechnic School, 10 Avenue Hassen Badi BP 182 El Harrach, 16200 Algiers, Algeria; ORCID orcid.org/ 0000-0001-5604-0210,
[2)] Mining Department of National Polytechnic School, 10 Avenue Hassen Badi BP 182 El Harrach, 16200 Algiers, Algeria; ORCID orcid.org/0000-0002-4245-476X
[3)] Mining Department of National Polytechnic School, 10 Avenue Hassen Badi BP 182 El Harrach, 16200 Algiers, Algeria; ORCID orcid.org/0000-0002-8770-5323
[4)] Environmental Research Center (C.R.E), Annaba, Algeria; ORCID orcid.org/0000-0002-7079-0488
[5)] Mining Department of National Polytechnic School, 10 Avenue Hassen Badi BP 182 El Harrach, 16200 Algiers, Algeria; ORCID orcid.org/0000-0001-5891-2860
* Correspondence: Dr.Aissa BENSEHOUB, Environment, Modeling and Climate Change Division, Environmental Research Center (C.R.E), sis at Campus Sidi Amar, 23001, Annaba, Algeria; email: aissabenselhoub@cre.dz

http://doi.org/10.29227/IM-2023-02-05

Submission date: 01-05-2023 | Review date: 05-06-2023

Abstract

The main purpose of our study is to treat the stability problem of the phosphate Kef Essennoun quarry in the mining field of Jebel Onk located in the Northeastern part of Algeria.
To achieve these objectives, we started by monitoring the unstable area, using two monitoring systems: control stations and inclinometer. We then carried out a digital assessment of the Northwestern edge stability of the quarry, under the current operating conditions of exploitation. After that, we proposed a new operating plan for the reopening of the depot under the required security conditions. At the end, we carried out an assessment of the edge stability, as the work to reopen and develop the Kef Essennoun quarry progressed.
The results show that, under the current operating conditions of exploitation, the Northwestern edge of the Kef Essennoun quarry is unstable (FS<1). The backfilling of the pilot pit of the mine, lead to the assurance of the mine walls stability, by increasing the values of safety factors with a rate of more than 30%.
The backfilling of the pilot pit of the mine and the resumption of top-down mining exploitation will ensure the stability of the quarry during and after the operating exploitation mining.
The study of the stability of the embankments bleachers, the edges of the quarries and the facings of the slag heaps during the open pit mining of useful ores deposits is an essential step that must be done gradually according to the development of mining works to guarantee the safety of personnel, materials, reserves and the environment.

Keywords: *Kef Essennoun, open pit mine, safety factor, embankments stability, mine reopening*

Introduction

The stability of quarries slopes and open-pit mines remains one of the crucial and fundamental questions for the useful mineral deposits exploitation. It has a direct influence on work security in the mine, on the techniques and technologies used and on the operating exploitation conditions of these deposits.

Given its importance, several authors have treated this topic during their research [1] [3] [4] [5] [6] [7] [8] [10] to optimize the parameters influencing the edge stability of opencast mining.

The determination of the optimal slope angle, ensuring the stability of the mining pit is a crucial step during the exploitation of the deposits because this angle has a double influence: 1 – Safety: an edge angle too high can become a bank deformation factor, resulting slippage on the mine edges and causing unpleasant damage. 2 – Economical: in very deep mines, a change in the slope angle by a few degrees leads to a change in the stripping volumes, amounting to millions of cubic meters, which influences the project's profitability.

The Kef Essennoun phosphate open pit mine has been a subject of a major landslide in 2007, which lead to the buried reserves and therefore the closure of the main pit [8]. After a brief observation and in order to ensure the continuity of production, the company SOMIPHOS ordered the resumption of the exploitation operations by reopening the quarry at another location. However, the problem stability has not been solved in a lasting reliable manner.

In the present study, we have dealt at the same time with a security, technical, technological and environmental problem concerning the assessment of edge stability and the reopening of the Kef Essennoun phosphate quarry in the Djebel Onk mine, in the aim to provide objective, solid and sustainable solutions for the maximum extraction of the reserves of the deposit under the best conditions.

Presentation of the study area

Geographical location

The Kef Essennoun phosphate deposit belongs to the Djebel Onk mining field in Northeastern part of Algeria. It is lo-

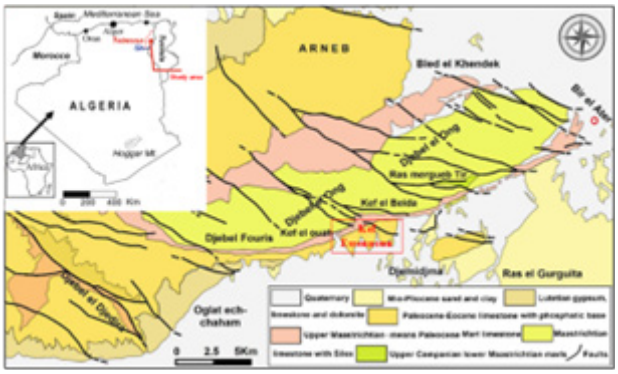

Fig. 1. Geographical and geological situation of the study area [6]
Rys. 1. Położenie geograficzne i geologiczne badanego obszaru [6]

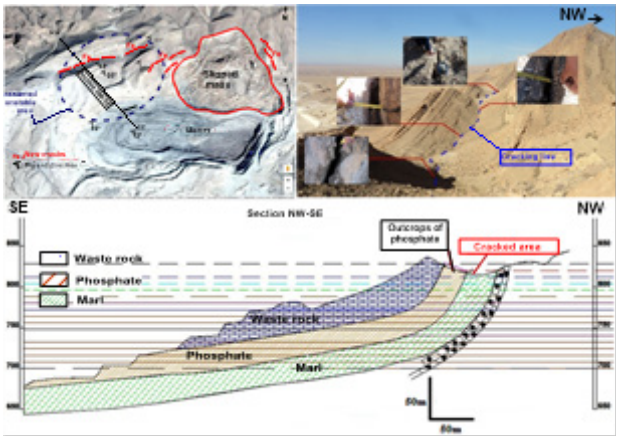

Fig. 2. Location of new cracks on the NW edge of the Kef Essennoun quarry
Rys. 2. Lokalizacja nowych pęknięć na NW krawędzi kamieniołomu Kef Essennoun

cated approximately 10 km southwest of the town of Bir El Ater, 100 km south of the town of Tebessa and 20 km from the Algerian-Tunisian border (Fig. 1).

Geomorphological context

The structure of the Jebel Onk region is an anticlinal stretching for about 20 km along an axis 70°E and a width of about 3 km [2]. This asymmetric anticline was described as a post--Pliocene anticlinal flexure. Morphologically, we can subdivide this area into two parts:

- The Southern part: where the mining operation takes place, this area is characterized by a simple structure and is in the form of monocline table with a regular dip from 5° to 10° toward the South.
- The Northern part: where the Kef Essennoun crest line is located (900 à 1000 m), is made up by massive Maastrichtian limestone and characterized by a more or less rugged morphology.

Geological setting

The stratigraphy series of the Jebel Onk region, in which the Kef Essennoun phosphate deposit belongs, is constituted by a stratification of layers that pass from Maastrichtian at the base to the Miocene at the top, surmounted by Quaternary deposits made up of scree and sandy alluvial formations (Fig. 1). The phosphate mineralization of the deposit is of an upper Thanetian age, represented by a layer that can rich more than 30 m thick.

Tectonic and structural aspect

The study area is located on the southern side of the Djebel Onk anticline. This zone is crossed by a three major NW-SE trending faults without distorting the geometry of the geological layers. On the other hand, in the Kef Essenoun area, extended northward (70°E), the flexible and fracturing tectonics has resulted in the abrupt change of the layers dipping with a nearly sub-vertical dip, steeply inclined to the southeast. Regarding the current tectonic activity, the deposit geological structure has not undergone any tectonic activity [8].

Socio-economic significance

Phosphate is one of the greatest Algerian mineral wealth with total geological resources estimated at 2 million tons. It is a fundamental pillar of the mining sector and of the national economy. The annual production of the phosphate ore exceeded two (2) million tones, in terms of exports in 2021, the majority of which came from the Kef Essennoun deposit.

As a result and with the objective of developing the extraction of this ore, Algeria launched in 2022 a mega project with an investment of approximately seven (07) billion USD. This project will induce a significant socio-economic growth in the eastern part of the country.

Methods

Appearance of recent cracks

After the gigantic slide of the northern edge of the quarry in 2007, the fronts of the bleachers were reoriented to-

Tab. 1. Location and depth of inclinometers
Tab. 1. Lokalizacja i głębokość inklinometrów

Inclinometer	X	Y	Z	Depth(m)
Inc-1	82620.52	69430.15	723.22	75
Inc-2	82627.62	69400.20	705.66	55
Inc-3	82279.63	69336.42	716.65	80
Inc-4	82418.96	69404.24	719.10	77

Tab. 2. Registered displacements at inclinometers
Tab. 2. Rejestrowane przemieszczenia na inklinometrach

Inclinometer	Cumulative displacement to the South (mm)	Cumulative displacement East-West (mm)	Depth (m)
1nc-1	53.83	43.85	55.5
1nc-2	10.10	4.03	33
1nc-3	6.64	0	72.5
1nc-4	16.47 (Sheared)	0	62

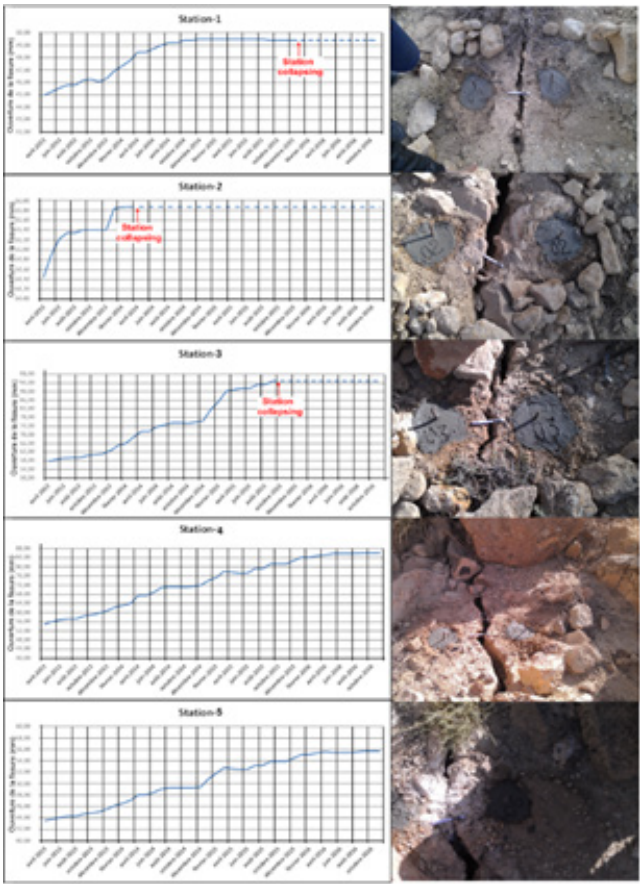

Fig. 3. Control stations from N°01 to 05 with the registration
Rys. 3. Stacje kontrolne od nr 01 do 05 wraz z rejestracją

wards the South, West and Northwest of the deposit. This solution, which seems suitable for the continued extraction of the ore, was hampered by the appearance, in 2013, of new cracks at the top of the Northwest edge of the new exploitation pit. These cracks are located at the phosphate/marl interface (Fig. 2).

Monitoring device

With the objective of monitoring the movement of the unstable rock mass, in amplitude and direction and to identify the location of the sliding surface two (02) monitoring systems have been set up: control stations and inclinometer.

Control stations. This device, installed along cracking line, is used to monitor the cracks progress in terms of spacing. These are steel stakes concreted in two points located on either side of a crack in which, periodic and continuous linear measurements are made of the distance between the two stakes, this method is widely used because of their low cost and ease of implementation. The measurements taken at these stations, between April 2013 and October 2016, showed that:

- The cracks diverge with a maximum speed of 14 cm/yr, recorded at the station number three (ST-3). Therefore, this area is unstable (Fig. 3);
- The progression of the cracking line follows the

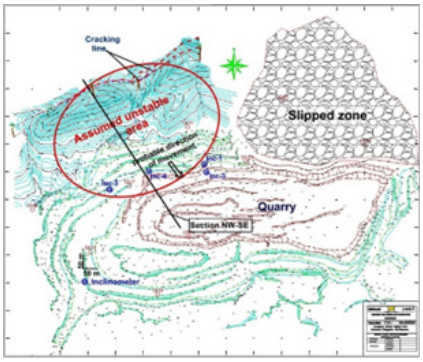

Fig. 4. Characteristics of the supposedly unstable area
Rys. 4. Charakterystyka rzekomo niestabilnego obszaru

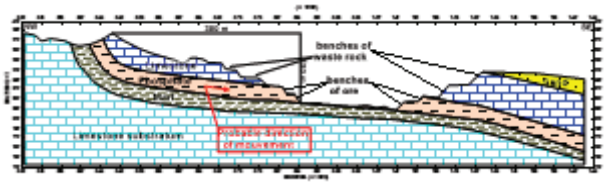

Fig. 5. Geometrical model adopted for the numerical modeling
Rys. 5. Model geometryczny przyjęty do modelowania numerycznego

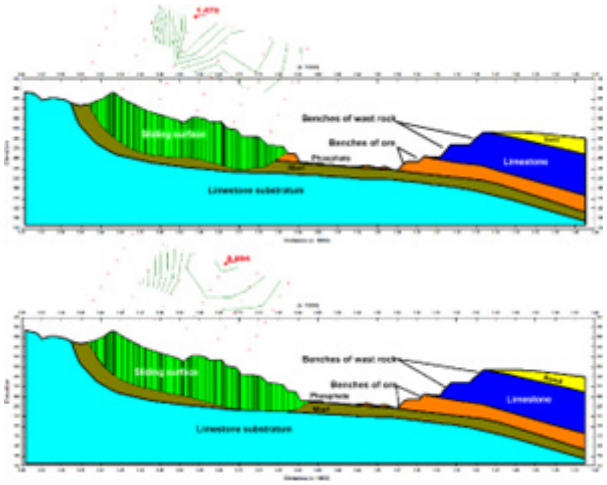

Fig. 6. Sliding surface (hatched in green) for the minimal factor of safety for both approaches: A) without the blasting effects; B) with the blasting effects
Rys. 6. Powierzchnia ślizgowa (zakreskowana na zielono) dla minimalnego współczynnika bezpieczeństwa dla obu podejść: A) bez efektów wybuchowych; B) z efektami wybuchowymi

advancement of the mining front of the phosphate stands on the west side of the mine (Fig. 2).

Inclinometers

In order to quantify the deformation rate and identify the exact location of the sliding surface, four (04) core drill holes equipped with inclinometers (Ic-1, Ic-2, Ic-3, Ic-4) were carried out between February and June 2014. These inclinometers were installed at the lower bench of the quarry (Tab. 1, Fig. 5). The main results are presented in the in table 2.

These measurements showed that:

- All the inclinometers have detected deformations of different degrees that are located in the marly layers.
- The most important deformation is of 53.38 mm towards the South, recorded at a depth of 55.5 m in the inclinometer.
- The likely movement is oriented to the feet of the stands (to the steepest slope).

Stability assessment of the northwestern edge of the kef essennoun quarry

For confirming the results obtained by the monitoring device, we carried out a digital assessment of the Northwestern edge stability of the Kef Essennoun quarry by using the Geo-Studio 7.10 software (Slope/W, 2007) [9]. This software calculates the edge safety factor by taking into account the integration of the geometric aspect (height and inclination of the embankment) and also the geo-mechanical aspect (cohesion and internal friction angle) [8].

Characteristics of the unstable area

Figure 4 shows a survey plan of the Kef Essennoun phosphate mine, updated in January 2016. The unstable zone is

Tab. 3. Geomechanical properties of rocks

Tab. 3. Geomechaniczne właściwości skał

Property / Layer	γ (kN/m^3)	C (MPa)	φ (°)
Altered limestone	22	8.24	39
Phosphate	23	7.35	39
Marl	20	1	15
Limestone substratum	26	5.6	33
Sand	18	1	27

Tab. 4. Simulation results

Tab. 4. Wyniki symulacji

Method	Security factor FS	
	Approach-1: without blasting effects	Approach-2: with the blasting effects
Ordinary	1.475	0.895
Bishop	1.919	1.081
Janbu	1.575	0.894
Morgenstern-Price	1.704	0.931

Tab. 5. Surface area to backfill and the necessary volume of waste rock fill

Tab. 5. Powierzchnia do zasypania i niezbędna objętość zasypki skałą płonną

Backfilling of the pilot pit			
Level	Surface (m^2)	height (m)	Volume (m^3)
N-1(705-690)	184 286	15	2 764 290
N-1(690-675)	116 033	15	1 740 495
Total	-	-	4 504 785

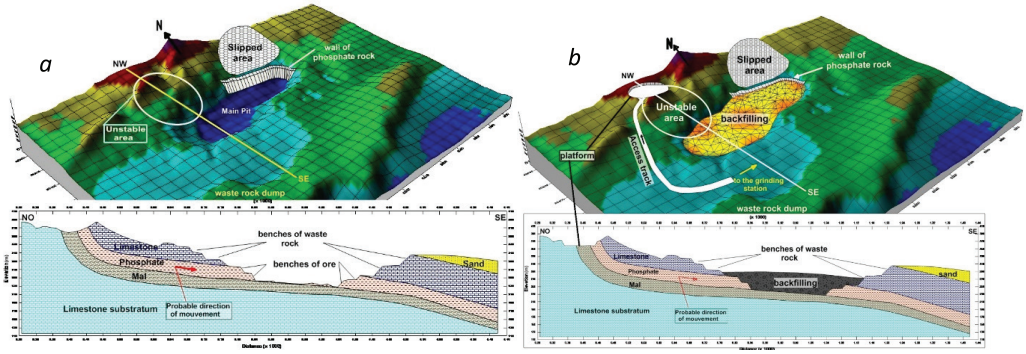

Fig. 7. Current situation of the phosphate quarry (a) and Condition of the quarry after backfilling and reopening of the initial platform (b)

Rys. 7. Obecna sytuacja kamieniołomu fosforytów (a) oraz stan kamieniołomu po zasypaniu i ponownym otwarciu platformy początkowej (b)

located in the Northwestern part of the new exploitation pit and extends over a surface area of more than 20 hectares with a total volume exceeding 10 million cubic meters, which risks being in motion.

This area is bounded at the bottom by the operating benches (free surface), at the top by the cracking line and to the left and right by a few thalwegs. Therefore, the only probable direction of the slide is from the North-West to the South-East (towards the feet of the benches).

Choice of the cross-section

The choice of such a profile for the slope stability study is justified by the characteristics of the study area, the instability indices observed in the field (observation of certain signs of sliding at the crest) and that it be representative for the different specificities, especially morphology and lithostratigraphy.

For the case of Kef Essennoun quarry, the selection of the profile location adopted for the modeling of the unstable area was made taking into account the location and direction of the cracking line, the probable direction of the slip (from the northwest to the southeast) (Fig. 2, 4).

For this purpose, we have used the survey plan of the mine, updated in January 2016, on which, we have drawn a northwest-southeast section.

The overall model adopted to calculate the safety factor with Geo-Studio software is an edge more than 150 m high with a spacing of 380 m, and a slope varying between 20° to 22°, consisting of five benches: two benches in the phosphate layer (H ~15 m and α = 75 to 85°) and three benches in the waste rock (H ~10 m and α = 70 to 80°). This heterogeneous edge is made up of four main layers: Limestone, Phosphate, Marl and limestone as the substratum (Fig. 5).

Results and discussion

Numerical calculation of the security factor

The calculation of the security factor (FS) of the Northwestern edge of the Kef Essennoun quarry was carried out on the basis of the geometrical model defined previously (Fig. 5). The main conditions of the calculation are the geomechanical parameters of the rocks (Tab. 3) and the anthropogenic seismicity due to blasting operations, represented by two horizontal and vertical components, (kh = 0.05 and kv= 0.0125). To this end, two approaches were considered, without and with the

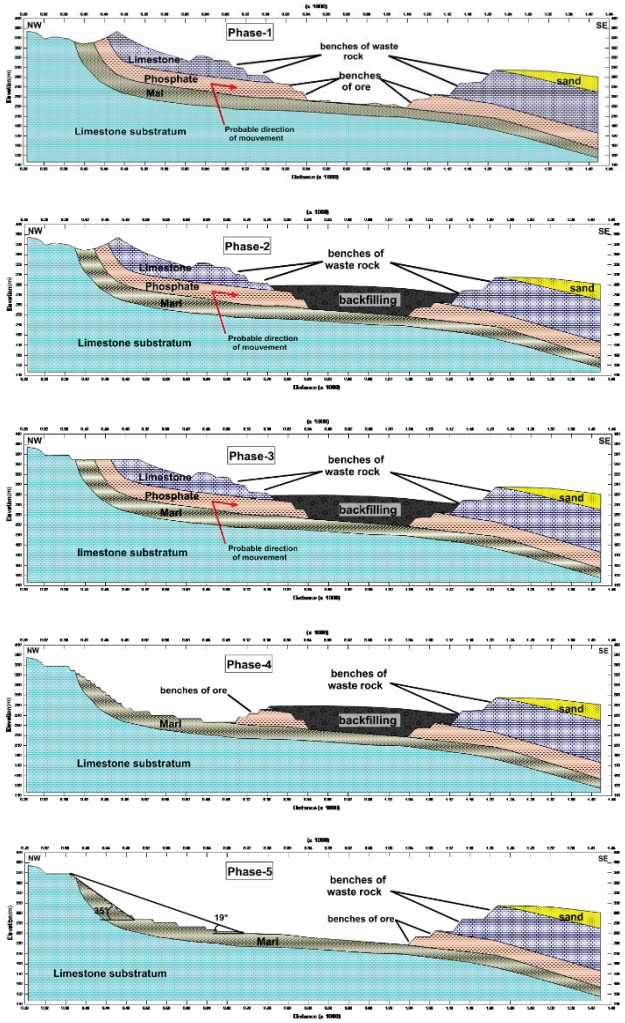

Fig. 8. Development stages of the mining exploitation of Kef Essennoun deposit
Rys. 8. Etapy rozwoju eksploatacji górniczej złoża Kef Essennoun

Tab. 6. Security factor of the different phases of development of Kef Essennoun's quarry
Tab. 6. Współczynnik bezpieczeństwa różnych faz rozwoju kamieniołomu Kef Essennoun

Method	Phase-1 (Before backfill)	Phase-2 (After Backfill)	Phase-3	Phase-4	Phase-5
ordinary	0.895	1.340	1.859	4.936	4.894
Bishop	0.981	1.559	1.884	4.819	4.795
Janbu	0.894	1.289	1.714	4.738	4.534
Morgenstern-Price	0.931	1.508	1.794	4.755	4.753

blasting effects. The obtained results are illustrated in the table 4 and figure 6.

According to the results obtained by the numerical modeling (Tab. 4 and Fig. 6), one notes that:

Approach-1: All security factors calculated by the different methods are greater than the minimum tolerated threshold for the slope stability (FS>1), with a minimum safety factor of 1.312, obtained by the Janbu method. Thus, the edge is stable.

Approach-2: All safety factors are critical (FS ≤1), with a minimum safety factor of 0.806, also obtained by the Janbu method. Thus, the edge is unstable.

The sliding surfaces given by these two approaches have a non-circular (polygonal) shape and located in the marly layer, with a slight difference in the volume of the unstable rock mass (Fig. 6) between the two approaches.

Reopening plan of the kef essennoun quarry

The results obtained previously have shown that, under the current operating conditions of exploitation, the Northwestern edge of the Kef Essennoun quarry is unstable (FS<1) (Tab. 4). This critical situation requires the proposal of a new exploitation plan for the reopening of the deposit under the required security conditions.

Current situation of the quarry

The Kef-Essennoun deposit is the only one which in exploitation among the five existing in the Jebel Onk mining field (Kef Essennoun, Djemi-Djema, Djebel Onk North, Bled Hadba and Oued Betita). The quarry is made up by several benches in the shape of a pit, with an overall surface area of over 35 hectares and a mean depth of 70 meters. In the Northeastern part of the pit, we have the gigantic landslide produced in 2007, estimated at 7.7 million cubic meters, blocked

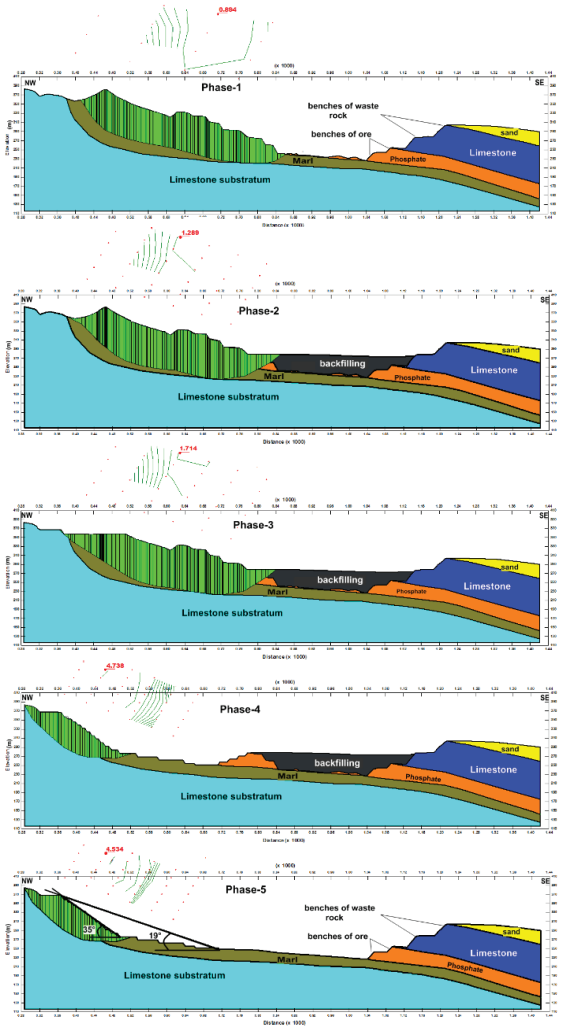

Fig. 9. Sliding surfaces for the minimum safety factor for the development phases of the Kef Essennoun quarry

Rys. 9. Powierzchnie ślizgowe dla minimalnego współczynnika bezpieczeństwa dla faz rozwoju kamieniołomu Kef Essennoun

by a wall of phosphate rock (security barrier). In the North-western side, we find the unstable zone and to the south the waste rock dump (Fig. 7-a).

Reopening of the deposit

The reopening of the Kef Essennoun quarry will need to go through the following four main steps:

- Backfilling of the pit;
- Creation of an access track at the upper level;
- Opening of a new platform ;
- Development of the mining operation exploitation from the top to bottom.

Backfilling of the pit. In order to stabilize the walls of the mine, we found it very useful to backfill the main mining pit. The economic and technical feasibility of this operation requires us to study carefully the surface and height to be backfilled, the type and volume of the backfill and the distance between the backfill and the pit. For this purpose, we recommend:

- Partial backfilling of the pit which affects only the first two benches with a height of 30 m and a volume of 4.6 million m^3 (Tab. 5).
- The use, as backfill, of the waste rock stored to the south of the quarry (dump), consisting mainly of limestones, dolomites and marly limestone.

Access track and working platform. After the backfilling work of the main exploitation pit, we will reopen the deposit by creating of another access track to the upper levels and re-opening a new working platform in the outcrop of the phosphates layer (Fig. 7-b).

Development of the mining operation. The development of the mining operation in the Kef Essennoun quarry goes through two principal steps:

- The reopening of an initial platform and the elimination of the overlying waste rock (hill), in order to reduce the load above the unstable zone (Fig. 10, 11; Phase 3).
- The continuation of the mining exploitation from the top to the bottom, level by level, in the dip direction of the phosphate layer, with bleachers not exceeding 12 m in height and an inclination βg of 70°. Regarding the security and cleaning berms (bs, bn) we take a minimum width of 8 m, these parameters give us a maximum ultimate edge which does not exceed 35° (Fig. 8, Phase 4, 5).

Stability assessment of the final edge considered. In order to prevent all critical situations of the stability of the mine walls, we carried out an assessment of the edge stability, as the work to reopen and develop the Kef Essennoun quarry

progressed, the results of which are shown in Table 6 and Figure 9.

From the results of table 6 and figure 9, we notice:

- The remarkable influence of the backfill operation on the stability of the Northwestern side of the Kef Essennoun quarry, where the safety factors were increased at a rate of over 30% after backfilling.
- After the backfilling of the pit, all the safety factors calculated by the different methods are much greater than 1 (FS>1), which means that the edge is stabilized.
- For the different development phases of the deposit (Phase 3, 4 and 5) (Tab. 6), all the safety factors are greater than 1 (FS> 1). Therefore, there will be no risk of instability at during mining operations, provided that we comply with the recommended technical and technological parameters (hg ≤ 12 m, βg ≤ 70°, bs, bn ≥ 8 m) and under current blasting conditions.

Conclusions

At the end of this study, we find that:

- The plan proposed by the company SOMIPHOS for the continuation of mining work in the Kef Essennoun deposit, after the sliding of the northern edge was not reliable, either, because as the pit was enlarged, new cracks appeared in the upper parts of the North and North-West of the quarry.
- The monitoring devices used (control stations and inclinometers) were complementary to each other and they showed that the northwest edge of the Kef Essennoun quarry is unstable, the sliding surface of which corresponds to the phosphate interface /marl.
- Numerical modeling carried out using the Geo-Studio 7.10 software showed that the north- west edge of the Kef Essennoun quarry is sensitive to mine blasting work and stable in the opposite case.

In view of this observation, we recommend:

- Partial backfilling of the pilot pit of the mine, up to the first two benches with a height of 30 m. This operation would lead to the assurance of stability, by increasing the values of safety factors with a rate of more than 30%.
- Re-study the mining work in order to find an optimal blasting plan, which ensures both the blasting operation and the stability of the mine walls.
- Resumption of top-down mining exploitation remains the appropriate method for this type of deposit, which will ensure the stability of the quarry during and after the operating exploitation mining.

Acknowledgements

We would gratefully acknowledging our colleagues of the study and development department of Phosphate Mining Company (SOMIPHOS) for technical support, especially Mr. BELGHITH Ali and MOHAMED Ali. Our big thank you also goes to Mr. CHANANE Larouci for their assistance in the translation of Article.

Literatura – References

1. Akbulut, I., Çam, I., Aksoy, T., Ölmez, T., Çağlan, D., Onak, A., Sezer, S., Yurtseven, N., Sülükçü, S., Çevik, M., & Çalişkan, V. (2014). Stability studies of the eastern slopes of afşin-elbistan, kişlaköy open-pit lignite mine (kahramanmaraş, se turkey), using the 'finite elements' and 'limit equilibrium' methods. Bulletin of the mineral research and exploration, 148, 107-118.
2. Dass Amiour, M., Mezghache, H. & Elouadi, B. (2013). The use of three physico-chemical methods in the study of the organic matter associated with the sedimentary phosphorites in Djebel Onk Basin, Algeria. Arab J Geosci 6, 309–319 (2013). https://doi.org/10.1007/s12517-011-0381-9
3. Fleurisson, JA. (2012). Slope Design and Implementation in Open Pit Mines: Geological and Geomechanical Approach, Procedia Engineering 46, p 27-38. https://doi.org/10.1016/j.proeng.2012.09.442
4. Fleurisson, JA. & Grenon M. (2014). Conception géomécanique des talus de mines à ciel ouvert. Apr 2014, Marrakech, Maroc. pp. 65-84. hal-00979370.
5. Fredj, M. & al. (2018). Influence of the failure surface choice on the safety factor value during slope stability studies, Naukovyi Visnyk NHU, 2018, N° 3. DOI: 10.29202/nvngu/2018-3/3
6. Gadri, L., Hadji, R., Zahri, F. & al. (2015). The quarries edges stability in opencast mines: a case study of the Jebel Onk phosphate mine, NE Algeria. Arab J Geosci 8, 8987–8997 (2015). https://doi.org/10.1007/s12517-015-1887-3.
7. Kiliç, A. (1999). Analyse de la stabilité des talus sous sollicitation dynamique:application à la mine de lignite d'Afsin-Elbistan,Turquie. Bull Eng Geol Env 57, p 327-336 (1999). https://doi.org/10.1007/s100640050055.
8. Mezam, MC. & Bachar Assed, M A. (2016). Étude Rétro-analytique du glissement du bord Nord de la mine à ciel ouvert de Kef Essennoun (Djebel Onk), Algérie. Bull Eng Geol Environ 76, 1307–1320 (2017). https://doi.org/10.1007/s10064-016-0988-x.
9. Slope/W., (2007). A software package for slope stability analysis. An Engineering Methodology. Seventh Edition, GEO-SLOPE International Ltd.
10. Shamsoddin Saeed, M., Maarefvand, P. & Yaaghubi, E. (2015). Two and three-dimensional slope stability analyses of final wall for Miduk mine. Geo-Engineering 6 9 (2015). https://doi.org/10.1186/s40703-015-0009-0.

Stabilność nasypów kopalni odkrywkowej wraz z propozycją nowej metody wydobycia dla jej ponownego otwarcia (Kef Essennoun, Algieria)

Głównym celem naszych badań jest rozwiązanie problemu stateczności kamieniołomu fosforytów Kef Essennoun w obszarze górniczym Jebel Onk zlokalizowanym w północno-wschodniej części Algierii. Aby osiągnąć te cele, rozpoczęliśmy od monitorowania niestabilnego obszaru przy użyciu dwóch systemów monitorowania: stacji kontrolnych i inklinometru. Następnie przeprowadziliśmy cyfrową ocenę stabilności północno-zachodniej krawędzi kamieniołomu w obecnych warunkach eksploatacji. Następnie zaproponowaliśmy nowy plan operacyjny dla ponownego otwarcia zajezdni w wymaganych warunkach bezpieczeństwa. Na koniec przeprowadziliśmy ocenę stabilności krawędzi w miarę postępu prac nad ponownym otwarciem i zagospodarowaniem kamieniołomu Kef Essennoun. Wyniki pokazują, że w obecnych warunkach eksploatacji północno-zachodnia krawędź kamieniołomu Kef Essennoun jest niestabilna (FS<1). Zasypanie wyrobiska pilotażowego kopalni doprowadziło do zapewnienia stabilności ścian kopalni poprzez zwiększenie wartości współczynników bezpieczeństwa o ponad 30%. Zasypanie wyrobiska pilotażowego kopalni i wznowienie odgórnej eksploatacji górniczej zapewni stateczność kamieniołomu w trakcie i po zakończeniu eksploatacji górniczej. Badanie stateczności obwałowań, krawędzi kamieniołomów i okładzin hałd żużla podczas odkrywkowej eksploatacji złóż rud użytecznych jest niezbędnym krokiem, który należy wykonywać stopniowo, zgodnie z rozwojem prac górniczych, aby zagwarantować bezpieczeństwo personelu, materiałów, zasobów i środowiska.

Słowa kluczowe: *Kef Essennoun, kopalnia odkrywkowa, współczynnik bezpieczeństwa, stateczność obwałowań, ponowne otwarcie kopalni*

Statistical Analysis of Selected Coal Charateristics and Toxic Compounds for FGX Air-Vibrating Separation

Waldemar MIJAŁ[1)], Tomasz NIEDOBA[2)], Daria POLEK[3)], Ireneusz BAIC[4)], Wiesław BLASCHKE[5)]*

[1)] Łukasiewicz Research Network - Institute of Non-Ferrous Metals, ul. Sowińskiego 5, 44-100 Gliwice, Poland; email: waldemar.mijal@imn.lukasiewicz.gov.pl
[2)] AGH University of Science and Technology, Faculty of Civil Engineering and Resources Management, al. Mickiewicza 30, 30-059 Kraków, Poland; email:tniedoba@agh.edu.pl
[3)] Polenergia Obrót S.A., ul. Krucza 24/26, 00-526 Warszawa, Poland; email:polek.daria@gmail.com
[4)] Łukasiewicz Research Network – Institute of Mechanised Construction & Rock Mining, al. Korfantego 193A, 40-157 Katowice, Poland; email: ireneusz.baic@imbigs.lukasiewicz.gov.pl
[5)] Łukasiewicz Research Network – Institute of Mechanised Construction & Rock Mining, al. Korfantego 193A, 40-157 Katowice, Poland; (R.I.P. 23.02.2021)
* Correspondence: Tomasz Niedoba; email: tniedoba@agh.edu.pl; +48 12 617 2056

http://doi.org/10.29227/IM-2023-02-06

Submission date: 01-05-2023 | Review date: 06-06-2023

Abstract

Dry beneficiation methods were popular in the first part of the 20th century. In the 1930s, before World War II, dry separators were used more commonly in the United States. Currently, this method is very popular in China, the United States, India, Russia and other places where its implementation is possible. In Poland, by contrast, dry separation still remains uncommon. However, during the last 30 years, dry separators have started to be more commonly used in coal beneficiation. One example of this type of separator might be the FGX air-vibrating separator. This type of separator uses air suspension to separate heavier particles (tailings) from lighter coal grains. The process of dry separation may depend on various parameters, e.g. particle size fraction, air supply, feed parameters, etc.. This paper describes the mathematical model which shows the scope for using this separation method for coal beneficiation. Mathematical models are based on dependencies between calorific value and ash content in the samples tested as well as relations between arsenic, thallium, mercury, lead and other coal characteristics. The latter parameters are of vital importance as Polish emission standards do not have any limits for the elements mentioned above (arsenic, thallium, mercury and lead).

Keywords: *dry separation, FGX dry separator, deshaling, statistical analysis, correlation, mercury, arsenic, thallium, calorific value, ash content*

1. Introduction

Coal preparation is based on many different methods, including the most common one, which is gravity separation (by using jigs, dense medium separators, dense medium cyclones, shaking tables) or a typical physio-chemical method like flotation (commonly used for coking coals). One of the oldest gravity separation methods is dry coal separation using air jigs or air tables. At the beginning of the 20th century, this method was used in the United States (air dense medium suspension created by air and sand in the Frazer-Yancey dry separator). In the 1930s, in the United States, few dry coal separation plants were built. The biggest dry separation plant was established in Lundale West Virginia, and the biggest separator in this plant had a total capacity of 200t/h. At the same time, in Europe, dry separators were used in countries such as Britain (1925), Belgium, Germany or Poland (1928). Dry enrichment is usually implemented in places where there are water shortages for wet beneficiation processes and in a harsh climate due to the possibility of freezing separation products after separation in a water. The raw materials that can go through beneficiation process using this method include mainly hard coals, with a large proportion of coal-fired or waste fractions, and brown coals (hard types) (Mijał & Tora, 2018; Mijał et al, 2019). In Poland, commonly used dry separation equipment includes the FGX air-vibrating separator and OSX optical sorter constructed by the Comex group company (difference in the colours and content of useful material in the tested feed are used for separation). Until now, those machines have not not used in existing coal separation plants (wide tests were conducted on steam and coking coal by Prof. I. Baic and Prof. W. Blaschke's team and the Institute of Mechanized Construction and Rock Mining, and optical separators were tested for pre-concentration of zinc and lead ore, for example).

The last 20 years become a period of fast development for new dry coal beneficiation equipment, especially ADMFB, CFX, TGX, FGX or KAT (Choung et al., 2006; Jambal et al., 2020; Mijał, 2018; Zhenfu et al., 2002). The FGX air-vibrating separator is becoming increasingly popular and is used in the United States, Turkey, India, South Africa, Vietnam, Russia, Mongolia and a dozen other countries (Baic et al., 2014; Baic et al., 2015; Krukowiecki, 1965; Mijał et al., 2018a; 2018b; Wieniewski et al., 2015; Tangshan, 2020). However, in Poland, it still remains uncommon.

Countries like the USA, India or China conduct research to analyse the scope for removing arsenic, mercury, lead and thallium from raw coal. These tests were conducted mostly using the FGX air-vibrating separator (with ADMFB or air jigs) which also shows the potential for using these jigs to re-

move this kind of contamination (Pan et al., 2020; Dey et al., 2020; Das et al., 2013; Mak et al., 2008; Luttrell et al., 1998; Zhang et al., 2011). Content of calorific value, ash, mercury, lead, thallium and arsenic in coal produced is very important, especially in view of the changes to environmental protection laws in Poland (new emission regulations, changing the quality of produced fossil fuels, implementing new EU regulations etc.). As an example, in Poland, between 2010 and 2014, mercury emission from combustion processes in the energy production and transformation sector alone reached an average amount of around 5,580.52 kg and a total amount(including all emission sources) of 10,014.98 kg. Combustion processes constitute 94% of all mercury emissions (54% of mercury emissions in the power generation sector). In Poland, the content of mercury in hard coal is proven to be between 10 and 800 μg/kg (Bukowski & Burczyk, 2008; Michalska & Białecka, 2012; Smoliński, 2007). Nowadays, in the European Union and Poland, there are currently no regulations concerning emissions of mercury or any other toxic elements. However, over the last few years, EU member states have been obliged to register emission data for the European Pollutant Release and Transfer Register system. This started after the introduction of the Regulation (EC) No 166/2006 of the European Parliament and of the Council (E-PRTR, 2020). In Poland, this kind of emission registration is run by the National Center for Emission Management (Polish: Krajowy Ośrodek Bilansowania i Zarządzania Emisjami – KOBiZE) (Mijal & Tora, 2018).

During the previous few years, some countries, e.g. the Netherlands, the United States or Germany, started implementing some basic regulations for mercury emission. After this, in 2013, the Minamata Convention on Mercury was accepted by some countries including Poland. As a consequence of the introduction of the Convention in the European Union, BAT conclusions have been created for mercury emissions from the combustion of solid fuels (Adamska, 2014; Chmielarz, 2014). Over the last 5 years, more significance has been attached to identifying the occurrence of mercury in raw coal and its beneficiation products (Dziok et al. 2017; 2019). At the same time, other studies focused on the economic scope for using dry coal beneficiation methods in the Polish mining industry (Blaschke & Baic, 2019; Buchalik et al. 2019), which show that dry separation can be applied, providing economic benefits for small private companies. The experiences of some foreign countries prove that investment and operating expenses for dry separation are 48 and 25% lower compared to wet beneficiation methods (Honaker, 2007; Honaker et al., 2010; Honaker et al. 2014) and results prepared by (de Korte, 2010; 2013; 2014) indicate that, when comparing dry separation method with the beneficiation method in dense medium cyclones, the investment and operating expenses can be 25 and 32% lower. Due to the above aspects, e.g. the economic benefits of dry separation and scope for removing mercury using beneficiation methods, this paper aims to describe correlations between different parameters of feed and beneficiation products from the FGX air-vibrating separator (calorific value, ash content, transient moisture, analytical moisture, operating moisture, volatile matter, heating value, coal content, hydrogen content, total sulphur content and mercury content), with a view to increasing the use of this method in Poland. All correlations are described in the next few chapters of this paper.

2. Materials and Methods

Dry beneficiation using an air table works by applying an ever-rising stream of air. A working plate can also get vibration movement to increase the accuracy of separation. The finished product depends on the construction of the table. One example of this type of separators might be the FGX air-vibrating separator. It consists of a funnel feed, dosing feeder, perforated working plate, vibrating element, air chambers, dust removal module and a mechanism that enables the angle of inclination of the working plate and the frequency of vibrations to be changed. The vibrating feeder delivers the feed material to the working plate, inclined at various lateral and longitudinal angles, set in a vibrating motion by means of a vibratory drive (Mijał & Tora, 2018).

In order to provide air supply, there are air chambers under the working plate, which are fed by a centrifugal fan. The fine carbonaceous material forms a fluidized bed (air solid slurry) on contact with the air. As a result, individual grains are similar to each other, depending on size or density. Under the influence of combined forces – air current and vibrations – the coal bed is raised and then, depending on density, it becomes stratified. The lighter material is suspended on the surface of the fluidized bed, while the grains with a higher density sink lie deeper. An additional phenomenon is the liquefaction effect resulting from the interaction of small grains between each other, i.e between the suspension and coarse grains. This phenomenon improves the efficiency of the separation of coarse fractions. Fine material located on the surface of the layer tends to slide over its surface and fall continuously, under the influence of gravity, through the partition at the edge of the plate (dumping of enriched coal). The heavy material falls to the bottom of the layer and is moved towards the waste collection point (gangue) (Baic et al., 2014; Baic et al., 2015; Sobko et al. 2016; Tangshan, 2019).

Air separators have low separation accuracy. This process needs to be conducted strictly following the rules of beneficiation. Other parameters affecting the separation process will only be briefly mentioned in the paper: initial preparation of the feed, grain size & weight feed composition, the amount of air for the separation process, the height of the bars, the angle of the working plate, the number of working plate swings and separation efficiency. Other factors are: total moisture, the dimension of the separated research material, grain size fraction, the amount of grain size fraction (0-6 mm in the feed), the relation between the amount of rock and coal grains in the feed, the total amount of ash in research material and the total amount of middlings in the raw feed. Other specific parameters and of the extent to which grain behaviour depends on the surface of the working board before and during the separation are described in this paper.

The research material used included steam coal extracted from three different coal mines in Poland. The first step was to check the quality of different samples, collected before the separation process (raw feed samples) and after dry beneficiation (concentrate, middlings, tailings or dust samples (the amount of separated product depends on selected parameters of beneficiation process)). All collected samples were subjected to technical and elementary analysis. The mercury content was determined using the MA-2 analyser which uses the atomic spectrometry method. Lead, zinc, copper, nickel and

Tab. 1. Analysis of linear regression between calorific value and ash content in the feed – Experiment 1

Tab. 1. Analiza regresji liniowej dla wartości opałowej i zawartości popiołu w nadawie – Eksperyment 1

N=12	Summary of regression of dependent variable: Q_{uF} R= 0.92914195 R^2= 0.86330475 Adjusted R^2= 0.84963523 F(1,10)=63.155 p<0.00001 Standard error of estimation: 564.22					
	b*	Standard error from b*	b	Standard error from b	t(10)	p
Constant term			29265.17	1626.577	17.99187	0.000000
A_F	-0.929142	0.116917	-340.52	42.849	-7.94704	0.000012

where: N – quantity of the sample; b – value of parameter; b* – value of parameter of normalised distribution; t – value of t-Student test; p – significance level; R – correlation index; R^2 – coefficient of determination; F – value of F-Snedecor test.

Tab. 2. Analysis of linear regression between calorific value and ash content in concentrate – Experiment 1

Tab. 2. Analiza regresji liniowej dla wartości opałowej i zawartości popiołu w koncentracie – Eksperyment 1

N=12	Summary of regression of dependent variable: Q_{uC} R=0.83327499 R^2= 0.69434720 Adjusted R^2= 0.66378192 F(1,10)=22.717 p<0.00076 Standard error of estimation: 660.50					
	b*	Standard error from b*	b	Standard error from b	t(10)	p
Constant term			26876.63	1428.484	18.81480	0.000000
A_C	-0.833275	0.174829	-255.87	53.684	-4.76622	0.000761

Tab. 3. Analysis of linear regression between calorific value and ash content in middlings – Experiment 1

Tab. 3. Analiza regresji liniowej dla wartości opałowej i zawartości popiołu w produkcie pośrednim – Eksperyment 1

N=12	Summary of regression of dependent variable: Q_{uM} R= 0.94597279 R^2= 0.89486451 Adjusted R^2= 0.88435096 F(1,10)=85.115 p<,00000 Standard error of estimation: 1405.4					
	b*	Standard error from b*	b	Standard error from b	t(10)	p
Constant term			29263.37	1806.529	16.19867	0.000000
A_M	-0.945973	0.102536	-342.66	37.142	-9.22580	0.000003

Tab. 4. Analysis of linear regression between calorific value and ash content in tailings – Experiment 1

Tab. 4. Analiza regresji liniowej dla wartości opałowej oraz zawartości popiołu w odpadach – Eksperyment 1

N=12	Summary of regression of dependent variable: Q_{uT} R= 0.98843110 R^2= 0.97699604 Adjusted R^2= 0.97469564 F(1,10)=424.71 p<0.00000 Standard error of estimation: 259.04					
	b*	Standard error from b*	b	Standard error from b	t(10)	p
Constant term			27839.13	1235.573	22.5314	0.000000
A_T	-0.988431	0.047962	-319.00	15.479	-20.6084	0.000000

Tab. 5. Analysis of linear regression between calorific value and ash content – Experiment 2

Tab. 5. Analiza regresji liniowej dla wartości opałowej i zawartości popiołu – Eksperyment 2

N=48	Summary of regression of dependent variable: Q_u= 0.91782903 R^2= 0.84241012 Adjusted R^2= 0.83898426 F(1,46)=245.90 p<0.0000 Standard error of estimation: 2904.4					
	b*	Standard error from b*	b	Standard error from b	t(46)	p
Constant term			27627.92	1046.856	26.3913	0.000000
A	-0.917829	0.058531	-314.67	20.067	-15.6811	0.000000

Tab. 7. Analysis of linear regression between arsenic content in middlings and mercury content in concentrate – Experiment 3

Tab. 7. Analiza regresji liniowej dla zawartości arsenu i zawartości rtęci w koncentracie – Eksperyment 3

N=5	Summary of regression of dependent variable: MAstd (data dry separation 2) R= 0.88757252 R^2= 0.78778499 Adjusted R2= 0.71704665 F(1,3)=11.,137 p<0.04448 Standard error from estimation 3.5230					
	b*	Standard error from b*	b	Standard error from b	t(3)	p
Constant term			-1.20900	3.494465	-0.345976	0.752202
CHg_t^d	0.887573	0.265967	0.11314	0.033904	3.337155	0.044482

Tab. 6. List of parameters included in the Experiment 3
Tab. 6. Lista parametrów mierzonych w Eksperymencie 3

Parameter	Index	Unit
Transient moisture	W_{ex}^{r}	%
Analytical moisture	W_a	%
Operating moisture	W_t^{r}	%
Ash content	A_a	%
Volatile matter	V^{daf}	%
Calorific value	Q_s^{a}	kJ/kg
Heating value	Q_i^{a}	kJ/kg
Coal content	C^{daf}	%
Hydrogen content	H^{daf}	%
Total sulphur content	S_t^{d}	%
Mercury content	Hg_t^{d}	µg/kg

chromium content was assessed by flame atomisation spectrometry (FAAS), and arsenic content by graphite cuvette atomisation (GFAAS). The Hitachi Z-2000 tandem spectrometer with Zeeman background correction was used for these determinations (Makowska et al., 2017). Other parameters were marked in accordance with PN-ISO standards applicable in Poland.

The first stage (Experiment 1) was based on samples divided into 12 feeds, 12 concentrates, 12 middlings and 12 tailings ones, and the minimum total weight of one sample used for the test was 25 Mg. Each sample had a different calorific value (Qu) and ash content (Ar). What is more, difficulties affecting the coal separation process also differed (it was difficult to obtain small samples for the research).

The samples used in phase 1 of the experiment might be considered as not applicable, but for the purpose of this research and discussion, their comparison by analysing correlation between calorific value (Qu) & ash content (Ar) was carried out. After this comparison of results, a theoretical mathematical equation defining the relation between calorific value (Qu) and ash content (Ar) during the dry separation process was developed. This can be treated as an introduction to the further research into the issue of dry coal separation efficiency. Secondly, the whole set of samples was used, but this time without dividing them into subproducts (48 samples, Experiment 2). Next, the mathematical model for the whole experiment was developed. Finally, arsenic, thallium and lead content were taken into account. One reason for this was that these elements had never been analysed using FGX methods in Poland before. Another reason is that emission norms for the aforementioned materials varied, thus relations with each product (feed, concentrate, middlings and tailings) were examined separately.

Furthermore, in 2017, the European Union adopted the IED Directive (Industrial Emission Directive), which contained the relevant BAT conclusions (Best Available Techniques) for emission limits for big power plants and other industrial factories. The BAT conclusions will be implemented in 2021. This creates the need to forecast the amount of the additional substances occurring in mineral products, including those presented in the paper. It will enable the clean coal to be obtained from the FGX dry separation process concerning the quality of the final beneficiation product.

The statistically significant models presented are result of the analysis.

3. Results and Discussion

3.1. Calorific value and ash content

Statistical methods in the processing of mineral resources are used to analyse experiments results. The possible main purposes of these works are to assess the enrichment of the raw material, to study the mechanism of phenomena occurring during processing, to assess process characteristics, to prepare nomograms and charts and to study the properties of new devices, etc (Foszcz et al., 2016; Marciniak-Kowalska et al., 2014; Tumidajski & Saramak, 2009; Niedoba, 2013; Niedoba et al., 2020; Öney et al. 2019; 2020).

The Authors selected one characteristic which proved to be a suitable basis for creating a theoretical mathematical model for dry separation. Concerning two first phases of the experiment, the main parameters taken into consideration were calorific value and ash content in raw feed and beneficiation products. The parameters mentioned and described in this chapter are described below:

- AF – ash content in the feed,
- QuF – calorific value in the feed,
- AC – ash content in concentrate,
- QuC – calorific value in concentrate,
- AM – ash content in middlings,
- QuM – calorific value in middlings,
- AT – ash content in tailings,
- QuT – calorific value in tailings.

Mathematical models were created for calorific value. To create these models, two experiments were taken into consideration. One consisted of 12 samples for which 4 models were created separately, for the feed, concentrate, middlings and tailings. The second experiment consisted of 48 samples, and the model created included the whole sample, without division of the products.

Looking at the results of correlation indices between calorific values and ash contents for experiment 1, one can observe that values of these indices for all products are high. The lowest results were achieved for the concentrate; nonetheless, their value is statistically significant. The same observations were established for experiment 2. The presented models enabled regressive models to be created. These are presented in Tables 1-5 and equations 1-5.

$$Q_{uf} = -340.52A_f + 29265.17; \quad R^2=86,33\% \qquad (1)$$

Tab. 8. Analysis of linear regression between lead content in middlings and transient moisture in concentrate – Experiment 3

Tab. 8. Analiza regresji liniowej dla zawartości ołowiu w produkcie pośrednim oraz wilgotnością przejściową w nadawie – Eksperyment 3

N=5	Summary of regresion of dependent variable: MPbtd (data dry separation 2) R= 0.92561196 R^2= 0.85675750 Adjusted R2= 0.80901000 F(1,3)=17.944 p<0.02408 Standard error from estimation: 3.1451					
	b*	Standard error from b*	b	Standard error from b	t(3)	p
Constant term			5.156418	2.769023	1.862180	0.159485
CW_{ex}^{r}	0.925612	0.218512	2.971642	0.701524	4.235977	0.024081

Tab. 9. Analysis of linear regression between thallium content in tailings and analytical moisture in feed – Experiment 3

Tab. 9. Analiza regresji liniowej dla zawartości talu w odpadach oraz wilgotności analitycznej w nadawie – Eksperyment 3

N=6	Summary of regresion of dependent variable: TTltd (data dry separation 2) R= 0.95372004 R^2= 0.90958192 Adjusted R2= 0.88697740 F(1,4)=40.239 p<0.00316 Standard error from estimation: 0.12609					
	b*	Standard error from b*	b	Standard error from b	t(4)	p
Constant term			0.464575	0.087915	5.284351	0.006152
FW[a]	0.953720	0.150348	0.117426	0.018512	6.343417	0.003163

Tab. 10. Analysis of linear regression between lead content in tailings and analytical moisture in feed – Experiment 3

Tab. 10. Analiza regresji liniowej dla zawartości ołowiu w odpadach oraz wilgotności analitycznej w nadawie – Eksperyment 3

N=6	Summary of regresion of dependent variable: TPbtd (data dry separation 2) R= 0.96334551 R^2= 0.92803456 Adjusted R2= 0.91004320 F(1,4)=51.582 p<0.00199 Standard error from estimation: 3.7572					
	b*	Standard error from b*	b	Standard error from b	t(4)	p
Constant term			6.314377	2.619664	2.410376	0.073525
FW[a]	0.963346	0.134132	3.961634	0.551600	7.182078	0.001991

Tab. 11. Analysis of linear regression between thallium content in tailings and analytical moisture in concentrate – Experiment 3

Tab. 11. Analiza regresji liniowej dla zawartości talu w odpadach oraz wilgotności analitycznej w koncentracie – Eksperyment 3

N=6	Summary of regresion of dependent variable: TTltd (data dry separation 2) R= 0.99009633 R^2= 0.98029074 Adjusted R2= 0.97536342 F(1,4)=198.95 p<0.00015 Standard error from estimation: 0.05887					
	b*	Standard error from b*	b	Standard error from b	t(4)	p
Constant term			0.265597	0.052041	5.10364	0.006965
CW[a]	0.990096	0.070195	0.142052	0.010071	14.10497	0.000147

Tab. 12. Analysis of linear regression between thallium content in tailings and total sulphur content in concentrate – Experiment 3

Tab. 12. Analiza regresji liniowej dla zawartości talu w odpadach oraz całkowitej zawartości siarki w koncentracie – Eksperyment 3

N=6	Summary of regresion of dependent variable: TTltd (data dry separation 2) R= 0.92876633 R^2= 0.86260690 Adjusted R2= 0.82825863 F(1,4)=25.114 p<0.00743 Standard error from estimation: 0.15543					
	b*	Standard error from b*	b	Standard error from b	t(4)	p
Constant term			-0.793805	0.347168	-2.28651	0.084180
CS_t^{d}	0.928766	0.185333	1.826127	0.364399	5.01134	0.007431

Tab. 13. Analysis of linear regression between lead content in taillings and operating moisture in concentrate – Experiment 3

Tab. 13. Analiza regresji liniowej dla zawartości ołowiu w odpadach oraz wilgotności operacyjnej w koncentracie – Eksperyment 3

N=6	Summary of regresion of dependent variable: TPbtd (data dry separation 2) R= 0.97641336 R^2= 0.95338305 Adjusted R2= 0.94172882 F(1,4)=81.806 p<0.00083 Standard error from estimation: 3.0239					
	b*	Standard error from b*	b	Standard error from b	t(4)	p
Constant term			-0.936800	2.777474	-0.337285	0.752858
CW_t^{r}	0.976413	0.107955	2.974026	0.328816	9.044651	0.000828

$$Q_{uc} = -255.87A_c + 26876.63;\ R^2=69.43\% \quad (2)$$

$$Q_{uM} = -342.66AM + 29263.37;\ R^2=89.49\% \quad (3)$$

$$Q_{uT} = -319.00AT + 27839.13;\ R^2=97.70\% \quad (4)$$

$$Q_u = -314.67A + 27627.92;\ R^2=84.24\% \quad (5)$$

Earlier studies have shown that it is not possible to assume a constant heat loss per 1% increase of ash content for various coals (Blaschke & Baic, 2020). The above-mentioned relationships show that using dry deshaling, as well as other beneficiation methods, will produce different effects. Results depend on the characteristics of the relationship between the calorific value and ash content of the specific type of coal being tested. The models obtained make it possible to establish whether the increase in calorific value is related mainly to the reduction of gangue content in the material, or whether the reduction of the value is low, which may be caused by incorrect separation parameters adopted before starting the process. If a significant relationship between the ash content and the calorific value is found, it can be concluded that the methodology of dry beneficiation adopted when using the FGX is accurate. Otherwise, the coal should be enriched using "wet" technology.

3.2. Arsenic, thallium, mercury and lead content in selected products of dry coal separation

As a basis for models, correlation matrices were created. Because of the size of the matrix, it was divided into subsections. Table 6 presents the list of parameters included in the analysis.

The following statistically important models (Tables 7-19; equations 6-18) were developed on the basis of correlation indices between arsenic, thallium and lead content as well as other characteristics of the samples. Notably, due to the small number of samples, only part of the relations are significant.

Concerning arsenic, only one correlation, observed in middlings, was significant. Other products did not show high correlation indices for arsenic content. Thus, one might say that it does not really correlate with other material characteristics; therefore, it is difficult to predict its content in the type of coal being tested. As far as other components are concerned, results showed that the most important relations included middlings, tailings and concentrates. Surprisingly, not so many relations were found for feed. Considering the components examined, the most statistically important equations were found for thallium, especially in the case of tailings.

It was also noteworthy that a significant number of relations were observed for lead content in tailings. This means that these components can be easier described by other characteristics of coal, especially when it has already been processed and divided into sub-products. However, a larger number of samples included in further experiments may assist in carrying out a more detailed analysis, and even some weaker relations may prove significant.

$$MAs_t^d = 0.11314\ CHg_t^d - 1.20900;\ R^2=78.78\% \quad (6)$$

$$MPb_t^d = 2.971642\ CW_{ex}^r + 5.156418;\ R^2=85.67\% \quad (7)$$

$$TTl_t^d = 0.117426\ FW^a + 0.464575;\ R^2=90.96\% \quad (8)$$

$$TPb_t^d = 3.961634\ FW^a + 6.314377;\ R^2=92.80\% \quad (9)$$

$$TTl_t^d = 0.142052\ CW^a + 0.265597;\ R^2=98.03\% \quad (10)$$

$$TTl_t^d = 1.826127\ CS_t^d - 0.793805\ ;\ R^2=92.88\% \quad (11)$$

$$TPb_t^d = 2.974026\ CW_t^r - 0.936800;\ R^2=97.64\% \quad (12)$$

$$TPb_t^d = 60.3096\ CS_t^d - 34.9234;\ R^2=84.34\% \quad (13)$$

$$TTl_t^d = 0.136645\ MW^a + 0.331830;\ R^2=96.87\% \quad (14)$$

$$TTl_t^d = -0.031248\ MA^a + 1.806443;\ R^2=86.44\% \quad (15)$$

$$TTl_t^d = 0.00011\ MQ_s^a - 1.38258;\ R^2=88.29\% \quad (16)$$

$$TPb_t^d = 4.545630\ MW^a + 2.115580;\ R^2=96.10\% \quad (17)$$

$$TPb_t^d = 0.0037\ MQ_s^a - 52.2748;\ R^2=81.71\% \quad (18)$$

The occurrence of the elements selected depends mainly on the form of their presence in the raw material used. For example, in the case of mercury, it may be removed when coal contains high amount of pyrite. Then, the efficiency of mercury removal oscillates within the limits of 90%. If there is a smaller amount of pyrite in the material then this level of efficiency decreases to approximately 10%. Another important factors is whether the form of pyrite is organic or mineral. If it is organic, then it is necessary to apply additional chemical or biological methods to the process (Blaschke & Baic, 2020).

As far as arsenic, lead and thallium are concerned, it should be noted that all of them are considered ecotoxic elements; therefore, their presence in coal is undesirable. In the case of Poland, the current production of energy – around 80% of all energy produced – is still based on coal combustion . The emission of these elements into the atmosphere can be lowered by introducing what is called pre-combustion processes, which include a type of mechanical processing that enables coal to be separated from the other particles. If the particles are pyrite, such processing is much easier; otherwise, more complicated expensive chemical or biological methods need to be used. Apart from mercury, this mainly applies to arsenic and lead; the analysis showed that these elements could be removed from the coal material, especially when they occurred in pyrite. As far as thallium is concerned, more research needs to be conducted in the future.

The models presented could be more statistically significant if the number of samples were larger. Observations based on the models presented can be used to forecast both the quality of the coal used in a power plant as well as selecting the appropriate beneficiation method. It also shows that the presence of additional elements in the material being analysed can influence the quality of the coal, measured by calorific value or analytic moisture (e.g., the presence of thallium). Furthermore, in Poland, the FGX method is still not common but could be effectively introduced in some cases. Statistical analysis would make such applications more justifiable.

Tab. 14. Analysis of linear regression between lead content in tailings and total sulphur content in concentrate – Experiment 3

Tab. 14. Analiza regresji liniowej dla zawartości talu w odpadach oraz wilgotności analitycznej w produkcie pośrednim – Eksperyment 3

N=6	Summary of regresion of dependent variable: TPbtd (data dry separation 2) R= 0.91836434 R^2= 0.84339306 Adjusted R2= 0.80424133 F(1,4)=21.542 p<0.00972 Standard error from estimation: 5.5425					
	b*	Standard error from b*	b	Standard error from b	t(4)	p
Constant term			-34.9234	12.37971	-2.82102	0.047779
CS_t[d]	0.918364	0.197868	60.3096	12.99413	4.64130	0.009725

Tab. 15. Analysis of linear regression between thallium content in taillings and analytical moisture in middlings – Experiment 3

Tab. 15. Analiza regresji liniowej dla zawartości talu w odpadach oraz wilgotności analitycznej w produkcie pośrednim – Eksperyment 3

N=5	Summary of regresion of dependent variable: TTltd (data dry separation 2) R= 0.98425066 R^2= 0.96874936 Adjusted R2= 0.95833248 F(1,3)=92.998 p<0.00237 Standard error from estimation: 0.08422					
	b*	Standard error from b*	b	Standard error from b	t(3)	p
Constant term			0.331830	0.073813	4.495573	0.020545
MW[a]	0.984251	0.102063	0.136645	0.014170	9.643549	0.002367

Tab. 16. Analysis of linear regression between thallium content in tailings and ash content in middlings – Experiment 3

Tab. 16. Analiza regresji liniowej dla zawartości talu w odpadach oraz zawartości popiołu w produkcie pośrednim – Eksperyment 3

N=5	Summary of regresion of dependent variable: TTltd (data dry separation 2) R= 0.92970543 R^2= 0.86435219 Adjusted R2= 0.81913625 F(1,3)=19.116 p<0.02214 Standard error from estimation: 0.17547					
		Standard error from b*	b	Standard error from b	t(3)	p
Constant term			1.806443	0.212292	8.50925	0.003409
MA[a]	-0.929705	0.212640	-0.031248	0.007147	-4.37220	0.022135

Tab. 17. Analysis of linear regression between thallium content in tailings and calorific value in middlings – Experiment 3

Tab. 17. Analiza regresji liniowej dla zawartości talu w odpadach oraz wartości opałowej dla produktu pośredniego – Eksperyment 3

N=5	Summary of regresion of dependent value: TTltd (data dry separation 2) R= 0.93961963 R^2= 0.88288505 Adjusted R2= 0.84384674 F(1,3)=22.616 p<0.01765 Standard error from estimation: 0.16304					
	b*	Standard error from b*	b	Standard error from b	t(3)	p
Constant term			-1.38258	0.494631	-2.79517	0.068126
MQ_s[a]	0.939620	0.197581	0.00011	0.000024	4.75561	0.017648

Tab. 18. Analysis of linear regression between lead content in tailings and analytical moisture in middlings – Experiment 3

Tab. 18. Analiza regresji liniowej dla zawartości ołowiu w odpadach oraz wilgotności analitycznej w produkcie pośrednim - Eksperyment 3

N=5	Summary regresion of dependent value: TPbtd (data dry separation 2) R= 0.98031244 R^2= 0.96101249 Adjusted R2= 0.94801665 F(1,3)=73.948 p<0.00331 Standard error from estimation: 3.1419					
	b*	Standard error from b*	b	Standard error from b	t(3)	p
Constant term			2.115580	2.753624	0.768289	0.498254
MW[a]	0.980312	0.113999	4.545630	0.528605	8.599286	0.003306

Tab. 19. Analysis of linear regression between lead content in tailings and calorific value in middlings – Experiment 3

Tab. 19. Analiza regresji liniowej dla zawartości ołowiu oraz wartości opałowej w produkcie pośrednim – Eksperyment 3

N=5	Summary regresion of dependent value: TPbtd (data dry separation 2) R= 0.90392637 R^2= 0.81708288 Adjusted R2= 0.75611051 F(1,3)=13.401 p<0.03523 Standard error from: 6.8054					
	b*	Standard error from b*	b	Standard error from b	t(3)	p
Constant value			-52.2748	20.64634	-2.53192	0.085281
MQ_s[a]	0.903926	0.246926	0.0037	0.00100	3.66072	0.035227

4. Conclusions

Based on the calculations performed for all experiments mentioned in this paper, it was found that there are high correlations between heating values and ash content. This means that it is possible to predict the calorific value of a coal sample by establishing its ash content. The dry coal separation method used in these experiments indicated that it can be an effective tool for separating feedstock into sub-products (concentrate, middlings, and tailings), and with the help of models, it is easier and more effective to select the appropriate tool or technique. Regarding arsenic, thallium, lead, and mercury – elements that have not previously been considered for the FGX dry separation method – few correlations were found to be statistically significant. However, relatively high quality models include thallium content, especially for tailings. The most difficult thing to predict is arsenic content but this situation may improve if more analyses of this kind are performed. This may help to find less correlated and more significant relationships between the carbon characteristics of all considered products, while more complex models may help to describe the problem more accurately.

The number of samples included in this paper was not sufficient to conclude that the results were representative of all circumstances. These samples were prepared specifically for the evaluation of the FGX dry separation method. If more samples with more variable process conditions were available, the results would enable the process to be defined more accurately. However, this particular method is still not common in Poland and therefore requires much more research.

Acknowledgements

The paper is the product of the Project No. 16.16.100.215.

To memory of Prof. Wiesław Blaschke (R.I.P. 23.02.2021)

Literatura – References

1. ADAMSKA B., 2014. Konwencja Minamata w sprawie rtęci. Rtęć w przemyśle – Konwencja, ograniczanie emisji, technologia, Warszawa, Poland, 26.11.2014.
2. BAIC I., BLASCHKE W., SZAFARCZYK J., 2014. Dry Coal Cleaning Technology, Inżynieria Mineralna - Journal of the Polish Mineral Engineering Society, vol. 2(34), 257-262.
3. BLASCHKE W., BAIC I., 2020. Gravity Concentration Technique. FGX Type Air-Vibration Separators, Studies, Dissertations, Monographs, vol. 212, IGSMiE PAN, Krakow, Poland, 9-171.
4. BLASCHKE W., BAIC I., 2019. FGX Air-Vibrating Separators for Cleaning Steam Coal – Functional and Economical Parameters, Inżynieria Mineralna - Journal of the Polish Mineral Engineering Society, vol. 2(44), 19-26.
5. BUCHALIK G., MOTYCZKA S., SZAFARCZYK J., BAIC I., BLASCHKE W., 2019. Economic efficiency of the dry separation process: Polish experience, Congress Proceeding Volume II - XIX International Coal Preparation Congress, New Delhi, India, 13-15.11.2019, Woodhead Publishing India. New Delhi, India, 54-63.
6. BUKOWSKI Z., BURCZYK A., 2008. Oznaczanie rtęci w węglach koksujących. Analiza korelacji. Konferencja Koksownictwo, Zakopane, Poland, 8-10.10.2008.
7. CHMIELARZ A., 2014. Propozycja BAT/BEP w dokumentach roboczych grupy eksperckiej konwencji Minamata w sprawie rtęci, Rtęć w przemyśle – Konwencja, ograniczanie emisji, technologia, Warszawa, Poland, 26.11.2014
8. CHOUNG J., MAK C., XU Z., 2006. Fine coal beneficiation using an air dense medium fluidized bed, Int. J. Coal Prep. Util., vol. 26, 1-15.
9. DAS T.B., PAL S.K., GOURICHARAN T., SHARMA K. K., CHOUDHURY A., 2013. Evaluation of reduction potential of selected heavy metals from an Indian coal by conventional coal cleaning. Int. J. Coal Prep. Util., vol. 33, 300-312.
10. DE KORTE G.J., 2010. Coal preparation research in South Africa, Proceedings of XVI International Coal Preparation Congress. Lexington. USA. 25-30.04.2010, 859-863.
11. DE KORTE G.J., 2013. Dry processing versus dense medium processing for preparing thermal coal. Proceedings of the XVII International Coal Preparation Congress. Istanbul. 1-6.10.2013, 301-308.
12. DE KORTE G.J., 2014. Dry processing of coal – status update, Report CSIR/Nre/Mmr/Er/2014/0040/B, Coaltech, South Africa.
13. DEY S., CHAURASIA B., SAHU L., 2020. Dry processing of high ash Indian coal by air fluidized vibrating deck, Int. J. Coal Prep. Util., vol. 42(6), 1675-1694..
14. DZIOK T., BAIC I., STRUGALA A., BLASCHKE W., 2019. Ekologiczne i ekonomiczne aspekty procesu suchego odkamieniania węgli kamiennych, Zeszyty Naukowe Instytutu Gospodarki Surowcami Mineralnymi Polskiej Akademii Nauk – The Bulletin of The Mineral and Energy Economy Research Institute of the Polish Academy of Sciences, vol. 108, 99-110.
15. DZIOK T., STRUGAŁA A., CHMIELNIAK T., BAIC I., BLASCHKE W., 2017. Koncepcja hybrydowego procesu usuwania rtęci z węgla kamiennego, Zeszyty Naukowe Instytutu Gospodarki Surowcami Mineralnymi Polskiej Akademii Nauk – The Bulletin of The Mineral and Energy Economy Research Institute of the Polish Academy of Sciences, vol. 98, 125-136.
16. E-PRTR - European Pollutant Release and Transfer Register, http://prtr.ec.europa.eu (available on-line 09.2020).
17. FOSZCZ D., DUCHNOWSKA M., NIEDOBA T., 2016. Accuracy Of Separation Parameters Resulting From Errors Of Chemical Analysis, Experimental Results And Data Approximation, Physicochem. Probl. Miner., vol. 52, no. 1, 98-111.
18. HONAKER R. Q., LUTTRELL G., MOHANTY M., 2010. Coal preparation research in the USA, Proceedings of XVI International Coal Preparation Congress. Lexington. USA, 25-30.04.2010, 864-874.
19. HONAKER R. Q., SARACOGLU M., THOMPSON E., BRATTON R., LUTTRELL G. H., RICHARDSON V., 2014. Dry coal cleaning using the FGX separator in "Thesis collection of FGX dry coal preparation technology", Tangshan Shenzhou Manufacturing Co., Ltd. China, 13-20.
20. HONAKER R.Q., 2007. Dry Coal Cleaning Technologies for India Coal; Workshop on coal beneficiation and utilization of rejects: initiatives, policies and best practices, Ranchi, India.
21. JAMBAL D, KIM B.-G., JEON H.-S., 2020. Dry beneficiation of coal on KAT air table, Int. J. Coal Prep. Util., 1-13 (available on-line: 31.11.2020).
22. KRUKOWIECKI W., 1965. Przeróbka Mechaniczna Kopalin; PWN: Warszawa, 154-159.
23. LUTTRELL G. H., VENKATRAMAN P., YOON R. H., 1998. Removal of hazardous air pollutant precursors by advanced coal preparation, Int. J. Coal Prep. Util., vol. 19, 243-255.

24. MAK C., CHOUNG J., BEAUCHAMP R., KELLY D. J. A., XU Z., 2008. Potential of air dense medium fluidized bed separation of mineral matter for mercury rejection from Alberta sub-bituminous coal, Int J Coal Prep Util., vol. 28, 115-132.

25. MAKOWSKA D., WIERONSKA F., DZIOK T., STRUGAŁA A., 2017. Emisja pierwiastków ekotoksycznych z procesów spalania paliw stałych w świetle regulacji prawnych, Polityka Energetyczna – Energy Policy Journal, vol. 20(4), 89-102.

26. MARCINIAK-KOWALSKA J., NIEDOBA T., SUROWIAK A., TUMIDAJSKI T., 2014. Multi-criteria evaluation of coal properties in terms of gasification, Arch. Min. Sci., vol. 59(3), 677-690.

27. MICHALSKA A., BIAŁECKA B., 2012. Zawartość rtęci w węglu i odpadach górniczych, Prace Naukowe GIG Górnictwo i Środowisko - Research Reports of Central Mining Institute. Mining & Environment, vol. 3, 73-87.

28. MIJAŁ W., 2018. Coal Mining and Coal Preparation in Vietnam. Inżynieria Mineralna-Journal of The Polish Mineral Engineering Society, vol. 41(1), 275-286.

29. MIJAŁ W., BLASCHKE W., BAIC I., 2018. Dry Coal Beneficiation Methods in Poland, 25th World Mining Congress Proceedings, Astana, Kazakhstan, 19-22.06.2018, 129-140.

30. MIJAŁ W., BLASCHKE W., BAIC I., 2018. Sucha metoda wzbogacania węgla w Polsce, Przegląd Górniczy – Mining Review, vol. 11(1152), 9-18.

31. MIJAŁ W., NIEDOBA T., POLEK D., 2019. Mathematical model of dry coal deshaling by using FGX vibrating air table, IOP Conf. Ser.-Mat. Sci., vol. 641, 1-11.

32. MIJAŁ W., TORA B., 2018. Development of dry coal gravity separation techniques. IOP Conf. Ser.-Mat. Sci., vol. 427, 1-8.

33. NIEDOBA T., 2013. Methodological Elements Of Applying Two- And Multi-Dimensional Distributions Of Grained Materials Properties To Coal Beneficiation, Gospod. Surowcami Min. – Mineral Resources Management, vol. 29(2), 155-172.

34. NIEDOBA T., PIĘTA P., SUROWIAK A., 2020. Factor Analysis and Mathematical Modeling in Determining the Quality of Coal, Inzynieria Miner., vol. 1, 151-160.

35. ÖNEY O., SAMANLI S., NIEDOBA T. SUROWIAK A, PIĘTA P., 2019. Optimization of reagent dosages with the use of response surface methodology and evaluation of test results with upgrading curves in graphite flotation, Particul. Sci. Technol., vol. 37(2), 171-181.

36. ÖNEY O., SAMANLI S., NIEDOBA T., PIĘTA P., SUROWIAK A., 2020. Determination of the Important Operating Variables On Cleaning Fine Coal by Knelson Concentrator and Evaluation Of The Performance Through Upgrading Curves, Int. J. Coal Prep. Util., vol. 40(10), 666-678.

37. PAN J., ZHOU C.-C., ZHANG N.-N., LIU C., TANG M.-C., CAO S.-S., 2020. Arsenic in coal: Modes of occurrence and reduction via coal preparation – a case study, Int. J. Coal Prep. Util., vol. 40(11), 766-779.

38. SMOLIŃSKI A., 2007. Energetyczne wykorzystanie węgla źródłem emisji rtęci – porównanie zawartości tego pierwiastka w węglach, Ochrona Powietrza i Problemy Odpadów, vol. 41(2), 45-53

39. SOBKO W., BLASCHKE W., BAIC I., 2016. Constructional Improvements of FGX-1 Air Concentrating Table Aiming at Optimization of Operation. Inżynieria Mineralna - Journal of the Polish Mineral Engineering Society, vol. 1(37), 37-46.

40. TANGSHAN KAIYUAN COAL PREPARATION TECHNOLOGY CO. LTD. Brochure and promotional materials. available on-line 2.12.2020 http://www.kyxuanmei.com/

41. TANGSHAN SHENZHOU MANUFACTURING CO. LTD., Brochure and promotional materials, http://www.tsshenzhou.com/en/enindex.htm (available on-line 11.2019).

42. TUMIDAJSKI T., SARAMAK D., 2009. Metody i modele statystyki matematycznej w przeróbce surowców mineralnych, Wydawnictwo AGH, Kraków, Poland, 7-295.

43. WIENIEWSKI A, SZCZERBA E, NAD A, ŁUCZAK R, KOŁACZ J, SZEWCZUK A., 2015. Ocena możliwości zastosowania nowoczesnych technik separacji do wstępnego wzbogacania rudy Zn-Pb, CUPRUM – Czasopismo Naukowo-Techniczne Górnictwa Rud, vol. 2(75), 109-122.

44. ZHANG B., AKBARI H., YANG F., MOHANTY M. K., HIRSHI J., 2011. Performance optimization of the FGX dry separator for cleaning high-sulphur coal, Int. J. Coal Prep. Util., vol. 31, 161-186.

45. ZHENFU L., QINGRU C., YAOMIN Z., 2002. Dry beneficiation of coarse coal using an air dense medium fluidized bed (ADMFB), Int. J. Coal Prep. Util., vol. 22, 57-64.

Analiza statystyczna wybranych charakterystyk i składników toksycznych węgla dla procesu separacji w separatorze powietrznym FGX

Suche metody wzbogacania były popularne w pierwszej połowie XX wieku. Separatory suche były używane zwłaszcza przed II Wojną Światową w latach 30-ych w USA. Obecnie, metoda ta jest bardzo popularna w Chinach, USA, Indiach, Rosji oraz w innych miejscach, gdzie możliwe jest jej zastosowanie. W Polsce proces ten jest wciąż bardzo mało popularny. Podczas ostatnich 30 lat systemy wzbogacania węgla zaczęły szerzej korzystać z separatorów suchych a przykładem bardzo popularnego urządzenia tego typu jest FGX – wibracyjny stół powietrzny. Ten typ separatora korzysta z zawiesiny powietrznej w celu wydzielenia cięższych ziaren (odpadów) od lżejszych ziaren węgla. Sucha separacja może zależeć od różnych parametrów, tj. klasa ziarnowa, zasoby powietrza, parametry nadawy itp. Artykuł ten opisuje model matematyczny, który pokazuje możliwości zastosowania tej metody separacji przy wzbogacaniu węgla. Modele matematyczne oparte były na zależnościach pomiędzy wartością opałową oraz zawartością popiołu w testowanych próbkach, jak również na relacjach pomiędzy zawartościami arsenu, talu, rtęci, ołowiu i innych charakterystyk węgla. Ostatnie parametry są bardzo ważne ponieważ polskie standardy emisji nie zawierają limitów dla pierwiastków wymienionych powyżej, a więc arsenu, talu, rtęci oraz ołowiu.

Słowa kluczowe: *separacja sucha, suchy separator FGX, odkamienianie, analiza statystyczna, korelacja, rtęć, arsen, tal, wartość opałowa, zawartość popiołu*

INŻYNIERIA MINERALNA
CZASOPISMO POLSKIEGO TOWARZYSTWA PRZERÓBKI KOPALIN

2(52)
2023

INŻYNIERIA MINERALNA
CZASOPISMO POLSKIEGO TOWARZYSTWA PRZERÓBKI KOPALIN

2(52)
2023